AD-A253 631

Volume 21

Ceramic Transactions

MICROWAVES: THEORY AND APPLICATION IN MATERIALS PROCESSING

David E. Clark • Frank D. Gac • Willard H. Sutton

DTIC
ELECTE
JUL 2 1 1992
S A D

92 7 20 183

92-19259

This document has been approved for public release and sale; its distribution is unlimited.

8000060 1004

Reproduced From
Best Available Copy

Volume 21

Ceramic Transactions

MICROWAVES: THEORY AND APPLICATION IN MATERIALS PROCESSING

Edited by David E. Clark, University of Florida;
Frank D. Gac, Los Alamos National Laboratory; and Willard H. Sutton, United Technologies Research Center

The American Ceramic Society, Inc.
Westerville, Ohio

Delete Available from The
American Ceramic Society Statement per
telecon Debbie Tyrrell AFOSR/XOT
Bolling AFB, DC 20332
NWW 7/29/92

DTIC QUALITY INSPECTED 2

Accesion For
NTIS CRA&I ☑
DTIC TAB ☐
Unannounced ☐
Justification
By
Distribution /
Availability Codes
Dist | Avail and / or Special
A-1

Approved for public release;
distribution unlimited.

REPORT DOCUMENTATION PAGE

Form Approved
OMB No. 0701 0188

Public reporting burden for this collection of information is estimated to average 1 hour per response, including the time for reviewing instructions, searching existing data sources, gathering and maintaining the data needed, and completing and reviewing the collection of information. Send comments regarding this burden estimate or any other aspect of the collection of information, including suggestions for reducing this burden, to Washington Headquarters Services, Directorate for information Operations and Reports, 1215 Jefferson Davis Highway, Suite 1204, Arlington, VA 22202-4302, and to the Office of Management and Budget, Paperwork Reduction Project (0704-0188), Washington, DC 20503.

1. AGENCY USE ONLY (Leave blank)	2. REPORT DATE	3. REPORT TYPE AND DATES COVERED
	27 April 1992	Final 28 April 1991 - 27 April 1992

4. TITLE AND SUBTITLE
Microwaves: Theory and Application in Materials Processing

5. FUNDING NUMBERS
AFOSR-91-0229 (G)
61102F
2306/A2

6. AUTHOR(S)
David E. Clark
Frank D. Gac
Willard H. Sutton

7. PERFORMING ORGANIZATION NAME(S) AND ADDRESS(ES)
The American Ceramic Society
735 Ceramic Place
Westerville, Ohio 43081

8. PERFORMING ORGANIZATION REPORT NUMBER
None
AFOSR-TR- 92 0370

9. SPONSORING/MONITORING AGENCY NAME(S) AND ADDRESS(ES)
Air Force Office of Scientific Research (AFSC)
AFOSR/NE, Building 410
Bolling Air Force Base
Washington, DC 20332-6448

10. SPONSORING/MONITORING AGENCY REPORT NUMBER
AFOSR-91-0229

11. SUPPLEMENTARY NOTES

12a. DISTRIBUTION/AVAILABILITY STATEMENT
Available to the Public from
The American Ceramic Society
Book Sales
735 Ceramic Place
Westerville, OH 43081 (614) 890-4700

12b. DISTRIBUTION CODE

13. ABSTRACT (Maximum 200 words)

The symposium was held during the 93rd Annual Meeting of The American Ceramic Society in Cincinnati, OH, April 29-May 3, 1991. One objective was to assemble the experts in this emerging technology for the purpose of identifying problem areas and defining potential solutions. A second objective was to explore new applications where microwave energy can have significant impact. A third objective was to bring together researchers, materials fabricators, and microwave equipment manufacturers for the purpose of expediting technology transfer and commercialization of important discoveries in this field.

Participants from 7 countries presented 80 papers at the symposium. A combination of keynote, invited, and contributed presentations provided excellent overviews of existing programs, microwave/materials interactions, measurements, equipment design, modeling, and applications.

14. SUBJECT TERMS Microwave/Material Interactions; Modeling; Dielectric Measurements; Microwave sintering; Microwave Processing of Nonoxides; Microwave Applications in Waste Management; Joining/Composite Fabrication with Microwave Energy; Novel(*) (*) Applications of Microwave Energy; Microwave Equipment Design

15. NUMBER OF PAGES
698

16. PRICE CODE
-

17. SECURITY CLASSIFICATION OF REPORT	18. SECURITY CLASSIFICATION OF THIS PAGE	19. SECURITY CLASSIFICATION OF ABSTRACT	20. LIMITATION OF ABSTRACT

NSN 7540-01-280-5500

Standard Form 298 (Rev. 2-89)
Prescribed by ANSI Std. Z39-18
298-102

Vol 21

Proceedings of the Symposium on Microwaves: Theory and Application in Materials Processing held during the 93rd Annual Meeting of The American Ceramic Society in Cincinnati, OH, April 29–May 3, 1991.

Library of Congress Cataloging-in-Publication Data

Symposium on Microwaves : Theory and Application in Materials Processing (1991 : Cincinnati, Ohio)
Microwaves: theory and application in materials processing / edited by David E. Clark, Frank D. Gac, Willard H. Sutton.
p. cm.—(Ceramic transaction ; v. 21)
"Proceedings of the Symposium on Microwaves: Theory and Application in Materials Processing held during the 93rd Annual Meeting of the American Ceramic Society in Cincinnati, OH, April 29–May 3, 1991"—T.p. verso
Includes index.
ISBN 0-944904-43-2
1. Ceramics—Congresses. 2. Microwaves—Industrial applications—Congresses. I. Clark, David E. II. Gac, Frank D. III. Sutton, Willard H. (Willard Holmes), 1930- IV. American Ceramic Society. Meeting (93rd : 1991 : Cincinnati, Ohio) V. Series.
TP786.S94 1991
666—dc20 91-25754
CIP

Copyright © 1991, The American Ceramic Society, Inc. All rights reserved.

No part of this book may be reproduced, stored in a retrieval system, or transmitted in any form or by any means, electronic, mechanical, photocopying, microfilming, recording, or otherwise, without written permission from the publisher.

Printed in the United States of America
1 2 3 4—95 94 93 92 91

ISBN 0-944904-43-2

Notice

The views, opinions, and findings contained in this book are those of the individual authors. The publishers, editors, and authors assume no responsibility or liability for errors or any consequences arising from the use of the information contained herein. Mention of trade names of commercial products does not constitute endorsement or recommendation for use by the publishers, editors, or authors.

Final determination of the suitability of any information, procedure, or product for use contemplated by any user, and the manner of that use, is the sole responsibility of the user. This book is intended for informational purposes only.

Expert advice should be obtained at all times when implementation is being considered, particularly where hazardous materials or processes are encountered.

Preface

Today there are numerous research teams worldwide investigating the use of microwave energy for processing materials. With a few obvious exceptions, such as food processing and wood drying (all low-temperature applications), the majority of the interest and activity began about ten years ago and has grown substantially in the last three years.

Research indicates that microwave energy offers many advantages over conventional heating methods. These advantages generally can be divided into two categories. One is the reduction in processing time and temperature, and the other the fabrication of materials with unique and/or superior properties. Further, microwave energy appears to be especially advantageous for the processing of many types of ceramics requiring high temperatures. This is due to the increased coupling efficiency of ceramics with microwaves as they are heated and to the more uniform (volumetric) heating provided by microwaves.

In spite of the great potential of microwave energy in the field of materials processing, there are engineering and cultural barriers that must be overcome before its widespread use will be realized. Examples of the barriers are the absence of a good database on dielectric properties in the microwave range and as a function of temperature; a poor exchange of information among researchers in the field; the absence of industrial equipment for large-scale/high-temperature manufacturing; and the reluctance on the part of materials manufacturers to change from a proven technology.

The mission of this symposium was to address some of these issues. One objective was to assemble the experts in this emerging technology for the purpose of identifying problem areas and defining potential solutions. A second objective was to explore new applications where microwave energy can have significant impact. A third objective was to bring together researchers, materials fabricators, and microwave equipment manufacturers for the purpose of expediting technology transfer and commercialization of important discoveries in this field.

Participants from seven countries presented 80 papers at the symposium. A combination of keynote, invited, and contributed presentations provided excellent overviews of existing programs, microwave/materials interactions, measurements, equipment design, modeling, and applications. This book contains 69 peer-reviewed papers from the symposium and will serve as an excellent reference source for both newcomers to the field and well-seasoned veterans.

Briefly, what we have learned is that

- There are differences between microwave and conventional heating, but we do not fully understand these differences or their origins. Although there is some agreement between models and data, much research is needed here.
- Substantial progress has been made in dielectric property measurements in the microwave range in the last few years, and these measurements should become more routine in the very near future.

- Exciting developments have occurred in equipment design at the research and development level, but more work is needed before equipment is available for large-scale manufacturing.
- Although the economics of microwave processing appear promising, more analyses are needed to nail down the benefits.
- As with any field, safety is a concern, but sufficient information is available to permit safe use of microwave energy. Investigations are likely to continue in this area as new equipment and applications emerge.

In order to ensure progress in this field, we plan to continue holding symposia on an annual basis, alternating between the American Ceramic Society, Inc., and the Materials Research Society.

David E. Clark
Frank D. Gac
Willard H. Sutton

Acknowledgments

The editors are grateful for the support provided by various professional societies, government agencies, and companies. We also thank the staff at The American Ceramic Society, Inc., for their assistance in organizing the facilities for the symposium and expediting the publication of the proceedings.

Of course, the most important constituents of any symposium are the speakers, authors, and session chairs. Thanks to the creativity and dedication of these individuals, the symposium was high-quality and smoothly run, resulting in an important and timely publication.

We extend special thanks to Lorie Stapler for assistance in organizing the symposium and for managing the collection and compilation of manuscripts.

Symposium on Microwaves: Theory and Application in Materials Processing

Sponsored by:

The Engineering Ceramics, Nuclear, and Whitewares Divisions of
The American Ceramic Society, Inc.

The National Institute of Ceramic Engineers

Endorsed by:

The Materials Research Society

The International Microwave Power Institute

Financial support provided by:

The American Ceramic Society, Inc.

Electronic and Material Sciences Directorate/
Air Force Office of Scientific Research

Advanced Industrial Concepts (AIC) Materials Program/
Conservation and Renewable Energy, DOE

3M Company

The University of Florida

Microwave Materials Technologies, Inc.

Session Chairs

Wayne R. Tinga
University of Alberta

David E. Clark
University of Florida

Frank D. Gac
Los Alamos National Lab

Peter Angelini
Oak Ridge National Lab

Ross H. Plovnick
3M Company

Claude P. Lorenson
Alcan International Ltd.

Ronald Snider
Raytheon Company

Richard S. Garard
Wavemat, Inc.

Mark A. Janney
Oak Ridge National Lab

Jes Asmussen Jr.
Michigan State University

Raymond Milleman
U.S. Department of Energy

Arthur C. Lind
McDonnell Douglas Research Labs

Richard Silberglitt
Technology Assessment & Transfer, Inc.

V.M. Kenkre
University of New Mexico

Gregory A. Kriegsmann
New Jersey Institute of Technology

D. Lynn Johnson
Northwestern University

Santosh Y. Limaye
Ceramatec, Inc.

Wesley P. Unruh
Los Alamos National Lab

Magdy F. Iskander
University of Utah

Contents

Section I. Program Overviews

An Overview of Microwave Applications Research in Canada 3
S.J. Oda
Microwave Processing of Ceramics at Northwestern University 17
D.L. Johnson
Microwave Processing Activities at the University of Florida 29
D.E. Clark and D.C. Folz
Microwave Processing of Ceramics at the University of Utah—Description of Activities and Summary of Progress 35
M.F. Iskander, O. Andrade, A. Virkar, H. Kimrey, R. Smith, S. Lamoreaux, C. Cheng, C. Tanner, R. Knowlton, and K. Mehta

Section II. Microwave/Material Interactions

Fundamental Interaction Mechanisms Between Microwaves and Matter 51
R.E. Newnham, S.J. Jang, M. Xu, and F. Jones
Theory of Microwave Interactions with Ceramic Materials 69
V.M. Kenkre
An Analysis of the Individual Grain Structure of an Oxide Heated Using Microwave Radiation and Heated Conventionally 81
T.T. Meek, X. Zhang, and M. Rader
Microwave Enhanced Diffusion? 95

J.D. Katz, R.D. Blake, and V.M. Kenkre
Activation Energies for the Dielectric Loss Factor/AC Conductivity of Some Polycrystalline Ceramics 107
R.W. Bruce
Microwave Enhanced Pyrochemical Reactions of PuO_2, UO_2, and U_3O_8 117
E.F. Sturcken and L.E. McCurry
Radiofrequency Safety Issues in Industrial Heating Systems 125
J.M. Osepchuk

Section III. Modeling

Computational Techniques in Modeling and Quantifying Microwave Interactions with Materials 141
M.F. Iskander, O. Andrade, H. Kimrey, R. Smith, and S. Lamoreaux
Electromagnetic Modeling of Single-Mode Excited Material Loaded Applicators 159
B. Manring and J. Asmussen, Jr.
Modeling Microwave Heating of Ceramics 167
X.D. Yu, V.V. Varadan, and V.K. Varadan
Microwave Heating of Ceramics 177
G.A. Kriegsmann
Models of Nonthermal Effects on Ionic Mobility During Microwave Processing of Crystalline Solids 185
J.H. Booske, R.F. Cooper, I. Dobson, and L. McCaughan
Numerical Methods for the Modeling of Microwave Fields 193
C. Lorenson and C. Gallerneault

Section IV. Dielectric Measurements

Measurement of Dielectric Properties in the Frequency Range of 300 MHz to 3 GHz as a Function of Temperature and Density 203
J.B. Salsman

A High Temperature Microwave Dielectrometer 215
W. Xi and W.R. Tinga
Effect of Powder Characteristics on Dielectric Properties of Alumina Compacts 225
R. Moreno, P. Miranzo, J. Requena, J.S. Moya, J. Mollá, and A. Ibarra
Dielectric Properties of Ceramics at Microwave Frequencies 235
N.H. Harris, J.R. Chow, R.L. Eisenhart, and B.M. Pierce
Free-Space Measurements of High-Temperature, Complex Dielectric Properties at Microwave Frequencies 243
R.D. Hollinger, V.V. Varadan, V.K. Varadan, and D.K. Ghodgaonkar
In Situ Measurement of the Dielectric Properties of Ceramics with a Single Mode Microwave Heating Device ...251
X.D. Yu, V.V. Varadan, V.K. Varadan, and D. Ghodgaonkar
Method for Calculating and Observing Microwave Absorption by a Sphere in a Single Mode Rectangular Cavity 261
H.W. Jackson and M. Barmatz
Measurement of Cavity Perturbation to Determine the Microwave Absorption of a Sphere in a Single Mode Resonator 271
J.L. Watkins, C.O. Hagenlocher, and M. Barmatz

Section V. Microwave Sintering

Practices of Ultra-Rapid Sintering of Ceramics Using Single Mode Applicators 283
Y.-L. Tian
Microwave Sintering of Alumina Ceramics in a Single Mode Applicator 301
D.S. Patil, B.C. Mutsuddy, J. Gavulic, and M. Dahimene
Microwave Sintering of Zirconia-8 Mol% Yttria 311
M.A. Janney, C.L. Calhoun, and H.D. Kimrey
Microwave (Hybrid) Heating of Alumina at 2.45 GHZ: I. Microstructural Uniformity and Homogeneity 319
A.S. Dé, I. Ahmad, E.D. Whitney, and D.E. Clark

Microwave (Hybrid) Heating of Alumina at 2.45 GHZ: II. Effect of Processing Variables, Heating Rates and Particle Size 329
A.S. Dé, I. Ahmad, E.D. Whitney, and D.E. Clark
Magnetite as a Sintering Aid for Microwave Consolidation of Soda-Lime Glass 341
Y.H. Kao and J.D. Mackenzie
Rapid Sintering of Hydroxyapatite Ceramics by Microwave Processing 349
Y. Fang, D.K. Agrawal, D.M. Roy, and R. Roy
Microstructural Evolution of $YBa_2Cu_3O_{7-x}$ Using Microwave Energy 357
A.D. Cozzi, D.K. Jones, Z. Fathi, and D.E. Clark
Microwave Plasma Sintering of Alumina 365
M.P. Sweeney and D.L. Johnson

Section VI. Microwave Processing of Nonoxides

"Ultra" High-Temperature Microwave Sintering 375
C.E. Holcombe and N.L. Dykes
Microwave Synthesis of Metal Carbides 387
H. Kozuka and J.D. Mackenzie
Production of Ultra-Fine Silicon Carbide by Fast Firing in Microwave and Resistance Furnaces 395
S.N. Kumar, A. Pant, R.R. Sood, J. Ng-Yelim, and R.T. Holt
Characterization of Silicon Nitride Synthesized by Microwave Heating 403
J.O. Kiggans, C.R. Hubbard, R.R. Steele, H.D. Kimrey, C.E. Holcombe, and T.N. Tiegs
Microstructure Development During Microwave Annealing of Dense Silicon Nitride 411
T.N. Tiegs, M.K. Ferber, J.O. Kiggans, K.L. More, C.M. Hubbard, and D.W. Coffey

Synthesis of Nonoxide Ceramic Powders by Nonthermal Microwave Plasma 421
A.K. Singh, P. Mehta, and A.I. Kingon

Section VII. Microwave Applications in Waste Management

The Use of "Self Heating" Ceramics as Crucibles for Microwave Melting Metals and Nuclear Waste Glass 433
F.F. Sturcken
Characterization of Radioactive Waste Melter Feed Vitrified by Microwave Energy 441
C.M. Jantzen and J.R. Cadieux
Microwave Processing of Simulated Nuclear Waste Glass 451
R.L. Schulz, Z. Fathi, D.E. Clark, and G.G. Wicks
Application of Microwave Heating Techniques to the Detoxification of Contaminated Soils 459
C.E. George, I. Jun, and J. Fan
Oxidative Degradation of Trichloroethylene Adsorbed on Active Carbons: Use of Microwave Energy 467
R. Varma and S.P. Nandi
Microwave Reactivation of CIP Spent Carbon 475
I.S. Balbaa, S.J. Oda, K.E. Haque, P.D. Kondos, and R.J.C. MacDonald

Section VIII. Joining/Composite Fabrication with Microwave Energy

Investigation of Interlayer Materials for the Microwave Joining of SiC 487
R. Silberglitt, D. Palaith, W.M. Black, H.S. Sa'adaldin, J.D. Katz, and R.D. Blake
Application of Microwave Processing to Simultaneous Sintering and Joining of Ceramics 497
X.D. Yu, V.V. Varadan, and V.K. Varadan

Microwave Joining of Si-SiC/Al/Si-SiC 507
T.Y. Yiin, V.V. Varadan, V.K. Varadan, and J.C. Conway
Microwave Joining of Ceramics 515
S. Al-Assafi, I. Ahmad, Z. Fathi, and D.E. Clark
Enhanced Microwave Absorption in Chiral Composite Materials 523
Y. Ma, V.K. Varadan, and V.V. Varadan
Parametric Experimental Study of Microwave Absorption in Chiral Composites 531
R. Ro, V.V. Varadan, and V.K. Varadan
Microwave Heating for Fiber-Placement Manufacturing of Carbon-Fiber Composites 539
A.C. Lind, F.C. Wear, and J.E. Kurz
Distribution of Dissipated Power in a Graphite Fiber Reinforced Epoxy Composite Heated in a Microwave Cavity 547
R. Fritz and J. Asmusser., Jr.
Microwave Heating of Cermets 557
E. Bescher and J.D. Mackenzie
Microwave Sintering of Al_2O_3:ZrO_2 Ceramics 565
D.S. Patil, B.C. Mutsuddy, J. Gavulic, and M. Dahimene
Microwave Sintering of Y_2O_3(3%)-ZrO_2 (TZP) 577
Y.-L. Tian, B.-S. Li, J.-L. Shi, Y.-P. Xu, J.-K. Guo, and D.-S. Yen

Section IX. Novel Applications of Microwave Energy

Microwave Processing of Polyester and Polyester/Glass Composites 587
U. Hottong, J. Wei, R. Dhulipala, and M.C. Hawley
Use of a TM_{010} Microwave Cavity at 2.45 GHz for Aerosol and Filament Drying 597
D.E. Christiansen and W.P. Unruh

Effect of Microwave Heating on Solid State Reactions of Ceramics 605
I. Ahmad and D.E. Clark
Applications of Microwaves in High Temperature Superconductor Materials and Devices 613
P.J. Gielisse, H. Niculescu, B. Roy, P. Pernambuco-Wise, J.E. Crow, G. Sykora, and R. Wahlers
Surface Modification of Sodium Aluminosilicate Glasses Using Microwave Energy 623
Z. Fathi, I. Ahmad, J.H. Simmons, D.E. Clark, and A.R. Lodding
Metallorganic and Microwave Processing of Ceramic Powders and Compacts 631
M.A. Willert-Porada and S. Vodegel

Section X. Microwave Equipment Design

Accurate High Temperature Measurements in Microwave Environments 641
J. Mershon
A Wide Range Tunable and Matchable High Temperature Applicator 647
B.Q. Tian and W.R. Tinga
Experimental Examination of Material Loaded Cylindrical Applicators and Comparison with Theoretical Models 655
J. Asmussen, Jr., B. Manring, R. Fritz, and M. Siegel
Techniques to Improve the Performance of Microwave Process Systems Which Utilize High Q Cavities 667
J.F. Gerling and G. Fournier
Microwave Thermogravimetric Analyzer (MTGA) 675
E.H. Moore, I. Ahmad, and D.E. Clark
An Applicator Design for Processing Large Quantities of Dielectric Material 683
V.N. Tran
Index 693

Ceramic Transactions *is a new proceedings series designed to meet two needs: high quality content and rapid publication. Volumes in the series come from meetings, symposia, and forums. Each paper is reviewed by two peers, and final manuscripts are prepared by authors in a "camera-ready" format. The volumes in this series would not be possible without the hard work, dedication, and cooperation of editors, reviewers, and authors, who all deserve a great deal of thanks.*

Your comments, questions, and suggestions for future ***Ceramic Transactions*** *volumes are welcomed and should be addressed to the Director of Publications, The American Ceramic Society, Inc.*

Section I. Program Overviews

AN OVERVIEW OF MICROWAVE APPLICATIONS RESEARCH IN CANADA

S.J. Oda, Ontario Hydro Research Division,
800 Kipling Ave., Toronto, Ontario
Canada M8Z 5S4

ABSTRACT

Examples of microwave applications research in Canada are described to help illustrate the reasons for the adoption of this energy efficient electrotechnology. Microwave processing of advanced ceramics, minerals, chemical synthesis and environmental wastes is being pursued as well as the more traditional (common) applications in the food and rubber industries.

INTRODUCTION

In Canada the development of industrial microwave heating applications has been undertaken by a number of research groups for over 25 years. Indeed, Edmonton, Alberta, Canada was the site for the founding of the International Microwave Power Institute in 1966. This organization continues to provide an international journal and annual symposium through which much of the world's industrial microwave heating activity is disseminated. This review describes some of the past and current Canadian activity in microwave heating. Table 1 summarizes the Canadian activity in industrial microwave heating by individual organizations including their areas of involvement. The following sections provide additional detail of microwave research activity involving Canadian government agencies, universities, electric utilities and private companies.

GOVERNMENT (FEDERAL AND PROVINCIAL) RESEARCH

Canadian government agencies, recognizing the potential benefits that industrial microwave processing can yield, have provided funding assistance and some technical support for the development of new innovative applications. As expected, these applications tend to emphasize the improved energy efficiency, selective and volumetric heating that microwaves can provide.

Atomic Energy of Canada Research Ltd. (AECL) at Chalk River, Ontario is currently involved in microwave applications research. Undertaking contract research for industry and government they have one of the largest resources of microwave and RF equipment design capability in Canada. One of AECL's laboratories has developed a microwave cavity system that can rapidly evaluate the permittivity and permeability of materials up to 1000°C at 2450 MHz [1]. Ceramics including aluminas, ferrites and silicon carbide are among the materials that have been successfully characterized. In addition, AECL together with Voss Associates Engineering Ltd. (VAEL) have recently produced a 2-part report reviewing the microwave heating and dielectric literature on

minerals, rocks, ceramics and related materials [2]. The report provides a good review of microwave heating studies related to minerals and suggests how available testing techniques can be used to examine potential applications. In addition to the review (contributed by VAEL), the report also includes tests performed by AECL on a selection of eight industrial minerals to determine both real and imaginary parts of the dielectric constant up to temperatures of about 800°C. The test procedure developed by AECL was used for the following mineral samples: serpentine, nepheline syenite, illite clay, kaolin, vermiculite, magnetite, talc, and talc plus 5% binder (sodium silicate). The technique is an effective and accurate method for obtaining fundamental properties of materials.

The Canadian Department of Energy, Mines and Resources, through their Canada Centre for Mineral and Energy Technology (CANMET), is also pursuing potential microwave applications. CANMET has conducted preliminary microwave tests to reactivate spent carbon from a gold mining operation [3,4]. More quantitative tests at Ontario Hydro's Research Division [5,48] provided the following: (1) microwave energy can reactivate spent carbon; (2) microwave heating provided a 95% regeneration of adsorption capacity (using the properties of virgin carbon) in 5 minutes as compared to 89% in 30 minutes for the conventional process; (3) microwave-reactivated carbon has superior properties versus conventional reactivation in terms of pH, apparent density and adsorption capacity; and, (4) based on greater energy efficiency, 915 MHz appears preferable over 2450 MHz. A second phase has been started in 1991 to bring this potential application closer to an industrial process.

The Ontario Waste Management Corporation sponsored a study to investigate the use of microwave heating to reactivate carbon and recover perchloroethylene solvent for the dry cleaning industry [49]. Preliminary test results indicate that a microwave energy requirement of 0.51 kWh/kg of carbon will reduce perchloroethylene concentrations in the spent carbon to that of fresh carbon. In addition, the initial results indicate that the important properties of the microwaved and fresh carbon are comparable (eg, colour removal efficiency and launderometer test).

The Ontario Ministry of Energy provides assistance to Ontario industry through its Enersearch program. This program has provided funding support for a number of potential microwave applications including drying of pharmaceutical hard gelatin capsules, joining of alumina and silicon nitride rods, sintering of alumina and silicon nitride ceramics, drying/slipcasting of whiteware and debarking of frozen timber [6,7,54,55,64]. One example of an Enersearch-funded project involved the use of microwave energy for drying of pharmaceutical capsules [7]. R & J Engineering Corp. built a microwave-assisted dryer that has provided an energy savings of 35% over the conventional drying system. (By incorporating microwave energy the drying time can be shortened from 35 minutes to about 11 minutes.) In addition, because the microwave-assisted equipment is shorter (6.6 m versus 12 m), the capsule production room can be smaller. This size reduction is claimed to provide a further 35-50% savings in energy attributable to climate control.

The National Research Council of Canada (NRCC), through its Division of Electrical Engineering, provided an invaluable technical resource for Canadian industry from 1965 to 1986 [8-23]. This facility helped Canadian users through education as well as through the development and design of a wide variety of microwave devices and instrumentation. Examples of their involvement ranged from development of a rotary microwave processor for processing granular materials [23], a waveguide applicator for sheet materials [17], to microwave instrumentation for measuring moisture contents in web processes [15].

UNIVERSITY RESEARCH

At the University of Alberta, W.A.G. Voss together with W.R. Tinga continue to lead much of the activity involving microwave heating technology. In 1966, with funding assistance from NSERC, Voss and Tinga helped to organize the International Microwave Power Institute which continues to provide a much needed technical resource for the international scientific community. Voss is credited with over 74 publications involving industrial processes and material properties, as well as biological effects. A few of the more recent publications are referenced [24-26]. W.R. Tinga is also very active in the field of microwave technology and is the head of the Microwave Power Laboratory at the University of Alberta (Department of Electrical Engineering) [25,27-30]. Of particular interest are two papers authored by these individuals at a recent Materials Research Society microwave symposium [25,26]. The first paper [25] describes the expanding application of microwaves for processing natural and synthetic solids. It provides an approach that gives attractive examples for potential microwave applications including: microwave-induced dry organic reactions; microwave heating of solvents to accelerate chemical reactions; mineral and ore processing with the zeolite family of particular industrial interest; and, advanced polymers, ceramics, and composites (eg, carbon-fibre based composites). The second paper [26] describes the development of a microwave materials analyser which promises to provide a more extensive empirical characterization of mixed (impure) material heating behaviour. The applicator has provided heating rates up to 700°C/s for various oxides and ceramic materials at 915 MHz. With microwave-transparent refractory materials surrounding the sample (solid, granular, liquid or gas), temperatures of greater than 1500°C can be maintained in some materials. A 60 W solid-state power source supplies the applicator with microwave energy and controls the temperature.

At the University of Waterloo D. Pei has been involved since the 60's in a number of microwave research activities [32-37]. Indeed in 1967, Pei and Ford were among the first to use microwave energy to heat solid compounds to temperatures of up to 1900°C [32] and to investigate its use for two chemical processes [33]: production of hydrogen cyanide from ammonia and carbon, and the direct dissociation of molybdenum disulphide. Among other microwave heating studies conducted at the University of Waterloo include: drying of sewage sludge and bread baking.

École-Polytechnique has been involved in microwave applications research since the early 60's. R. Bosisio is credited for much of the activity at this university in the field of microwave plasma and dielectric methods and measurement at high temperature [38-45]. A recent paper [38] involving his group gives data on a 'model' dielectric/ohmic loss material (NaI in ethanol) from which are predicted heating patterns at the two ISM frequencies, 915 and 2450 MHz. According to Voss [31], 'this is an important contribution in the most difficult area of electroheat'. Another effort involves a collaboration between École-Polytechnique's LAIMO (Laboratoire d'applications industrielles des micro-ondes) and Hydro-Québec's LTÉÉ (Laboratoire des technologies électrochimiques et des électrotechnologies d'Hydro-Québec) facility (see Hydro-Quebec entry). The involvement at LAIMO is led by M. Giroux of the Department of Electrical Engineering [52,53].

At Queen's University J. Wan is utilizing microwave energy in catalytic processes and destruction of environmental contaminants including: methane decomposition to C_2 and C_3 hydrocarbons; dehalogenation of trichlorobenzene; and destruction of SO_2 and NO_x by reduction rather than conventional oxidative methods [46-49]. Research activities concerning the latter rely on the selectivity and efficiency of microwave heating. By selecting a 'catalyst' that facilitates the particular reaction as well as containing a strongly absorbing microwave sensitizer, the bulk of the

reaction can take place at ambient temperature. A second benefit provided by microwave energy is its ability to be pulsed, which provides some control of reaction temperature and reaction selectivity.

At Laurentian University in Sudbury, Ontario, Smith, Gedye et al reported the use of microwave energy (from a standard domestic microwave oven) to synthesize some organic compounds up to 1240 times faster than conventional reflux techniques [50,51]. According to the authors, reaction rate enhancement is possible because the polar molecules in certain solvents can absorb microwave energy very rapidly (eg, water, methanol). This high rate of absorption is said to cause superheating of the solvent when contained in a microwave-transparent pressure vessel. Reaction rates of polar molecules in non-polar solvents were not increased appreciably by the microwave technique. By optimizing the conditions of the reaction the authors believe that rate enhancements of 200 are possible. One example cited is the reaction of benzyl chloride and 4-cyanophenoxide dissolved in methanol and heated to form 4-cyanophenylbenzyl ether. This reaction, which conventionally takes about 12 hours to produce 65% of the theoretical yield, required only 35 seconds to produce the same yield in a standard household microwave oven. As in many other potential microwave applications, one of the major challenges will be to scale-up the process without affecting technical or economic feasibility.

ELECTRIC UTILITY RESEARCH

Two of the larger Canadian electric utilities, Ontario Hydro and Hydro-Québec, have invested in research facilities to provide technical support and development activities not only for the supply of electrical energy but also for its effective utilization. A number of other utilities have provided co-funding for projects carried out by others.

Ontario Hydro has been involved in industrial microwave applications research for the past several years in order to help its customers use this electrotechnology effectively and efficiently [52-59]. While the initial focus of this research was to improve productivity of industrial processes, the current activity is emphasizing the use of microwaves for environmental applications. The more successful investigations conducted by Ontario Hydro include: microwaves to accelerate the drying, and slipcasting of traditional ceramics that provided a 30-minute cycle compared to the multi-day cycle common to a traditional ceramics plant [53]. Microwave heating trials were also performed to reduce the volume of a hazardous sludge material to eliminate a potential environmental impact [55]. Using the actual 45-gallon waste drum as the 'oven' or applicator and installing a suitable source to heat the drum contents, microwave heating provides one approach that can dry the sludge in the waste drums without removing the material. The obvious advantage of this approach is to minimize handling and possible exposure and contamination. In a third application a hybrid kiln combining microwaves with resistance heating to process advanced ceramics was developed at Ontario Hydro [54]. This new heating device was built and tested to investigate the effect of this hybrid technology on production rates and energy requirements for calcining and sintering a selected number of ceramic materials. Even without any process optimization, test results on the ceramics revealed significant reductions in both processing time and energy consumption. Based on these promising results, a second phase was started to further refine kiln operation and expand the range of materials tested in this device. An environmental application currently being pursued on behalf of the Ontario Waste Management Corporation is described in a previous section.

Hydro-Québec's LTEE laboratories are involved in dielectric heating applications through a university-utility collaboration [60]. LTÉÉ and LAIMO (of the École-Polytechnique) are partners

in promoting the use of dielectric heating for industrial processes to help its industrial customers improve productivity and remain competitive. As in the case of Ontario Hydro's Research Division this collaboration has supplied R&D support for various dielectric heating applications as well as conducting testing on behalf of industrial customers who wish to assess the feasibility of a particular application. One investigation conducted by this partnership involves the microwave preheating of shredded rubber. Used in the manufacture of carpets, the shredded rubber must be mixed with vulcanizing agents and pressed into molds. Microwave heating was investigated to preheat the rubber prior to molding and reduce pressing time. Preliminary test results indicate that the pressing time can be reduced by more than 20%. Another evaluation conducted by LAIMO and LTEE involved drying of the paper in damaged transformer bushings. A microwave applicator was designed at LAIMO to facilitate drying which can be completed in less than 8 hours compared to the days or months required by conventional convective oven drying.

Powertech (BC Hydro) has recently become involved in dielectric heating through a Canadian Electrical Association state-of-the-art review that will identify existing and potential applications of radio-frequency and microwave heating for hazardous waste treatment. The review will provide a technical and economic assessment for each identified opportunity in comparison to conventional treatment processes and include an estimate of the market and electrical load impact in Canada over the next five years. Recommendations for further research and development on new applications will be made and include suggestions for future work in cost-effective waste management systems.

The Canadian Committee on Electrotechnologies (CCE), as part of the International Union for Electroheat (UIE), provides a coordinating function in Canada to provide a better understanding of industrial electroheat technologies and their uses. These electroheat technologies include microwave and radio-frequency heating. A portion of the CCE activities is promoting the efficient and effective use of electrotechnologies by education (eg, annual visits to major engineering faculties across Canada) and published material (a bimonthly publication entitled 'Electroflash').

The Canadian Electrical Association (CEA) sponsors research and development activities in support of its Canadian electrical utility membership. Over the past several years, a number of investigations has been conducted to support the development and understanding of microwave and radio-frequency heating applications [52,54,75,77].

PRIVATE COMPANY RESEARCH

A number of Canadian companies are currently involved in microwave applications research. Obviously many of these companies do not wish to divulge their exact involvement for proprietary reasons; however, there are a few examples that can be cited.

Alcan International (Kingston Research and Development Centre) has been involved in microwave applications research in food [62-64,67] and advanced ceramics [65,66,68,69]. The latest reference in the first set [67] involves microwave oven modelling systems for optimizing packaging design that provides good background information (and references) on the value of mathematical modelling systems. Although it will never replace experimental work, modelling can help to provide a direction for empirical testing. The second set of references describe activity in microwave processing of advanced ceramics. The joining of both high-purity alumina and hot-pressed silicon nitride rods (12 mm diameter) using microwave radiation at 2450 MHz is described [65]. Powers of 200 to 300 W resulted in joints with strengths up to 220 MPa and 600 MPa for

alumina and silicon nitride, respectively. The use of microwave radiation at 2450 MHz is described to sinter a large variety of ceramic materials to produce materials approaching theoretical densities [66]. Up to 40 powder compacts averaging 10 grams in weight have been sintered simultaneously to demonstrate the feasibility of process scale-up. Both alumina and silicon nitride were rapidly heated and sintered in times of approximately 60 minutes. Typically, energy consumption can be as low as 3.8 kWh/kg. A comparison of the energy requirement for conventional versus microwave sintering, based on multiple samples is included. References [68,69] detail the properties of the alumina sintered at 2.45 GHz, indicating that sintering densities in excess of 98% theoretical have been obtained in times of between 6 and 120 minutes; however, only with sintering times greater than 30 minutes does the product have a uniform grain structure. Based on sintering of 400 gram batches, microwave processing is estimated to provide a 90% savings over conventional sintering in an electric resistance furnace.

Ceramics Kingston, also located in Kingston, Ontario has also been quite active in microwave processing [70-74]. One reference [70] describes the preconditioning of ceramic powders using non-intrusive microwave coupling agents to improve the microwave absorption characteristics. The preconditioning technique for Alcoa A-16 alumina is described. This technique involves mixing small quantities of a preconditioning agent with the ceramic powder. The mixed powder can then be heated in a 2.45 GHz system either as a powder or a preform shape. Preliminary test results suggest that the energy required for microwave sintering/annealing of alumina can be reduced by as much as 10 to 20 times simply by replacing conventional powders with preconditioned ones. With the addition of an 'appropriate' coupling agent, microwave sintering at 2.45 GHz of pure alumina samples (1.5" green diameter) up to 98% of theoretical density has been reported [71]. Because of the amount of time and care required to produce an economic benefit, this type of processing was questioned. In a third reference [73] the microwave calcination of Gibbsite to produce α-alumina was shown to be feasible at the bench-scale. Maximum surface area and weight loss occur after about 5 minutes at a microwave power level of between 400 to 600 W. Development for both sintering and calcination is being pursued by Ceramics Kingston. Finally, Ceramics Kingston has reported the use of microwave technology (2.45 GHz) to sinter metal oxide varistors [72,74]. The electrical properties of the microwave-sintered products are comparable with conventionally sintered varistors. Energy savings, productivity increases and added manufacturing flexibility are also claimed by the authors.

Wardrop Engineering Ltd. is investigating the use of microwave energy for rendering meat, poultry and fish by-products [75]. The objective of the study, sponsored in part by the Canadian Electrical Association, is to develop a microwave process that has the potential to improve environmental control and product quality as compared to conventional rendering operations.

SUMMARY

This paper has reviewed the impressive amount of Canadian research into microwave heating. The references provide an additional source of more detailed information. It is apparent from this information that Canadian researchers have potential microwave applications that can meet the needs of Canadian industry. New applications being actively pursued range from the processing of ceramics, minerals and food to the development of more energy efficient ways to produce chemicals, and manage hazardous wastes. As in most countries, the microwave oven has promulgated experimentation in Canada that has been partly responsible for the recent popularity (ie, affordability) of microwave heating for some researchers. The benefits of the technology, such as selective and volumetric heating, are being recognized and adapted to meet the diverse

requirements of materials processing. However, the particular advantages (and disadvantages) of microwave heating at this scale should not be confused with the operation of large-scale industrial processes. One of our main challenges is to more clearly understand what is happening on a small scale in order to confidently transfer the application to a large-scale industrial process (while maintaining the advantages observed in the laboratory). In Canada, this opportunity is being pursued.

TABLE 1
MICROWAVE HEATING RESEARCH IN CANADA

GOVERNMENT RESEARCH	
Atomic Energy of Canada Research Ltd.	dielectric property measurement, applicator design
Canadian Department of Energy, Mines and Resources (CANMET)	mineral processing
Ontario Ministry of Energy (Enersearch program)	funding assistance program for energy-efficient technologies
Ontario Waste Management Corporation (Ministry of the Environment)	processing of dry cleaning waste
National Research Council (Division of Electrical Engineering)	biomedical effects, feasibility assessment, equipment design
UNIVERSITY RESEARCH	
Queen's University	microwave 'catalysis', environmental applications, chemical synthesis
École-Polytechnique (LAIMO)	plasma, dielectric property measurement, industrial dielectric heating assessments (in cooperation with Hydro-Quebec's LTEE)
University of Alberta	dielectric properties of materials, applicator design, microwave theory & instrumentation
Laurentian University	microwave chemical synthesis
University of Waterloo	biomedical effects, industrial process feasibility assessment and equipment design

TABLE 1 (CONT'D)

ELECTRIC UTILITY RESEARCH	
Ontario Hydro's Research Division	environmental applications, advanced ceramics, mineral processing
Hydro-Québec's LTÉÉ	rubber processing, paper drying, design
Powertech (BC Hydro)	environmental applications
Canadian Committee on Electrotechnologies	education in industrial electrotechnologies
Canadian Electrical Association	electric utility research & development
CANADIAN COMPANY ACTIVITIES	
Voss Associates Engineering Ltd	consultation, design, feasibility assessments
Alcan Research	advanced ceramics, food product packaging
Ceramics Kingston Inc.	processing of advanced ceramics
Wardrop Engineering	rendering of meat, poultry and fish by-products
MBM Ceramics	slip-casting and drying of whiteware
R&J Engineering	drying of pharmaceutical hard capsules

REFERENCES

Atomic Energy of Canada Research Ltd

1. Hutcheon, R.M., de Jong, M.S., Adams, F.P. et al, "A Technique for Rapid Scoping Measurements of RF Properties up to 1000°C", Electromagnetic Energy Reviews, 2(4), December 1989.

2. Atomic Energy of Canada Ltd Research Company and Voss Associates Engineering Ltd., "Microwaves and Minerals: I. Technology Review, II. Tests of Ontario's Industrial Minerals", Ontario Ministry of Northern Development and Mines, Industrial Mineral Background Paper 14, 1990.

Energy, Mines and Resources

3. Haque, K.E., "Microwave irradiation pretreatment of a refractory gold concentrate", Proceedings of the International Symposium on Gold Metallurgy, edited by R. Slater, D.M. Wyslouzil and G.W. McDonald, Winnipeg, Manitoba, August, 1987.

4. Haque, K.E., Kondos, P., MacDonald, R.J.C. and LaForest D., "Microwave Activation of Carbon", MSL-89-76 (OP&J) draft, CANMET, Energy Mines and Resources Canada, 1989.

5. Haque, K.E., Kondos, P., MacDonald, R.J.C. et al, "Evaluation of Microwave Reactivated Carbon", Mineral Sciences Laboratories Division Report MSL 90-27(CR), CANMET, Energy Mines and Resources Canada, July 1990.

Ontario Ministry of Energy - ENERSEARCH

6. Gilbert, A.F., "Microwave Assisted Debarking of Wood", Ontario Ministry of Energy - Enersearch Program, Project #600102, June 1989.

7. Hradecky, J.J., "Microwave Drying in Pharmaceutical Hard Gelatin Capsule Production", Ontario Ministry of Energy - Enersearch Program, Project #ES 035, January, 1989.

National Research Council of Canada - Division of Electrical Engineering

8. VanKoughnett, A.L., "A microwave applicator for filamentary materials", J. Microwave Power, 7, 1972.

9. VanKoughnett, A.L. and Wyslouzil, W., "An automatic tuner for resonant microwave heating systems", ibid, 6, 1971.

10. VanKoughnett, A.L., Bleackley, W.J. and Wyslouzil, W., "Ridged Exposure Chamber", ibid, 7, 1972.

11. VanKoughnett, A.L. and Wyslouzil, W., "A Waveguide TEM Mode Exposure Chamber", ibid, 7, 1972.

12. VanKoughnett, A.L. and Wyslouzil, W., "Microwave Dryer for Ink Lines", ibid, 7, 1972.

13. VanKoughnett, A.L. and Dunn, J.G., "Doubly Corrugated Chokes for microwave heating systems", ibid, 8, 1973.

14. VanKoughnett, A.L., Dunn, J.G. and Woods, L.G., "A microwave applicator for heating filamentary materials", ibid, 9, 1974.

15. Wyslouzil, W. and VanKoughnett, A.L., "An Attenuation Based Microwave Moisture Gauge for Sheet Materials", ibid, 9, 1974.

16. VanKoughnett, A.L., "Fundamentals of Microwave Heating", Trans. IMPI 1, 1973.

17. Kashyap, S.C. and Dunn J.G., "A waveguide applicator for sheet materials", IEEE Trans, MTT-24, 1976.

18. Kashyap, S.C. and Wyslouzil, W., "Automatic Control of Nonresonant Dryers", J. Microwave Power, 11, 1976.

19. Kashyap, S.C. and Wyslouzil, W., "Methods for Improving Heating Uniformity of Microwave Ovens", J. Microwave Power, 12, 1977.

20. Kashyap, S.C., Wong, J.W. and Dunn J.G., "Microwave Leakage Indicating Strip", ibid, 13, 1978.

21. Kashyap, S.C. and Vachon, F., "A microwave method for grading agricultural products", ibid, 14, 1979.

22. Luter, L., Wyslouzil, W. and Kashyap, S.C., "The Destruction of Aflatoxins in Peanuts by Microwave Roasting", Journal Can. Inst. Food Sci. Tech., 15, 1982.

23. Wyslouzil, W. and Kashyap, S., "A cascading rotary microwave processor", Proc. Symp. Microwave Power, Chicago, IL, August 1985.

University of Alberta - Voss/Tinga

24. Voss, W.A.G., "Electroheat Development in Canada", Electroheat Education Newsletter, 12, August 1989, published by the British National Committee on Electroheat, 30 Millbank, London.

25. Tinga, W.R., Tian, B.Q. and Voss, W.A.G., "A New High Temperature Multipurpose Applicator", presented at the Materials Society Spring Meeting, San Francisco, CA, Section L, Microwave Processing of Materials, April 16-21, 1990.

26. Voss, W.A.G., "Model-Informed Microwave Processing of Materials", presented at the Materials Society Spring Meeting, San Francisco, CA, Section L, Microwave Processing of Materials, April 16-21, 1990.

27. Tinga, W.R., "Solid State Microwave Generators", ibid, 5, 1970.

28. Tinga, W.R. and Nelson, S.O., "Dielectric Properties of Materials for Microwave Processing - Tabulated", ibid, 8(1), 1973.

29. Tinga, W.R., "Microwave Dielectric Constants of Metal Oxides at High Temperatures: Part I", Electromagnetic Energy Reviews, 1(5), 1988.

30. Tinga, W.R., "Microwave Dielectric Constants of Metal Oxides at High Temperatures: Part II", Electromagnetic Energy Reviews, 2(1), 1989.

31. Electromagnetic Energy Reviews, Voss, W.A.G. and Fisher, P. editors, 2(3), 1989.

University of Waterloo - Pei

32. Ford, J.D. and Pei, D.C.T., "High Temperature Chemical Processing via Microwave Absorption", J. Microwaev Power, 2, 1967.

33. Pei, D.C.T. and Ford, J.D., "Evaluation of Microwave Power for High-Temperature Chemical Reactions", J. Microwave Power, 4(3), 1969.

34. Pei, D.C.T., "Microwave Vacuum Drying vs. Heated-Air Drying for Soybeans", University of Waterloo Research Institute, February 1983.

35. Pei, D.C.T., "A Study on the Potential of Microwaev Grain Dryers", University of Waterloo Research Institute Project No. 112-01, August 1982.

36. Pei, D.C.T., "Method of Baking Bread", United States Patent 4,419,374, Dec 6, 1983.

37. Ang, T.K., Pei, D.C.T. and Ford, J.D., "Microwave Freeze Drying: An Experimental Investigation", Chemical Engineering Science, 32, 1977.

École-Polytechnique

38. Bose, T.K., et al, "Computer-based Permittivity Measurements and Analysis of Microwave Power Absorption in Conductive Dielectrics", IEEE Trans. Elect. Insulation, 1987.

39. Bosisio, R.G., Wertheimer, M.R. and Weissfloch, C.F.,"Generation of large volume microwave plasmas", Journal of Physics E: Scientific Instruments 6, 1973.

40. Bosisio, R.G., Barthakur, N. and Spooner, J., "Microwave Protection of a Field Crop against Cold", J. Microwave Power, 5, 1970.

41. Bosisio, R.G. and Barthakur, N. "Microwave Protection of a Field Crop against Cold", J. Microwave Power, 8, 1973.

42. Bosisio, R.G., Spooner, J. and Granger, J., "Asphalt Road Maintenance with a mobile microwave power unit", J. Microwave Power, 9, 1974.

43. Wertheimer, M.R., Bosisio, R.G. and Rouleau, D., "Production of Nitrogen Atoms in a Discharge", ibid, 10, 1975.

44. Bosisio, R.G., Kutlu, E et al, "A vulcanization analyser for microwave power heated rubber compounds", International IFAC Conference in Instrumentation and Automation in the Paper, Rubber and Plastics Industry, Brussels, May 24-26, 1976.

45. Bosisio, R.G., Cambon, J.L., Chaverie, C. and Klvana, D., "Experimental Results on the Heating of Athabasca tar sand samples with microwave power", J. Microwave Power, 12, 1977.

Queens University - Wan

46. Wan, J., Tse, M., Husby, H. and Depew, M., "High-Power Pulsed Microwave Catalytic Processes: Decomposition of Methane", J. Microwave Power and Electromagnetic Energy, 25, (1), 1990.

47. Wolf, K., Choi, H.K.J. and Wan, J.K.S., " Microwave Assisted Catalytic Conversion of Cyclohexane", AOSTRA Journal of Research, 3, 1986.

48. Tse, M.Y., Depew, M.C. and Wan, J.K.S., "Applications of High Power Microwave Catalysis in Chemistry", Research on Chemical Intermediates, Elsevier Science Publishers B.V., Amsterdam, 13, 1990.

49. Depew, M.C., Dineson, T., Tse, M.Y. and Wan, J.K.S., " Microwave-Induced Decomposition of Some Gaseous Air Pollutants", Research on Chemical Intermediates, 15, p 113-127, 1991.

Laurentian University - Gedye et al

50. Gedye, R.N., Smith, F.R. and Westaway, K.C., "The rapid synthesis of organic compounds in microwave ovens", Can.J.Chem, 66, 1988.

51. Emsley, J., "The chemist's quick cookbook", New Scientist, 12, November 1988.

Ontario Hydro
52. Oda, S.J. and Chen R.C., "Microwave, Radio-frequency and Infrared Devices: Their Uses and Potential in Industry", Canadian Electrical Association Report No. 411 U 481, Montreal, 1986.

53. Oda, S.J. and Balbaa, I.S., "Microwave Processing at Ontario Hydro Research Division", Mat. Res. Soc. Symp. Proc., 24, 1988.

54. Oda, S.J. and Balbaa, I.S., Microwave-Resistance Heating for Advanced Ceramic Processing, Phase I: System Development, Canadian Electrical Association Project No. 709 U 603, January 1990.

55. Oda, S.J., Balbaa, I.S. and Barber B.T, "The Development of New Microwave Heating Applications at Ontario Hydro's Research Division", presented at the Materials Research Society Spring Meeting, San Francisco CA, Microwave Processing of Materials, Apr 16-21, 1990.

56. Oda, S.J. and Balbaa, I.S., "Microwave Power Optimization for Carbon Activation", report for the Canadian Department of Energy, Mines and Resources, CANMET - MSL Division, SSC File No.: 006SQ.23440-9-9126, October 1990.

57. Oda, S.J., "Microwave Heating for Removal of Perchloroethylene from Activated Carbon", Ontario Hydro Research Division Report No. 90-242-P, November 1990.

58. Sanio, M.R. and Schmidt, P.S., "Procedure for Estimating the Capital and Operating Costs of Dielectric Heating Equipment", Ontario Hydro Report no. TSDD-89-011, 1989.

59. Sanio, M.R. and Michelussi, I., "Microwave Applications in the Food & Beverage Industry", Ontario Hydro Report No. TSDD-89-010, August 1989.

Hydro-Québec
60. Girard, R.J., Giroux, M. and Leclerc, P., "Development of Dielectric Heating Applications Through a Utility-University Collaboration", presented at the International Microwave Power Institute Annual Symposium, Denver, CO, August 1990.

61. "Microwaves and Radio Frequency at your Service", LTEE/LAIMO publication, 1990.

Private Canadian Companies
Alcan International Ltd. - Kingston Research & Development Centre
62. Herzig, R., Keefer, R. and Lorenson, C., "Oven Effects Affecting Power Distribution in Microwave Cooking", presented at the International Microwave Power Institute 23rd Symposium, Ottawa, Canada, 1986.

63. Lorenson, C., Lacroix, C., Ball M. and Keefer, R., "Applications of Electromagnetic Theory to Microwave Heating Distributions inside Containers of Different Geometries", ibid, 1986.

64. Ball, M., Hewitt, B, Lorenson, C. and Keefer, R., "Factors Relating to the Performance of Thin Metallized (Susceptor) Films in the Microwave Oven", ibid, 1986.

65. Apte, P.S., Kimber, R.M. and Patterson, M.C.L., "Microwave Heating for Ceramic Joining", Ontario Ministry of Energy Enersearch Program, Project #600049, December 1988.

66. Apte, P.S., Kimber, R.M., Patterson, M.C.L. and Roy, R.Y., " Multicavity System for the Sintering of Advanced Ceramic Shapes", Ontario Ministry of Energy Enersearch Program, Project #600048, March 1989.

67. Lorenson, C., "The Why's and How's of Mathematical Modelling for Microwave Heating", Microwave World, 11(1), 1990.

68. Patterson, M.C.L., Kimber, R.M. and Apte, P.S., "The Properties of Alumina Sintered in a 2.45 GHz Microwave Field", presented at the Materials Research Society Spring Meeting, San Francisco, CA, Section L, Microwave Processing of Materials, April 16-21, 1990.

69. Apte, P.S., Kimber, R.M. and Patterson, M.C.L., "Mechanical Properties of Microwave Sintered Alumina", Proc. 11th Rise International Symposium on Metallurgy and Materials Science: Structural Ceramics - Processing, Microstructure and Properties, Rise National Laboratory, Roskilde, Denmark, 1990.

Ceramics Kingston Ltd.

70. Li, J., McMahon, G., Pant, A., et al, "Preconditioning of Powders for Microwave Processing", Ontario Ministry of Energy Enersearch Program, Project #600066, January, 1988.

71. Pant, A., McMahon, G., et al, "Microwave Sintering of Alumina Using 2.45 GHz Radiation", presented at the Materials Society Spring Meeting, San Francisco, CA, Section L, Microwave Processing of Materials, April 16-21, 1990.

72. McMahon, G., Pant, A. Sood, R. et al, "Microwave Sintering Technology for the Production of Metal Oxide Varistors", presented at the Materials Society Spring Meeting, San Francisco, CA, Section L, Microwave Processing of Materials, April 16-21, 1990.

73. McMahon, G., Lee, J., Saleem, M., Kuriakose, A.K. et al, "Microwave Calcination of Gibbsitic Material Using 2.45 GHz Radiation", AIME Meeting Salt Lake City, UT, 1990.

74. Bratt, J., Corrigan, D., McMahon, G., Pant, A. Sood, R. et al, "Novel Sintering Technology for the Production of Electronic Ceramics", AIME Meeting Salt Lake City, UT, 1990.

Wardrop Engineering Ltd.

75. Private communication with H. Hussein (project leader): Canadian Electrical Association Project No 8927U33, "Development of the Microwave Rendering Process", March 1991.

Dofasco Ltd.

76. Parr, J., "Use of Microwave Technology at Dofasco's Foundry", Proc. Industrial Workshop on Electroheat, Ontario Ministries of Energy and Industry and Trade, November, 1984.

77. Bilgen, E., "Microwave and Radio-frequency Curing of Polymers", CEA Report No. 634 U, Canadian Electrical Association, Montréal, 1986.

MICROWAVE PROCESSING OF CERAMICS AT NORTHWESTERN UNIVERSITY

D. Lynn Johnson
Northwestern University
Department of Materials Science and Engineering
Evanston, IL 60208-3108

ABSTRACT

Ceramic rods have been sintered in cold wall single mode microwave cavities under a variety of conditions, including microwave heating and plasma heating. High sintering rates, high density and fine grain sizes were achieved for β-alumina and Al_2O_3-TiC composites under favorable conditions. Thermal runaway often was observed in alumina during microwave heating if the heating rate was more than a few degrees per second. On the other hand, microwave plasma sintering of alumina was accomplished at very high heating rates (100 K/s).

INTRODUCTION

Berteaud and Badot used a TE_{10n} (the value of n was not specified) cavity to sinter alumina, and reported that a stable temperature near 1700 C could be maintained with about 100 W/cm^3.[1] At higher powers a runaway phenomenon took place. Colomban and Badot[2] followed this work by firing β-alumina in the same type of cavity. Their microstructures appear to indicate that melting had occurred on the interior of the specimens. In 1979 they published the paper with the optimistic title "Le Chauffage par microondes methode de cuisson des ceramiques en 1990!" (Microwave Heating: Firing Method for Ceramics by 1990!), in which they outlined the basic principles of microwave heating of ceramics.[3] Perhaps their dream has not yet been realized.

EXPERIMENTAL PROCEDURES

Following the initial work of Berteaud and Badot, the present author and Professor Morris E. Brodwin of the Department of Electrical Engineering and Computer Science began a microwave sintering program, commencing with the design and construction of a TE_{102} rectangular cavity with a set of replaceable apertures and a moving short circuit. (Eventually an adjustable aperture was designed, built and utilized to significant advantage.) Specimens in the form of tubes or rods were passed through the broad faces of the cavity at a position corresponding to a maximum in the electric field of the empty cavity. Choke tubes were utilized to mitigate leakage of microwave energy out of the cavity. No insulation was used so that the temperature of the surface of the sample could be monitored continuously by an optical pyrometer through choked peepholes in the narrow walls of the cavity. For some experiments the choke tubes were extended into the cavity, as shown schematically in Fig. 1, leaving a gap of 25 mm where the sample was exposed to the microwave energy.[4]

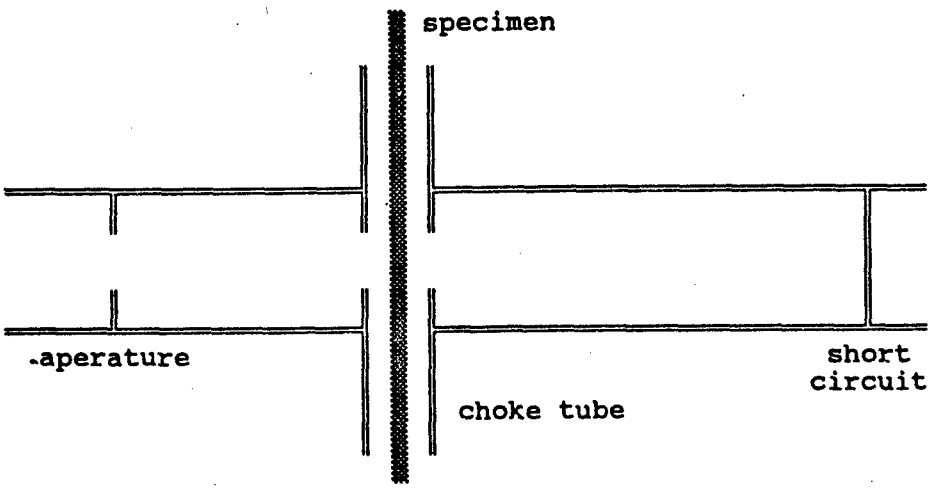


Fig. 1. Vertical cross section of TE_{103} rectangular cavity.

A cylindrical TE_{111} cavity was designed and constructed for the sintering of SiC rods (see Fig. 2). When insufficient heating was observed, the interior of the cavity was polished and silver plated. The cavity also was sealed so that pressures up to 1 MPa could be achieved to suppress electrical breakdown of the sintering atmosphere.

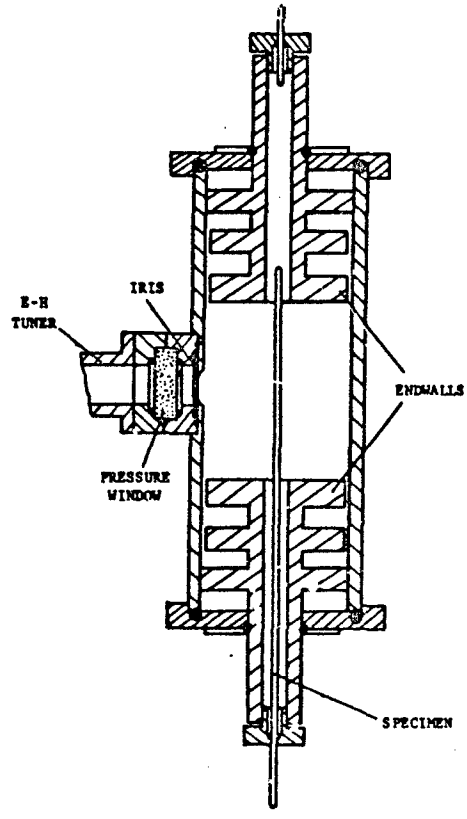


Fig. 2. Vertical cross section of cylindrical TE_{111} cavity.

In an independent study, alumina rods were sintered in gas plasmas excited by microwaves. Initially, a reduced height waveguide applicator terminated by a fixed short circuit was used for rapid pass-through sintering.[5] Recently, a cylindrical TM_{012} cavity was designed following Asmussen, et al.[6] and used to sinter stationary alumina rod and thimble specimens in a variety of plasma gas compositions.[7]

RESULTS AND DISCUSSION

The first specimens attempted were isostatically pressed tubes of β-alumina*. It was found that uniform heating was impossible to obtain. A localized high temperature zone would develop on the side of the tube facing the microwave source, but failed to spread around the tube. Increasing the power eventually resulted in local melting. A similar result obtained even if the specimen was rotated before and during heating. However, isostatically pressed 4 mm diameter rods of the same material were heated and sintered successfully by rapid pass-through sintering.

Specimens were rotated and translated through the cavity at velocities of 10-40 mm/min. The surface temperature and final linear shrinkages are plotted in Figs. 3 and 4. The shrinkage plateau of Fig. 4 corresponded to a final average relative density of 92%.

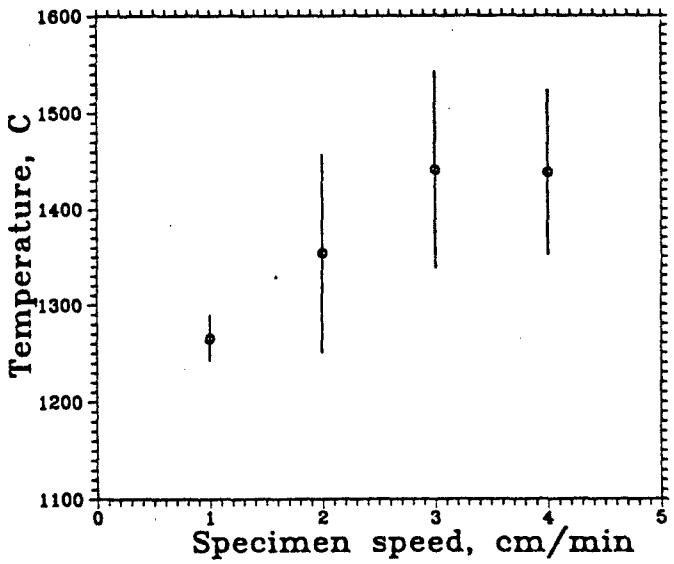


Fig. 3. Surface temperature of β-alumina rods as a function of velocity through the cavity.

* Alcoa Industrial Chemicals, Bauxite, AR 72011

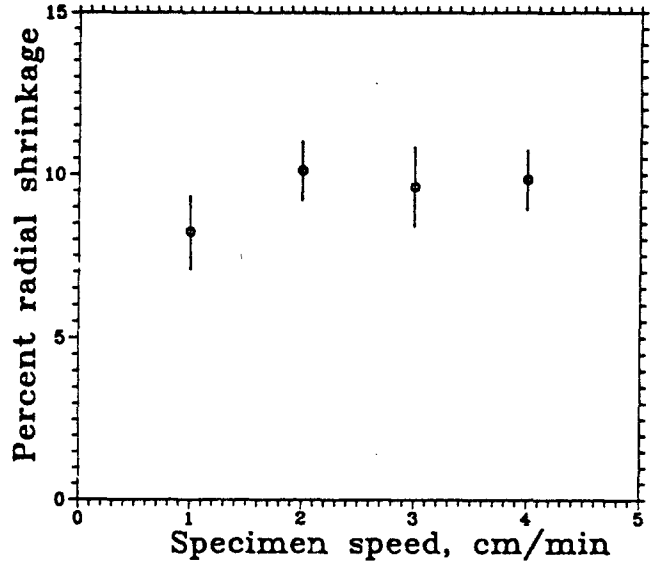


Fig. 4. Radial shrinkage of β-alumina rods as a function of translation velocity through the cavity.

Although the heating rate was not measured directly, average values can be obtained from the peak temperature measurements, translation rates, and gap width over which the sample received microwave excitation. By this means it was estimated that the highest average heating rate was on the order of 50 C/s, but peak heating rates were probably in the range of 100 C/s at the highest translation velocity. Stable hot zones could not be maintained at higher translation rates.

Maximum temperatures within the specimens obviously were higher than the surface temperatures. For instance, large grains indicative either of runaway grain growth or melting were observed on the interior of specimens which had a surface temperature of 1800 C. However, at the surface temperatures shown in Figs. 3 and 4, the interior grain size was on the order of only 30% greater than the surface grain size. This may indicate an axial temperature gradient greater than the radial gradient in these rapid pass-through experiments. In parallel with the observed density, the grain size also was independent of specimen translation velocity, with the center grains being on the order of 2 μm in diameter.

Our attention was then turned to the sintering of SiC in the TE_{111} cavity. It was immediately observed that SiC could not be heated adequately in argon, the atmosphere of choice in conventional sintering of SiC, because of breakdown. All further studies were conducted in nitrogen because of its higher breakdown strength, recognizing that a higher temperature would be required for sintering. Rods 4 mm in diameter could be heated to about 1700 C in the as-machined cavity. The interior of the cavity was then polished and silver plated, after which the maximum temperature achievable rose 200 C. Finally, pressurization to about 1 MPa made it possible to heat specimens to 2000 C, as shown in Fig. 5.[8],[9] Of course, it is well known that SiC does not sinter in nitrogen at this temperature.

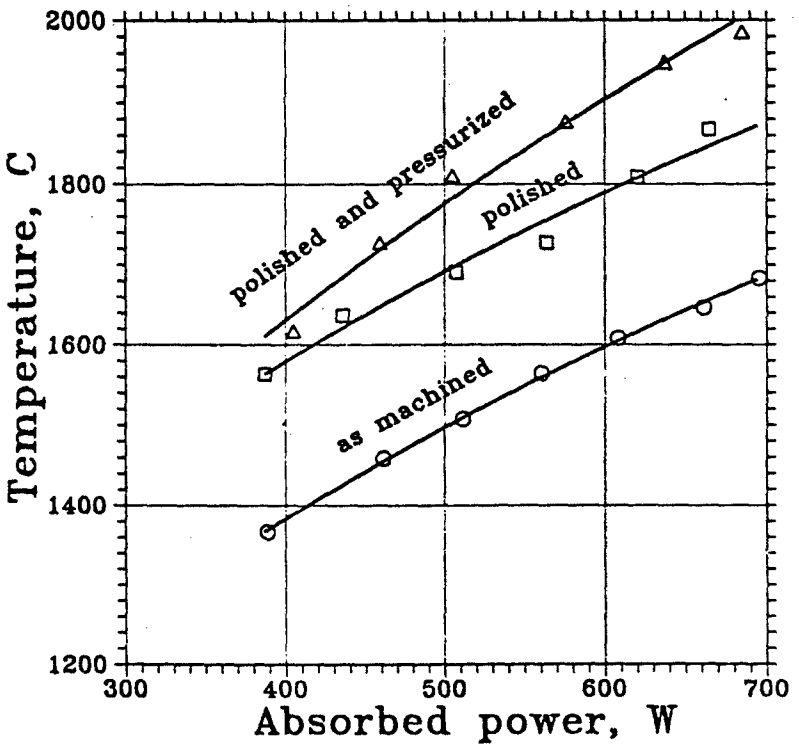


Fig. 5. Surface temperature of SiC rods as a function of power absorbed for the cavity as-machined, as-polished and silver plated, and as-pressurized with nitrogen.

Rods of α-alumina were sintered successfully if adequate precautions to avoid thermal runaway were taken.[10] A final grain size of 2 μm was achieved at densities of 99.9% for Baikowski CR30 alumina* containing 0.25% MgO, see Fig. 6.

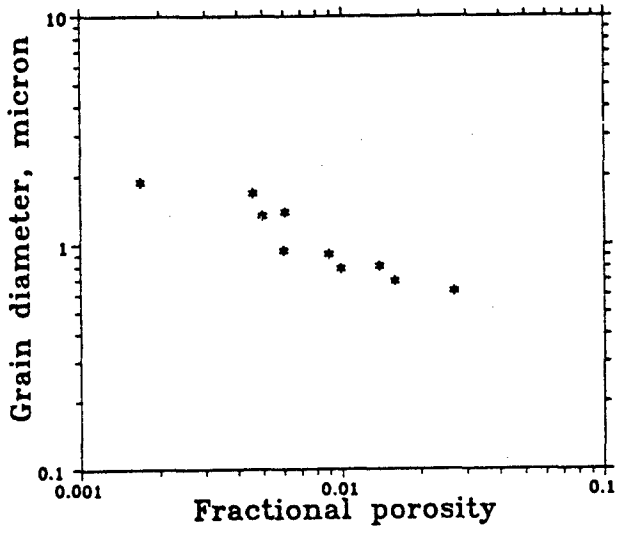


Fig. 6. Grain size as a function of porosity for microwave sintered Baikowski CR30 alumina.

The best results were obtained with Al_2O_3-TiC composites.[11],[12] Here it was observed that the presence of the lossy TiC suppressed thermal runaway. Thermal runaway was not observed in 4 mm diameter rods with TiC concentrations of 30% by volume or greater. Stable heating rates as high as 50 C/s could be achieved, as can be inferred from Fig. 7.

Two factors may have contributed to this result. First, the temperature dependence of the effective electrical conductivity at the microwave frequency probably is significantly less in TiC than in alumina, which would reduce preferential heating of local hot spots. Second, the thermal conductivity is greater in the composite than in alumina, which would permit more rapid dissipation of the extra heat generated at a local hot spot.

---

*Baikowski Industrial Corp., Charlotte, NC 28210

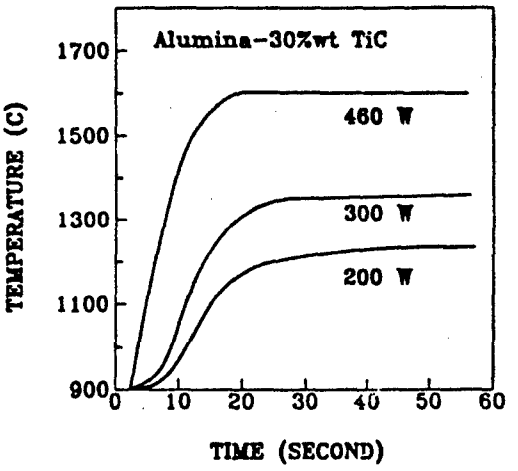


Fig. 7. Temperature as a function of time for rods of alumina-30% TiC as a function of time at various input power levels.

Temperature distributions in semi-infinite solids, slabs and cylinders was modeled by Watters.[13] The general result for finite specimens was that temperature gradients in alumina can be quite high. Further modeling of steady state temperature distributions have included the effects of thermal insulation. Heat at the surface of the specimen was assumed to be dissipated by both convection and radiation. Figure 9 shows the computed difference between the steady state center and surface temperatures as a function of thermal conductivity for a 4 mm diameter infinite cylinder for the following conditions: center line temperature 1600 C, dielectric loss proportional to exp(-1eV/RT), surface emissivity 0.6, temperature of surroundings 300 K, no thermal insulation, and uniform microwave field throughout the specimen.

Of course, the temperature gradients can be reduced by enclosing the specimen in thermal insulation. The calculated temperature difference is plotted as a function of thickness of thermal insulation in Fig. 9. Here the density and temperature dependent thermal conductivity of SALI* alumina fiber insulation were used. The insulation was assumed to have the same activation energy of dielectric loss as the specimen (1 eV), and its absorption of microwave power at

*Zircar Products, Inc., Florida, NY 10921

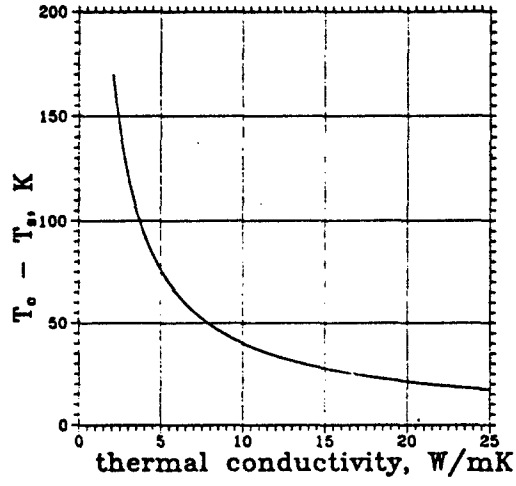


Fig. 8. Computed steady state difference between the center temperature, T_c (1873 K), and the surface temperature, T_s, of a 4 mm diameter rod as a function of thermal conductivity. See text for a description of the assumptions used.

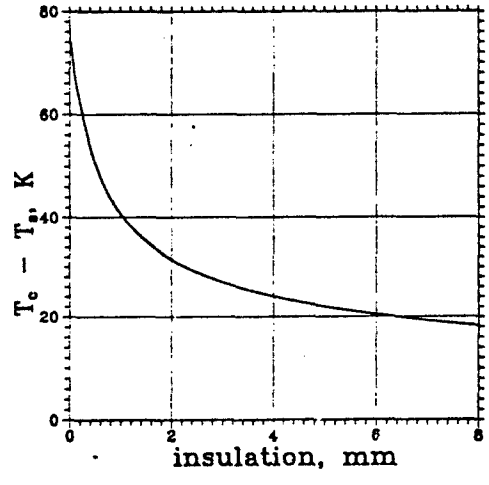


Fig. 9. Computed steady state difference between center and surface temperature of 4 mm diameter rods with a thermal conductivity of 5 W/mK as a function of insulation thickness. See text.

any given temperature and field was assumed to scale as its relative density (12% of theoretical). The thermal conductivity of the specimen was chosen to be 5 W/mK (approximates nearly dense alumina at the temperatures of interest), while that of the insulation varied from 0.33 to 0.43 W/mK from 1[illegible] to 1600 C. It is interesting to note that substantial temperature gradients exist even with thick insulation covering this small specimen. There certainly must be gradients if any microwave power is absorbed by the specimen, since this power must be transferred into the insulation at the surface of the specimen in the steady state.

An alternative method of reducing temperature gradients that has been studied in some detail is to immerse the sample in a plasma excited by the microwave field. Kemer investigated the sintering of α-alumina in a nitrogen plasma using both translation and stationary specimens.[5] He observed stable heating rates probably in excess of 100 C/s, with final temperatures possibly exceeding 1900 C. Sintered densities in excess of 99% were observed under these conditions for Baikowski CR30 alumina doped with MgO. The average grain growth rates during sintering were on the order of 1.5 μm/min with final grain sizes averaging <3 μm. Instantaneous linear shrinkage rates as high as 2.4%/s were measured at a translation rate of 30 mm/min. Densities approaching 99.9% of theoretical were achievable in less than 10 min in stationary specimens at power levels of 400 W absorbed in the plasma. However, alumina was corroded extensively by the nitrogen plasma if the specimen was held fixed in the plasma.

Kemer observed that alumina could not be heated to the sintering temperature range in a pure argon plasma. Recently Sweeney [7] completed a study of microwave plasma sintering of alumina in argon plasmas to which diatomic gases were added, and observed the conditions under which suitable heating can be attained. She confirmed that alumina will not sinter in a pure argon microwave plasma, but that additions of oxygen or nitrogen will raise the specimen temperature and permit sintering. At low concentrations (10% and less) oxygen results in higher densities than nitrogen, but the results converge at 15% and above.

Finally, Hsu investigated the heating of a variety of oxide ceramic materials in He, H_2, N_2, and O_2 plasmas.[14] Among other things, he showed that the penetration of microwave energy through the plasma to directly heat the specimen can be controlled to some extent by controlling the pressure and composition of the plasma. It should be mentioned that microwave excitation was used in the first plasma sintering study, and that a significant reduction in sintering temperature was observed for alumina.[15],[16] It remains to be seen

whether that enhancement was due primarily to the plasma or to the microwave energy that penetrated the plasma to heat the specimen directly.

CONCLUSIONS

Rod specimens of β- and α-alumina and alumina-TiC composites can be sintered rapidly in cold wall single mode applicators under certain conditions. Alumina-TiC is particularly amenable to this procedure, since thermal runaway is easily avoided. High densities and fine grain sizes can be realized. The sintering of alumina specimens in a microwave excited plasma is much more easily controlled than by microwave heating alone in the single mode applicators.

ACKNOWLEDGEMENTS

The research was supported in part by the Electric Power Research Institute under Contract No. RP2730-1, the National Science Foundation under Grants Nos. DMR-7918403 and DMR-8326710, and the United States Army Research Office under Grant No. DAAG29-80-K-0031.

REFERENCES

1. A. J. Berteaud and J. C. Badot, "High Temperature Microwave Heating in Refractory Materials," J. Microwave Power, 11 [4] 315-20 (1976).

2. P. Colomban and J. C. Badot, "Elaboration of Anisotropic Superconducting Ceramics (Na^+ β-alumina) by Microwave Heating," Mat. Res. Bul. 13 135-139 (1978).

3. P. Colomban and J. C. Badot, "Microwave Heating: Firing Method for Ceramics by 1990!", L'industrie Ceramique, 725 101-107 (1979).

4. John Bumgarner, "Microwave Sintering of Alumina Ceramics", MS Thesis, Northwestern University (1984).

5. E. L. Kemer and D. L. Johnson, "Microwave Plasma Sintering of Alumina," Am. Ceram. Soc. Bull., 64 [8] 1132-36 (1985).

6. J. Asmussen, Jr., R. Mallavarpu, J. R. Hamann, and H. C. Park, "The Design of a Microwave Plasma Cavity," Proceedings of the IEEE 1, 109-117 (1974).

7. M. P. Sweeney and D. L. Johnson, "Microwave Plasma Sintering of Alumina," to be published Ceramic Transactions, Proceedings of 93rd Ann. Mtg. of the Am. Ceram. Soc., Cincinnati, OH, (April 1991).

8. D. L. Johnson and M. E. Brodwin, "Microwave Sintering of Ceramics," Electric Power Research Institute Research Project 2730-01, Interim Report, March 1987

9. Y.-L. Tian, M. E. Brodwin, H. S. Dewan, and D. L. Johnson, "Microwave Sintering of Ceramics Under High Gas Pressure," in Microwave Processing of Materials, Mat. Res. Soc. Symp. Proc. Vol. 124, Eds. W. H. Sutton, M. H. Brooks, and I. J. Chabinsky, (1988) pp. 213-218.

10. Y. L. Tian, D. L. Johnson, and M. E. Brodwin, "Ultrafine Microstructure of Al_2O_3 Produced by Microwave Sintering," in Ceramic Transactions Vol. I, Ceramic Powder Science 2, Part B, The American Ceramic Society, Inc., Westerville, Ohio, (1988) pp. 925-932.

11. Y. L. Tian, D. L. Johnson, and M. E. Brodwin, "Microwave Sintering of Al_2O_3-TiC Composites," in Ceramic Transactions Vol. I, Ceramic Powder Science 2, Part B, The American Ceramic Society, Inc., Westerville, Ohio, (1988) pp. 933-938.

12. Y. L. Tian, H. S. Dewan, M. E. Brodwin, and D. L. Johnson, "Microwave Sintering Behavior of Alumina Ceramics," Ceramic Transactions, Vol. 7, Sintering of Advanced Ceramics,", The American Ceramic Society, Westerville, Ohio, (1990) pp. 391-401.

13. D. G. Watters, "An Advanced Study of Microwave Sintering," Ph.D. Thesis, Northwestern University, June 1989.

14. Matthew Hsu, "Heating Effects During Microwave Plasma Sintering of Ceramics," Ph.D. Thesis, Northwestern University, June 1991.

15. C.E.G. Bennett, N. A. McKinnon, and L. S. Williams, "Sintering in Gas Discharges," Nature, 217, 1287-88 (1968).

16. C.E.G. Bennett and N.A. McKinnon, "Glow Discharge Sintering of Alumina," in Kinetics of Reactions in Ionic Systems, Edited by T. J. Gray and V. D. Frechette, Plenum Press, New York, (1969) pp. 408-12.

MICROWAVE PROCESSING ACTIVITIES AT THE UNIVERSITY OF FLORIDA

D.F. Clark and D.C. Folz, Dept. of Materials Science and Engineering, University of Florida, Gainesville, FL 32611.

ABSTRACT

Specific projects where emphasis is placed on the use of microwave energy as an alternative heat source will be reviewed. Areas of interest include sintering and annealing of superconductors, solid-state reactions, joining, self-propagating high temperature synthesis, surface modification and white-wares fabrication.

BACKGROUND

Our program in microwave processing was initiated in 1987 with one graduate student working with a 700 watt 2.45 GHz home microwave oven. A significant effort was expended during the first six months in modifying this oven in order to achieve and contain the high temperatures required for processing ceramics.

The material that we selected for preliminary investigation was $YBa_2Cu_3O_{7-x}$, a superconductor below ~92K. The rationale for this selection was two-fold. Previous work by other investigators indicated that CuO was a fairly good susceptor of microwave energy, and thus it should be possible to microwave heat mixtures of CuO, Y_2O_3 and $BaCO_3$. Indeed, this proved to be the case. A second reason for selecting this material system was the enormous market potential. Figure 1 illustrates that ceramic superconductors can be sintered and annealed in a microwave oven. Considerably less time and somewhat lower temperatures are required to yield equivalent properties as compared to conventional heating methods.

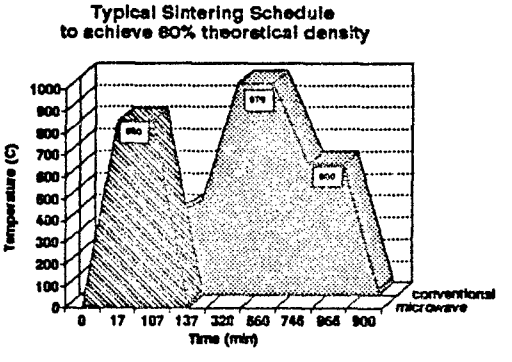


Figure 1. Time versus temperature curve for $YBa_2Cu_3O_{7-x}$ processed using microwave and conventional techniques.

By 1989, we had learned to process a wide variety of materials in the microwave oven. These included whitewares, electro-optic ceramics, powdered metals, alumina and glasses. One of the most exciting discoveries was that microwave energy could be used to ignite and combust mixtures of Ti and C, Mo and Si, TiO_2, Al and C, and other powdered mixtures exhibiting exothermic behavior. In one specific system, we ignited the interior of powder compacts and controlled the radial propagation of reaction from the inside to the external surfaces. The reaction is shown below.

$$TiO_2 + Al + C \rightarrow Al_2O_3 + TiC + \text{heat} \quad (1)$$

Samples prepared by this method are shown in Figure 2.

PROCESSING TIME:



0:00 min. 6:00 min. 8:00 min. 12:00 min.

Light Area: $4Al + 3TiO_2 + 3C$ (reactants)

Dark Area: $2Al_2O_3/3TiC$ (products)

Figure 2. Samples of Al_2O_3/TiC processed by combustion synthesis in a 700 watt microwave oven.

The University of Florida sponsored a July 1989 workshop on microwave processing. Engineers and scientists from national laboratories, equipment manufacturers and material manufacturers were invited. The major conclusions from this workshop are summarized below.

- Companies are interested in using microwave processing if it offers advantages in the form of energy and time savings, or if it results in materials with superior properties.
- There is a need for basic science research to develop a better understanding of microwave/material interaction.
- Equipment manufacturers must work more closely with materials processors for scale-up and product analyses.

As a result of this workshop, the University of Florida established a close working relationship with Raytheon Company, a major manufacturer of microwave equipment. Also, a project was initiated with Florida Tile Division of Sikes Corporation, a leading U.S. producer of ceramic tiles.

EQUIPMENT DEVELOPMENT

Our microwave processing facility consists of a 700 watt, single-mode applicator, a 6.4 kw multimode oven and several low power (500 - 800 watt) home microwave ovens modified to meet specific requirements. The single-mode unit was installed recently and no studies have been completed to date. However, we expect to use it for basic science studies in the near future. One of the home microwave ovens was modified to provide in situ weight changes in the material during heating. Its design and use is described in another paper in these proceedings. It is referred to as a microwave thermogravimetric analyzer (MTGA).

The major workhorse of our group is the 6.4 kw, 2.45 GHz multimode unit acquired from Raytheon Company. This oven was designed originally to cure rubber and dry wood. We have modified it for use at higher temperatures. A schematic is shown in Figure 3. A shielded thermocouple and optical pyrometer have been installed to monitor and control temperature inside a ceramic cavity. This cavity was designed to be transparent to microwaves and opaque to infrared. We also have the option of using a cavity lined with a thin coating of SiC powder that results in microwave hybrid heating of the sample. The atmosphere can be controlled to a certain extent by flowing various gases such as argon and oxygen through the cavity. Temperatures as high as 2000°C have been attained within moments, but it is more routine to operate in the range of 800 - 1650°C.

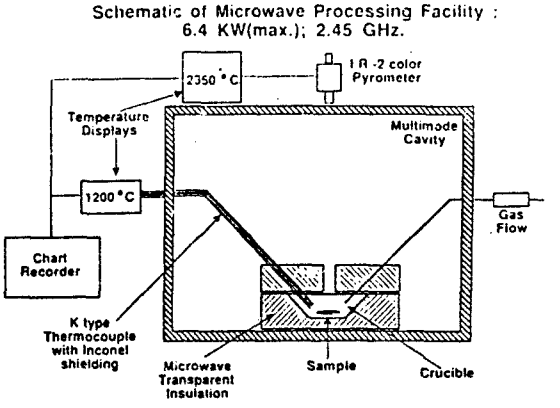


Figure 3. Schematic of the microwave cavity design used at the University of Florida.

FOCUS AREAS

Our major interest in microwave energy is its use in materials processing. We have selected several areas of ceramic processing that we believe can benefit by the use of microwave energy, either economically or through improved materials properties. These include:

- Solid State Reactions
- Joining
- Superconductors
- Binder Burnout
- Surface Modification
- Ultra-rapid Sintering
- Glass Melting

Each of these areas is more fully described in other papers in these proceedings. Some significant points of the research in these areas are highlighted below.

Solid-state reactions. Materials used in this study were Al_2O_3 powders, single crystals of Al_2O_3 and ZnO powders. Mixtures of Al_2O_3 and ZnO were heated in a microwave oven to yield the following reaction.

$$ZnO + Al_2O_3 \rightarrow Zn\,Al_2O_3 \quad (2)$$

Both Zn diffusion and the reaction site were found to be enhanced under certain conditions [1].

Joining. Materials used in this study were 94 percent alumina substrates and alumina-containing sols. The substrates were joined together with the sol and subsequently heated in a microwave oven to high temperatures. Joints nearly as strong as that of the bulk materials were obtained when the materials were heated to 1600°C [2].

Superconductors. Materials used in this study were $YBa_2Cu_3O_{7-x}$ powders. Both sintering and annealing were accomplished in shorter times than with conventional methods. Comparable superconducting and environmental stability properties were observed [3].

Binder burnout. Materials used in this study were Al_2O_3 powders and polymethyl methacrylate (PMMA). The objective of the research was to determine if microwaves offer any advantage over conventional heating methods for the removal of binders. We constructed a microwave thermogravimetric analyzer (MTGA) to facilitate data collection. We expect binder burnout to become more efficient in the microwave oven as the sample size is increased [4].

Surface modification. Materials used in this study were various compositions of Na_2O - Al_2O_3 - SiO_2 glasses and KNO_3. Microwave energy was used to carry out the following reaction that resulted in chemically strengthened glass.

$$\text{glass} - Na^+ + K^+_{(\text{molten salt})} \rightarrow \text{glass} - K^+ + Na^+_{(\text{molten salt})} \qquad (3)$$

When this reaction was carried out in a microwave oven, the rate of ion exchange was about four times faster than in a conventional oven under equivalent conditions. Additionally, the microwave enhanced effects were glass-composition (structure)-dependent [5].

Ultra-rapid sintering. Materials used in this study were Al_2O_3 powders of various particle sizes. The objective of this study was to use a combination of microwave and conventional heat to result in ultra-rapid and uniform heating. Using this technique, referred to as microwave hybrid heating (MHH), samples with superior microstructure and properties were produced, as compared to equivalent samples produced by conventional fast firing methods [6].

Glass melting. Materials used in this study were simulated nuclear waste glass frits obtained from Savannah River Laboratory. We demonstrated that these frits can be melted and homogenized using microwave energy. Leaching performance of these glasses was at least as good as those prepared with conventional methods [7].

SUMMARY

We have presented a very brief overview of the activities in microwave processing at the University of Florida. Each of the focus areas will result in a master's or doctoral degree. In some cases, a focus area will result in several degrees. Importantly, the results to date appear sufficiently promising in some areas to suggest that technology transfer should be rapid. Results from these studies will lead most certainly lead to a better understanding of microwave/ material interactions and reveal new applications for microwave processing.

ACKNOWLEDGEMENTS

The microwave processing research at the University of Florida has been supported by the Defense Advanced Research Projects Agency (DARPA), the Florida High Technology and Industry Council (FHTIC), the Space Research Institute (SRI), Raytheon Company, Engelhard Corporation, Florida Tile and AlSiMag.

REFERENCES

1. Ahmad, I. and Clark, D.E., Effect of Microwave Heating on Solid State Reactions of Ceramics, this volume.

2. Al-Assafi, S. and Clark, D.E., Microwave Joining of Ceramics, this volume.

3. Cozzi, A.D., Jones, D.K. and Clark, D.E., Microstructural Evolution of $YBa_2Cu_3O_{7-x}$ Using Microwave Energy, this volume.

4. Moore, E.H., Ahmad, I. and Clark, D.E., Microwave Thermogravimetric Analyzer (MTGA), this volume.

5. Fathi, Z. and Clark, D.E., Surface Modification of Glasses, this volume.

6. De, A.S., Ahmad, I., Whitney, E.D. and Clark, D.E., Microwave (Hybrid) Heating of Alumina at 2.45 GHz; II. Effect of Processing Variables, Heating Rates and Particle Size, this volume.

7. Schulz, R.L., Fathi, Z. and Clark, D.E., Microwave Processing of Simulated Nuclear Waste Glass, this volume.

MICROWAVE PROCESSING OF CERAMICS AT THE UNIVERSITY OF UTAH -- DESCRIPTION OF ACTIVITIES AND SUMMARY OF PROGRESS

M. F. Iskander, O. Andrade
Department of Electrical Engineering
University of Utah
Salt Lake City, UT 84112

A. Virkar
Department of Materials Science and Engineering
University of Utah
Salt Lake City, UT 84112

H. Kimrey
Oak Ridge National Laboratory
Oak Ridge, TN 37831

R. Smith, S. Lamoreaux, C. Cheng
Department of Electrical Engineering
University of Utah
Salt Lake City, UT 84112

C. Tanner, R. Knowlton, K. Mehta
Department of Materials Science and Engineering
University of Utah
Salt Lake City, UT 84112

ABSTRACT

An interdisciplinary effort to address certain modeling, measurements, and characterization aspects of microwave processing of ceramics was initiated at the University of Utah almost a year ago. The FDTD method was used to model EM power deposition patterns in single-mode cavities, some microwave sintering experiments were conducted in a multimode cavity and using SiC rods as process stimulus, and a wide variety of dielectric and thermophysical properties were measured on microwave- and conventionally sintered samples. This paper summarizes these efforts and presents initial results.

INTRODUCTION

Approximately a year ago an interdisciplinary team from the Electrical Engineering and Materials Science and Engineering Departments at the University of Utah initiated a focused effort to address certain modeling, measurements, and characterization aspects of microwave processing of ceramics. This activity was motivated by an Engineering Clinic research grant from Oak Ridge National Laboratory (ORNL). The Engineering Clinic team first identified areas where available measurement research facilities and computer codes can effectively contribute to the overall project

objectives of simulation of the microwave processing procedure and characterization of the sintered ceramics. Research in the following areas was pursued:

- Simulation of microwave processing of ceramics in single- and multi-mode cavities.
- Microwave sintering experiments.
- Dielectric properties measurements as a function of temperature and over a broad frequency band.
- Thermophysical and microstructural characterization of microwave-sintered ceramics.

SIMULATION OF MICROWAVE PROCESSING OF CERAMICS IN SINGLE- AND MULTI-MODE CAVITIES

It is believed that the simulation of the microwave processing procedure would provide valuable information that may help in characterizing the heating process, identification of critical parameters, and hopefully lead to future optimization of the process. Presently, sample sizes and shapes, type and thickness of the surrounding insulation, and the desirability of including a process stimulus such as SiC rods are considered forms of art and highly dependent on human expertise. Modeling and simulation of the microwave heating process may help identify critical parameters and stimulate critical thinking towards their optimization.

The simulation of the microwave sintering process consists of two parts. This includes the calculation of the electromagnetic (EM) power deposition pattern which is then used to calculate the thermal pattern. Solution procedures of these two calculations and samples of obtained results are described in the following sections.

Calculation of the EM Power Deposition Pattern

After careful examination of available options in computational electromagnetics, the Clinic team decided to use the Finite-Difference Time-Domain (FDTD) method to model the ceramic-insulation samples in single- and multi-mode cavities. Figure 1 shows the modeled geometries where

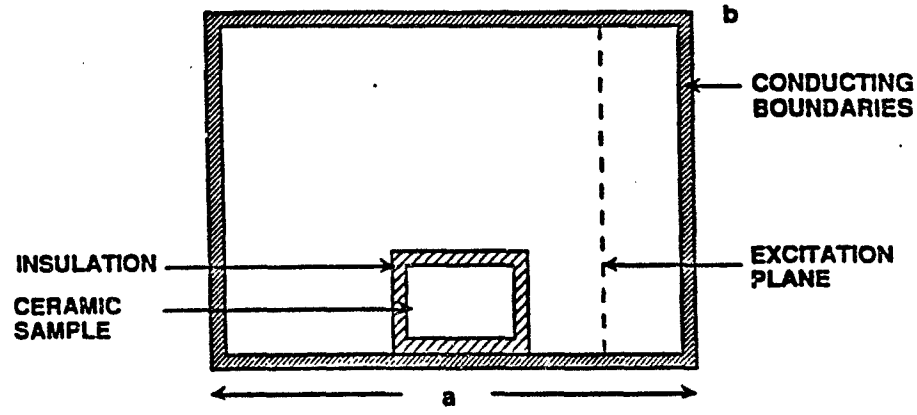


Fig. 1. The geometry of a microwave sintering process modeled using FDTD. The conducting boundaries of the cavity may be assumed perfect conductors or conductors of practical conducting values (10^7 S/m). The excitation plane was placed inside the cavity.

it is clear that rectangular cavities of various dimensions were used in these analyses. The FDTD solution procedure is described elsewhere [1-3] and a 3D computer code available at the University of Utah was used for these calculations. The excitation plane was used to assume an arbitrary incident electric field that is needed to initiate the iterative solution procedure.

Solution convergence to modes of empty cavities. To examine the convergence of the solution procedure and in particular the effect of the initially assumed fields on the convergence rate, solutions for several modes of an empty cavity were first calculated. Figure 2 shows the results obtained where it is clear that convergence was achieved for several cavity modes regardless of the initially assumed fields on the excitation planes. The possibility of using more than one excitation plane was also examined and small differences on the convergence rates were observed. It should also be noted that at frequencies off resonance, the field distribution in the cavity was much smaller than that predicted at resonance.

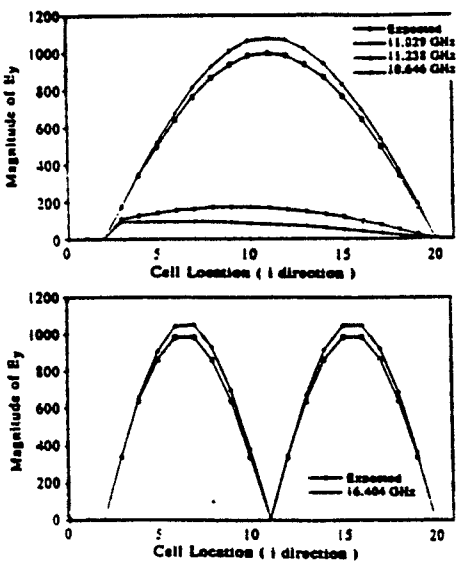


Fig. 2. Convergence of the FDTD solution to cavity modes predicted analytically, (top) TE_{101} mode ,(bottom) TE_{201} mode.

Field distribution in a dielectric object within the cavity. We examined next the accuracy of the calculated electric field distribution in a dielectric object placed inside the cavity. To help in this evaluation a spherical object, for which an approximate analytical solution is available, was utilized. Figure 3 shows the results obtained for three different values of ε_r of the dielectric sphere. In general, good agreement can be observed with equation (1), the expression used as the analytical solution.

$$\left|E_{in}\right| = \frac{3}{\varepsilon_r + 2}\left|E_{out}\right| \qquad (1)$$

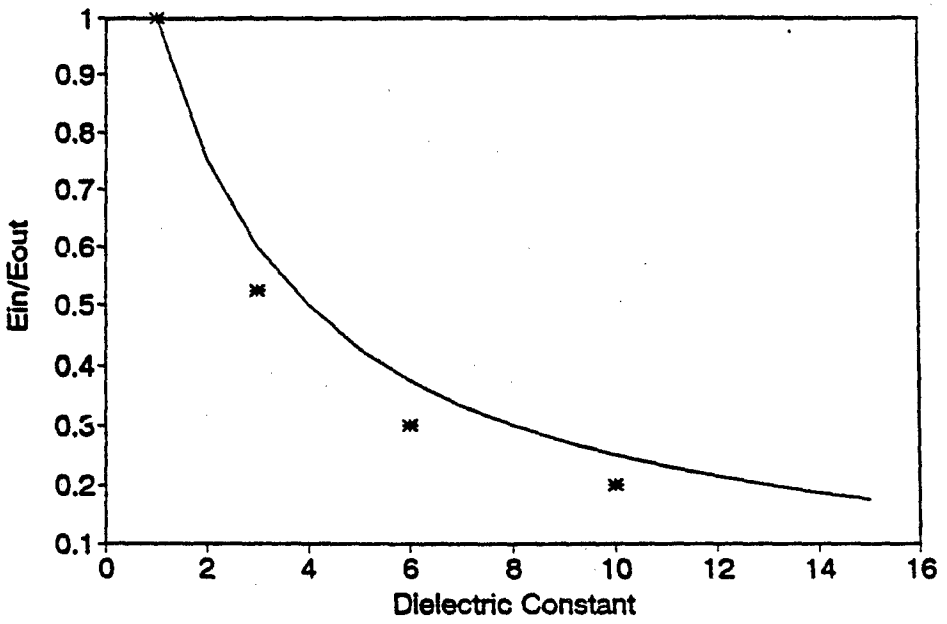


Fig. 3. Electric field distribution in a small spherical object placed inside a cavity operating at TE_{101} mode. Obtained results when averaged throughout the sphere agreed with equation (1) to within 15 percent. Data was calculated for $\varepsilon_r = 3, 6$, and 10.

Field continuity at the dielectric boundaries. Another validation that needs to be checked in the adopted solution is the accuracy of the results obtained in satisfying the boundary conditions for the tangential and normal field components. For this purpose field components were calculated at the dielectric interface. The results showed that the tangential component of the electric field is continuous to within 8 percent error, and that the normal component of the electric flux density is continuous to within 5 percent error. These calculations were made for values of ε_r varying between 3 and 10.

Typical specific absorption rate (SAR) results in ceramic samples. The absorbed power in ceramic samples surrounded with insulation was then calculated for typical ceramic samples sintered in a single-mode cavity. Typical results are shown in Figs. 4 and 5.

These results may then be used as an input in a thermal model to calculate the thermal pattern (temperature distribution) in the ceramic-insulation object. These thermal calculations are described in the next section.

Calculation of the temperature distribution pattern

The following heat transfer equation was solved numerically using the finite-difference approach [4].

$$\rho C \frac{\partial T}{\partial t} - K\nabla^2 T = W_{EM} \qquad (2)$$

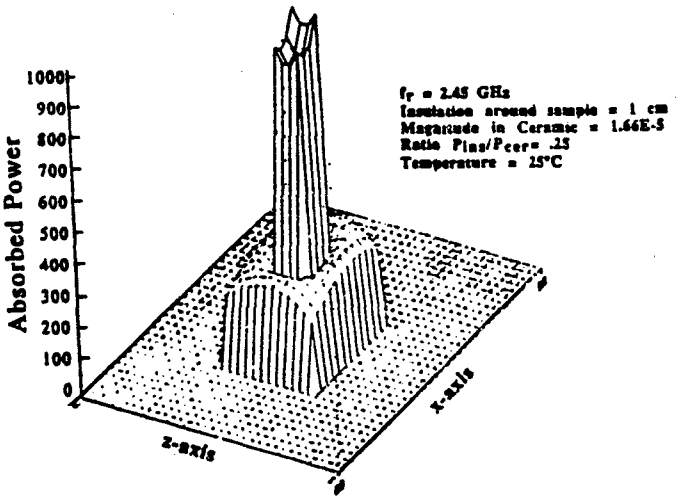


Fig. 4. Absorbed power distribution in a ceramic sample and surrounding insulation at the start of a sintering process (room temperature). The ceramic sample is 1 cm^3 cube and the insulation in this case is 1 cm thick surrounding the sample. Using mixing rules, ε_r and σ for the sample were 4.13 and $64e10^{-4}$ s/m, respectively, while ε_r and σ for the surrounding insulation were assumed 1.557 and $15.374e10^{-6}$ s/m, respectively.

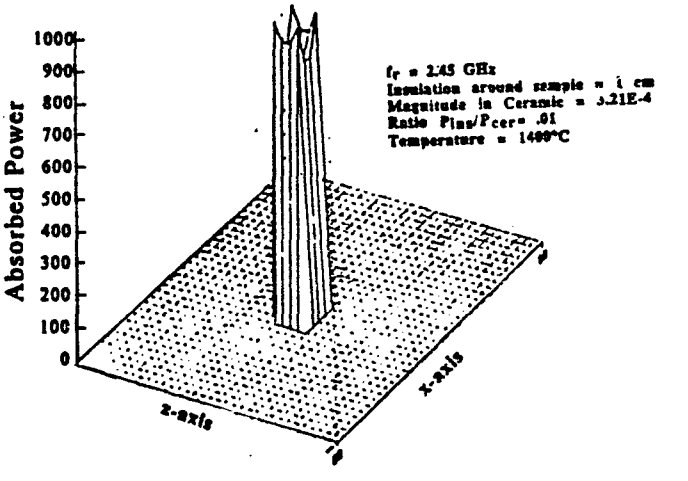


Fig. 5. Absorbed power distribution in a ceramic sample and surrounding insulation at 1400°C. The ceramic sample is 1 cm^3 cube and the insulation in this case is 1 cm thick surrounding the sample. Using mixing rules, ε_r and σ for the sample were 11.3 and $4.8e10^{-3}$ s/m, respectively, while ε_r and σ for the surrounding insulation were assumed 1.557 and $15.374e10^{-6}$ s/m, respectively.

where ρ, C, K are the density, specific heat, and thermal conductivity, respectively. W_{EM} is the input electromagnetic power distribution calculated using the EM simulation described earlier. Initial results are available from the developed thermal code. Additional validation of the results is, however, still needed before their final publication.

MICROWAVE SINTERING EXPERIMENTS

The Oak Ridge National Laboratory arranged to loan the University of Utah Clinic team a microwave sintering system. The system consists of a modified General Electric microwave oven and a programmable microwave-temperature controller (Micristar) with a dual-channel strip-chart recorder for monitoring both temperature and input power vs. time. The dimensions of the microwave sintering cavity are $40 \times 40 \times 24.5$ cm^3 operating at 2.45 GHz. Several ceramic samples of 2.3 cm diameter, and 0.7 to 0.9 cm in height were sintered in the oven. In all cases samples were surrounded with cylindrical insulations of 7.5 cm outer diameter and 2.5 cm inner diameter. The insulation height was 4.5 cm and four rods of SiC were inserted in the insulation in a picket-fence arrangement to aid the microwave heating process. The temperature was monitored using a Pt-Rh (R-type) thermocouple. Alumina and zirconia samples were heated to temperatures as high as 1475°C. Typical temperature and input power profiles during the sintering experiments are shown in Fig. 6. In all cases ceramic samples were glowing red to white hot while the insulation stayed near ambient, thus indicating appropriate microwave coupling to samples with negligible coupling to the insulation. This also indicates that the actual sintering occurred under microwave heating conditions and not by radiative transfer from the surrounding material.

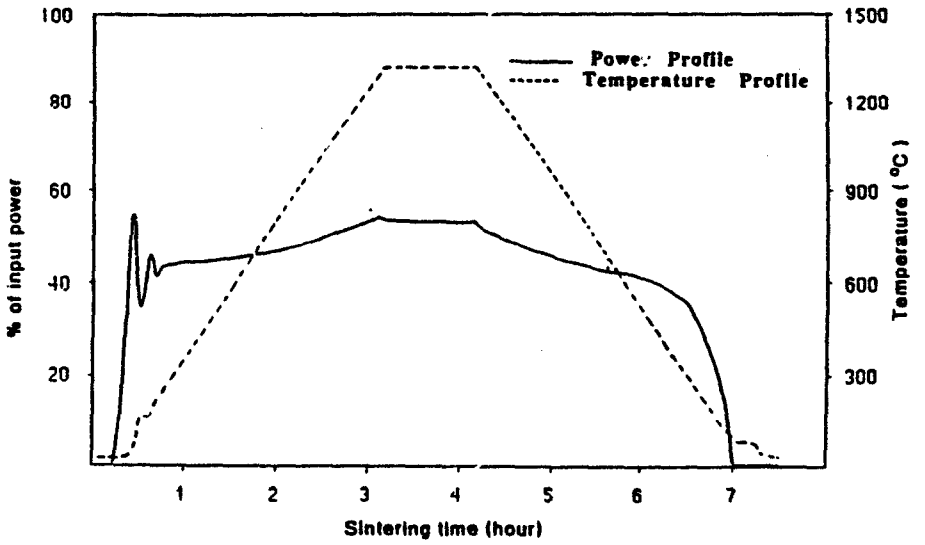


Fig. 6. Percentage input power and temperature profiles adopted in the microwave sintering experiments at the University of Utah. With the presence of the SiC rods in the insulation surrounding the sample, sintering to 1475°C was consistently achieved. The desired temperature and power profiles were programmed in the Micristar unit.

DIELECTRIC PROPERTIES MEASUREMENTS

Knowledge of the dielectric properties of ceramic samples and insulation and their variation with temperature and frequency is crucial in performing the EM and thermal simulation described above. To help further develop the available data base, the Engineering Clinic team took on the task of performing dielectric properties measurements. Extensive measurement facilities are available at the University of Utah including the HP 8510B Network Analyzer (45 MHz to 40 GHz) and the HP 8753 Network Analyzer (300 kHz to 6 GHz). A wide variety of sample holders for dielectric properties measurements is also available, including a lumped-capacitance sample holder terminating a Kovar section of a transmission line (for frequencies up to 4 GHz and temperatures up to 400°C). For cavity perturbation measurements an S-band rectangular cavity is used for measurements at 2.45 GHz and a cylindrical cavity with an adjustable plate covers the frequency range from 9 to 11 GHz. Free-space measurement techniques are also available for measurements at X-band and higher frequencies.

To demonstrate the accuracy of the measurement procedures, sample results are given in Tables 1-3. These results are given for standard materials of known dielectric properties and over various frequency ranges to demonstrate the available capabilities. In addition, preliminary results for ceramic samples are given in Table 4.

Table 1. Measurement Results of the Dielectric Constant of Teflon using Lumped-Capacitance Sample Holder.

Sample -- Teflon

Published value ($\varepsilon_r' = 2.1$, $\varepsilon_r'' \sim 2e10^{-4}$)

Frequency	ε_r'	ε_r''
0.8 GHz	1.88	0.0147
1.0 GHz	1.96	0.0221
1.2 GHz	2.09	0.0242
1.4 GHz	2.19	0.0250
1.6 GHz	2.20	0.0210
1.8 GHz	2.22	0.0188
2.0 GHz	2.23	0.0188
2.2 GHz	2.25	0.0198
2.4 GHz	2.30	0.0205
2.6 GHz	2.32	0.0228

THERMOPHYSICAL AND MICROSTRUCTURAL CHARACTERIZATION OF MICROWAVE-SINTERED CERAMICS

For complete thermophysical and microstructural characterization of microwave-sintered ceramics, the materials science group of the Clinic team conducted the following measurements:

Table 2. Measurement Results of the Dielectric Constant of Polystyrene and Lucite using the Free-Space Method.

Frequency: 10.0 GHz

Material	Thickness	Distance between antennas	ε_r'	ε_r''
Polystyrene	2.662 cm	36.5 cm	2.39	0.0611
Polystyrene	2.662 cm	41.5 cm	2.42	0.0848
Lucite	0.7228 cm	36.5 cm	2.72	0.0618
Lucite	0.7228 cm	41.5 cm	2.75	0.0387

Table 3. Measurement Results of the Dielectric Constant of Standard Materials using a Rectangular Cavity in the 2.45-GHz Frequency Range (Perturbation Method).

	fs (GHz)	Q factor	ε_r'	ε_r''
Empty Cavity	2.43992	1030.38		
Insulation Material	2.43784	1026.03	1.557	0.0002–0.0008
Empty Cavity	2.43606	1114.74		
Teflon	2.42885	1111.29	2.03	0.00049
Glass	2.40369	827.72	6.147	0.059
Silicon Carbide	2.2681	25.67	29.36	–

- Thermal diffusivity using camera-flash technique
- Density by fluid immersion
- Grain size using micrographs and linear intercept method
- Indentation fracture toughness.

Photo-Flash Procedure for Measuring Thermal Diffusivity

The measurement procedure basically involves coating a mildly polished cylindrical ceramic sample with a thin (500 angstroms) layer of gold and coloring the gold surface with black ink [5]. The sample is then exposed to a pulse of heat from a camera flash. The light is expected to be absorbed efficiently and the heat to be initially uniformly distributed on the front face of the sample. The sample is enclosed in a plastic box covered on the inside by black felt to protect the sample from outside heat and light. A type-E thermocouple is then attached to the back of the sample and recorded temperature is plotted as a function of time. Using the best fit linear approximation of the temperature vs. time curve, the thermal diffusivity is calculated from [5]

Table 4. Measurement Results of the Dielectric Constant of Si_3N_4-Based Ceramic Materials using a Rectangular Cavity in the 2.45-GHz Frequency Range (Perturbation Method).

Base material Si_3N_4

	fs (GHz)	Q factor	ε_r'	ε_r''
1. SC-111A AY_6 2% Al_2O_3 6% Y_2O_3	2.419136	1021.59	8.03	0.01146
1. SC-111A AY_6 Microwave annealed	2.419776	1021.86	7.91	0.01151
2. SC-128 AY_3L_4	2.420816	1039.87	7.93	0.00475
2. SC-128 AY_3L_4 Microwave annealed	2.420856	916.99	8.47	0.06621
3. SC-127 AL_8	2.419328	1028.63	8.22	0.00904
3. SC-127 AL_8 Microwave annealed	2.420768	1005.3	8.07	0.01962
4. SC-147 α' - β' AlN Y_2O_3	2.42384	1033.56	7.874	0.00805
Empty cavity	2.43992	1051.69		

$$a = 0.1388\, L^2/t_{1/2} \qquad (3)$$

where L is the length of the sample and $t_{1/2}$ is the half-time required for the sample to reach half of its maximum temperature increase.

Measurements were performed on a 17.6-mm-long section of a 6.2-mm-diameter sample of microwave-sintered SiC and the results are shown in Table 5. In two of the eight runs, aluminum foil was used to reflect light onto the thermocouple to improve the observed flash point. Measurements were also made on Si_3N_4 samples. One set of samples was thermally annealed in a microwave cavity. Work at ORNL has shown that this procedure leads to enhanced creep resistance. Annealing procedure is expected to alter the microstructure; in particular, the grain size and the nature of the grain boundary phase. For example, it is conceivable that crystallization of the grain boundary glassy phase would occur during annealing. The objective of the thermal diffusiv-

Table 5. Thermal Diffusivities of Si_3N_4 Sample.

Material	Thermal Diffusivity (mm^2/sec)
1. As - Received Si_3N_4 (3% Al_2O_3 - 6% Y_2O_3	12.736 ± 0.164
As - Annealed Si_3N_4	13.905 ± 0.217 (8.4% increase)
2. As - Received Si_3N_4 (2% Al_2O_3 - 3% Y_2O_3 - 4% La_2O_3)	12.974 ± 0.238
As - Annealed Si_3N_4	14.265 ± 0.391 (9.1% increase)
3. As - Received Si_3N_4 (2% Al_2O_3 - 8% La_2O_3)	11.519 ± 0.154
As - Annealed Si_3N_4	12.64 ± 0.131 (8.9% increase)

ity measurements was to determine the effect of microwave annealing, if any, on the thermal diffusivity. For comparison, therefore, measurements were also made on as-fabricated Si_3N_4 materials. Since cylindrical-shaped samples were not available, measurements were made on parallelpipeds. As a result, the values obtained are rather approximate. Even so, the experiments showed that there was ~8% increase in the thermal diffusivity upon microwave annealing. These data are given in Table 5.

Density Measurements

Density was measured on zirconia and alumina samples. Density measurements were conducted using a simple fluid immersion technique. The following equation was used to determine density, ρ, from measured weights.

$$\rho = \frac{w_{dry}}{w_{wet} - w_{H_2O}} \qquad (4)$$

where w_{dry} = dry weight of the sample
w_{wet} = weight in air after having the sample boiled in water
w_{H_2O} = weight while suspended in water.

The densities are given in Table 6. The zirconia samples sintered to near theoretical density at 1475°C/1 hr. Alumina samples were sintered at two temperatures: 1100°C and 1475°C. At 1100°C, the sample sintered to 3.72 gm/cm^3 which is ~93% of theoretical density, while at 1475°C it sintered to 3.93 gm/cm^3 which is ~98.25% of theoretical density. Density of ~93% at

Table 6.

Microwave Sintered

Material	Conditions	Density (g/cm^3)	Fracture Toughness ($MPa\sqrt{m}$)	Grain Size (μm)
ZrO_2-2 mol% Y_2O_3	1475°C 1 hour	5.92	14.5	1.10
Al_2O_3	1475°C 1 hour	3.93	4.5	3.60
Al_2O_3	1100°C 5 hours	3.72	3.7	0.85

Silicon Nitride hot pressed at 1725°C for 1 hour, later microwave annealed at 1400°C for 20 hours

Material	Density (g/cm^3)	Fracture Toughness ($MPa\sqrt{m}$)
Si_3N_4 - 2 wt% Al_2O_3, 6 wt% Y_2O_3	3.35	–
Si_3N_4 - 2 wt% Al_2O_3, 3 wt% Y_2O_3, 6 wt% La_2O_3	3.34	–
Si_3N_4 - 2 wt% Al_2O_3, 8 wt% La_2O_3	3.37	–
Si_3N_4 - 6.5 wt% AlN, 4 wt% Al_2O_3	3.33	6.9

Silicon Nitride hot pressed at 1725°C for 1 hour, no microwave processing

Material	Density (g/cm^3)	Fracture Toughness ($MPa\sqrt{m}$)
Si_3N_4 - 2 wt% Al_2O_3, 6 wt% Y_2O_3	3.33	–
Si_3N_4 - 2 wt% Al_2O_3, 3 wt% Y_2O_3, 6 wt% La_2O_3	3.38	–
Si_3N_4 - 2 wt% Al_2O_3, 8 wt% La_2O_3	3.45	–
Si_3N_4 - 6.5 wt% AlN, 4 wt% Al_2O_3	3.32	7.2

1100°C is well above what is expected in conventional sintering at this temperature. No significant difference in densities of Si_3N_4 samples was observed.

Determination of Grain Size using Micrographs and Linear Intercept Method

SEM fractographs of zirconia and alumina samples are shown in Figures 7 and 8. Zirconia sample, which sintered to near theoretical density, exhibited a very fine grain size (~1.1 μm) and intergranular failure. Grain size was measured by the linear intercept method which is strictly applicable to flat surfaces and not fracture surfaces. Thus, the measured grain sizes are rather approximate. Grain sizes are given in Table 6. Alumina samples sintered at 1100°C exhibited a very fine grain size (~0.85 μm) while that sintered at 1475°C had a significantly larger grain size (~3.60 μm). An examination of SEM fractograph shows a substantial amount of transgranular fracture in the sample sintered at 1475°C. Also, some porosity is seen trapped within grains, indicative of grain boundary breakaway from pores.

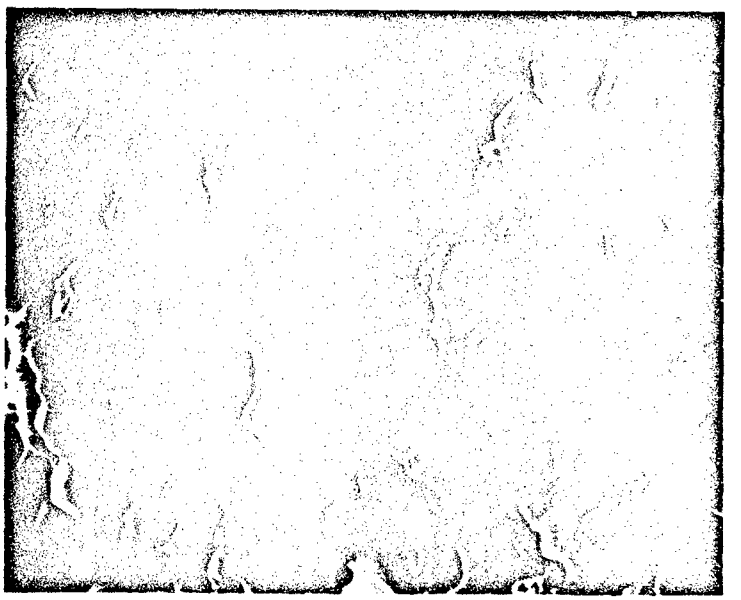


Fig. 7. An SEM fractograph at a microwave-sintered TZ2Y: 1475°C/2 hours.

Measurement of Fracture Toughness by Indentation

Indentation techniques, as described by Anstis, *et al.* [6], was used for the determination of fracture toughness on zirconia, alumina, and Si_3N_4 ceramics. Zirconia exhibited K_c of ~14.3 MPa$\sqrt{m}$ as shown in Table 6. This value is probably too high on account of the transformation

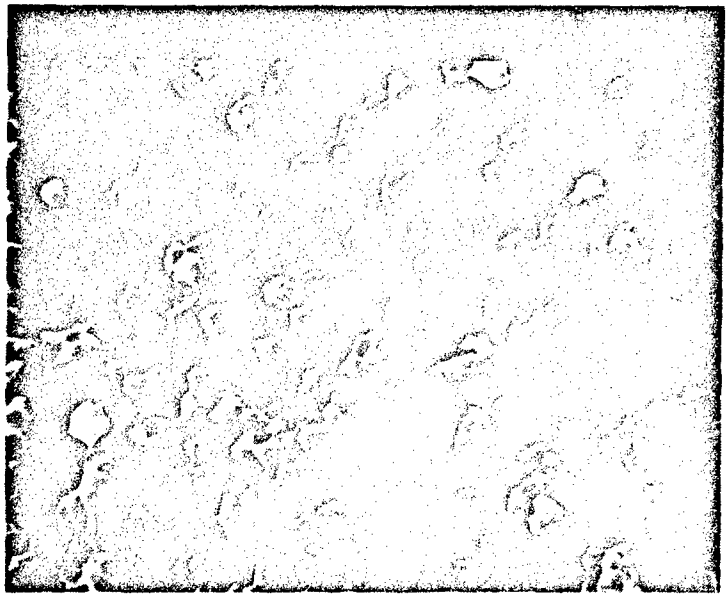


Fig. 8. An SEM fractograph at a microwave-sintered alumina: 1475°C/2 hours.

which occurs under the indent, which tends to introduce uncertainties in the indentation technique. Even so, the K_c obtained on microwave-sintered zirconia is similar to that sintered conventionally and measured in a similar manner. The indentation K_c of alumina is between 3.7 and 4.5 MPa$\sqrt{m}$, again in the same range as for conventionally sintered alumina. The K_c of Si_3N_4 was ~7.0 MPa$\sqrt{m}$ regardless of the thermal treatment.

SUMMARY AND CONCLUSIONS

A focused effort to model and simulate microwave sintering of ceramics in single- and multi-mode cavities and to measure dielectric properties and thermophysical properties of conventionally and microwave-sintered samples was initiated at the University of Utah as a result of an Engineering Clinic grant from Oak Ridge National Laboratory almost a year ago. To date, the FDTD has been used to model and calculate EM power deposition patterns in insulated ceramic samples in single-mode cavities, and a finite-difference program was used to calculate the temperature distribution patterns. The accuracy of the solution procedure has been checked and sample results for actual ceramic samples have been presented. Results of dielectric properties measurements and thermophysical characterization of both microwave and conventionally sintered samples have also been tabulated.

Although significant progress has been made, challenges still remain. In the numerical simulation area the Clinic team was unable to model large samples or overmoded cavities even with the IBM 3090 Supercomputer. Along these lines, a research team at Jet Propulsion Laboratory (JPL) was able to parallel process various sections of the FDTD program to overcome memory limitation and considerably shorten the Central Processing Unit (CPU) time. These parallel processing aspects of the FDTD code will be implemented in Utah. In the dielectric properties measurements area, accuracy of high-temperature measurements and problems with the thermal

gradient along samples are still under investigation. Other remaining problems include the measurement of temperature by a nonintrusive method. Finally, determination of whether improved properties can be realized in a variety of ceramics sintered by microwave heating is the central part of the future work. With continued support by ONRL of the interdisciplinary efforts at Utah, additional dielectric and thermophysical characterizations of conventionally and microwave-sintered samples will be reported soon.

* The Engineering Clinic Program supports teams of undergraduate seniors at the University of Utah. Mr. Hal Kimrey from Oak Ridge National Laboratory has sponsored a clinic project in 1990 and is continuing his sponsorship through the 1991/1992 academic year. For more information regarding the Clinic Program, please contact Dr. Magdy F. Iskander, program director. Research sponsored by the U.S. Department of Energy, Assistant Secretary of Conservation and Renewable Energy, Office of Industrial Technologies, Advanced Industrial Technologies, Advanced Industrial Materials Program under contract DE-AC05-840R21400 with Martin Marietta Energy Systems, Inc.

REFERENCES

1. K. S. Yee, "Numerical Solution of Initial Boundary Value Problems Involving Maxwell's Equations in Isotropic Media," IEEE Transactions on Antennas and Propagation, Vol. AP-14, pp. 302-307, (1966).

2. A. Taflove and K. R. Umashankar, "The Finite-Difference Time-Domain Method for Numerical Modeling of Electromagnetic Wave Interactions with Structures," Chapter 8 in *Progress in Electromagnetic Research*, M. Morgan, Ed., New York, NY, Elsevier Science Publication Co., (1990).

3. P. Cherry and M. F. Iskander, "FDTD Analysis of Power Deposition Patterns of an Array of Interstitial Antennas for Use in Microwave Hyperthermia," IEEE Transactions on Microwave Theory and Techniques, accepted for publication, (1990).

4. M. F. Iskander and O. Khoshdel-Milani, "Numerical Calculations of the Temperature Distribution in Realistic Cross Sections of the Human Body," Int. J. Radiation Oncology, Biol., Phys., Vol. 10, pp. 1907-1912, (1984).

5. T. Log and T. B. Jackson, "Photo Flash Technique for the Measurement of Thermal Diffusivity," submitted for publication, J. Am. Ceram. Soc., (1990).

6. G. R. Anstis, P. Chantikul, B. R. Lawn, and D. B. Marshall, "A Critical Evaluation of Indentation Technique for Measuring Fracture Toughness: I. Direct Crack Measurements," J. Am. Ceram. Soc. 64, Vol. 9, pp. 533-538, (1981).

Section II. Microwave/Material Interactions

FUNDAMENTAL INTERACTION MECHANISMS BETWEEN MICROWAVES AND MATTER

R.E. Newnham, S.J. Jang, Ming Xu, and Frederick Jones

Materials Research Laboratory
The Pennsylvania State University
University Park, PA 16802

ABSTRACT

A molecular and crystallographic view of the absorption of microwave energy by ceramic materials is presented, with examples drawn from both structural and electronic ceramics, together with the liquid and polymeric materials used in processing them. Among the absorption mechanisms discussed are dipole reorientation, space charge phenomena, ferrimagnetic resonance, and tails from the far infrared. Other important topics include relaxation spectra, field partitioning, and thermal runaway.

INTRODUCTION

Many different physical phenomena are involved in the microwave processing of ceramics. Microwaves are electromagnetic waves ranging from 1m to 1mm in wavelength at frequencies from 0.3 to 300 GHz. The interaction with matter takes place through the electric field vector E(V/m) and the magnetic field vector H(A/m) belonging to the microwave. The purpose of this paper is to review the fundamental interaction mechanisms between microwaves and matter.

ELECTRIC LOSS

When subjected to an electric field, materials polarize creating an electric polarization $P(C/m^2)$ equal to the dipole moment (C-m) per unit volume (m^{-3}).

There are four important polarization mechanisms in solids , and three of them lead to losses in the microwave region: (1) space charges arising from localized electrical conduction, (2) rotating electric dipoles, and (3) ionic polarization associated with far-infrared vibrations.

In discussing these phenomena, it is helpful to describe the losses in terms of the real and the imaginery parts of the dielectric constant K*. The electric field of the microwave is given by

$$E = E_0 e^{i\omega t} \qquad (1)$$

where E_0 is the amplitude of the field, ω is the angular frequency, t the time, and $i = \sqrt{-1}$. The resulting electric flux density is

$$D = D_0 e^{i(\omega t - \delta)} \tag{2}$$

where δ is the phase angle associated with the time lag in polarizing the material. The electric flux density (electric displacement) comes from the applied electric field and the electric polarization:

$$D = \varepsilon_0 E + P = \varepsilon E \tag{3}$$

where ε_0(= 8.85 x 10^{-12} F/m) is the permittivity of free space, and the dielectric constant is the relative permittivity of the material

$$K^* = \frac{\varepsilon}{\varepsilon_o} = \frac{D}{\varepsilon_o E} = \frac{D_o e^{-i\delta}}{\varepsilon_o E} = K' - iK'' \tag{4}$$

The real part of the dielectric constant is in phase with the field

$$K' = \frac{D_o}{\varepsilon_o E} \cos\delta \tag{5}$$

and the imaginary part is out of phase

$$K'' = \frac{D_o}{\varepsilon_o E} \sin\delta \tag{6}$$

The loss factor tan δ is K''/K'.
As pointed out by Sutton (1989), the power absorbed per unit volume is

$$W = \frac{1}{2} E_o^2 \omega \varepsilon_o K'' = \frac{1}{2} E_o^2 \omega \varepsilon_o K' \tan\delta \tag{7}$$

Microwave absorption therefore increases with field intensity, frequency, loss factor and dielectric constant . It is also important to realize, however, that in microwave processing we are dealing with inhomogeneous materials. Generally there are ceramic particles, organic vehicles, and porosity present in the green ceramic body. In this case we must be aware that electic fields are also inhomogeneous (Meek, 1987). Flux continuity ($D_1 = D_2$) is required across

interfaces if both phases are insulators. This means that electric fields are largest in regions of small permittivity.

CONDUCTION LOSSES

Most ceramics are wide band gap semiconductors with resistances that decrease rapidly with temperature. Sintered alumina is an excellent high voltage insulator with resistivity in excess of 10^{14} Ω-m at room temperature, but it drops to less than 10^{10} Ω-m at 400°C and 10^{5} Ω-m at 1000°C. Other ceramic insulators such as steatite and procelain decrease even faster. At 400°C the resistivity of steatite is about 10^{8} Ω-m, and porcelain with its mobile alkali ions is only about 10^{4} Ω-m.

Metallic behavior is observed in some transition metallic oxides. Rhenium trioxide (ReO_3) is comparable to silver and gold with resistivity less than 10^{-8} Ω-m at room temperature. RuO_2, Ti_2O_3, PdO, and tungsten bronzes such as $Na_{0.8}WO_3$ are also excellent conductors.

The importance of conduction losses in microwave heating is borne out in the experiments of Walkiewicz, Kazonich and McGill (1988). In this study a wide variety of metal powders, inorganic chemicals, and mineral specimens were heated in a microwave oven and the temperatures recorded as a function of time. The results are summarized in Table 1.

Table 1. Microwave heated minerals, chemicals, and metal powders. Temperatures were recorded after a few minutes heating at power levels near 1kW. (McGill, et al, 1988) approximate resistivities are given in parentheses.

Metal powders (10^{-6} - 10^{-8} Ω-m)	Oxide minerals (10^{4} - 10^{14}Ω m)
Al, Co, Cu, Fe, Mg, Mo	SiO_2, Al_2O_3, $KAlSi_3O_8$, $CaCO_3$
Moderate heating to about 400°C	Very little heating only about 80°C.
Alkali Halides (10^{4} - 10^{5}Ω-m)	Sulfide semiconductors (10^{-3} - 10^{-5}Ω-m)
KCl, KBr, NaCl, NaBr, LiCl	FeS_2, PbS, $CuFeS_2$
Very little heating. Only about 50°C.	Easily heated to about 1000°C.
Mixed Valent Oxides (10^{-2} - 10^{-4}Ω-m)	Carbon and Graphite (~10Ω-m)
Fe_3O_4, CuO, Co_2O_3, NiO	Easily heated to 1000°C.
Easily heated to about 1000°C	

It is apparent from these observations that conduction promotes the coupling of microwave energy into the powder. Transition metal oxides and sulfides such as magnetite and pyrite are easily heated, but insulators like alumina and silica are not.

Note, however, that metal particles are not heated as well, despite their high electrical conductivity.

Metals do not heat as well as semimetals and narrow-band semiconductors because electric fields cannot penetrate much below the surface. Skin depth, δ, is defined as the depth at which the electric field drops to $1/e = 0.368$ of the surface value. It is related to frequency f, permeability μ and conductivity σ by the relation

$$\delta = 1/\sqrt{\pi f \mu \sigma} \tag{8}$$

For copper, $\sigma = 5.8 \times 10^7\ \Omega^{-1}m^{-1}$, $\mu \equiv \mu_0$, where μ_0 is the permeability of free space, and the skin depth is approximately 1 cm at 60 Hz and less than 1 μm at microwave frequencies. Since field penetration is proportional to $\sigma^{(-1/2)}$, microwave energy heats semimetals and semiconductors better than copper. Note also that the resistance of metals increases with temperature, unlike that of semiconductors which show a rapid decrease. This promotes rapid heating and thermal runaway for the latter, as explained later.

The inhomogeneous nature of green ceramics can be understood using the Maxwell-Wagner model (von Hippel, 1954). For a two-layer system consisting of equal amounts of conducting high-permittivity material (e.g., ferrite) and an insulating low-permittivity material (air or polymer), the relaxation frequency at which absorption occurs is

$$\omega = \sigma/\varepsilon. \tag{9}$$

This lies in the microwave region when the resistivity ρ, expressed in Ω-m, is about $10/K$, where K is the dielectric constant. Hence, semiconductors and semimetals have about the optimum conductivity for ceramic processing at microwave frequencies.

OXIDE SEMICONDUCTORS

Transition metal oxides like magnetite with mixed cation valences are among the best microwave absorbers with very rapid thermal runaway. In electroceramic technology these mixed valency oxides are used as NTCR (negative temperature coefficient of resistance) thermistors. The electrical resistance decreases exponentially with increasing temperature. Typical of the NTCR thermistor materials, also know as controlled valency semiconductors, are titanium-doped hematite (Fe_2O_3:Ti) and lithium-doped bunsenite (NiO:Li). Reacting hematite with rutile in air yields

$$(1-\frac{x}{2})Fe_2O_3 + xTiO_2 \rightarrow Fe^{3+}_{2-x}Fe^{2+}_{x}Ti^{4+}_{x}O_3 + \frac{x}{4}O_2 \tag{10}$$

This is an n-type semiconductor in which electrons are transferred between iron atoms of different valence

$$Fe^{3+} + e^- \rightleftarrows Fe^{2+} \tag{11}$$

p-type NTC thermistors are made from nickel oxide doped with lithium.

$$(1-x)NiO + \frac{x}{2}Li_2O + \frac{x}{4}O_2 \rightarrow Ni^{2+}_{1-2x}Ni^{3+}_{x}Li^{+}_{x}O \tag{12}$$

The hole conduction process involves charge transfer between trivalent and divalent nickel ions.

$$Ni^{2+} + h^{\cdot} \rightleftarrows Ni^{3+}. \tag{13}$$

Doped nickel oxide has the rocksalt structure with lithium partially replacing nickel in the cation sites. Ionic radii for Ni^{2+}(0.84Å), Ni^{3+}(0.74Å), and Li^{+}(0.88Å) all favor octahedral coordination with oxygen.

The resistivity of $Ni_{1-x}Li_xO$ ceramics decreases drastically with increasing lithium content. The restivity at $x=10^{-4}$ is about 1000 Ωm and at x=0.1 it drops to 0.01 Ωm. The color is another indication of increased conductivity. The green color of pure nickel oxide deepens to black with increased doping.

For semiconducting compositions near $Ni_{0.95}Li_{0.05}O$, the band gap is about 0.15eV. The physical origin of this narrow band gap is attributed to the weak attractive forces between the negatively charged portion of the lattice where Li^{+} dopant ions are located, and positively charged regions occupied by the compensating Ni^{3+} ions. Charge is neutralized best when these ions are next, nearest neighbors, but under the action of electric field or temperature, the electron hole located at the Ni^{3+} drifts away rather easily to other nickel sites. Polarization of the surrounding oxide lattice also contributes to the band gap energy.

Electrical conductivity σ is proportional to the charge carrier concentration n, the charge of each carrier q, and the mobility μ:

$$\sigma = n\,q\,\mu. \tag{14}$$

In thermistors and other materials subject to thermal runaway, the temperature dependence of the conductivity is of great importance. Both n and μ are strongly dependent on temperature. For a semiconductor, the carrier concentration varies exponentially with temperature

$$n \sim \exp(-E/kT) \tag{15}$$

where E is the energy required to liberate charge carriers, k is Boltzman's constant and t is the absolute temperature. The temperature dependence of the mobility depends on its physical origin. For most scattering processes, mobility follows an inverse power law

$$\mu \sim T^{-b} \tag{16}$$

in which mobility decreases with increasing temperature because of atomic thermal vibrations, but a different temperature dependence is observed for hopping processes. Here the mobility depends on thermal excitation, and increases exponentially with temperature

$$\mu \sim \exp(E'/kT). \tag{17}$$

E' is the energy observed in the hopping process. Summing up, the temperature dependence of the electrical conductivity is

$$\sigma(T) \sim T^{-b}\, e^{-(E+E')/kT} \tag{18}$$

Since exponentials tend to dominate, the electrical resistance of a mixed valency oxide can be described by

$$R = Ae^{B/T}. \tag{19}$$

For the transition metal oxides used as NTC thermistors, R lies in the range $1\text{-}10^4$ ohms, and B is 2000 - 6000°K. The temperature coefficient α describes the fractional change in resistance with increasing temperature:

$$\alpha = \frac{1}{R}\frac{dR}{dT} = \frac{B}{T^2} \tag{20}$$

At room temperature, the resistance drops by 2-6%/°K for a typical thermistor. Resistance changes typical for thermistors made from transition metal oxides are shown in Fig. 1

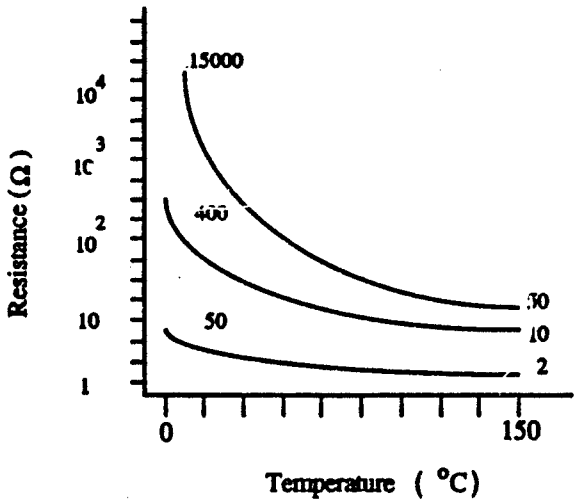


Fig. 1. Temperature dependence of typical NTC thermistors.

THERMAL RUNAWAY

A typical current-voltage relationship for a transition metal oxide thermistor is shown in Fig. 2. This is a so-called static characteristic in which the current is set to constant value and the system is equilibrated. The steady state voltage and temperature are then recorded for each current setting. Runaway takes place if the current is not carefully controlled.

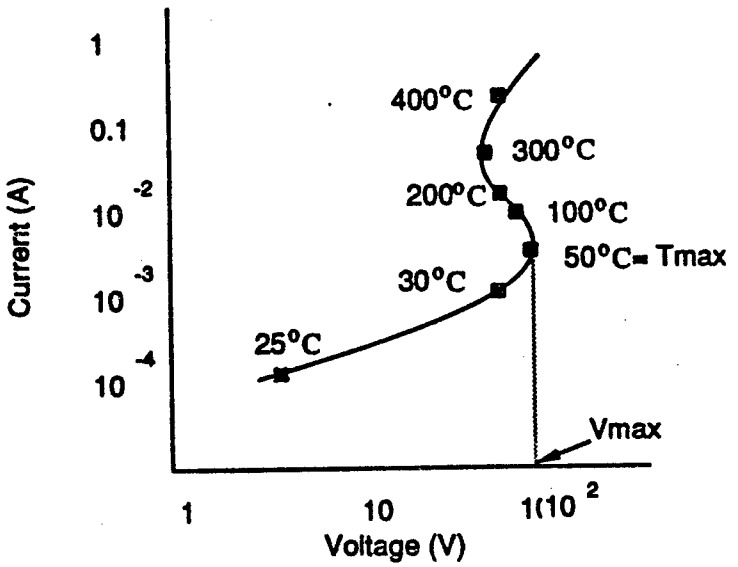


Fig. 2. Current-voltage characteristic for a transition metal oxide thermistor. Runaway takes place above T_{MAX} and V_{MAX}.

The relationship between the I-V characteristic (Fig. 2) and the R-T relationship (Fig. 1) is established by through Ohm's Law and the power balance equation:

$$R = V/I = Ae^{B/T} \tag{21}$$

$$W = VI = AD(T-T_0). \tag{22}$$

W is the input power (watts), T the specimen temperature, T_0 the temperature of ambient, and D the coefficient in Newton's law of cooling. D is a measure of the thermal coupling to the surroundings per unit surface area of the specimen. When surrounded by air, the specimen is cooled by convective air currents, and D ranges from 5 W/m^2K for free convection to 50 W/m^2K for forced convection (Tummala). The values of D are substantially higher, typically 100 - 10,000 W/m^2K, when in thermal contact to the surroundings takes place through solids or liquids.

Converting Ohm's law and the power balance equation to logarithmic form and summing the two, we obtain an expression relating voltage and temperature:

$$2\ln V = \ln AD + \ln (T-To) + B/T. \tag{23}$$

Thermal runaway takes place when T exceeds T_{MAX} and V exceeds V_{MAX}. To determine these conditions, we take the derivative of the voltage-temperature relation at $T = T_{MAX}$, $V = V_{MAX}$ and

$$2\frac{d}{dT}\ln V = 0 = \frac{1}{T_{MAX} - T_0} - \frac{B}{T_{MAX}^2} \tag{24}$$

$$T_{MAX} = \frac{B}{2} \pm \sqrt{\frac{B^2}{4} - BT_0} \tag{25}$$

For B = 2000 - 4000 K, and T_0 = 30°C, T_{MAX} is in the range 45-85°C, which is not far above room temperature. Therefore many transition metal oxides are on the verge of thermal runaway, as evidenced by the microwave heating experiments. The corresponding values for input current and power are obtained from the equation balancing input and output power using the appropriate value for D.

MICROWAVE ABSORPTION IN SILICATES

Conduction losses are important in glasses as well. Fused silica has very low tan δ values (<0.001) over wide frequency and temperature ranges. Alkali ions promote dielectric loss in glass. At low frequencies the loss is associated with ion transport through the silicate network giving a space charge contribution to the

dielectric permittivity. At 1 MHz the dielectric constant of sodium silicate glasses containing 30 mol% Na_2O. 70 mol% SiO_2 are about twice as large as SiO_2 glass.

Vibration losses become important at higher frequencies. Localized motion of the alkali ion in silicate cages can lead to strong absorption in the microwave range. The undesirable heating of Corning 9609 glass-ceramic cooking ware is an excellent example (MacDowell, 1984). Sodium nepheline ($Na_4Al_4Si_4O_{16}$) is the crystalline phase in this ceramic whose microwave losses are far higher than those of natural nephaline ($KNa_3Al_4Si_4O_{16}$). The glass-ceramic has a tan δ of about 7% at 2.45 GHz compared to 1% for the mineral nepheline. The high loss is attributed to the "rattling" motion of the smaller Na^+ ion occupying the crystallographic site of the larger K^+ ion. Sodium nepheline dishes are unsuitable for use in microwave ovens because of the high heat-up rate. The rattling motion of alkali ions can be pictured as localized conduction, or as a reorientable dipole between the cation and the coordinating anion cage. In this respect it bears a similarity to the double potential model used to describe proton motion in ice and ferroelectric potassium dihydrogen phosphate.

In most glasses, the tan δ values continue to climb with higher frequency. These losses are especially prominent in lead-bearing glasses and can be thought of as tails from far infrared spectra. The atomic motion associated with these losses involve motions of heavy ions, or in some cases loosely bonded fragments of the silicate network, against the more tightly bonded portions of the network.

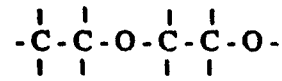
TAILS FROM THE FAR INFRARED

Most people have watched the ghostly "Tales from the Crypt," but few have given much thought to tails from the far infrared. They, too, are rather cryptic in that their origin is very obscure.

In crystals, infrared resonances involve the interaction of electromagnetic waves and the electric dipoles associated with lattice vibrations. The "reststrahlen" in alkali halides come from the excitation of a mode in which alkali ions vibrate out of phase with halogens. The frequency of this peak moves toward the far infrared and microwave region for heavy ions like Cs^+ and I^-. Weaker bonding and heavier masses both contribute to the frequency shift. This idea is utilized in choosing infrared windows for optical systems.

Similar relationships are observed in polymer and composite systems. Vibrational motions in polymers involve large numbers of atoms (and hence large masses) and weak secondary bonding forces between polymer chains. The dielectric properties of polymers at microwave frequencies have been reviewed by A.J. Bur (1985). High frequency dielectric losses arise from various portions of the polymer structure. These include pendulum-like motions of bulky side groups, crankshaft motions of the main chain, "freezing-in" motions accompanying the rubber to glass transformations, and oscillations of the tiny crystallites present in semicrystalline polymers. Generally speaking, the smaller segments of polymer chains resonate at higher frequencies and are the last to be frozen out at low temperatures.

Poly (ethylene oxide) or PEO is a typical crystalline polymer with a melting point of 60°C and Tg near -67°C. The helical chain has a backbone of carbon and oxygen atoms:



PEO has a modest dielectric constant of 4.3 at room temperature but a large absorption factor (tan δ~0.1) in the GHz range. Microbrownian motions of the main chain has been suggested as the cause of this absorption peak. Like glycerine, this peak is strongly dependent on temperature and frequency. At -50°C, the loss peak in PEO has dropped six orders of magnitude to the kilohertz range. (Connor, et al., 1964).

In amorphous polymers it is often difficult to identify the origin of microwave losses. Low density polyethylene $(CH_2)_n$ has twice the microwave loss level of high density polyethylene. (Amrhein, 1972). The tan δ values increase slowly with frequency similar to the behavior of the high Q resonator ceramics. The higher losses of low density polyethylene have been attributed to the amorphous regions where portions of polymer chains are able to oscillate in response to the microwave field.

DIPOLE REORIENTATION

The loss spectrum of water illustrates the contributions of conductivity and dipole reorientation to the dielectric constant. Fig. shows the classical relaxation spectrum at room temperature. Water molecules have large dipole moments because of their nonlinear molecular geometry. Under an electric field the dipoles reorient easily at room temperature producing a large dielectric constant of nearly 80. At microwave frequencies there is a rapid decrease in the dielectric constant accompanied by a large loss peak which is utilized in cooking foods. The presence of water in meat and vegetables couples the microwave energy into the food. At lower frequencies there is additional loss arising from conduction. The temperature dependence of the dielectric properties at 3GHz and 1MHz are quite different. The microwave loss peak moves to higher frequencies with increasing temperature causing the 3GHz loss to decrease. On the other hand the 1 MHz loss increases with temperature as the water becomes more conducting. It is interesting to note that the dipole reorientation effects in water persist below the freezing point. The dielectric constant of ice is almost as high as water but the relaxation frequency drops rapidly into the kilohertz range and no longer couples strongly to microwaves.

Other polar liquids behave in a manner similar to water. Table 2 lists the microwave properties of several polar and non-polar liquids. Both the real and the imaginary parts of the dielectric constant of polar liquids are orders of magnitude larger than nonpolar liquids. Dipole reorientation is one of the dominant absorption mechanisms in the microwave region.

Many organic liquids show strong dispersion effects. Glycerol ($CH_2OHCHOHCH_2OH$) is a highly viscous polar liquid with a boiling point of 290°C and a melting point of 18°C. Dielectric spectra taken over a wide range of temperatures resemble the curious frequency - dependent curves of lead magnesium niobate (PMN) and other relaxor ferroelectrics. The broad, diffuse melting transition is accompanied by peaks in K' and K" which depend strongly on both temperature and measuring frequency. When measured at 100 Hz, K" peaks at -60°C, and then shifts rapidly to higher temperatures for higher frequencies. At 10 kHz the peak is at -40°C at 10 MHz, 0°C, and at 100 MHz, 25°C. Thus the absorption maximum in glycerol moves rapidly toward the microwave region as the temperature rises (Morgan and Yager, 1940).

It is this "tunability" of energy absorption that makes microwave processing especially interesting. Unlike normal furnaces with broad band heat sources, monochromatic sources such as microwave ovens and high power lasers offer the possibility of shifting the heating from one constituent to another as reaction and densification take place. Exploitation of this time-temperature-frequency feature seems likely.

Table 2. Microwave dielectric properties of liquids at 3 GHz and 25°C (vonHippel, 1954)

	K	tan δ
Polar Liquids		
Water (H_2O)	77	0.16
Methyl Alcohol (CH_3OH)	24	0.64
Ethyl Alcohol (CH_3CH_2OH)	6.5	0.25
Nonpolar Liquids		
Heptane ($CH_3(CH_2)_5CH_3$)	2.0	0.0001
Carbon Tetrachloride (CCl_4)	2.0	0.0004

MICROWAVE RESONANCE SPECTRA

Piezoelectric resonances also give rise to loss spectra, sometimes at very high frequencies. For thickness resonance, the fundamental frequency f is

$$f = \frac{1}{2t}\sqrt{\frac{c}{\rho}} \text{ (Hz)} \qquad (26)$$

where c is the stiffness (approximately 10^{11} N/m^2 for an oxide), ρ the density (~5000 k_g/m^3) and t refers to the specimen thickness in meters. Millimeter thick transducers have resonant frequencies in the MHz range, and extrapolating these results to the microwave range, it is apparent that micron-size piezoelectric particles will resonate at GHz frequencies. Ceramic grain sizes and ferroelectric domain sizes are in the micron range and therefore show electromechanical losses in the

microwave range. Experiments on $LiNbO_3$ crystals, bicrystals and ceramics confirm these ideas (Yao Xi thesis).

The microwave losses in $BaTiO_3$ are shown in Fig.3. Note the drastic reduction in loss in specimens placed under DC bias. With domain walls locked in position there is a large decrease in K.

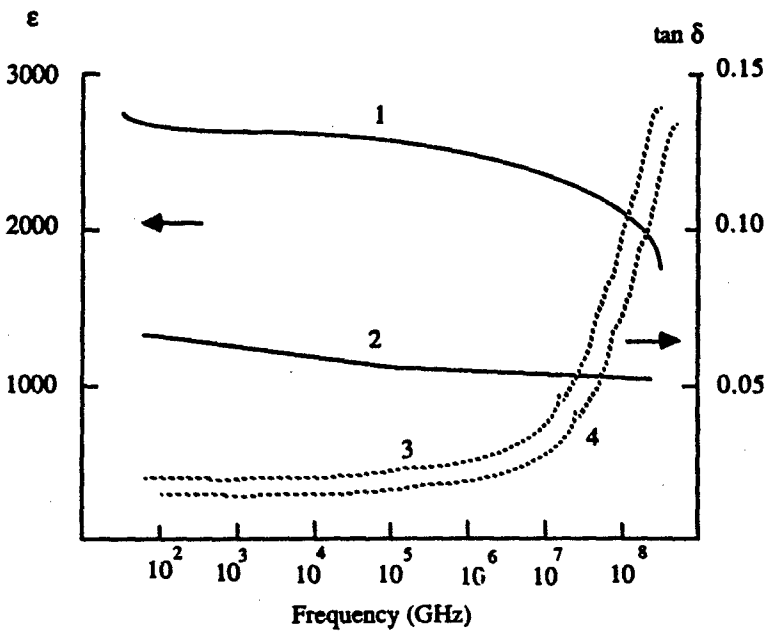


Fig. 3. Frequency dependence of the parameters of a poly-domain barium titanate crystal in weak fields. 1) Permittivity; 2) permittivity in a bias field of 10 kV/cm; 3) loss-angle tangent; 4) loss-angle tangent in a bias field of 10 kV/cm.

Fig. 3 Dielectric permittivity and loss tangent of $Ba(Ti_{0.85}Zr_{0.11}Sn_{0.04})O_3$ ceramics change rapidly in the microwave region. Poling the ceramics inhibit domain wall motion and lowers both K and Tan δ. (Poplavko, 1964).

Dimensional resonances of a different sort are employed in the dielectric resonators used in cellular mobile radios, marine satellite communications, and microstripline filters for SHF-TV converters. Dielectric resonance involves electromagnetic waves rather than the acoustic waves utilized in piezoelectric devices. The resonant frequency is controlled by the dielectric constant K ($= \varepsilon/\varepsilon_0$) and relative magnetic permeability $\mu_R = \mu/\mu_0$.

$$f = \frac{c}{\lambda \sqrt{K^{*} \mu_R}} \qquad (27)$$

where c is the speed of light in vacuum and λ the wavelength. Resonance occurs when the specimen size corresponds to an integral number of wavelengths. High K dielectrics reduce the wavelengths and miniaturize the microwave filters.

The microwave loss spectra of typical dielectric resonators are shown in Fig. 4. Note that high K ceramics have higher losses than do low K materials, and that the losses generally increase at higher frequencies suggesting that the origin of these losses is in the far infrared. Tan δ values for dielectric resonators are very small, typically 10^{-3} to 10^{-4}, and are probably associated with low frequency tails of far infrared absorption peaks.

The lowest frequency infrared mode involves vibrations of the large cation against the oxygen octahedra (Fig.5). The mode softens in high permittivity ferroelectric perovskites and eventually condenses at the Curie temperature to give spontaneous polarization. This helps to explain why high K dielectrics are generally more absorbing than Low K solids in the microwave region. The infrared peaks of dielectric resonator materials have been investigated by Wakino (1986).

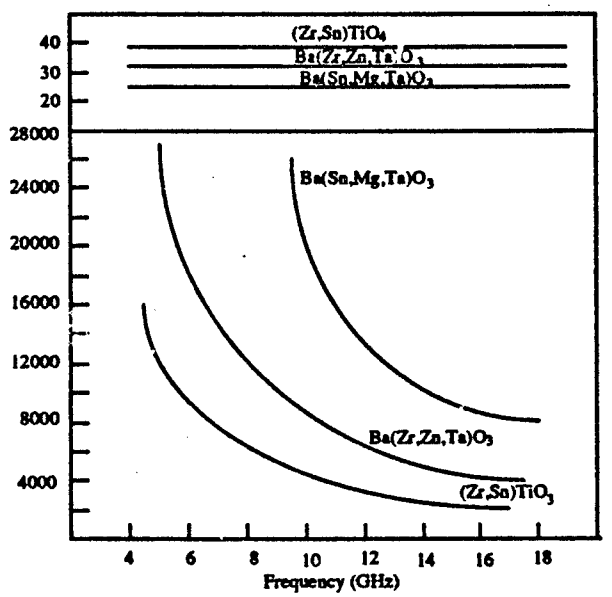


Fig.4.Microwave dielectric constants and loss spectra for ceramics used as dielectric resonators (Wakino,1986).

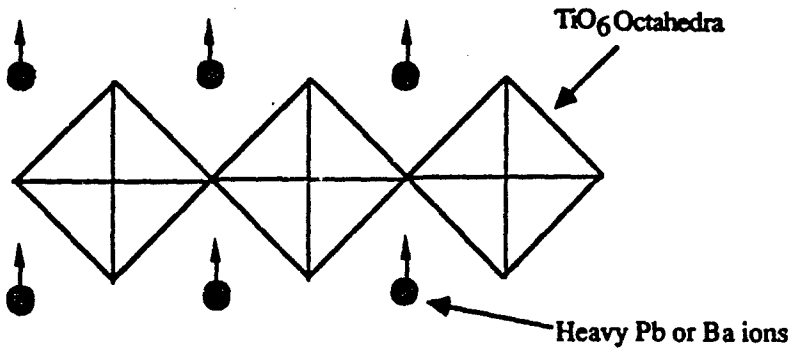


Fig. 5. Far infrared vibration mode for oxide perovskites. The vibrational mode of heavy ions of Pb or Ba, and TiO_6 octahedra in the oxide perovskites.

MAGNETIC LOSS

Most of the interactions between microwaves and matter take place through the electric vector of the electromagnetic wave, but the magnetic field vector can also induce substantial microwave losses, especially in magnetic materials with aligned spins. Some of the loss mechanisms in magnetic materials are listed in Table 3.

Table 3. Loss mechanisms in magnetic solids (Chikazumi, 1964)

Hysteresis loss rising from irreversible domain wall displacements

Eddy current loss from field-induced electric currents

Magnetic aftereffects associated with electron diffusion, usually from Fe^{2+} to Fe^{3+}

Dimensional resonances coming from electromagnetic standing waves

Magnetic resonance from precessional motion of unpaired dipole magnetic moments

Domain wall oscillations

The magnetic field vector of the microwave is represented by

$$H = H_0 e^{i\omega t} \tag{28}$$

The resulting magnetic flux density is

$$B = B_0 e^{i(\omega t - \delta)} = \mu_0 H + I \tag{29}$$

where μ_0 is the permeability of free space ($4\pi \times 10^{-7}$ H/m) and I is the magnetization (magnetic dipole moment per unit volume).

The magnetic permeability μ is analogous to the electric permittivity E.

$$\mu = \frac{B}{H} = \frac{B_o e^{-i\delta}}{H_o} = \mu' - \mu'' , \tag{30}$$

and the magnetic loss factor

$$\tan\delta_m = \frac{\mu''}{\mu'} \tag{31}$$

The relative permeability $\mu_R = \mu/\mu_0$ is the magnetic equivalent of the dielectric constant.

The magnetic permeability of ferrites is strongly dependent on frequency. The resulting losses arise from conduction, ferrimagnetic resonance, and domain wall oscillations.

In magnetic ceramics, much of the microwave loss is associated with ferrimagnetic resonance which is observed in ferrites with the spinel, magnetoplumbite and garnet structures. As illustrated in Fig.6, ferrimagnetic resonance involves precessional motions of the sublattice magnetization vectors about an effective internal magnetic field H_e. The effective field is caused by domain wall resonance or by magnetocrystalline anisotropy. High frequency absorption in the microwave region is found in magnetic materials with large anisotropy coefficients K_1. Soft ferrites such as the manganese ferrites with the spinel structure generally show the highest loss in the MHz region whereas hard ferrites with the magnetoplumbite structure have much higher resonant frequencies up in the GHz range.

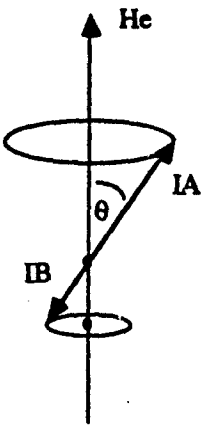


Fig. 6. Microwave resonance in ferrimagnetic oxides in which the sublattice magnetizations I_A and I_B precess about an internal effective field H_e.

Summary

The interactions between microwaves and matter are many and various. Conduction losses from localized space charge effects are responsible for microwave loss in transition metal oxides with mixed valence states. The inhomogeneous nature of green ceramics can be modeled using Maxwell-Wagner theory and thermal runaway follows a process similar to that observed in NTC thermistors.

Alkali ions cause microwave loss in glasses and other silicates, especially when loosely coordinated in a manner allowing considerable rattling room. Oscillating Na ions can be pictured either as localized conduction or as reorientable dipoles. The two polarization mechanisms lose their identity in situations like this.

Organic compounds and polymers are useful in ceramic processing. Dipole relaxation spectra are common in water, alcohol and other polar liquids, leading to intense energy absorption in the microwave regions. Polymers also absorb in this region of the electromagnetic spectrum with smaller segments of the polymer chain resonating at higher frequencies and continuing to lower temperatures.

Localized resonances caused by piezoelectric electromechanical coupling can also cause microwave loss. Domains in ferroelectric ceramics are on the right size scale to promote loss in the GHz region.

Dielectric resonator materials such as $ZrTiO_4$ utilize electromagnetic resonance rather than electromechanical resonance. These are generally low - loss ceramics but the tan δ values increase with frequency, suggesting a loss mechanism associated with infrared vibrations. Soft mode condensation in ferroelectrics has a similar origin.

Finally, not all microwave losses take place through the electric vector of the wave. The magnetic field vector can initiate energy transfer through magnetic resonance effects in which the unpaired electron spins precess about internal fields.

Anisotropy effects in hard ferrites and oscillating domain walls often create the internal fields.

References

E.M. Amhein, Ann. N.Y., " High Frequency Microwaves", Acad. Sci. 196 179 (1972).

A.J. Bur, "Dielectric Properties of Polymers at Microwave Frequencies: A Review", Polymer 26 (7) 963-977 (1985).

S. Chikazumi, Physics of Magnetism, Wiley, New York , (1964).

T.M. Conner, et. al., " Microwave Loss in Polymers", J. Appl. Chem., 14, 74 (1964).

Morgan and Yager, " Organic Dielectrics", Ind. Eng. Chem. 32, 1519 (1940).

W.H. Sutton, Microwave Processing of Ceramic Materials. Ceram. Bull. 68 (2)376-386(1989).

J.F. MacDowell, Microwave Heating of Nepheline Glass-Ceramics, Ceram. Bull. 63 (2) 282-286 (1984).

S.L. McGill, J.W. Walkiewicz, and G.A. Smyres ,The Effects of Power Level on the Microwave Heating of Selected Chemicals and Minerals in Microwave Processing of Materials, Vol. 124. Mat. Res. Soc., Pittsburgh PA, 1988.

T.T. Meek, Proposed Model for the Sintering of a Dielectric in a Microwave Field. J. of Mat. Sci. Lett. 6 638-640 (1987).

Y.M. Poplavko, "Permittivity Dispersion of Barium Titanate Type Ferroelectric", Sov. Phy. - Solid State 6 [1] 45-49 (1964).

R. Tummala and E. Rymazewski, Microelectronic Packaging Handbook, p. 171

A.R. von Hippel (Ed.) Dielectric Materials and Applications M.I.T. Press, Cambridge, MA 1954.

K. Wakino, "High Frequency Dielectrics and Their Applications", Proc. ISAF, 1986.

Xi Yao, Dielectric and Piezoelectric Behavior of Lithium Niobate Bicrystals and Polycrystal Ceramics, Ph.D., Thesis, The Pennsylvania State University, (1982).

THEORY OF MICROWAVE INTERACTIONS WITH CERAMIC MATERIALS

V. M. KENKRE
Department of Physics and Center for MicroEngineered Ceramics
University of New Mexico, Albuquerque, NM 87131

ABSTRACT

Very little is known about how microwaves interact with ceramics. We have recently developed a theory of these processes on the basis of Debye relaxation of interstitials, vacancies and bivacancies, and explained successfully thermal runaway observations on silica, alumina, strontium titanate, zinc oxide and iron oxide, as well as dielectric constant and loss factor observations on alumina, silica, and boron nitride. The article addresses these results as well as their satisfactory correlation with potentials for atomic motion and diffusion barriers obtained on the basis of ab initio computer calculations, and our recent exploration of structure effects on the phenomena of thermal runaway and microwave absorption.

INTRODUCTION

The following is a description of a theoretical attempt carried out in our group within the last year to understand the interaction of microwaves with ceramic materials. The motivation came from reported, in some cases suspected, in others expected, and always, surely, desired, enhancement in sintering temperatures and times under the action of microwaves. The context came from two specific phenomena: thermal runaway, and loss factor measurements. The techniques used were a combination of ab initio computations involving numerical methods, Langevin procedures applied to stochastic nonlinear equations, and simple model calculations of absorption of electromagnetic radiation. Results have been satisfactory. They show agreement of the theory with reported findings in a variety of materials and promise further insights into microwave interactions with ceramics. Whether microwave sintering does or does not become a feasible industrial method in the near future, the analysis reported below should find use in the difficult but important business of the construction of a general picture of the way ceramics behave under electromagnetic radiation in the microwave range.

For the sintering background, we refer the reader to reports in the recent literature [1-3] that microwave heating can lower the sintering temperature in several materials by several hundreds of degrees and shorten the sintering time by several hours. It has been suspected that microwaves not only increase the heating efficiency by concentrating the heating process within the material rather than in the furnace in which the material is placed, but also have basic consequences such as more efficient atomic diffusion within the material. To understand microwave effects on sintering, one must understand microwave effects on atomic diffusion. To understand the latter, one must, in turn, acquire a comprehensive picture of the general phenomenon of microwave absorption in ceramics. Of the two areas we have targeted for study, one is rather dramatic and consists of the finding that, during microwave heating of a number of materials, the increase of temperature is found to be gentle at first but explosive later when a threshold is reached, the sudden rise of temperature being referred to as thermal runaway [1,4,5]. The other target of our study has been dielectric measurements of ceramics, in particular the temperature and frequency dependence of the loss factor and the dielctric constant.

RELAXATION OR RESONANCE ?

The first question that a theory of microwave interaction with ceramic materials must address is related to an apparent paradox: there appear to be no oscillations in ceramic materials with characteristic frequencies in the microwave range. Standard resonance absorption theory is based on an evolution equation of the form:

$$\frac{d^2x}{dt^2}+\alpha\frac{dx}{dt}+\omega_0^2x=\frac{q}{m}E\cos\omega t \qquad (1)$$

Resonance absorption means that the (microwave) radiation with electric field E is absorbed by the material possesing an oscillation of a coordinate x with characteristic frequency ω_0 when the radiation frequency ω is essentially equal to ω_0. The effective charge and mass are, respectively, q and m. The primary effect of the damping rate α is to broaden the absorption line, a secondary effect being to impose a slight shift (to the low-frequency side) on the resonant frequency. Typical ω_0's such as those of vibrations in the ceramic are larger by 2 to 3 orders of magnitude than microwave frequencies ω which lie in the GHz range. In light of this disparity, it is obvious that a resonance mechanism is unable to provide an

explanation of the source of microwave interactions in ceramics.

The resolution of this paradox lies in understanding that absorption of microwaves in ceramics can occur by the relaxation mechanism [6] rather than by resonance. The simplest way to understand relaxation is to notice that damping, which merely broadens the resonance line when small, has a profound effect on the *location* of the absorption peak when large. In the large damping limit, equation (1) is well represented by

$$\frac{dx}{dt} + \Gamma x = cE\cos\omega t \qquad (2)$$

c being $q/m\alpha$ and Γ being $\omega_0{}^2/\alpha$. The absorption peak is now nowhere near ω_0 but at Γ, which, in this limit of large α (relative to ω_0), can be considerably smaller – indeed by orders of magnitude as is the case in microwave absorption – than the characteristic frequency ω_0 of the material oscillation. It is important to observe that, in this limit, absorption can occur at field frequencies which cannot be identified with, and are much lower than, all frequencies in the system except the quantity Γ which one could call the relaxation frequency or, more appropriately, the relaxation rate. The terminology arises because the physical origin of the absorption is through a matching of the field period to a time characteristic of the relaxation process that the oscillator undergoes under the combined action of damping and natural oscillatory tendencies.

NONLINEAR POTENTIAL AND STOCHASTIC EVOLUTION

Through model calculations we have explored various possibilities regarding characteristic motions within the ceramic materials. That work has resulted in our suggesting vacancy or interstitial motion, e.g. bivacancy rotation, as being responsible for microwave interaction through the Debye relaxation mechanism explained above. This is in agreement with earlier ideas. As an initial step in our analysis, we carried out a first-principles determination of the features of the potential felt by these moving entities in several materials, a particularly simple example being MgO which has a rock salt structure with a lattice constant of 4.21 Å. In order to describe vacancy motion, we chose the CNDO/2 method (Complete Neglect of Differential Overlap version 2) as a reasonable compromise between the level of sophistication and the amount of computational time, and considered clusters of up to 30 atoms. The method and details of the results of the numerical

calculation may be found elsewhere [7]. The important characteristic of the potential which emerges from the numerical work is that it is generally periodic and obviously nonlinear, i.e. anharmonic. The appropriate force term to be used in the equation of motion is therefore NOT of the Hooke's form as in (1) or (2), but possesses nonlinearity. The potential to be used is not of the harmonic form $(1/2)\omega_0{}^2x^2$ but may be modelled simply by the sinusoidal form

$$U(x) = -\frac{1}{2}\Delta\left(1+\cos\frac{2\pi}{a}x\right) \tag{3}$$

where a describes the periodicity of the potential and Δ measures its height. The evolution equation on which one may base a theory of microwave absorption is

$$\frac{d^2x}{dt^2}+\alpha\frac{dx}{dt}+\frac{dU(x)}{dx}=\frac{q}{m}E\cos\omega t+R(t) \tag{4}$$

Two characteristics of (4) distinguish it from earlier starting points such as (1). The first is the nonlinearity of the potential U which is a consequence of the *mechanical* interaction of the moving entity with the rest of the lattice. The second stems from the term R(t). That term represents the random force which describes the *thermal* interaction of the moving entity with the rest of the solid. Our theory of microwave absorption in ceramics is based on the interplay of these two interactions. It will be seen that the coexistence of nonlinearity and stochasticity is responsible for such behavior as thermal runaway.

TWO-STATE ANALYSIS AND THE T(t) EQUATION

The solution of (4) presents a non-trivial task. Contrary to the case of the harmonic (1), on which most of the textbook descriptions of the absorption of electromagnetic radiation are based, one cannot find exact solutions even for the simple case of the sinusoidal potential given by (3). Analytic solutions are known in terms of Jacobian elliptic functions for the undamped ($\alpha = 0$), homogeneous ($E = 0$), and deterministic ($R = 0$) limit. The introduction of low damping allows one to use the averaging method [8] to find approximate solutions. Scientists interested in chaos have studied the deterministic undamped case. But their results are appropriate for high electric fields which are not attained in microwave interactions with ceramics since field intensities are limited by breakdown. Scarcity of available results has led us to study (4) in a variety of new ways including the development

of nonlinear Fokker-Planck equations to treat the stochastic element and the use of perturbation techniques supported by numerical simulation. Rather than describe that work here, we will consider a simplified two-state analysis which can capture the essence of the evolution and lead us rapidly from (4) to an understanding of phenomena such as thermal runaway.

An important feature of the nonlinear potential U(x) in (3) or (4) is that the interstitial atoms or vacancies which are subjected to it, lie in the binding part of the wells at low temperatures but may be freed from them at high temperatures. With attention on the two states provided by the nonlinear potential, let us make the reasonable assumption that the relative population in the two states is given statistically as a result of thermal quasi-equilibrium. A simple expression for the fraction f(T) of the number of free entities to the total (both free and bound) number is given, through Boltzmann considerations, by

$$f(T)=\frac{e^{-\frac{\Delta}{T}}}{1+e^{-\frac{\Delta}{T}}} \tag{5}$$

where, for simplicity, we have absorbed the Boltzmann constant k through a redefinition of Δ. Clearly, Δ measures the barrier the absorbing entity must surmount to become free of its binding well. The role of the stochastic force R is to maintain thermal equilibrium.

One can now address a phenomenon such as thermal runaway in terms of the physical model which is a consequence of the above considerations. We assume that the system consists of two species which we call the A-species and the M-species. The former consists of absorbing entities and is typified by impurities and inclusions whose relaxation times match the period of the microwaves and which therefore absorb microwave radiation via the Debye relaxation mechanism. These entities are absent in systems which are found to be transparent to microwaves. In such cases, the A-species entities are provided by aids which, when introduced into ceramics which are naturally transparent to microwaves, cause the absorption of radiation. Absorption by this A-species leads to an initial slow rise of temperature with respect to time as the absorbed energy is redistributed in the form of thermal energy by the stochastic interactions. The increase in temperature causes an increase in the fraction f(T): more carriers tend to be free. Straightforward considerations to be detailed below show that absorption in the free state is much larger than in the bound state. This means that absorption increases substantially as more entities

become free. Stochastic redistribution of the absorbed energy in the thermal form increases T which in turn increases f(T) which *in its turn* increases absorption. The nonlinear feedback is responsible for the possibility of an explosive acquisition of energy , i.e. for the dramatic phenomenon of thermal runaway.

It is important to understand that the behavior described is a direct consequence of the interplay of the nonlinearity of the potential and the stochasticity of the random term. The latter is responsible for the redistribution of the absorbed energy in thermal form while the former provides the disparity in absorption between the free and bound states. The statement made above about the drastic difference between absorption of electromagnetic radiation by free versus bound charges can be understood easily as follows. When an electric field representative of the incident electromagnetic radiation is applied to the charge in question, the charge is accelerated. The movement is opposed by friction forces which increase as the velocity increases until the friction forces balance the electric force. A d.c. electric field thus brings a free charge in equilibrium to a state of non-zero velocity. The product of this non-zero velocity and the electric force is the rate at which power is absorbed by the charge from the electromagnetic field. In the case of a charge trapped in a potential well on the other hand, the effect is different. The velocity increases under the action of the electric field but this increase is opposed by another agent in addition to the friction force, viz. the binding force which constrains the particle to the well. In the absence of friction, an oscillation of the charge occurs around the potential minimum. This minimum is displaced from the original minimum. In the presence of friction, the oscillation decreases in amplitude until the particle comes to rest at the new potential minimum. Thus, under the combined action of the electromagnetic force, the binding force and the friction force, the equilibrium state for a bound absorber is that of rest. Once this state is reached, there is no absorption. By contrast, the equilibrium state for a free absorber involves, as we have seen above, non-zero velocity. Heating continues in this state.

When we incorporate these features into an evolution equation for the temperature T(t), we obtain

$$\frac{dT}{dt} = P[k_A + f(T)k_M] - \sigma_1 T^4 \qquad (6)$$

Here P is the power and k_A and k_M are proportional to the absorption coefficients of the A-species and M-species, respectively, as well as to their total number in the material. The last term in (6) describes losses through radiation pathways. Its form

and dependence on T would be generally different from that used in (6) if other modes such as convective decay were dominant. However, we use the form shown both in order to follow standard procedure and because excellent confirmation for the term is found in our applications to specific observations.

APPLICATION TO THERMAL RUNAWAY OBSERVATIONS

We have encountered rather diverse shapes of the time-temperature curve in our study of the data on various materials and equation (6) has been able to describe them all satisfactorily. One of the types is characterized by a sudden increase in temperature and no saturation within the reported observations. It is typified by chromia. Another shows only a slight effect, i.e. near-linear rise of temperature. Silica provides an example of this behavior. A third kind of observation, exemplified by iron oxide, is a rise followed by temperature saturation. A fourth type combines all these tendencies into an S-shaped curve which includes the gentle rise, the steep increase and the saturation. Alumina typifies this behavior.

Equation (6) addresses all these shapes naturally. If k_M f(T) is dominant, and is not overwhelmed by the T^4 term within the range of observations the sudden rise and no saturation appear as obvious consequences of (6). If k_M and the T^4 terms are both negligible the linear rise arises naturally. If k_M alone is negligible, but the T^4 term does dominate at high temperatures, the rise and saturation emerge as a consequence. Finally, the full equation (6), with all terms significant, corresponds to the S-shaped curve as in alumina.

The specific observations we analyzed are on strontium titanate of initial porosity of 53% during the process of sintering via microwave heating [4], on silica for microwave heating [5] at 500 W for 7 min; on zinc oxide [1], the heating time being also 7 min; on silica at power levels of 1000 W, 1500 W, and 2000 W respectively [5], on iron oxide [1], and on alumina of initial porosity 50% undergoing microwave sintering [4]. A comparison of the observed curves and the theoretical fits shows excellent agreement. We refer the reader to refs. 9 and 10 for the relevant figures. The results are summarized in Table 1.

Table 1. Parameters Deduced from Thermal Runaway Observations.

material	k_A(deg/min/W)	k_M(deg/min/W)	Δ(deg)	σ_1(1/s/deg^3)
silica	3.9×10^{-2}	8.5	5400	0.35×10^{-12}
silica*	1.8×10^{-2}	8.8	5600	0.35×10^{-12}
zinc oxide	9×10^{-2}	30	2800	0.46×10^{-12}
ferric oxide	1.6	0.96	1.7×10^{-3}	0.5×10^{-12}
alumina	8.1×10^{-6}	72	2600	1.9×10^{-12}
str. titanate	1.1×10^{-2}	230	3600	4.1×10^{-12}

*multiple power levels

Several comments are in order. Although σ_1 has been taken as a fitting parameter it is related to the Stephan-Boltzmann constant σ through

$$\sigma_1 = \sigma \frac{S}{V} \frac{1}{C_v} \tag{7}$$

where S and V are the surface and volume of the sample and C_V is its specific heat. The magnitude of the universal constant σ is known to be

$$\sigma = 5.68 \times 10^{-12}\ Wcm^{-2}\deg^{-4} \tag{8}$$

We have been able to show that typical values of the surface-volume ratio and known values of the specific heat lead to extremely good agreement of σ_1 with values obtained from our fits. An example is alumina in which the value deduced from the above calculation is $2 \times 10^{-12}\ s^{-1}\ deg^{-3}$ whereas the value obtained from the fits is 1.9 x 10-12 $s^{-1}\ deg^{-3}$. This agreement certainly supports the view in the literature that the loss of heat by radiation is indeed the major factor responsible for temperature saturation in thermal runaway. Furthermore this means that σ_1 need not be taken to be a fitting parameter in our theory [9,10]. The deduced magnitudes of Δ also appear

to be compatible with usually accepted values of energy barriers for defect formation. While not identical to the latter, they do not differ by order-of-magnitude factors. It is remarkable that a two-parameter theory (the adjustable parameters being k_M and k_A) fits the large variety of observed shapes of the temperature-time curves so well. A complete microscopic theory of the phenomenon, which is under way, is expected to obtain these two adustable parameters also from ab initio calculations, making this theoretical development free of adjustable quantities.

APPLICATION TO DIELECTRIC LOSS MEASUREMENTS

In order to provide independent experimental suport for the basic assumptions of our theory described above, we have applied them in a context different from that of thermal runaway, viz. dielectric measurements on ceramics.For reasons of space we do not describe the relevant formulae here, except for mentioning that they involve straightforward application of the ideas explained above and that they address the complex dielectric constant

$$\varepsilon = \varepsilon_r - i\varepsilon_i \tag{9}$$

and the loss factor

$$\tan\delta = \frac{\varepsilon_i}{\varepsilon_r} \tag{10}$$

which is related to the absorbed power P through the well-known relation

$$P = \frac{1}{2} E^2 \omega \ \varepsilon_0 \varepsilon_r \tan\delta \tag{11}$$

Reference 11 may be consulted for full details of this part of our theory. We have found reasonable fits to data on both the real part of the dielectric constant and the loss factor in several materials including sapphire, boron nitride, and fused silica. Experiments are available [12] at 3.5, 35 and 94 GHz. In our fits to observations of Ho^{12} on alumina at 3.5 and 35 GHz we find that the deduced values of the energy barrier Δ in units of temperature lie between 3000 and 7000 K and that the relaxation time τ responsible for absorption through Debye relaxation is

$$\tau = 0.8 \times 10^{-10} s \tag{12}$$

This latter result is particularly satisfactory because $1/\tau$ lies close to the frequency of microwaves used in the experiments, thus ensuring internal consistency of the theory. The value of the energy barrier Δ also agrees with values for ionic and vacancy motion [13].

GENERALIZATION FOR f(T) AND STRUCTURE EFFECTS

Among the directions in which we have extended the theory explained above is the exploration of structure effects through the generalization of the simple two-state assumption of our model and of the corresponding expression (5) for the fraction f(T). It is clear that such a generalization based on phase space considerations leads to

$$f(T) = \frac{\int_{\text{free region}} dx\, dp\; e^{-\frac{(p \cdot p/2m) + U(x)}{kT}}}{\int_{\text{entire region}} dx\, dp\; e^{-\frac{(p \cdot p/2m) + U(x)}{kT}}} \tag{13}$$

The phase space integration is carried out over the entire region available to the moving entity in the denominator of (13) but only over the "free" region in the numerator. For a representative 1-dimensional system one can reduce (13) to

$$f(T) = \frac{\int_{\text{entire region}} dx\; e^{-\frac{U(x)}{kT}} erfc\sqrt{-\frac{U(x)}{kT}}}{\int_{\text{entire region}} dx\; e^{-\frac{U(x)}{kT}}} \tag{14}$$

The integrations over the momentum have been carried out and the complementary error function introduced in (14). For the sinusoidal potential U(x) given by (3) it is possible to obtain

$$f(T) = \frac{\int_{-\pi}^{\pi} dy\; e^{\frac{\Delta \cdot \cos y}{2kT}} erfc\sqrt{\frac{\Delta(1+\cos y)}{2kT}}}{2\pi I_0\left(\frac{\Delta}{2kT}\right)} \tag{15}$$

which involves the modified Bessel function I_0 while for the square well potential in 3 dimensions one gets

$$f(T)=\frac{re^{-\frac{\Delta}{kT}}+erfc\sqrt{\frac{\Delta}{kT}}+\frac{2}{\sqrt{\pi}}\sqrt{\frac{\Delta}{kT}}\,e^{-\frac{\Delta}{kT}}}{1+re^{-\frac{\Delta}{kT}}} \tag{16}$$

In appropriate limits these expressions can be shown to lead to

$$f(T)=\frac{e^{-\frac{\Delta}{kT}}}{\frac{1}{r}+e^{-\frac{\Delta}{kT}}} \quad \Rightarrow (r=1) \Rightarrow \quad f(T)=\frac{e^{-\frac{\Delta}{kT}}}{1+e^{-\frac{\Delta}{kT}}} \tag{17}$$

In the first form of (17) we explicitly see the effect of the structure factor r which is the ratio of the volume of the free region to that of the bound region. In the simple case r = 1, we recover the two-state result of (5). This theory [11] has been used to extract the value of the geometrical factor r for alumina (found to be 0.58) by fitting the predictions to observations of the loss factor at 3.5 and 35 GHz.

CONCLUSIONS

We have described a simple theory of microwave interactions with ceramic materials. Debye relaxation as the mechanism for absorption and a crucial interplay of the nonlinearity of the potential and the stochasticity of the random force are its essential elements. A simplified treatment based on a two-state description of the phase space available to the absorbers subjected to the nonlinear potential was found to lead to a satisfactory explanation of thermal runaway and dielectric observations on a wide variety of materials. Extensions of the theory along generalized phase space considerations were also described. Among the topics currently under investigation are ab initio calculations of the parameters of the theory for a wide range of materials and the study of anomalous power dependence and saturation effects observed in several materials.

ACKNOWLEDGMENTS

The work described here was the result of an active collaboration with Joel Katz, Lubosh Skala, Marty Weiser and Jim Warsa. It is a pleasure for me to thank them for their help. In particular, the numerical ability and analytical assistance of L. Skala, and the experimental knowhow and general microwave expertise of J. Katz were invaluable in this research. This work was part of a collaboration of the Center for Micro-Engineered Ceramics at UNM and the Los Alamos Nati onal Laboratories.

REFERENCES

1. L. M. SHEPPARD, Ceramic Bulletin, 67 , 1656 , (1988).
2. R. W. BRUCE, in Mat. Res. Soc. Symp. 124, Materials Research Society, (Pittsburgh 1988), p. 3.
3. J. D. KATZ, R. D. BLAKE, J. J. PETROVIC and H. SHEINBERG, in Mat. Res. Soc. Symp. 124, Materials Research Society, (Pittsburgh 1988), p. 119.
4. V. K. VARADAN, Y. MA, A. LAKHTAKIA and V. V. VARADAN, in Mat. Res. Soc. Symp. 124, Materials Research Society, (Pittsburgh 1988), p. 45.
5. S. L. MCGILL, J. W. WALKIEWICZ and G. A. SMYRES,in Mat. Res. Soc. Symp. 124, Materials Research Society, (Pittsburgh 1988), p. 247.
6. See, e.g., H. M. ROSENBERG, The Solid State, 3d ed., Oxford University Press, (Oxford, 1988), p.226.
7. L. SKALA, V. M. KENKRE, M. WEISER and J. D. KATZ, Proc. Materials Research Society (San Francisco 1990) to be pubiished.
8 See, e.g., H-L WU, P. GRIGOLINI and V. M. KENKRE, J. Phys. Condens. Matter, 2, 4417, (1990).
9. V. M. KENKRE, L. SKALA, M. WEISER and J. D. KATZ, Proc. Materials Research Society (San Francisco 1990) to be published.
10. V. M. KENKRE, L. SKALA, M. WEISER and J. D. KATZ, J. Materials Science, 26, 2483, (1991).
11. V. M. KENKRE, L. SKALA, M. WEISER and J. D. KATZ, J. Materials Research, submitted for publication
12. W.W. HO, in Microwave Processing of Materials, Eds. W.H. Sutton, M.H. Brooks and I.J. Chabinsky, Materials Research Society, Pittsburgh 1988, p.137
13. Structure and Properties of MgO and Al_2O_3 Ceramics, ed. W. D. Kingery, (The American Ceramic Society, Columbus 1984).

AN ANALYSIS OF THE INDIVIDUAL GRAIN STRUCTURE OF AN OXIDE HEATED USING MICROWAVE RADIATION AND HEATED CONVENTIONALLY

T. T. Meek*, X. Zhang* and M. Rader**
*Department of Materials Science and Engineering
**Department of Electrical Engineering
The University of Tennessee, Knoxville
Knoxville, TN 37996-2200

ABSTRACT

This work examines the structure of an oxide material heated conventionally and in a 2.45 GHz electromagnetic field. Also examined is the structure of the initial starting powder. Of particular interest is the surface structure and the interior bulk structure. TEM analysis indicates that the particle structure differs depending on the processing technique. Based on these findings, a preliminary heating model is introduced which is based on the presence of a liquid phase during sintering. The presence of this liquid phase may account for the apparent lower activation energy for sintering others have reported since their work presumes sintering is due to solid sate processes.

INTRODUCTION

The technology of microwave processing of ceramics, glasses and composite materials is of great interest because of the real advantages that have been demonstrated by many researchers. Many of the claimed benefits depend on an accurate measurement of temperature in the piece being processed. A number of methods are used to measure temperature in a microwave field. In the author's opinion all of these methods, in one way or another, have serious deficiencies. During the years that one of us (Meek) has been involved in this area he has seen numerous examples of where the apparent temperature measured did not reflect the microstructure observed. This paper will give examples of the above and discuss recent work that shows that the temperature in a dielectric material composed of more than one grain or composed of more than one dielectric constant region will differ. In practice the proposed model put forth by Meek [1] suggests that the local temperature depends most importantly on the local dielectric constant and other secondary properties such as heat capacity and density (which also affects local dielectric constant).

BACKGROUND

Over the course of several years one of the authors (Meek) has observed microwave sintered microstructures which appear to only be possible if higher than measured temperatures were reached during the process cycle. Some examples appear in earlier papers by Meek and his co-workers [2-5].

Figure 1 shows the fracture surface of a sample of zirconia sintered at 1800°C (as determined using an IR meter) in a 60 GHz electromagnetic field. The sample took ten minutes to heat from room temperature to 1800°C and was held at 1800°C for 1 second The microstructure appears to be one that would occur at a much higher temperature. Similarly, Figure 2 shows the microstructure of a fractured surface of a sample of Apollo 11 simulant material sintered at 1150°C (as

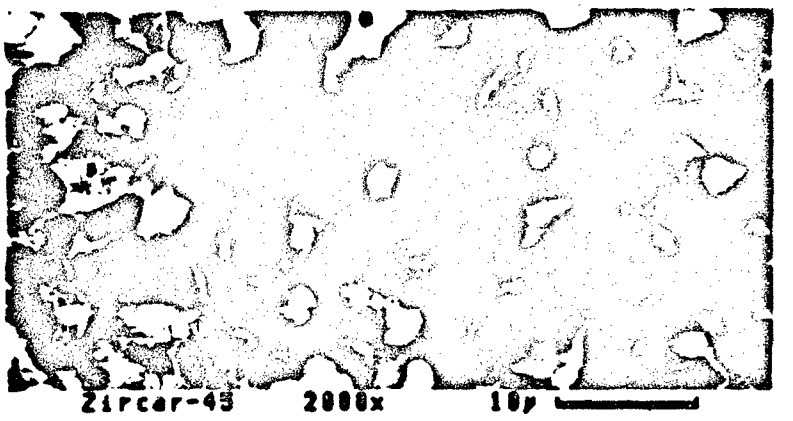


Figure 1. Fractured surface of zirconia sintered at 1800°C for 1 second.

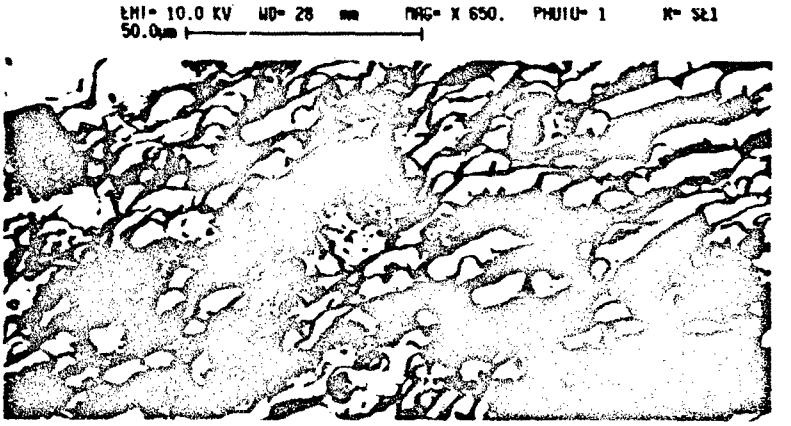


Figure 2. Fractured surface of Apollo 11 simulant material sintered at 1150°C for 45 minutes.

determined using an IR meter) for forty-five minutes in a 2.45 GHz electromagnetic field. Here it appears that the intergranular regions were melted during sintering. This material was examined to determine if the individual grain structure differed from the conventionally sintered material.

EXPERIMENTAL

The material used in this work is Apollo 11 lunar simulant powder with composition as shown in Table 1. The details of sample preparation are described elsewhere [6]. The initial powders were in the form of pellets of 0.9 cm diameter and approximately 2 cm length. These pellets were made by cold pressing in a piston-cylinder apparatus at 700 psi and then isostatically pressing in rubber sleeves to 50,000 psi.

Table 1. Simulated Compositions (weight percent).

	A11	A15	A16
SiO_2	42.03	46.52	45.26
TiO_2	7.48	1.40	0.58
Al_2O_3	13.59	17.10	26.22
FeO	15.74	12.05	5.82
MnO	0.20	0.17	0.07
MgO	7.86	10.42	6.39
CaO	11.98	11.17	14.76
Na_2O	0.44	0.43	0.45
K_2O	0.14	0.20	0.13
Cr_2O_3	0.30	0.27	0.12
P_2O_5	0.11	0.20	0.13
S	0.13	0.07	0.07

One set of samples was then sintered in a 2.45 GHz microwave furnace. Another set of samples was sintered conventionally at 1150°C for 4 hours. The sintered samples were then ground to small agglomerates using a pestle and mortar. A small amount of agglomerates was further put into a small test tube, methanol was added and the tube immersed in an ultra-sonic bath. After 30 minutes of vibration the liquid appeared cloudy. The cloudy suspension was then poured onto a small piece of mica and dried. A very thin carbon film (about 100 Å) was evaporated onto the mica and finally the thin film was floated off the mica substrate into clean distilled water. A small piece of thin film was then picked up with a copper grid. In this way we are able to break up the agglomerates into small individual grains or small grain clusters. The unsintered powder specimen was also made by this method.

An Hitachi H-800 scanning transmission electron microscope (STEM) was used to evaluate the sintered samples. The accelerating voltage was 200 KeV and electron probe size was about 40 Å. Under the STEM dark field image mode, we

used the convergent beam electron diffraction (CBED) method to study the sintered powders because by using this method one can analyze very small regions of the order of the probe size (in this case around 40 Å).

RESULTS AND DISCUSSION

Analysis of the Grain Structure

For conventionally sintered samples using TEM the CBED patterns obtained from both edge and center of the particle showed several diffraction discs which commonly occur in a crystal structure (see Fig. 3a edge and 3b center). Comparing these CBED patterns with those for unsintered particles, the unsintered particles also showed similar crystal diffraction features as found in the conventionally sintered Apollo 11 simulant material.

In the case of microwave sintered samples, the CBED patterns obtained from the edge of a particle showed a central diffused disc (Figure 4) which indicates an amorphous structure. The center of the particle had similar diffraction discs (Figure 5) indicating a crystalline structure. The estimated thickness of the amorphous surface layer is in the range of 500 Å.

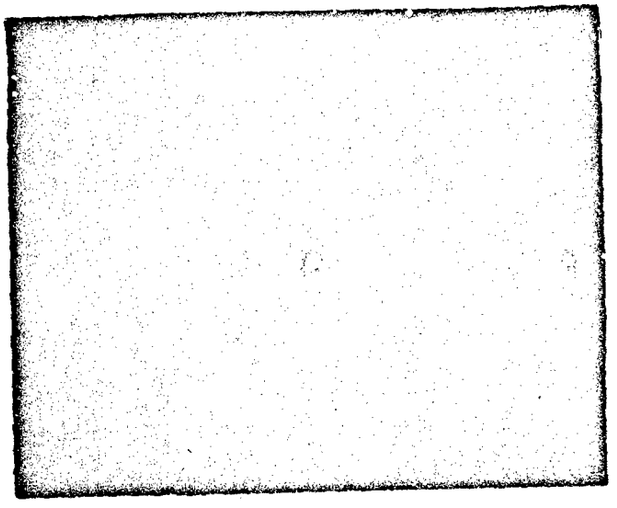


Figure 3a. CBED pattern obtained from edge of conventionally sintered Apollo 11 simulant particle indicating a crystalline structure.

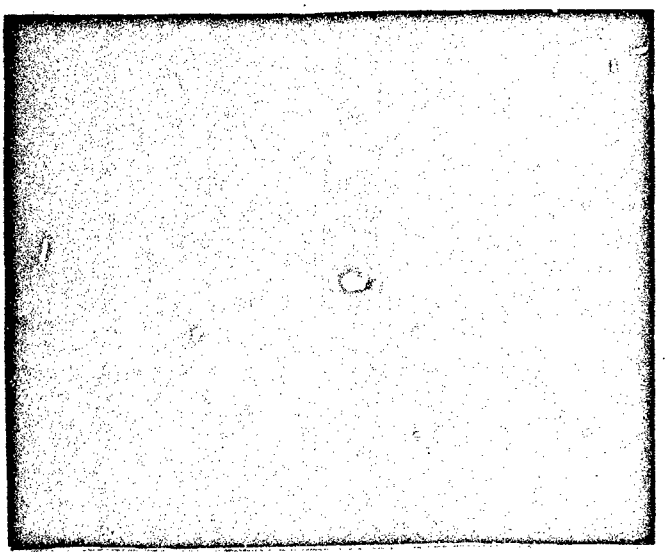


Figure 3b. CBED pattern obtained from center of conventionally sintered Apollo 11 simulant particle indicating a crystalline structure.

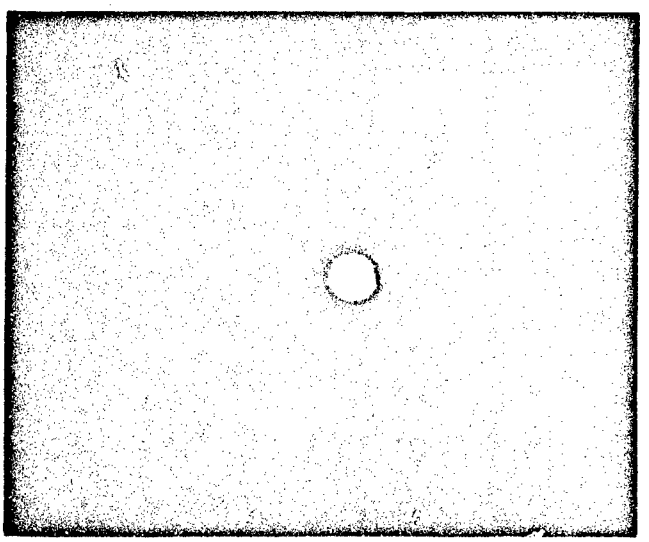


Figure 4. CBED pattern obtained from the edge of a microwave sintered Apollo 11 simulant particle indicating an amorphous structure.

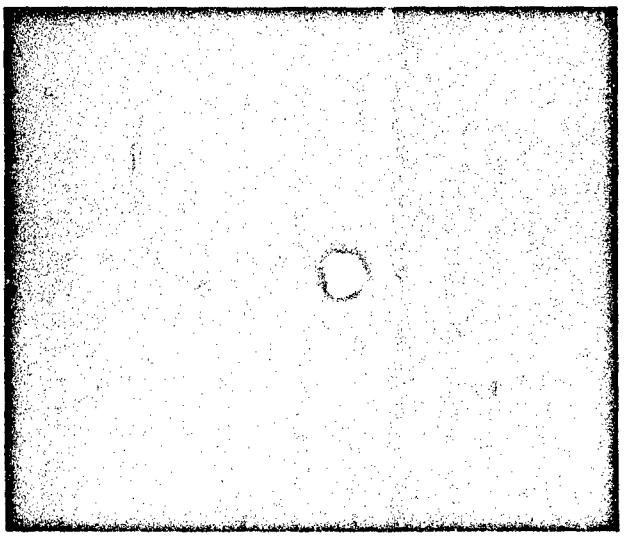


Figure 5. CBED pattern obtained from the center of a microwave sintered Apollo 11 simulant particle indicating a crystalline structure.

The existence of a surface amorphous layer suggests the possibility that the microwave sintered samples may have undergone transient liquid phase sintering during a portion of the sintering process. This phenomenon may help explain the so-called "apparent lower activation energy for sintering" as reported by others [3]. Generally, the activation energy of liquid phase sintering is lower than that of solid state sintering, although in the case of microwave sintering the occurrence of a liquid may be in a transient manner.

Based on the above results we introduce some thoughts on sintering in a microwave field where a transient liquid phase may occur.

The Interaction of Two Dielectric Particles with a Microwave Field

Figure 6 shows two spherical particles of a dielectric material present in a microwave field. Equation 1 (Kelvin eq.) relates the partial pressure over the curved particle surface to a flat surface where X is the neck radius and r_n is the capillary radius. P_o is the pressure over the flat surface for the condition $X >> r_n$, and $\frac{1}{r_n} >> \frac{1}{X}$

$$\ell n \frac{P}{P_o} \equiv \frac{\gamma M}{\rho R T} \frac{1}{r_n} \qquad (1)$$

Where γ = surface energy of particle
M = molecular weight of material
ρ = density of material
R = gas constant
T = temperature in Kelvin

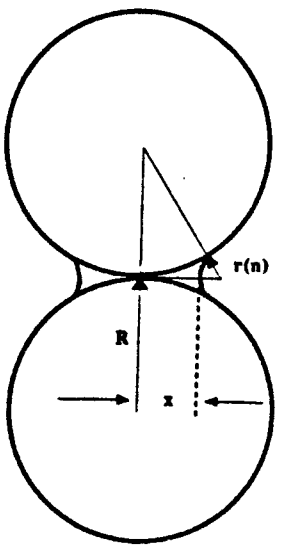


Figure 6. Two spherical dielectric particles in a microwave field.

From Eq. 1 we see that since r_n has a negative curvature then $\ell n \frac{P}{P_o}$ is and negative therefore $\frac{P}{P_o}$ will be less than 1.

Following this argument we see from Fig. 6 that the work of one particle against the other is [7]

$$\Delta P_c dV_n = \gamma dA_n \tag{2}$$

where ΔP_c is the variation in the capillary vapor pressure, dV_n is the change in the neck volume, γ is the surface free energy and dA_n is the incremental change in the neck area. The volume of the neck region is $\pi x^4/2R$ and the surface area of the neck region is $\pi^2 x^3/R$ where R is the particle size. Substituting dA_n and dV_n into Eq. (2) we have

$$\Delta P_c \approx \frac{3}{4}\pi \frac{\gamma}{X} = \frac{3}{8}\pi\gamma \frac{1}{\sqrt{Rr_n}} \tag{3}$$

Consider now the Clapeyron equation which is

$$\frac{dT}{dP} = T\frac{\Delta V}{\Delta H} \tag{4}$$

where T is temperature in Kelvin, P is pressure, ΔV is the volume change for the phase change from solid to liquid and ΔH is the heat of fusion.

Then we have

$$\ell n \frac{T_m'}{T_m} = \frac{M}{\Delta H_f}\left(\frac{1}{\rho_L} - \frac{1}{\rho_S}\right) \cdot \Delta P_c \tag{5}$$

where T_m' is the melting temperature of the material which makes up the capillary region and T_m is the melting temperature of the particle bulk region. For the case where $T_m' \neq T_m$ a temperature gradient will be set up across the particle from its center to its surface. M here is the particle mass, ρ_L and ρ_S are the densities of the liquid and solid materials in the capillary region and ΔP_c again is the change in the capillary vapor pressure. It should be emphasized here that ΔP_c is negative due to the concave curvature of the surface. Substituting ΔP_c of equation (3) into (5) we have

$$\ell n \frac{T_m'}{T_m} = \frac{M}{\Delta H_f}\left(\frac{1}{\rho_L} - \frac{1}{\rho_S}\right) \cdot \left(-\frac{3\pi}{8}\gamma\right)\frac{1}{\sqrt{R r_n}} < 0 \tag{6}$$

Therefore, $T_m' < T_m$.

Consider the affect on the capillary pressure of an applied microwave field. From Panofsky and Phillips [8] we have equation (7) which relates the change in capillary pressure between two dielectric plates submerged in a dielectric liquid.

$$P_A - P_D = \frac{g\varepsilon_o}{2}\left[E^2 \frac{dk}{dg}\right]_1^2 \tag{7}$$

We assume here that the liquid is incompressible and $P_A - P_D$ is the change in the capillary pressure where P_A is the maximum pressure in the capillary under the influence of the electrostatic field and P_D is the capillary pressure in a region outside of the electrostatic field. Here g represents the affect of gravity on the liquid, ε_o is the permittivity of free space, E is the electric field intensity, and dk/dg is the rate of change of the local dielectric constant with respect to g. Using the Clausius-Mossotti relation for an incompressible fluid results in

$$P_A - P_D = \frac{\varepsilon_o (k-1)}{2}\left[E_t^2 + k E_n^2\right]_B \tag{8}$$

where E_t and E_n are the tangential and normal components of the electric field intensity on the surface.

$P_A - P_D$ is the capillary pressure induced by the presence of an electrostatic field in the liquid. While the affect here is due to an electrostatic field, the presence of a superimposed microwave field may create a higher concentration of point imperfections at the particle surfaces which could enhance the electrostatic field. Let ΔP_E represent this contribution to the capillary pressure. Sintering in a microwave field then may cause an increase in the capillary pressure by the amount ΔP_E. This increase will affect the vapor pressure over the liquid in the neck region and from equation (5) the ratio of T_m'/T_m will also be affected. For example, an electrostatic field of 0.2V across a space charge region of 50Å will result in a reduction of the melting temperature of the material in the interparticle region of 222°C if that material is aluminum oxide.

The next section divides the sintering process into three stages and introduces steady state relationships which describe the heat input from the electromagnetic field during each stage.

Preliminary Model for Transient Liquid Phase Sintering

The steady state equations presented below are meant to be only the initial part of a general sintering model in which the time varying nature of the heat flow and temperature gradients formed during sintering are taken into account. Ultimately a set of general expressions such as equation (9) will be developed.

$$dQ = d\,(t, T, M_i, C_i, \ldots) \tag{9}$$

$$\frac{\Delta L}{L} = f\,(t, T, M_i, \Delta P_e, \ldots) \tag{9'}$$

where Q = heat input into particles
$\frac{\Delta L}{L}$ = shrinkage of particulate system
t = time
M_i = mass of ith material
C_i = heat capacity of ith material
ΔP_e = contribution to capillary pressure to electromagnetic field

Recognizing from the above that the electric field intensity and power density is a point function varying with local dielectric constant lets start with a model which expresses the heat input into dielectric particles in the presence of a 2.45 GHz electromagnetic field. We will examine how this distribution of heat input takes place over the course of the sintering process. For the first stage we have:

$$Q = CM\Delta T \tag{10}$$

where Q = the heat input to a particle
C = the particle heat capacity
M = particle mass
ΔT = particle temperature minus the particles initial temperature

Further we may now express the partitioning of the available energy (in the form of heat) to the particle-air matrix as follows. We consider the region between the grains to include a small surface layer of each grain

$$Q = M_S C_S (T_S - T_O) + M_A C_A (T_A - T_O) \tag{11}$$

where M_S = mass of solid particles
T_S = temperature of solid particles
T_O = initial temperature of solid particles and interparticle medium
C_S = heat capacity of solid particles
M_A = mass of interparticle medium
C_A = heat capacity of interparticle medium
T_A = temperature of interparticle medium

Changing equation (11) to a unit volume basis by dividing by the bulk volume V_B yields:

$$\frac{Q}{V_B} = \rho_S C_S \frac{V_S}{V_B}(T_S - T_o) + \rho_A C_A \frac{V_A}{V_B}(T_A - T_o) \tag{12}$$

where ρ_S = density of solid particles
V_S = volume of solid particles
V_B = bulk volume
ρ_A = density of interparticle medium.

We now introduce η, the total porosity as:

$$\eta = \frac{V_A}{V_B} = 1 - \frac{V_S}{V_B} \tag{13}$$

and equation (12) becomes

$$\frac{Q}{V_B} = \rho_S C_S (1-\eta)\,\Delta T_S + \rho_A C_A \eta\,\Delta T_A \tag{14}$$

Equation (14) describes the first stage of the sintering process from a non-dynamic point of view in that it shows how the heat is divided between the solid particles and the interparticle media without any liquid forming.

The next stage of sintering may be described as solid state with the introduction of a liquid phase. This liquid phase may or many not be transient depending on the system under study. We will assume for this analysis, however, that it is transient.

In this stage the interparticle media contributed by each particle surface results in a liquid formed by the melting of a thin surface layer of each solid particle and the heat input is expressed as:

$$Q = (M_S - M_L)\, C_S \Delta T_S + M_A C_A \Delta T_A + M_L\, \Delta H_f \qquad (15)$$

where M_L = the mass of the liquid
ΔH_f = heat of fusion of the solid

Again converting to a per unit volume basis we have

$$\frac{Q}{V_B} = \left(\rho_S \frac{V_S}{V_B} - \rho_L \frac{V_L}{V_B}\right) \Delta T_S C_S + \rho_A C_A \frac{V_A}{V_B} \Delta T_A + \frac{M_L}{V_B} \Delta H_f \qquad (16)$$

and expressing this in terms of porosity we have

$$\frac{Q}{V_B} = \rho_S C_S (1\text{-}n)\, \Delta T_S - \rho_L C_S \frac{V_n}{V_B} \Delta T_S + \rho_A C_A \cdot N \Delta T_A + \rho_L \frac{V_n}{V_B} \Delta H_f \qquad (17)$$

where V_n = the neck volume and in this case is equal to V_L for a transient liquid.

During stage two, a liquid emerges due to the preferential coupling of the electromagnetic field to the particle surface. Once the liquid forms, the capillary pressure is enhanced in the electromagnetic field by ΔP_E and the capillary vapor pressure is also enhanced further driving down the melting temperature of the material between the particles. This also increases the temperature gradients present in the powder compact.

The last stage then will be a combination of solid state sintering and liquid phase sintering. During this stage the heat input may be described in a similar manner as above.

Starting again with the heat input expression we have

$$Q = (M_S - M_L)\, C_S \Delta T_S + M_L C_L \Delta T_L + M_A C_A \Delta T_A + M_L \Delta H_f \qquad (18)$$

where ΔT_L = the liquid temperature minus the melting temperature
C_L = heat capacity of the liquid

Again considering heat per unit volume we have

$$\frac{Q}{V_B} = \left(\rho_S \frac{V_S}{V_B} - \rho_L \frac{V_L}{V_B}\right) \Delta T_S C_S + \rho_C C_L \frac{V_L}{V_B} \Delta T_L + \rho_A C_A \frac{V_A}{V_B} \Delta T_A + \rho_L \frac{V_L}{V_B} \Delta H_f \quad (19)$$

and introducing η the total porosity yields.

$$\frac{Q}{V_B} = \rho_S C_S (1-\eta) \Delta T_S - \rho_L C_S \frac{V_L}{V_B} \Delta T_S + \rho_L C_L \Delta T_L + \rho_A C_A N . \Delta T_A + \rho_L \frac{V_L}{V_B} \Delta H_f \quad (20)$$

Equation (20) relates the partitioning of the available energy in the electromagnetic field between the various phases (or regions) present in the dielectric media. Very likely large temperature gradients exist on a microscale within this dielectric media. These temperature gradients may act as a driving force for sintering according to Searcy [9]. He reported that relatively small temperature gradients influenced sintering of various ceramic materials. Braudeau, Morell and Monty [10] reported that a 6°C/mm temperature gradient near 1600°C measurably increased the rate at which 10 μm grooves in alumina surfaces decayed. Very likely the local temperature gradients present in dielectric materials heated using microwave radiation far exceed 6°C/mm.

CONCLUSIONS

Based on the experimental results of TEM analysis of microwave sintered and conventionally sintered oxide material, there exists a difference in grain structure between these two methods of heat treatment. The microwave heated grains have an amorphous surface layer that is approximately 10% of their diameter while the conventionally heated grains appear to be all crystalline. The presence of a amorphous surface layer on the surface of the microwave sintered grains suggests the presence during sintering of either a transient liquid or a permanent liquid phase. If one assumes the presence of a transient liquid phase during sintering, then the preliminary model developed here offers an initial description of the heat distribution during the sintering process in a microwave environment.

REFERENCES

1. T. T. Meek, "A Proposed Model for the Sintering of a Dielectric in a Microwave Field," Journal of Materials Science Letters, 6, pp. 638-640, 1987.

2. T. T. Meek and R. D. Blake, "Ceramic-Ceramic Seals by Microwave Heating," Journal of Materials Science Letters, 5, pp. 270-274 , 1986.

3. M. A. Janney and H. D. Kimrey, "Microwave Sintering of Alumina at 28 GHz," pp. 919-24 in Ceramic Transactions, Vol. I. *Ceramic Powder Science II*. Edited by G. Messing, E. Fuller, and H. Hausner. American Ceramic Society, Westerville, OH, 1988.

4. T. T. Meek, et al. "Microwave Processing of Ceramics," The International Microwave Powder Institute, 21, No. 3, pp. 193-194, 1986.

5. R. D. Blake and T. T. Meek, "Microwave Processed Composite Materials," Journal of Materials Science Letters, 5, pp. 1097-1098, 1986.

6. T. T. Meek, C. F. Holcombe, N. Dykes, "Microwave Sintering of Some Oxide Materials Using Sintering Aides," Journal of Materials Science Letters, 6, pp. 1060-1062, 1987.

7. W. D. Kingery, H. K. Bowen and D. R. Uhlmann, "Surfaces, Interfaces, and Grain Boundaries," p. 185 in Introduction to Ceramics, 2nd Edition, John Wiley and Sons, 1976.

8. W.K.H. Panofsky and M. Phillips, "Energy Relations and Forces in the Electrostatic Field," pp. 95-117 in Classical Electricity and Magnetism, 2nd Edition, Addison-Wesley Publishing Co., Inc., 1962.

9. A. W. Searcy, ""Theory for Sintering in Temperature Gradients: Role of Long-Range Mass Transport," Journal of the American Ceramic Society, 70, No. 3, pp. C-61-C-62, 1987.

10. P. Braudeau, A. Morell, and C. Monty, "Influence of a Temperature Gradient on the Transport of Matter on Alumina," (in Fr.), Ann. Chim. Fr., 10, pp. 261-63, 1985.

MICROWAVE ENHANCED DIFFUSION?

J. D. Katz and R. D. Blake
Los Alamos National Laboratory
Los Alamos, NM 87544

V. M. Kenkre
Department of Physics
University of New Mexico
Albuquerque, NM 87544

The observation of more rapid reaction and/or sintering during microwave processing of ceramics has lead to speculation that microwave processing results in "enhanced diffusion".

The loss mechanisms by which microwaves interact with a crystal lattice have been reviewed. These mechanisms were evaluated with regard to the atomic theory of diffusion. The potential for these loss mechanisms to influence atomic diffusion, and thus produce enhancement will be discussed.

Existing evidence, both direct and indirect, regarding microwave enhanced diffusion has been reviewed and will be discussed along with recent experimental data.

INTRODUCTION

The use of microwave radiation for materials synthesis and processing is a rapidly expanding field. There have been numerous reports of enhanced diffusion during microwave processing. These reports fall into two categories. The first consists of indirect evidence of diffusion such as observations of enhanced sintering, grain growth or reaction zones[1-3]. These types of observations do not provide clear evidence of enhanced diffusion since interpretation is difficult for complex processes such as sintering, grain growth and chemical reaction.

The second body of evidence is much smaller and comprises direct measurements of diffusivities and activation energies for diffusion during microwave heating[4-6]. Fathi and Clark[4] report an increase in width of the reaction zone of approximately 3 times for the ion exchange of potassium into a sodium-aluminum-silicate glass. This data indicates an increase in the diffusivity of approximately one order of magnitude. Patterson and McCallun[5] have implanted titanium in sapphire and studied the diffusion after conventional and 2.45 GHz microwave annealing at 1000°C. Preliminary results from this study indicate that there is no difference in the concentration profiles between the conventionally and microwave annealed samples. Janney and Kimrey[6] report activation energies 40% lower for the tracer diffusion of

oxygen in alumina annealed using 28 GHz microwaves. They obtained activation energies of 710 and 410 kJ/mol for the conventional and microwave samples respectively which is equivalent to an increase of approximately two orders of magnitude in the diffusivity for the temperatures studied.

To understand how a microwave field might influence diffusion it is helpful to look at the factors which control diffusion. Substitutional diffusion can be represented by the following atomistic formula:

$$D = fA_0^2 N\omega \qquad (1)$$

where D is the diffusivity, f is the correlation factor, A_0 is a geometric constant, N is the concentration of vacancies (i.e., the probability that an ion has a vacant next nearest neighbor,) and ω is the jump frequency. The correlation factor corrects for the fact that only vacancy diffusion is purely random. The jumps of a diffusing ion are dependent on its previous jumps, and hence, "correlated". It follows from the above formula that a microwave field can only influence the rate of diffusion in two ways. The first and most obvious is by altering the jump frequency, ω, and the second is by changing the correlation factor, f.

Electromagnetic energy can be dissipated in a crystalline dielectric through several loss mechanisms. These mechanisms include electronic polarization, ionic vibration, ion jump relaxation, conduction and interfacial polarization.

Electronic polarization and ionic vibration are resonance phenomenon and if operable during microwave heating have the potential to directly change the ion jump frequency. Electronic polarization would alter the energy barrier to be overcome by the jumping ion and ionic vibration would alter the frequency of attempted jumps. Microwave frequencies are in the range of 10^9 to 10^{10} Hz and the ion jump frequency is of the order of the Debye frequency which is about 10^{13} Hz. Application of resonance theory shows that resonance, and hence, an ionic vibration loss mechanism, is not possible for any reasonable damping force since these two frequencies differ by three to four orders of magnitude. This has been explained in detail by Kenkre[7]. (It will be shown later that in the unlikely event that ionic resonance did occur it would actually result in a lower diffusivity.) Since electronic polarization occurs at even higher frequencies than ionic vibration, this loss mechanism is not thought to be operable at microwave frequencies either. It can thus be concluded that electronic polarization and ionic vibration are not important loss mechanisms for microwave heating, and therefore, microwave heating does not influence diffusion by altering the jump frequency.

The second way by which the diffusivity might be altered is by changing the correlation factor. This is a much more plausible way of causing an alteration in the diffusivity when considering the remaining loss mechanisms. Ion jump relaxation in a crystalline ceramic occurs when an aliovalent ion and vacancy form an associated pair. (An aliovalent ion is an impurity cation or anion with a valence different from that of its host sublattice.) An aliovalent ion-vacancy pair has a dipole moment associated with it which responds to the applied electric field. The vacancy is thought to jump around the aliovalent ion to align its dipole moment with the electric field[8]. Interfacial polarization occurs at a structural inhomogeneity such as a grain

boundary, dislocation, or vacancy cluster. In an ionic lattice there will be a localized disruption in electroneutrality at such a structural inhomogeneity with a net dipole moment which will align itself with the applied field.

An example of ion jump relaxation might occur due to the solution of impurity $CaCl_2$ in a KCl lattice as follows:

$$CaCl_2 \xrightarrow{KCl} Ca_K^{\cdot} + V_K^{'} + 2Cl_{Cl} \qquad (2)$$

Where $Ca_K^{\cdot}$ is a calcium ion on a potassium ion site with a +1 net charge and $V_K^{'}$ is a vacancy on a potassium ion site with a -1 net charge. For reasons of electroneutrality the calcium ions and the vacancies form pairs which have a net dipole moment. This situation is illustrated in Fig. 1. For the case of no applied electric field the dipoles are randomly oriented. Figure 2 illustrates the situation after the electric field has been applied. The dipole pairs are aligned in the direction of the electric field.

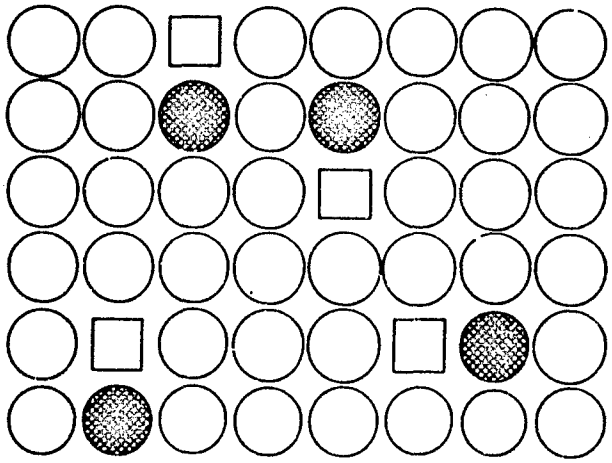


Figure 1. Schematic representation of vacancy-impurity pairs with random orientations.

Ion jump relaxation can also result from the formation of intrinsic Schottky or Frenkel pairs. An example for the case of Schottky pairs in alumina is as follows:

$$null = V_{Al}^{'''} + 1.5V_O^{\cdot\cdot} \qquad (3)$$

Where V_{Al}''' is an aluminum ion vacancy with -3 net charge and $V_O^{\cdot\cdot}$ is an oxygen ion vacancy with a +2 net charge. Each aluminum ion would associate with an average one and a half oxygen ion vacancies to form a dipole. The loss tangent of Coors AD-995 alumina[9] is reproduced in Fig. 3. The loss is seen to increase exponentially with temperature. This behavior can be explained by extrinsic defects in the linear region of the curve and the formation of intrinsic Schottky type defects in the exponential region[10].

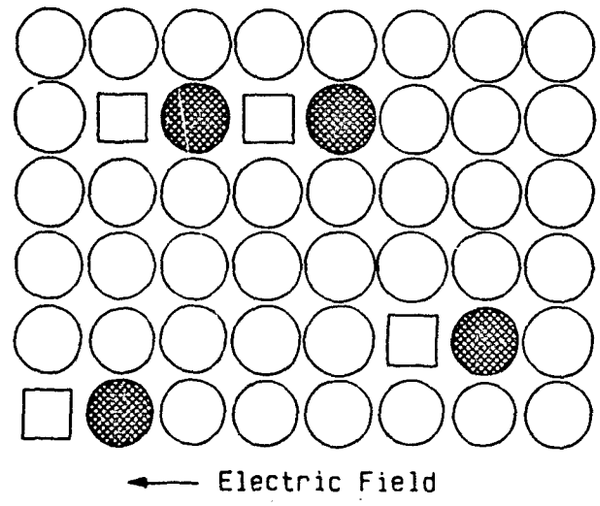


Figure 2. Schematic representation of vacancy-impurity pairs aligned with the applied electric field.

Conduction is mostly of interest at low frequencies. This type of loss mechanism occurs when vacancies are not associated with other defects, and hence are not localized. Unassociated vacancies are much more mobile than associated pairs and migrate to align themselves with the electric field.

Since both intrinsic vacancy formation and lattice jumps are thermally activated we may express them by Arrhenius type equations as follows:

$$N = \exp(-G^f/kT) \tag{4}$$

$$\omega = \nu\exp(-G^m/kT) \tag{5}$$

Where G^f and G^m are the Gibbs Free Energies for vacancy formation and motion

respectively and ν is the Debye frequency*. Equations 1, 4 and 5 may be combined to produce the following equation:

$$D = fA_0^2 \nu \exp[-(G^f + G^m)/kT] \quad (6)$$

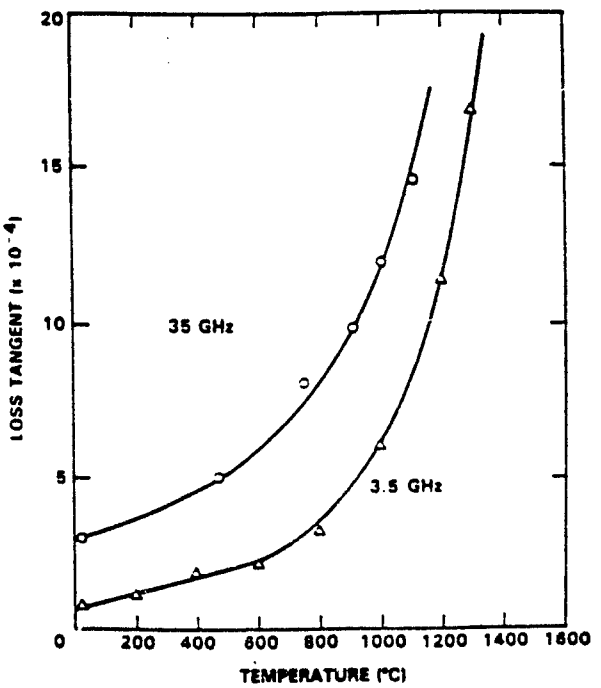


Figure 3. Loss tangent of Coors AD-995 alumina as a function of temperature at 35 and 3.5 GHz. From reference 6.

*The effect of an ion resonance loss mechanism would be to replace the Debye frequency with a lower primary lattice vibration frequency. The lower frequency would result in a decrease in the jump frequency (as calculated from equation 5) and a commensurate decrease in the diffusivity. Any forced oscillations induced by a microwave field can be described by an equation of the type used for a damped harmonic oscillator which is as follows:

$$dx^2/dt^2 + 2\beta dx/dt + \nu x = 0$$

where 2B is the damping factor and ν is the Debye frequency. The solution to this equation is:

$$x = x_0 \exp(-\beta t)\cos\nu'' t$$

where the new primary vibration frequency, $\nu'' = (\nu^2 - \nu'^2)^{1/2}$ and ν' is the frequency of the forced oscillation. If $\nu' < \nu$, then $\nu > \nu''$.

The Gibbs Free Energies may be expressed in terms of the enthalpies (H^f, H^m) and the entropies (S^f,S^m) for formation and motion as follows:

$$G^f = H^f - TS^f \tag{7}$$

$$G^m = H^m - TS^m \tag{8}$$

Substituting equations 7 and 8 into equation 6, we obtain the following equation for the case of intrinsic vacancy concentration controlling:

$$D = fA_0^2 \nu \exp(S^f/k + S^m/k)\exp-[(H^f + H^m)/kT] \tag{9}$$

For the case where extrinsic vacancy concentration controls, the concentration of vacancies, N, is as follows:

$$N = [C_i] \tag{10}$$

Where $[C_i]$ is the concentration of impurity ions. Equations 1, 5 and 10 may be combined to produce the following equation:

$$D = fA_0^2 [C_i] \nu \exp(S^m/k)\exp-(H^m/kT) \tag{11,}$$

Since the diffusivity has been shown on numerous occasions to be thermally activated we may express the diffusivity by an Arrhenius type equations as follows:

$$D = D_0 \exp(-Q/kT) \tag{12}$$

Where D_0 is the pre-exponential factor and Q is the activation energy for diffusion. By comparing equations 9 and 12, we see that the pre-exponential factor can be expressed as follows for the intrinsic case:

$$D_0 = fA_0^2 \nu \exp(S^f/k + S^m/k) \tag{13}$$

and for the extrinsic case comparing equations 11 and 12,

$$D_0 = fA_0^2[C_i]\nu\exp(S^m/k) \quad (14)$$

Similarly the activation energy for diffusion is the sum of the enthalpies for vacancy formation and motion.

$$Q = H^f + H^m \quad (15)$$

The model of the ion jump relaxation loss mechanism involves a vacancy jumping around the aliovalent ion to align its dipole moment with the electric field. Clearly such a loss mechanism would involve a change in the correlation factor. Similarly, the interfacial polarization loss mechanism would alter the correlation factor. Conversely, these two loss mechanisms do not involve any enthalpy changes, therefore, any alteration to the diffusivity would result from changes in "D_0" the pre-exponential factor, rather than to the activation energy for diffusion.

EXPERIMENTAL

Some preliminary experiments have been performed using the alumina(Al_2O_3)-chromia(Cr_2O_3) system. This system was chosen for two reasons. First, the alumina-chromia system is ideal, and therefore, as will be shown later, the comparison of chemical and tracer diffusivities is much easier. Second, this system is something of a model system in the field of ceramics and much information is available on it including diffusion data from studies by Oishi and Kingery,[11] and by Stubican and Osenbach[12] among others.

In the alumina (or Corundum) crystal structure, the oxygen ions reside in a close packed hexagonal lattice and the smaller aluminum ions occupy 2/3 of the octahedral interstices. Since the alumina-chromia system is "ideal", it exhibits complete solid-state solubility with chromium ions substituting for aluminum ions on octahedral interstitial sites.

The alumina used in this work was Sumitomo grade AKP-50*. The diffusion couples were prepared by conventionally sintering green alumina pellets in air to full density to produce 1 cm X 1 cm right circular cylinders. Chromia was then plasma sprayed onto the top surface of the cylinders. The as-sprayed layer was about 30 microns in thickness and relatively uniform.

The microwave annealing was performed under flowing argon in a facility consisting of a 2.45 GHz, 6 kilowatt microwave power supply and a cubic, 2 ft on side resonant cavity. Temperature was measured with an Accufiber Model 100 Multi-Channel Optical Fiber Thermometer§. The diffusion couples were enclosed in a low density insulation casket made from yttria stabilized zirconia board supplied by Zicarζ. The insulation casket comprises a black body so temperature measurements could be made using an uncoated optical fiber.

---

*Sumitomo Chemical Company, Ltd., Osaka, Japan.
§Accufiber, Inc., Beverton, OR.
ζZircar Products, Inc., Florida, NY.

RESULTS AND DISCUSSION

The concentration versus distance profile for an alun :-chromia diffusion couple, which has been microwave annealed at 1750°C for twenty mini s, was obtained by microprobe analysis and is presented in Fig. 4.

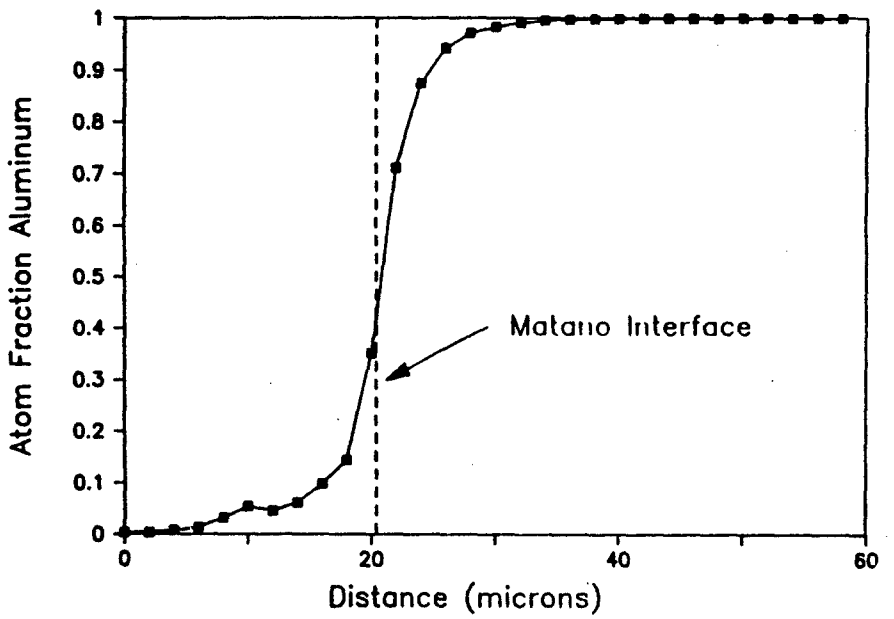


Figure 4. Cation concentration profile for a chromia-alumina diffusion couple microwave heated to 1750°C and held for twenty minutes.

Boundary conditions were satisfied for a Boltzmann-Matano[13,14] diffusion analysis. This type of analysis yields the interdiffusivity which was defined by Darken[15] as follows:

$$\tilde{D} = D_{Cr}N_{Al} + D_{Al}N_{Cr} \qquad (16)$$

where D_{Al} and D_{Cr} are the chemical diffusivities and N_{Al} and N_{Cr} are the mole fractions of aluminum and chromium respectively. The interdiffusivities for $N_{Al}=N_{Cr}=0.50$ obtained in this study are presented in Figure 5.

The data available in the literature for aluminum and chromium ion diffusion in alumina are for tracer diffusivities. The interdiffusivity is related to the more familiar tracer diffusivity as follows. First we define the relationship between the chemical and tracer diffusivity after Darken[15]:

$$D_{Cr} = D^{*}_{Cr}(1 + d\ln\gamma_{Cr}/d\ln N_{Cr}) \quad (17)$$

where D^{*}_{Cr} is the tracer diffusivity and γ_{Cr} is the activity coefficient of chromium in the alumina-chromia system. Since the alumina-chromia system is ideal, $\gamma_{Al} = \gamma_{Cr} = 1$, and therefore, $\ln \gamma_{Al} = \ln \gamma_{Cr} = 0$, and equation 16 simplifies to:

$$\tilde{D} = D^{*}_{Cr}N_{Al} + D^{*}_{Al}N_{Cr} \quad (18)$$

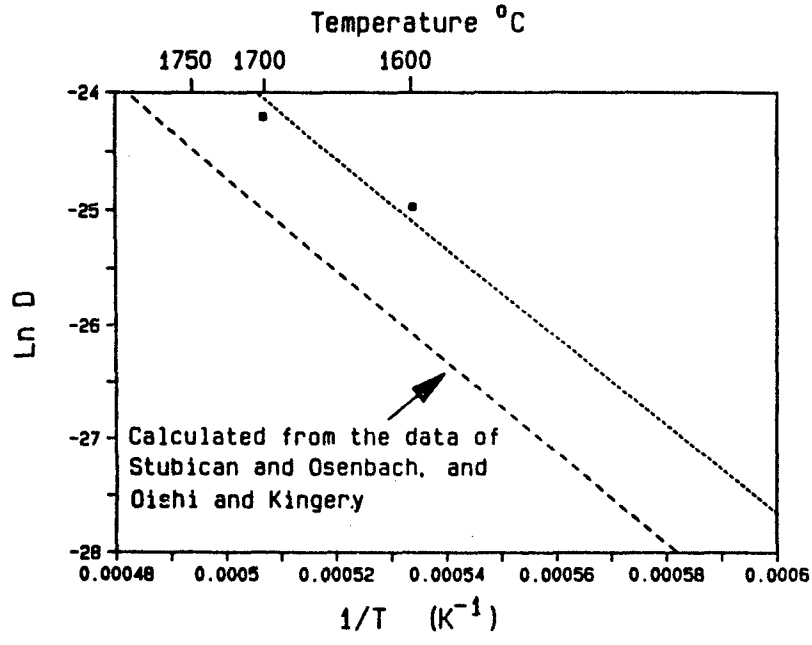


Figure 5. Calculated and measured interdiffusivities for the alumina-chromia system.

We may now calculate the interdiffusivity for the alumina-chromia system at $N_{Al} = N_{Cr} = 0.50$ using data from Oishi and Kingery, and from Stubican and Osenbach. This data is indicated by the dashed line in Fig. 5. Two interdiffusivities obtained to date in this study, appear to lie on a line parallel to the interdiffusivity calculated from the literature. The interdiffusivities measured in this study are approximately three times that of the literature values. Since the two lines are parallel the activation energy for diffusion is the same, the pre-exponential is greater for the microwave case by a factor of three.

In the unlikely event that vacancy defects are intrinsically controlled (i.e., Schottky defects dominate) the observed enhancement is due to a correlation effect. For extrinsic defects dominating, the observed enhancement simply means the concentration of extrinsic defects is three times higher.

While this preliminary data seems to indicate that a microwave field does not lead to an enhancement in diffusion it is by no means conclusive. One major criticism involves the use of a susceptor to heat the high purity alumina, which has a very low dielectric loss at room temperature, to a temperature where it will couple to the microwave field. Because of the use of a susceptor it is not certain how much of the heating was due to the microwave field. For future experiments a hybrid microwave-electric resistance furnace will be constructed. Using this furnace a diffusion couple could be heated conventionally by electric resistance elements to a temperature at which it couples to microwaves and then the resistance elements would be turned off.

CONCLUSIONS

Relaxation type loss mechanisms are thought to be operable during microwave heating of crystalline ceramics. These loss mechanisms will influence the correlation factor for diffusion. To estimate the magnitude of the change to the diffusivity, the correlation factor must be recalculated. It should be noted, however, that the correlation factor usually has a small effect on the diffusivity, less than an order of magnitude. Any alteration to the correlation factor would show up as a change in the pre-exponential factor of the diffusivity.

In order for resonance type loss mechanisms to occur, unrealistically high damping forces would have to be present because of the large difference between the natural lattice vibration frequency and the microwave heating frequencies. For this reason resonance type loss mechanisms are not thought to occur during microwave heating.

The experimental results reported herein show a small, factor of 3 increase in the interdiffusivity of microwave annealed samples. The observed enhancement was minimal and may have been caused by an increase in the correlation factor as a result of a relaxation type loss mechanism. A more plausible explanation for the observed increase in interdiffusivity, however, is a higher concentration of extrinsic defects in the diffusion couples used in this study then in those used by Oishi and Kingery and by Stubican and Osenbach.

ACKNOWLEDGEMENTS

The authors would like to thank Carolynn P. Scherer for reviewing the manuscript and Bill Hutchinson for performing the microprobe measurements. The authors would also like to thank the Department of Energy for supporting this work.

REFERENCES

1. T.T. Meek, R.D. Blake, J.D. Katz, J.R. Bradberry and M.H.Brooks, "Cation Diffusion in Glass Heated Using 2.45 GHz Radiation", J. of Mater. Sci. Lett., Vol. 7, No. 9, pp. 928-931, (1988).

2. B. Swain, "Microwave Sintering of Ceramics", Advanced Materials & Processes, Vol. 2, No. 9, pp. 76-82, (1988).

3. I. Ahmad and D.E. Clark, "Effect of Microwave Heating on Solid State Reactions of Ceramics", This Volume.

4. Z. Fathi and D.E. Clark, "Surface Modification of Glasses", This Volume.

5. M.C.L. Patterson and J.C. McCallun, Private Communication.

6. M.A. Janney and H.D. Kimrey, "Diffusion- Controlled Processes In Microwave-Fired Oxide Ceramics", Materials Research Society Proceedings, Vol. 189, Spring 1990 Meeting.

7. V.M. Kenkre, "Theory of Microwave Interactions With Ceramic Materials", This Volume Paper.

8. O. Stasiw and J. Teltow, "Uber Felordnungserscheinungen in Silberhalogeniden mit Zusatzen", Ann. der Phys., Vol. 1, p. 261-272, (1947).

9. W.W. Ho, "Millimeter Wave Dielectric Property Measurement of Gyrotron Window Materials", Rockwell Report SC5357.2TR, April 1984.

10. V.M.Kenkre, L.Skala, M.W.Weiser and J.D.Katz, "Theory of Microwave Effects on Atomic Diffusion in Sintering: the Phenomenon of Thermal Runaway", J. Materials Science, Vol. 26, pp. 2483-2489, 1991.

11. Y. Oishi and W.D. Kingery, "Oxygen Diffusion in Periclase Crystals", J. Chem. Phys., Vol. 33, pp. 905-906, (1960).

12. V. S. Stubican and J. W. Osenbach, "Grain-Boundary and Lattice Diffusion in ^{51}Cr in Alumina and Spinel", Advances in Ceramics, Vol. 10, pp. 406-417, American Ceramic Society, 1984.

13. L. Boltzmann, Ann. Physik, Vol. 53, p. 960, (1894).

14. C. Matano, Japan. Phys., Vol. 8, p. 109, (1933).

15. L. Darken, "Diffusion, Mobility and Their Interrelation through Free Energy in Binary Metallic Systems", Trans. AIME, Vol. 174, pp. 184-194, (1948).

ACTIVATION ENERGIES FOR THE DIELECTRIC LOSS FACTOR/ AC CONDUCTIVITY OF SOME POLYCRYSTALLINE CERAMICS

Ralph W. Bruce, Electrical Engineering Department, MS 14B, United States Naval Academy, Annapolis, MD 21402-5000

ABSTRACT

By analyzing the temperature dependence of the dielectric loss factor/AC conductivity, the activation energy can be determined. Analyses will be presented based upon material type, % of the major phase, density and frequency. Trends in the material's behavior, when placed in a microwave field, can be determined from these analyses. Additionally, from the determination of the temperature at which a material's AC conductivity begins to change rapidly, the onset of a material's change in phase may be indicated, e.g., the onset of sintering. In particular, it has been determined that the dielectric loss constant of Al_2O_3 has two activation energies, one in the range of .16 to 1.15 Kcal/mole for low temperatures (< 700°C) and one in the range of 9.22 to 69.2 Kcal/mole for high temperatures (> 700°C) at a frequency of 3.5 GHz and samples from 85% to 100% Al_2O_3.

INTRODUCTION

Various authors have referred to the activation energies of the electrical conductivity of ceramic systems that can be sintered in a microwave furnace [1-3]. In reviewing these comments, the question arises whether or not the use of an activation energy (E_A) model could adequately represent the electrical dynamics of a ceramic during sintering. In knowing something about the E_A's of a material, some relation could be developed that would predict how the material would behave in the presence of a strong microwave field. The purpose of this paper is to therefore look at the activation energies of some polycrystalline alumina and describe the resulting trends. In this way,

it is hoped that a better theoretical understanding could be achieved about the interaction of ceramics with strong microwave fields while at high temperatures.

To accomplish this objective, the equation relating the interaction of microwaves with materials is stated and secondly, data from known sources on the dielectric behavior of ceramics as a function of temperature are presented. From these data are derived the activation energies of the materials which are then interpreted.

MICROWAVE-MATERIAL INTERACTIONS

The basic reason for the current interest in microwave-material interactions is the energy absorption that occurs when a material is placed into a strong electromagnetic field at microwave frequencies (300 Mhz to 30 Ghz). It is the resulting temperature rise that is being exploited to bring the ceramic material to the temperature at which it will sinter. This temperature rise (ΔT) can be expressed as a function of the power absorbed (P_{abs}), the time of exposure to the microwave energy (Δt), the density of material (ρ) and the specific heat (C_p) by the following equation [4]:

$$\Delta T = \frac{P_{abs}\,\Delta t}{\rho C_p} \qquad (1)$$

The power absorbed, P_{abs}, is related to the dielectric properties of the material (the relative dielectric constant, ϵ_r', and the effective dielectric loss factor , ϵ_{eff}''), the frequency of the incident microwave energy (f in Hz), the permittivity of free space (ϵ_0 = 8.854 x 10^{-12} F/m), the internal electric field strength (E in Volts/m), and the volume of the material (V in m^3) by [5]:

$$P_{abs} = 2\pi f \epsilon_0 \epsilon''_{eff} |E|^2 V \qquad (2)$$

This relationship holds under the assumptions of an incident uniform plane wave and for a constant E field within the volume of the material. It is the effective dielectric loss factor (ϵ''_{eff}) that is of most interest in the present discussion. This parameter is comprised of several factors having to do with various electrical relaxation mechanisms in solids. It is expressed as [5]:

$$\epsilon''_{eff} = \epsilon''_{MW} + \epsilon''_{d} + \epsilon''_{i} + \epsilon''_{e} + \frac{\sigma}{2\pi f \epsilon_0} \qquad (3)$$

Where: ϵ_{MW}": Maxwell-Wagner interfacial polarization loss This phenomena is normally noted in heterogeneous materials

ϵ_d": Dipolar losses which are usually encountered in the microwave region of the frequency band

ϵ_i": Ionic losses which are usually encountered in InfraRed portion of the frequency band

ϵ_e": Electronic polarization losses which are encountered in the optical region of the frequency band

σ: The DC electrical conductivity of the material which is temperature and material dependent.

Finally, the AC (alternating current as compared to the DC-direct current) conductivity is that portion of Equation 2 given as:

$$\sigma_{AC} = 2\pi f e_0 e''_{eff} \tag{4}$$

It is this conductivity, comprised of several factors, that is the focus of the present study.

ACTIVATION ENERGY

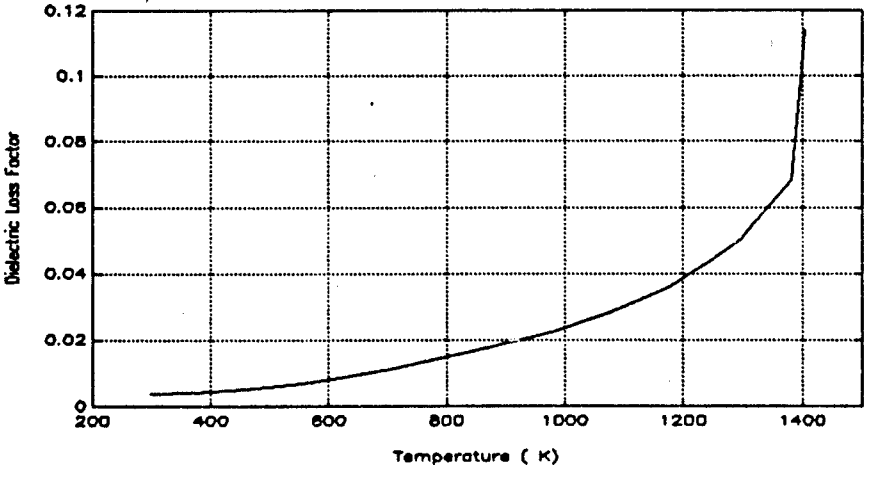


Figure 1. Plot of ϵ_{eff}" versus Temperature at 3.55 GHz [7]

Table 1. Values for ϵ_r', ϵ_{eff}'', σ_{AC}, $\ln(\sigma_{AC})$, and 1/T versus Temperature (T) for General Electric Alumina A-923 (97%) at 3.55 GHz [7]

Temp. (°K)	ϵ_r'	ϵ_{eff}'' (x10^3)	σ_{AC} (mS/m)	$\ln(\sigma_{AC})$	1/T (1/°K x10^3)
298	9.31	3.63	.717	-7.240	3.355
372	9.41	3.95	.781	-7.156	2.688
457	9.58	5.08	1.003	-6.905	2.188
554	9.72	6.80	1.344	-6.612	1.805
629	9.84	8.86	1.749	-6.349	1.590
703	9.96	11.16	2.203	-6.118	1.422
835	10.17	16.27	3.214	-5.740	1.198
978	10.42	22.40	4.424	-5.421	1.022
1073	10.63	28.17	5.563	-5.192	.932
1176	10.86	35.84	7.078	-4.951	.850
1246	10.98	43.92	8.674	-4.747	.803
1298	11.17	50.27	9.927	-4.612	.770
1323	11.22	56.10	11.079	-4.503	.756
1382	11.38	68.28	13.485	-4.306	.724
1405	11.41	114.10	22.534	-3.793	.712

By plotting the natural logarithm of σ_{AC} versus the inverse temperature (1/T), the activation energies of the materials can be derived and compared as a function of % of the major phase. The AC conductivity is derived from the data for the dielectric loss factor (ϵ_{eff}'') using Equation 4. Data for dielectric loss factor, the AC conductivity, its' natural logarithm, the temperature (T) and the inverse temperature (1/T) for Alumina[1] is given in Table 1. The

---

General Electric A-923 (97%) [7]

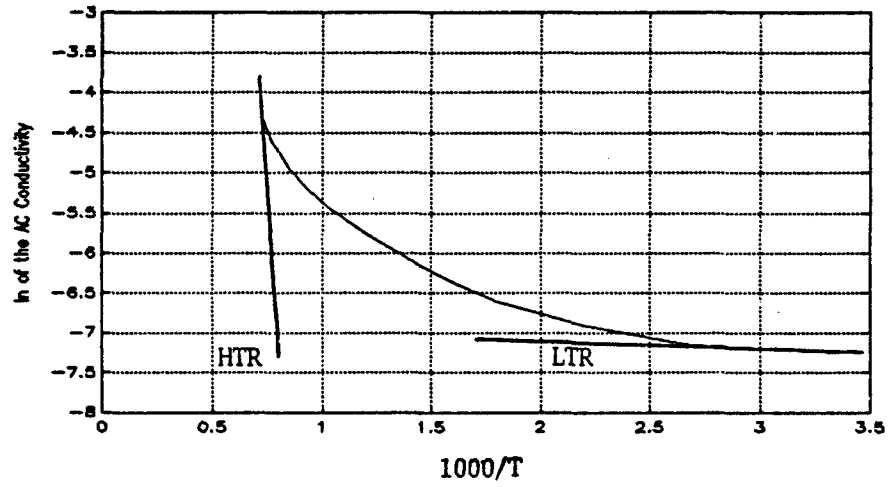


Figure 2: Plot of $\ln(\sigma_{AC})$ versus $10^3/T$
for General Electric Alumina A-923 (97%)

plot of ϵ_{eff}" versus temperature is given in Figure 1. This graph shows the typical exponential increase that is common to oxide ceramics. Above 973 K, the very sharp increase in $\epsilon"_{eff}$ depicts what has been termed "thermal runaway". The plot of $\ln(\sigma_{AC})$ vs 1/T is given in Figure 2. From this graph, it can be seen that there are two linear segments, designated the High-Temperature Region (HTR) and the Low-Temperature Region (LTR), indicating two activation processes. Using the following equation and standard techniques for determining activation energies, the E_A for the LTR is .57 Kcal/mole and 31.99 Kcal/mole for the HTR [6].

$$E_A = -k(SLOPE) \qquad (5)$$

k is Boltzman's constant and SLOPE is the slope of the line. The lowest three temperature values were used to calculate E_A for the LTR and the three highest values for the HTR. This analysis was extended to look at the E_A's of a number of other aluminas from a number of manufacturers. These data are given in Table 2.

DISCUSSION

In reviewing the data form Table 2, it quite obvious that the E_A's do not follow a set pattern though some general comments can be made. As all these

Table 2. Data for Al_2O_3 from various manufactures

Manufacturer and Type	% Al_2O_3	ρ (gm/cm^3)	Frequency (GHz)	E_A (LTR) (Kcal/mol)	E_A(HTR) (Kcal/mol)	Temp.* (°C)	tan δ*	Reference
Alberox								
950	95.0	3.663	3.75	.65	19.37	892	.0100	[7,p. 5]
962	96.2	3.731	3.77	.54	14.30	828	.0105	[7,p. 5]
American Lava Co.								
AlsiMag614	96.0	3.725	3.34	.96	9.92	1035	.0100	[7,p. 6]
AlSiMag719	94.0	3.586	3.54	-.20**	26.29	967	.0114	[7,p. 6]
Coors								
AD99	99.6(est.)	3.795	3.92	.24	59.73	1300	.0100	[7,p. 19]
AD995	99.5(est.)	3.840	3.57	.99	22.60***	1400	.0028	[7,p. 20]
US Ceramic Tile Co.								
B-890-2	90.0-95.0	3.583	3.59	.26	19.37	960	.0100	[7,p. 21]
P-3142-1	95.0-97.0	3.706	3.52	.22	29.06	965	.0100	[7,p. 21]
G. E.								
A-923	97.0	3.740	3.52	.57	43.82	1132	.0100	[7,p. 26]
A-1004	94.0	3.649	3.70	.14	28.37	700	.0093	[7,p. 29]

Table 2 (continued)

Honeywell								
A-127	85.0	3.326	3.91	.38	17.30	800	.0097	[7,p. 31]
A-203	95.0	3.589	3.67	.92	9.69	930	.0100	[7,p. 31]
Norton Co.	99.5	3.828	3.32	****	23.98	1300	.0100	[7,p. 31]
US Stoneware								
A-212	96.0	3.583	3.59	.94	28.60	1235	.0100	[7,p. 34]
A-216	85.0	3.457	3.74	.24	14.53	665	.0100	[7,p. 34]
A-312	96+	3.508	3.73	.71	6.92	675	.0100	[7,p. 34]
Western Gold and Platinum								
AL-300	97.6	3.765	3.37	.24	45.20	1100	.0100	[7,p. 36]
AL-400	95.0	3.687	3.48	.22	32.75	1030	.0100	[7,p. 37]
AL-995	99.5	3.758	3.44	.62	46.81	1280	.0100	[7,p. 37]
AL-1000	99.85	3.816	3.40	1.43	39.66	1390	.0100	[7,p. 37]

NOTES:

* The temperature at which the loss tangent ($\tan \delta = \epsilon''_{eff}/\epsilon'_r$) $\approx$ .0100, the upper limit of accuracy.

** Shows a slight downward slope for low temperatures which is not the normal case for oxide ceramics.

*** Upper limit for temperature measurement (1400 °C) reached, thus all data not available.

**** Data shows resonance absorption at low temperatures thus can not be accurately modelled.

data are in the 3.0 to 4.0 GHz, frequency effects are not demonstrated. Since density and $\%Al_2O_3$ are generaliy related, the discussion will be limited to the $\%Al_2O_3$. This $\%Al_2O_3$ shows a trend of increasing E_A with increasing purity for both temperature regions. What can not be said, specifically, is why there is such variation between samples of the same purity but from different sources. In general, each manufacturer adds different materials to affect the sintering rate. As these specific compositions are generally proprietary, correlating these data with specific sintering aides can not be done at this time, though that is one specific goal for subsequent study. Additionally, microstructural effects such as grain size, porosity, etc., may also play a role. These last parameters are not determinable from the electrical data published.

One limitation of this data is that the tan δ is limited to a practical upper value of .01 due to the accuracy of the measuring equipment [8]. This restricts the upper limit of temperatures for which data could be obtained especially for the low E_A materials. This results in limiting the accuracy of the determination of the activation energy for these materials. Included in the data in Table 2 is the temperature at which tan δ equaled .01 (in most cases). Like the E_A's, there is little correlation between this temperature and the % purity.

The final topic for discussion is the meaning of the existence of E_A's for the two temperature regions. According to most discussions in this area, the E_A for the LTR is due to dipolar losses [9]. But as the temperature rises, the conductivity of the material increases significantly due to dipolar relaxation losses, charge transfer and a broadening of the infrared absorption spectra [9]. These would account for this very large increase in the conductivity though the extent of each contribution is not easily determined. The effects of charge transfer can be differentiated to some degree by looking at the effects of purity for a given manufacturer upon E_A. From this it can be deduced that this large increase in conductivity is directly related to charge transfers which are more pronounced in materials of lesser purity. Additionally, as the purity is changed by adding conductivity modifiers (i.e., sintering aids), so is the temperature at which sintering begins to occur. It could therefore be said that by modifying the conductivity in known ways, a convenient sintering temperature can be chosen.

As a final note, the modeling of the AC conductivity would be based upon two separate thermal rate equations for each of the temperature regions rather than just one as has been indicated in previous work [1-3]. The above

analysis assumes that the rate equations are driven by Boltzman's statistics which give rise to the two activation energies. More recent work suggests that traditional Boltzman's statistics do not completely hold for ceramic materials at high temperatures in high strength microwave fields [10]. In this recent analysis, nonlinear effects of the interaction of microwave energy with lattice phonons could explain, in part, the very rapid increase in temperature seen during microwave sintering. Whether or not this new view or a more traditional approach is the most appropriate, the modeling of this sintering process is not easily accomplished.

CONCLUSION

By looking at the E_A's of polycrystalline ceramics, two temperature regions directly related to dipolar relaxation in the lower region and dipolar relaxation, charge transfer and infrared spectra broadening in the upper region are evident. A further study relating specific sintering aides to each of the activation energies would be needed to pin down the direct contribution of each conductivity mechanism to the E_A.

REFERENCES

1. H.D. Kimrey, M.K. Ferber and M.A. Janney, Sintering Dilatrometry in a High-Frequency Microwave Field, Presented at the 91st Meeting of the American Ceramic Society, Symposium on Microwave Processing of Ceramics, Indianapolis, IN, April 25th-27th, 1989.

2. W.R. Tinga, Theory of Microwave Absorption in Sintering Ceramics, Presented at the 91st Meeting of the American Ceramics Society, Symposium on Microwave Processing of Ceramics, Indianapolis, IN, April 25th-27th, 1989.

3. R.J. Brook, Sintering Cycles and Ceramic Microstructures, Presented at the 91st Meeting of the American Ceramics Society, Symposium on Microwave Processing of Ceramics, Indianapolis, IN, April 25th-27th, 1989.

4. E.P. Bescher, Y.-H. Kao, C.Y. Li and J.D. Mackenzie, The Use of Transition Metal Oxides in Microwave Sintering of Coal Ash-Derived Bricks and Tiles, Materials Research Society Symposium Proceedings, Vol. 178, Pittsburgh, PA, 1990, pp. 279-288.

5. A.C. Metaxas and R.J. Meredith, Industrial Microwave Heating, Peter Peregrinus, Ltd., London, UK, 1983.

6. G.G. Koerber, Properties of Solids, Prentice-Hall, Englewood Cliffs, NJ, 1962, pp. 201-205.

7. W.B. Westphal and A. Sils, Dielectric Constant and Loss Data, Tech. Rep. AFML-TR-71-66, April, 1972.

8. W.B. Westphal, Dielectric Constant and Loss Measurements on High-Temperature Materials, Tech. Rpt. 182, Laboratory for Insulation Research, MIT, Cambridge, MA, October, 1963, p. 4.

9. J. Iglesias and W.B. Westphal, Supplementary Dielectric-Constant and Loss Measurements on High-Temperature Materials, Tech. Rpt. 203, Laboratory for Insulation Research, MIT, Cambridge, MA, January, 1967, p. 2.

10. J.H. Booske, R.E. Cooper, I. Dobson, and L. McCaughan, Models of Nonthermal Effects on Ionic Mobility During Microwave Processing of Crystalline Solids, presented at the 93rd Meeting of the American Ceramics Society, Symposium on Microwaves: Theory and Application in Materials Processing, Cincinnati, OH, April, 1991.

MICROWAVE ENHANCED PYROCHEM CAL REACTIONS OF PuO_2, UO_2, AND U_3O_8

E. F. Sturcken, L. E. McCurry
Building 773-A, Rm C-160
Westinghouse Savannah River Company
Aiken, South Carolina 29808-0001

ABSTRACT

Experiments in the high level cells at WSRC have established that PuO_2 has an extremely high absorption factor for microwaves: temperatures in excess of 1000°C were reached in less than 5 minutes with a multi mode, 2450 MHz, 600 watt, microwave oven. In other microwave heating experiments, stoichiometric compositions of PuO_2-UO_2 were prepared and U_3O_8 was reduced to U_4O_9.

BACKGROUND

A strong coupling of microwave energy with uranium oxide was reported by Paul A. Haas[1]. Haas observed a "glowing" area in a sample of UO_3 gel spheres being microwave dried as part of a nuclear fuel preparation process. Dry UO_3 did not heat, but U_3O_8 and UO_2 heated strongly so Haas deduced that the UO_3 was reduced by traces of NH_3 and organic materials remaining in the gel after washing..

COUPLING MICROWAVE ENERGY WITH PuO_2

Experiments in the high level cells (HLC) of the Savannah River Laboratory (SRL) demonstrated that PuO_2 had an extremely high absorption factor for microwaves.

Note: This paper also appears in Ceramic Transactions Vol. 23: Nuclear Waste Management IV.

The experiments were performed in a microwave oven* that was remoted, [2], for use in high radiation fields. The oven had a nominal power rating of 600 watts. A 17.6 gram sample of PuO_2 was inserted into a cylindrical MgO crucible, .032 m (1.25 in.) OD X .025 m (1.00 in.) ID X .064 m (2.5 in.) length, and the crucible was mounted in a block of fused quartz foam insulation. The sample was run at a microwave power setting of 100 percent. The sample heated rapidly and glowed with a cherry red color in less than 3 minutes,Figure 1. The photograph is of poor quality due to its being taken behind 4 ft of lead glass shielding in the SRL high level cells.



Fig. 1 Plutonium dioxide heating in a microwave oven.

The power was turned off to prevent damage to the microwave oven, since for this first experiment, a cover of insulation had not been placed over the MgO crucible. The experiment was repeated two more times and gave the same result. The sample was located near the center of the microwave cavity but was insensitive to position because of the small amount of power absorbed.

* Model MDS-81, CEM Corp., Matthews, N.C. 281205

One can calculate the microwave power absorbed, P_{ab} , by the PuO_2 using the expression:

$$P_{ab} = C_p K m (T_f - T_i) m / t \qquad (1)$$

where C_p is the specific heat , K is the conversion factor from calories to watts, so K = 4.184 joules/cal, T_i and T_f are the initial an final temperatures in degrees centigrade, m, is the sample mass in grams and, t , the time in seconds required to heat the sample from T_i to T_f .

Using equation (1), the power absorbed by the 17.6 grams of PuO_2 in going from room temperature to 1000 ° C, in 200 seconds, is about 25 watts, where C_p for PuO_2, [3], is 0.0811 at 23° C and 0.0810 at 1000 ° C. Hence, assuming the majority of power delivered to the microwave cavity is absorbed by the sample and the heat transfer within the sample is good, one should be able to rapidly heat kilogram quantities of plutonium oxide to 1000 ° C with a 2 kilowatt microwave power source.

FORMING PuO_2-UO_2 SOLID SOLUTION

In a second HLC experiment, 17.6 grams of UO_2 was added to the 17.6 grams of PuO_2 in the MgO crucible and the mixture stirred thoroughly. The MgO crucible was fit snugly into a cylindrical hole in a fused quartz foam insulation block and a second fused quartz foam insulation block, with a cylindrical hole, was fit snugly over the top of the crucible.

The assembly was inserted in the microwave oven and heated at a power setting of 100 percent for 30 minutes. At the completion of the experiment, it was discovered that the top and bottom insulation blocks had melted next to the MgO crucible and fused to it; indicating that the crucible temperature had reached a minimum of 1600 ° C and probably much higher. The PuO_2-UO_2 mixture appeared to be a sintered mass in the bottom of the crucible, Figure 2 . Scanning electron microscope (SEM) analysis in the SRL "Contained" SEM and x-ray diffraction confirmed the formation of a one to one solid solution between PuO_2 and UO_2 .

Chikalla's phase diagram, [4] , of the system PuO_2-UO_2 indicates that the solid to liquid transition temperature for a one to one solid solution is 2600 ° C. The melting point of PuO_2 is near 2300 ° C and the melting point of UO_2 near 2700 ° C.

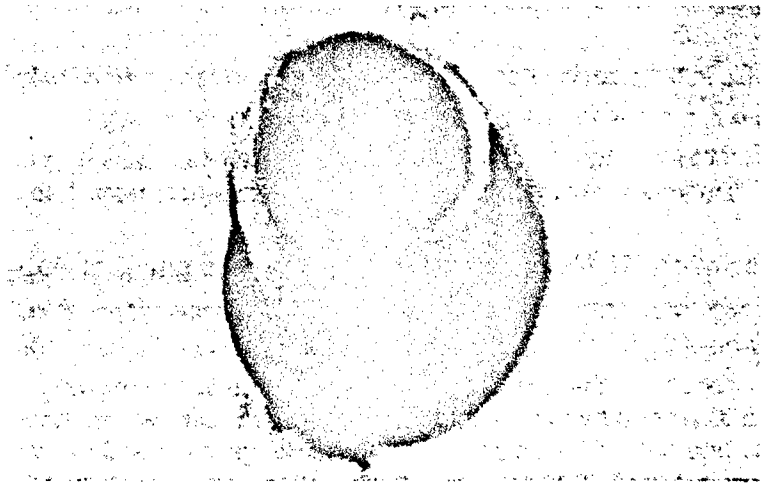


Fig. 2 Microwave sintered PuO_2-UO_2 in MgO crucible. Note the space adjacent to the crucible where the insulation melted away.

MICROWAVE REDUCTION OF U_3O_8 TO U_4O_9

A 3.36 gram sample of "depleted" U_3O_8 powder was heated in a 600 watt, microwave oven* for 30 minutes at 100% power. The sample was contained in a 0.016 m (0.625 in.) OD X 0.010 m (0.375 in.) ID X 0.051 m (2.00 in.) length boron nitride, BN, crucible.

The BN crucible and cover was contained in a 0.032 m (1.25 in.) OD X 0.025 m (1.00 in.) ID X 0.064 m (2.5 in.) length MgO cylindrical crucible. The MgO crucible was fit snugly into a cylindrical hole in a block of fused quartz foam insulation. A fused quartz foam cover was also fit snugly on top of the MgO crucible.

* Model RMS-150, Floyd Inc., Lake Wylie, S. C., 29710

The three walled containment was designed to keep the fused quartz foam insulation from melting.

Boron nitride was selected because it is transparent to microwaves and sublimes at 3000 °C. The sample was small because only a .016 m diameter rod of BN was available to fabricate the BN crucible.

Scanning electron micrographs were taken of the sample after microwave heating. The grain boundary structure, Figure 3, showed that the U_3O_8 powder had sintered.

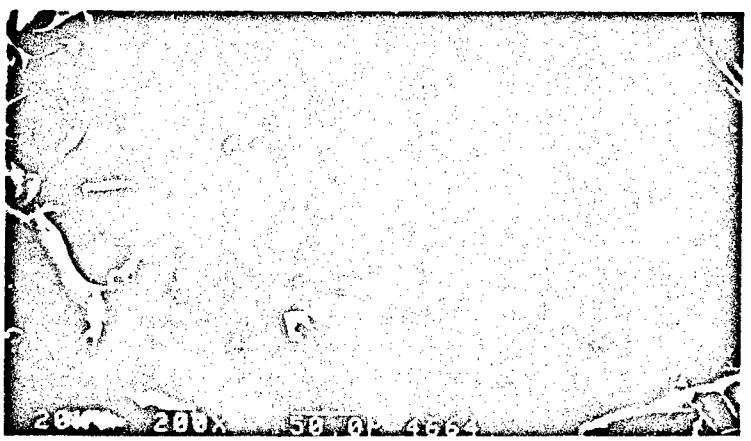


Fig. 3. SEM back scattered electron image of, U_4O_9, microwave sintered from U_3O_8 powder.

X-ray diffraction patterns of the sintered material showed that the structure was U_4O_9. According to the literature, U_3O_8 begins to decompose at 1300° C and continues to decompose with increasing temperature until it becomes UO_2 which then melts at 2700 ° C. Some melting of the fused quartz foam insulation occurred adjacent to the MgO crucible so the sample reached a minimum of 1600 ° C.

It was also noteworthy that such a small quantity of material, 3.36 grams, was adequate to develop temperatures in the neighborhood of 1600 ° C and higher in the crucibles and insulation.

UNUSUAL OBSERVATIONS

Even though the U_3O_8 powder was dry in the experiment described above, the lid was pushed off of the BN crucible and a small amount of oxide escaped when the microwave power was first turned on. The power was turned off, the lid placed back on and the experiment continued with no further problems.

To investigate the cause of this behavior, thirty grams of the U_3O_8 stock powder, from which the above sample was taken, was microwave heated in an alumina crucible for one minute and the sample observed through the microwave oven window.

As soon as the microwave power was turned on, particles throughout the powder began to spark and occasionally light up like tiny arcs or flames and some fine particles on the sample surface became airborne. The "start up" behavior of the U_3O_8 powder was reproducible, even after it was heated to cherry red, in less than 3 minutes, and cooled down. The rapid heating may be a kind of plasma heating, in which the U_3O_8 particles, interacting with the microwaves, discharge small "lightening bolts".

CONCLUSIONS

The strong coupling of PuO_2, UO_2, and U_3O_8 with microwave energy has many practical applications in the nuclear industry. Some of these applications are discussed in the following paragraphs.

Remote Operation in Nuclear Pyrochemical Facilities-Microwave technology offers the potential to considerably reduce furnace heating times; to "pipe" microwaves into high radiation cells and glove boxes and thereby greatly simplify equipment maintenance; to reduce facility size and nuclear wastes and to develop new and more efficient chemical technology, e.g., in the area of recovery and purification of plutonium.

Microwave Sintering of PuO_2 for Space Applications- PuO_2 pellets,clad in iridium, are the heat source for a number of thermoelectric generators in spacecraft.

PuO_2 is produced by plutonium oxalate precipitation and calcination. PuO_2 ,with a larger particle size, is needed to simplify pellet fabrication , improve safety and increase the power density of the pellets.

Microwave Heating to Produce Nuclear Fuels and Other Nuclear Alloys- Nuclear fuels are prepared by alloying PuO_2, UO_2, or U_3O_8 with the desired material, e.g., aluminum, in conventional furnaces. The heat treatments are lengthy and require remote operation of electrical and mechanical equipment that is large and maintenance-intensive.

The solution chemistry of PuO_2, produced by "firing" at high temperature, may be improved by alloying it with UO_2 as shown above.

It may be possible to heat lossy ceramics located in outer space with microwaves transmitted from the earth and use them as heat sources for thermolectric devices in space vehicles.

ACKNOWLEDGMENTS

The information contained in this article was developed during the course of work under contract number DE-AC09-89SR18035 with the U.S. Department of Energy. The authors wish to express their appreciation to Dr. Samuel. D. Fink, John H. Gray and Dan F. Steedly of WSRC for their assistance with the experiments.

REFERENCES

1. P. A. Haas, "Heating of Uranium Oxides in a Microwave Oven", Am.Ceram. Soc. Bull., 58 [9] 873 (1979).
2. E. F. Sturcken, T. S. Floyd, D. P. Manchester, Chapter 9, "Remote Operation of Microwave Systems", pp. 188-202, "Introduction to Microwave Sample Preparation", H.M. Kingston, L.B.Jassie, ACS Professional Reference Book, American Chemical Society, Washington, D. C., 1988.
3. T. K. Engel, "The Heat Capacities of Al_2O_3, UO_2 and PuO_2 from 300 to 1100 °K", J. Nucl. Mat., 31, pp. 211-214, (1969).
4. T. D. Chikalla, " System PuO_2-UO_2 in He", J. Am. Ceram. Soc., 46 [7] 326 (1963).

RADIOFREQUENCY SAFETY ISSUES IN INDUSTRIAL HEATING SYSTEMS

John M. Osepchuk, Raytheon Research Division,
131 Spring Street, Lexington, Massachusetts 02173

ABSTRACT

Potential RF hazards for industrial heating systems become especially noteworthy as microwave/RF power in the realm of 10's of kilowatts are employed. A review of the RF bioeffects literature and safe exposure and emission standards is presented. Techniques for suppression of RF leakage are discussed. Thresholds for sensation, pain and RF burns, particularly under conditions of field concentration, are reviewed.

INTRODUCTION

The use of electromagnetic energy in the radiofrequency range of the spectrum (0-3000 GHz) for purposes other than information handling has spread slowly from power frequencies (25-400 Hz) upward. The startling success[1] of the microwave oven at 2.45 GHz has led to an explosion of activity, ranging from food processing and medical applications to diamond growing and a variety of ceramics applications[2]. Although ISM (Industrial, Scientific, and Medical) applications exist[3] at a broader range of assigned ISM frequencies (see Table 1), most activity exists at 2.45 GHz. The frequencies, 5.8 GHz and higher, are relatively unused, but it is important to preserve more optimum alternative frequencies to 2.45 GHz.

Although ISM industrial practices are somewhat standardized (see reference texts[4]), power levels up to now have been "high" (many kilowatts) mostly at non-microwave frequencies. There are some very high power (>100 kW) systems[2] at 0.915 GHz, but at 2.45 GHz most of the activity is exploratory at levels less than 5 kW.

In time, many applications will go to high power (25, 50, 100 kW . . .) for better process efficiency and economy. In addition, there are some signs[5] (world-wide) of the resurgence of the Solar Satellite Power System Concept, where gigawatts of microwave power would be transferred from space systems to earth.

Table 1. Frequency Allocations for ISM Applications[a] PBN-91-1026

Frequency, MHz	Region	Conditions
6.765–6.795	worldwide	special authorization with CCIR[b] limits; both in-band and out-of-band
13.553–13.567 26.957–27.233 40.66–40.70	worldwide	free radiation bands
433.05–434.79	selected countries in Region 1[c]	free radiation bands
433.05–434.79	rest of Region 1[c]	special authorization with CCIR[b] limits
902–928	Region 2[d]	free radiation band
2.40–2.50 × 10^3	worldwide	free radiation band
5.725–5.875	worldwide	free radiation band
24.0–24.25	worldwide	free radiation band
61.0–61.5 122–123 244–246	worldwide	special authorization with CCIR[b] limits; both in-band and out-of-band

[a] Ref. 13.
[b] CCIR = "International Radio Consultative Committee" of the International Telecommunications Union (ITU).
[c] Region 1 comprises Europe and parts of Asia; the selected countries are the Federal Republic of Germany, Austria, Liechtenstein, Portugal, Switzerland, and Yugoslavia.
[d] Region 2 comprises the Western hemisphere.

RF BIOEFFECTS AND HAZARDS

Thousands of papers on RF bioeffects, most in the "microwave" range, have been published—most of them in the last twenty years. Surveys and reviews[6,7] of this literature show that RF bioeffects are thermal in nature. Even if some of the "non-thermal" effects

exist, they play a significant role in hazards only in the presence of heating. Radiofrequency heating effects, however, may not always be equivalent to that from other forms of heating because of the greater penetration of RF heating and heterogeneous heating.

There are subtle aspects of thermal damage[6,7], but we will concentrate on classical burn thresholds.

The temperature of biological cell death is where the rate of protein destruction exceeds the rate of repair to such a degree that cell metabolism fails. This threshold temperature is a function of time at temperature, and is best estimated from the classic work of Moritz and Henriques[8]. This threshold curve is shown in Figure 1. One can see that a skin temperature of 65°C will produce a burn in one second, but a temperature of 45°C results in a burn only after 3 hours.

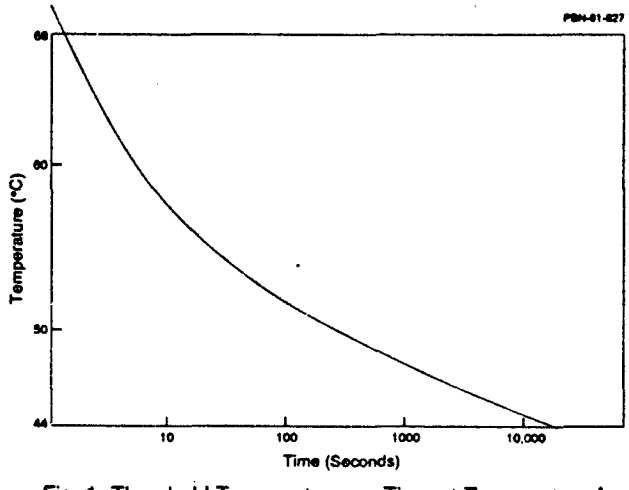


Fig. 1: Threshold Temperature vs. Time at Temperature for Skin Burns (Moritz and Henriques)

For very short exposure time or for very high frequencies where penetration is only skin deep, it may be useful to employ the heating equation for water

$$\frac{dT}{dt} = 0.239\times10^{-3}\text{SAR (watt/kg) (°C, sec.)} \quad , \quad \text{(i)}$$

Note that the ANSI C95 parameter of 0.4 W/kg corresponds to less than 0.0001°C per second rate of temperature rise. (SAR ≡ specific absorption rate.)

Burns require less power in the case of high frequency radiation (e.g. >10 GHz) where absorption is only skin deep and energy focusing to small areas is possible. Above 300 GHz the safety rules[9] for laser energy absorption applies, where a few joules or less can result in burns if the spot is small enough. In practice RF burns are most likely when contact with a "hot" conductor or aperture is made by the human body. Contact or quasi-contact exposures thus present more potential hazard than "radiant" exposure.

The estimates of contact burn threshold come from the work of Rogers[10]. For body impedance 500 Ω, the burn threshold corresponds to 20 watts dissipated in a few seconds in a volume of 1 cc.

If the energy is concentrated at a point, then burns can occur with absorbed powers as low as 0.20 watts[11]. The threshold measured above 0.25 GHz should roughly apply at lower frequencies as well.

Rogers[10] points out that the threshold sensation for low frequency currents (<100 kHz) is variously described as "tingling or pricking" (a shock-like sensation, Reference 5), but high frequency currents at >100 kHz produce a threshold sensation of warmth.

Thresholds for sensation, pain, and burns from contact currents have been detailed in the literature[10-13]. Thresholds for sensation of discharges between a conductor and the body are also discussed[11,14].

Classical studies[15] show that at frequencies above 10 GHz, sensations are perceived at a few mW/cm^2 in a few seconds, but at 2.45 GHz sensation is perceived at 20-50 mW/cm^2 in a few seconds. Pain is perceived when the skin temperature exceeds 45°C[16]. Studies at 2.45 GHz show that tissue exposures at several hundred mW/cm^2 and minutes of exposure, are required to

heat the tissue to pain. Above 10 GHz, because absorption is superficial, pain will occur in seconds.

In microwave or RF diathermy, it is said[17] that "the pain sensors are a reliable and sensitive means for alerting the patient to an unsafe temperature." This applies where heating is normally maximum near the skin. In the unusual situation of a focused deep heating spot, this rule would be controverted. This is possible in some cases[18] of animal heating but has not been reported in the case of diathermy or hyperthermia. Thus the suggestion[19] that it is possible or probable for a microwave heating injury to occur without pain is not well founded.

Little data on sensation and pain thresholds exists below 2.45 GHz. Protection against damage afforded by sensation and pain may be reduced at lower frequencies[20].

CAVEATS ON THERMAL BASIS FOR INJURY

Injury from microwave/RF exposure has a thermal basis in addition to deleterious effects from sensations, for example, the "startle" effect. One new confirmed microwave effect that might be undesirable[15] is the microwave auditory effect[21]. For short pulses (<30 μsec) of energy at frequencies between 0.3 GHz and 3.0 GHz, one can induce in some animals and man an auditory sensation if the energy flux density exceeds 0.04 mJ/cm^2. This is unlikely to happen with ordinary radar pulses without exceeding average power exposure limits.

There have been and continue to be reports of "non-thermal" effects in bioeffect experiments[7], sterilization[21], and more recently polymer processing[22]. Up to now, such confirmed effects have eventually been found associated with non-uniform heating. It remains to be seen if there are effects associated with "micro-thermal" principles[23,24].

SAFETY STANDARDS

Safety of microwave equipment is generally assured by an emission standard such as that imposed on microwave ovens[25] by the FDA—that is, 5 mW/cm^2 at 5 cm from the surface of the oven. The primary reference for safety is the exposure standard. In this country the generally applicable standard is ANSI C95.1-1982. In Figure 2 there is presented a capsule guide of the proposed revision[26], depicting maximum exposure levels (MPE). The reduction of averaging time at frequencies above 10 GHz is necessary to prevent skin burns.

HAZARDOUS INTERFERENCE

Actual hazardous aspects of ambient microwave/RF radiation derive more from interference phenomena[27] or the more remote possibility of sparking[28] and ignition of fires. Sensitive instrumentation, without shielding and filtering, can suffer interference at levels as low as 1 $\mu W/cm^2$. In fact, early demand pacemakers were reported to be inhibited at such low power densities by many RF sources. Extensive studies[29] by the Air Force have shown that modern pacemakers which incorporate shielding and filtering are unlikely[30] to suffer interference even at 10 mW/cm^2.

Some new issues relate to pressure for spectrum sharing with communications systems and the possibility of new sources of hazardous interference[31].

HAZARDS PECULIAR TO MICROWAVE HEATING

There are some peculiar hazards related to overheating (time). One is the possibility of superheating in small objects. As shown in the literature[32], at 2.45 GHz small objects approximating a sphere can develop peak heating in the center. This can lead to superheating (above boiling point) and the

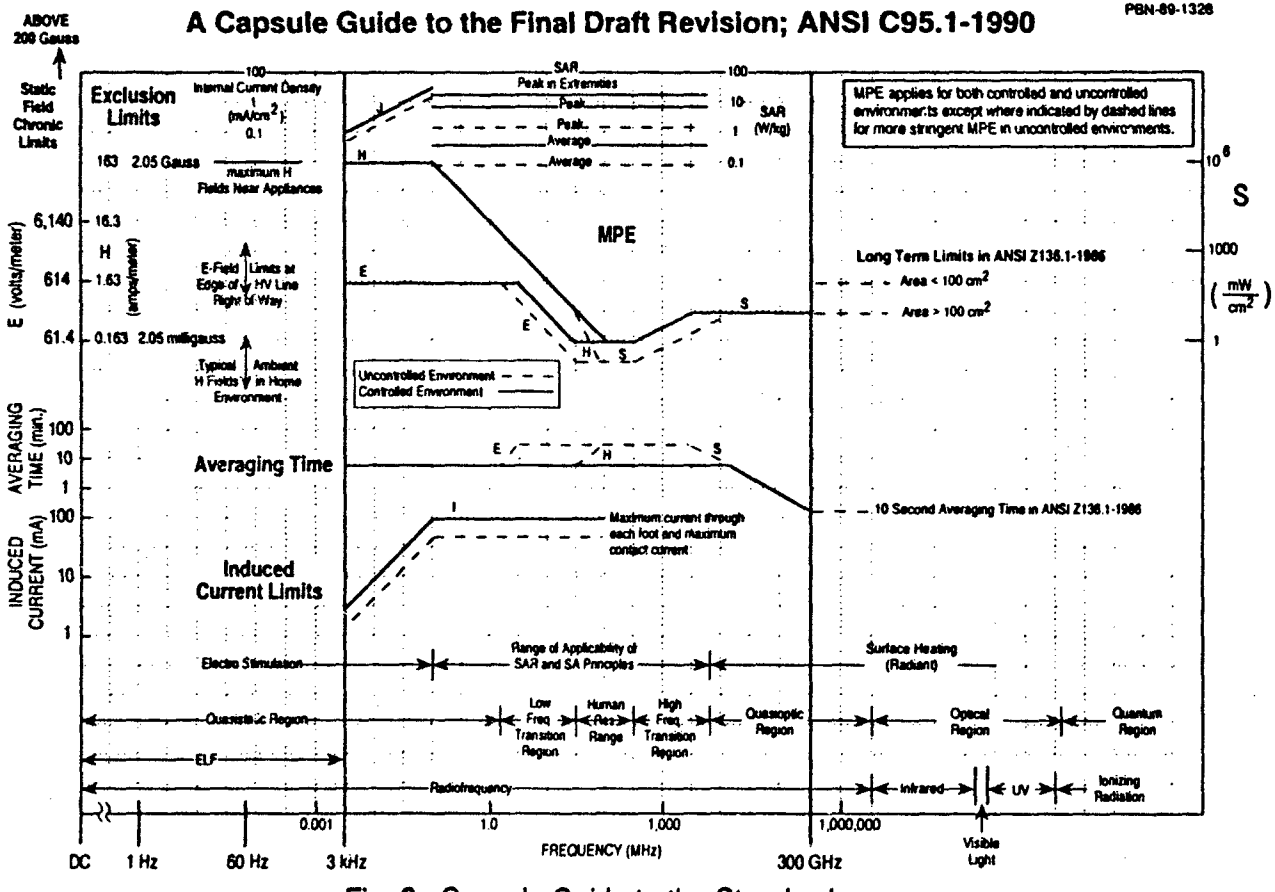


Fig. 2: Capsule Guide to the Standard

subsequent release of energy in a small explosion. This can be demonstrated with a small beaker of water ~100-200 ml in microwave ovens under the right conditions[33].

This phenomenon is illustrated in Figure 3 where spherical phantoms with a cloud point at 51°C are heated so as to show internal hot spots.

LEAKAGE SUPPRESSION

In order to minimize personnel exposure and interference, it is important to achieve good seals[25] in the microwave power apparatus and appropriately designed screens for viewing or ventilation. The proper use of interlock systems on all doors or access apertures becomes increasingly important as power levels rise into the tens or hundreds of kilowatts. Accidental absorption of such power may cause significant injury in seconds. Occasionally, introduction of glass or plastic tubing for gas or liquid flow is done by creating a circular hole in the oven wall and then attaching a metal tube with

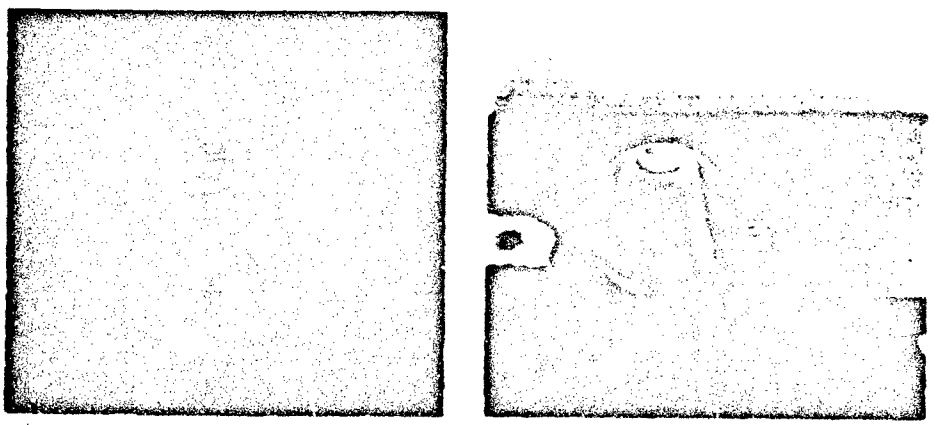


Fig. 3. Samples of Phantom Material Heated in a Microwave Oven
Sekusui Glue R-500 (water and polyvinyl alcohol), cloud temperature of 51 C

proper gasketing. If the tube inner diameter is well below the cut-off dimension for the fundamental waveguide mode (TE_{11}), then the leakage is attenuated roughly by 32 L/d dB at 2.45 GHz, where L is the length of the tube and d is the inner diameter of the tube. If the metal tube contains a plastic tube carrying the liquid, then one should consult the literature[34] for more specific design information.

ELECTROPHOBIA

This is a phenomenon in which there is widespread fear of electromagnetic fields.

Science-based standards for EM fields are based on presumed thresholds of effects and hazards. Recently, these standards have been attacked by a provocative journalist and some unwitting allies from the engineering community. These attacks center around uncritical acceptance of recent research suggesting weak field effects and a proposed policy of "prudent avoidance."

The restoration of a rational approach to EM fields has been a goal of various organizations like the IEEE Committee on Man and Radiation (COMAR), the International Microwave Power Institute (IMPI), and the Electromagnetic Energy Policy Alliance (EEPA).

CONCLUSIONS

Heating of personnel during brief exposure (seconds) to microwave/RF power can be a serious hazard as system power levels increase to many 10's of kilowatts. Protective measures include use of interlocks, leakage detectors, and personnel training. Hazards related to explosive or flammable properties of materials being processed are a possibility but difficult to generally predict. In contrast to these real hazards, most of today's public concern about

exposure to microwave/RF energy is part of an Electrophobia for which public education is the ultimate antidote.

REFERENCES

1. J. M. Osepchuk, "A History of Microwave Heating Applications," IEEE Trans., MTT-32 (9), 1200-1224 (Sept. 1984).

2. R. H. Edgar and R. Snider, "The Economics of Microwave Processing in the Ceramics Industry," Ceramics Trans., this issue.

3. M. A. Stuchly and S. S. Stuchly, "Industrial, Scientific, Medical, and Domestic Applications of Microwaves," IEE Proc., 130 (8), 467-503 (Nov. 1983).

4. A. C. Metaxas and R. J. Meredith, Industrial Microwave Heating. Peter Peregrinus, London, 1983.

5. SPS-91, Power from Space, Proceedings of the Second International Symposium, August 1991, Paris, France, Societe des Electriciens et des Electroniciens.

6. S. M. Michaelson and J. C. Lin, Biological Effects and Health Implications of Radiofrequency Radiation. Plenum Press, New York, 1987.

7. CRC Handbook of Biological Effects of Electromagnetic Fields. Edited by C. Polk and E. Postow. CRC Press, Boca Raton, Florida, 1986.

8. A. R. Moritz and F. C. Henriques, Jr., "Studies in Thermal Injury II. The Relative Importance of Time and Surface Temperature in Causation of Cutaneous Burns," Am. J. Pathol., 23, 695 (1947).

9. D. Sliney and M. Wolbarsht, 163-168, Safety with Laser and Other Optical Sources. Plenum Press, New York, 1980.

10. S. J. Rogers, "Radiofrequency Burn Hazards in the MF/HF Band," pp. 3-81; in Aeromedical Review, Proceedings of a Workshop on the Protection of Personnel Against Radiofrequency Electromagnetic Radiation. Edited by John C. Mitchell. Research Study Group, Panel VIII Defense Research Group, NATO, Sept. 1981.

11. J. M. Osepchuk, "The Microwave Stimulus," 35-56, Microwaves and Thermoregulation. Edited by E. R. Adair. Academic Press, New York, 1983.

12. I. Chatterjee, D. Wu and O. P. Gandhi, "Human Body Impedance and Threshold Currents for Perception and Pain for Contact Hazard Analysis in the VLF-MF Band," IEEE Trans. Biomed. Eng., BME-33, 486-494 (May 1986).

13. J. Bernhardt, "The Direct Influence of Electromagnetic Fields on Nerve and Muscle Cells of Man within the Frequency Range of 1 Hz to 30 MHz," Radiat. Environ. Biophys., 16 (3), 309-323 (1979).

14. J. P. Reilly, "Human Sensitivity to Electric Shock Induced by Power-Frequency Electric Fields," IEEE Trans., EMC-29 (3), 221-232 (Aug. 1987).

15. S. M. Michaelson, "Cutaneous Perception of Microwaves," J. Microwave Power, 1 (2), 67 (1972).

16. J. D. Hardy, "Thermal Radiation: Pain and Injury," 170, Therapeutic Heat. New Haven.

17. A. W. Guy and C. K. Chou, "Electromagnetic Heating for Therapy," 57-94, Microwaves and Thermoregulation. Edited by E. R. Adair. Academic Press, New York, 1983.

18. A. R. Shapiro, R. F. Lutomirski, and H. T. Yura, "Induced Fields and Heating within a Cranial Structure Irradiated by an Electromagnetic Wave," IEEE Trans. Microwave Theory Tech., MTT-19, 187-196 (Feb. 1971).

19. D. R. Justesen, "Microwave and Infrared Radiation as Sensory, Motivational, and Reinforcing Stimuli," Electromagnetic Fields and Neurobehavioral Function. Edited by M. E. O'Connor and R. H. Lovely. Alan R. Liss, Inc., New York, 1988.

20. E. R. Adair, Ph.D., John B. Pierce Foundation, New Haven, CT; Personal Communication.

21. J. C. Lin, Microwave Auditory Effects and Applications. Charles C. Thomas, Springfield, Illinois, 1978.

22. R. Decareau, Microwaves in the Food Processing Industry. Academic Press, New York, 1985.

23. D. A. Lewis, T. C. Ward, J. D. Summers, and J. E. McGrath, "Cure Kinetics and Mechanical Behavior of Electromagnetically Processed Polyimides, Polymer Reprints, 29 (1), 174-175 (1988).

24. P. Czerski and C. C. Davis, "Interaction of Electromagnetic Fields with Genetic Information," 231-248, Mechanistic Approaches to Interactions of Electric and Electromagnetic Fields with Living Systems. Edited by M. Bland and E. Findl. Plenum Press, New York, 1987.

25. J. M. Osepchuk, "A Review of Microwave Oven Safety," J. Microwave Power, 13 (1), 13-26 (March 1978).

26. IEEE SCC 28; "Safety Levels with Respect to Human Exposure to Radiofrequency Electromagnetic Fields, 3 kHz to 300 GHz."

27. R. Reis, "Potential Interference with Medical Electronics Devices," Bull. New York Acad. Med., 55 (11), 1216-1221 (Dec. 1979).

28. Radio Electron. Eng., 49 (6), 264 (1979).

29. J. C. Mitchell, "Part VII: Interference Effects; Electromagnetic Compatibility of Cardiac Pacemakers," 557-584, Biological Effects of Electromagnetic Radiation. Edited by J. M. Osepchuk. IEEE Press, New York, 1983.

30. J. M. Osepchuk, "Debunking a Mythical Hazard," Microwave World, 16 (Nov.-Dec. 1981).

31. Supplemental Notice of Inquiry, FCC Gen. Docket No. 89-554, March 14, 1991 and D. White, "HERF and Electromagnetic Terrorism," EMC Technology, 10 (1), 7 (Jan.-Feb. 1991).

32. H. N. Kritikos and H. P. Schwan, "The Distribution of Heating Potential Inside Lossy Spheres," IEEE Trans. Biomed. Eng., BME-22, 457-463 (1975).

33. C. R. Buffler and T. Lindstrom, "Experimental Evidence of Water Eruption Caused by Super-Heating," Microwave World, 9 (4), 10-11 (1988).

34. K. W. White, Electromagnetic Wave Propagation Through Circular Waveguide Containing Radially Inhomogeneous Lossy Media, Report USACERI TM M-89/11, U.S. Army Corps. of Engineers, Sept. 1989, Available from NTIS; AD-A213062.

Section III. Modeling

COMPUTATIONAL TECHNIQUES IN MODELING AND QUANTIFYING MICROWAVE INTERACTIONS WITH MATERIALS

M. F. Iskander, O. Andrade
Department of Electrical Engineering
University of Utah
Salt Lake City, UT 84112

H. Kimrey
Oak Ridge National Laboratory
Oak Ridge, TN 37831

R. Smith, S. Lamoreaux
Department of Electrical Engineering
University of Utah
Salt Lake City, UT 84112

ABSTRACT

Computational techniques and numerical modeling are expected to play a significant role in developing the area of microwave sintering of ceramics. There is no doubt that before the full commercial utilization of this technology, detailed understanding of the basic nature of the microwave interactions with materials as a function of frequency, geometry, and temperature must be developed. Tradeoffs between the use of single- and multi-mode cavities should be clearly understood and the shapes and sizes of ceramic samples suitable for this technology must be identified. To this end, numerical techniques may help in a wide variety of ways including modeling realistic sintering experiments, the development of a basic understanding of the physical and geometrical aspects of microwave interactions with materials, and in the development of an expert system that integrates simulation and analysis software with the developing human expertise and material data base. This paper describes roles that may be played by computational techniques and software tools in the area of sintering of ceramics. In particular, a simulation software package based on the Finite-Difference Time-Domain (FDTD) method will be discussed. The CAEME (Computer Applications in Electromagnetics Education) software for EM education/training will be described and the advantages of developing an expert software system that emulates humans by logically performing tasks, accessing simulation software, and by interfacing with dielectric and thermal materials data bases will be described. Example results of simulated sintering experiments in single-mode cavities are also presented.

INTRODUCTION

With the continued interest in the area of microwave sintering of ceramics and the continued publication of results inferring advantages of microwave over conventional sintering, there has

been a significant need to better model the microwave sintering process and simulate these interactions in a realistic fashion. Modeling a microwave sintering process in a single- or multi-mode cavity is not a simple task, particularly for cases where insulation is used to contain the heat and when complex sintering arrangements such as those that utilize silicon carbide (SiC) rods to initiate and/or accelerate the heating process. Simple models and one- or two-dimensional numerical codes are often useful but three-dimensional models and solution procedures are certainly needed to reasonably and accurately model realistic sintering experiments. There are several electromagnetics techniques that may be used in 3D modeling of a microwave sintering process. This includes techniques based on an integral equation formulation, on the direct solution of Maxwell's equations in differential form, and on the utilization of vector spherical wave expansions to describe the fields inside and outside the dielectric object (ceramic sample and surrounding insulation). Table 1 summarizes the basic features of these solution procedures and outlines advantages and limitations of each [1, 2].

Based on the comparison described in Table 1, the group at the University of Utah decided to use the Finite-Difference Time-Domain (FDTD) method to model the microwave sintering process in a single-mode cavity. The following section describes the solution procedure and presents the models used and some of the obtained results.

In addition to the use of computational techniques to simulate sintering processes, these techniques, when used in an education/training mode, can provide significant insight into the fundamental aspects of microwave interactions with materials. For example, FDTD has been used to demonstrate wave reflection/transmission at dielectric interfaces and the Finite-Difference method has been used to calculate electric field distribution in a 2D parallel plate capacitor with a dielectric object of arbitrary dimensions placed between the plates [3]. A large collection of software has been developed by the NSF/IEEE CAEME Center on Computer Applications in EM Education. The Center's objectives, avenues for participation, and a list of the available software are described as is a brief proposal for establishing a knowledge-based system [4] for microwave processing of ceramics. Aspects of a desirable knowledge-based system for microwave sintering are summarized and an example of a similar system recently developed by the Utah group for electronic package design is described.

FINITE-DIFFERENCE TIME-DOMAIN MODELING OF MICROWAVE SINTERING IN A SINGLE-MODE CAVITY

From Table 1 it may be seen that modeling microwave sintering using FDTD provides the following advantages:

a. The technique is particularly adequate for modeling inhomogeneous objects which is important in simulating real sintering experiments involving ceramic samples surrounded by insulations of different materials.

b. It is based on the solution of Maxwell's equations in differential form. The numerical solution is hence localized in nature and the resulting matrix is sparse. Such a matrix characteristic is attractive from the parallel processing point of view which may turn out to be essential in modeling of large samples in multi-mode cavities.

Table 1. Comparison between basic formulation, applicability, and computational efficiency of numerical techniques based on integral, differential, and spherical wave expansion formulations.

	Integral Operator	Differential Operator	Spherical Expansions
Basic formulation	Using Green's function	Directly from Maxwell's differential equation	Multiple [illegible]pan-sions [illegible]re used inside [illegible]side the dielectric object
Application	Suitable for interior and exterior boundary value problems Special efforts are needed for handling inhomogeneous media	Suitable for interior problems and bounded regions including inhomogeneous Special efforts are needed for handling exterior and unbounded regions	Suitable for interior and exterior boundary value problems Special effort is needed near convex surfaces
Computational Efficiency	The resulting matrix equation is smaller but dense The choice of the appropriate Green's function may result in sinificant reduction in matrix size	The resulting matrix is larger but sparse Lends itself directly to efficient iterative solution procedures Finite-difference time-domain and finite element methods are attractive for parallel computing	Expansion functions are complete and procedure uses much fewer (10-15%) of the number of terms used in integral operator techniques Self-validation is yet another attractive feature of this technique
Time and frequency domain solutions	Has been applied for both, but most commonly used in frequency domain Used for both perfectly conducting and penetrable objects	Has been applied for both and its time-domain solution is gaining popularity Used for both dielectric and conductivity objects	Frequency-domain technique is suitable for perfectly conducting and penetrable objects
Additional characteristics	Highly adaptable for hybridization with other techniques to improve its accuracy and numerical efficiency. Examples include hybridization with physical optics, geometrical theory of diffraction and the use of a wide variety of approaches to deal with edge singularities and to handle electrically large objects	Some efforts need to be focused on its hybridization with other modal expansion or boundary value techniques to help apply it to exterior problems. Efficient time-domain analysis procedure is needed to deal with dispersive dielectrics	The expansions used near convex boundaries and within an artificial spherical boundary surrounding the 3D objects are of questionable accuracy, although in many cases provide practical results

The limitations of the FDTD procedure are often associated with modeling exterior and open-space type problems, such as those of scattering by perfectly or highly conducting objects. In microwave sintering in a single-mode cavity, however, the calculation domain is well defined by the cavity walls and neither the sample nor the surrounding insulation is perfectly conducting [5, 6]. In other words, the questionable accuracy of absorbing boundaries and staircase-type modeling of the FDTD is not expected to play a role in our present application [2].

Mathematical formulation of the FDTD is based on the finite-difference representation of the time and spatial derivatives in Maxwell's equations [7]. We, like others, used Yee's cell to systematically relate the various electric and magnetic field components at different time steps. In modeling microwave sintering experiments in single-mode cavities, we initially used Model 1 of Figure 1 and subsequently improved the calculations by utilizing a more accurate feed model as

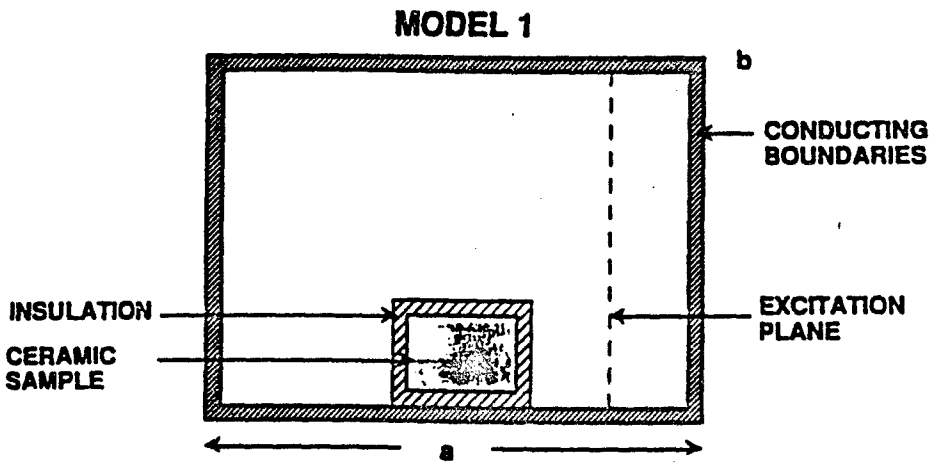


Figure 1. A model of microwave sintering experiment in a single-mode cavity. Two rectangular cavities were used for these calculations. An X-band cavity of dimensions 2.286 × 1.016 × 1.524 cm^3 and TE_{101}-mode resonance at 11.829 GHz, and an S-band cavity of dimensions 9.144 × 4.064 × 8.128 cm^3 and TE_{101}-mode resonance at 2.45 GHz. Insulated samples of different dimensions were modeled.

shown in Figure 2 [8]. In Figure 1, a 1 × 1 × 1 cm^3 ceramic sample was surrounded by insulation of variable thickness. Rectangular cavities of two different dimensions were used to model sintering experiments in the X and S bands. The first cavity is 2.286 × 1.016 × 1.524 cm^3, suitable for modeling sintering at 11.829 GHz (TE_{101} mode), while the other is 9.144 × 4.064 × 8.128 cm^3, suitable for modeling sintering experiments at 2.45 GHz. The excitation plane was placed inside the cavity as shown in Figure 1. The cavity walls were assumed to be

made of copper of conductivity $\sigma = 5.7 \times 10^7$ S/m. The FDTD computation domain was designed to include a volume of width equals to three cell sizes to simulate the wall losses and account for the field's penetration in the cavity walls.

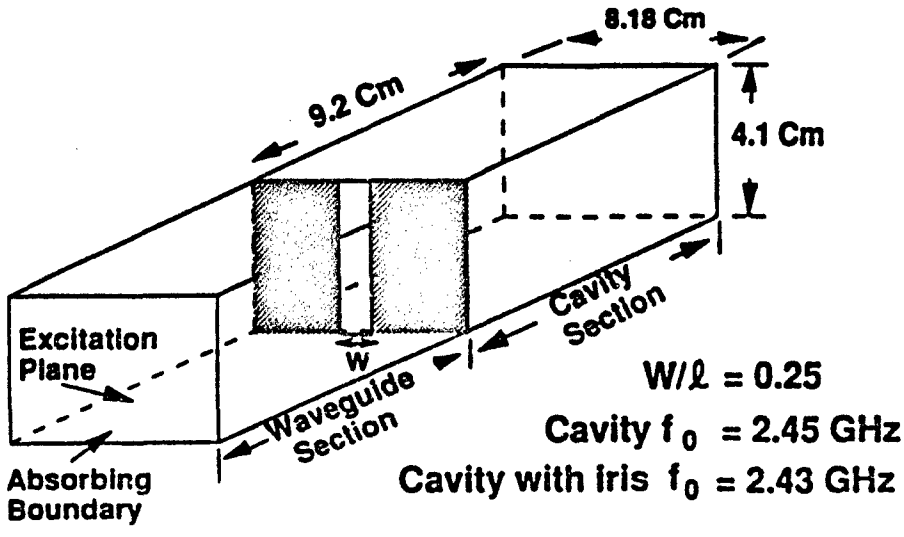
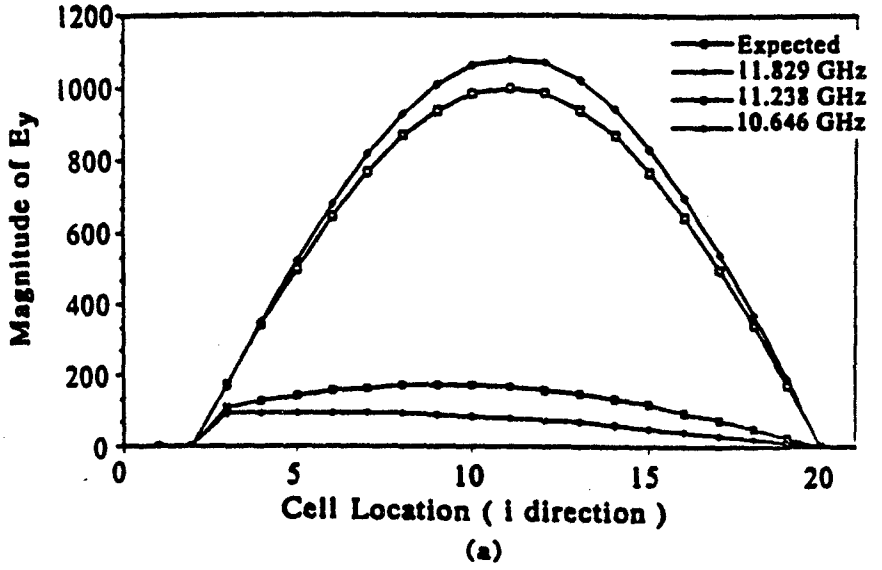


Figure 2. An improved model for simulating microwave sintering of insulated ceramic samples in single-mode cavities. The model utilizes realistic feed arrangement to help improve the calculation of the SAR distribution, the cavity Q, and the shift in resonant frequency as a result of the coupling iris.

To examine the convergence and accuracy of the solution procedure, an empty cavity was considered first. Figure 3 shows the convergence of the FDTD solution to a cavity mode irrespective of the initially assumed fields on the excitation plane. In addition, a dielectric sphere was placed at the location of maximum electric field in the cavity, and the obtained FDTD solution of the internal fields was compared with the expression $|E_{in}| = \frac{3}{\varepsilon_r + 2} |E_{out}|$ based on the quasi-static approximation [8]. The obtained results are shown in Figure 3 of a companion paper in this proceedings [8] where it may be seen that the FDTD results are in good agreement with the quasi-static values. Figure 4 shows that the FDTD results satisfy the boundary conditions. Specifically, the tangential electric fields on boundary A are continuous, and the normal electric field components on boundary B are discontinuous by the ratio of ε_r. The convergence of the solution to the appropriate cavity modes, and the agreement of the calculated electric-field components with the quasi-static calculations for the special case of a dielectric sphere, provided confidence in the accuracy of the developed FDTD code.



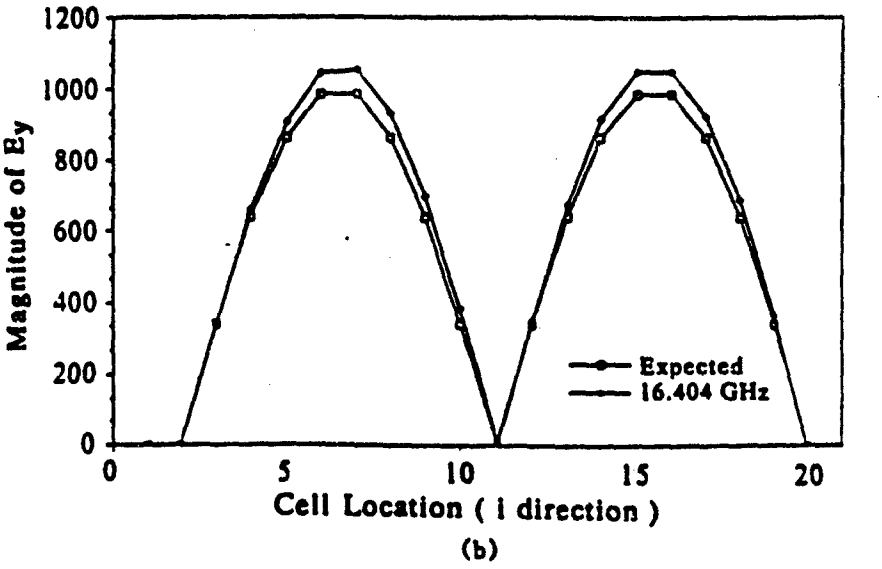


Figure 3. Convergence of the FDTD solution to the cavity mode regardless of the initially assumed incident fields on the excitation plane . (a) Convergence to the expected TE_{101} mode at 11.829 GHz and to almost zero fields at two other frequencies, 11.238 and 10.646 GHz. (b) Convergence to the TE_{201} mode at f = 16.404 GHz.

With this confidence in the accuracy of the FDTD solution, realistic microwave sintering experiments were simulated. Figure 5 shows the field distribution inside a TE_{101}-mode cavity with the sample, and Figures 6 and 7 show the specific absorption rate (SAR) in ceramic samples surrounded by 0.5-cm-thick insulation. Figures 6 and 7 illustrate the relative SAR in both the ceramic sample and the surrounding insulation at two different temperatures and for a specific case of an insulation thickness of d = 0.5 cm. Several other results for varying thicknesses of the insulation have also been calculated.

In Model 1, however, it was observed that the presence of the excitation plane within the cavity is similar to the case of strongly coupling the EM fields in an experimental cavity. It results in lowering the cavity Q. Therefore, to improve the ability of the developed FDTD model to accurately calculate the Q of the cavity, a new excitation procedure was utilized. This is shown in Figure 2, where an inductive iris was used to facilitate exciting the cavity from a waveguide section. An absorbing boundary was used at the end opposite to the excitation aperture in the waveguide section to eliminate reflections from this end. It was, however, observed that with this new excitation, the FDTD solution did not converge in the cavity region. Oscillations occurred and the fields inside the cavity failed to reach steady state. Upon careful examination of the frequency of the oscillating fields, it was observed that the frequency slightly shifted from 2.45 GHz to 2.43 GHz due to the reactive impedance of the iris. Changing the excitation frequency to 2.43 GHz resulted in a convergent solution and accurate calculation of the cavity Q as well as the SAR distribution in the sample and the surrounding insulation. Based on an assumed cavity walls made of copper of conductivity equals to 5.7×10^7 S/m, the cavity Q was calculated to be approximately 8000 which is in good agreement with experimental expectations. With this, it is believed that the developed

j cell \ i cell	21	22	23	24	25	26	27	28	29	30	31	32	33	34	35	36	37
18	599	628	661	700	743	788	822	841	850	848	838	816	780	734	689	648	613
19	593	624	661	708	769	843	885	905	911	910	900	879	834	759	697	648	609
20	584	614	653	709	792	945	983	985	982	981	980	975	935	781	697	640	599
21	569	595	632	689	761	546	421	382	369	369	380	418	540	751	678	619	580
22	549	566	592	664	486	417	416	407	401	401	405	413	412	478	652	579	551
23	526	525	504	414	385	407	416	417	416	416	415	412	402	378	405	492	510
24	507	497	468	412	404	412	420	423	424	424	421	416	407	397	403	457	483
25	496	482	453	412	411	417	423	427	428	428	424	418	411	404	403	442	468
26	492	477	450	412	413	418	424	428	430	429	426	419	412	406	403	438	463
27	496	482	454	412	411	417	423	427	429	428	425	418	411	404	403	442	468
28	507	497	468	412	405	413	420	424	425	424	421	416	407	397	403	457	483
29	526	525	504	414	385	407	416	418	417	416	415	412	402	378	406	492	511
30	549	566	592	664	486	417	417	407	402	401	405	413	412	478	652	579	551
31	569	596	632	690	762	547	422	382	370	369	380	418	540	751	678	619	580
32	584	614	654	709	792	946	983	986	983	982	981	976	936	782	698	640	599
33	594	625	662	709	770	843	886	905	912	911	901	880	835	760	697	648	609
34	599	629	662	701	744	789	822	842	850	849	839	817	781	735	689	649	614

Figure 4. Internal and external electric field distributions inside a dielectric sphere of ϵ_r = 3. The results were obtained using the FDTD solution and illustrate the continuity of the tangential electric field components at boundary A and normal electric flux density component $\bar{D} = \epsilon\bar{E}$ at the interface B. FDTD results thus satisfy the boundary conditions.

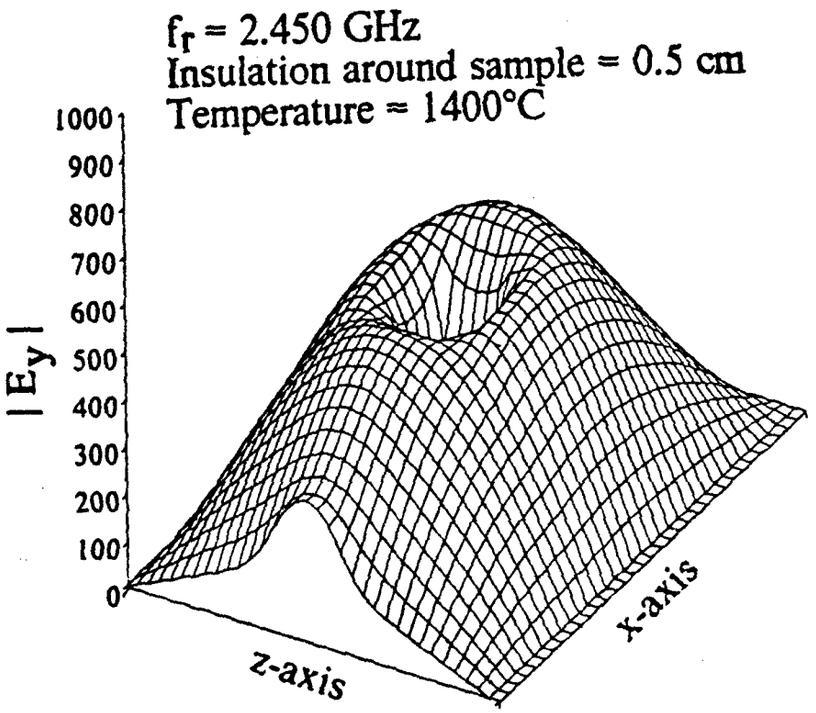


Figure 5. Field distribution inside a TE_{101}-mode cavity with a ceramic sample inside. The sample is 1 cm^3 cubic alumina surrounded by 0.5-cm-thick insulation. The dielectric properties of the sample and the insulation at 1400° C are

Ceramic 50% dense alumina	$\varepsilon_r = 4.13$ $\sigma = 64.06 \times 10^{-6}$ S/m
Insulation 12% dense alumina fibers	$\varepsilon_r = 1.557$ $\sigma = 15.37 \times 10^{-6}$ S/m

and at 1400° C are

Ceramic 96% dense alumina	$\varepsilon_r = 11.327$ $\sigma = r.80 \times 10^{-3}$ S/m
Insulation 12% dense alumina fibers	$\varepsilon_r = 1.557$ $\sigma = 15.37 \times 10^{-6}$ S/m

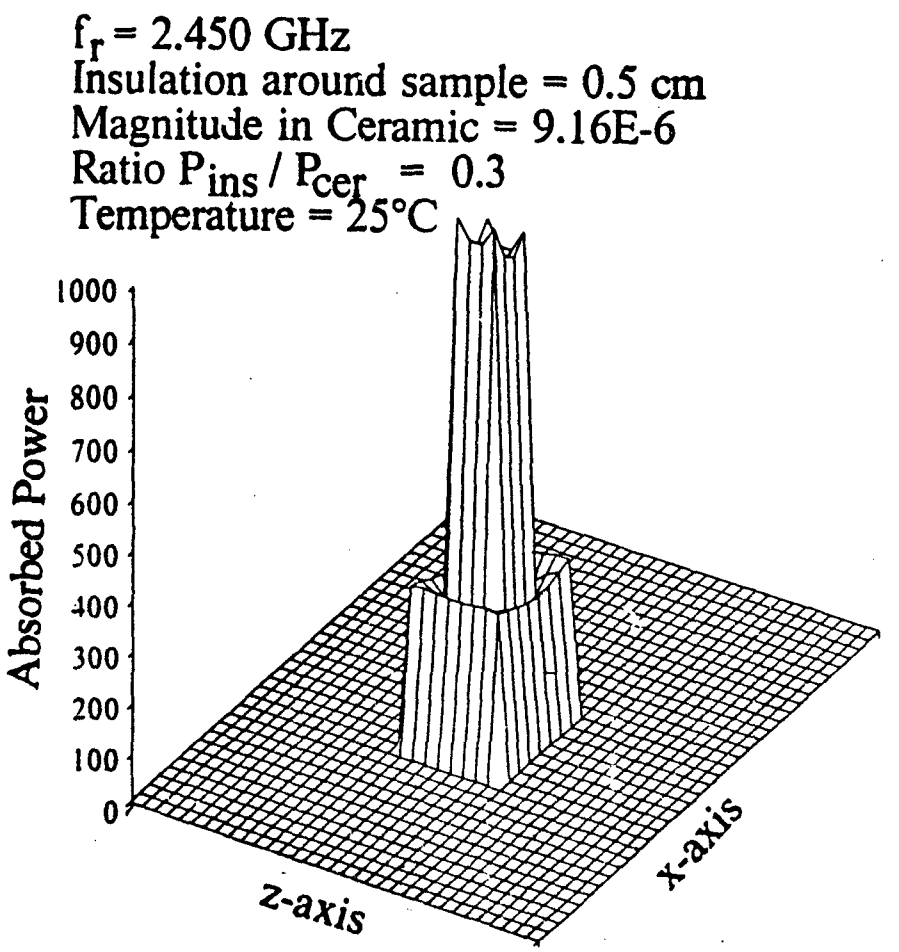


Figure 6. The specific absorption rate (SAR) of an insulated alumina sample at 25° C. Dielectric properties of the sample and insulation are given in Figure 5.

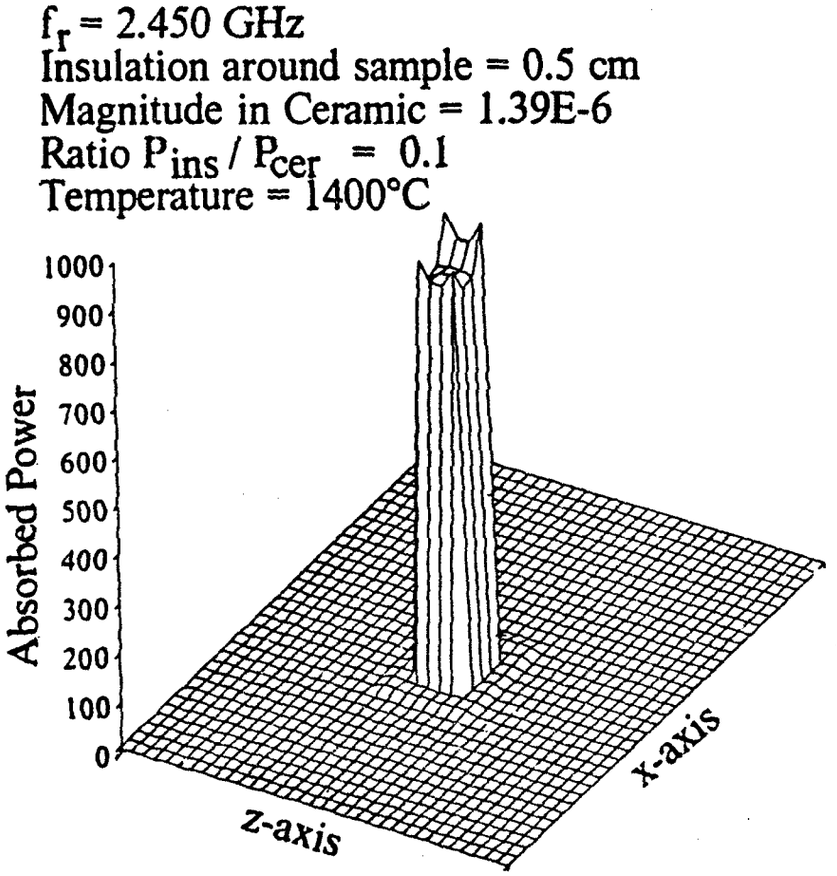


Figure 7. The specific absorption rate (SAR) of an insulated alumina sample at 1400° C. Dielectric properties of the sample and insulation are given in Figure 5.

single-mode microwave processing model is the most accurate one available to date. The field distribution and SAR results for insulated ceramic samples heated at 2.43 GHz are shown in Figures 8 and 9.

With the successful development of the FDTD model, efforts are now under way to extend this model to multi-mode cavities. Initial experience with a new multi-mode cavity has been very exciting and detailed results will be presented in future publications.

OTHER APPLICATIONS OF COMPUTATIONAL TECHNIQUES AND SOFTWARE TOOLS

Besides using computational techniques to model and simulate microwave sintering of ceramics, computers and software tools may be used as educational/training aids to help inter-disciplinary groups review and understand fundamental aspects of microwave interactions with materials. To date, there is also commercially available software that may aid in the development of an expert system that emulates human expertise and logically integrates available software and the developing data bases. This section will briefly summarize some ongoing activities in these areas.

COMPUTER APPLICATIONS IN DEVELOPING A FUNDAMENTAL UNDERSTANDING OF THE PHYSICAL ASPECTS OF MICROWAVE INTERACTIONS WITH MATERIALS

Computational techniques and modern software tools including computer graphics and authoring software may provide a unique opportunity for an interdisciplinary group, such as those working in our area of microwave sintering, to carefully examine and fully understand the complex nature of microwave interaction with materials. Through preliminary microwave sintering experiments, say in home-type microwave ovens, may of us learned the complex nature of this process and its high dependence on the material type and shape, as well as on the type and size of the surrounding insulation. The behavior of the electric- and magnetic-field components at dielectric interfaces between samples and insulations needs to be understood to help explain some thermal runaways at these interfaces, as well as to optimize the role of insulation in a microwave sintering process. In addition, many of us encountered problems with the use of thermocouples when used in monitoring sample temperatures. In single-mode cavity sintering experiments, it may be noticed that the orientation of the thermocouple inside the cavity plays a role in its level of interference with the electromagnetic fields and in the magnitude of the resulting temperature measurement errors. In addition, difficulties are often encountered in tuning cavities and in predicting the effect of sample size, loss tangent, on the Q and the resonance frequency of the cavity.

Many of these physical and geometrical aspects of microwave interaction with materials are available in textbooks. Most of the available presentations are made in an abstract and highly mathematical fashion that often obscures the underlying physical aspects of these interactions. Modern computational techniques and software tools with their attractive features such as interactivity, visualization, graphical presentation of results can play a significant role in helping interdisciplinary groups such as ours to understand the physical aspects of microwave interaction with materials.

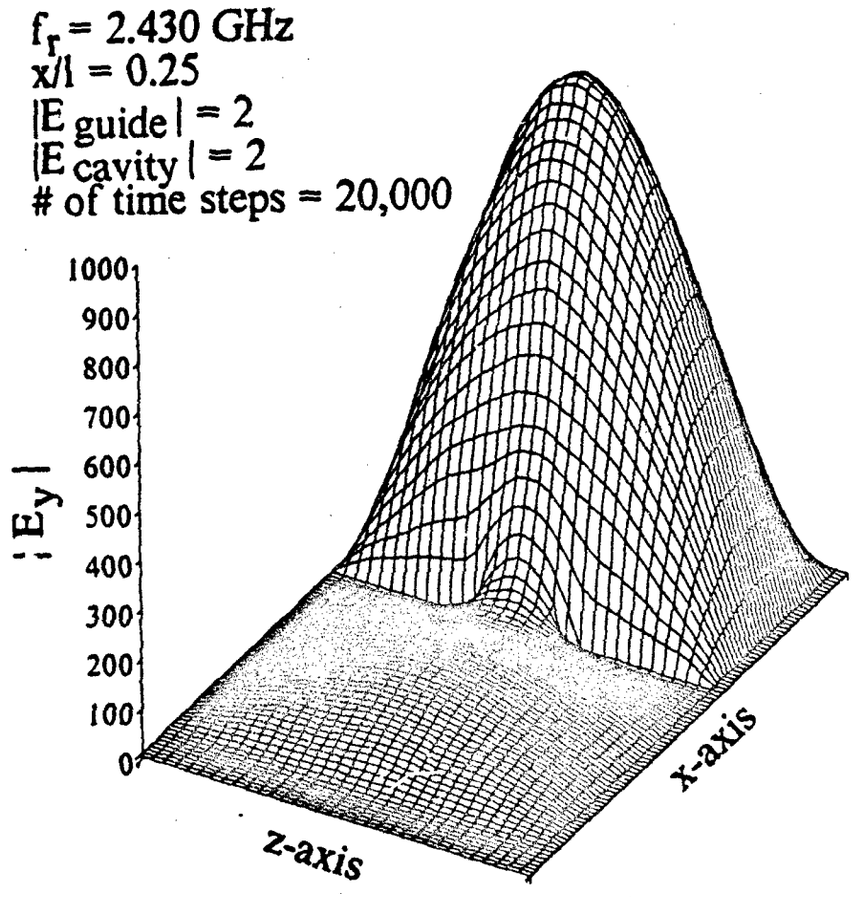


Figure 8. Field distribution inside an empty cavity at f = 2.43 GHz. The displayed electric field has a magnitude of 10 after 20,000 time steps in the FDTD solution. This value reaches 100 at steady state after 200,000 time-step calculations.

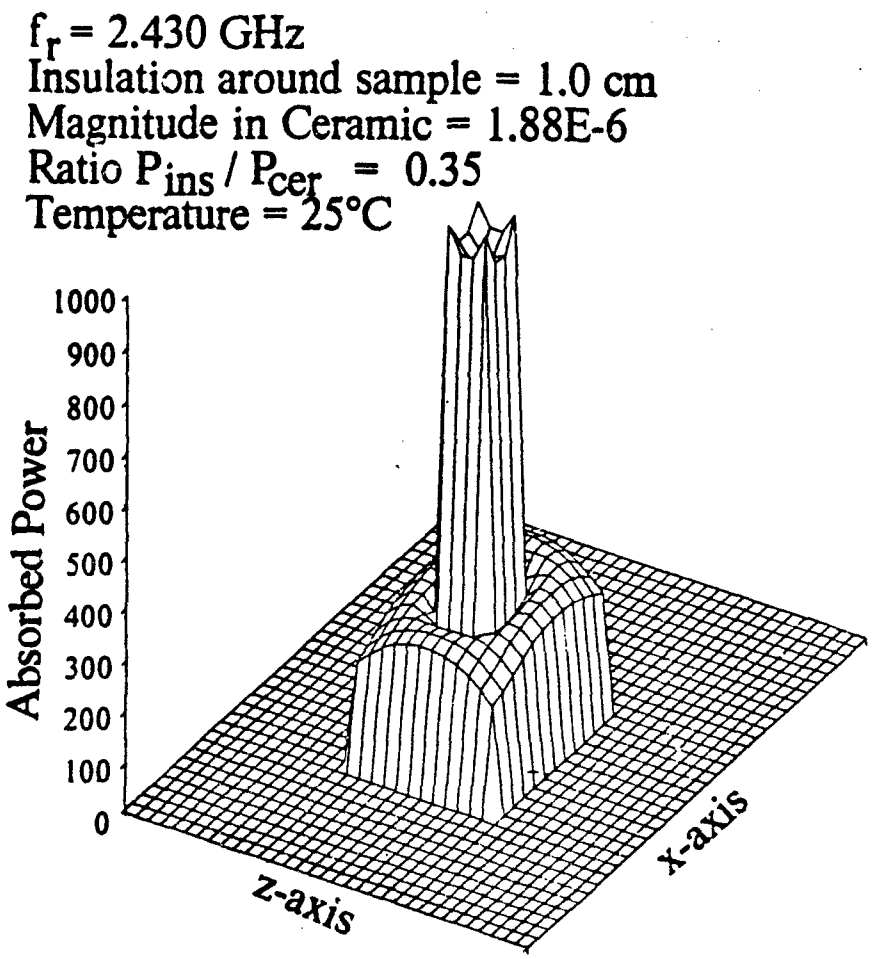


Figure 9. The specific absorption rate in a 1 cm^3 cube ceramic sample surrounded by 1-cm-thick insulation. At 25° C, the dielectric constant of the insulation was taken as e_r = 1.557 and the conductivity $\sigma = 15.37 \times 10^{-6}$ S/m and for the ceramic sample, e_r = 4.13 and $\sigma = 64.06 \times 10^{-6}$ S/m

To this end, a large collection of software packages developed by the NSF/IEEE Center for Computer Applications in Electromagnetic Education (CAEME) may be of great value. The CAEME Center, funded by NSF, is managed by the Institute of Electrical and Electronics Engineers (IEEE) to provide broad participation by universities and professional societies across the country. The Center is in its second year of operation, and thus far has sponsored the development of more than 15 software packages for electromagnetics education. These packages cover broad aspects of EM interactions with materials including fundamental aspects of fields, wave propagation and reflections, solutions of electrostatic and magnetostatic problems, transmission lines, waveguides, and concepts of radiation. A list of the packages is included in Table 2. To illustrate the relevance of the CAEME software to the area of microwave sintering of ceramics, let us consider a few examples. Consider the placement of an insulated ceramic sample in a microwave cavity. It is desired to visualize the electric-field distribution with and without the sample. If we assume an approximate 2D analysis, software packages such as Nos. 1, 12, and 15 listed in Table 2 may help in the visualization of fields within and around a dielectric object. They may also be used to demonstrate the role of the sample dielectric properties and the shape and size on the field distribution. Field values at interfaces between different materials may be calculated and the effect of placing a metallic fin (simulating the insertion of a thermocouple) near the sample may be investigated. Software packages such as Nos. 7, 8, and 12 may be used to demonstrate the significant difference in placing the metallic fin parallel or perpendicular to the electric field in a waveguide. Field configurations in different modes in waveguides of different cross sections, including rectangular, circular, and sectoral waveguides, may be visualized using software package No. 7.

Other software packages, such as Nos. 1, 2, 4, and 13 in Table 2 may be used to study the fundamental aspects of electromagnetic fields and to visualize their reflection, transmission, standing-waves, and polarization properties in dynamic fashion. The question-and-answer sections in software package No. 4 and the laboratory experience in software package No. 2 significantly help in emphasizing basic ideas and enhance the ability to physically interpret obtained results. A study of the fundamentals of transmission lines and their transient and steady-state analysis are discussed in software packages No. 5 and 6 of Table 2. Many interesting aspects of reflection, standing waves, and impedance-matching techniques may be studied using these packages.

An introduction to computational techniques that may be used to simulate realistic sintering experiments (such as the finite difference method described in an earlier section of this paper and also the method of moments) is included in the software package No. 10 in Table 2. In addition to tutorial sections, examples illustrating the various aspects of the solution procedure were given. The user may then use the software for designing or simulating cases of interest, including microstrip lines, ridge waveguides, and TM scattering by dielectric objects. The two videos in software packages No. 3 and 11 of Table 2 provide an exciting opportunity for reviewing tutorials on the basic concepts and fundamental aspects of electromagnetics. Video 3 is based on laboratory demonstrations, while Video 11 was prepared based on dynamic computational simulations using the FDTD method described in earlier sections of this paper.

CAEME is in the process of publishing the developed software in a book which will include diskettes of the software [8][1].

---

1 For more information on CAEME and the availability of the software, please contact one of the authors (M. F. Iskander) at (801) 581-6944.

Table 2. List of Software Packages Available from the NSF/IEEE CAEME Center.

Software Package Number	Description
1	"Electromagnetic Code for Solving Static and 2D Dynamic Field Problems on a Personal Computer," (IBM PC and compatibles), J. E. Lebaric, M. Melton, and J. Engel, Rose Hulman Institute of Technology
2	"Electromagnetic Waves" (IBM PC and compatibles), W. L. Stutzman, Virginia Polytechnic
3	"Experimental Demonstrations for Teaching Electromagnetic Fields and Waves," Video, Markus Zahn, MIT
4	"Visualization of Fields and Waves Using Hypercards" (Macintosh), Rodney Cole, University of California at Davis
5	"Nuline --- A Time- and Frequency-Domain Transmission-Line Analysis" (IBM PC and compatibles), F. M. Tesche, Tesche Associates, Dallas, Texas
6	"Simulator for Signal Propagation on General Multiconductor Transmission Lines" (IBM PC and compatibles), L. Carin, Polytechnic University, New York
7	"Interactive Software Package for the Analysis and Visualization of Electromagnetic Fields Inside Cylindrical Waveguides" (IBM PC and compatibles), A. Z. Elsherbeni, University of Mississippi
8	"Finite-Difference Solution of Rectangular Waveguides with Metallic Fins" (IBM PC and compatibles), Syracuse University
9	"Three-Dimensional Antenna and EM Field Displays on Personal Computers" (IBM PC and compatibles), J. C. McKeeman, Virginia Polytechnic
10	"Software Package for Introductory Course on Computational Electromagnetics" (IBM PC and compatibles), M. F. Iskander and O. Andrade, University of Utah
11	"Computer Generated Video for Teaching Some Concepts in Fundamental Electromagnetics" (Video, V. Cable, Lockheed Corporation
12	"Simulation of EM Phenomena Using FDTD Technique" (IBM PC and compatibles), K. Li and R. Shin, Massachusetts Institute of Technology
13	"MacEM" (Macintosh), K. Lonngren, University of Iowa
14	"Computer-Aided Instruction for Theory and Design of Linear Antenna Arrays" (IBM PC and compatibles), S. J. Blank, New York Institute of Technology
15	"Boundary Element Software Package for Solving Electrostatic Problems" (IBM PC and compatibles), P. Levin, Worcester Institute of Technology

DEVELOPMENT OF A KNOWLEDGE-BASED SYSTEM TO DESIGN EXPERIMENTS FOR MICROWAVE SINTERING

The development of a knowledge-based system for designing experiments for microwave sintering of ceramics in single- and multi-mode cavities represents another aspect of the role that may be played by software in this area. A knowledge-based system is a software that simulates the performance of a human expert and makes effective use of available information. It logically integrates analysis software, educational software, and data bases, and may be designed to provide nonlinear program navigation. It may also provide other benefits, including:

a. Integration of available software that addresses various aspects of the sintering process. This may include microwave simulation software, software for calculating temperature distribution patterns, and materials properties data base. With the continued developments in this area, additional software may be added or modified to improve modeling, simulation, and understanding capabilities.

b. The availability of a knowledge-based system helps in the propagation of knowledge and consequently speeds up commercialization of this technology.

c. Knowledge-based systems help in the capture and distribution of expertise and in an interdisciplinary area such as microwave sintering of ceramics may help preserve experiences by individuals and some of the knowledge otherwise considered endangered.

d. Knowledge-based systems may also be designed to include tutorials, possibly using CAEME educational software.

At the University of Utah a knowledge-based system for electronic package design was developed for IBM. Figure 10 shows the various components of this system. Electronic package design is similar to the microwave sintering process technology insofar as its interdisciplinary aspect. In the software developed at the University of Utah, NEXPERT [9] was used to develop the shell that contains the logical interaction between the various software packages and the design rules. The shell also coordinates access to the devices and materials data base included in the knowledge-based system. The shell was designed to access software for electrical, mechanical, and thermal analysis of electronic packages as well as a broad data base for material properties and device characteristics. Many design rules and checkpoints were included in the shell to help evaluate the obtained results from the simulation software and route consequent evaluation steps in a logically structured fashion. For example, if the electronic package design passes the wireability test and constraints, the knowledge-based shell may focus the analysis on electrical characterization of the packages to examine parameters such as cross-talk and various impedance mismatches. Based on the results from the electrical analysis, the expert system may suggest changes in the package design and hence rerun and check the wireability tests, or, if successful, will continue with other characterization aspects such as thermal and mechanical analysis. From the above discussion, it may be seen that considerable experience and a large number of evaluation rules go into the development of the shell. It simply emulates human expertise in the electronic package design.

We believe that the development of a knowledge-based system for microwave sintering of ceramics is timely and may have a significant impact on the rapid and effective commercial utilization of this technology.. The availability of software such as NEXPERT for the development of the shell, the inclusion of the FDTD 3D modeling software, and the inclusion of tutorial software such as that available from CAEME as well as dielectric and thermal properties

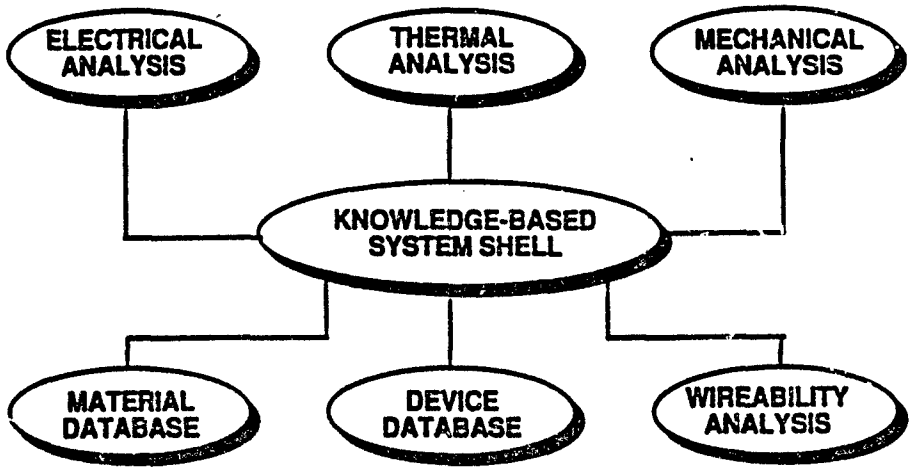


Figure 10. General flow chart of a knowledge-based system for electronic package analysis.

data bases, make the development of a useful and self-contained knowledge-based system possible and certainly within reach.

CONCLUSIONS

In this paper we presented various different roles that may be played by computer modeling, numerical techniques, and available software tools in the area of microwave processing of materials. In the area of training and understanding the fundamental aspects of EM interactions with materials, we described the CAEME software that provides a broad coverage of the fundamentals of electromagnetics theory and engineering. Videos of computer-generated movies and of experimental demonstrations of basic concepts and laws of electromagnetics are among the products of the CAEME Center.

The use of the FDTD method to model and simulate realistic microwave sintering in single-mode cavities was also discussed. It is believed that the developed model which accounts for the coupling characteristics of the feed iris, and accurately calculates the SAR distribution in insulated ceramic samples of complex geometries is the most accurate available to date. The developed model also calculates the Q of the cavity and the shift in the resonance frequency as a result of the reactive coupling of the iris. Results illustrating many of these features were presented.

Finally, the idea of developing a knowledge-based system to help maintain progress in the area of microwave processing of ceramics was discussed. A well-designed knowledge-based system mimics human expertise and may provide effective use of the developed simulation software, including tutorials and dielectric and thermal properties data bases. With the availability of

software such as NEXPERT suitable for the development of the system's shell, we believe that this suggestion is timely and is certainly worthy of serious consideration.

REFERENCES

1. M. F. Iskander, "Computational Techniques in Bioelectromagnetics," *J. Computer Physics Communication*, Special issue on Computational Electromagnetics, L. Shafai, Editor, 1991.

2. M. F. Iskander, "Computer Modeling and Numerical Techniques for Quantifying Microwave Interactions with Materials," *Microwave Processing of Materials*, W. Snyder, W. Sutton, M. F. Iskander, and L. Johnson, Coeditors, MRS Publication, Vol. 189, 1991.

3. M. Melton, J. E. Lebaric, and J. Engel, "Electromagnetic Code for Solving Static and Dynamic 2D Field Problems on a Personal Computer," presented at the 1991 ACES Symposium, Naval Postgraduate School, Monterey, CA, March 19-22, 1991. The paper and software will be included in the first CAEME book to be published soon.

4. L. Bielawski and R. Leward, *Intelligent Systems Design, Integrating Expert Systems, Hypermedia, and Database Technologies*, John Wiley and Sons, New York, 1991.

5. A. Taflove and K. R. Umashankar, "The Finite-Difference Time-Domain Method for Numerical Modeling of Electromagnetic Wave Interactions with Arbitrary Structures," in *Progress in Electromagnetic Research*, M. Morgan, Editor, Elsevier Science Publishing Co., New York, 1990.

6. D. H. Choi and W. J. R. Hoefer, "The Finite-Difference Time-Domain Method and its Application to Eigenvalue Problems," *IEEE Transactions on Microwave Theory and Techniques*, Vol. MTT-34, pp. 1464-1470, 1986.

7. K. S. Yee, "Numerical Solution of Initial Boundary Value Problems Involving Maxwell's Equations in Isotropic Media," *IEEE Transactions on Antennas and Propagation*, Vol. AP-14, pp. 302-307, 1966.

8. M. F. Iskander, O. Andrade, A. Virkar, H. Kimrey, R. Smith, S. Lamoreaux, C. Cheng, C. Tanner, R. Knowlton, and K. Mehta, "Microwave Processing of Ceramics at the University of Utah -- Description of Activities and Summary of Progress," *Proceedings of Symposium on Microwaves, Theory, and Applications in Materials Processing*, American Ceramic Society Meeting, April 28-May 2, 1991. Also in the *Proceedings of the 93rd American Ceramic Society Meeting*, this issue, 1991.

9. NEXPERT is available from Neuron Data Inc., 156 University Avenue, Palo Alto, CA 94301, (415) 321-4488.

ELECTROMAGNETIC MODELING OF SINGLE-MODE EXCITED MATERIAL LOADED APPLICATORS

Ben Manring and Jes Asmussen, Jr.
Michigan State University, Dept. of Electrical Engineering
East Lansing, MI 48824-1226.

Numerical modeling of the electromagnetic fields is investigated for a circular cylindrical cavity loaded with a coaxially positioned, circular cylindrical, homogeneous, lossy dielectric. Solution for the eigen-frequencies is accomplished by mode-matching techniques where the cavity is divided into a coaxial material-loaded waveguide region terminated on either end by an empty waveguide region. Fields in each region are expressed as infinite modal expansions. Appropriate field components are matched across the region boundaries to form an infinite characteristic matrix whose complex determinant is zero for each of the complex resonant eigenfrequencies. The model is used to describe resonant conditions for conductors and lossy dielectrics including nylon and alumina.

INTRODUCTION

Even though microwave cooking, drying, material processing, and other applications have been common uses of microwave power for over forty years, the design of specific microwave applicators is usually an empirical process. Whether multimode or single mode, microwave processing applicators are designed by a trial and error procedure. This experimental methodology is necessary because exact theoretical models have not been developed for applicators loaded with lossy materials. The development of models for such applicators would improve the understanding of microwave processing/heating and would enable the rapid design of optimized and controllable microwave processing systems.

As an initial attempt to model a lossy material loaded cavity the present investigation is concerned with the mode-matching solution for a circular cylindrical cavity of radius b and length L_s, loaded with a coaxially positioned, circular cylindrical,

isotropic, homogeneous, lossy dielectric of radius *a* and length *l* located at height h above the cavity bottom. The general loaded cavity configuration is pictured in Figure 1. A numerical model for such an applicator is described and single mode solutions are investigated as functions of load dimensions and complex dielectric constant. The importance of these solutions becomes apparent when it is recognized that microwave energy is transferred to the material through these single mode coupling windows.

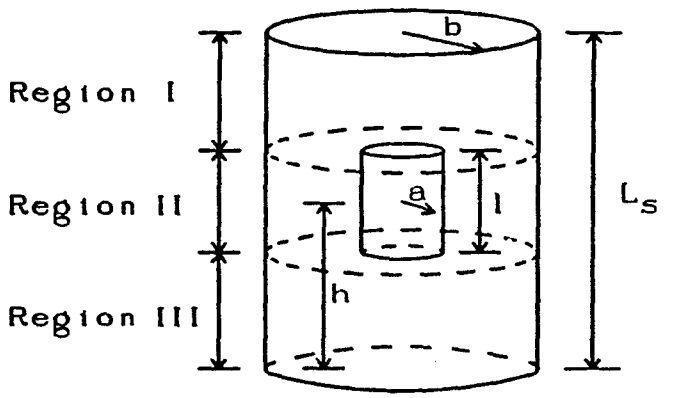


Figure 1. Coaxially Loaded Circular Cylindrical Cavity.

METHODOLOGY

The solution of electromagnetic boundary value problems in a region enclosed by conducting walls is usually accomplished in one of two ways: 1) finite element methods, or 2) mode-matching techniques. In cases where either the enclosing region or the material inside the region is irregular in shape or highly inhomogeneous in composition there is little choice but to use finite element methods to determine the resonant characteristics of the structure. However, if it is possible to consider the structure as a series of contiguous regions where the electromagnetic fields in each region can be written in terms of an expansion of simple modes, then the resonant characteristics of the system may be determined by mode-matching techniques.

If the nature of the resonant structure meets the above conditions, mode-matching offers the advantage over finite element analysis in understanding the modal composition of the electromagnetic fields. Knowledge of the modal composition of the fields

can be extremely useful in understanding and designing applicators for optimal processing of a variety of loads. By examining the modal coefficients and how they change with applicator and load parameters, process cycles can be intelligently designed and predicted.

LOADED CAVITY CONFIGURATION VARIATIONS

The general configuration of Figure 1 may assume one of two special cases depending upon the shape of the load. Figure 2 shows the case where the load length is equal to the cavity length, i.e., $h = \frac{1}{2} L_s$ and $l = L_s$. This configuration is referred to as cavity-short type. When $l < L_s$, as shown if Figure 1, the configuration is referred to as cavity-open type. The cavity-open type configuration includes cases where the load is more elongated and rod-shaped and cases where the load is flat and disk-shaped.

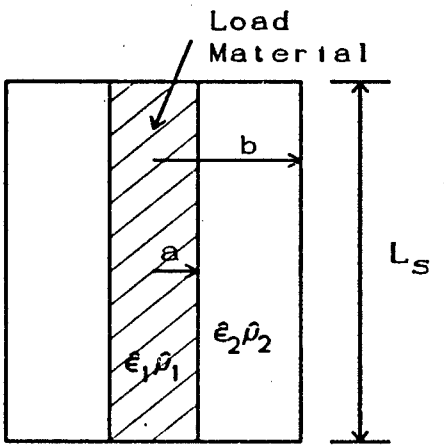


Figure 2. Cavity-Short Type.

In addition to the various geometrical configurations of the cavity and load, the dielectric constant of the load must be considered. For lossy materials, the dielectric constant, $\hat{\epsilon}$, is complex.

$$\hat{\epsilon} = \epsilon' - j\epsilon''. \tag{1}$$

For most materials, ϵ' falls into the range of 1 to over 100 while ϵ'' varies from 0, for a lossless dielectric, to over 10,000 for a good conductor. It should be noted that in general ϵ' and ϵ'' can also be functions of spacial coordinates (non-homogeneous) and directional (non-isotropic), although here we consider only homogeneous and isotropic cases.

NUMERICAL MODEL

As shown in Figure 1 the cavity is divided into three regions. Regions I and III are empty waveguide regions while region II is a coaxially loaded waveguide region. In order to solve for the eigenvalues of the cavity system, the eigenvalues for each of the waveguide regions must be found first. The empty region solutions can be either TM or TE with eigenvalues given by the zeros of Bessel's functions of the first kind and their derivatives. The constitutive relationship between the wavenumber and the propagation constants in the empty regions is[1]

$$\omega^2 \mu \epsilon_0 = k^2 = k_z^2 + k_\rho^2, \tag{2}$$

where $k_\rho = \frac{\lambda}{b}$ with b the cavity radius and λ a zero of an ordinary Bessel's function for TM modes or of the derivative of an ordinary Bessel's function for TE modes.

The fields in the coaxially loaded region can also be divided into TM and TE solutions for phi-symmetric (n=0) modes. For non-phi-symmetric modes the fields are neither TE nor TM and the eigenvalue equation is more complicated. The coaxially loaded waveguide eigenvalue equation is given in Equation (3) where $\hat{\epsilon}$ is the complex dielectric constant in the load region and the F's are combinations of Bessel's functions of the first and second kind using Harrington's notation.[2]

$$\begin{aligned}
&V_n W_n - U_n^2 = 0 \\
&V_n = k_{\rho 1} k_{\rho 2} \mu_0 (k_{\rho 2} F_2' F_4 - k_{\rho 1} F_2 F_4') \qquad (=0 \text{ for } TE_{n=0} \text{ solutions}) \\
&W_n = k_{\rho 1} k_{\rho 2} (\hat{\epsilon} k_{\rho 2} F_1' F_3 - \epsilon_0 k_{\rho 1} F_1 F_3') \qquad (=0 \text{ for } TM_{n=0} \text{ solutions}) \\
&U_n^2 = \left[\frac{n\gamma}{\omega a}\right]^2 F_1 F_2 F_3 F_4 (k_{\rho 1}^2 - k_{\rho 2}^2)^2 \\
&k_1^2 = \omega^2 \mu_0 \hat{\epsilon} = k_{\rho 1}^2 + \gamma^2 \\
&k_2^2 = \omega^2 \mu_0 \epsilon_0 = k_{\rho 2}^2 + \gamma^2
\end{aligned} \tag{3}$$

Equation (3) is also the characteristic equation for the cavity-short type geometrical configuration with

$$\gamma = \frac{q\pi}{L_s} \tag{4}$$

where L_s is the cavity length and q is an integer.

The solution to the general open-type configuration (Figure 1) involves finding the waveguide modes in each of the three regions, writing the field solution in each region as a sum over all of the modes for the region, and matching E_{tan} and H_{tan} fields at the region boundaries. The field matching equation yields an infinite matrix, which must be truncated to finite dimensions for calculation. The determinant of the matrix set equal to zero is the eigenvalue equation for the cavity system. This equation must be solved using a complex root-finding routine. Convergence to a solution determines how large the matrix must be to provide an accurate result.[3] The results in Figure 6 below were for a 5x5 matrix. The eigenvalue equation is solved after the following configuration variables have been specified: a, b, L_s, l, h, ϵ', and ϵ''. The numerical solution to the eigenvalue problem computes the loaded cavity complex resonant frequency and coefficients for the modal expansions.

EXAMPLE SOLUTIONS

Cavity-Short Type

A resonant frequency solution to the cavity-short type configuration for nylon is shown in Figure 3. The inside diameter of the cavity is 6" while the nylon rod through the cavity axis is 1" in diameter. Empty cavity and short-type numerical solutions from equations (2) and (3) are plotted as shown by the solid lines indicated in Figure 3 while the experimentally measured points are represented by open squares for the empty cavity and crossed circles for the short-type loaded cavity. Figure 3 demonstrates excellent agreement between theory and experiment.

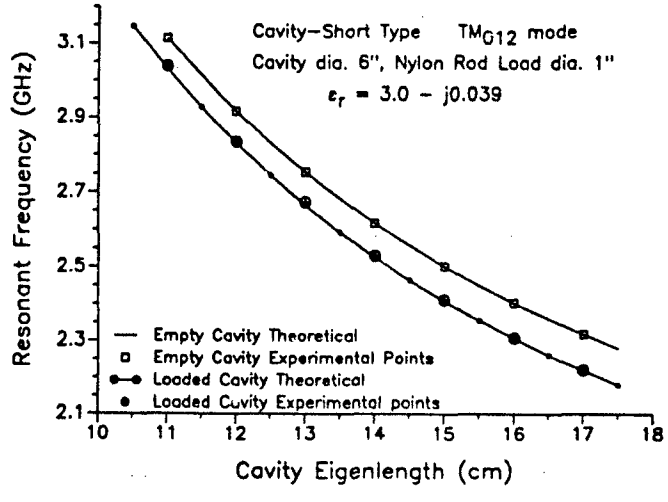


Figure 3. Cavity-Short Solution for Nylon.

A similar plot for alumina is shown in Figure 4. Figure 4 shows how the resonant frequency would change with a hypothetical change in the imaginary part of the dielectric constant for a cavity-short type heating configuration. It is interesting to note that as the loss factor increases from zero, the resonant frequency for a constant cavity length first drops, then rises again as the loss factor continues to increase into the range where the material becomes a good conductor.

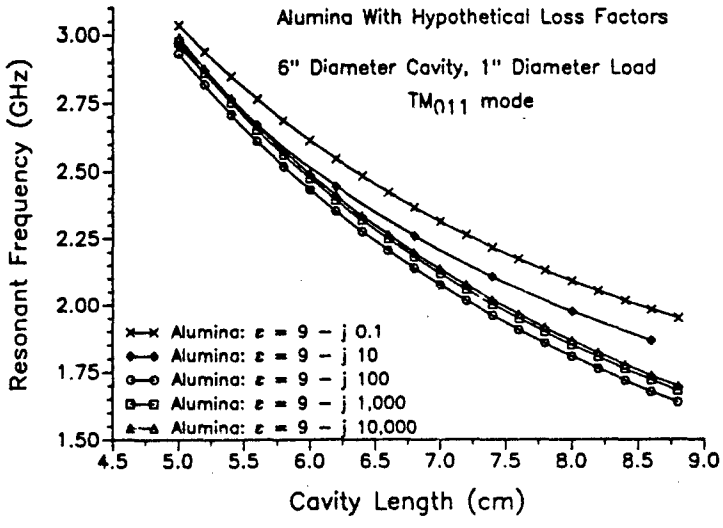


Figure 4. Cavity-Short Solution for Alumina with Hypothetical Losses.

Cavity-Open Type

A solution for cavity-open type TM modes when the load is a conductor has been attempted in the past.[4] However, due to a neglect of the TEM contribution in the loaded region, the solutions were in error. Figure 5 shows a plot of the open-type solution for the TM_{012} mode in a 6" diameter cavity with a 0.5" diameter conducting rod in the center for various rod lengths. As can be seen by examining Figure 5, experimental points coincide very well with the theoretical solution.

Figure 6 contains a plot of the resonant frequency versus load length for a cavity-open type configuration with a 0.5" diameter nylon load in a 6" diameter cavity. Experimental points are included for comparison with the theory. At either extreme, when the load length was zero (empty cavity) or when the load extended the cavity length (cavity-short type), the open-type solution gives the correct result. For other load lengths there is also good agreement between theory and experiment, although it must

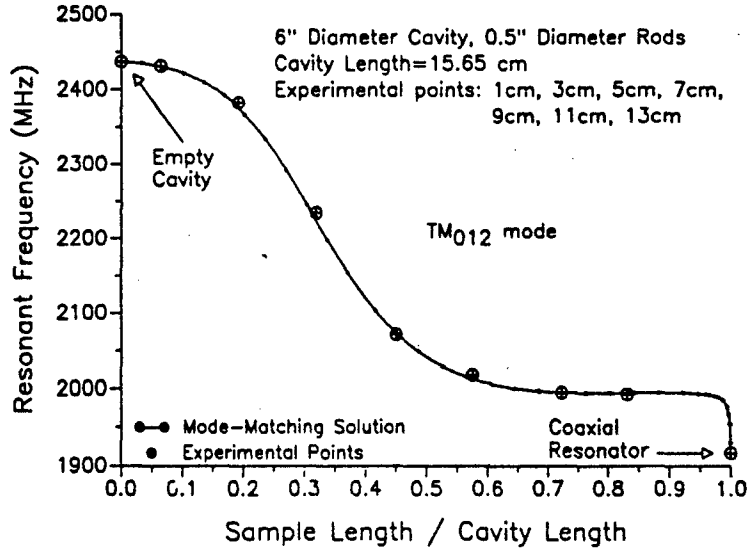


Figure 5. Cavity-Open Solution for Conducting Load.

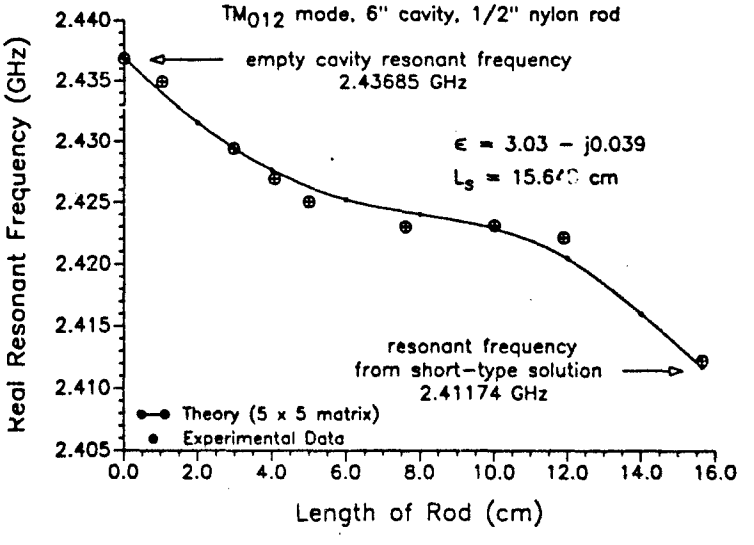


Figure 6. Cavity-Open Solution for Nylon Load.

be noted that the condition number of the characteristic matrix becomes too large to give accurate results at 16 digit precision if the matrix is truncated at more than five by five.

CONCLUSIONS

It has been shown that mode-matching provides an accurate means of calculating the modal wavenumbers and resonant frequencies of circular cylindrical cavities coaxially loaded with conductors or lossy dielectric materials. From this information the modal fields can be calculated and spatial energy dissipation in the load determined. Although there exists a numerical instability for large characteristic matrices for the dielectric load open-type solution, good agreement between theory and experiment is still possible. It is hoped that by using extended precision in the numerical calculations, even better agreement will be achieved.

The information made available by this technique is a valuable contribution to a more precise understanding of electromagnetic cavity heating of lossy materials. In addition to an exact understanding of heating materials in the circular cylindrical cavity, general trends in the change of resonant conditions with dielectric properties and load size and shape provide insight into the microwave heating of other materials variously configured in other applicators. This information should make predictive control and design of microwave applicators a viable alternative to the trial and error methods of the current technology.

References:

1. R. F. Harrington, *Time-Harmonic Electromagnetic Fields*, McGraw-Hill, 1961, 199.

2. Ibid., 221.

3. K. A. Zaki and A. E. Atia, "Modes in Dielectric-Loaded Waveguides and Resonators," *IEEE Trans. Microwave Thry. Tech.*, MTT-31, no. 12 (December 1983), 1039-1045.

4. D. M. Bolle, "Eigenvalues for a Centrally Loaded Circular Cylindrical Cavity," *IRE Trans. Microwave Thry. Tech.*, MTT-10, no. 3 (March 1962), 133-138.

MODELING MICROWAVE HEATING OF CERAMICS

Xiang Dong Yu ,Vasundara V. Varadan, Vijay K. Varadan
227 Hammond Building
Research Center for the Engineering of Electronic and Acoustic Materials &
Department of Engineering Science and Mechanics
The Pennsylvania State University
University Park, PA 16802

ABSTRACT

A method to simulate microwave heating of ceramics which has a temperature dependent dielectric property is developed here. In this simulation study, the impedance method is used to find the microwave energy absorbed by ceramics and a non-linear finite element method is used to determine the dynamic temperature profile in the ceramics during microwave heating. Using the developed method, the thermal runaway phenomenon in the microwave heating of ceramics is successfully simulated.With detailed analysis of the microwave energy absorption pattern in the ceramics, the effects of dielectric properties on microwave energy absorption by ceramics are discussed. The causes of non-uniform heating with microwave energy that has been observed in our laboratory are also investigated.

INTRODUCTION

The use of microwave energy is a new and exciting approach in ceramic processing. It has already been used in sintering, joining and melting of ceramics[1]. Since microwave heating is a volumetric process, it could provide uniform heating so that the temperature gradient which is observed in conventional rapid heating methods can be avoided. Rapid and uniform heating are important in the joining and sintering of ceramics. On the contrary, non-uniform heating is often observed in our laboratory with microwave sintering or joining. Therefore, it is of practical interest to simulate the phenomenon of microwave heating for better control and more efficient use. In spite of the significance of the problem, there is no comprehensive analysis available which would describe the behavior of ceramic materials exposed to electromagnetic radiation. Research by Iskander [2] and Watters et al. [3] has revealed some of the mechanisms of microwave heating of ceramics. However, the simulation of microwave heating of ceramics with a temperature dependent dielectric property is still lacking. In this paper, a method of simulating microwave heating of ceramics with temperature dependent dielectric properties is developed here. The impedance method is used to find the microwave

energy absorbed by ceramics. A non-linear finite element method is developed to determine the dynamic temperature profile in the ceramics during microwave heating. Using this developed method, the thermal runaway phenomenon in the microwave heating of ceramics is successfully simulated.With detailed analysis of the microwave energy absorption pattern in the ceramics, the effects of dielectric properties on microwave energy absorption by ceramics are discussed. The causes of non-uniform heating using microwave energy that has been observed in our laboratory are also investigated. In doing so, a better understanding of microwave heating of ceramics is realized.

THEORY

In order to simulate microwave heating of ceramics, it is necessary to find the electric and magnetic field strength inside ceramics and the absorbed microwave energy. Electric and magnetic fields are linked by Maxwell's equations, a group of linear differential equations. Assuming an $e^{-i\omega t}$ harmonic time dependence, Maxwell's equations can be expressed as follows,

$$\nabla \bullet (\varepsilon_0 \varepsilon_r E) = \rho_e \qquad (1)$$

$$\nabla \bullet (\mu_0 \mu_r H) = 0 \qquad (2)$$

$$\nabla \times E = j\,\omega \mu_0 \mu_r H \qquad (3)$$

$$\nabla \times H = \sigma E - j\,\omega \varepsilon_0 \varepsilon_r E \qquad (4)$$

where ε_0 and μ_0 are the permitivity and permeability in the vacuum, ε_r and μ_r are the relative permitivity and permeability of the material, σ is the conductivity of the material. **E** and **H** are the electric and magnetic field strength, respectively. The propagation of energy in the electromagnetic field can be deduced from this equation system and leads to Poynting's theorem

$$P = -\int_S [E \times H^*]\, dS \qquad (5)$$

which states that the mean energy, P, flowing into a surface, S, depends on the amplitude, distribution and prevailing phase of the electric and magnetic field.
By using Gauss' law, equation 5 can be converted into the volume integral which can then be resolved into three single integrals

$$P = j\omega \int \mu_0 \mu_r (H \bullet H^*)\, dv - j\omega \int \varepsilon_0 \varepsilon_r' (E \bullet E^*) dv$$

$$+ \omega \int \varepsilon_0 \varepsilon_r'' (E \bullet E^*) dv \qquad (6)$$

The first two integrals take account of the magnetic and electric fields respectively while the third represents the necessary dissipation in the dielectric in a general form. Therefore, the energy converted into heat by the alternating field is

$$P = \omega \varepsilon_0 \varepsilon_r'' \int_V (E \bullet E^*) dv \ (W) \qquad (7)$$

It increases according to the frequency , the square of the electric field strength and the imaginary part of the dielectric constant. Once the profile of ε'' as function of temperature and the electric field strength in the homogeneous body are known, it may be possible to study the thermal runaway conditions through the source-incorporated heat-diffusion equation. The diffusion of thermal energy in a homogeneous bound volume V is determined by the partial differential equation

$$\rho C_p \frac{\partial T}{\partial t} - K_h \nabla^2 T = p \qquad (8)$$

where ρ, C_p and K_h are the mass density , specific heat and thermal conductivity of the material, respectively. p is the microwave energy density absorbed by the material. At the boundary of the volume V, the boundary condition

$$K_h \, n \bullet \nabla T = h(T - T_0) + \varepsilon \sigma_r (T^4 - T_0^4) \qquad (9)$$

must be satisfied , in which h is the heat convection coefficient, ε and σ_r are the emissivity of the material and Stefan-Boltzmann constant. T_0 is the ambient temperature. The initial condition is

$$T(r, 0) = T_i \qquad (10)$$

This heat diffusion equation is analogous to the forced Fisher equation

$$T_t = T_{xx} + G(T) \qquad (11)$$

which is known to have chaotic behavior for specific initial and boundary conditions as investigated by Fisher [4] in 1937 and Rothe [5] in 1981.

DESCRIPTION OF THE MODEL

For simplicity, a ceramic slab with finite thickness under plane wave radiation is considered here as depicted in figure 1. The incident electric field is a monochromatic plane wave propagating in the z-direction and is polarized along the x-axis. To account for material non-linearity during microwave heating, the slab is further divided into layers so that the finite element method can be used accurately. It is assumed that each element has the same material properties during the microwave heating process at each temperature step. Since the ceramic slab is assumed to be very large, the problem becomes one-dimensional. In the following discussion, layers with smaller thicknesses will be considered as different media since they may have different material properties such as dielectric constant and loss factor which are functions of temperature during the microwave heating process.

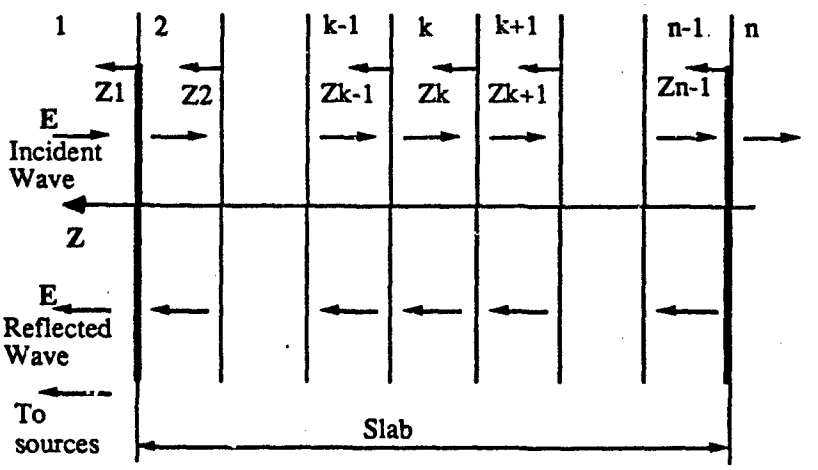


Figure 1. Ceramic Slab.

To simulate microwave heating of ceramics, the microwave energy absorbed by the ceramic slab must first be calculated. Therefore, the electric and magnetic fields in the ceramic slab have to be determined first. The electromagnetic field inside a dielectric body of arbitrary shape is difficult to determine. For the model considered here, an impedance method [6] is applied and proven to be effective to account for material non-linearity.

The application of the impedance method can be described as follows. When an electric field is incident on the ceramic slab, which is now assumed to be composed of several different layer, multiple reflection will occur in the different layers leading to positive and negative traveling waves. A generalized reflection coefficient is defined for any layer as the ratio of the incident and reflected field. Hence, the

total field can be represented by the positive traveling wave and the generalized reflection coefficient. In the first layer, the incident field is known and the reflected field is unknown. For the Nth layer, the generalized reflection coefficient is zero because there is no negative traveling wave. The total field impedance, which is complex and position dependent, is defined as the ratio of electric field over the magnetic field. For the Nth layer, the total field impedance will be equal to the field impedance for that layer. At an interface, the total field impedances for adjacent layers are equal due to the field boundary condition at that interface. With this boundary condition, the total impedance at different interfaces can be found. Hence, the reflected field in the first layer is found. By using the boundary condition that the electric field is continuous at each interface, the electromagnetic field strength in each layer is readily found. The resulting field can then be used to calculate the microwave energy absorbed by that layer.

When the microwave energy absorbed by the slab is known, the heat diffusion equation can be used to calculate the temperature variation with time and position. Since the dielectric constant and loss factor are functions of temperature, the microwave energy absorbed by the ceramic slab is also a function of temperature. Hence, the heat diffusion equation becomes non-linear. A non-linear finite element method is therefore needed to find the dynamic temperature distribution profile. At the surface of the ceramic slab, radiation link elements are used to account for radiation heat loss. Conduction loss is neglected since the radiation loss is the prime heat loss at high temperature. The detailed implementation of the non-linear analysis is as follows. The time step to do the non-linear analysis is designated first. The temperature at the end of time step is then estimated. The material properties at the middle of the temperature increment are used for each media. The microwave energy absorbed by each media with different dielectric properties is calculated according to the technique described above. The temperature distribution is then obtained by using power absorption data. The computed results will be compared with the prior estimated temperature. Such an iteration procedure will continue until the difference between the estimated and calculated temperature reaches a prescribed value.

RESULTS AND DISCUSSION

Microwave Energy Absorption by Ceramics

By using the technique stated above, the effects of the dielectric constant and the loss factor on the power absorption by ceramics are considered. Figure 2 gives the comparison of power absorption by ceramic slabs with the same dielectric constant and different loss factors. The increase in loss factor will dramatically increase the ability of the ceramic slab to absorb microwave energy. Figure 3 shows that with the increase of both dielectric constant and loss factor, the uniformity and ability of power absorption by ceramics are also increased.

Simulating Microwave Heating of Ceramics

The developed non-linear finite element method is used in this case to find the dynamic temperature profile of a ceramic slab under plane wave radiation

considering changes in both the dielectric constant and the loss factor with temperature. The analysis procedure is displayed in figure 4. The data of dielectric constant and loss factor change with temperature are taken from Fukushima et al.[7]. The incident microwa ve power flux is 30kw/m^2. The microwave frequency is taken to be 6 GHz to be consistent with the dielectric data.

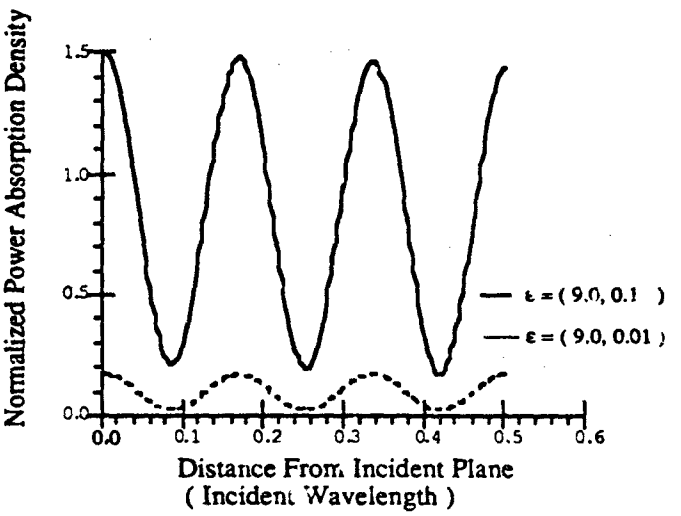


Figure 2. Microwave Power Absorption for Slabs with Different Loss Factors.

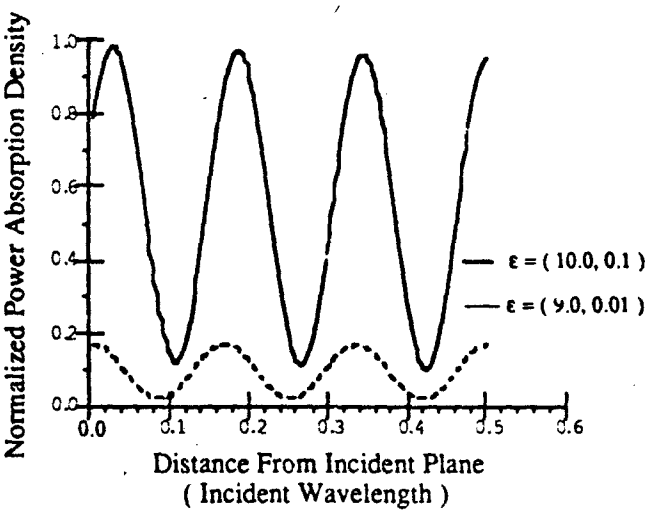


Figure 3.Microwave Power Absorption for Slabs with Different Dielectric Properties.

The mass density, specific heat and thermal conductivity are taken to be 4g/cm^3, 1.125 j/g °C and 10w/cm^2, respectively. The thickness of the plate is taken to be 5.08 cm. The finite element analysis routine on ANSYS is implemented in the calculation. The calculation is done on a VAX-11/780 computer. The CPU time is 79 seconds.

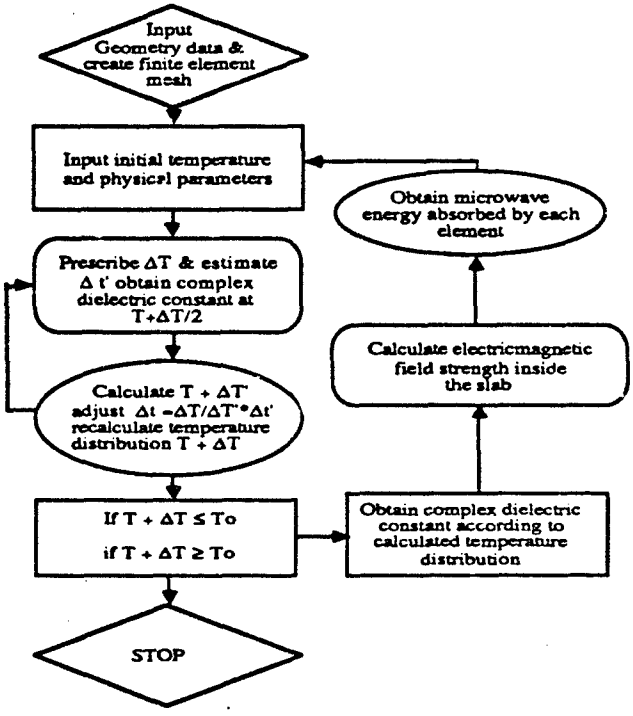


Figure 4. Procedures for Simulating Microwave Heating of Ceramics.

Figure 5 gives the temperature variation with time at 0.01m inside the slab from the microwave incident plane. The temperature increases slowly at the beginning and rapidly after 600°C.

Figure 6 displays the temperature profile over the thickness of the slab. An appreciable temperature gradient is observed. This temperature gradient is caused by non-symmetric microwave radiation of the ceramic slab and radiation heat loss at the boundary, which subsequently results in a non-uniform power absorption by the ceramic slab. If symmetric radiation is realized, i.e., microwave radiation is from both sides of the slab, the uneven heating will result from boundary radiation heat loss only and the center of slab will have the highest temperature. Hence, the radiation heat loss at the boundary is the main contribution to the non-uniform heating with microwaves observed in our laboratory where the ceramic sample is melted at the center while the boundary is still intact. In order to prevent this effect, good insulation must be used at the boundary. Also, in practice, the ceramic sample needs to be rotated continuously to prevent any uneven radiation. Figure 7 shows

the variation of total microwave energy absorbed by the ceramic slab verse the temperature variation at 0.01m inside the slab from microwave incident plane. It indicates that as the ceramic becomes hot, its energy absorption ability is increased. Therefore, thermal runaway is realized in microwave heating.

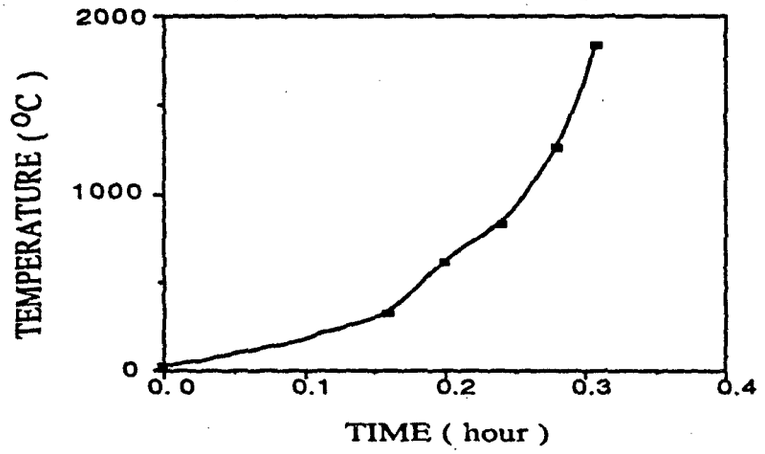


Figure 5. Dynamic Temperature Profile 0.01m inside the Slab from the Incident Plane.

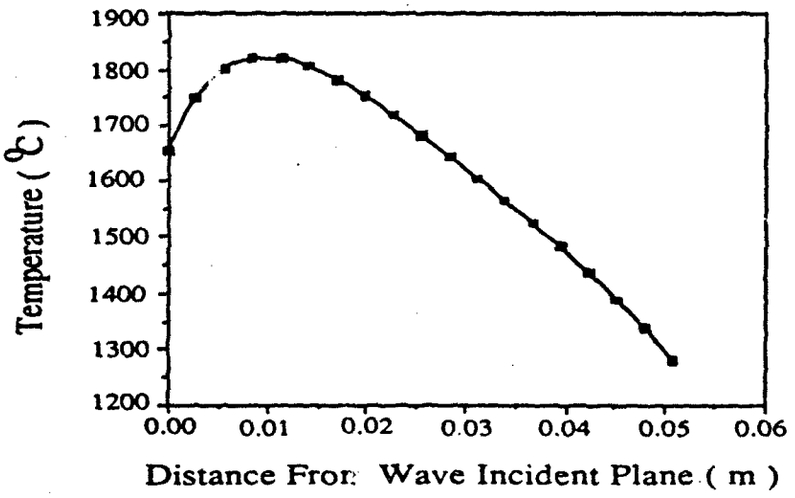


Figure 6. Temperature Distribution over the Thickness of the Slab.

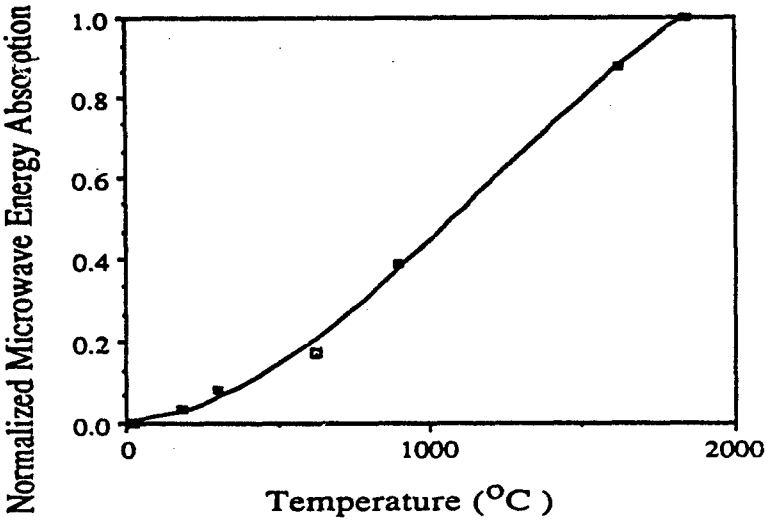


Figure 7. Total Microwave Energy Absorbed by slab vs. Temperature.

CONCLUSION

A method of modeling microwave heating of ceramics is developed here. The results show that increasing the dielectric constant could increase microwave power absorption uniformity while increasing the loss factor could increase the material's ability to absorb microwave energy. It is found that non-uniform heating observed in the laboratory can be caused by boundary radiation loss and non-uniform radiation by the microwave source. Through this research, it is observed that the dielectric property of a material at elevated temperature has a very important role in designing microwave processing technique. In microwave sintering of ceramics, the green sample changes its microstructure during microwave heating. Its dielectric properties change with not only temperature but also microstructure. Hence, the characterization of the dielectric property of ceramics during microwave sintering is very important . In doing so, we are not only able to control the sintering process but also able to understand thoroughly the mechanism of microwave sintering. Therefore, we need to develop a method to dynamically characterize the dielectric property of materials with temperatures as well as model microwave heating for the ceramic samples of complicated shapes.

REFERENCES

1.W.H Sutton, M.H. Brooks and Irving J. Chabinsky, Microwave Processing of Materials, Mat. Res. Soc. Symp. Proc., Vol.124 , 1988.
2. Magdy F. Iskander, "Medical and Biological Application of Electromagnetic Techniques -- A Relevant Experience to the Microwave Processing of Material Research", Mat. Res. Soc. Symp. Proc., Vol. 124, pp.69-119,1988 Material Resaerch Society.

3. D.G. Watters, M.S. Brodwin and G.A. Kriegman, "Dynamic Temperature Profiles for a Uniformly Illuminated Planar Surface", Mat. Res. Soc. Symp. Proc., Vol.124. pp. 129-34, 1988 Material Research Society.
4. R.A.Fisher , " The Waves of Advance of Advantageous Genes", Ann. Eugenics,Vol. 7, pp.355-68, 1937.
5. F. Rothe, " Convergence to Pushed Fronts", Rocky Mt. J. Math, Vol.11, pp.617-33, 1981.
6. V.V.Varadan," Wave Propagation and Scattering", Lecture Notes.
7. H. Fukushima, T. Yamanaka and M. Matsui, " Measurement of Dielectric Properties of Ceramics at Microwave Frequency", J. Japan Soc. of Prec. Eng., Vol.53, pp.743-48 , 1987.

Microwave Heating of Ceramics

GREGORY A. KRIEGSMANN
Department of Mathematics
Center for Applied Mathematics and Statistics
New Jersey Institute of Technology
University Heights
Newark, NJ 07102

ABSTRACT

The heating of a ceramic slab under TM-illumination is modeled and analyzed in the small Biot number regime. The steady state temperature is nearly constant in this limit and its value is a function of the microwave power. This function is multivalued when the electrical conductivity is modeled as an exponential function of temperature. Limiting cases and examples are presented and physically interpreted.

INTRODUCTION

Although the use of microwaves to heat and dry materials has gained acceptance in many industries, the basic understanding of these processes still remains somewhat empirical due to their highly nonlinear character. This is certainly the case with ceramic sintering. The mathematical description of this process is fraught with nonlinearities; the electrical conductivity which is present in both Maxwell's equations and the heat equation is highly temperature dependent at the temperatures required for sintering. Moreover, the thermal boundary conditions must take into account both convective and radiation heat loss. The result is a highly nonlinear initial-boundary value problem.

In previous works we have studied the heating of both electrically very thin [1,2] and very thick [3] ceramic slabs. In both cases the temperature distribution had little or no effect on the electric field. In this paper we will give the results for a slab of thickness comparable to a wave length where the temperature distribution significantly affects the electric field. For conductivities which increase with temperature we deduce an S-shaped response curve relating the slab temperature to the microwave power. The upper branch of this curve owes its existence to a nonlinear skin effect wherein the interior of the slab is shielded from the microwaves. Under the proper conditions this curve clearly explains the experimentally observed

phenomenon of thermal runaway which results in the destruction of the ceramic by melting [4,5].

FORMULATION

The formulation we now present assumes a time harmonic electric field and, in general, a time dependent temperature distribution. Although the governing equations do not admit exactly such a physical solution, the equations we present are in fact the leading order equations of an asymptotic theory. This theory is based upon the fact that the time required for heat to diffuse an electromagnetic wavelength is much larger than the period of a microwave. It yields the standard time harmonic vector wave equation for the electric field and an averaged diffusion equation for the temperature distribution in which the electromagnetic source term has been integrated over a microwave period.

Within this framework, we assume that a plane, time harmonic electromagnetic wave of frequency ω impinges normally upon an isotropic ceramic material which fills the region $0 < x < d$. A portion of the wave scatters from the interface $x = 0$, a portion penetrates the slab and heats the material, and the remaining portion is transmitted through the interface $x = d$. In the free space regions $x < 0$ and $x > 0$, the electric field is given by the real parts of

$$\mathbf{E} = E_0[exp(ikx - i\omega t) + \rho\, exp(-ikx - i\omega t)]\mathbf{k}, \quad x < 0, \tag{1}$$

$$\mathbf{E} = E_0[\tau\, exp(ikx - i\omega t)]\mathbf{k}, \quad x > d, \tag{2}$$

respectively, where E_0 is the strength of the incident field, $k = \omega/\sqrt{c}$, c is the speed of light in free space, τ is the transmission coefficient, and ρ is the reflection coefficient. Both τ and ρ are to be determined.

The electric field which penetrates the ceramic and interacts with the material is given by the real part of $\mathbf{E} = [U(x)exp(-i\omega t)]\mathbf{k}$, where U satisfies

$$\frac{d^2U}{dx^2} + k_1{}^2[1 + i\frac{\sigma(T/T_A)}{\omega\epsilon_1}]U = 0, \qquad 0 < x < d. \tag{3}$$

In this equation ϵ_1 is the permittivity of the ceramic, which is assumed to be constant, $k_1 = \frac{\omega}{c}\sqrt{\epsilon_1/\epsilon_0}$, ϵ_0 is the permittivity of free space, T_A is the ambient temperature in the absence of microwave radiation, T is the temperature of the slab in the presence of radiation, and $\sigma(T/T_A)$ is the conductivity of the slab. At the ambient temperature, T_A, the conductivity takes the value σ_A, i.e., $\sigma(1) = \sigma_A$. Implicit in the definition of k_1 is our assumption that the magnetic permeability of the ceramic is identical to that of free space, μ_0.

From the continuity of the tangential electric and magnetic fields at $x = 0$ and $x = d$, we deduce that U and its derivative are continuous there. Combining this fact with (1-2) and eliminating τ and ρ , we find that U satisfies the boundary conditions

$$\frac{dU}{dx} + ikU = 2ikE_0, \qquad x = 0, \tag{4}$$

$$\frac{dU}{dx} - ikU = 0, \qquad x = d. \tag{5}$$

Within the ceramic region the electromagnetic wave interacts with the material and increases its temperature through ohmic and dipolar heating. The temperature evolves according to the equation

$$\frac{\partial T}{\partial t} = \frac{\partial^2 T}{\partial x^2} + \frac{\sigma(T/T_A)}{2K}|U|^2, \qquad 0 < x < d, \tag{6}$$

where t is the nondimensional time which was scaled with respect to the time required for heat to diffuse an electromagnetic wavelength. In (6) K is the thermal conductivity which is assumed to be constant. We also require that the temperature satisfies the surface heat balances

$$K\frac{\partial T}{\partial x} = h(T - T_A) + se(T^4 - T_A^4), \qquad x = 0, \tag{7}$$

$$-K\frac{\partial T}{\partial x} = h(T - T_A) + se(T^4 - T_A^4), \qquad x = d, \tag{8}$$

where h is the convective heat constant, s is the radiation heat constant, and e is the emissivity of the surface.

The nonlinear character of the problem is now apparent: the electric field propagates through the ceramic and affects the temperature distribution through its presence in (6). This in turn changes the electrical conductivity of the material, σ, which affects the propagation through its presence in (3).

Analysis

We begin by integrating the equation (6) across the width of the slab. Then, using integration by parts on the term involving the second derivative and applying the boundary conditions (7-8), we obtain

$$\frac{\partial}{\partial t}\int_0^d T\,dx = -N(T_1) - N(T_0) + \frac{1}{2K}\int_0^d \sigma(T/T_A)|U|^2\,dx \tag{9}$$

$$N(Z) = \frac{h}{K}(Z - T_A) + \frac{se}{K}(Z^4 - T_A^4) \tag{10}$$

This states that the rate of increase of thermal energy equals the power added by the microwave source minus that which is removed at the surface by convection and radiation. A steady state temperature distribution will be achieved when these powers are equal. When this occurs we have

$$N(T_1) + N(T_0) = \frac{1}{2K}\int_0^d \sigma(T/T_A)|U|^2\,dx. \tag{11}$$

The form of (10) suggests that the two nondimensional parameters

$$B_1 = hd/K \quad \text{and} \quad B_2 = sedT_A^3/K \tag{12}$$

play a fundamental role in the description in the heating process. The parameter B_1 is the Biot number [6], which is a measure of the relative effects of convection and conduction, the constant B_2 is the radiation equivalent of the Biot number which is a measure of the relative effects of convection and radiation. Typical values for B_1 and B_2 of a ceramic slab are of the order of 0.0001 [2,7]. In a recent study [8] we have exploited the size of these parameters to obtain an asymptotic approximation to the steady state solution of (3-8) as $B_1 \to 0$ with B_2/B_1 held fixed. That is, the effects of radiation and convection were weighed equally. In this limit we found

$$T = T_0 + O(B_1) \quad \text{and} \quad U = U_0 + O(B_1) \tag{13}$$

where the term $O(B_1)$ represents an error which is of the same order as B_1, T_0 is a constant, and U_0 is the electric field satisfying (3-8) with T replaced by T_0. We note here that the temperature is nearly constant because the slab is almost thermally insulated when $B_1 \to 0$.

We obtain the relationship between the steady state temperature T_0 and the applied microwave power, in this limit, by combining (11) and (13). It is

$$2N(T_0) = \frac{\sigma(T_0/T_A)}{2K} \int_0^d |U_0|^2 \, dx. \tag{14}$$

This formula implicitly gives T_0 as a functional of the electric field U_0 within the slab. A more transparent version of this relationship is

$$p = 2\frac{(v-1) + \frac{B_2}{B_1}(v^4 - 1)}{\frac{\sigma(v)}{\sigma_A} Q} \tag{15}$$

$$Q = \frac{1}{d} \int_0^d |U_0/E_0|^2 \, dx \tag{16}$$

where $v = T_0/T_A$ and $p = d\sigma_A E_0^2/hT_A$. The parameter p is the dimensionless ratio of the power generated by a uniform electric field in a slab of thickness d and conductivity σ_A to the power lost by conduction at the slab surface with temperature T_A. Since p is proportional to E_0^2, the relationship (15-16) implicitly gives the temperature T_0 as function of the incident power. This is our fundamental relationship which we have also derived in a more rigorous mathematical manner in Reference 8.

LIMITING CASES

We shall now deduce from our above results two limiting cases which we have studied elsewhere. In the first limit we take $d \to 0$ and hold k_1 and k fixed. This is the thin slab approximation in which the solution of (2) reduces to $U_0 = E_0$. In this limit the electric field is uniform throughout the ceramic. Equation (16) remains

valid and Q becomes one. The resulting expression is identical to the one obtained in Reference [1] which was deduced by a formal mathematical approach.

The second limit is the case where $d \to \infty$ and $\sigma \to 0$, independently. First, we let $d \to \infty$ with k and k_1 held fixed. In this limit we deduce that U_0 behaves as a damped plane wave which propagates into the slab. Computing Q and inserting the results into (15-16) we obtain an expression for p as a function of v. Taking the limit of this formula as $\sigma \to 0$, we obtain the result presented in [3] which was obtained by completely different reasoning. This is the case of a very thick ceramic slab with weak losses.

EXAMPLES AND DISCUSSIONS

An examination of the conductivity data in [9] shows that the exponential representation

$$\sigma(T/T_A) = \sigma_A exp[\chi(T/T_A - 1)] \tag{17}$$

is an appropriate conductivity model for certain ceramic materials. Substituting (17) into (15-16), performing the necessary integration to obtain Q from (16), and inserting these expressions into (15) implicitly gives v as a function of p. Figure 1 displays this relationship for $B_2/B_1 = \alpha = 0.1$, $\sigma_A/\omega\epsilon_1 = \mu = 0.001$, $k_1 d = 1.414$, $kd = 1$, and $\chi = 0.78$. We observe from the figure that v is a multivalued function of p; the lower and upper branches represents stable steady state temperatures by virtue of our analysis found in Reference 8. The middle branch accordingly is unstable. When the power is increased steadily from zero the temperature follows the lower branch until reaching the first critical power, p_{c1}. At this point the process of loosing thermal energy to the surrounding medium is saturated, in the sense that any increase in microwave power will destroy the possibility of a steady state temperature distribution. Thus, when the power is increase beyond this point the temperature jumps to the upper branch at v_{c2}. If the temperature v_{c2} is greater than the melting temperature, then the sample will melt and the ceramic slab will be destroyed.

We next show the effect of changing the thickness of the slab, d, in Figure 2. In all three cases we kept $\alpha = 0.1$, $\chi = .78$, and $\mu = 0.001$ and set $(kd, k_1 d) = (1., 2.), (.25, .5)$, and $(.0625, .125)$. We find that the effect of decreasing d is to decrease p_{c2} and increase the corresponding temperature. Thus, as $d \to 0$ the curve approaches the result of the thin slab [8] where the hysteresis effect is lost. Since the electric field is a constant in the thin slab model, it is clear that the hysterisis effect is caused by the temperature dependence of the electric field in the present theory. The upper temperature branch comes about because the electrical conductivity begins to quench the electric field within the ceramic and this in turn reduces heating.

On the other hand, we observe from Figure 2 that p_{c2} increases and v_{c2} decreases as d is made larger. In the limit as $d \to \infty$ the curve will become monotonic so that a given p yields only one value of v. Thus in this limit, we reproduce the thick slab results [3].

CONCLUSIONS

We have presented a simple mathematical analysis of a microwave irradiated ceramic slab in the small biot number limit in which the slab is essentially insulated. The relatively small amount of heat loss at the surface accounts forthe multivalued temperature response as a function of microwave power. The upper branch of the temperature response curve owes its existence to a nonlinear skin effect which tends to shield the ceramic at high temperatures from the incident microwave. This multivalued response gives a plausible explanation for the thermal runaway phenomenon which often occurs in the microwave sintering of ceramics.

This work was supported by the Air Force Office of Scientific Research Under Grant No. AFOSR 91-0252

REFERENCES.

1. Brodwin, M. E., Kriegsmann, G. A., and Watters, D. G., "Temperature Instabilities in a Thin, Uniformly Illuminated Ceramic Slab", **IEEE MTT**, submitted.
2. D. G. Watters, "An Advanced Study of Microwave Sintering", Ph.D. Dissertation, Northwestern University, 1988.
3. Kriegsmann, G. A., Brodwin, M. E., and Watters, D. G., "Microwave Heating of a Ceramic Half-Space", **SIAM J. Appl. Ma.**, Vol. 50, No.4, pp.1088-98,(1990).
4. Brodwin, M. E. and Johnson, D. L., "Microwave Sintering of Ceramics", MIT-S, K-5, pp. 287-288, (1988).
5. Roussy, G., Bennani, A., and Thiebiant, J., "Temperature Runaway of Microwave Irradiated Materials", **Journal of Applied Physics**, Vol. 62, pp. 1167-1170,(1987).
6. Incropera, F. P. and DeWitt, D. P., "Introduction to Heat Transfer", Wiley, N.Y., 1985.
7. Kingery, W. D., Bowen, H. K., and Uhlman, D. R., "Introduction to Ceramics", Wiley, N.Y., 1976.
8. Kriegsmann, G. A., "Microwave Heating of a Ceramic Slab", Proceedings of the Eleventh Dundee Conference on Differential Equations, Dundee, Scotland, July 1990, in press; Report No. 27, Center for Applied MAthematics and Statistics, New Jersey Institute of Technology, Newark, 1990.
9. W. B. Westphal, "Dielectric constant and loss measurements on high-temperatu materials", Laboratory for Insulation Research Technical Report, MIT, October 1963.

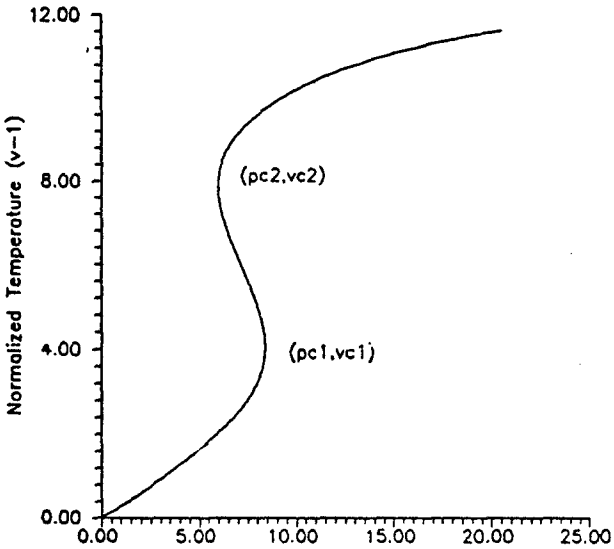


Figure 1. Normalized Power(p)

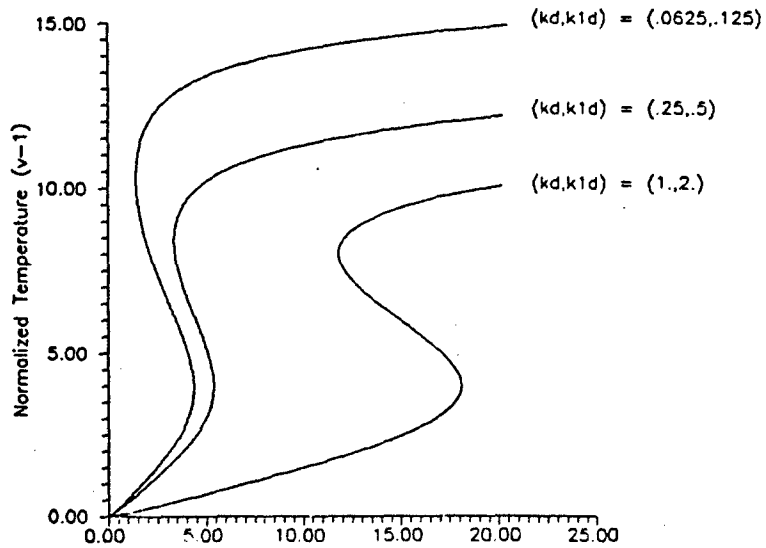


Figure 2. Normalized Power(p)

MODELS OF NONTHERMAL EFFECTS ON IONIC MOBILITY DURING MICROWAVE PROCESSING OF CRYSTALLINE SOLIDS

J.H. Booske,* R.F. Cooper,** I. Dobson,* and L. McCaughan*
* Department of Electrical and Computer Engineering
**Department of Materials Science and Engineering
University of Wisconsin
Madison, WI 53706

ABSTRACT

Models for nonthermal effects on ionic motion during microwave heating of crystalline solids are proposed to explain the anomolous reductions of activation energy for diffusion and the overall faster kinetics noted in microwave sintering experiments and other microwave processing studies. Radiation energy couples into low frequency elastic oscillations, generating a nonthermal phonon distribution that enhances ion mobility and diffusion rates. It is argued that the effect of the microwaves is not to reduce the activation energy, but rather to render the use of a "Boltzmann" thermal model inappropriate for the inference of activation energy from sintering-rate or tracer-diffusion data. Mechanisms are discussed for how such photon/phonon coupling might occur.

INTRODUCTION

Numerous researchers have investigated the use of microwave radiation for sintering ceramics.[1] Most of these studies have been motivated by the expectation of more uniform and rapid heating, since the microwave radiation is absorbed directly inside the object, rather than depending on inward conduction from the surface. Thus, microwave sintering might yield some of the advantages of hot pressing (microstructural uniformity, strength, theoretical density, etc.) while permitting efficient, pressureless processing of complicated, premachined shapes, as in conventional sintering.

Experimental results supporting such expectations have been recently reported.[2-4] Moreover, the data reported in these studies suggest that different microscopic mechanisms for the motion of ions are responsible for the differences between microwave and conventional sintering. For example, experiments with alumina suggest an apparent reduction in activation energy of 60-70% during microwave sintering when compared with conventional (pressureless) sintering.[2] Specifically, the activation energy inferred from Arrhenius plots of densification rates for the conventional process was 575 kJ/mole (~ 6 eV), compared to an inferred activation energy of 170 kJ/mole (~ 1.8 eV) for the microwave process. In both approaches equal bulk "temperatures" were maintained based on thermocouple measurements. In similar measurements with single crystal sapphire,[3] microwave heating was observed to yield enhanced tracer diffusion kinetics for $^{18}O^{2-}$.

For the single crystal experiments, empirically inferred activation energies for ion diffusion based on a thermal process model were 20% lower for microwave versus conventional heating.[3]

NONTHERMAL HYPOTHESIS

In another paper,[5] we argued that for the parameter regimes relevant to sintering, the activation energy is largely determined by intrinsic characteristics of the polycrystalline compound--i.e., the atomic bonds and molecular structure. Hence, it is very improbable that microwave heating alters either the atomic/molecular structure or the activation energy. For an alternative explanation, we must recognize that inferring activation energy values from plots of logarithms of densification rates versus inverse thermocouple readings assumes two things:

1. the ion thermal motions are characterized by a thermalized Maxwell-Boltzmann energy distribution, and

2. the measuring device (e.g., thermocouple, IR pyrometer, optical fiber) provides an accurate measure of the average kinetic energy of the ions--specifically, the "temperature" for a Maxwell-Boltzmann distribution.

In the case of microwave sintering, it is possible that one or both, of these assumptions is incorrect. Thus, the effects of the microwaves would not be to reduce the activation energy, but rather to render the use of a "Boltzmann-like" thermal model inappropriate for the inference of activation energy. In particular, we propose that the microwave radiation excites a nonthermal phonon distribution in the (poly)crystalline lattice. This translates into a nonthermal (i.e., non-Boltzmann) energy distribution, thereby enhancing the mobility of crystal lattice ions. Ultimately, this leads to enhanced point defect diffusion and to enhanced sintering rates. It is also believed that similar nonthermal effects are responsible for unusual observations reported in other microwave heating processes.[6] In the remainder of this paper, we briefly review candidate channels for resonant generation of nonthermal phonon distributions and then outline how the corresponding nonthermal ion energy distribution, can lead to apparent enhancement of point defect mobility.

GENERATION OF NONTHERMAL PHONON DISTRIBUTIONS

In conventional sintering, hot gas molecules collide with surface ions of the ceramic compact. Thus, kinetic energy first transfers to those ions on the macroscopic surface, followed by subsequent conduction to the ceramic bulk interior. Since the surrounding gas molecules have a Boltzmann distribution of random thermal motion, it is reasonable to assume that this heating process maintains a thermal, Maxwell-Boltzmann distribution for the random vibrations of ions in the (poly)crystalline lattice, i.e.,

$$f_{th}(E) = \frac{2}{\sqrt{\pi}\, T^{3/2}} \sqrt{E}\, e^{-E/T} \qquad (1)$$

where E is the ion energy and T is the temperature (in energy units). Corresponding to this thermal distribution of ion vibrational energy is a "thermal" partitioning of ion vibrations amongst

the lattice phonon frequencies--i.e., a thermal phonon distribution.[7] Since the phonons obey Bose-Einstein statistics, the thermal phonon distribution can be written in the form[8]

$$f_{th}(\omega) = \frac{3V}{2\pi^2 v_a^3} \frac{\omega^3 \, d\omega}{e^{\hbar\omega/T} - 1} \qquad (2)$$

where V is the volume, v_a is the acoustic speed, and we have used the Debye approximation.[9] For conventional vacuum sintering, radiant heat transfer would dominate. However, one can expect that the resistively heated oven element--characterized by a thermal energy distribution--will radiate a "thermal" photon spectrum. In heating the ceramic specimen, this thermal radiation spectrum should also lead to a thermal Boltzmann energy distribution--i.e., "reciprocity". Hence, conventional heating can be expected to lead to thermal ion energy and crystal phonon distributions, regardless of whether conduction or radiant heat transfer dominates.

Microwave heating, however, involves a time-harmonic perturbation of the lattice through ionic polarization. If the microwave frequency satisfies resonance with one or more normal mode oscillations, then a considerable amount of coherent, oscillatory motion will be pumped into those resonant modes. The resulting nonthermal phonon distribution will be determined by dynamic balance between the excitation of the resonant phonons and the nonlinear "thermalization" of these driven phonons into other phonons. It is also reasonable to expect that the net ion *energy* distribution resulting from microwave heating will not be a pure Maxwell-Boltzmann distribution. This is usually the case in resonant microwave heating of other kinetic dielectric media (e.g., plasmas).

Elsewhere, we have analyzed channels for resonant coupling of microwave radiation to normal lattice modes.[5] Here, we will summarize the results of that discussion. In general, there are two classes of possible resonant coupling. The first possibility involves direct resonance between the microwave field and localized normal oscillations in the lattice. Localized normal lattice modes at microwave frequencies may be associated with "weak" surface bonds or concentrations of point defects. This is more likely to occur in polycrystalline ionic solids, especially in the green, pre-sintered state. Localized excess charge concentrations can also lead to direct microwave frequency resonance with phonons.[5] Causes of localized charge imbalance may include transition metal impurities, although we expect the impurity fraction to be extremely small in high-purity ceramics. Free surface, grain boundaries and dislocations (because of their structural role in the creation of lattice vacancies and because of the difference in formation energy of intrinsic cation and anion vacancies) can create localized excess charge in the lattice even in high-purity compounds not containing transition metal cations. Thus, in polycrystalline compounds, the possibility exists for stimulating microwave-frequency phonons near extended lattice defects. Further discussions on these and other "microwave-regime" lattice resonances can be found elsewhere.[10]

The second possible class of resonant microwave coupling involves coupling between electromagnetic (microwave) and elastic (phonon) traveling waves.[11,12] Because of the large difference in phase velocities of the electromagnetic wave (near speed of light) and the elastic wave (acoustic speed), such coupling is necessarily a nonlinear, multi-wave mixing process (e.g., inverse Brillioun scattering). Ordinarily, one does not consider structural ceramics as examples of nonlinear dielectric media. At the elevated temperatures characteristic of sintering, however, a nonlinear dielectric response can be expected due to the large ion vibration amplitudes.[5,12]

We have identified several candidate channels for nonlinear three-wave resonance. First is a mode in which two large amplitude electromagnetic waves with frequencies ω_1 and ω_2 couple with a low frequency (radio frequency or lower) elastic wave having frequency Ω_a. The feasibility

of this process depends on the microwave power source having an operating frequency bandwidth, $\Delta\omega/\omega$ in the range $10^{-6} \le \Delta\omega/\omega \le 10^{-2}$ (a very realistic assumption). The two electromagnetic frequencies would fall within the microwave source bandwidth $|\omega_1 - \omega_2| \le \Delta\omega$. Resonant energy transfer to the elastic wave would occur when $\omega_1 - \omega_2 = \Omega_a$.

A second three-wave mixing channel is possible between two elastic waves, with frequencies Ω_1 and Ω_2, and the electromagnetic wave with (microwave) frequency ω_{em}. In this case, energy is resonantly transferred from the electromagnetic wave to one of the elastic waves--say, the second one at Ω_2--if $\omega_{em} = |\Omega_1 - \Omega_2|$.

NONTHERMAL ION ENERGY DISTRIBUTIONS

It can be expected that a lattice characterized by a nonthermal phonon distribution will be likewise characterized by a nonthermal ion energy distribution. We are unsure (at this time) what forms the nonthermal phonon distribution and nonthermal ion energy distribution acquire during intense microwave heating. However, it is clear that point defect mobility (and thus sintering rates) is most sensitive to the high energy tail of the distribution, while measurements with standard temperature diagnostics (such as thermocouples) are more sensitive to "bulk" features of the distribution. This distinction has important implications which we illustrate by *assuming* a particular form for the nonthermal ion energy distribution and showing the implications for enhanced ion mobility.

To begin with, we imagine an idealized crystal lattice in which an ion finds itself situated beside a point defect (vacancy), as in Fig. 1. The mobility of the point defect--directly relevant to the diffusion flux and sintering rates--is proportional to the probability that a neighboring ion will surmount the potential energy barrier V_b and thereby effect an ion/vacancy exchange. The probability that a neighboring ion will occupy the vacancy can be calculated by integrating the ion energy distribution function f(E):

$$P(E > V_b) = \int_{V_b}^{\infty} f(E)\, dE \qquad (3)$$

For a thermal process, we can take the ion energy distribution to be the Maxwell-Boltzmann distribution of Eq.(1).

As mentioned earlier, we are still uncertain of the form of the nonthermal energy distribution induced by microwave heating. However, for illustrative purposes, we assume that the energy distribution induced by microwave heating consists of an energetic, superthermal ion population superimposed on a "thermalized" background of ion energies. We model this by a "two-temperature" energy distribution:

$$f_{nt}(E) = \frac{2}{\sqrt{\pi}\, T_b^{3/2}} \sqrt{E}\ \left\{ (1 - \Delta)\, e^{-E/T_b} + \Delta \left(\frac{T_b}{T_{st}}\right)^{3/2} e^{-E/T_{st}} \right\} \qquad (4)$$

where T_b is the "bulk temperature" in energy units (as measured by a thermocouple, for example), T_{st} is the characteristic energy of the superthermal (nonthermal) component of ion energies, and Δ is the fraction of ions in the superthermal component of the distribution function. As we shall see, even small deviations from a thermal energy distribution (i.e., small values of Δ) can significantly affect point defect mobility, as characterized by the probability of ion/vacancy exchange--i.e., Eq.(3). Examples of the two distributions are portrayed in Fig. 2.

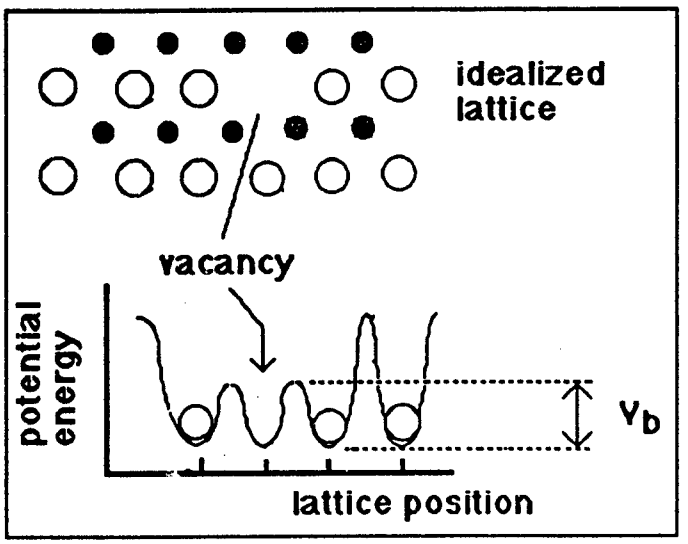


Fig.1. Idealized crystal lattice and associated potential energy function in the presence of a point defect (vacancy)

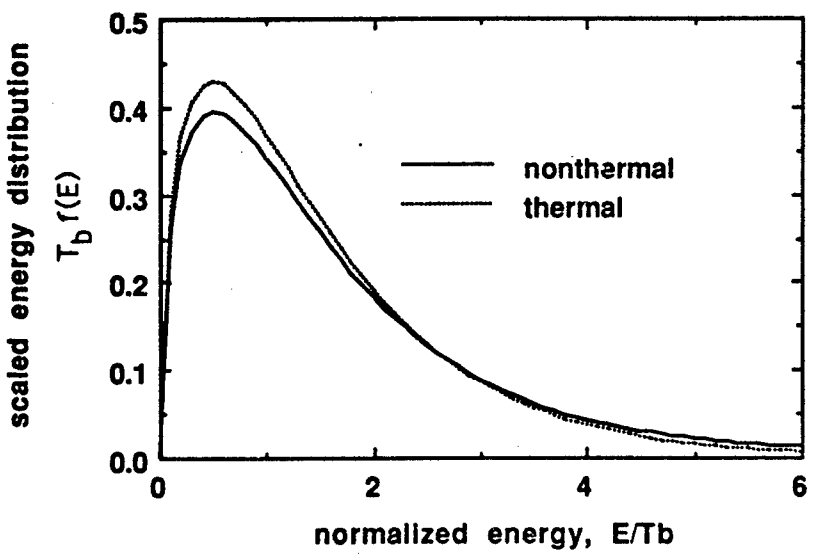


Fig. 2. Examples of thermal and nonthermal distributions, according to Eqs. (1) and (4). For the nonthermal case, $\Delta = 0.1$ and $T_{st} = 4\,T_b$.

For illustration, we calculate Eq.(3) for both a thermal [Eq.(1)] and a nonthermal [Eq.(4)] ion energy distribution. For the nonthermal case, we consider the particular distribution plotted in Fig. 2, for which $T_{st} = 4\ T_b$ and $\Delta = 0.1$ (a small deviation from the thermal distribution). For both distributions, it is assumed that a conventional "temperature" diagnostic (such as a thermocouple) would measure the mean energy of the distribution, $\langle E \rangle$. For the thermal distribution, $\langle E \rangle_{th} \sim T_b$, while for the nonthermal distribution, our particular choices of Δ and T_{st} yield $\langle E \rangle_{nt} \sim 1.3T_b$ which we approximate as $\langle E \rangle_{nt} \sim 1.3T_b \approx T_b$ (for reasons that will be clear shortly). In Fig. 3, we plot Eq. (3) as a function of the normalized bulk temperature T_b/V_b for both the thermal and nonthermal distributions. We observe that the probability of point defect motion is significantly enhanced (by orders of magnitude) for the nonthermal distribution, especially at lower values of T_b/V_b. In view of this large difference, the 30% error associated with the approximation $\langle E \rangle_{nt} \sim 1.3T_b \approx T_b$ is not considered serious.

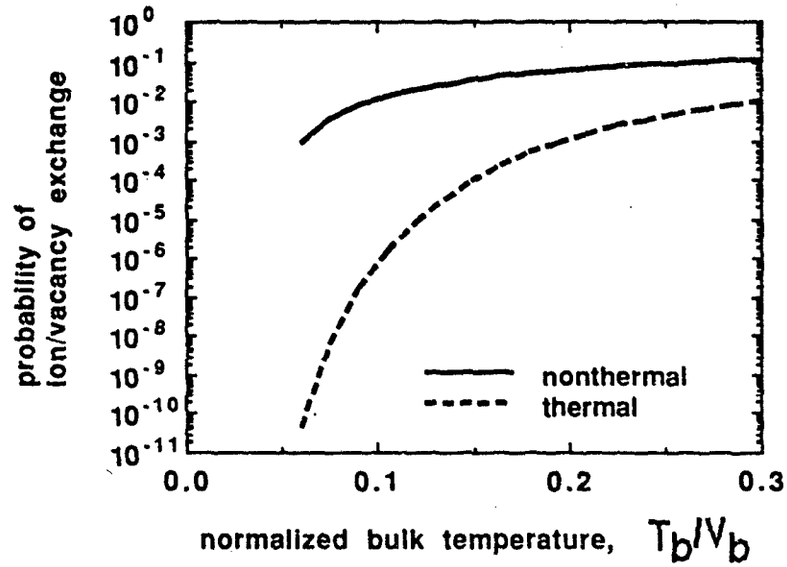


Fig.3. Probability of point defect motion for both a thermal energy (Maxwell-Boltzmann) distribution [Eq.(1)] and a "two-temperature" nonthermal distribution [Eq.(4)]. For the nonthermal case the deviation from thermal distribution is slight: $T_{st} = 4\ T_b$ and $\Delta = 0.1$.

The reason that a small, 30% difference in the mean energy $\langle E \rangle$ (between the thermal and nonthermal distributions) leads to orders of magnitude difference in the probability of point defect motion, $P(E > V_b)$, is that the excess energy in the nonthermal case is distributed in the high energy tail, where $P(E > V_b)$ is most sensitively affected. In like manner, we hypothesize that a similar phenomenon is responsible for the observations of apparent enhancement of diffusion and sintering rates during a comparison of microwave versus conventional heating of ionic solids.

SUMMARY

We have proposed that observations of enhanced diffusion and sintering rates in microwave (versus conventional) sintering are due to a nonthermal energy (or phonon) distribution induced by the intense microwave radiation field. This is most likely the case if the microwave radiation resonantly couples to specific elastic waves or normal modes of oscillation in the crystal lattice. The possibilities for coupling to normal mode oscillations appear greater in polycrystalline media (versus single crystal) due to additional effects associated with surfaces, grain boundaries, and concentrations of point defects. Alternatively, microscopic spatial nonuniformity in microwave heating may yield several populations of ions, each characterized by a different "temperature". Averaged over a macroscopic region, this would appear as a nonthermal energy distribution, similar to the one considered in this paper [cf. Eq. (4)].

While the exact nonthermal energy (or phonon) distribution during intense microwave heating is still unknown, we have explored a hypothetical nonthermal ion energy distribution. This exercise established that even small deviations from a thermal distribution could lead to large changes in the mobility of point defects. Several important questions can now be posed: (1) what are the exact forms of the lattice phonon and ion energy distributions during intense microwave heating of ionic solids?, and (2) what are the exact mechanisms for microwave-to-phonon energy transfer during microwave sintering? Future work at the University of Wisconsin is focused on these and related questions.

ACKNOWLEDGEMENTS

Two of the authors (JHB, RFC) acknowledge the support of NSF Presidential Young Investigator Awards (ECS-9057675 and MSM-8657164, respectively). The authors would like to express their appreciation for helpful discussions with Drs. R. Agrawal, A. Wendt, and T.M. Antonsen, Jr.

REFERENCES

1. See. for example, papers presented in "Microwave Processing of Materials," Materials Research Society Symposium Proceedings, Vol. 124, Ed. W.H. Sutton, M.H. Brooks, and I.J. Chabinsky, (Materials Research Society, Pittsburgh, PA, 1988), as well as references cited therein.

2. B. Swain, "Microwave Sintering of Ceramics," in *Adv. Materials and Proc. incorporating Metal Progress* magazine, September issue (1988).

3. M.A. Janney, "Microwave Processing of Ceramic Materials," Materials Science Seminar Series, University of Wisconsin-Madison (1989).

4. D. Palaith, R. Silberglitt, C.C.M. Wu, R. Kleiner, and E.L. Libelo, "Microwave Joining of Ceramics," in Ref. 1, pp. 255-266 (1988).

5. J.H. Booske, R.F. Cooper, and I. Dobson, "Mechanisms for Nonthermal Effects on Ionic Mobility During Microwave Processing of Crystalline Solids," submitted to *J. Mat. Res.* (1990).

6. T. Schneider, EPRI, private communications (1990); also, K. Wolf, H.K.J. Choi, and J.K.S. Wan, "Microwave Assisted Catalytic Conversion of Cyclohexene," *AOSTRA J. Res.* Vol. 3, pp. 53-59 (1986).

7. M. Born and K. Huang, Dynamical Theory of Crystal Lattices, (Oxford Clarendon Press, London, 1954), Chap. 2.

8. J.P. McKelvey, Solid State and Semiconductor Physics, (Krieger Pub. Co., Malabar, FL, 1966), p. 171.

9. P. Debye, "Zur Theorie der spezifischen Wärmen," *Ann. d. Phys.* Vol. 39, pp. 789-839 (1912).

10. See other papers presented in this *Ceramic Transactions*, e.g., by Newnham, Meek, Katz, etc.

11. R. Stolen and K. Dransfeld, "Far-Infrared Lattice Absorption in Alkali Halide Crystals," *Phys. Rev.* Vol. 139, pp. 1295-1303, (1965).

12. M. Sparks, D.F. King, and D.L. Mills, "Simple theory of microwave absorption in alkali halides," *Phys. Rev. B* Vol. 26, pp. 6987-7003, (1982).

NUMERICAL METHODS FOR THE MODELLING OF MICROWAVE FIELDS

Claude Lorenson, Christine Gallerneault
Alcan International Limited, Kingston R&D Centre
PO Box 8400, Kingston, Ontario Canada K7L 5L9

ABSTRACT

The popularity of microwave processing of materials continues to grow and as a result there is a need for numerical models that can help the design of cavity and applicators for specific applications. The Method of Moments and a Finite Element Method have been used to predict the heating behaviour of dielectric materials in multi-mode cavities at 2.45 GHz. A brief description of each method will be given and comparative strengths and weaknesses will be discussed.

INTRODUCTION

There is a continued growth in the popularity of microwave processing of materials. The potential for increased productivity, reduced costs and improved material performance are the major reasons for interest in this technology. In order for these benefits to manifest themselves in the end products, there is a need to improve our basic understanding of the radiation/matter interaction and to improve the distribution of electric fields inside microwave furnaces. Mathematical modelling can be a very useful tool with which to improve our understanding of these problems. Until recently, there was very little activity in the modelling of microwave heating phenomena in multi-mode cavities. This paper will briefly describe two techniques that can be applied to such problems and will present some examples in the use of modelling for materials processing.

NUMERICAL TECHNIQUES

Mathematical modelling is the representation of real life phenomena in terms of a set of mathematical expressions. The degree of complexity that can be included in a model is related to the computer memory needed to specify the problem (geometry) and the processing time needed to obtain solutions. Because of these limitations, the degree of reality incorporated in a model can be limited. These limitations can also influence the choice of numerical techniques used in solving a problem. A Finite Difference method (refs. 1 and 2), a Finite Element method or the Method of Moments could be used. We will describe the latter two techniques that have been used for material applications in our research effort.

THE METHOD OF MOMENTS

This method has been used extensively for electromagnetic modelling in the field of radar cross-section and to predict radiation patterns of antennae. In these applications the scattering bodies are far away from the source and the electric field of interest is in the far field regime, which is the simplest numerical condition. However in microwave processing near field regions must be included since typically the load to be treated is close to the source (~30 cm). In an application like radar cross-section, the interesting quantities are the reflected fields, all surfaces modelled are good conductors and there is no need for loss mechanisms to be included. In microwave processing, the load to be treated is lossy and this, in addition to the need to examine near fields, poses an additional complexity in the use of the Method of Moments.

In order to simplify the numerical computations, many electromagnetic scattering problems are solved in the wire-grid approximation. Since a conducting wire mesh behaves electromagnetically approximately like a solid surface, it is possible to replace the surfaces of interest with a coherent wire grid. Some care has to be taken with respect to the mesh size (smaller then the wavelength), the wire spacing and the wire radius. Good operating rules are known for these parameters and the theoretical work deriving them can be found in refs. 3 and 4. When building a model, the furnace walls and any reflecting elements inside the cavity are replaced by a wire grid (figure 1). As far as the load is concerned, you can also replace the solid with a wire grid but typically the grid has a higher density (because the wavelength is smaller in the material). This is apparent in figure 1 where the load here has $\varepsilon'_r=9$ and the density is higher then the walls of the cavity. At 2.45 Ghz, λ=12.2 cm so the walls need tc have a wire spacing of ~3cm and about ~1cm in the load (i.e. $\lambda_{air}\cong 12$ and $\lambda_{load}\cong 4$). In order to predict the power density in the load, it is necessary to add lumped elements to the load wires to represent the dielectric material properties. A resistor and a capacitor in parallel are added at each node of the wires. The resistor is related to ε''_r and the capacitor to ε'_r.

The source of microwaves in this particular model is represented by a number of strong emitting dipoles (4 typically) located near the roof of the furnace. Some empirical work is needed in the beginning to test which configuration of antenna give the most realistic field (infra-red imaging is a useful technique here). When this configuration is known, all models for a given furnace can use the same. In the Method of Moments, plane waves emitted from the antenna propagate in the space defined by the wire grid, some fields are reflected and some are absorbed in the load. This electromagnetic scattering problem is formulated in terms of induced currents in all the parts present (load and walls). The field absorbed by the load induces current in the lumped wires and the power absorbed can be calculated. There are many ways to solve for these induced currents (see refs. 5 and 6) and most of them are based on integral equations. These integral equations are derived from Maxwell's equations and the boundary conditions of the problem of interest. The Method of Moments is a set of procedures to transform these integral equations into a set of linear equations from which the currents can be extracted using known matrix algebra techniques. The mathematical details of

this technique is beyond the scope of this paper but the interested reader can consult ref. 7. The model developed using this technique for the material described above required 1550 dipole modes (number of unknowns) with storage requirements of 10 Mb for the complex array to be inverted.

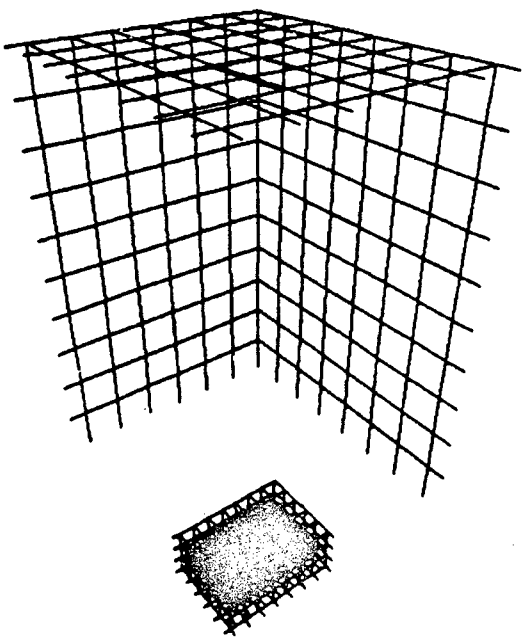


Figure 1. Moment method wire grid model for 1/4 oven and load.

RESULTS

Figure 2 shows the electric field in the empty furnace. This type of computation is necessary to make sure that the model can reproduce the incoherent mode pattern found in a multimode cavity.

In this figure, the bottom plane is the reflecting surface at the bottom of the cavity and the light gray pattern represents a certain (iso-surface contour) value of the electric field for a 5 cm region above the cavity bottom.

Figure 3 shows the power density inside the load (in this case the extent of the boundaries represent the load not the oven walls), it is quite clear that we have two hot spots near the edge of the load (ε'_r=9,ε''_r=1.6). Again the bottom plane represents the

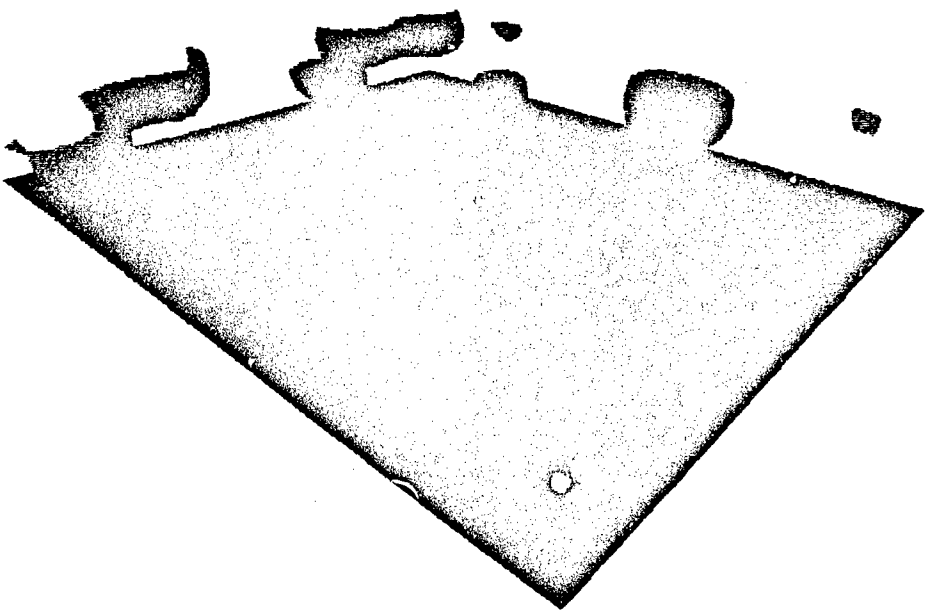


Figure 2. Electric field for an empty oven.

bottom of the load and iso-surface contours (the light gray 3D shape) emerging from the bottom represent the high values of the power absorbed through the depth of the load. Obviously, in order to reduce thermal stress, we would like to "spread" this heating zone and that can be accomplished experimentally by adding reflecting elements on top of the load. The model prediction for the power absorbed in the presence of these reflecting elements is shown in figure 4. Clearly the load will now be able to heat more uniformly (at least until the dielectric properties change!). Heat transfer and temperature dependence of the dielectric properties is not taken into account here. Furthermore all of the results are qualitative since we are interested in the spatial distribution of the power delivery rather than the absolute values of the fields or absorbed power. This example shows how a modelling technique can help in designing improvements inside the furnace.

There are three important limitations related to the application of this technique. They are geometric, microwave source and materials modelling constraints. The modelling of circular or elliptical shapes is difficult because of the way we build our grid, i.e. it is difficult to handle curved surfaces and have the correct lumped impedances. For the same reasons we are limited to rectangular furnaces. This is an important limitation since in some applications for continuous processing we need more freedom in our choice of geometry. In terms of materials, it is easy to model homogenous, "non-composite" materials but other kinds of materials are either impossible (metallic laminates) or a giant "bookeeping nightmare", as it is difficult to keep track of the

different impedances needed in the model and furthermore the boundaries between different types of materials become nebulous. In terms of modelling the source, it would be desirable to have the physical waveguide launch itself modelled instead of relying on secondary effects from antennas because it would then be possible to test how the power level has an effect on the processing and also if there is advantage in using shields near the launch. By relying on a secondary technique to represent the source as we do in the Method of Moments, neither of these tests are available.

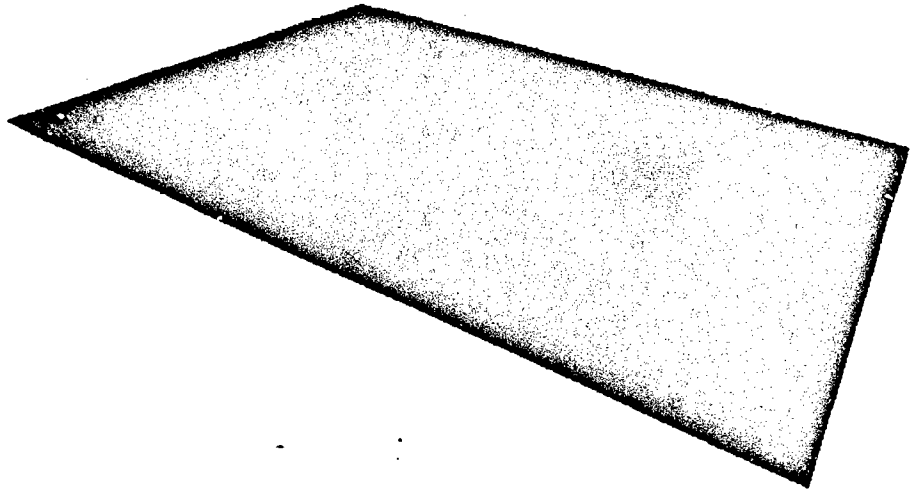


Figure 3. Power density for the load calculated by the method of moments.

THE FINITE ELEMENT METHOD (FEM)

Knowledge of the limitations inherent in the Method of Moments leads one to examine other techniques such as the finite element method in order to address these issues. The finite element method is based on variational principles. A finite element analysis determines the electric field distribution by minimizing the energy in each element. To calculate the field it is necessary to build a model of the furnace, the air and the load with threedimensional pieces that can have various shapes and sizes. As in the previous technique when the dielectric constant is higher, the mesh density is higher. Because

the elements are not confined to be rectangular prisms, different shapes of furnaces or loads can be modelled which is a big advantage for this technique. Figure 5 shows a quarter model of a rectangular furnace with a dielectric load in the centre (the centre line is the closest to the viewer). This model consisted of 6700 elements and required 2 hours of CPU time on a convex C240. Notice the higher mesh density in the load and the transition mesh from dielectric to air. In this model the waveguide feed is located in the centre on the roof of the oven. Using this technique, the exact electric field at the launching point can be used. In this case it is a TE_{10} mode in a WR-284 waveguide. In FEM, we can put the waveguide feed anywhere and also we can use any shape of furnace we need which is important when considering continucus processing.

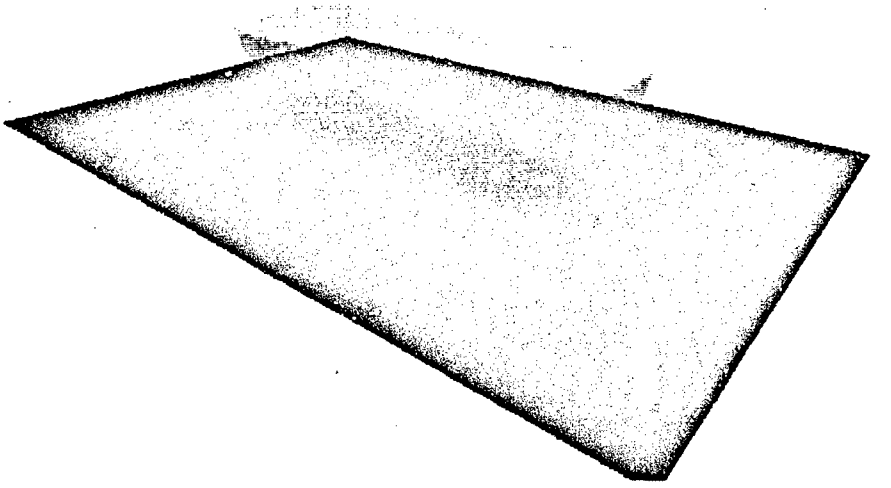


Figure 4. Power density for the load in the presence of reflecting elements calculated by the method of moments.

The transition mesh from high to lower mesh density can be a source of problems when calculating the electric field. A "non-physical" mesh would manifest itself by a very high density of electric field in that region when there is no reason for such behavior. Such a transition mesh creates artificial boundaries that breaks the piecewise continuity needed for a coherent solution throughout the model.

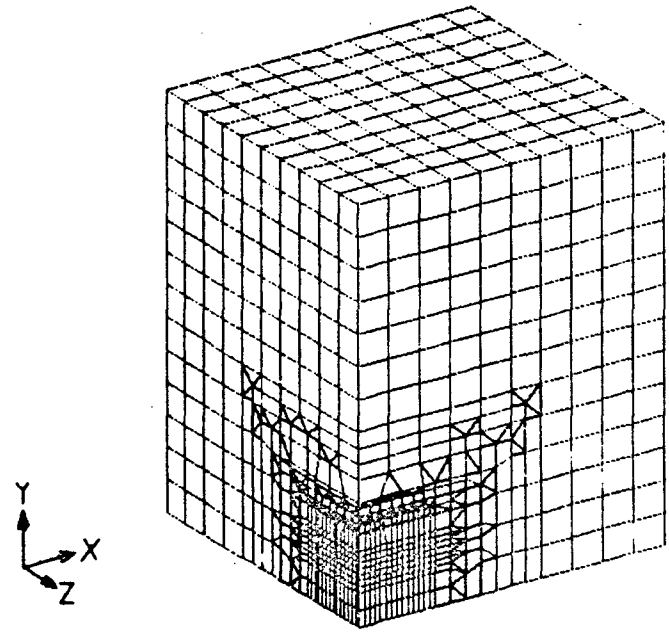


Figure 5. Finite element mesh for 1/4 oven and load.

In terms of material modelling, FEM can handle a larger variety of problems because of the ability to mix layers of different materials with different conductivities or dielectric values easily. If we want to model metallic laminates, all there is to do is to use surface elements for the metallic parts. In FEM we can use line, surface or 3 dimensional elements, bringing versatility to the different configurations of materials that can be treated. Of course not only the electric field can be deduced but also the power absorbed in the load and the induced current in the different conductors if there are some in the model. When looking at magnetic materials, FEM gives the best way to predict the magnetic energy density since all elements have their own material properties, including permeability, attached to them.

One of the drawbacks of FEM is that model building is more tedious especially with regards to construction of the transition mesh or air present in the furnace. As a result "quick runs" to test a few alterations to a furnace are not as practical. However commercially available preprocessors and automatic meshers are available and do help.

CONCLUSION

Because of the current interest in microwave processing and the challenging problems that lurk in the future in terms of scale-up and continuous processing, there is a need to establish mathematical models that can guide our understanding of heating mechanisms and the design of applicators. This paper presented two techniques that have proven

useful in our experience. Specific applications have been presented or discussed and the limitations of the techniques have been explained. Mathematical modelling will never replace experimental work, but it can provide direction for the selection of the important tests to be performed experimentally.

REFERENCES

1. M. DePourcq, "Field and Power Density Calculations in Closed Microwave Systems by Three-Dimensional Finite Differences", IEE Proc. H. -Microwave Antennas and Propagation, 132(6):360, (1985)

2. R.W. Lau, et al.,. "The Modelling of Biological Systems in Three-Dimension Using the Time Domain Finite-Difference Mehtod: II. The Application and Experimental Evaluation of the Method in Hyperthermia Appicator Design", Phys. Med. Biol., 31(19) 1257, (1986).

3. K.S.H. Lee, L. Marin, J.P. Castillo,"Limitations of Wire Grid Modelling of Closed Surface", IEEE Transactions on Electromagnetic Compatibility , EMC-18, 123 (1976)

4. J. Mayham, "Characteristic Modes and Wire Grid Modelling", IEEE Transactions on Antennas and Propagation, AP-38, (4) 457, (1990).

5. I. Tatsuo,"Numerical Techniques for Microwaves and Millimiter Wave Passive Structures", John Wiley and Sons, 1989

6. R.F. Harrington,"Field Computations by Moment Method", R.E. Krieger Publishing Company, 1968

7. J.M. Moore and R. Pizer, "Moment Methods in Electromagnetics", John Wiley and Sons, 1984, Research Studies Press

Section IV. Dielectric Measurements

MEASUREMENT OF DIELECTRIC PROPERTIES IN THE FREQUENCY RANGE OF 300 MHz TO 3 GHz AS A FUNCTION OF TEMPERATURE AND DENSITY

Johanna B. Salsman
U. S. Bureau of Mines
Tuscaloosa Research Center
Tuscaloosa, AL 35486.

ABSTRACT

As part of the research effort on investigating the effects of microwave energy on the chemical and physical properties of minerals and ores, the U. S. Bureau of Mines, Tuscaloosa Research Center has conducted an extensive research program on identifying those properties of minerals that are affected by microwave energy, namely the dielectric constant and loss tangent. The objective was to establish a reliable data base for predicting the effects of microwave heating on minerals.

The dielectric constant and loss tangent of minerals, commonly referred to as the dielectric properties, were determined utilizing the theory of microwave propagation through an open-ended air filled coaxial line that was terminated at its open end with the particular mineral under investigation and measuring the reflection coefficient of the mineral with a network analyzer. From the measured values of the reflection coefficient, the dielectric properties of the mineral could be determined.

The dielectric properties of powdered minerals with medium to high electrical conductivities ($\tan\delta \geq .01$) were measured in the frequency range of 300 MHz to 3 GHz. Since the minerals were prepared as powders, techniques were used to relate the measured dielectric properties of the powdered minerals to the dielectric properties of the mineral at its theoretical or natural density. Also, these measurements were performed as a function of temperature, from 25° to 325° C.

The results of the dielectric constants and loss tangents using this method were determined to be precise within ±5 pct. This report describes the method of measurement and discusses the results of the Bureau's investigations into dielectric properties of minerals with the inclusion of typical measured data.

INTRODUCTION

Major research efforts are underway worldwide on the use of microwave energy in various processing techniques. Deterrents to these research efforts are the lack of sufficient data on the

electrical properties of materials (including minerals) and the lack of personnel trained in microwave processing technology. It is very likely that microwave energy may offer many advantages to minerals beneficiation and processing techniques; however, it is difficult to exploit these advantages without an understanding of the electrical properties of minerals. At the microwave heating frequencies, 30 MHz to 3 GHz, these properties are often referred to as the dielectric properties of minerals, namely the dielectric constant and the loss tangent. The dielectric constant determines how much energy can be stored in a material while the loss tangent is proportional to the amount of energy that is lost as heat. The product of these two terms, the dielectric loss factor, determines how well a material will absorb microwave energy.

Microwave technology is beginning to find many successful uses in industrial applications other than food preparation. Recent investigations of the use of microwave energy as a heat source in materials processing techniques have shown several advantages over conventional methods of heating. For example, studies conducted on microwave processing of ceramics and composite materials have shown improved microstructural properties in the final product along with a reduction in energy requirements and processing times [1-3]. However, research is limited in this area because the dielectric properties of minerals and most materials at microwave heating frequencies are virtually unknown. In order to predict whether microwave energy may be a viable tool for use in the minerals industry, these properties must be known, otherwise trial and error methods are the only alternative.

MEASUREMENT OF THE DIELECTRIC PROPERTIES OF MINERALS

The Bureau of Mines, Tuscaloosa Research Center has developed a successful method for measuring the dielectric constant and loss tangent of minerals using an open-ended coaxial line and a network analyzer that has an operational frequency range of 300 kHz to 3 GHz. This method is very versatile since it allows for the measurement of the dielectric properties of minerals at microwave heating frequencies. It is also capable of measuring liquids, solids, and powders. The measurement system incorporated a heating device and a variable density chamber to allow for the measurement of dielectric properties as a function of temperature and density. The combination of all these various capabilities in the measurement system significantly adds to its overall effectiveness and versatility.

Theory of Measurement

The method of measuring the dielectric constant, ε_r', and loss factor, ε_r'', involves placing the mineral sample, the load shown in figure 1, at the end of an open-ended coaxial line and measuring the input reflection coefficient, Γ^*, as seen at the end of the line. By knowing Γ^*, the dielectric properties can be determined.

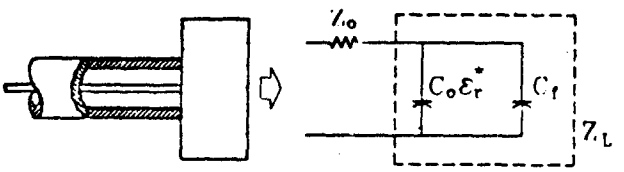


Figure 1. The Equivalent Circuit of a Sample at the End of a Coaxial Line.

Mathematically, the input reflection coefficient can be calculated from the expression given in the following equation [4]:

$$\Gamma^* = \frac{1 - j\omega Z_o(C_o\varepsilon_r^* + C_f)}{1 + j\omega Z_o(C_o\varepsilon_r^* + C_f)} \quad (1)$$

where Γ^* is the complex input reflection coefficient, ω is the angular frequency, $= 2\pi f$, f is the frequency, C_o and C_f are fringing capacitances associated with the coaxial line, Z_o is the impedance of the coaxial line, and ε_r^* is the complex dielectric constant.

Rearranging equation 1 and solving for ε_r^* yields:

$$\varepsilon_r^* = \frac{1 - \Gamma^*}{j\omega Z_o C_o(1 + \Gamma^*)} - \frac{C_f}{C_o} \quad (2)$$

The complex dielectric constant, ε_r^*, can also be expressed by:

$$\varepsilon_r^* = \varepsilon_r' - j\varepsilon_r'' \quad (3)$$

where ε_r' is the dielectric constant, and ε_r'' is the loss factor. Similarly the complex input reflection coefficient can be expressed as:

$$\Gamma^* = \Gamma\cos\varphi + j\Gamma\sin\varphi \quad (4)$$

where Γ is the magnitude of the complex input refection coefficient and φ is the phase. By substituting equations 3 and 4 into equation 2 and separating equation 2 into its real and imaginary parts, the dielectric properties can be determined. Equations 5 and 6 are the mathematical representation of the dielectric constant and loss factor, respectively, and may be used to calculate the dielectric properties of the load at the end of the coaxial line, given all other terms in the equations are known or can be evaluated.

$$\varepsilon_r' = \frac{-2\Gamma\sin\varphi}{\omega Z_o C_o(1 + 2\Gamma\cos\varphi + \Gamma^2)} - \frac{C_f}{C_o} \quad (5)$$

$$\varepsilon_r'' = \frac{1 - \Gamma^2}{\omega Z_o C_o(1 + 2\Gamma\cos\varphi + \Gamma^2)} \quad (6)$$

Since Z_o is the impedance of the line and is constant and the values of Γ and φ are measured, one only needs to determine the values of C_o and C_f, the fringing capacitances of the line, to determine the dielectric constant, loss factor, and thus the loss tangent of the material at the end of the open-end coaxial line.

Determination of C_o and C_f

The determination of C_o and C_f can become quite cumbersome and tiring; however, it is crucial to the measurement technique [5]. First, solve equations 5 and 6 in terms of the capacitances C_f and C_o, respectively.

$$C_o = \frac{1 - \Gamma^2}{\omega Z_o \varepsilon_r''(1 + 2\Gamma\cos\varphi + \Gamma^2)} \tag{7}$$

$$C_f = \frac{-2\Gamma\sin\varphi}{\omega Z_o \varepsilon_r''(1 + 2\Gamma\cos\varphi + \Gamma^2)} - \varepsilon_r' C_o \tag{8}$$

From equations 7 and 8, C_o and C_f can be determined through an iterative process. The procedure begins with placing materials of known dielectric properties at the end of the open-ended coaxial line and measuring the magnitude and phase of the reflection coefficient at the end of the line, i.e. the input reflection coefficient.

For a first approximation, assume C_f equal to zero. Using equation 7 and a material with high dielectric properties, calculate a value of C_o. Using this value of C_o, place a material with low dielectric properties at the end of the coaxial line and measure the input reflection coefficient. From equation 8 calculate a value of C_f. Using equation 8 again and this new value of C_f, calculate a new value of C_o with measured reflection coefficient data from a new material with high dielectric properties. Call this new C_o, C_{oi}. In order to judge whether these values of capacitances are suitable values of C_o and C_f, compare C_o and C_{oi}. If they are not equal, the iteration must continue a number of times using the last calculated values of C_o, or C_{oi}, and C_f until the values of the capacitances C_o and C_{oi} converge. This process must be repeated for every measurement frequency since the fringing capacitances change with frequency.

Selection of Reference Materials for Determining Capacitances

The high loss materials chosen to determine the fringing capacitance were saline solutions since their dielectric properties could be calculated as a function of temperature, normality, and frequency [6]. Two of the low loss materials used were obtained from the National Institute of Standards and Technology and were cyclohexane and 1,2 dichloralethane. Other low loss reference materials used were air, perchloralethylene, and teflon. The dielectric properties of the perchloralethylene and teflon were measured previously by a technique developed by the Bureau and compared favorably to referenced data [7]. Saline solutions of normalities other than those used to determine the values of the fringing capacitances were used to evaluate the errors in the measurement procedure. Table 1 gives the error for a 0.2 normal saline solution measured by this technique.

Table 1. A Comparison of the Dielectric Properties of Measured and Calculated Data for a 0.2 N Saline Solution

	Dielectric constant			Loss factor		
Frequency, MHz	Measured value	Known value	Pct diff.	Measured value	Known value	Pct diff.
36.07	71.5	75.86	5.72	928.29	914.73	1.48
45.41	73.49	75.86	3.12	736.57	726.66	1.36
57.16	74.35	75.86	1.99	584.69	577.30	1.28
71.97	75.14	75.86	.95	464.34	458.67	1.24
90.60	75.46	75.85	.51	368.88	364.47	1.21
114.05	75.58	75.85	.36	293.07	289.68	1.17
143.59	75.64	75.85	.28	233.00	230.31	1.17
180.77	75.74	75.85	.15	185.33	183.21	1.16
227.57	75.78	75.84	.08	147.62	145.86	1.21
286.50	75.78	75.84	.08	117.74	116.29	1.25
360.68	75.81	75.83	.03	94.14	92.90	1.33
454.07	75.75	75.81	.08	75.55	74.46	1.46
571.64	75.79	75.78	.01	60.81	59.99	1.37
719.65	75.66	75.74	.11	49.45	48.71	1.52
905.98	75.55	75.67	.16	40.65	40.02	1.57
1,089.23	75.41	75.59	.24	35.19	34.63	1.62
1,309.55	75.24	75.47	.30	31.08	30.40	2.24
1,648.62	74.83	75.25	.56	27.04	26.55	1.85
2,075.49	74.85	74.90	1.40	23.85	24.09	1.00
2,612.89	74.81	74.35	.62	22.37	22.86	2.14
3,000.00	74.43	73.88	.74	22.74	22.67	.31

Determination of Density Effects

Natural minerals come in all shapes and sizes. Many minerals are not found in nature as large solid pieces, but as tiny fragments mixed with all types of other minerals which have to be separated in order to acquire a pure sample. In the process of separating the minerals, the samples had to be pulverized to a powder. However, the measured dielectric properties of this powdered mineral did not represent those properties of that mineral found in its natural state; thus methods needed to be explored for determining the dielectric properties of a material at its natural or theoretical density using data on a powdered sample, (i.e. without the influence of porosity and high surface area effects).

Stuart Nelson [8] has been conducting research on evaluating the dielectric properties of various materials for the U. S. Department of Agriculture for several years. During his studies, the need arose to determine dielectric properties as a function of density and relate this information to

those properties at a different density. After considerable evaluation, the Bureau used Nelson's technique and incorporated the method into its measurement system.

It was found that the linearity of ε_r' with the density of a powdered-air mixture can be expressed as

$$\sqrt{\varepsilon_r'} = m\rho + 1 \tag{9}$$

where m is the slope of the line and ρ is the density of the air-powder mixture. The dielectric constant for air at zero density is unity for the mixture.

The quadratic dependence of ε_r' and ε_r'' on density was expressed by Kent [9] as

$$\varepsilon_r' = a\rho^2 + b\rho + 1 \tag{10}$$

$$\varepsilon_r'' = c\rho^2 + d\rho + 0 \tag{11}$$

since at zero density, $\varepsilon_r' = 1$ and $\varepsilon_r'' = 0$. (a, b, c, and d are constants for a given material at a given frequency.)

It becomes obvious that when squaring equation 9, equations 9 and 10 become equivalent, where $a = m^2$ and $b = 2m$. Thus, if this relationship holds, measurements of the dielectric constant of a powdered sample at any one bulk density, along with the $\rho = 0$ and $\varepsilon_r' = 1$ intercept, will provide enough information to determine the dielectric constant at any density including that of a solid material.

A linear relationship between the loss factor and density can also be obtained by completing the square of equation 11 as shown below.

$$\sqrt{\varepsilon_r'' + e} = \sqrt{c}\rho + \sqrt{e} \tag{12}$$

where $e = d^2/4c$. However, a single measurement will not suffice for the evaluation of ε_r'' since the constant e must be determined. Two measurements will be sufficient for the determination of the loss factor although, as more measurements are taken at different densities the evaluation of the slope term for both the dielectric constant and loss factor becomes more precise.

EXPERIMENTAL PROCEDURE

The measurement system consisted of an open-ended coaxial line that was connected to a computer controlled network analyzer where the opposite end of the coax was placed against the mineral sample. The reflection coefficient at the coax-mineral interface was measured by the network analyzer in the frequency range of 300 MHz to 3 GHz and the dielectric constant and loss factor of the mineral were computed as described in the theoretical section of this paper.

The Coaxial Line

The air filled coaxial line was constructed of type 307 stainless steel and was fitted with a 7 mm APC flange in order that it could be easily fitted to the network analyzer. It was necessary to have a very rigid coaxial line since hard, solid samples were to be measured. The termination port on the network analyzer had an impedance of 50 ohms. For matching purposes, the coaxial line was designed and constructed to maintain the same impedance by the expression given in equation 13 and shown in figure 2 [10].

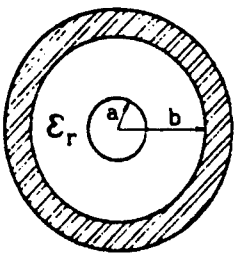


Figure 2. A Cross-Section of A Typical Coaxial Line

$$Z_o = 60 \ln(b/a)/\sqrt{\varepsilon_r'} \qquad (13)$$

ε_r' in equation 14 is the dielectric constant of the material filling the coaxial line, 'b' is the radius of the outer conductor, and 'a' is the radius of the inner conductor. In order to maintain an impedance of 50 ohms, from equation 14, it was necessary to maintain a ratio of 2.3 of the conductor radii, b to a.

It became necessary, however, to insert a thin spacer at the end of the coaxial line. The purpose of the spacer was twofold: 1) it held the center conductor in place preventing it from moving off center inside the coaxial line, and 2), it prevented materials from creeping up into the line during the measurement procedure. To compensate for the spacer at the end of the line, the conductor ratio in equation 13 was adjusted to maintain the 50 ohm impedance. Using 2.1 for the dielectric constant of the spacer material, the ratio was calculated to be 3.54. Thus the radius of the inner conductor was reduced by an amount to maintain this ratio, but only for the end of the line where the spacer was positioned as shown in figure 3.

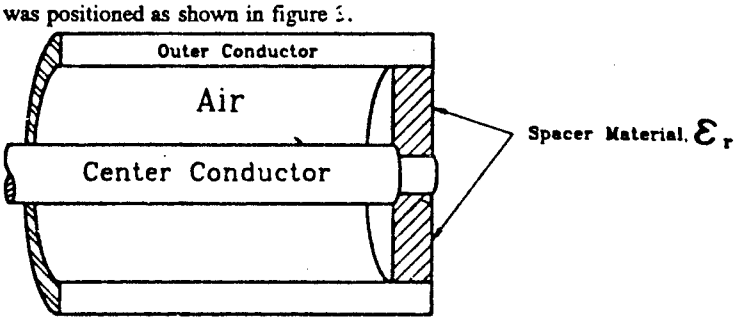


Figure 3. The End of the Coaxial Line Where the Spacer Was Placed.

The coaxial line was also designed so impedance standards for calibration of the test equipment such as a short circuit and a 50 ohm matching load could be secured at its end. Calibrating the system at the end of the coaxial line enabled the measurement of the reflection coefficient at the end of the line. This eliminated the necessity of dealing with signal delays that are inherent in the system when adding an electrical device of a given length away from the calibration port of the measurement equipment.

The Network Analyzer

The reflection coefficients were measured with a network analyzer[1] in conjunction with a transmission/reflection test set[2]. The network analyzer had an operational frequency range of 300 kHz to 3 GHz. The test set was connected to the coaxial line. The analyzer supplied a signal to the end of the coaxial line and measured the magnitude and phase of the applied and reflected voltage by means of a high resolution synthesized signal source and a dual channel three-input receiver. Comparison of these voltages gave the complex reflection coefficient at the end of the coaxial line. The reflection coefficient could be displayed as real and imaginary parts or as magnitude and phase in rectangular or polar/Smith chart formats. In addition, a microprocessor within the network analyzer could compute the impedance at the end of the line from the reflection coefficient data. Through design, the coaxial line was capable of fitting impedance standards at its end which enabled reflection coefficient measurements at the end of the coaxial line.

The network analyzer was controlled by minicomputer that was programmed to transmit the control signals necessary to sweep the analyzer frequency and record the reflection coefficient data at each frequency step. Data from the analyzer were transmitted to the computer where they were analyzed to determine the dielectric properties of the material at the end of the coaxial line.

The Heating Device

The heating device consisted of two small semi-circular electric heaters 7.5 cm in height that, when placed together, left a 5 cm opening in the center. The opening provided enough space to place the mineral sample and the coaxial line. The coaxial line was mounted on a stand which also supported the heaters. An insulating box housed the heaters and coaxial line, and was sealed to maintain an inert atmosphere around the sample during the heating period. A positive pressure of argon was maintained in the box to eliminate oxidation of the sample while heating. A K-type thermocouple was positioned along the side of the coaxial line to measure the surface temperature of the material during the heating and measurement cycle.

The Density Chamber

In order to vary the densities of the powdered mineral samples and measure the dielectric properties of the minerals at various densities, a variable density chamber was designed and constructed. A cylindrical chamber was constructed of a very low-loss material. The choice of

[1]Hewlett Packard Model #HP8753A*
[2]Hewlett Packard Model #HP85044A*
*Reference to specific products does not imply endorsement by the U.S. Bureau of Mines.

the low-loss material ensured that none of the transmitted signal was reflected from the density chamber which would interfere with the dielectric property measurements. The density measurements were accomplished by placing a predetermined amount of the powdered mineral into the chamber of known volume. The floor of the chamber was actually a piston that allowed a volume change inside the density chamber. The open end of the coaxial line was fitted with a grounding plate and was secured on the top of the density chamber. Once the chamber was filled with a mineral sample, the piston was moved in a vertical direction until the sample was seated against the coaxial line. The Smith Chart display on the network analyzer indicated when the coaxial line and the mineral were in contacted electrically. The movement of the piston floor was calibrated to determine the volume change inside the chamber. By knowing the weight and volume of the sample, the density of the powder-air mixture was calculated. Figure 4 is a drawing that depicts the apparatus including coaxial line, heating device, and density chamber. Figure 5 is a photograph of the complete measurement system.

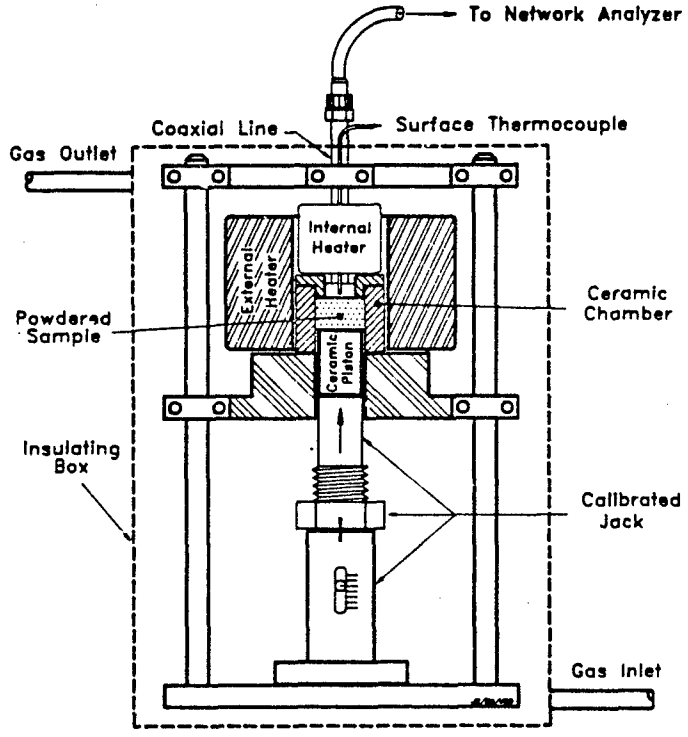


Figure 4. The Holding Apparatus Constructed for Measuring the Dielectric Properties of Minerals as a Function of Temperature and Density.

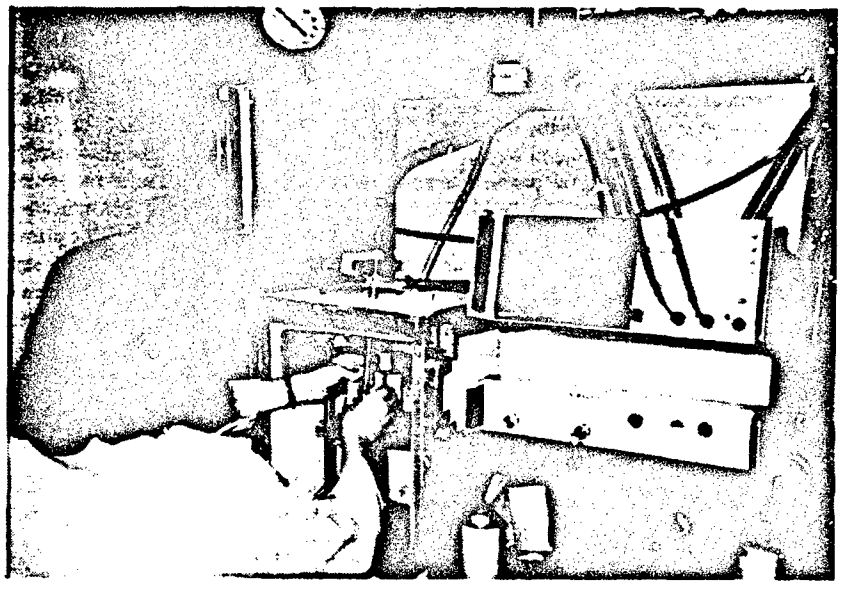


Figure 5. The Equipment for Measuring Dielectric Properties.

RESULTS

The dielectric properties of over 60 minerals have been measured using the technique described above. For every mineral measured, the measurement frequency was swept from 300 MHz to 3 GHz at 27 MHz intervals. Each mineral was measured at a minimum of three different densities and, at each density, dielectric property data was taken at temperatures of 25°, 75°, 100°, 125°, 175°, 200°, 225°, 275°, 300°, and 325° C. It was found that the dielectric properties of the minerals generally increased with increasing temperature, indicating that the materials become more absorbent of microwave energy as they were heated. However, the mineral chalcocite, Cu_2S, displayed a very different trend. While heating the Cu_2S, the dielectric constant and loss factor decreased after the mineral reached 100° C instead of increasing as was expected. After investigating this phenomena, it was found that Cu_2S experienced a phase change at 100° C, where its crystalline structure changed from an orthrombic to isometric [11]. None of the other minerals evaluated displayed similar characteristics. However, crystalline phase changes of the other minerals occurred at a much higher temperature than the capabilities of the measurement system. If the heating device were capable of temperatures above 325° C, it is believed that similar changes would have been observed. Figure 5 depicts the dielectric constant and loss factor in graphic form for the mineral chalcocite as a function of frequency and at different temperatures.

As an example of typical dielectric property data, figure 6 displays the measured data in graphic form of the dielectric constant and loss factor for the mineral chalcopyrite, CuFeS, in the frequency range of 300 MHz to 3 GHz. The data is shown for the temperatures of 25°, 100°,

200°, and 300° C. The trends in the dielectric properties for chalcopyrite were similar to those observed in all the minerals measured by the Bureau.

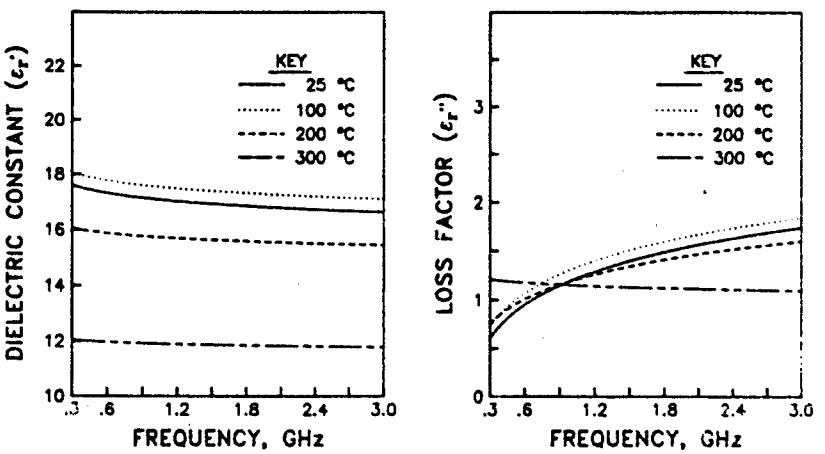


Figure 6. The Dielectric Properties of Chalcocite at Elevated Temperatures

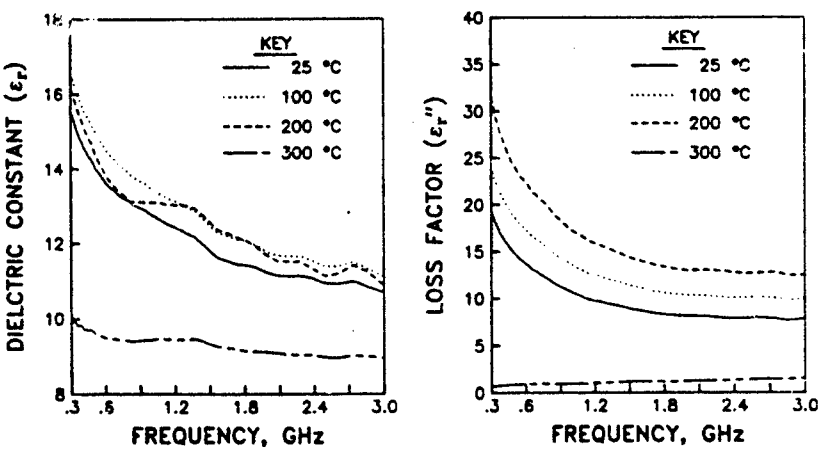


Figure 7. The Dielectric Properties of Chalcopyrite at Elevated Temperatures.

CONCLUSIONS

A technique for measuring dielectric properties at microwave heating frequencies was developed. The measurement system is completely computer controlled and will allow for the measurement of materials ($\tan\delta \geq 0.01$) in the temperature range of 25° to 325° C. The measurement system was designed to measure the dielectric properties of liquids, solids, and powders and techniques

to determine powder density effects on dielectric properties was incorporated into the system. To date, the Bureau of Mines' Tuscaloosa Research Center has measured the dielectric properties of over 60 medium to high-loss minerals and will continue to provide basic data on the dielectric properties of materials at microwave heating frequencies as a function of temperature. It is the desire of the Bureau to aid in developing new and improved minerals and materials processing techniques and it is believed that an understanding of the dielectric properties of materials at microwave heating frequencies is one of the ways to accomplish this goal.

REFERENCES

1. Nippon Steel Corp, "Hot Pressing of Inorganic Materials," Japanese Patent 74/100, 727, (Sept. 2, 1974).

2. T.T. Meek, "Sintering of a Refractory in a Microwave Field," UNITECR '89, pp. 1411-1416, (1989).

3. J.D. Katz, R.D. Blake, and C.P. Scherer, "Microwave Sintering of Titanium Diboride," Presented at the 13th Annual Conference on Composites and Advanced Ceramics (Cocoa Beach, FL, Jan. 15-18, 1989). OSTI, LA-UR-89-533, (1989).

4. T.W. Athey, M.A. Stuchly, and S.S. Stuchly, "Measurement of Radio Frequency Permittivity of Biological Tissues with an Open-Ended Coaxial Line: Part I," IEEE Tran. Microwave Theory and Tech., Vol. MTT-30, No. 1, pp. 82-86, (1982).

5. M.A. Stuchly, T.W. Athey, G.M. Samaras, and G.E. Taylor, "Measurement of Radio Frequency Permittivity of Biological Tissues with an Open-Ended Coaxial Line: Part II - Experimental Results," IEEE Tran. Microwave Theory and Tech., Vol. MTT-30, No. 1, pp. 87-91, (1982).

6. A. Stogryn, "Equations for Calculating the Dielectric Constant of Saline Water," IEEE Tran. Microwave Theory and Tech., Vol. MTT-19, No. 9, pp. 733-736, (1971).

7. R.H. Church, W.E. Webb, and J.B. Salsman, "Dielectric Properties of Low-Loss Minerals," BuMines RI 9194, 23 pp, (1988).

8. S.O. Nelson, "Observation of the Density Dependence of Dielectric Properties of Particulate Materials," J. Microwave Power, Vol. 18, No. 2, pp. 143-152, (1983).

9. M. Kent, "Complex Permittivity of Fish Meal: A General Discussion of Temperature, Density and Moisture Content," J. Microwave Power, Vol. 12, No. 4, pp. 341-345, (1977).

10. R.G. Brown, R.A. Sharp, W.L. Hughs, and R.E. Post. Lines, Waves, and Antennas - The Transmission of Electric Energy. John Wiley & Sons, New York, pp. 259, (1973).

11. E.S. Dana, Dana's Manual of Minerology, 15 ed, John Wiley & Sons, New York, p. 151, (1944).

A HIGH TEMPERATURE MICROWAVE DIELECTROMETER

Weiguo Xi, and W.R. Tinga
Elec.Eng.Dept., University of Alberta, Edmonton, AB, Canada, T6G 2G7

ABSTRACT

A microwave dielectrometer has been developed for measuring dielectric properties of various oxides and ceramics at up to at least 1200°C. This system uses a re-entrant coaxial cavity with a hollow center conductor both as a microwave heater and as a test chamber. A small cylindrical sample is easily introduced into the cavity through an insertion hole and tested in the frequency band of 3GHz while being heated by a tunable 60W solid state source of 915MHz. The sample temperature is measured with an optical fiber thermometer. The speed, convenience and accuracy of this system may make instant on-line measurements possible.

In this paper, the sample loading effect and the hole effect on the characteristics of the cavity are discussed based on the results from our mode-matching analysis. The theoretically predicted calibration curves for determining dielectric constants and loss tangents are provided in polynomial form. Error estimations are also included. The system setup is described and part of our experimental results are presented to demonstrate the system performance.

INTRODUCTION

Dielectric measurements at room temperature and at high temperature differ in techniques rather than in principles. However, only little research has been done on high temperature methods due to technical difficulties. Some researchers used electrical heaters and invariably met with difficulties due to thermal insulation and expansion. Others utilized microwave heating which is obviously fast and well localized. However, this approach has also encountered certain difficulties. The main problems involved are the interference of the heating power with the test signal and the microwave heating dependence on the varying material properties. Though some progress has been made, temperatures can only reach several hundred degrees and the range of measurable materials is limited [1-3].

Our microwave dielectrometer discussed in this paper is able to

heat various materials, including oxides and ceramics, and measure their dielectric constants and loss factors to temperatures above 1200°C. Three main features characterize this system. (1) A coaxial re-entrant cavity serves both as a microwave heater and as a sample test chamber. By virtue of a strongly focused E-field in the re-entrant gap, a heating rate up to 700°C/sec. can be achieved. The high heating rate, together with the small sample volume used, alleviates problems due to the cavity's thermal expansion, thus ensuring a higher measurement accuracy. (2) Heating and testing are conducted at the same time but in different frequency bands — 915MHz and 3GHz. As a consequence, the test signal can be easily separated from the heating power by a high pass filter. (3) The use of the sample insertion hole greatly eases sample preparations and avoids the typical air gap problem, making instant on-line measurements possible.

CAVITY CHARACTERISTICS

The re-entrant coaxial cavity shown in Fig.1 is a quasi-TEM resonator with TEM field in the coaxial section and TM fields in the gap section if the wavelength $\lambda > 2(r_2 - r_1)$. Consequently, it can be represented by a section of uniform transmission line terminated by a capacitance which expresses the effect of the gap field. Unfortunately, such a capacitance is not only frequency dependent but also varies nonlinearly with sample load [4]. It is further complicated by the modified gap fields due to the presence of the insertion hole. Experimental results have shown that the sample inserted through the holes results in significantly different loading effects on the cavity [5]. To understand these characteristics, we resort to a numerical approach for field analysis, using a mode-matching formulation. The resonant frequencies calculated by this program are virtually the same as those measured. The following discussion is based on the numerical results [6].

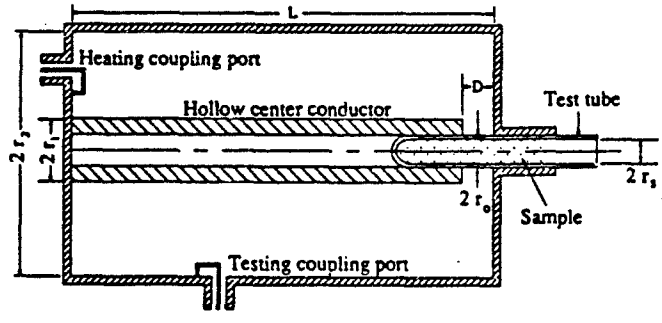
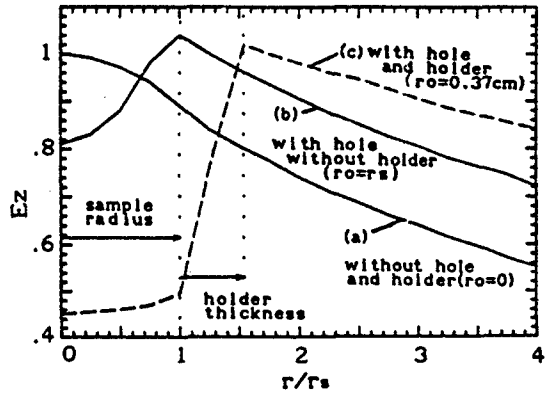


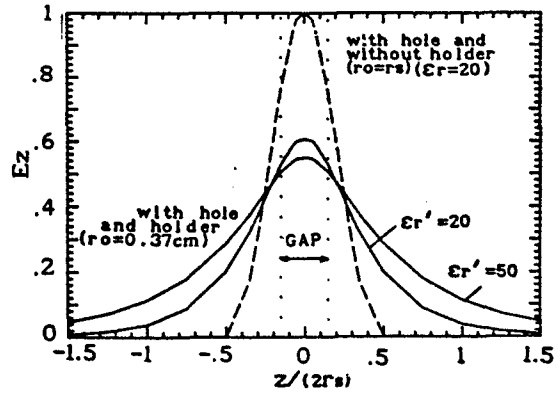
Figure 1. Cross section of coaxial cavity used as high temperature dielectrometer; r_s=0.25, r_o=0.375, r_1=1.244, r_2=20.0, D=0.3, in cm.

Numerical results show that the presence of the holes in the

re-entrant gap causes the gap capacitance or the gap E-field to decrease but the effective sample length to increase. This can be demonstrated by the calculated Ez field distribution shown in Fig.2. It shows that (1) the peak gap field moves from the center to the edge of the hole;(2) the field propagation into the hole is cutoff; (3) the insertion of high permittivity samples and the use of a test tube enhance the hole effects. To maintain an insertion hole below cutoff, the hole diameter should be kept under $\lambda/(1.31\sqrt{\varepsilon_r'})$.



(a) radial distribution at the midplane of the gap.



(b) Axial distribution along the axis (z=0, gap center).

Figure 2. Distribution of E-field in the gap and hole area; r_s=0.24, r_1=1.23, r_2=4.51 L=20.5, D=0.3, in cm, ε_r'=20; in the test band at about 3GHz.

The resonant frequency shift produced by a sample is plotted in Fig.3. These results reflect the gap field variations shown in

Fig.2, which means the weaker the gap field, the smaller the shift in resonant frequency. Dielectric measurement sensitivity is determined by the slope of the frequency shift curve. Therefore,the hole effects lower the sensitivity but extend the measurable range because a smaller degree of detuning tends to lessen some difficulties such as mismatch and bandwidth requirement for the heating source in practical measurements. More significant is the extended linear range caused by the hole's presence. We see that curve(c) is almost a straight line up to ε_r'=80. This is not only a consequence of a reduction of the gap field but also an outcome of an extension of the hole field upon insertion of higher permittivity samples which offsets the saturation phenomena evident for the normal case of curve (a).

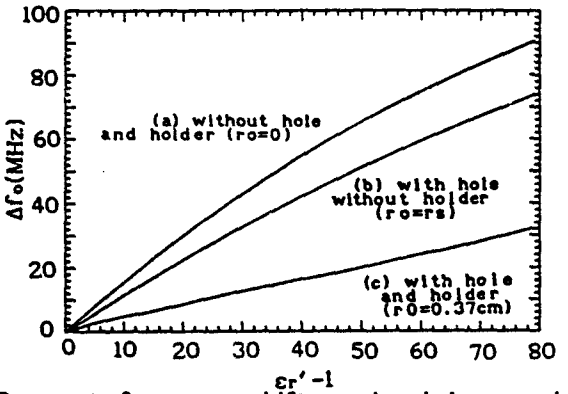


Figure 3. Resonant frequency shift produced by sample in the test band at about 3GHz; r_s=0.24, r_1=1.23, r_2=4.51, L=20.5, D=0.3, in cm.

The loading effects in the heating band are demonstrated in Fig.4 by the resonant frequency shift and the filling factor. The frequency shift does not increase linearly with ε_r' because the hole effects are less significant at a lower frequency but the detuning for ε_r'=80 is nearly the same as in the test band. The filling factor, F,is defined here as the ratio of stored energy in a sample, Ws, to that in the whole cavity, Wc, i.e, F=Ws/Wc. According to perturbation theory, the energy dissipated in a sample, W_D, is directly proportional to its stored energy and W_D=Wstanδ=WcFtanδ. This indicates that, for a constant loss tangent, a higher filling factor means more energy dissipated in a sample. Fig.4 shows that the filling factor increases non-linearly with the dielectric constant. Therefore, the dissipated energy increases not only with the the loss tangent but also with the dielectric constant; both are normally temperature dependent. As a result, the matching condition of a sample loaded cavity will vary greatly while the sample is being heated. A dynamic matching scheme is usually required.

DIELECTRIC DETERMINATION

For a given cavity and frequency band, the resonant frequency shift produced by a sample can be readily calculated by the mode-matching analysis and thus a calibration curve can be established for determining

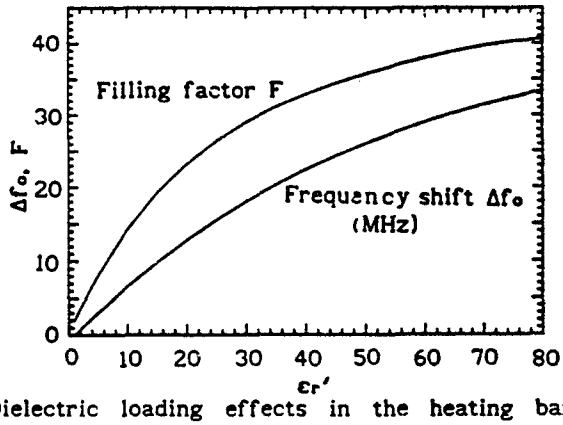


Figure 4. Dielectric loading effects in the heating band at about 915MHz; r_s=0.24,r_0=0.37, r_1=1.23, r_2=4.51, L=20.5, D=0.3, cm.

the dielectric constant from the measured frequency shift. For convenience, this curve can also be expressed by linear equations

$$\varepsilon_r' = 1+1.77(\Delta f_0) \qquad 1 \le \varepsilon_r' \le 10 \qquad (1)$$

with an absolute error ≤±0.1 and

$$\varepsilon_r' = 2.687(\Delta f_0)-3.9 \qquad 10 < \varepsilon_r' \le 75 \qquad (2)$$

with a relative error <2%, where Δf_0 is the absolute frequency shift in MHz. These equations correspond to our cavity dimensions shown in Fig.1 and to the frequency band of 3GHz in which we measure. The accuracy of the determined dielectric constant depends on the uncertainties of both calculated and measured Δf_0, i.e.,

$$\Delta f_0 = \frac{\partial \varepsilon_r'}{\partial(\Delta f_0)}(\delta(\Delta f_0)_{calc.}+\delta(\Delta f_0)_{meas.}) \qquad (3)$$

Since Δf_0 is a relative parameter which can be calculated and measured quite accurately, the uncertainties of $\delta(\Delta f_0)_{calc.}$ and $\delta(\Delta f_0)_{meas.}$ can be made less than ±0.05MHz which produces a maximum $\delta\varepsilon_r'$ of ±0.13. It should be noted that a 1% of variation in sample radius as seen in the unavoidable looseness of a solid sample will cause a 2% error in ε_r'. This error would be much larger if a sample holder was not used [6].

The loss factor can be determined from the drop in cavity Q after

a sample is loaded. Using the perturbation theory, the loss factor can be written as

$$\varepsilon_r'' = \frac{f_0(\varepsilon_r'-1)}{2\Delta f_0}(1/Q_0'-1/Q_0) \qquad (4)$$

where Q_0 and Q_0' are the cavity Q before and after the sample is loaded. This equation is found to be a valid approximation only for $\varepsilon_r' \leq 30$ if $r_s=0.25$ and D=0.3cm. For better accuracy, the loss factor can be calculated from

$$\varepsilon_r'' = \frac{\varepsilon_r'}{F}(1/Q_0'-1/Q_0) \qquad (5)$$

where the filling factor, F, can be calculated by the mode-matching program and expressed by a polynomial

$$\varepsilon_r''/F = 1000X(2.1+0.128\varepsilon_r'-0.00277\varepsilon_r'^{2}+2.525X10^{-5}\varepsilon_r'^{3}-1.108X10^{-7}\varepsilon_r'^{4})$$

The accuracy in the determined loss factor is mainly affected by the errors in Q measurements. In a reflectometer setup, the maximum error of measured Q is estimated to be ±10% and ±4% if the directivity of the directional coupler is 30dB and 40dB, respectively.

SYSTEM DESCRIPTION

The testing and heating system is shown in the block diagram of Fig.5. A scalar network analyzer (HP 8756A) is used in a reflectometer setup to measure the reflection spectrum of the cavity before and after a sample is inserted, from which the frequency shift and Q change, and therefore, the dielectric constant and loss factor are determined.

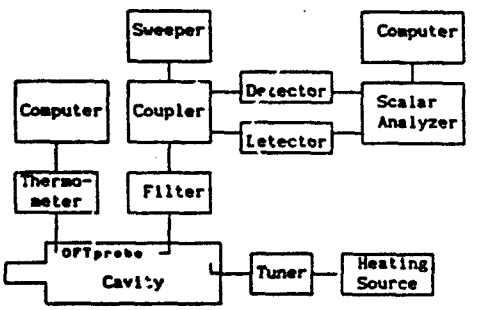


Figure 5. Measurement system.

The cavity is the coaxial re-entrant cavity discussed above and its

dimensions are given in Fig.1. The gap width is adjustable via a non-contact movable bucket short circuit which is designed to give an effective short at both the heating and testing frequencies. The inner surface of the cavity is gold-plated, giving a Q-factor of about 3000 and 1500 at 3GHz and 915MHz, respectively, when it is empty. The cavity has two coupling loops, one for the testing and the other for the heating channel.

The sample is contained in a fused quartz tube with 0.71cm OD X 0.5cm ID. As it is tested, the sample is heated simultaneously by a 60W solid state 915 ±20MHz power source. The heating source provides readouts of the incident and reflected power. A three stub tuner is used for matching the loaded cavity.

A high pass filter is connected between the analyzer and the cavity to prevent the heating power from being coupled into the analyzer which is operated at the test band. It presents very low insertion loss at 3GHz but about 60dB insertion loss at 915MHz.

The surface temperature of the sample is measured with an optical fiber thermometer* . A lightpipe probe is positioned at the gap center and the edge of the inner conductor and hardly disturbs the microwave field. It has a temperature range from 500 - 2000^{0}C and responds almost instantaneously. Its resolution is as high as 0.1^{0}C at 2000^{0}C but accuracy depends on the placement. We found that the temperature reading does not vary greatly with the probe-sample distance from the sample but will be misleading if the probe does not aim at the sample properly.

Dielectric and temperature measurements are carried out automatically via computer control. The maximum sampling time is one second and would be less if the analyzer could transfer its data faster. Conversely, the heating rate can be slowed down by reducing the output level of the heating source.

EXPERIMENTAL RESULTS

Using the high temperature dielectric measurement system described above, various materials, such as zeolite, silicon carbide, mullite, alumina, cupric oxide, soda lime glass and the like, have been tested. The system is first checked by measuring a number of well characterized liquids at room temperature and the obtained results are found to agree well with the published data [6].

Dynamic data of zeolite powder (3A, 0.88g/cm^{3}) being heated by a fixed power level of 25W at 915MHz are presented in Fig.6 to demonstrate the inter-relationship among dielectric properties, temperature and heating rate, and the reflected power from the cavity. When the heating starts, the loaded cavity is tuned to be overcoupled and 20% incoming power is reflected. As the temperature of the sample is rising, the sample becomes lossier, whereby the cavity is first

* Model 100C, Accufiber, Beaverton, OR, U.S.A.

brought into a critical coupling or matched condition and then shifted into an over-coupled condition which again raises the reflection. At a critical temperature (about 200°C for zeolite), the sample's loss and heating rate increase exponentially. Temperature run-away would take place if the net power into the sample was increased and the heat loss was eliminated. Instead, the heating enters a stable phase. We found that local melting of zeolite occurs around 700°C and cavities may thus formed in the sample. Density changes will invariably lead to erroneous dielectric data. Therefore, local melting should be prevented. Moreover, a significant thermal expansion occurs in most powder samples. To control the density, it is necessary to press the sample before heating it.

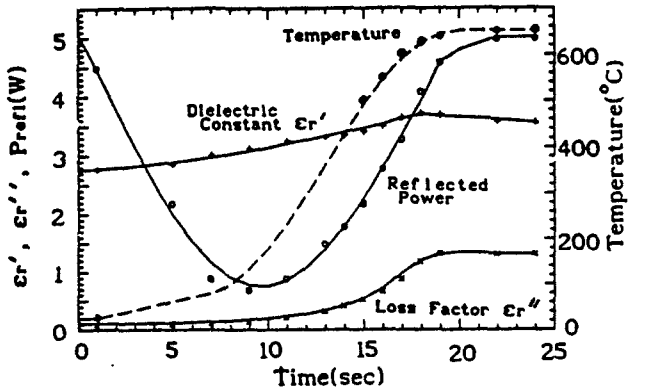


Figure 6. Dynamic heating curve of zeolite powder at a fixed input power of 25W at 915MHz, showing varying dielectric properties, temperature and power reflection.

Fig.7 is the heating curve of mullite rod (MV20, McDanel) up to 1300°C. It is difficult to heat the sample at the begining due to the sample's low loss at room temperature and the heat loss via conduction. Therefore, the sample is inserted without using the holder to avoid the contact with metal walls. During heating, the power level is adjusted to maintain a moderate heating rate of about 30°C/s. The frequency of the heating source is tuned to follow the changes in resonant frequency. The stub tuner is held at a fixed but optimum position which can keep the reflection less than 10% for an entire period of the test. For a long heating period, the cavity's thermal expansion will cause the measured dielectric constant to be higher than the true value. This error can be counteracted by adjusting the gap width.

Fig.8 shows the temperature dependence of the dielectric properties of silicon carbide powder (500mesh, 1.88g/cm^3). The data are taken while the sample is cooling down after being heated to about 1000°C. The cooling curve is selected because the dielectric

properties of silicon carbide during heating are found to be rather unstable. Besides, the sample seems to have a high thermal

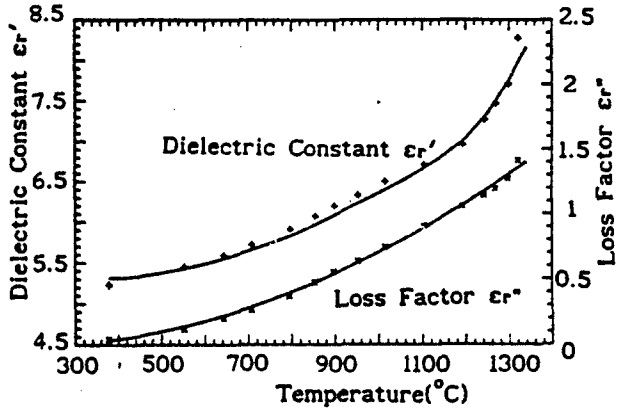


Figure 7. Temperature dependence of dielectric properties of mullite, measured while the sample is being heated by a 60W, 915MHz heating source.

conductivity which means that the heat loss via conduction becomes more significant. In order to heat the sample to as a high temperature as possible, matching has to be conducted dynamically. However, the

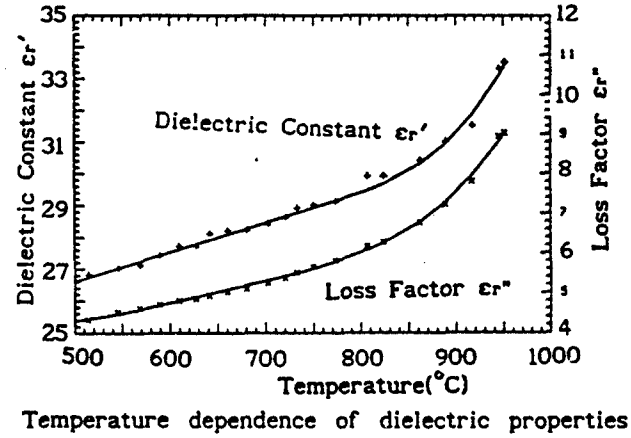


Figure 8. Temperature dependence of dielectric properties of silicon carbide powder, measured while the sample is cooling.

adjustment of the tuner may disturb the resonant curve in the testing band, thus endangering the measurement reliability. On the other hand, the measurement taken during the cooling period is far more stable and consistent, but it is applicable only to thermally reversible materials. The microwave heating behavior of SiC needs to

be investigated further.

CONCLUSION

A high temperature microwave dielectrometer design has been presented which is shown to be capable of measuring the complex dielectric constant versus temperature curve up to at least 1200°C, in about 20 seconds, while the sample is being rapidly heated by 60 w of 915 MHz microwave power. Small cylindrical samples, of non-critical length, are easily inserted via the use of a hollow coaxial center conductor. Calibration of the cavity is based on a mode matching analysis which accurately predicts the sample loading and hole effects on the cavity characteristics. Dielectric data on the behavior of silicon carbide and mullite with temperature are given to 1300°C. The use of a hollow center conductor is also shown to linearize the dielectrometer response up to a dielectric constant value of 80.

ACKNOWLEDGEMENT

This work was sponsored by the Natural Scientific and Research Council of Canada.

REFERENCES

1 D.Couderc, M.Giroux and R.G.Bosisio, "Dynamic high temperature permittivity measures on samples heated via microwave absorption", J. of Microwave Power, 8(1), 69-82, 1973

2 J.Jaw, M.Finzel, J.Asmussen and M.C.Hawley,"Dielectric and temperature measurements during microwave curing of epoxy in a sweeping resonant cavity", IEEE MTT-S Digest, 465-468, 1987

3 M.Ollivon, S.Quinquenet, M.Seras, M.Delmotte and C.More, "Microwave dielectric measurements during thermal analysis", Thermochimica Acta, 125, 141-153, 1988

4 W.Xi and W.R.Tinga, "New results on coaxial re-entrant cavity", tc be published

5 W.R.Tinga, B.Q.Tian and W.A.G.Voss, "New high temperature multipurpose applicator", Materials Research Society Proceedings, Symposium L, 1990

6 W.Xi and W.R.Tinga, "Field analysis of new dielectrometer", to be published

EFFECT OF POWDER CHARACTERISTICS ON DIELECTRIC PROPERTIES OF ALUMINA COMPACTS

R. Moreno, P. Miranzo, J. Requena, J.S. Moya
Instituto de Cerámica y Vidrio, C.S.I.C.
28500 Arganda del Rey, Madrid (SPAIN)

J. Mollá & A. Ibarra
Asociación EURATON-CIEMAT para Fusión
Avda. Complutense 22, 28040 Madrid (SPAIN)

Abstract

Three different submicronic alumina powders have been analyzed. The sintering and microstructural evolution of the different green compacts have been studied by dilatometry and SEM, respectively. Dense (>99 %th) alumina samples were used for the measurement of the dielectric properties at 20 GHz. The dielectric properties have been related to the impurities content, grain size distribution, porosity, etc. The important effect of small quantities of MgO in solid solution on the microwave absorption of alumina compacts has been pointed out.

INTRODUCTION

The characterization of the dielectric properties of ceramic materials at high frequencies (1-100 GHz) has recieved an increasing interest in the last few years due to the needs of very different emerging technologies like microwave heating for fusion applications, microelectronics, microwave sintering, warm superconductors, etc. Alumina is one of the best known ceramic materials although with respect to its high frequency dielectric properties (specifically the loss tangent) it does not show a reliable behaviour in different samples of the same quality produced by different suppliers and even in samples of the same origin but different batches.

The origin of the observed microwave absorption and the effect of the different types of defects, dopants or microstructural characteristics of alumina ceramics are not clearly defined at present. As an example of this situation, the dependence of the loss tangent with the grain size is a matter of controversy. Some authors claim that fine grained alumina has

increased losses due to the higher number of grain boundaries [1]; however, recent results indicate that it is possible to obtain fine grained alumina with low losses and even that there is no grain size dependence [2].

In the present work the effect on the dielectric properties of the sintering time, grain size and microstructure of several alumina samples produced using high purity powders of different origin and characteristics has been studied.

MATERIALS AND METHODS

Aluminas with similar characteristics and different MgO content have been selected for this study. These powders have been labeled as follows: (1) Condea HPA-0.5 without MgO, (2) Condea HPA-0.5, Mg with 0.05 wt% MgO as sintering aids and (3) Baikalox (Baikowski) powder with very low MgO content (0.003 wt%).The characteristics of these powders are reported in Table I.

Table 1. Characteristics of the Alumina Powders.

ALUMINA POWDER	SAMPLE 1*	SAMPLE 3
CHEMICAL ANALYSIS (wt%)		
SiO_2	0.006	0.054
Fe_2O_3	0.002	0.1
TiO_2	-	0.01
CaO	0.002	0.008
MgO	0.002	0.003
Na_2O	0.004	0.02
K_2O	-	0.01
Al_2O_3	99.97	99.36
SPECIFIC SURFACE AREA (m^2/g)	10	9
MEAN PARTICLE SIZE (μm)	0.5	0.25

* Sample 2 has the same characteristics with 0.05% of MgO.

Green compacts have been obtained by wet bag isostatic pressing at 207 MPa (30.000 psi). Dynamic sintering has been studied by means of dilatometric measurements. Static sintering behaviour has been also investigated by heating samples at 1550°C for holding times 1, 1.5, 4 and 50 hours in an electric furnace. The green and final densities have been determined by Hg and H_2O immersion methods, respectively.

The microstructure of the sintered samples has been observed by scanning electron microscopy (SEM) on polished and thermally etched surfaces. Grain size distribution have been evaluated on SEM micrographs by using an image analyzer. By this method the spherical equivalent diameter is evaluated considering that the area enclosed by the closed

boundary of a grain is equal to that of a circle. At least 150 grains per sample have been measured.

The dielectric properties (permitivity and loss tangent) have been measured at 20 GHz at room temperature from the resonant frequency and quality factor of the cavity with and without the sample inside the cavity [3]. Our cylindrical cavities work in the TE_{012} mode with halfwidth around 1 MHz. The diameter of the cavity is 20 mm and the length can be varied between 9 to 45 mm. They are made of brass and the powder is coupled through a longitudinal slot situated in the cylinder wall. With this system it is possible to measure the permitivity in the range between 1 to 30 with errors lower that 0.5 % and loss tangent values as low as 10^{-4} with 10% error [4]. The samples are disk shaped with 10 mm radius and 3mm height. The flatness between the samples faces is better than 5 μm.

RESULTS AND DISCUSSION

Dynamic sintering measurements reveal that no significant differences between the starting alumina compacts with and without MgO addition exist. The addition of MgO does not modify the sintering rate of alumina, although it leads to slightly higher final densities. This is in good agreement with other authors [5], but no reduced initial sintering rate for doped alumina has been observed, as proposed by other authors [6]. The resulting fired densities were higher than 99%th.

Figures 1-3 show the grain size distributions of samples 1, 2 and 3 at different sintering times. As can be observed, when MgO is added the grain size distribution shifts to lower values. Small MgO additions prevent discontinuous grain growth and allow the material to be sintered to nearly theoretical density. The effect of MgO can be observed in Figure 4, in which SEM micrographs of samples 1 and 2 heated at 1550°C/50h are shown. Discontinuous grain growth occurs in the undoped samples. Also, there are pores inside the large grains. For these trapped pores the diffusion distance to the next grain boundary is very large and nearly impossible to eliminate. The effect of the dopant is that pores remain at grain boundaries until they are eliminated.

The obtained permitivity values are the typical ones observed for policrystalline alumina [7]. There is neither dependence on the powder origin nor on the sintering time. The small differences between the samples can be correlated with density effects (Figure 5). Theoretical estimations for ceramic materials with spherical pores predict a linear relationship between porosity and permitivity as long as the porosity does not exceed 10% [8]. In the case of alumina a linear relationship with a slope of about 0.13 [9] has been observed, which is in good agreement with that obtained in the present work ($\approx$0.17).

Conversely, the loss tangent values show a marked dependence on the powder origin. Figure 6 shows the loss tangent as a function of sintering time. For the powders 1 and 3 there is no dependence on the sintering time, whereas powder 2 shows a slight dependence for very long times. The powder 2 (MgO doped sample) has loss tangent over a factor of 2 greater than the others. This can explain the differences observed between the samples obtained from differents companies or even between different batches of the same material.

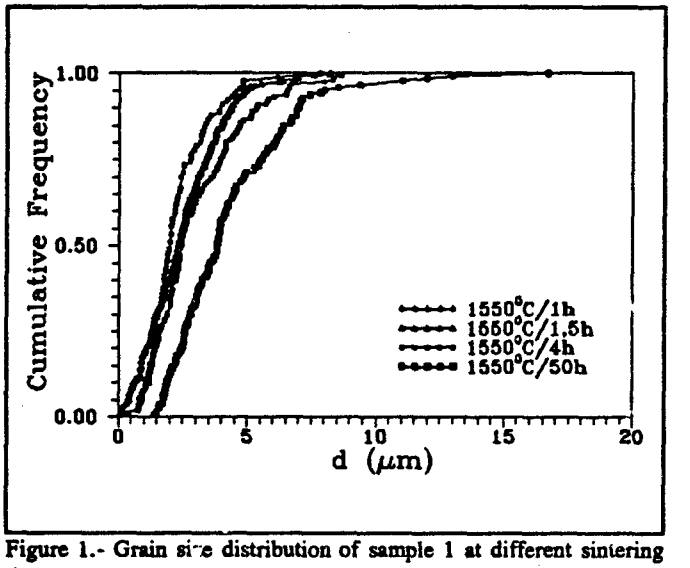


Figure 1.- Grain size distribution of sample 1 at different sintering times.

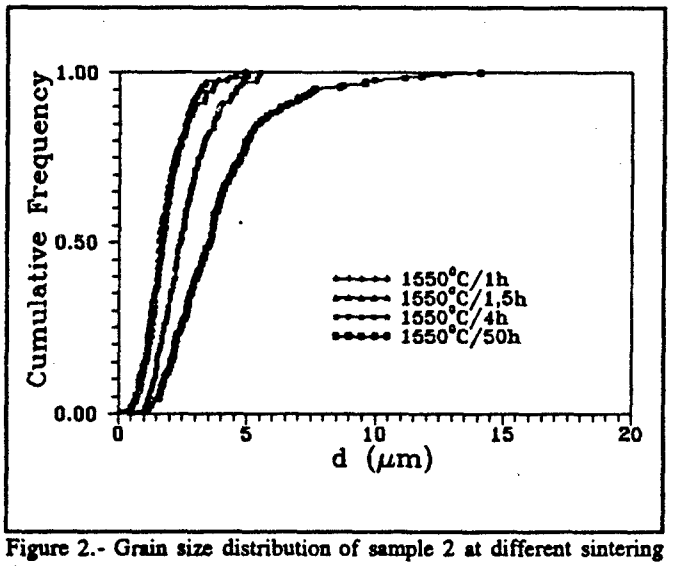


Figure 2.- Grain size distribution of sample 2 at different sintering times.

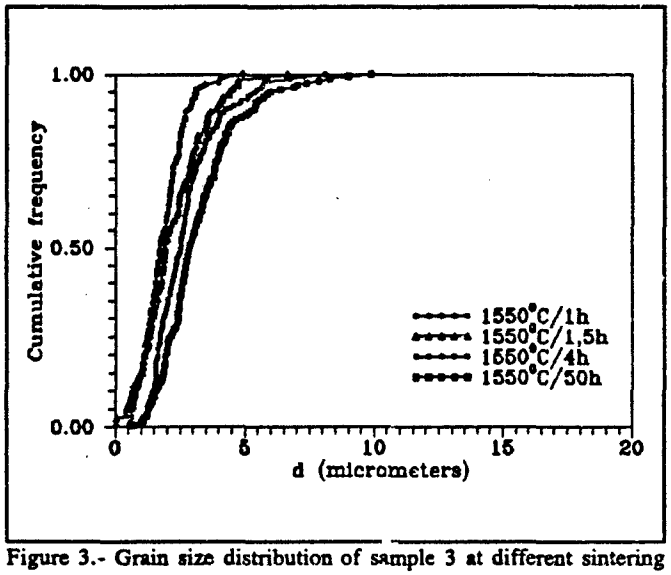


Figure 3.- Grain size distribution of sample 3 at different sintering times.



Figure 4.- SEM micrographs of samples 1 (a) and 2 (b) heated at 1550°C/50h.

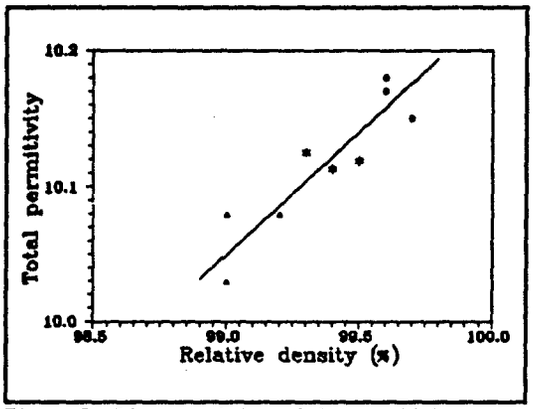


Figure 5.- Linear variation of the permitivity versus total density for samples 1 (*), 2 (o) and 3 (▵).

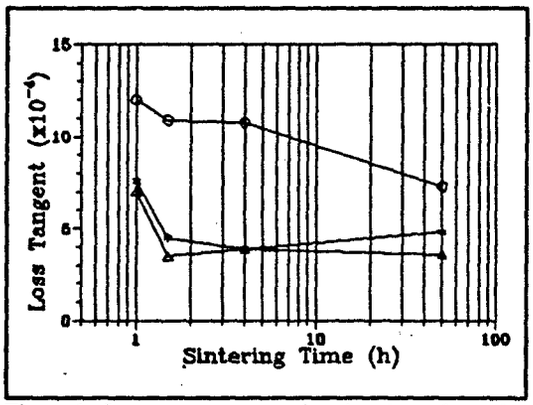


Figure 6.- Loss tangent versus sintering time of samples 1 (*), 2 (o) and 3 (▵).

Figure 7 shows the loss tangent values as a function of grain size. From this figure it is clear that there is no dependence of the loss tangent on the grain size distribution. This result is in agreement with previously mentioned results for high purity alumina grades [2].

It is interesting to point out that the only difference between the powders 1 and 2 is the addition of MgO to 2 as a sintering aid. This indicates that MgO is responsible for the observed increase in the loss tangent values. Many authors agree that precipitation of spinel at grain boundaries takes place for MgO concentrations $\geq$ 0.1%. Consequently the MgO in sample 2 (0.05 wt%) must be in solid solution [10,11].

Solid solution of MgO in Al_2O_3 lattice induces the formation of oxygen vacancies and

prevents exaggerated grain growth and consequently affects the microstructure of the fired compacts. Therefore, the observed increase in the loss tangent values can be explained by either the microstructure changes or the increase in the concentration of oxygen vacancies. The first possibility can be disregarded because no dependence on the grain size from the samples prepared using the same starting powder has been observed (Figure 7). Then, the higher losses observed in sample 2 must be related to the high oxygen vacancy concentration. The slight decrease of loss tangent value detected in MgO-containing samples with the sintering time may be associated with precipitation phenomena.

It is also interesting to point out that powders 2 and 3 have been produced by different suppliers and the type and amount of impurities are quite different. However, there are no significant effects on the dielectric properties, indicating that not all the impurities induce the effect observed for MgO.

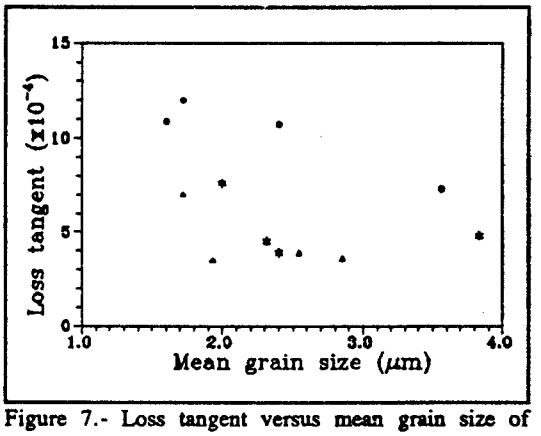


Figure 7.- Loss tangent versus mean grain size of samples 1(*), 2(o) and 3(Δ).

The microwave absorption (directly related to the loss tangent) can be expressed as the sum of contributions from the conductivity of electrons or ions and relaxation processes. With respect to the last one, two kinds of contributions can be identified: 1) large defects like clusters and dipoles and 2) polarization mechanisms associated to point defects or intrinsic polarizability of the lattice. The formation of oxygen vacancies gives rise to Mg-vacancy dipoles and different types of clusters [12]. These defects induce very strong absorption processes at low frequencies as well as changes in the polarizability, which means that the effect of MgO on the high frequency dielectric properties can be associated with a low frequency maximum or with a higher lattice polarizability around the MgO. The low frequency maximum could be due to the ionic conduction induced by the presence of the oxygen vacancies or dipolar effects that appear as a consequence of charge trapping at the Mg-vacancy sites. It is known that MgO can induce very strong absorption processes at low frequencies (1Hz to 10 KHz) [13]. It seems reasonable to relate the observed effect of MgO in the loss tangent with these types of defects.

These results open the possibility to control the microwave absorption of alumina by the control of dopants. This fact can be considered of great interest in emerging technologies like microwave sintering, radiofrequency heating, etc. More reseach is required in order to clarify the role of other possible dopants and the mechanism by which MgO changes the high frequency loss tangent of alumina ceramics.

CONCLUSIONS

From the results obtained in the present work, the following conclusions can be drawn:

(i) It has been proved that permitivity does not change with the powder origin; it only changes with the density.

(ii) Loss tangent depends neither on grain size nor on sintering time, but shows a marked effect (increases by a factor of ~ 2) with the addition of small quantities (0.05 wt%) of MgO.

ACKNOWLEDGMENTS

The CIEMAT work has been made in the frame of the CEE Fusion Technology Research Program. This work has been partially supported by CICYT (Spain).

REFERENCES

1. W.W. Ho, "MMW Dielectric Property Measurement of Gyrotron Window Material", ORNL/Sub/83-51928/2, Report (1985).

2. J. Mollá and A. Ibarra, "Dielectric Properties of Insulators for Fusion Applications", EUR-CIEMAT, Report 89/14 (1989).

3. R.J. Cook, in "Microwave Cavity Methods", Proceedings of a Tutorial Conference on Measurements of High Frequency Dielectric Properties of Materials, J. Chamberlain and G.W. Chantry, eds., NPL, Teddington, UK (1972).

4. J. Mollá and A. Ibarra, "A System for the Measurement of Insulator Materials Permitivity", EUR-CIEMAT Report 89/13 (1989).

5. P.A. Lessing and R.S. Gordon, in "Deformation of Ceramic Materials", pp. 271-96, R.C. Bradt and R.E. Tressler, eds., Plenum, New York (1974).

6. P.J. Jorgensen, "Modification of Sintering Kinetics by Solute Segregation in Al_2O_3", J.Am.Ceram.Soc., 48 (4) 207-10 (1965).

7. A.R. Von Hippel, "Dielectric Materials and Applications", Cambridge MIT Press (1966).

8. G. Ondrack, Reviews on Powder Metallurgy and Physical Ceramics, 3, 205-322 (1987).

9. R. Heidinger, private communication.

10. A.H. Heuer, "The Role of MgO in the Sintering of Alumina", J.Am.Ceram.Soc., 62 (5/6) 317-18 (1979).

11. W.C. Johnson and R.L. Coble, "A Test of the Second-Phase and Impurity Segregation Models for MgO-Enhanced Densification of Sintered Alumina", J.Am.Ceram.Soc., 61 (3/4) 110-14 (1978).

12. H.A. Wang, C.H. Lee, F.A. Kröger and R.T. Cox, "Point Defects in Al_2O_3:MgO Studied by Electrical Conductivity, Optical Absorption and ESR, Phys.Rev., 27 (6) 3821-41 (1983).

13. R. Vila and M. Jimenez de Castro, "Dielectric Polarization of Magnesium doped Aluminium Oxide", in "VI Europhysical Topical Conference on Lattice Defects in Ionic Crystals", Groningen (The Netherlands) sept. 1990. To be published in Rad. Effects and Def. in Sol.

DIELECTRIC PROPERTIES OF CERAMICS AT MICROWAVE FREQUENCIES

N. H. Harris, J. R. Chow, R. L. Eisenhart and B. M. Pierce
Materials Science Department, E1/F150
Hughes Aircraft Company
El Segundo, CA 90245

The dielectric properties of alumina and silicon nitride have been determined using modified rectangular microwave waveguide techniques from 22° to 900°C over 8-12 GHz and modified coax techniques from 25° to 500°C over 2-18 GHz. The coax techniques were used to determine the temperature and frequency dependence of the dielectric properties of silicon nitride and of phosphate bonded alumina reinforced with silicon carbide whiskers. The coax techniques provide broadband dielectric property data that can be applied to the understanding and enhancement of the coupling behavior of ceramics, especially in the initial heat-up period of microwave processing.

INTRODUCTION

In a recent review of the state-of-the art in microwave processing of ceramics by Sutton, it was pointed out that one of the major obstacles to its widespread application in the ceramics industry is the lack of dielectric properties data for many ceramic materials [1]. The objective of our study was to develop a method for high temperature dielectric property measurements over 2 to 18 GHz at elevated temperatures and to perform measurements on silicon nitride and a silicon carbide reinforced alumina composite. Measurement of the dielectric properties becomes particularly important when considering the effect of impurities or the addition of sintering aids on the microwave coupling of these materials as a function of temperature [2,3].

In Table 1 the advantages and disadvantages of three measurement techniques are compared. The resonant cavity is best for low loss tangent materials but is limited to a very narrow band, is very dimension sensitive and requires multiple fixtures and samples to cover the 2 to 18 GHz frequency range.

The waveguide method has the advantages of a convenient rectangular sample shape and is the least sensitive to the sample dimensions. However, a disadvantage of the waveguide method is that it requires five sets of waveguides, samples, calibrations, and measurements to cover the 2 to 18 GHz range. In addition the size of sample required for the lower frequency waveguides becomes very large.

In contrast the coaxial fixture covers the full bandwidth with only one small (7 mm outside diameter) sample and one measurement. More importantly the correction for the air gap is much less complex than for the rectangular waveguide due to the radial symmetry of the electric field.

Table 1. Transmission Line Measurement Approach Comparison

1. RESONANT CAVITY	BEST FOR LOW LOSS TANGENT (<0.1)	VERY NARROW BAND REQUIRES MULTIPLE FREQUENCY SAMPLE POINTS VERY DIMENSION SENSITIVE
2. WAVEGUIDE FIXTURE	SIMPLE SAMPLE SHAPE LEAST SENSITIVE TO DIMENSIONS	MODERATE NUMBER OF BANDS - REQUIRES 5 OF EACH TO COVER 2 TO 20 GHz WAVEGUIDES SAMPLES CALIBRATIONS, MEASUREMENTS
3. COAXIAL FIXTURE	COVERS FULL BAND REQUIRES ONLY ONE SAMPLE EASIEST TO CALIBRATE	COMPLEX SAMPLE SHAPE VERY DIMENSION SENSITIVE SOME COMPLEXITY WITH CENTER CONDUCTOR

The disadvantages of the coaxial fixture include the sample shape complexity, the dimensional sensitivity and some complexity with the center conductor.

Measurements were based on a modification of standard transmission methods [4] in specially prepared high temperature waveguide and coax fixtures at Hughes. The Hughes coaxial fixture differs from other high temperature coax fixtures in that it involves a dual port transmission measurement which inherently provides greater sensitivity than the commonly used single port techniques.

The free space method used by W. Ho is readily adaptable to the use of a furnace to obtain dielectric properties measurements at elevated temperatures [5]. However the free space method is limited to frequencies greater than 30 GHz. Since most commercial microwave heating equipment operates at 0.915 and 2.45 GHz, some at 5.8 GHz and a very few at 28 GHz, the dielectric properties obtainable by the 7 mm coax in the 2 to 18 GHz range would be quite useful in developing the data base necessary for widespread utilization of microwave processing in ceramics.

While the Hughes coax is limited to ultimately 900°C, by its current materials of construction, it has only been used in dielectric measurements to 500°C. The temperature range of ambient to 500°C is of interest in studying the behavior of ceramic materials during the initial heating period in the sintering process. It is expected that the Hughes coax fixture will be useable to 900°C with further refinements.

EXPERIMENTAL PROCEDURE

The elevated temperature transmission line microwave measurements system schematic diagram is shown in Figure 1. The transmission line measurement utilizes an HP8510B network analyzer, an

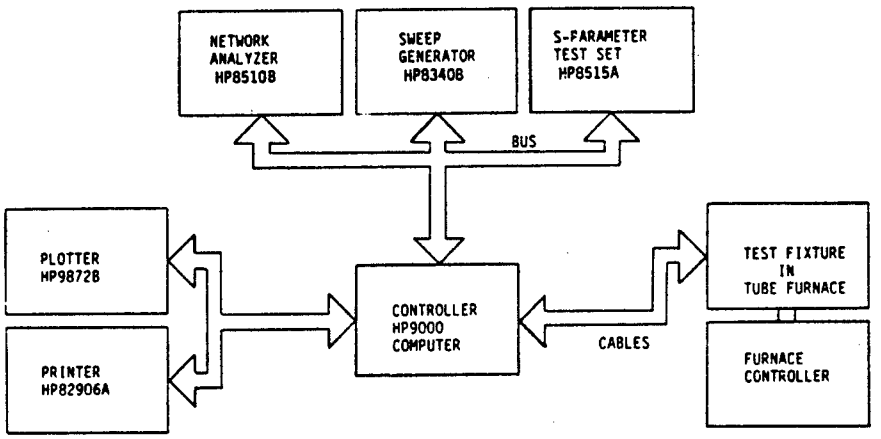


Figure 1. Elevated Temperature Transmission Line Microwave Measurement System.

HP8340B sweep generator and other associated components controlled by an HP9000 computer.* The primary source of error which must be taken into consideration is that of the air gap. The air gap error was not corrected in the waveguide but was corrected in the coax fixture based upon the radial symmetry of the electric field. A diagram representing the cross-section through the coax fixture and the test specimen is shown in Figure 2. The relation for the effective dielectric constant, ε_{eff}, relative to the magnitude of the air gaps is given as follows:

$$\varepsilon_{eff} = \frac{\ln(d/a)}{[\ln(d/e) + (1/\varepsilon_a)\ln(c/b) + \ln(b/a)]} \qquad (1)$$

where a is the outside diameter of inner conductor, b is the inside diameter of the sample, b - a is the inner air gap, d is the inside diameter of the 7 mm coax fixture, c is the outside diameter of the sample and d - c is the outer air gap. These dimensions are shown in Figure 2. The usefulness of this relation in providing an air gap correction was demonstrated first for the outside diameter (OD) correction in Figure 3 and for the inside diameter (ID) correction in Figure 4 using a series of specially machined Rexolite** specimens. The correction in the measurement software controlling the network analyzer totally eliminated the air gap effect for up to a 5.5% OD gap [(d - c)/c] and for as much as a 13.5% ID gap [(b - c)/a]. The magnitude of the gap correction can be seen by comparison of the corrected and uncorrected data in Table 2 and in Figures 3 and 4. The program was able to correct for air gap dimensions larger than the anticipated gaps resulting from thermal expansion mismatch between the metal fixture and the ceramic specimen.

* HP denotes products of Hewlett-Packard Co., Palo Alto, CA.

**Rexolite is a polymer product of Union Carbide Co., Danbury, CT.

Table 2 Gap Dimensions of Rexolite in Coax Fixture at 22°C.

NUMBER	LENGTH(mm)	OUTSIDE DIAMETER(mm)	INSIDE DIAMETER(mm)
RX-01	4.059	7.264	3.200
RX-02	4.084	7.264	3.272
RX-03	4.064	7.264	3.594
RX-04	4.069	7.264	4.572
RX-05	4.072	7.209	3.175
RX-06	4.069	6.858	3.175
RX-07	4.072	5.842	3.175

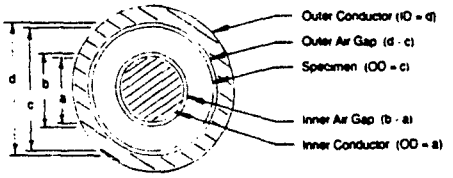


Figure 2. Coax Gap Error Considerations (Coax Gap Error Relationship).

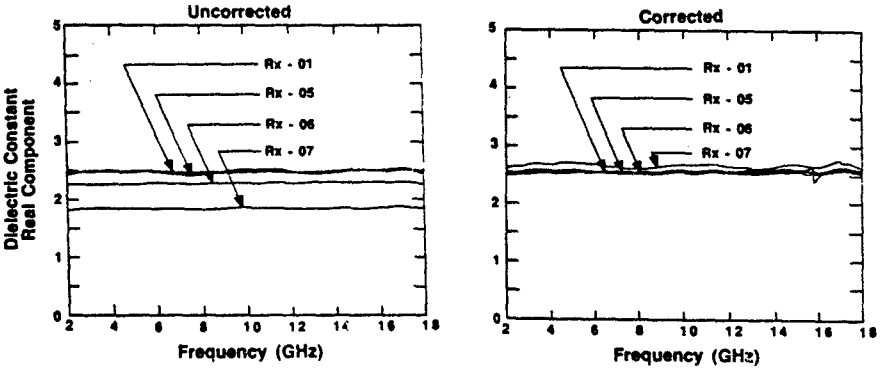


Figure 3. Coax Gap Error Considerations (Outside Diameter Correction).

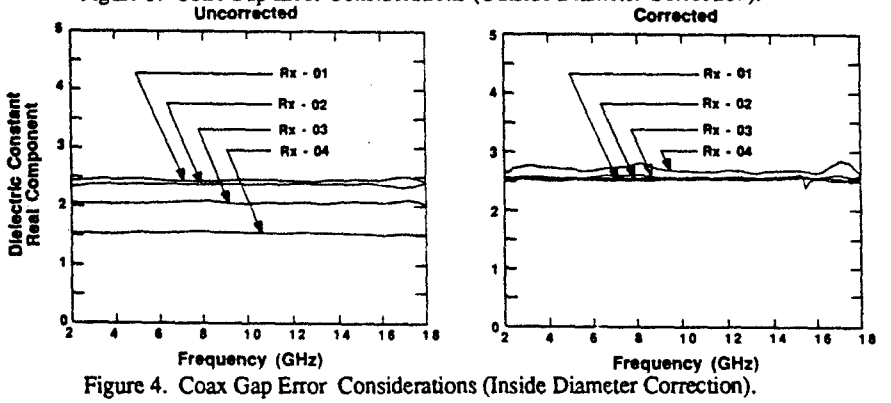


Figure 4. Coax Gap Error Considerations (Inside Diameter Correction).

In the present study specimens were machined from disks prepared from submicron alumina*** mixed with 10% phosphoric acid**** and from 0 to 5 weight percent silicon carbide whiskers*****. The materials were mixed, screened -200 mesh, and then cold pressed with a uniaxial pressure of 10,000 psi. The disks were then cured at 750°C for 4 hours. After machining, the specimens were dried in a vacuum oven at 150°C for more than 24 hours. The specimens were stored in a desiccator until the dielectric measurements were performed to prevent misleading results due to the absorption of moisture from the atmosphere.

The dielectric properties of silicon nitride* were determined from 25° to 900°C in the X-band waveguide. The same silicon nitride* was measured in the coax fixture along with a silicon nitride** and mixtures of phosphate bonded alumina with 0, 1.0, 2.5, and 5.0% (by weight) SiC whiskers. The gap sensitivity measurements for the coax fixture dielectric properties were performed on a series of Rexolite specimens at 22°C. The air gaps in the Rexolite specimens were machined so that they accounted for the anticipated gaps resulting from the difference in thermal expansion coefficients of the metal coax fixture and various ceramic test specimens.

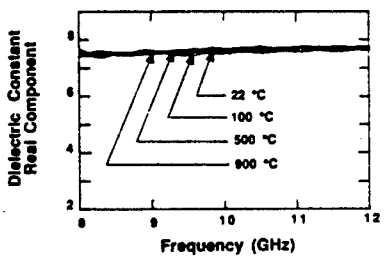


Figure 5. Dielectric constant (real component) of silicon nitride (Kyocera 220) over 8-12 GHz from 22° to 900°C.

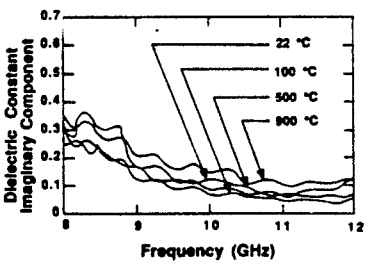


Figure 6. Dielectric constant (imaginary component) of silicon nitride (Kyocera 220) over 8-12 GHz from 22° to 900°C.

---

* Silicon nitride 220M, slip cast, Kyocera, Nagoya, Japan.

** Silicon nitride, Toshiba Ceramics, Tokyo, Japan.

*** Alumina, Grade A-16-SG, ALCOA, Bauxite, AR.

**** Phosphoric acid, reagent grade, J. T. Baker Co., Phillipsburg, NJ.

***** Silicon nitride whiskers, ARCO Specialties Co., NC.

RESULTS AND DISCUSSION

The results of the dielectric constant determination (real and imaginary components respectively) are shown in Figures 5 and 6 for the silicon nitride* in the X-band waveguide with temperatures from 25° to 900°C. These results are uncorrected for air gaps. The air gap between the test sample and the waveguide increases with higher temperatures due to the higher thermal expansion coefficient of the metal waveguide compared with the ceramic test specimens.

The same silicon nitride* was measured in the coax fixture with the results shown in Figure 7 for both the real and imaginary components of the dielectric constant for 25°, 200° and 500°C each over the 2 to 18 GHz frequency range. The coax results for another silicon nitride** are shown at 25° and 500°C over the 2 to 18 GHz frequency range in Figure 8. The values obtained were 7.5 +/- 0.5 for the real and 0.2 +/-0.1 for the imaginary component of the dielectric constant which compare favorably with the values reported by W. Ho at 35 GHz (ε_r = 7.5 - 8.8 at 23°C), [5]. The

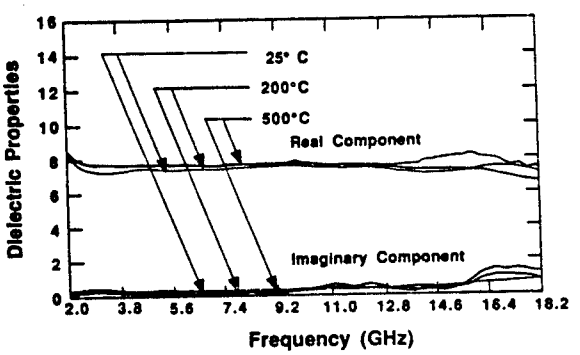


Figure 7. Dielectric constant vs. frequency (2-18 GHz) of silicon nitride (Kyocera 220) at 25°, 200°, and 500°C.

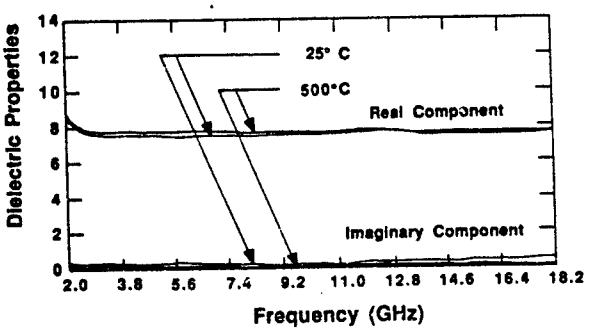


Figure 8. Dielectric constant vs. frequency (2-18 GHz) of silicon nitride (Toshiba) at 25° and 500°C.

* 220M, slip cast silicon nitride, Kyocera, Nagoya,Japan.
** Silicon nitride, Toshiba Ceramics, Tokyo, Japan

broad spectral results of the coax method points out that the narrow band waveguide results may be in question. As seen in Figure 6 the imaginary component of the dielectric constant as measured in a waveguide increases anomalously at lower frequencies but remains relatively constant when measured in a coax as shown in Figure 7. It has been determined that this effect is caused by the controller software and that it can be resolved with program modification.

The dielectric constant real and imaginary components were determined for a series of phosphate bonded alumina samples with silicon carbide reinforcing from 0 to 5.0% by weight. The real components are shown at 25°C and 500°C in Figure 9. The imaginary components are shown at 25° and 500°C in Figure 10. It can be seen that at 25°C the effect of the SiC whisker additions is

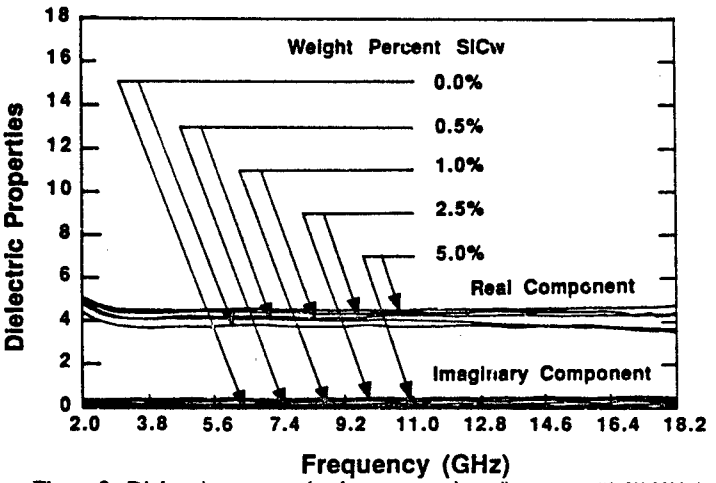


Figure 9. Dielectric constant (real component) vs. frequency (2-18 GHz) at 25°C for 1-5% SiCw/Al_2O_3 + 10% H_3PO_4. (Gap error correction and 10% curve smoothing).

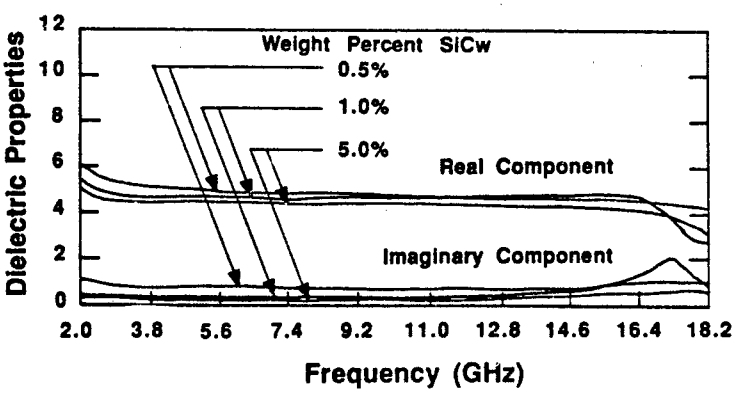


Figure 10. Dielectric constant (imaginary component) vs. frequency (2-18 GHz) at 500°C for 0-5% SiCw/Al_2O_3 +10% H_3PO_4. (Gap error correction and 10% curve smoothing).

negligible. However at 500°C the increasing SiC content resulted in a clearly discernable increase in both the real and imaginary components of the dielectric constant. The higher imaginary component values for the dielectric constant would be expected to enhance the coupling of the composite with microwave radiation so that faster heating rates would result. It is apparent that modification of the composition of ceramic materials is a critical part of optimizing a material system for microwave processing.

Microwave processing of ceramic composites is a complex process. However it is possible, with semi-empirical shape factors, to develop methods for predicting the dielectric properties of discontinuous fiber, whisker and particulate reinforced composite systems. The Hughes coax measurement technique can be used to determine the shape factors necessary to design composites optimized for microwave processing.

CONCLUSION

A high temperature broad frequency band dielectric properties measurement capability has been achieved with a Hughes coax fixture design. A method for correcting coax air gap errors was developed and incorporated into the measurements software. The coax fixture demonstrated sensitive broad band capability to 500°C for silicon nitride with dielectric constant values which compared favorably with published data. Increasing concentrations of SiC whiskers in a phosphate bonded alumina composite resulted in an increase in both the real and imaginary dielectric constant values at 500°C. The Hughes coax design was shown to be a useful method for determining the dielectric properties of ceramic materials up to 500°C in the frequency range of 2 to 18 GHz. The dielectric properties data obtained with the Hughes coax system will be useful in predicting the response of ceramic materials during the initial heat up period of microwave processing

REFERENCES

1. W. H. Sutton, "Microwave Processing of Ceramic Materials" Am. Ceram. Soc. Bul. **68** (2) 376-86 (1989).

2. T. T. Meek, C. E. Holcomb, and N. Dykes, "Microwave Sintering of Some Oxide Materials Using Sintering Aids," J. Mater. Sci. Lett., **6**, 1060-62 (1987).

3. T. T. Meek, R. D. Blake, and J. J. Petrovic, "Microwave Sintering of Al_2O_3 and Al_2O_3-SiC-Whisker Composites," Ceram. Eng. Sci. Proc., **8** [7-8] 861-71 (1987).

4. Product Note 8510-3, Materials Measurement, "Measuring the Dielectric Constant of solids with the HP 8510 network analyzer", Hewlett-Packard Company, 3000 Hanover St., Palo Alto, CA 944304 (August 1, 1985).

5. W. W Ho, "High Temperature Dielectric Properties of Polycrystalline Ceramics", Materials Research Society, Pittsburgh, PA, Symposium Proceedings - Microwave Processing of Materials **124**, ed. by W. H. Sutton, M. H. Brooks, and I. J. Chabinsky, 137-48 (1988).

FREE-SPACE MEASUREMENTS OF HIGH-TEMPERATURE, COMPLEX DIELECTRIC PROPERTIES AT MICROWAVE FREQUENCIES

R. D. Hollinger, V. V. Varadan, V. K. Varadan, and D. K. Ghodgaonkar
The Research Center for the Engineering of Electronic and Acoustic Materials &
The Department of Engineering Science and Mechanics
The Pennsylvania State University
University Park, PA 16802

ABSTRACT

A free-space microwave setup has been used to measure the dielectric constant and loss tangent at temperatures up to 850 °C in the frequency range 8 - 40 GHz for several ceramic materials. The setup and technique are described, and results are presented for both commercially available fired ceramics and a green alumina sample during and after initial binder burnout and firing.

INTRODUCTION

As higher demands are placed on the properties of ceramics, more techniques for *in situ* monitoring of these properties during processing and sintering must be employed for real time feedback and quality control. Recently, microwaves have been investigated for use in industrial processing of ceramics, glasses, and composites. The main advantages of microwave heating already explored include reduction of sintering time with very low grain growth and a reduction of input energy. These advantages result from the rapid increase of the loss tangent with increasing temperature resulting in thermal runaway. The thermal runaway depends on the dielectric properties, size, and shape of the ceramic particles as well as the porosity of the pressed ceramic. It is not yet well understood how these parameters affect sintering. Varadan *et al.* [1] have suggested that since experimental determination of loss tangent during sintering is time consuming, theoretical research involving computer simulation should be employed. However, some benchmark data must be collected to verify and refine theoretical models.

Even when microwave power is not being used to process the materials, remote microwave sensors can be used to measure the properties of the material during processing. This is the situation for the present study. Microwave sensors are ideally suited for this because the antennas can easily be thermally isolated from the process. Also, for anisotropic materials such as composites,

polarization effects can be measured to characterize the anisotropic properties.

In addition to process control, microwave characterization as a function of temperature is important for measuring a material's performance and suitability for particular applications. These include radomes, high temperature absorbers, microwave joining of thermoplastics, and basic materials research.

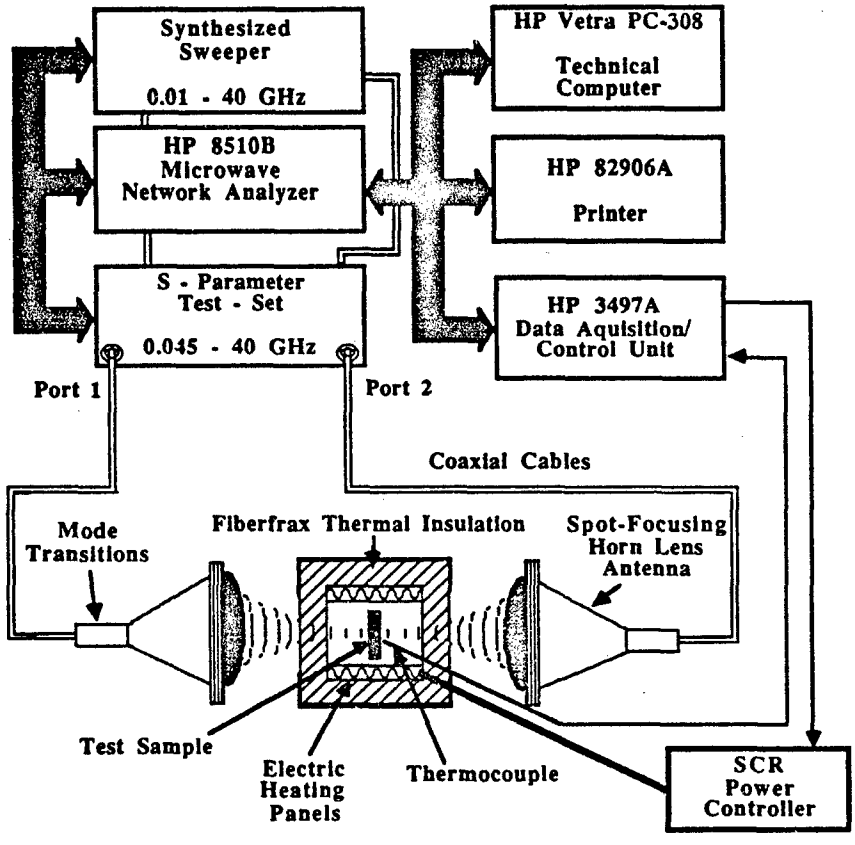


Figure 1. Schematic diagram of high temperature, free-space, microwave setup.

EXPERIMENTAL

The experimental setup is shown in Fig. 1. The spot-focusing horn lens antennas have a 3-dB beamwidth of approximately one wavelength, a focal distance of 30.5 cm., and a depth of focus up to ten wavelengths. Diffraction effects at the edges of the sample are negligible if the minimum transverse dimension of the sample is greater than three times the E-plane 3-dB beamwidth of the antenna at its focus [2]. The antennas are separated by a distance equal to twice the focal distance (61 cm) with a sample hoider placed at the common focal

plane of the two antennas for measurements at room temperature. For high-temperature measurements, the furnace with a high temperature (HT) sample holder is placed at the common focal plane of the antennas. The HT sample holder is made from quartz and it can hold planar samples of cross section 15.2 cm × 15.2 cm. The furnace uses resistive heating panels on the top, bottom, and two sides. The front and back are enclosed only by a glass wool thermal insulation which is virtually transparent to microwaves due to its low density.

The measurement system is fully computer automated. An HP 3497A Data Acquisition/Control Unit (DA/C) is used for interfacing the computer with a thermocouple and SCR current controller. The thermocouple is placed in contact with the test sample near the spot focus of the antennas. The temperature control algorithm has been tailored to this particular furnace for optimal convergence and control. The computer is also interfaced with the HP 8510B Network Analyzer (NA). When the temperature reaches the set point, the NA is prompted to take a sweep. The computer then sets the time domain gating and downloads and stores the S-parameters. The furnace is again heated and the process continues until the maximum desired temperature is reached.

The measurement system is calibrated using a free–space TRL calibration technique. The letters 'TRL' represent the three standards used in the calibration, namely Through connection, Reflect or short, and Line delay. A detailed discussion of this technique as applied to this setup and the resulting accuracy is described by Ghodgaonkar *et al.* [2-3]. However, due to the design of the furnace, the sample holder is freestanding and it is difficult to place the sample holder exactly at the reference plane during and after calibration. Therefore, some additional steps are taken to minimize errors due to the incorrect positioning the sample. The first step is to perform free-space TRL calibration with the standard room temperature sample holder and measure S_{11} and S_{21} of the sample. Next, the furnace and HT sample holder are placed between the antennas and TRL calibration is performed again. Then the sample is placed in the HT sample holder in the furnace. The position of the sample is adjusted such that the measured S_{11} and S_{21} are close to the values obtained with the standard sample holder. Then S_{11} and S_{21} are measured at room temperature and stored in the computer. The sample is heated from ambient temperature to 850°C in steps of 50°C and the S–parameters are measured at the 50°C intervals.

Because it is impossible to place the sample exactly at the reference plane a correction factor is used to numerically introduce an electrical delay and magnitude offset to account for the slight mis-positioning of the sample. The measured data is corrected as follows.

$$S_{11}^{C} = \frac{S_{11}^{STD}}{S_{11}^{FRT}} S_{11}^{HT} \tag{1}$$

$$S_{21}^{C} = \frac{S_{21}^{STD}}{S_{21}^{FRT}} S_{21}^{HT} \tag{2}$$

where the superscripts C, STD, FRT, and HT indicate corrected, standard room temperature sample holder, furnace room temperature, and furnace HT data,

respectively. From Eqs. (1) and (2) it can be seen that when the furnace room temperature data is substituted for the raw HT data the corrected data is identical to the standard room temperature data.

The transmission coefficient (S_{21}) is less affected by sample placement errors because translation of the sample does not change the beam path length and small angle rotations only refracts the beam slightly. The same is not true for S_{11}. This was seen experimentally in that the correction coefficients were an order of magnitude smaller for S_{21} than for S_{11}. Therefore, complex S_{21} only was used in the calculation of the complex dielectric constant, but the correction factors were still used.

DATA INVERSION

In deriving the equations to be solved for computing relative complex permittivity ($\varepsilon_r = \varepsilon_r' + i\,\varepsilon_r''$) from the measured values of S_{21} we refer to Ghodgaonkar *et al.* [2]. We assume that the relative magnetic permeability of the planar sample of thickness d is $\mu_r = 1+0i$. S_{21} is measured using the measurement system described above. The complex transmission coefficient, S_{21}, can be written in terms of the parameters Γ and T:

$$S_{21} = \frac{T(1-\Gamma^2)}{1-\Gamma^2 T^2} \tag{3}$$

where Γ, the reflection coefficient of the air-sample interface, and T are given as

$$\Gamma = \frac{Z_{sn}-1}{Z_{sn}+1} \tag{4}$$

$$T = e^{ikd} \tag{5}$$

In Eqs. 4 and 5, Z_{sn} and k are the normalized characteristic impedance and propagation constant of the sample, respectively, and are related to ε_r by

$$Z_{sn} = \frac{1}{\sqrt{\varepsilon_r}} \tag{6}$$

$$k = k_0\sqrt{\varepsilon_r} \tag{7}$$

where $k_0 = (2\pi / \lambda_0)$ and λ_0 is the wavelength in free-space. By use of Eqs. 3 through 7 we obtain S_{21} in terms of ε_r. However, this cannot be solved explicitly for ε_r so an iterative technique using an initial guess for ε_r is used. Unique determination of ε_r can be achieved using the time domain response of the NA.

The method given by Eqs. 3-7 is not very accurate for loss tangents less than 0.025. So, where possible the thickness resonance method was used. This technique utilizes the minimum in the magnitude of S_{11} when the thickness of the sample is an integer multiple of a half-wavelength. The sharpness of this minimum can be related to the loss tangent ($\tan\delta$) of the material by the following formula,

$$\tan\delta = \frac{\varepsilon_r''}{\varepsilon_r'} = \frac{\Delta f}{f_o} \tag{8}$$

where f_0 is the frequency at the minimum and Δf is the difference in frequency between the two points which are 3 dB above the minimum. Note that this is not a Q-factor which uses the frequencies at the half power points. Equation 8 can be derived analogously to the resonances on transmission lines derived by Jordan [4].

Free space TRL calibration accounts for the errors in the S–parameter measurements due to multiple reflections between the horn lens antennas and the surface of the sample, sample placement errors and the effect of the glass wool windows at the front and back of the furnace. Other sources of errors are temperature gradients in the sample and the thermal expansion of the sample. The spot-size of the focused beam is around one wavelength (2-4 cm range for 8-18 GHz frequency range). The estimated temperature gradient across the 2-4 cm spot-size region of the sample is less than 50° C for a temperature of 850 ° C. The materials tested have coefficients of thermal expansion in the range 10^{-5} to 10^{-7} /°C which results in negligible error in dielectric measurement.

In order to see how the properties of the glass wool insulation change at elevated temperatures, the empty furnace was heated from room temperature to 850°C making measurements every 50°C. This data shows that the phase of S_{21} varies by ±3.5° and its magnitude by ± 0.1dB. The magnitude of S_{11} is nearly –60 dB at room temperature and increases to –40 dB at 850°C. From these error limits the resulting errors in dielectric constants and loss tangents can be calculated.

For the samples discussed in this paper the accuracy of dielectric constant measurement is better than ±2%. For materials with loss tangents greater than 0.025, the measurement accuracy in loss tangent is better than ±2%. The measurement uncertainties are large for materials with loss tangent less than 0.025. For low-loss materials, the loss tangent can be calculated from the thickness resonance whenever the sample is an integer multiple of a half-wavelength thick. This method gave more accuracy for low loss materials down to loss tangents of 0.005. This was verified by measuring several known materials using this method. The lowest loss tangent that could be measured satisfactorily was that of a PVC (polyvinyl chloride) sample, which we measured to be 0.005 at 14.4 GHz and which has been reported [3] to be 0.0051. Factors limiting the accuracy of this method are that the minimum dips below the noise floor or near the noise floor where measured values S_{11} are sensitive to the type of time domain gating used. In the case of HT loss tangent measurements, the accuracy is limited by the somewhat large uncertainties in S_{11}, but this is moderated by the fact that this method depends more on relative magnitudes of S_{11} rather than the absolute magnitude. In case of very low-loss materials ($\tan \delta < 0.004$), the thickness resonance gives a definite conclusion regarding the maximum value of the loss tangent .

RESULTS

Figure 2 shows the variation of the dielectric constant with temperature for quartz (sample thickness is 0.653 cm) at 15 GHz. The data deviation is within 1% of a straight line fit and the overall trend is an increase of about 5% from 25 to 850 °C. The loss tangent of 3×10^{-4} is too small for any present free-space

method. Variations of the dielectric constant for quartz are similar to the variations measured by other investigators at 35 GHz [5].

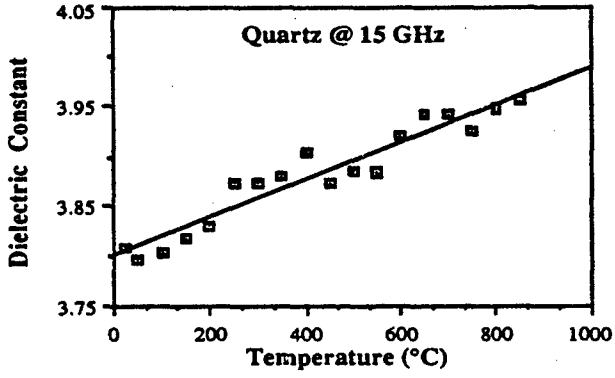


Figure 2. Dielectric constant of quartz at 15 GHz. for temperatures 25 to 850 °C.

Figure 3 shows the dielectric constant and loss tangent for silicon carbide Hexoloy SA (sample thickness 1.27 cm) plotted from 8 to 40 GHz. Because SiC is a semiconductor, even just a small increase in temperature causes it to become highly conductive. In fact, above 150°C it is so conductive that the transmission is near the noise floor of the NA (-60 dB). It is also interesting to note that the dielectric constant and loss tangent decrease with increasing frequency which is expected for the frequency regime above the dipolar relaxation frequency.

Figure 4 shows the dielectric constant and loss tangent for a green alumina sample. The 11.5 cm. diameter by 0.75 cm. thick sample was prepared by pressing 0.1 μm high purity α-alumina powder[1] mixed with 2% (wt.) poly vinyl alcohol to a pressure of 172 MPa (25000 psi.). The density was calculated to be about 45% of the theoretical density. The curve labeled 'Green' shows the dielectric properties of the sample with the binder still present while the curve labeled 'Pre-Fired' is for the same sample measured a second time when the binder had been burned out. The effect of the binder is easily seen by comparing the two plots. At around 500°C the binder has burned away and the two curves agree very closely. The reason the pre-fired curve changes suddenly at 100°C is most likely due to absorbed moisture being driven out. The dielectric properties of a commercially obtained 98% dense fired alumina sample were also measured. The dielectric constant varied linearly from 9.4 at 25°C to 10.6 at 850°C while the loss tangent varied linearly from about 1.2×10^{-3} at 25°C to 20×10^{-3} at 850°C as measured using the thickness resonance. Comparison of these values to the ones shown in Fig. 4 indicates how the dielectric properties change with density.

[1]Baikowski International Corporation, Charlotte, N. C.

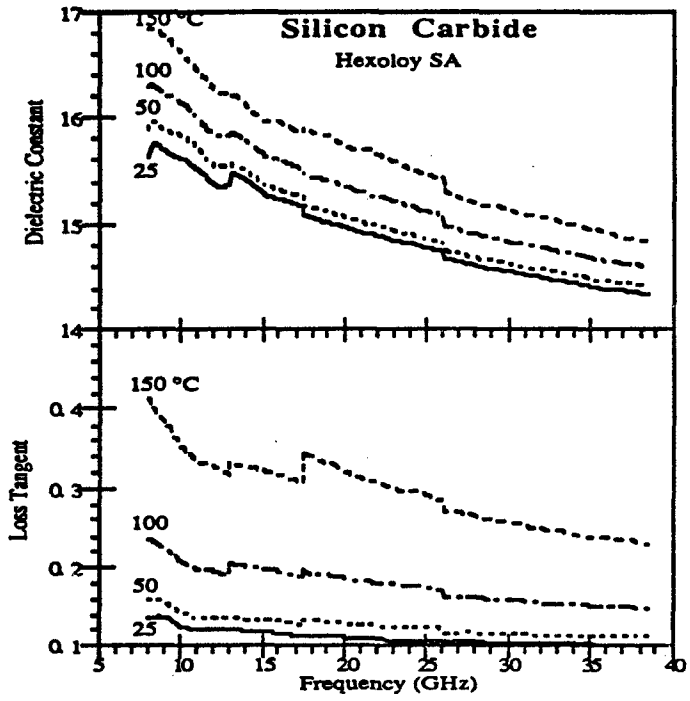


Figure 3. Dielectric constant and loss tangent of Silicon Carbide Hexoloy SA for frequecies 8 - 40 GHz and temperatures 25 - 150 °C.

CONCLUSIONS

It has been shown that free-space microwave techniques have the capability of accurately measuring the complex dielectric properties of materials at high temperatures. Some preliminary results have also been shown for monitoring the binder burn out in a green alumina sample. The limited maximum temperature in this paper is due to the limitations of the furnace, not of the measurement technique or thermal isolation, and modifications would allow monitoring of sintering also. Here we emphasize free-space techniques because neither waveguides nor any other guided wave structures permit *in situ*, thermally isolated process monitoring. In cases where microwaves are used for the processing, the same microwaves can be used for measuring dielectric properties and tuning the system for optimum performance.

ACKNOWLEDGEMENTS

The authors acknowledge the help of Dr. H. S. Dewan in the design and construction of the high-temperature sample holder and the furnace.

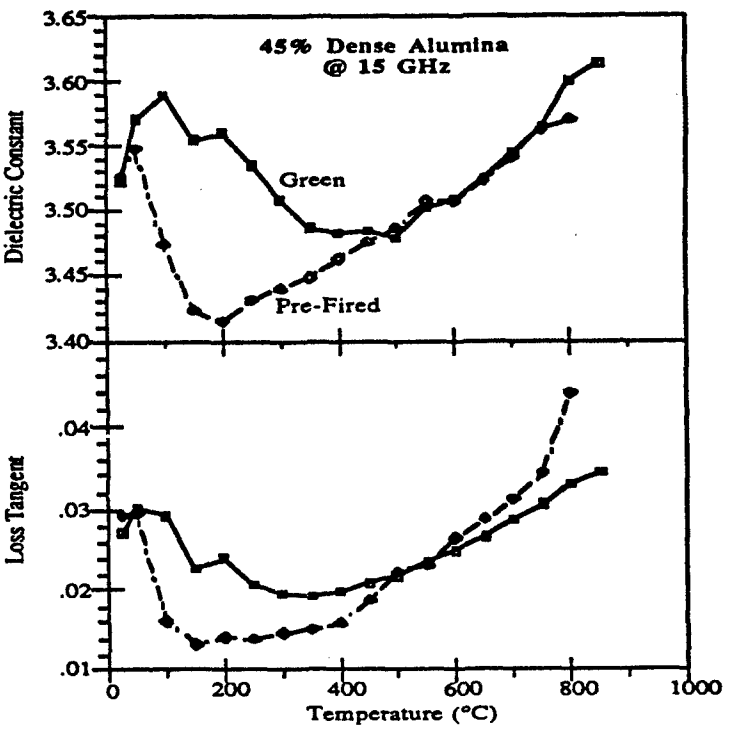


Figure 4. Dielectric constant and loss tangent of a 45% dense alumina sample both in the green state during initial burnout and firing and after the first firing.

REFERENCES

1. V.K. Varadan, Y. Ma, A. Lakhtakia, and V.V. Varadan, "Microwave Sintering of Ceramics," MRS Symp. Proc., Vol. 124, pp. 45-57, (1988).
2. D.K. Ghodgaonkar, V.V. Varadan and V.K. Varadan, "Free-Space Measurement of Complex Permittivity and Complex Permeability of Magnetic Materials at Microwave Frequencies," IEEE Trans. Instrum. Meas., Vol. 39, pp. 387-394, (1990).
3. D.K. Ghodgaonkar, V.V. Varadan and V.K. Varadan, " A Free-Space Method for Measurement of Dielectric Constants and Loss Tangents at Microwave Frequencies," IEEE Trans. Instrum. Meas., Vol. 38, pp. 789-793, (1989).
4. E.C. Jordan, *Electromagnetic Waves and Radiating Systems*, Prentice-Hall, New York, pp. 236-239, (1950).
5. W.W. Ho, " High temperature millimeter wave characterization of the dielectric properties of advanced window materials," Technical Interim Report, AMMRC Contract No. DAAG46-79-C-0077, SC5235.5IRD, February 1981.

IN SITU MEASUREMENT OF THE DIELECTRIC PROPERTIES OF CERAMICS WITH A SINGLE MODE MICROWAVE HEATING DEVICE

X. D. Yu, V.V.Varadan , V.K. Varadan and D. Ghodgaonkar
227 Hammond Building
The Research Center for the Engineering of Electronics and Acoustic Materials &
Department of Engineering Science and Mechanics
The Pennsylvania State University
University Park, PA 16802

ABSTRACT

A single mode microwave heating device which operates at 2.45 GHz was modified to simultaneously heat and characterize ceramic materials. The equivalent circuit derived by Marcuvitz [9] to model the ceramic rod in the waveguide was used in the formulation. Three crystal detectors on the impedance analyzer were used as a reflectometer to measure the reflection coefficient of the load, so that transmission line measurements can be automated. The measured reflection coefficient at different temperature is a function of the dielectric constant and loss tangent of the ceramic material. The Newton-Raphson method was successfully used to solve a nonlinear complex equation. By using this system, a 94% alumina rod was heated and characterized and experimental results are presented.

INTRODUCTION

Microwave processing is receiving more and more attention in the material research field, especially in ceramic processing. Microwave heating has many advantages such as rapid and uniform heating. It is useful in the sintering and joining of ceramics. Research work by Tian et al.[1] has shown that microwave sintering results in rapid densification and ultra-fine microstructure. Fukushima [2] has shown that by using microwave heating, ceramics can be joined and a higher strength than conventional joining can be obtained. Theoretical work by Yu et al.[3] has shown that the increase of dielectric constant and loss tangent with temperature can lead to uniform and enhanced microwave power absorption in ceramics. Hence, the dielectric properties of the ceramics at high temperature must be known so that microwave processing can be controlled.

Dynamic heating and characterizing of ceramics has the advantages of obtaining a high heating rate and requiring a simple sample. It allows for measuring dielectric properties of ceramics at elevated temperature, monitoring the puzzling microwave sintering ceramics process and studying the variation of dielectric properties with

temperature, heating rate and microstructure. It has been studied by D. Couderc et al.(1973)[4] , Areneta et al (1984) [5], Fukushima et al. (1987) [6], J. Jow et al [7] as well as J. Asmusse et al. [8]. Here, a single mode microwave heating device which operates at 2.45 GHz was modified to simultaneously heat and characterize ceramics materials. The equivalent circuit derived by Marcuvitz [9] to model the ceramic rod in the waveguide was used in the formulation. Three crystal detectors on the impedance analyzer were used as a reflectometer to measure the reflection coefficient of the load, so that transmission line measurements can be automated. The measured reflection coefficient at different temperature is a function of the dielectric constant and loss tangent of the ceramic material. The Newton-Raphson method was successfully used to solve a nonlinear complex equation. By using this system, a 94% alumina rod was heated and characterized. The experimental results are presented.

MODEL DESCRIPTION

The model to be used to characterize ceramic dielectric properties is depicted in figure 1. As given by Marcuvitz [9], the effect of a ceramic rod in the waveguide can be modeled as the electric elements ZA and ZB in the equivalent circuit. In this model, ZS is the impedance of the variable short, whereas ZI is the impedance of the iris. P1 and P2 are the distances from the center of the ceramic rod to the position of iris and variable short respectively. The measured reflection coefficient, Γ, and resulting impedance, Z , can be expressed in terms of ZI, ZS, ZA and ZB, i.e,

$$\frac{1}{Z_c} = \frac{1}{ZI_c} + \frac{1}{ZAB} \qquad (1)$$

where

$$Z_c = Z_0 \frac{Z - Z_0 \tanh(\gamma P1)}{Z_0 - Z \tanh(\gamma P1)} \qquad (2)$$

$$ZI_c = Z_0 \frac{ZI - Z_0 \tanh(\gamma P1)}{Z_0 - ZI \tanh(\gamma P1)} \qquad (3)$$

$$ZAB = ZB + \frac{ZA(ZB + ZS_c)}{(ZA + ZB + ZS_c)} \qquad (4)$$

$$ZS_c = Z_0 \frac{ZS + Z_0 \tanh(\gamma P2)}{Z_0 + ZS \tanh(\gamma P2)} \qquad (5)$$

In the case when the dielectric constant and loss tangent are small, which is true for many ceramics, ZA is also very small and can be neglected in the calculation. Hence

$$\frac{1}{Z_t} = \frac{1}{ZI_c} + \frac{1}{ZS_c} + \frac{1}{ZA} \qquad (6)$$

By solving the complex equation

$$F(\varepsilon', \varepsilon'') = \frac{1}{Z_t} - \frac{1}{ZI_c} + \frac{1}{ZS_c} + \frac{1}{ZA} = 0 \qquad (7)$$

the complex permittivity (ε'-jε'') can be deduced. The impedance of the iris and variable short can be obtained by measuring the reflection coefficient with a network analyzer system. The system was calibrated by using a one port calibration technique before making the measurement. It is displayed in figure 2.

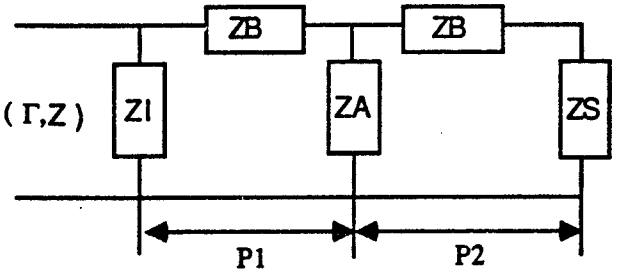


Figure 1. Dielectric Characterizing Model.

MEASUREMENT OF REFLECTION COEFFICIENT

The reflection coefficient can be measured by obtaining the voltages from the microwave detectors on the impedance analyzer. In the transmission line as described in the figure 3, the voltage [10] at the position of the detector is

$$V_n = V\left(1 + \rho \exp\left(j(\theta - \phi_n)\right)\right) \qquad (8)$$

$$|V|_n^2 = |V|^2\left(1 + \rho^2 + 2\rho\cos(\theta - \phi_n)\right) \quad (n = 1, 2, 3) \qquad (9)$$

where ρ and θ are the magnitude and phase of the reflection coefficient of the load and ϕ_n is the phase shift corresponding to the distance from the nth detector to the load and back. By solving Eq. 9 for three detectors, ρ and θ can be found.

For a crystal detector, the input microwave power is linearly proportional to $|V|_n^2$. In the low microwave power region, the output voltage from the detector is

linearly proportional to the input power passing through it. Because the range of the voltage from the detector is large in this experiment, the linear relation between the output voltage and input microwave power will not exist. Therefore, the nonlinear relationship between output voltage and input microwave power must be obtained.To acquire this relationship, a matched load was connected to the position of the cavity in the microwave heating device. The input microwave power from the reading of the control panel and output voltage from the detector were recorded simultaneously. A typical relation is displayed in figure 4.

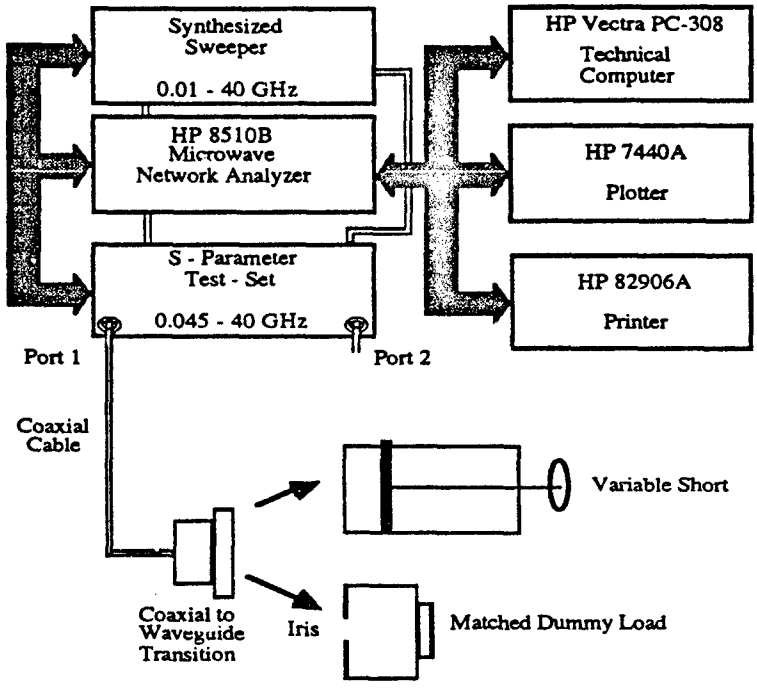


Figure 2. Network Analyzer System Measuring impedance of the Iris and Variable Short.

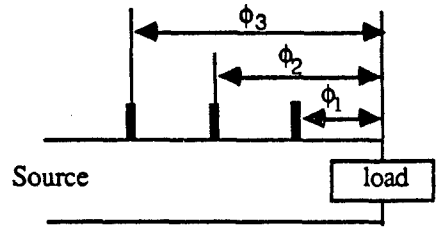


Figure 3. Three Detector Reflectometer.

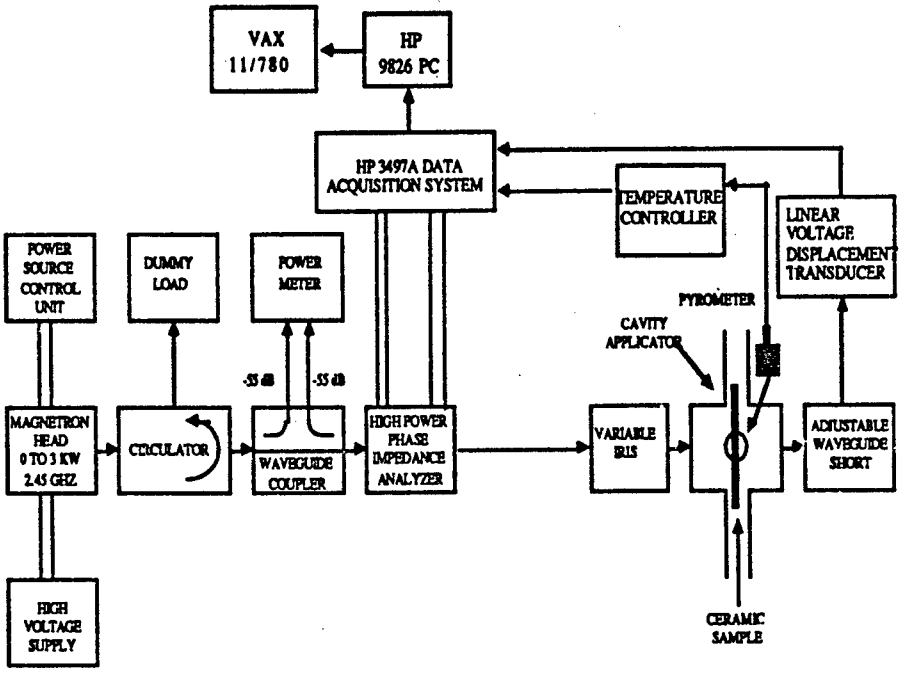


Figure 5. High Temperature Material Characterizing System.

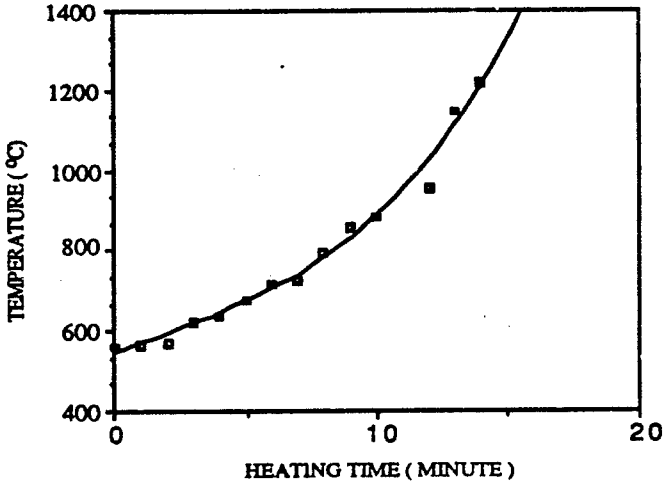


Figure 6. Thermal Runaway Data.

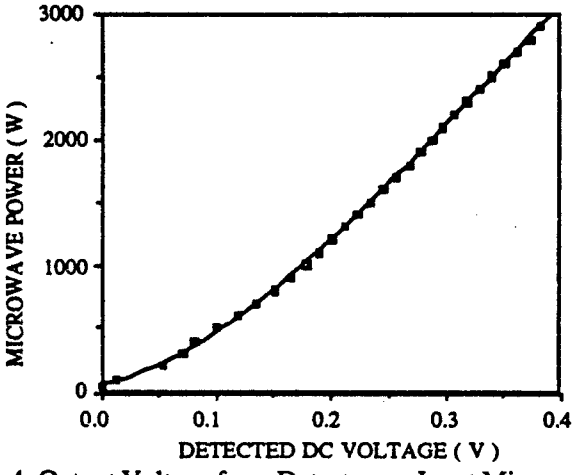


Figure 4. Output Voltage from Detector vs. Input Microwave Power.

EXPERIMENTAL SET-UP AND CHARACTERIZING PROCEDURES

A schematic diagram of the automated dielectric characterization system is shown in the figure 5. As a main controller, we use the combination of a HP9826 personal computer and a HP3494 data acquisition system. The output voltages from crystal detectors are related to the input microwave power. The voltage from the temperature controller is linearly related to the temperature . The voltage from the linear voltage displacement transducer indicates the position of the variable short. Those voltages will be collected by a HP3494 data acquisition system controlled by the algorithm written in HP BASIC. The geometric data of the ceramic rod, waveguide dimensions and operating frequency are inputted in advance to the data file. To increase the experimental accuracy, the EIP578 frequency counter is connected to the characterizing system to monitor operating frequency.

Upon turning on the microwave generator, the variable short is adjusted to the resonating position so that the microwave power can be absorbed by the ceramic rod efficiently. The output voltages from the three detectors, the voltage from the temperature controller and the voltage from the linear voltage displacement transducer were acquired by the data acquisition system at the prescribed temperatures. These raw data were then transformed to the input microwave power at each detector, temperature at the time of measurement and the position of the variable short respectively according to the proper calibration formulas. The magnitude and phase of the reflection coefficient were found by solving the nonlinear Eq.9. Eq. 7 is used to set up a complex nonlinear equation to find the real and imaginary parts of the complex dielectric constant

In solving the complex equation, the real and imaginary parts of the function $F(x_1, x_2)$ are assumed to be f_1 and f_2. The complex equation therefore becomes

$$f_1(x_1, x_2) = \mathrm{Re}\left(F(x_1, x_2)\right) = 0$$
$$f_2(x_1, x_2) = \mathrm{Im}\left(F(x_1, x_2)\right) = 0 \qquad (10)$$

Let X denote the vector of value (x_1, x_2) then, in the neighborhood of X, each of the function f_i can be expanded in Taylor series

$$f_i(X + \delta X) = f_i(X) + \sum_{j=1}^{2} \frac{\partial f_i}{\partial x_j} \delta x_j + O(\delta X^2) \qquad (11)$$

By neglecting terms of order δX^2 and higher, a set of linear equations for the corrections δX that moves each function closer to zero simultaneously, namely

$$\sum_{j=1}^{2} \alpha_{ij}\, \delta x_j = \beta_i \qquad (12)$$

where

$$\alpha_{ij} \equiv \frac{\partial f_i}{\partial x_j} \qquad \beta_i = -f_i \qquad (13)$$

Matrix equations can be solved by Krammer's rule. The corrections are then added to the solution vector,

$$x_i^{new} = x_i^{old} + \delta x_i \;, \; i = 1, 2 \qquad (14)$$

and the process is iterated to convergence.

RESULTS AND DISCUSSION

A Coors AD-998 alumina rod with a diameter 0.8 cm was used in this characterization experiment. Since the imaginary part of the complex dielectric constant is usually small, the simplified formulation was used to retrieve dielectric properties. The thermal run away phenomenon was observed during the experiment. Figure 6 gives the temperature rise with time. The measured real and imaginary parts of the complex dielectric constant are given in figures 7 and 8. They both increase with rising temperature which agrees with the afore mentioned theoretical prediction.

CONCLUSION

The system developed here can be used to measure the dielectric properties of ceramic rods. It is also applicable for characterizing the microwave sintering process which should shed light on the mechanism of sintering during microwave heating.

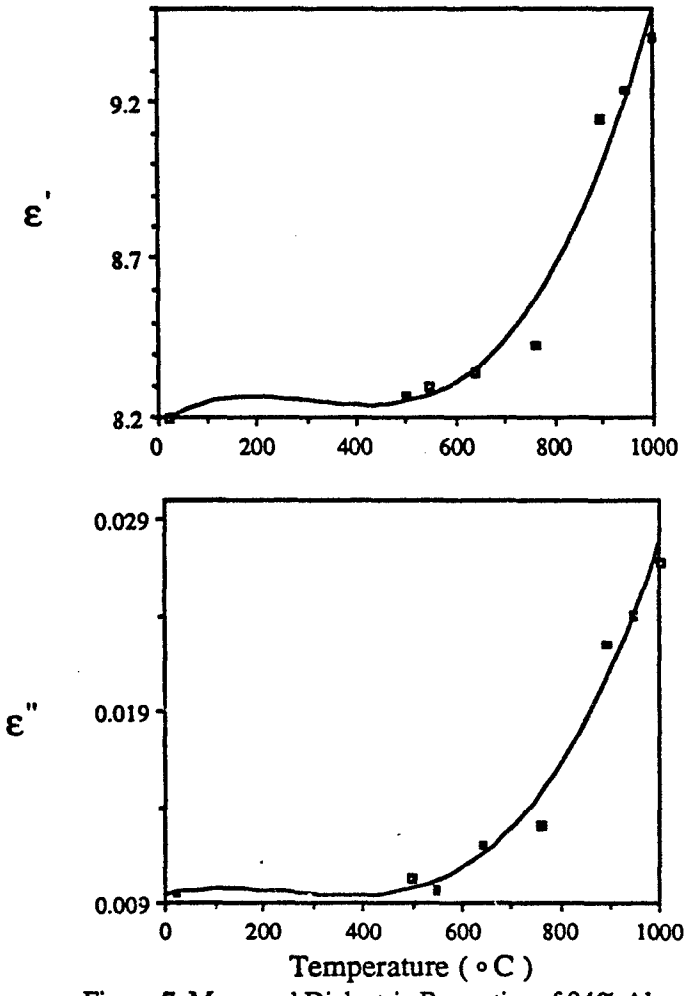


Figure 7. Measured Dielectric Properties of 94% Alumina.

REFERENCES

1.Y.L. Tian, D. Lynn Johnson, and M.E. Browin, "Ultra Microstructure of Al_2O_3 by Microwave Sintering", in Ceramic Powder Science II (Ceramic Transaction Vol.1), Eds. G.L. Messing, E.R. Fuller, Jr., and H.Hausner, American Ceramic Society, Inc., PP. 925-932 ,1987.

2.H. Fukushima, T.Yamanaka and M.Matsui, "Microwave Heating of Ceramics and its Application to Joining", pp.267-72 in Microwave Processing of Materials, Symposium Proceedings, Vol.124. Edited by W.H. Sutton, M.H. Brooks, and I.J. Chjabinsky. Material Research Society, Pittsburgh, PA 1988.

3.X.D. Yu, V.V. Varadan, V.K.Varadan, " Non-linear Finite Element Method

Modeling Microwave Heating of Ceramics". In this Symposium.
4.D. Couderc, M. Giroux and R.G. Bosisio, " Dynamic High Temperature Microwave Complex Permitivity Measurement on Samples Heated via Microwave Absorption", J. Microwave Power, 8(1), pp.69-82, 1973.
5.J. C. Araneta, M. E. Brodwin and G. A. Kriegsmann, " High-Temperature Microwave Characterization of Dielectric Rods", IEEE . Vol. MTT-32, NO.10, October, pp.1328-35 , 1984.
6.H. Fukushima, T. Yamanaka and M. Matsui, "Measurement of Dielectric Properties of Ceramics at Microwave Frequency", J. Japan Soc. Prec. Eng. 53, pp.743-48 , 1987.
7. J. Jow, M.Finzel, J. Asmussen and M.C. Hawley," Dielectric and Temperature Measurements During Microwave Curing of Epoxy In Sweeping Resonant Cavity", IEEE. Vol.1 MTT-S Digest, pp.465-68, 1987.
8.J. Asmussen , H.H. Lin, B. Manring and R.Fritz, " Single-Mode or Controlled Multimode Microwave Cavity Applicators for Precision Material Processing", Rev. Sci. Inst. 58, pp.1477-86, 1987.
9.N. Marcuvitz, Chapter 5 Four-Terminal Structures, Page 266-67," Waveguide Handbook", Edition 2. Edited by P.J.B Clarricoats, E.D.R. Sherman and J.R.Wait, Published by Peter Peregrinus., London, UK, 1986.
10.R. Caldecott, " The generalized Multiprobe Reflectometer and Its Application to Automated Transmission Line Measurements", IEEE Trans. Antennas Propagat., Vol. ap-21, NO.4, pp.550-54, 1973.

METHOD FOR CALCULATING AND OBSERVING MICROWAVE ABSORPTION BY A SPHERE IN A SINGLE MODE RECTANGULAR CAVITY

H. W. Jackson and M. Barmatz
Jet Propulsion Laboratory, California Institute of Technology
Pasadena, CA 91109

A new theory of microwave absorption by a lossy dielectric sphere in a single mode rectangular cavity has been recently developed. The absorption was treated in the framework of an electromagnetic scattering problem. That theory is summarized here and calculated results that bear on optimizing the processing of materials are illustrated. Methods for observing power absorption and other results predicted by the scattering model are discussed. Cavity perturbation theory provides a bridge between theoretical calculations and experimental observations, and a special problem that arises when an established version of cavity perturbation theory is applied to spheres is identified, analyzed, and resolved. The direct problem of predicting shifts in frequency and Q from model calculations is discussed for a sphere in a cavity when the sphere's complex dielectric constant is known. Also, the inverse problem of determining the complex dielectric constants from measured values of those shifts is considered. The small sphere limit, where an electrostatic or quasistatic model is valid, is treated in detail, and planned work on parallel problems for larger spheres is described.

INTRODUCTION

Microwave heating in single mode cavities is being studied at the Jet Propulsion Laboratory as part of NASA's Microgravity Science and Applications program. A goal of this program is to develop efficient techniques for containerless processing of materials in the microgravity environment of space. In a typical containerless processing application, a material will be positioned inside a chamber, for example by acoustic forces.[1] Then microwaves will heat the isolated sample to elevated temperatures where the material may be melted, sintered, or dried without being contaminated by a supporting crucible and some of its physical properties may be measured in a noncontact manner. Predicting, monitoring, and controlling each of these processing stages so that the quality of the processing is improved with optimum heating efficiency are areas where theory can contribute to this developing technology. For example, predicting and controlling the temperature profile inside a sample to prevent cracking while cooling are areas where theoretical results should be beneficial. The complex dielectric function is part of the input data for theoretical calculations bearing on these matters. In some applications, these data are not available, particularly at high temperatures, and it will be important to determine the complex dielectric function from a combination of experimentally

measured shifts in frequency and Q, and results of a theoretical model and cavity perturbation theory. Results of this research have a broad range of applicability including contained as well as containerless processing.

Subsequent sections of this article report on progress that we have made in treating some of these matters. First, a recently developed theory of microwave absorption by a spherical sample in a rectangular cavity is summarized. Next calculated results of that theory relevant to improving efficiency of microwave heating are illustrated. Then cavity perturbation theory is considered as an aid in predicting and monitoring microwave absorption by a sample. First, general theory is treated, and then perturbation theory results are applied to small spherical samples.

THEORY OF MICROWAVE ABSORPTION BY A SPHERE IN A SINGLE MODE RECTANGULAR CAVITY

Scattering Model

Absorption of microwave power by a lossy dielectric sphere in a resonant rectangular cavity has recently been treated by a new method based on electromagnetic scattering theory.[2] In this model, a resonant mode of the empty cavity is resolved into plane wave fields and results of Mie's[3] scattering theory for a transversely polarized plane progressive electromagnetic wave incident on a sphere are utilized. The electromagnetic fields in the cavity containing the sphere are expressed approximately as a superposition of fields from the individual Mie scattering problems. Absorbed power is calculated by evaluating the time average Poynting vector and integrating its radial component over the surface of the sphere. Results of this model will be most accurate when the sample is much smaller than the cavity and is far from all cavity walls, so that effects of multiple scattering will be minimized.

Calculated Results for Microwave Power Absorption

The usefulness of the scattering model[2] can be illustrated with calculations of microwave absorption that exhibit dependences on the complex dielectric function, position of a sample in a cavity, sample radius, and other experimentally controllable parameters. A variety of structure is exhibited in the calculated results and much of that structure has obvious utility in optimizing conditions for heating a sample efficiently. Examples of that structure for a range of dielectric constants are displayed in Figs. 1 - 3. All of these results are for spherical samples of radius a = 3 mm. The cavity has perfectly conducting walls, and edge lengths of L_x = 10.250 cm, L_y/L_x = 1.776, and L_z/L_x = 1.463. The cavity is excited in a TM_{550} mode at frequency f = 8.39 GHz, with empty cavity wave number k = 1.759 cm^{-1}, which yields ka = 0.528. The dimensions of the cavity were chosen so that the TM_{550} mode is separated from the nearest mode by ≈ 180 MHz. A characteristic electric field strength in the cavity is fixed at 20 V cm^{-1}. For this particular mode, the field strength is equivalent to the maximum electric field intensity.

Each figure shows the power absorbed by a sample and the quality factor Q_s associated with absorption by the sample in the loaded cavity as the sample moves on a straight line path that passes through the center of the cavity, that path being

parallel to the x-axis. The calculated curves predict that the samples of alumina and coal will be maximally absorbing where the electric field intensity E takes on its maximum value. On the other hand, barium titanate, having a larger imaginary component of the dielectric constant, ε_r'', is predicted to be minimally absorbing at the same location and maximally absorbing where E assumes its minimum value.

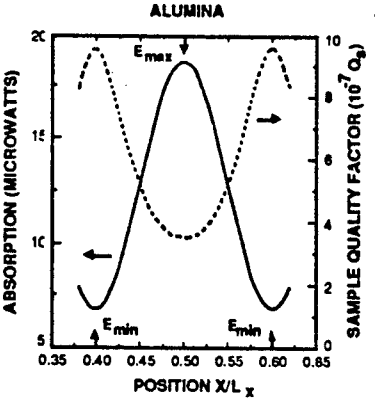


Figure 1. Absorption and sample Q versus position for alumina using $\varepsilon_r' = 9.0$ and $\varepsilon_r'' = 0.0018$.

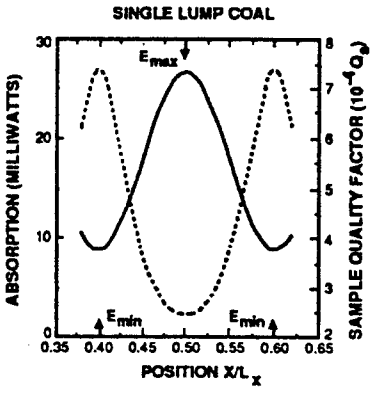


Figure 2. Absorption and sample Q versus position for single lump coal using $\varepsilon_r' = 8.4$ and $\varepsilon_r'' = 2.47$.

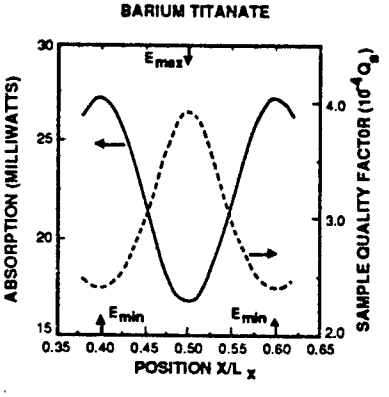


Figure 3. Absorption and sample Q versus position for barium titanate using $\varepsilon_r' = 300$ and $\varepsilon_r'' = 159$.

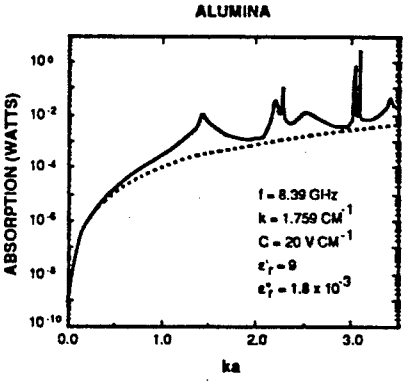


Figure 4. Microwave absorption versus ka for alumina sample at cavity center.

Figure 4 displays another kind of interesting structure in the microwave absorption as a function of ka. Other than the radius, the parameters used in these calculations were the same as for Figs. 1 - 3. The peaks and valleys in the absorption curve

reflect the resonance structure of the alumina sphere. Some of the peaks are very sharp, and they are associated with resonances in the sphere involving spherical harmonics Y_{lm} with high values of l. That sharp structure may have useful practical implications not only in materials processing to achieve efficient heating, but also in device applications. An electrostatic approximation, based on Eqs. (9b) and (10), was used to calculate the dashed curve in Fig. 4. The electrostatic results account for a background on which resonance effects are superimposed.

METHODS FOR OBSERVING ABSORPTION AND OTHER PREDICTED RESULTS

Cavity Perturbation Theory

Methods for observing power absorption and other predicted results of the new scattering theory will be discussed in this section. Such methods are directly applicable in verification tests of the theory and in monitoring and controlling materials processing. They can also be applied to the inverse problem of determining the complex dielectric constant from experimentally measured shifts in frequency and Q. Cavity perturbation theory can provide connections between theoretical predictions and experimentally observable quantities, and will be considered in this context in what follows.

In Altman's[4] treatment of perturbation theory for a sample inserted in a cavity, one considers electric and magnetic fields such that

$$\boldsymbol{E}(\mathbf{r},t) = \mathbf{E}(\mathbf{r})e^{-i\omega t}, \quad \boldsymbol{H}(\mathbf{r},t) = \mathbf{H}(\mathbf{r})e^{-i\omega t}, \tag{1}$$

together with

$$\varepsilon = \varepsilon' + i\varepsilon'' = \varepsilon_0\varepsilon_r = \varepsilon_0(\varepsilon_r' + i\varepsilon_r''), \quad \varepsilon'' = \frac{\sigma}{\omega'}, \tag{2}$$

$$\mu = \mu' + i\mu'' = \mu_0\mu_r = \mu_0(\mu_r' + i\mu_r''), \tag{3}$$

$$\omega = \omega' - i\omega'', \quad \omega'' = \frac{\omega'}{2Q}. \tag{4}$$

The following fundamental formula of cavity perturbation theory is derived from Maxwell's equations when those equations are applied to a small sample in a high Q cavity:

$$\frac{\omega - \omega_0}{\omega} = -\frac{\int_{V_s}\left[(\varepsilon - \varepsilon_0)\,\mathbf{E}_0^{*}\cdot\mathbf{E} + (\mu - \mu_0)\,\mathbf{H}_0^{*}\cdot\mathbf{H}\right]dv}{4U}. \tag{5}$$

In Eq. (5), ω_0, ε_0, μ_0, $\mathbf{E}_o$, and $\mathbf{H}_o$ refer to the empty cavity, whereas ω, ε, μ, $\mathbf{E}$, and $\mathbf{H}$ refer to the cavity containing the sample. V_S and V are the volumes of the sample and cavity, respectively, and U is approximately the time average energy stored in the cavity. U is essentially the same whether the cavity is empty or loaded, and is given approximately by

$$U = \frac{1}{4}\int_V \left[\varepsilon_0 \mathbf{E}_o^* \bullet \mathbf{E}_o + \mu_0 \mathbf{H}_o^* \bullet \mathbf{H}_o\right] dv. \tag{6}$$

Next, Eqs. (2) - (4) are substituted into Eq. (5) and it is tacitly assumed that the integrals $\int_{V_s} \varepsilon_0 \mathbf{E}_o^* \bullet \mathbf{E}\, dv$ and $\int_{V_s} \mu_0 \mathbf{H}_o^* \bullet \mathbf{H}\, dv$ are real-valued. Equating real and imaginary parts of the ensuing equation, one finds the following results when the sample is non-magnetic, so that $\mu = \mu_0$:

$$\Delta \equiv \frac{\omega' - \omega_0'}{\omega'} = -\frac{\varepsilon_0(\varepsilon_r' - 1)}{4U}\int_{V_s} \mathbf{E}_o^* \bullet \mathbf{E}\, dv \tag{7a}$$

$$Q_s^{-1} \equiv Q^{-1} - Q_o^{-1} = \frac{\varepsilon_0 \varepsilon_r''}{2U}\int_{V_s} \mathbf{E}_o^* \bullet \mathbf{E}\, dv. \tag{7b}$$

The two left hand members of Eqs. (7a) and (7b) respectively define Δ, the relative real-valued frequency shift, and Q_s^{-1}, the change in Q^{-1} associated with power absorbed in the sample. Eqs. (7a) and (7b) can be combined to obtain

$$Q_s^{-1} \equiv Q^{-1} - Q_o^{-1} = -\frac{2\varepsilon_r''}{(\varepsilon_r' - 1)} \frac{(\omega' - \omega_0')}{\omega'} \tag{8}$$

A fundamental formula for Q_s^{-1} based on W_{abs}, the power absorbed by the sample, is given by

$$Q_s^{-1} = \frac{W_{abs}}{\omega' U}. \tag{9a}$$

In view of Eqs. (8) and (9a), it appears that one can directly obtain information on Q_s^{-1}, and in turn W_{abs}, by measuring the relative frequency shift. Since Q_s^{-1} is hard to measure accurately, but Δ is easy to measure accurately, this could be a very useful result, not only for verifying the scattering model, but for other purposes as well. However, we have found that Eqs. (7a), (7b), and (8) are of limited validity, and are correct only for certain special experimental conditions. For example, it turns out that they are valid for a cylindrical sample of small radius in an axial electric field. However, they are not correct for spheres, even for very small spheres, whenever $\varepsilon_r'' \neq 0$. This will be explained shortly. For spheres, one must measure Q_s^{-1} itself to obtain direct data on W_{abs}.

Understanding and eliminating the source of failure of perturbation theory for spheres is still important if one wishes to predict the frequency shift or solve the inverse problem of determining the complex dielectric constant from measurements of Q_s^{-1} and Δ. These matters will be analyzed next.

The power, W_{abs}, can be evaluated directly from the joule heat, $\mathbf{j} \bullet \mathbf{E}$, in the sample. This provides a fundamental formula for Q_s^{-1}, as follows:

$$Q_s^{-1} = \frac{W_{abs}}{\omega' U} = \frac{\frac{1}{2}\sigma \int_{V_s} \mathbf{E}^* \bullet \mathbf{E}\, dv}{\omega' U} = \frac{\varepsilon_0 \varepsilon_r''}{2U} \int_{V_s} \mathbf{E}^* \bullet \mathbf{E}\, dv. \qquad (9b)$$

Eqs. (7b) and (9b) contain two different expressions for Q_s^{-1}, and under some conditions they represent quite different numbers.

Notice that Eq. (7b) contains $\mathbf{E}_o^*$, referring to the empty cavity, but Eq. (9b) contains $\mathbf{E}^*$, referring to the field inside the sample. To understand the importance of this difference, consider a small spherical sample and suppose that ka<<1. In this case, it is usual to assume that an electrostatic approximation is valid. In electrostatics, the electric field $\mathbf{E}$ inside a dielectric sphere placed in a previously constant field $\mathbf{E}_o$ satisfies[5]

$$\mathbf{E} = \frac{3}{\varepsilon_r' + 2} \mathbf{E}_o. \qquad (10)$$

The fields $\mathbf{E}$ and $\mathbf{E}_o$ usually differ appreciably. In an extreme case, for barium titanate where $\varepsilon_r' = 300$, they differ by a factor of about 100. Similarly large discrepancies also occur in results for Q_s^{-1} calculated using Eqs. (7b) and (9b). This suggests that something is not quite right with cavity perturbation theory, and that it needs to be generalized. This issue cannot be settled completely within the context of electrostatics.

We shall consider the hypothesis that these cavity perturbation results are of limited validity because the integral $\int_{V_s} \mathbf{E}_o^* \bullet \mathbf{E}\, dv$ is treated as real-valued in deriving Eqs. (7a) and (7b). One can show that $\mathbf{E}$ will not be real-valued inside a sample if $\varepsilon_r'' \neq 0$ there unless the condition $Q^{-1} = \varepsilon_r''/\varepsilon_r'$ is accidently met. This result can be established by considering the wave equation

$$\nabla \times \nabla \times \mathbf{E} - k^2 \mathbf{E} = 0 \qquad (11)$$

where

$$k^2 = \mu_0 \varepsilon_0 \varepsilon_r \omega^2 \qquad (12)$$

and using Eqs. (2) and (4). A corollary to this result is that $\mathbf{E}_o$ can be chosen as real-valued since $\varepsilon_r'' = 0$ for the empty cavity. From these conditions it follows

that $\int_{V_s} \mathbf{E}_o^* \cdot \mathbf{E}\, dv$ is complex-valued in general, although in special cases it may be real-valued as a result of integrating. These results can be expressed by writing

$$\int_{V_s} \mathbf{E}_o^* \cdot \mathbf{E}\, dv = R + iI \tag{13}$$

where R and I are real numbers.

Substituting Eqs. (2) - (4) and (13) into Eq. (5) and then equating real and imaginary parts of the ensuing equation, one obtains the following results for a non-magnetic sample where $\mu = \mu_0$:

$$\Delta = -\frac{1}{4U}\left\{\varepsilon_0\left[(\varepsilon_r' - 1)R - \varepsilon_r''I\right] + \frac{\omega''}{\omega'}\varepsilon_0\left[\varepsilon_r''R + (\varepsilon_r' - 1)I\right]\right\}. \tag{14}$$

For a high Q cavity, the term involving $\omega''/\omega' = (2Q)^{-1}$ is negligible, and one finds that to good approximation

$$\Delta \equiv \frac{\omega' - \omega_b'}{\omega'} = -\frac{\varepsilon_0}{4U}\left[(\varepsilon_r' - 1)R - \varepsilon_r''I\right]. \tag{15}$$

Also, one can show that

$$Q_s^{-1} \equiv Q^{-1} - Q_o^{-1} = \frac{\varepsilon_0}{2U}\left[\varepsilon_r''R + (\varepsilon_r' - 1)I\right]. \tag{16}$$

The quantities R and I are given by Eq. (13). The modified cavity perturbation formulas in Eqs. (15) and (16) are valid under more general conditions than those found in the version of perturbation theory that yielded Eqs. (7a) and (7b).

Perturbation Theory Applied to a Sphere

The generalized cavity perturbation theory developed above will now be applied to a lossy dielectric sphere. First, we will consider small spheres, where ka<<1; and later we will briefly consider a relaxation of this condition, where the sphere radius may be larger.

Altschuler[6] has treated small spheres by perturbation theory in an approximation where the field inside the sphere is given by

$$\mathbf{E} = \frac{3}{\varepsilon_r + 2}\mathbf{E}_o = \frac{3}{(\varepsilon_r' + 2) + i\,\varepsilon_r''}\mathbf{E}_o. \tag{17}$$

We will call this a quasistatic model. In this formula for **E**, the complex dielectric constant occurs rather than just ε_r', as in the electrostatic model, Eq. (10). For Eq. (17), **E** is complex-valued inside the sphere whenever $\varepsilon_r'' \neq 0$ and $\mathbf{E}_o$ is real valued.

As a partial check on the quasistatic model, we have calculated the microwave absorption for barium titanate, for which ε_r'' is large. In Fig. 5, those results are compared with a curve based on our scattering theory with the same parameter set as used for Fig. 3. The penetration depth δ for barium titanate is 0.638 mm, and the product $k\delta$ is indicated by the arrow in the figure. Agreement between the curves is very good at small radii, about up to $a = \delta$, but rapidly deteriorates beyond that. In the quasistatic model, the electric field is constant inside the sample. Therefore, one expects this model to deteriorate and ultimately fail for $a > \delta$.

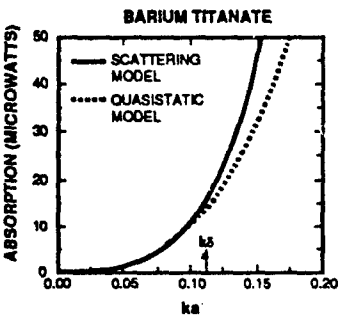


Figure 5. Absorption versus ka for barium titanate for scattering and quasistatic models. The sample is at the cavity center.

When the quasistatic model formula for **E** is used in our modified version of cavity perturbation theory, Eqs. (13), (15), and (16) yield

$$\Delta = -\frac{\varepsilon_0}{4U}\frac{\left[3(\varepsilon_r' - 1)(\varepsilon_r' + 2) + (\varepsilon_r'')^2\right]}{(\varepsilon_r' + 2)^2 + (\varepsilon_r'')^2} V_s \, |\mathbf{E}_o|^2 \tag{18}$$

and

$$Q_s^{-1} = \frac{\varepsilon_0 \varepsilon_r''}{2U}\frac{9}{(\varepsilon_r' + 2)^2 + (\varepsilon_r'')^2} V_s \, |\mathbf{E}_o|^2 . \tag{19}$$

Also, Eqs. (9b) and (17) give precisely the same results for Q_s^{-1} as Eq. (19), thus demonstrating that for this model, the modified cavity perturbation theory results for Q_s^{-1} are consistent with direct evaluation of joule heating of the sample.

As Altschuler[6] has shown, the inverse problem of determining the complex dielectric constant from measured values of Δ and Q_s^{-1} can be easily solved in the case of the quasistatic model. This will be demonstrated next. Substituting Eq. (17) for **E** into Eq. (5), evaluating the integral, and defining a quantity G by

$$G \equiv -\frac{4U}{3\varepsilon_0 V_s \, |\mathbf{E}_o|^2}\left[\Delta - i\frac{1}{2}Q_s^{-1}\right], \tag{20}$$

one can solve the ensuing equation for ε_r. The result is

$$\varepsilon_r = \varepsilon_r' + i\,\varepsilon_r'' = \mathrm{Re}\left(\frac{1 + 2G}{1 - G}\right) + i\,\mathrm{Im}\left(\frac{1 + 2G}{1 - G}\right). \qquad (21)$$

These results are valid for small spheres, where the quasistatic model is applicable. The sphere radius must satisfy $ka << 1$ and $a < \delta$ in this case. The restriction to small radii is a serious disadvantage when ε_r'' is so large that the penetration depth is very small.

In conclusion, we have presented predictions from a new microwave scattering model for absorption by a spherical sample in a rectangular cavity. The results cover a range of values of the complex dielectric constant and indicate an inverted absorption behavior as a function of position for certain materials. Additional results for absorption versus radius for alumina exhibit sharp resonance behavior superimposed on a smooth background. We have also derived modified cavity perturbation expressions as a bridge between theory and experiment and applied them to small spheres. The good agreement found with known results helps establish confidence in this approach. We plan to extend these methods to larger spheres, where the electric field inside a sample can be evaluated from the scattering model. We have already treated shifts in Q for larger spheres. Using the modified cavity perturbation theory, we will also predict shifts in frequency and determine complex dielectric constants from measured shifts in frequency and Q for larger lossy dielectric spheres inserted in a cavity.

ACKNOWLEDGMENT

We wish to acknowledge P. Wagner for computer support and Dr. J. L. Watkins for enlightening discussions. The research described in this article was carried out at the Jet Propulsion Laboratory, California Institute of Technology, under contract with the National Aeronautics and Space Administration.

REFERENCES

1. M. Barmatz, "Overview of Containerless Processing Technologies," in Materials Processing in the Reduced Gravity Environment of Space, edited by G.E. Rindone (Elsevier, New York, 1982), pp. 25-37.
2. H.W. Jackson and M. Barmatz, "Microwave Absorption by a Lossy Dielectric Sphere in a Rectangular Cavity," Submitted for publication.
3. G. Mie, Ann. Phys. 25, 377 (1908).
4. J.L. Altman, Microwave Circuits (Van Nostrand, New York, 1964), pp. 409 -416.
5. J.A. Stratton, Electromagnetic Theory (McGraw Hill, New York, 1944), p. 206.
6. H. Altschuler, in Handbook of Microwave Measurements, edited by M. Sucher and J. Fox (Polytech. Press; Brooklyn, New York, 1963) Vol. 2, pp. 530 - 536.

MEASUREMENT OF CAVITY PERTURBATION TO DETERMINE THE MICROWAVE ABSORPTION OF A SPHERE IN A SINGLE MODE RESONATOR

J. L. Watkins, C. O. Hagenlocher, and M. Barmatz
Jet Propulsion Laboratory, California Institute of Technology
Pasadena, CA 91109

Experiments have been conducted on materials in a single mode microwave resonator to test predictions of a new theory of microwave absorption by a lossy dielectric sphere. Two different experiments are reported here. An analysis of cavity perturbation for verifying the new absorption model revealed a limitation of a standard form of cavity perturbation theory and led to a modification which generalized its application. The first experiment tested the validity of the modified theory. The cavity perturbations of a nylon sphere were used to calculate the complex permittivity using the standard perturbation theory and the modified form. These permittivity values were compared to that determined from cavity perturbation using a thin nylon rod where the standard and modified forms agree. The results show that the modification is necessary to correctly apply perturbation theory to spherical samples.

The second experiment confirmed the theoretical prediction that under certain sample conditions the power absorbed by a sphere in a resonant cavity can be maximum at a location in the cavity where the empty cavity electric field intensity is a minimum. The prediction was checked by comparing the measured power absorbed by a nylon sphere and a graphite sphere as a function of position in a single mode resonator under identical conditions.

INTRODUCTION

As part of NASA's Microgravity Science and Applications program to develop efficient methods of processing materials containerlessly positioned in the space environment, the Jet Propulsion Laboratory (JPL) is studying the use of microwave technology as applied to material processing. Requirements for space-based processing include the ability to position, heat and remotely measure the thermophysical properties of a material. Microwave technology can be used to help satisfy all three of these requirements and offers a number of features that make it attractive for space-based material processing. When considering the efficiency, weight, and size of microwave ovens versus alternative methods of heating, microwaves are superior for many applications. The complex permittivity of processing materials can be determined in a non-contact manner and microwaves can even be used to exert positioning forces on most materials. Current embodiment of these ideas is an integrated single mode microwave oven/acoustic positioner which includes the ability to rapidly measure cavity perturbations for determining the complex permittivity of heated samples. Figure 1 diagrams a ground-based prototype of this device. The cavity acts as both an acoustic and microwave resonator. The moveable plunger is used to tune the acoustics for sample positioning

while a tunable microwave source provides energy for heating. In order to better apply microwave methods to this type of cavity, it is necessary to understand the microwave behavior of materials in a resonator. Recently, a theory of microwave absorption by a sphere in a rectangular cavity has been developed at JPL.[1] Application of this theory [2] has led to some new predictions on the behavior of materials in a single mode resonator. Experimental work done to support some of the predictions of this theory is described in this paper. First a description of the apparatus is presented followed by a discussion of cavity perturbation experiments prompted by theoretical issues and results of sample heating as a function of position in the single-mode resonator.

EXPERIMENTAL APPARATUS

The microwave oven system shown in Fig. 2 is designed to be able to heat materials and also permit measurement of the cavity perturbations for determining dielectric properties. The output of the microwave sweep oscillator is amplified by the 40 watt TWT and applied to the resonant cavity oven through a critically coupled inductive loop. The incident and reflected power are sampled at the cavity entrance and each is detected by both a power meter and a diode. The incident power is used to level the sweep oscillator output. In addition, power in the cavity is measured using an under-coupled transmission probe. All power measurements can be read and stored by the computer.

The oven itself is a cylindrical cavity with the length and diameter both equal to 4.78 cm. Both the heating and reflected power measurements described in this paper were done with the cavity excited in the TM_{010} mode at 4.8 GHz. Small holes in the cavity walls provide optical and mechanical access to the sample. Samples under study are supported in the oven by a thin (1 mm diameter) quartz pedestal. The temperature of the sample is monitored by a remote IR temperature sensor* through one of these holes. The temperature can be fed to a furnace controller which adjusts the microwave power so that the sample follows a programmed temperature profile.

Cavity perturbation measurements are made by taking a swept-frequency reflected power spectrum of the cavity. These spectra are taken automatically and very rapidly; the computer steps the microwave frequency via the dc FM control and then reads the incident and reflected power at each frequency step. By fitting the resultant reflected power spectrum to a Lorentzian curve, the cavity resonant frequency and quality factor can be determined. When these parameters for both the empty cavity and the cavity with a sample inserted are combined with a suitable cavity perturbation model, the complex permittivity of the sample can be determined as described below.

CAVITY PERTURBATION MEASUREMENTS

Examples of reflected power spectra are shown in Fig. 3 and Fig. 4. The Lorentzian fits provide the cavity resonant frequency and quality factor. The measurements shown were made on a nylon ball located at the center of the cavity and a thin nylon rod located on the axis and extending all the way through the cavity. These two geometries were used to test cavity perturbation theory.

The established form of the cavity perturbation equations we used is for non-magnetic materials and can be written as [3]

* Everest Interscience Inc., Fullerton, CA Model 2401

$$\Delta \equiv \frac{\omega' - \omega_o'}{\omega'} = -\frac{\varepsilon_o(\varepsilon_r' - 1)}{4U}\int_{V_s} \mathbf{E}_o^* \bullet \mathbf{E}\, dV \qquad (1)$$

$$Q_s^{-1} \equiv Q^{-1} - Q_o^{-1} = \frac{\varepsilon_o \varepsilon''}{2U}\int_{V_s} \mathbf{E}_o^* \bullet \mathbf{E}\, dV \qquad (2)$$

where $\omega', Q^{-1}, \mathbf{E}$ and $\omega_o, Q_o^{-1}, \mathbf{E}_o$ are the resonant frequency, quality factor, and electric field of the cavity with the sample present and absent respectively, Q_s^{-1} is the quality factor due to the sample itself, $\varepsilon = \varepsilon_o(\varepsilon_r' + i\,\varepsilon_r'')$ is the complex permittivity of the sample, and the integral is over the volume of the sample. U is the time averaged energy stored in the cavity and can be calculated from knowledge of the unperturbed cavity field $\mathbf{E}_o$. By measuring Δ and Q_s^{-1} and assuming a form for $\mathbf{E}$, one can determine ε_r' and ε_r''.

These equations were examined to see if they could be used to connect predictions of the microwave absorption theory developed at JPL with experimental measurements. In this process, it was recognized that the equations were not valid for all sample geometries. The problem lies in the fact that their derivation assumes

$$\int_{V_s} \mathbf{E}_o^* \bullet \mathbf{E}\, dV \qquad (3)$$

is real. This assumption is only true for limited sample geometries and cavity modes; in particular, it is valid for a thin cylindrical rod on the axis of a cylindrical cavity excited in the TM_{010} mode where the electric field is axial everywhere but it is not valid for a sphere under the same conditions. By allowing the integral to be complex, the equations can be rederived in a form applicable to the spherical sample.

Using $\mathbf{E} = \mathbf{E}_o$ for the nylon rod, the integral discussed above is real and both forms of perturbation theory give the correct values for the real and imaginary parts of the permittivity

$$\varepsilon_r' = 2.99,\ \varepsilon_r'' = 0.0276. \qquad (4)$$

For the nylon sphere, however, the standard perturbation theory gives

$$\varepsilon_r' = 2.99,\ \varepsilon_r'' = 0.0177. \qquad (5)$$

Comparison to the values found for the rod yields

$$\frac{\varepsilon_r''(\text{rod}) - \varepsilon_r''(\text{ball})}{\varepsilon_r''(\text{rod})} = 0.357. \qquad (6)$$

Using the modified cavity perturbation theory for the sphere

$$\varepsilon_r' = 3.03,\ \varepsilon_r'' = 0.0297. \tag{7}$$

Again comparing to the rod values gives

$$\frac{\varepsilon_r''\ (\text{rod}) - \varepsilon_r''\ (\text{ball})}{\varepsilon_r''\ (\text{rod})} = -0.076. \tag{8}$$

It can be seen from these data that the modified theory gives consistent values for the complex permittivity for both geometries and that this more general form is a more correct application of perturbation theory.

POWER ABSORPTION MEASUREMENTS

In the treatment of absorption by a non-magnetic material in a microwave field, the absorbed power is simply the Joule heating in the sample which is written

$$P_{abs} = \frac{1}{2}\varepsilon_o \varepsilon_r'' \omega \int_{V_s} \mathbf{E}^* \bullet \mathbf{E}\, dV, \tag{9}$$

where $\mathbf{E}$ is the electric field inside the material, ε_r'' is the relative loss factor and the integral is over the volume of the sample. The above expression is exact, however, in general $\mathbf{E}$ is not known and some assumptions must be made to use Eq. 9. For small samples, it is customary to assume that (1) the sample radius is much smaller than the microwave wavelength $a/\lambda << 1$ so that the integral can be approximated by

$$\int_{V_s} \mathbf{E}^* \bullet \mathbf{E}\, dV = |\mathbf{E}_{rms}|^2\ V_s \tag{10}$$

and (2) the field in the sample is proportional to the unperturbed field

$$\mathbf{E} = A\mathbf{E}_o, \tag{11}$$

where A is real-valued and depends on the geometry of the sample. (An additional assumption here is that ε_r'' remains constant. In general it changes with temperature and can affect the relative power absorption.) For a sphere, one usually assumes the electrostatic approximation

$$\mathbf{E} = \frac{3}{\varepsilon_r + 2}\mathbf{E}_o. \tag{12}$$

In the approximation of this treatment, the absorbed power, which is proportional to the electromagnetic energy that would be found in the volume occupied by the sample if the sample were removed, is given by

$$P_{abs} \propto |E_o|^2 . \quad (13)$$

According to this argument, the relative power absorption of a material can be determined at each point in a cavity in which the unperturbed fields are known.

When microwave power is applied to the cavity the sample will reach a steady-state temperature which can be determined by considering the energy balance, (Power lost by radiation, conduction, and convection) = (Microwave Power absorbed). If the temperature difference between the walls and the sample remains small enough, the thermal losses will be dominated by the conduction and convection terms which are linear in temperature. In this case, we expect

$$T \propto P_{abs} \propto |E_o|^2 . \quad (14)$$

Figures 5 and 6 show the temperature and power absorption profile of a 3.3 mm nylon ball and a 3.3 mm graphite ball along the radius of the cylindrical cavity compared to the energy distribution in the empty cavity. The electric field strength is held constant inside the resonator. The linear dependence of temperature with absorbed power is clearly seen.

The nylon heats qualitatively in accordance to the simple power absorption model presented above. The graphite, however, behaves in exactly the opposite manner, i.e. its maximum power absorption occurs where $|E_o|^2$ is a minimum. (The temperature decrease near the cavity wall is where the ball is physically exiting the cavity.) These experimental data show that the standard power absorption model breaks down in the case of graphite. Apparently the presence of the graphite sample modifies the local electric field in a non-negligible way and the assumption that

$$E_{rms} \propto E_o \quad (15)$$

becomes invalid. A microwave absorption model which can predict this type of "inverted" behavior needs to take into account perturbations to the local field caused by the presence of the dielectric material. In fact, a theory of microwave absorption by a lossy dielectric sphere in a single mode rectangular cavity [1,2] which directly handles the interaction of the microwave field with the sample has been developed at JPL and does predict this behavior.

Future work is planned to extend these measurements to a sphere in a rectangular single mode cavity to allow quantitative comparisons to the microwave absorption theory.

CONCLUSIONS

The first experiment demonstrates that a proposed modification to a standard form of cavity perturbation theory is required in order to properly treat the case of a sphere in a resonant cavity. The second set of experiments show that nylon and graphite heat maximally in different positions in our resonant cavity and demonstrate the weakness of the usual assumptions made in treating the absorption of microwaves by an arbitrary material. These experiments support the prediction of a new theory [1], reported at this symposium [2], of microwave absorption by a sphere in a resonant cavity.

ACKNOWLEDGMENT

We wish to acknowledge Dr. H. W. Jackson for many helpful discussions and Richard Zanteson for design and fabrication of the experimental apparatus. The research described in this article was carried out at the Jet Propulsion Laboratory, California Institute of Technology, under contract with the National Aeronautics and Space Administration.

REFERENCES

1. H.W. Jackson and M. Barmatz, "Microwave Absorption by a Lossy Dielectric Sphere in a Rectangular Cavity," submitted for publication.
2. H.W. Jackson and M. Barmatz, "Method for Calculating and Observing Microwave Absorption by a Sphere in a Single Mode Rectangular Cavity," submitted for publication in the Proceedings of the Microwave Symposium of the 93rd meeting of the American Ceramics Society.
3. J.L. Altman, Microwave Circuits (Van Nostrand, New York, 1964), pp. 409-416.

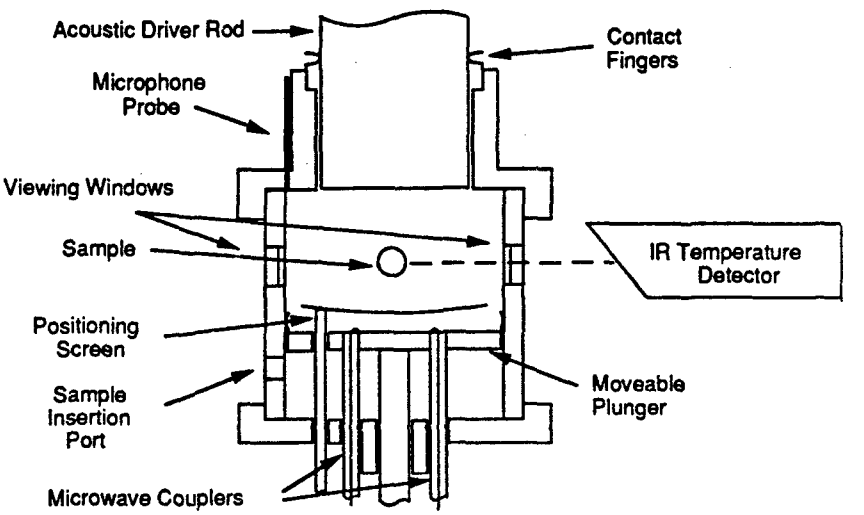


Figure 1. Single Mode Microwave Oven/Acoustic Levitator.

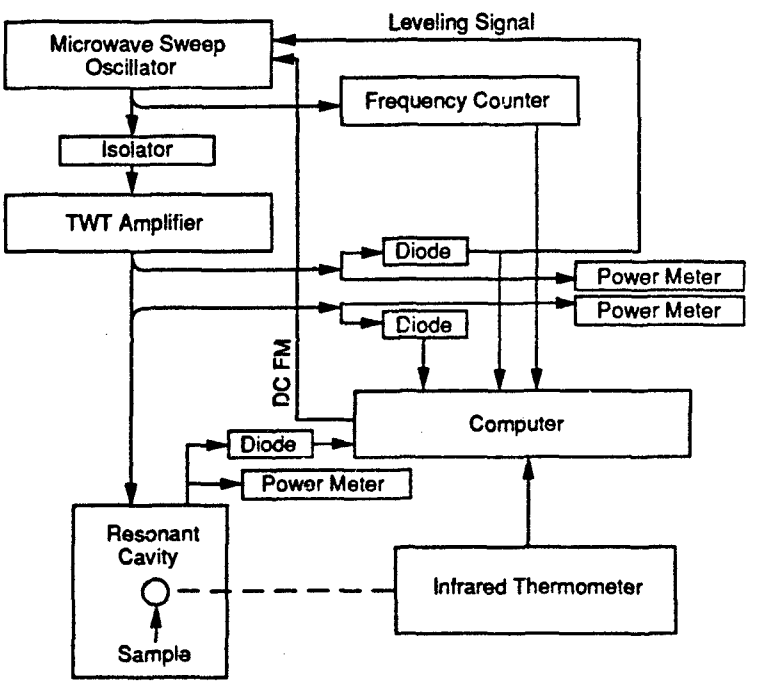


Figure 2. Resonant Microwave Oven System.

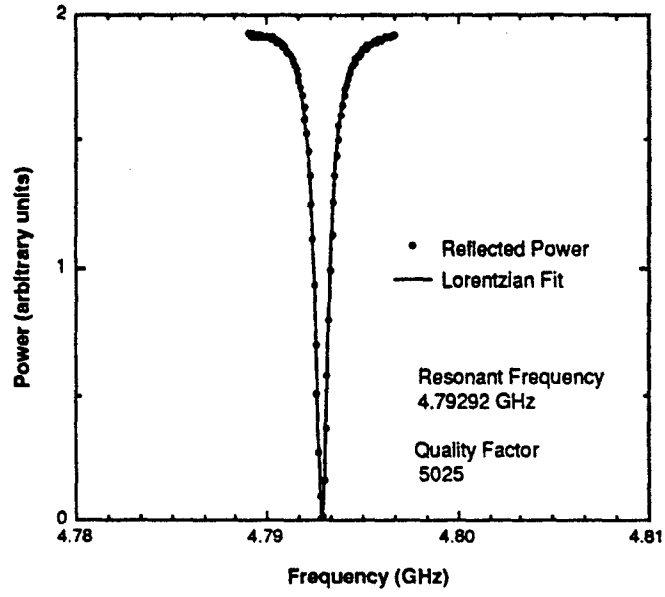


Figure 3. Reflected power versus frequency for a nylon sphere (d=3.3 mm) located in the center of a cylindrical cavity excited in the TM 010 mode.

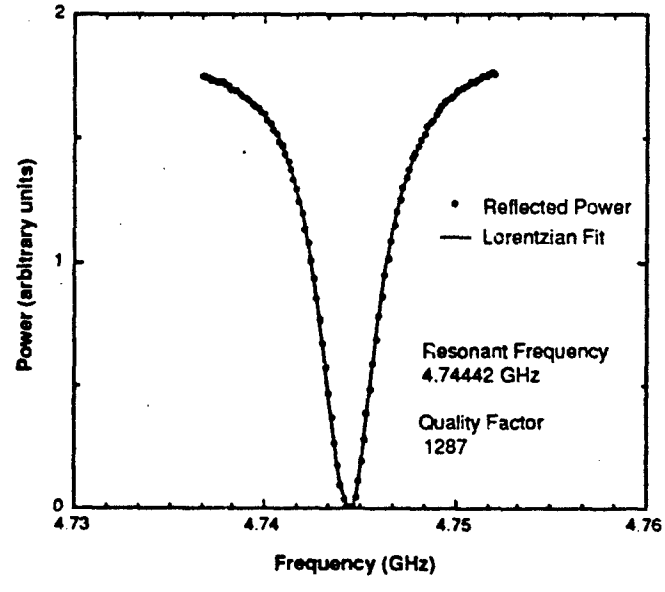


Figure 4. Reflected power versus frequency for a cylindrical nylon rod (d=2.5 mm) located on the axis of a cylindrical cavity excited in the TM 010 mode.

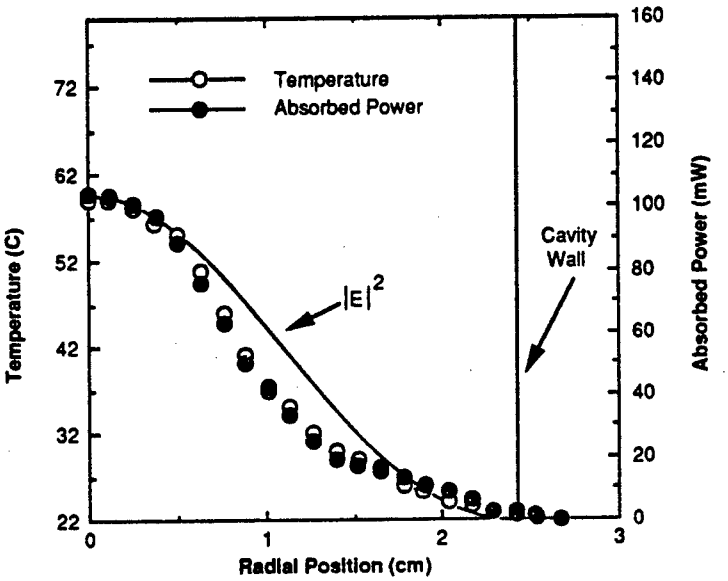


Figure 5. Microwave heating of a nylon sphere (d=4.8 mm) in a cylindrical cavity excited in the TM 010 mode.

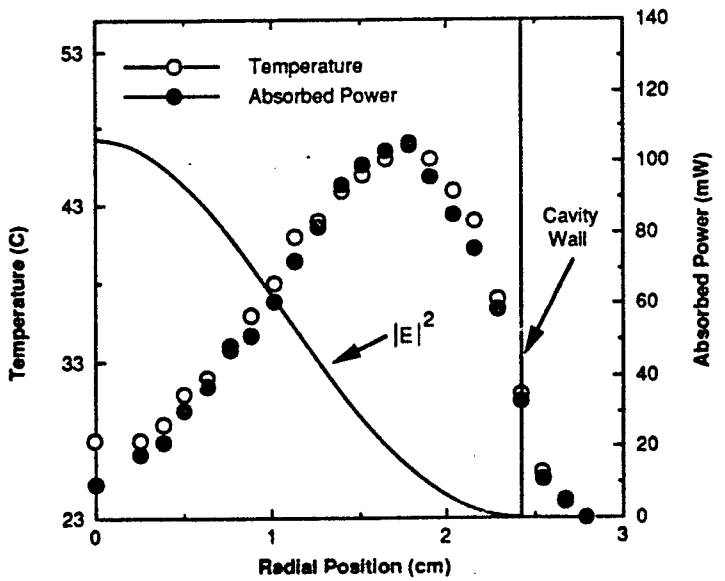


Figure 6. Microwave heating of a graphite sphere (d=4.8 mm) in a cylindrical cavity excited in the TM 010 mode.

Section V. Microwave Sintering

PRACTICES OF ULTRA-RAPID SINTERING OF CERAMICS USING SINGLE MODE APPLICATORS

Yong-Lai Tian
Shanghai Institute of Ceramics, Chinese Academy of Sciences, Shanghai, China, 200050.

ABSTRACT

This is an overview of practical aspects for ultra-rapid sintering of ceramics in single mode applicators. The efficiency and performance of microwave systems can be markedly improved by innovative designs. Discussion will focus on the main problems and their solutions in microwave sintering such as arcing, temperature heterogeneity, thermal runaway, cracking and inability to heat up ceramics with low loss factors.

INTRODUCTION

Rapid sintering of ceramics using microwave energy offers many advantages which are impossible with conventional heating techniques. Fine grain size , high toughness and substantial energy saving have been achieved by microwave sintering[1,2]. A high heating rate and a short processing time are crucial for these applications[2,3]. Microwave sintering of ceramics can be performed in both multimode applicators and single mode applicators. In review of the literature[1,4], it is interesting to note that most of the rapid processing of ceramics were carried out in single mode applicators. This may be attributed to the fact that a single mode applicator has some advantages over a conventional multimode applicator in rapid processing[5]. For instance, the single mode applicator can yield higher electric field strength and couple more energy into ceramic samples than the multimode applicator can. High heating rates of 10^2-10^3° C/min can be readily achieved in a single mode applicator whereas the heating rates in multimode applicators are much lower. The single

mode applicator allows on-line electric feedback for a precise control of the process. In addition, a single mode applicator can be used to diagnose the variation of material properties with electromagnetic field that may lead us to a better understanding of some fundamental principles of the microwave-materials interaction[6].

The control of rapid sintering of ceramics in a single mode applicator is technically more complicated than that of other heating processes. Due to the complexity of the microwave-materials interaction, many practical problems are encountered in the process of microwave sintering such as thermal runaway, sample cracking, arcing and plasma, and inability to heat ceramics with low dielectric loss factors. Although many theories have been put forth and numerous experiments have been reported in the microwave sintering field, little has been mentioned about the practical problems. The purpose of this paper is to discuss, based on the author's own research experience, the following aspects which are indeed very important for performing rapid sintering of ceramics in single mode applicators.

(1) How to heat ceramics which are nearly microwave transparent at ambient temperature.
(2) How to improve the energy efficiency of a single mode applicator.
(3) How to improve the temperature uniformity and avoid thermal runaway.
(4) How to avoid the cracking induced by thermal stress and phase transformations.

SINGLE MODE APPLICATORS USED IN RAPID SINTERING

Various types of single mode applicators, e.g. TE_{10n}, TM_{010}, TE_{011} and TE_{111}, have been applied to rapid sintering of ceramics. The configurations of two commonly used single mode applicators, TE_{10n} and TE_{011}, are schematically illustrated in Fig.1 and Fig.2, respectively. TE_{10n} rectangular cavity exhibits a uniform electric field parallel to the axial direction of the sample. It can also be precisely tuned and coupled for high energy efficiency. TE_{011} cylindrical applicator shows a special electric field pattern which has a maximum field strength at the sample surface and a minimum in the sample center. The high field at the surface can compensate for the surface energy loss due to radiation and convection and thus improve the temperature uniformity. Cylindrical

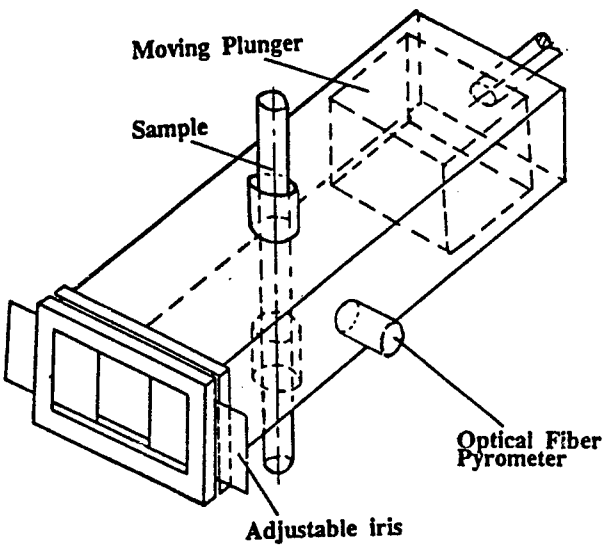


Fig.1 Configuration of a TE_{10n} rectangular single mode applicator.

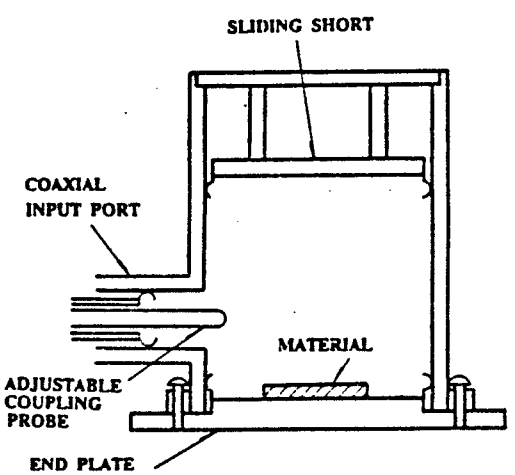


Fig.2 Cross-section of a TE_{011} cylindrical single mode applicator.

applicators with mirror coated inner walls may offer additional energy savings by reflecting the thermal radiation back to the sample[7].

HEATING CERAMIC SAMPLES

The first step of microwave sintering is to rapidly heat the sample to a high sintering temperature. Some ceramics e.g. SiC and β-Al_2O_3, are microwave absorbers. Heating these ceramics in a single mode applicator would not be difficult. However, some other ceramics, e.g. pure α-Al_2O_3, are nearly transparent to microwaves at ambient temperature. Heating these ceramics from room temperature to sintering temperature is very difficult. The possible approaches for intensifying the energy absorption of ceramics are as follows:

(1) Raising microwave power input.
(2) Improving the energy efficiency of the applicator.
(3) Raising microwave frequency.
(4) Using microwave absorbers as additives.
(5) Protecting samples with insulation to save energy losses.
(6) Microwave and conventional hybrid heating.

Approaches 3,4,5, and 6 will not be discussed in this article due to the limitations of their specialized applications.

ENERGY EFFICIENCY OF SINGLE MODE APPLICATORS

The energy efficiency of a single mode applicator, E_{ff}, is given by the equation[8-10],

$$E_{ff}=\frac{P_s}{P_i}=\frac{4\beta'}{(1+\beta')^2+[2Q_0(\frac{\Delta\omega}{\omega_0})]^2}(1-\frac{Q_0'}{Q_0}) \qquad (1)$$

where P_s is the energy absorbed by the sample, P_i is the incident power, β' is the coupling parameter, Q'_0 and Q_0 are the unloaded quality factor for an applicator with and without the sample inside the applicator, respectively; ω_0 is the resonant frequency and $\Delta\omega$ is the difference between the working frequency and resonant frequency.

The energy absorption of the sample, P_s, can be increased by either raising the incident power, P_i, or improving the energy efficiency of the applicator, E_{ff}. Raising the incident power would seem to be a simple way to couple more energy into a sample. However, it was experimentally demonstrated that the increase of incident power P_i was limited by arcing and the plasma generated in the applicator[11]. In order to increase the incident power, either high vacuum ($< 10^{-5}$ torr) or high pressure can be introduced to suppress the arcing and plasma generation. For some ceramics, e.g. SiC and Si_3N_4, sintering in high vacuum may cause the problems of decomposition and vaporization. The pressurization not only suppresses the plasma generation but also inhibits the decomposition and the vaporization. However, the use of vacuum and pressurization in regular sintering processes is not convenient or necessary. By improving the energy efficiency of the applicator, E_{ff}, some ceramics with low loss factors have been successfully sintered in a single mode applicator[10].

It is seen from Eq (1) that a high E_{ff} mainly depends on (1) a critical tuning and coupling ($\Delta\omega=0$, $\beta'=1$) for a minimum power reflection, (2) a low ratio of Q'_0/Q_0 for less wall loss. Since Q'_0 is proportional to the reciprocal of the dielectric loss factor ($1/\epsilon_r \tan\delta$), therefore for samples with high loss factor, $Q'_0 \ll Q_0$, the wall loss is negligible and the energy efficiency is not sensitive to Q_0. For samples with low loss factors, E_{ff} becomes sensitive to Q_0. A high Q_0 factor is necessary to achieve a high energy efficiency, E_{ff}.

CRITICAL TUNING AND COUPLING

Tuning is performed by moving a short circuit to compensate for the shifting of the resonant frequency ($\Delta\omega$). The shifting of the resonant frequency, $\Delta\omega$, is mainly caused by two factors: (a) the stability of the magnetron frequency and (b) the dielectric constant, ϵ_r[12]. Since the variation of ϵ_r with temperature for many ceramics is insignificant[4], only a slight adjustment of the position of the short circuit is needed during the sintering process. However, for sintering ceramics with low loss factors, the wall loss of the short circuit must be minimized in order to ensure a high Q_0 factor for the energy efficiency. Many designs of the short circuit have been well established[6,9]. Tuning of a cavity is usually not difficult in microwave sintering.

Coupling is performed to compensate for the shifting of the impedance of the applicator. The shifting of the impedance mainly depends on the dielectric loss factor, $\epsilon_r \tan\delta$[12]. Since the dielectric loss factor, $\epsilon_r \tan\delta$, for many ceramics changes markedly with temperature, the impedance of the applicator is widely shifted during heating. A plate iris has been long used for coupling. It has the advantage of negligible wall loss and thus can be used to construct a high Q_0 applicator for sintering of low loss factor ceramics[2]. However, the use of the plate iris is limited because its size can not be adjusted to compensate for the wide shifting of impedance during the sintering process. Alternatively the adjustable iris has been developed for continuous coupling adjustments. The design of the adjustable iris consists of two sliding gates and two choked flanges as shown in Fig.1[6,10]. The size of iris can be changed by moving the gates. The use of an adjustable iris significantly improved the coupling efficiency as shown in Fig.3. With a plate iris of 37.5 mm , the maximum temperature of a Y-TZP sample was 1250° C with 800 W incident power and it was 1800° C with 200 W power when an adjustable iris was used[13].

INFLUENCE OF Q FACTOR ON ENERGY EFFICIENCY

Although the adjustable iris improves the coupling efficiency significantly, it may also reduce the Q_0 factor because of its complex structure. This complex structure causes additional energy losses on the wall of the component. For instance, when an plate iris of 25 mm was replaced by an early designed adjustable iris, the Q_0 factor dropped from 2400 to 300. This adjustable iris worked well in sintering of Y-TZP, β-Al_2O_3 and Al_2O_3-TiC composites, but was incapable of heating pure Al_2O_3 samples because of arcing and rapid warming of the adjustable iris itself. In contrast, the samples of pure Al_2O_3 were successfully sintered in the same applicator with a plate iris of 25 mm^2. This example confirmed the fact mentioned earlier that the energy efficiency becomes very sensitive to the Q_0 factor when heating microwave transparent materials. Therefore, for the purpose of sintering low loss factor ceramics, the internal structure of the adjustable iris has to be optimally designed to minimize the energy loss. We modified the early version adjustable iris and developed a new version through the use of some innovative design. The tests of the new adjustable iris exhibited some encouraging

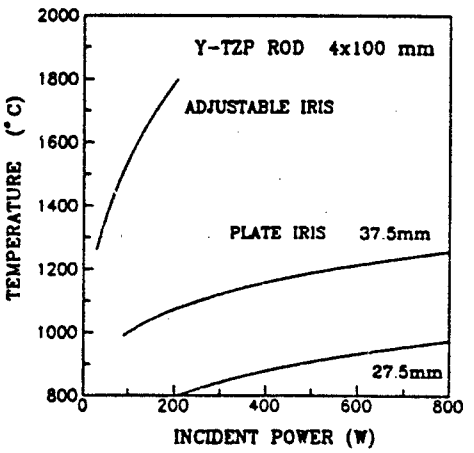


Fig.3 Variation of temperature with incident power using different iris in microwave sintering of Y-TZP.

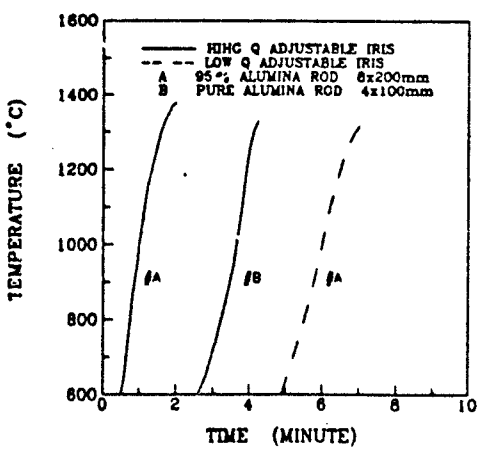


Fig.4 Temperature curves for heating pure alumina and 95% alumina rods with modified (high Q) adjustable iris and unmodified (low Q) adjustable Iris. Pure alumina (sample B) was not able to be heated up by the unmodified iris.

results, the Q_0 factor was raised to 1700 which is close to the value, of 2400 for a near lossless plate iris. Using this new adjustable iris, pure alumina (CR30) samples ($\tan\delta \sim 5\times10^{-4}$) have been rapidly heated and sintered at 1700° C. Fig.4 shows the difference in heating rates using the new design 'high Q' adjustable iris and the old 'low Q' adjustable iris[10].

TEMPERATURE HETEROGENEITY

It was generally observed from our rapid sintering experiments that the temperature of ceramic samples was often radially and axially nonuniform. The temperature was always higher in the center of the samples than at the surface. Fig.5 shows an example of the variation of axial temperature profiles of Al_2O_3-TiC rod samples with different compositions and temperatures in a TE_{10n} applicator. Although the radial temperature gradient is difficult to measure experimentally, it may be inferred from the grain size measurements. It was observed that the surface grains of a microwave sintered alumina sample were smaller than those in the center[2]. Based on the experimental observation, we hypothesized the thermal dynamics, as shown in Fig.6, to display the variation in radial temperature of a rod sample during a microwave sintering process[14]. At first, the temperature gradient increases with the increasing temperature, t=1. At the transition stage t=2, where sintering has begun, the temperature gradient reaches its maximum. As the sample densifies in the stable sintering stage, the thermal conductivity increases and the temperature gradient decreases.

THERMAL RUNAWAY

Thermal runaway was a serious problem often observed in microwave sintering in those ceramics which had a low thermal conductivity and whose dielectric loss factor was strongly temperature dependent. Fig.7 shows a typical temperature profile of thermal runaway in an alumina sample[14]. At temperature below 1000° C, heating was slow because the dielectric loss factor was very low in this temperature regime. A uniform hot zone in the center of cavity was observed. In the temperatures range from 1100 to 1400° C, the heating rate was markedly accelerated. The hot zone started to shrink rapidly to a tiny bright spot and the temperature reached the melting point almost instantly (10-20 seconds as shown in Fig.7). The melting

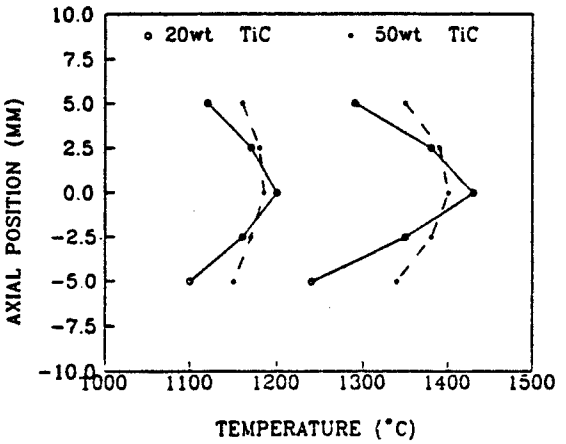


Fig.5 Axial temperature distribution for different compositions of Al_2O_3-TiC samples heated in a TE_{10n} applicator.

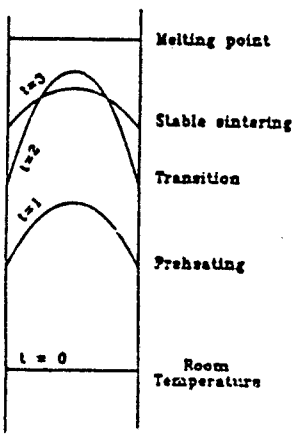


Fig.6 Schematic representation of radial temperature distributions in rod samples at various arbitrary times during microwave heating from room temperature to the stable sintering temperature.

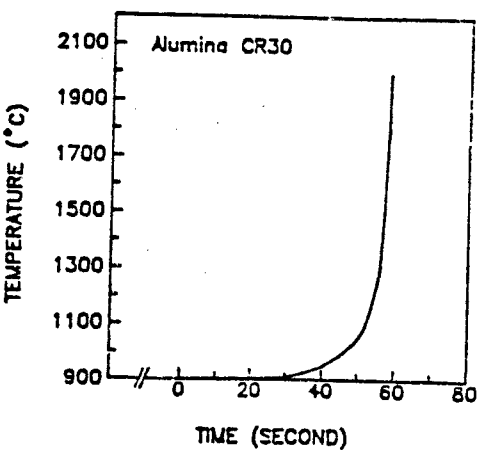


Fig.7 Thermal runaway of Al_2O_3 at constant input power. The zero of time was defined at 900 C, which occurred approximately 5 minutes after the application of power.

usually started in the center and spread rapidly outward.

FACTORS AFFECTING THE TEMPERATURE UNIFORMITY

The temperature heterogeneity and the instability of ceramic samples during microwave sintering are influenced by many factors related to both the operation parameters of microwave hardware and the properties of materials. It was concluded in our previous experimental study that the following conditions were the major causes of the temperature heterogeneity and thermal runaway[14].

(1) Low thermal conductivity.
(2) Rapid increase in dielectric loss factor with increasing temperature.
(3) Large size and complex geometry of the sample.
(4) High heating rate and high processing temperature.
(5) Nonuniform electromagnetic field.

COMPUTER SIMULATION OF TEMPERATURE PROFILES

It is difficult to experimentally measure the temperature distributions and variations inside ceramic samples during rapid sintering. As a result of the limitations of the experiments, a numerical program has been developed to compute the dynamic temperature profiles of a microwave heated ceramic rod[15,16]. This numerical thermal analysis makes it possible to quantitatively evaluate the contribution of each factor listed above.

The thermal physical model of this computation is illustrated in Fig.8. A cylindrical ceramic sample, e.g. Al_2O_3, is placed in a rectangular applicator. Heat is generated within the shaded area of the sample, where a constant electric field is assumed for simplicity. The instantaneous temperature distribution T(r,z,t) inside the sample is a solution of the heat equation:

$$\rho C_p(T)\frac{\partial T}{\partial t}=\frac{1}{\rho}\frac{\partial}{\partial r}\left[K(T)\,r\frac{\partial T}{\partial r}\right]+\frac{\partial}{\partial Z}\left[K(T)\frac{\partial T}{\partial Z}\right]+Q \qquad (2)$$

where $C_p(T)$ and K(T) are the specific heat and the thermal conductivity of the material, respectively. Both are temperature dependent. ρ is the density of the sample assumed constant during heating. The heat generated

inside the material, Q, due to the absorption of microwave energy, is given by

$$Q = K' \epsilon_r \tan\delta E^2 \qquad (3)$$

where K' is a constant and the electric field, E is assumed as a uniform distribution, $\epsilon_r \tan\delta$ is the dielectric loss factor which is also a function of the temperature. Eq(2) is subject to the following boundary condition:

$$K(T) \frac{\partial T}{\partial R}\Big|_{r=d/2} = 1.49 \frac{(T_s - T_0)^{5/4}}{L^{1/4}} + \epsilon_\lambda \sigma_0 (T_s^4 - T_0^4) \qquad (4)$$

where the first and second terms on the right hand side are energy loss at the surface through convection and radiation, respectively. T_s is the surface temperature and T_0 is the ambient temperature. ϵ_λ is the emissivity and σ_0 is the Boltzmann constant.

This equation was numerically solved by an explicit finite difference method[16]. Some typical results, illustrated below, show the behavior of the temperature distribution of various samples under different heating conditions.

Fig.9 shows the dynamic temperature variation of an 8mm alumina sample with the coupled microwave power. At low power levels (100W and 200W) the steady state temperatures were reached. As power increased to 400W thermal runaway occurred within 40 seconds.

Fig.10 shows computed two dimensional temperature distributions of an 8mm alumina rod heated under different microwave power levels. It can be seen that even in a uniformly distributed electric field, nonuniform temperature distributions were observed in both the radial and the axial directions. It can also be seen that a high heating rate and a high temperature may enhance the temperature gradient.

Fig.11 shows a plot of the radial temperature profiles for different sizes and densities of samples. It can be

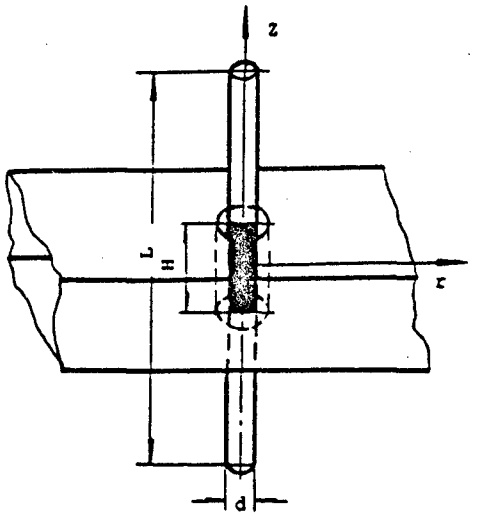


Fig.8 Thermal physical model for a ceramic cylinder under a uniform microwave heating.

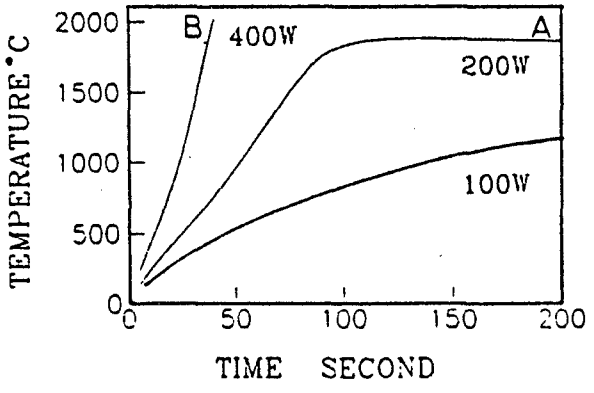


Fig.9 Variation of temperature with time at the center of an Al_2O_3 rod (d=8mm, L=22cm, H=5.5cm)

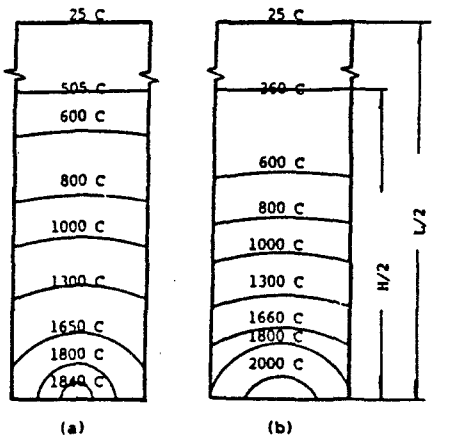


Fig.10 Two dimensional temperature distributions of 8 mm Al_2O_3 rod heated with different power levels. (a) Heated at 200W for 200 seconds, a steady temperature state at point A as shown in Fig.9. (b) Heated with 400W for 40 Seconds, a transient temperature at point B of Fig.9.

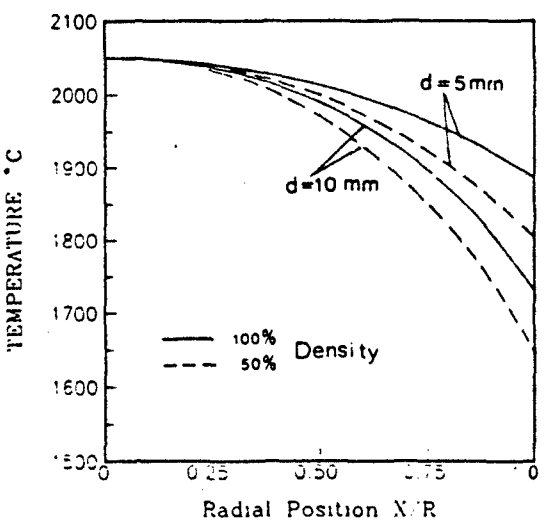


Fig.11 Radial temperature distributions for different sizes and densities of Al_2O_3 samples with 400W absorbed power. (X is the distance to the central axis and R is the radius).

seen that the temperature difference between the surface and the centers of the samples increased with the increasing sample size and porosity. These results indicated that for those samples of large size and poor thermal conductivity, the center of the sample might start to melt while the surface is still well below the normal sintering temperature. The stress between the shrunken part in the center and the un-shrunken part at the surface might cause cracking.

All the foregoing computed results are consistent with our previous experimental observations. Fig.12 shows a good agreement between the computed results and the experimental measurement for the axial temperature profiles of an 8 mm alumina rod heated with 200 W.

CRACKING INDUCED BY THERMAL STRESS AND PHASE TRANSFORMATIONS

Cracking of ceramic samples frequently occurred during rapid sintering of ceramics. Once the cracking initiated, arcing and plasma generation occurred simultaneously in the local cracked area. This resulted in a rapid drop of the sample temperature. A high temperature gradient and a rapid heating rate are the major causes of cracking. This type of cracking usually begins at the onset of densification and grows along the boundary between the hot zone and dark area where the highest stress is induced as a result of difference in shrinkage between the hot area and the cold area.

Phase transformation induced cracking was observed in microwave sintering of Y-TZP samples[13]. Commercial Y-TZP powder always contains a few percent of residual monoclinic phase. When the ZrO_2 monoclinic phase transformed into the tetragonal phase during heating, the high volume change (9%)[17] associated with this transformation induced high stress and thus caused the cracking. This type of cracking usually occurred in the center of the sample where the phase transformation temperature was first reached.

SOME PRACTICAL APPROACHES TO AVOID THERMAL RUNAWAY AND CRACKING

The thermal runaway and cracking may be avoided by two major approaches: (a) changing the properties of materials to improve the thermal conductivity, and (b)

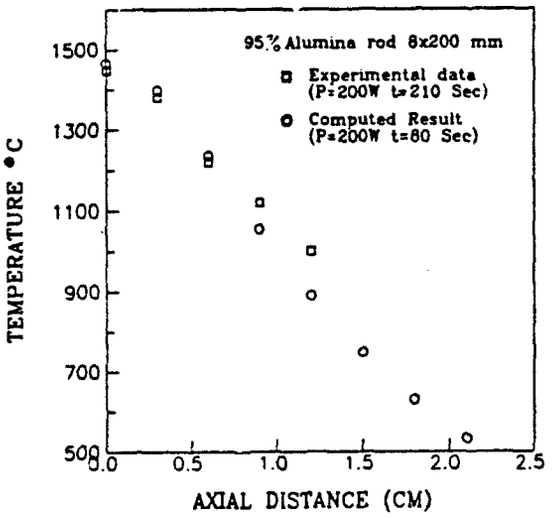


Fig.12 A comparison of computed results with experimental data for axial temperature profiles of a 95% Al_2O_3 rod heated with 200 W microwave power.

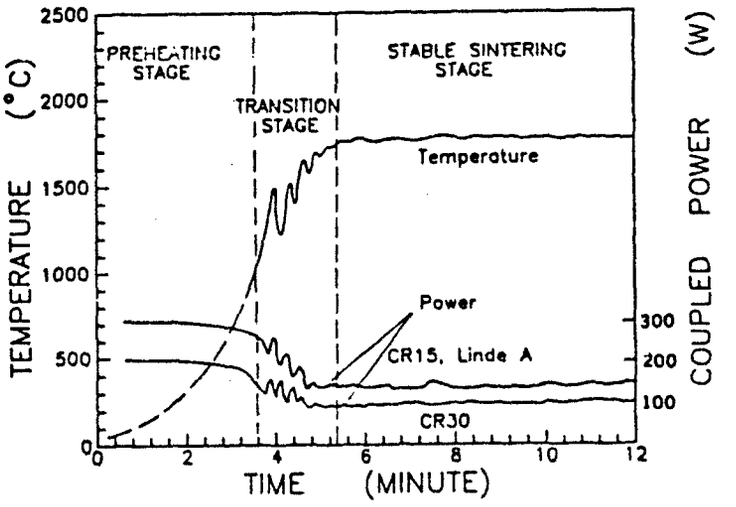


Fig.13 Temperature profile of Al_2O_3 sample controlled by varying microwave input power.

carefully controlling the heating rate by varying the input power.

Thermal runaway did not occur in high thermal conductive ceramics, e.g. SiC and ZrO_2. Therefore, adding conductive fiber or powder into low thermal conductive matrix not only improves the microwave absorption of the sample, but also eliminates the thermal runaway. For instance, 20 wt% TiC was found to be a transition composition for Al_2O_3-TiC composites above which thermal runaway was eliminated[14].

For low thermal conductive ceramics, such as alumina and mullite, thermal runaway can be avoid by a careful control of the input power during the sintering process. Fig.13 shows a typical example for the sintering of α-Al_2O_3[2]. A large constant power was applied in the preheating stage of a low temperature regime. In the transition stage of 1000-1400° C, the heating rate was reduced by varying or pulsing input power, as shown in Fig.13, to avoid the acceleration of the temperature rise and thermal runaway. As the sample began to densify, the thermal conductivity increased and the temperature gradient decreased. The sample finally reached a steady state temperature in the stable sintering stage.

As mentioned earlier, the thermal stress induced cracking was mainly caused by either large temperature gradients or high heating rates. Therefore, the two approaches mentioned above can be used for avoiding cracking. In addition, by improving the strength of green samples before rapid sintering, such as presintering green samples to 70-80% TD using either conventional or microwave heating, the chances of cracking may be reduced significantly[11].

ACKNOWLEDGMENTS

The author is grateful to Professors D.L. Johnson, M.E. Brodwin, D.S. Yen, J.K. Guo, J.L Tao and B.S. Li for their advice in his research and Dr. W.H. Sutton for his encouragement to prepare this paper. The financial support from the Electric Power Research Institute under contract No. RP2730-1 and National Natural Science Foundation of China under No. 58972097 are acknowledged.

REFERENCES

1. W.H.Sutton et al, Microwave Processing of Materials, Symposium Proceedings. Vol. 124. Materials Research Society, Pittsburgh, PA, 1988.

2. Y.L.Tian, D.L.Johnson and M.E.Brodwin, "Ultrafine Microstructure of Al_2O_3 Produced by Microwave Sintering", Ceramic Powder Science II, p925-932, 1987.

3. Y.L.Tian, D.L.Johnson and M.E.Brodwin, "Microwave Sintering of Al_2O_3-TiC composites", ibid, p933-938, 1987.

4. W.H. Sutton, "Microwave Processing of Ceramic Materials", Ceramic Bulletin, Vol.68, No.2, p376-386, 1989.

5. J.Asmussen and R.Garard, "Precision Microwave Applicators and Systems for Plasma and Materials Processing", Microwave Processing of Materials, MRS Symposium, Vol.124, p347-352, 1988.

6. J.C.Araneta, Ph.D. Dissertation, Northwestern University, 1984.

7. K.Y.Tu, Y.L.Tian, M.E.Brodwin and D.L.Johnson, "A Circular Cylindrical Applicator for Enhanced High Temperature Processing", J. Microwave Power, Vol.22, No.3, P177, 1987.

8. L.Quéméneur, et al "Microwave Clinkering with a Grooved Resonant Applicator", J. Am. Ceram. Soc., 66 [12], p855-859, 1983.

9. A.C.Metaxas and R.J.Meredith, Industrial Microwave Heating, Peter Peregrinus Ltd., London, 1983.

10. Y.L.Tian, B.S.Li, J.K.Guo and D.S.Yen, "A Microwave Processing System for ceramics with Improved Energy Efficiency and Process Control", Proceedings of the 25th Microwave Power Symposium, p13-14, Denver, 1990.

11. Y.L.Tian, M.E.Brodwin, H.S.Dewan and D.L.Johnson, "Microwave Sintering of Ceramics under High Gas Pressure", Microwave Processing of Materials, MRS Symposium, Vol.124, p213-218, 1988.

12. H.Fukushima, T.Yamanaka, and M.Matsui, "Measurement of Dielectric Properties of Ceramics at Microwave Frequency", J. Japan Soc. of Precision Engr., 53 [5], p1-6, 1987.

13. Y.L.Tian, B.S.Li, Y.P.Xu, J.K.Guo and D.S.Yen, "Microwave Sintering of Y(3%)-ZrO_2(TZP)", to be published in this proceedings, 1991.

14. Y.L.Tian, M.E.Brodwin, H.S,Dewan and D.L.Johnson, "Sintering Behavior of Alumina Ceramics in Microwave Processing", Sintering of Advance Ceramics, Advances in Ceramics, Am. Ceram. Soc., 1988 (in press).

15. Y.L.Tian, J.H.Fang, B.S.Li, J.K.Guo and C.J.Tu, "Dynamic Temperature Profiles for a Microwave Heated Ceramic Cylinder", Presented at the 25th Microwave Power Symposium, Denver, 1990.

16. J.H.Fang, Y.L.Tian, B.S.Li, L.C.Sun and C.J.Tu, "A Two Dimensional Numerical Model and Computation for Thermal Dynamics of Microwave heated Ceramics", Proceedings of the 7th Annual Meeting of Chinese Eng. Thermal Physics Soc., p824-829, 1990.

17. T.K.Gupta, J.H.Bechtold, R.C.Kuznicki, L.H.Cadoff and B.R. Rossing, "Stablization of Tetragonal Phase in Polycrystalline Zirconia", J. Materials Science, Vol.12, p2421-2426, 1977.

MICROWAVE SINTERING OF ALUMINA CERAMICS IN A SINGLE MODE APPLICATOR

D. S. Patil*+, B. C Mutsuddy+
Institute of Materials Processing
Michigan Technological University
Houghton, Michigan 49931

James Gavulic, M. Dahimene
Wavemat Inc., Plymouth, Michigan 48170

ABSTRACT

High purity submicron powders were sintered in a single mode cylindrical cavity applicator CMPR-250 operating at 2.45 GHz in the TM012 mode. The alumina powders could be sintered from an initial green density of 60 % to a final density close to theoretical. Rapid heating rates at very low power level were achieved. Uniform microstructure and relatively small grain size in the microwave sintered alumina were evident. The initial results of this study demonstrate the potential applicability of a single mode applicator for sintering alumina ceramics.

INTRODUCTION

When microwaves penetrate and propagate through a dielectric material, the internal electric fields generated within the affected volume induce translational motions of free or bound charges and rotate charge complexes such as dipoles. The resistance of these induced motions causes losses and attenuates the electric field, and volumetric heating results due to these losses. Absorption of the electromagnetic energy inside the material is direct when the material couples with the microwaves, consequently, high heating rates can be achieved. The interaction being a direct one, this particular kind of heating source has a low thermal inertia. Energy can be quickly deposited or removed from the material. These are the advantages of microwave heating. However the heating is limited by several factors in certain materials that are transparent to the microwaves at room temperature, and would require preheating to some critical temperature.

* Permanant address : Laser and Plasma Technology Division
Bhabha Atomic Research Centre, Trombay, Bombay 400 085, INDIA.
+ Member, American Ceramic Society.

Microwave and radio frequency dielectric heating is easy when a material is polarizable, which efficiently converts the energy absorbed from the oscillating electric field into the thermal energy in the lattice [1, 2].
The power absorbed by a dielectric in an electric field is given by :

$$P = 2 \Pi f \varepsilon (\bar{E}^2/2) \tan \partial \qquad (1)$$

where
P = power absorbed in the material
ε = dielectric permittivity
f = frequency of the incident radiation
E = electric field strength
$\tan \partial$ = loss tangent of the material

The equation (1) provides an approximation of P and shows it's dependence on the variables. The losses in the ceramics at microwave frequencies are not fully understood and are possibly due to ionic migration, ionic vibration and electronic polarization. It is evident that many ceramics do not display high loss factors [3, 4]. The absoption of microwave energy in the material is determined by the depth of wave penetration which varies with temperature and frequency. The power available at the surface falls off exponentially. Therefore, size of a given sample will determine the frequency f at which the sample can be effectively heated. For the frequencies in the r.f. band, the dimensions are in meter. At microwave frequencies dimensions decrease to a few centimeters.

Temperature and impurities, however, can have a significant effect on the energy losses in ceramics. Conduction losses are typically found to be predominant at higher temperatures. The loss tangent and conductivity are directly related. In some cases introduction of impurities can be used to increase the conductivity and loss factor to the desired level. As the losses go up the depth of penetration decreases, opposing uniform sintering. On the other hand decreases in the thermal conductivity of the material with temperature plays a significant role in obtaining the desired heating profile.

The rate of heating increases with temperature for ceramics like Al_2O_3. It is therefore necessary to control the power to prevent thermal runaway. Again, in order to induce absorption of the microwave energy in the materials it is sometimes necessary to preheat the material before it effectively starts to couple with the microwaves [5]. Sintering aids which might couple at low temperatures and burn off at higher temperature may be an alternative to the preheating problem.

Rapid heating of materials minimizes segregation of the impurities to the grain boundaries while a decrease in sintering time reduces grain growth [5]. Temperature gradients in conventional heating cause greater pore elimination at the surface [6]. Heating internally (thereby creating higher internal temperatures) while cooling the surface will definitely be helpful in providing

more uniform final pore elimination. Good uniformity of the microwave sintering is not an easy objective to achieve and requires a knowledge of the material's high temperature microwave properties as well as ability to modify and control them.

Microwave applicator and system design allow significant flexibility (depending on the designer's ingenuity) in controlling these factors. Many ingenious designs for applying the microwave power to process materials have been reported in the literature. The difficulties encountered in efficient microwave heating of the ceramics can be reduced by using a tunable resonant cavity. Single mode resonant systems can be designed to yield very high electric field strength. Since, power absorbed by the material is proportional to the square of the electric field strength as shown in equation (1), use of a single mode applicator helps in inducing absorption in materials having low dielectric loss.

Microwave sintering of Al_2O_3 has been tried by several investigators [7, 8]. The purpose of this study is to show the feasibility of using a single mode applicator for sintering alumina. The objectives are also to avoid the use of binders and/or susceptors around the samples.

EXPERIMENTAL PROCEDURE

Equipment set up

Single mode/controlled multimode cavities appear to have an advantage over conventional multimode applicators. In a single mode cavity one has the flexibility of focusing energy at a given location of the sample. We used Wavemat's single mode, internally tuned resonant cavity CMPR-250 described by Asmussen et.al. [9]. Some of the empty cavity modes that are individually excited in this applicator are TE_{110}, TM_{012}, TE_{211}, TE_{011}&TM_{111} (degenarate mode) and TE_{111}.

The experimental system consists of a variable power-CW microwave power supply 3 KW-operating at 2.45 GHz, 2 circulators and matched dummy loads, power meters (that measures the incident power P_i and the reflected power P_r), a coaxial input coupling system, single mode cavity and Accufibre temperature measurement system*.

When the applicator is loaded with a material, the resonant modes are shifted from empty cavity resonant modes and probably become hybrid (combination of more than one) modes. Depending on the material's properties and position in the cavity, new cavity modes may be encountered. The material is kept on the cavity base plate on a boron nitride platform in the centre of the cavity. The material can be viewed through a copper screen window. Power is fed to the cavity through an adjustable coaxial input probe.

Adjustment of the short length L_s and coupling probe position L_p are made manually. Short and the probe positions are measured within 0.1 mm by micrometer indicators.

---

* Model 100 C, Accufiber, Inc., Beaverton, OR 97005.

To provide uniform heating, the sample dimensions are limited to half a wavelength. At 2.45 GHz dimensions are limited to approximately 6 cm. A larger size sample will require lower frequencies.

This single mode applicator has the ability to focus and match the incident microwave energy into the process material. This is accomplished with single mode excitation and internal cavity matching. The matching is labelled "internal cavity" since all tuning adjustments take place inside the cavity.

The input impedance of the microwave cavity is given by

$$Z_{in} = R_{in} + j X_{in} \qquad (2)$$

R_{in} and $j X_{in}$ are the cavity input resistance and reactance and represent the complex load impendance as seen by the feed transmission line. At least two independent adjustments are required to match this cavity load to a transmission line. The probe and sliding short tuning of the cavity applicator provide these two required degrees of freedom. Continuous tuning is required as the material's dielectric properties change during processing.

The ceramic pellet is encapsulated in a small amount of fiber insulation and the sample is irradiated by the microwave energy by first adjusting the probe and cavity length positions to excite a specific loaded cavity resonance (to match the cavity applicator to the input transmission system). The specific mode selection depends on the shape and location of the ceramic pellet. For a cylindrical pellet kept in the center of the cavity, the TM_{012} mode with its electric field along the cavity axis is a logical processing mode. For flat samples, TE modes will be a suitable choice.

Once adjusted for a match in the pre-specified mode, microwave power is applied and is absorbed in the cavity with minimum reflected power, and heating of the material begins. This changes the material properties and the Q of the cavity. The change in materials complex dielectric constant results in the shift in the cavity resonance and hence the change in the applicator input impedance. During heating, the applicator length L_s and probe length L_p are adjusted manually to maintain reflected power to a minimum (i.e. the applicator is kept tuned as the material's properties change). Since the tuning distances are a few mm, the tuning process can be quickly performed either manually or with small motors. Thus tuning also can be utilized as a sample input power control technique.

The ability to tune a cavity gives freedom of mode selection and also allows different material loads to be matched to a constant frequency power source. The flexibility in tuning during the operation cancels the variation in the cavity resonant frequency caused by cavity expansion or contraction due to changes in ambient temperature. The changes due to relative humidity in air inside the cavity can also be cancelled.

Sample preparation and experiment

We used two grades of Al_2O_3 powders for this sintering study. A16SG* (Alcoa) and Sumitomo alumina grade AKP-30MG**. The manufacturers quote the surface

area of the powders to be 8.6 and 7.1 m^2/gm, respectively. Average particle size is 0.52 and 0.41 μm, respectively.

The powders were rolled with the alumina grinding media and isopropyl alcohol. The slurries were dried under an IR lamp and the powders were sieved through a 100 mesh screen. The sieved powders were cold isostatically pressed into 25.4 mm dia. x 25.4 mm height pellets at a pressure of 276 MPa. The A16SG Al_2O_3 pellets were calcined at 1000 C for 1 hour. The AKP-30MG pellets were kept in the oven at 100 C for 12 hours to remove the moisture. No binder was added during processing. The green densities of the pellets were around 60 % of the theoretical density.

The pellets were embeded in the Al_2O_3 fiber insulation and the insulated pellet was kept in the centre of the base plate of the cavity. The incident microwave power was coupled with the help of the coupling probe. Tuning of the particular mode was accomplished by adjusting the position of a sliding short and the coupling probe. A hole of ~ 3 mm diameter was drilled through the insulation to view the sample surface by the accufiber optical pyrometer through a non-radiating opening on the wall of the cylindrical cavity.

Accurate temperature measurement was restricted by three factors. First, a thermocouple was tried but the leads started to act as antenna causing a loss of microwave energy from the cavity. Second, error in the sample temperature measurement was due to the interference from luminous fiber insulation at high temperature. Third, the emissivity of the sample which is also temperature dependent, varies during sintering due to morphological changes.

Nonetheless, the recorded temperatures which were probably below their true value did provide some relative temperature differences between the samples. Efforts are now being directed to get the true estimate of the temperature and with some more improvements we will be able to measure the temperature of the sample to a reasonably good accuracy.

The samples were processed according to the schedule shown in Figure 1. To compare the results of the microwave processing with the conventional sintering, a similar sample of A16SG was sintered at 1650 C for 1 hour with the heating and cooling rate of 200 C/hour.

The densities of the samples were measured by the Archimedes principle. Specimens were cut from the sintered samples and the surfaces were polished to a 0.25 μm finish with diamond paste. The samples were chemically etched to reveal the microstructure. Both the chemically etched and fractured surfaces were examined using a scanning electron microscope (JEOL***, JSM-820).

---

* Alcoa, Aluminium Company of America, Pittsburgh, PA.
** Sumitomo Chemical Company, Ltd., Osaka, Japan.
*** JEOL, USA, Inc., Peabody, MA 01960.

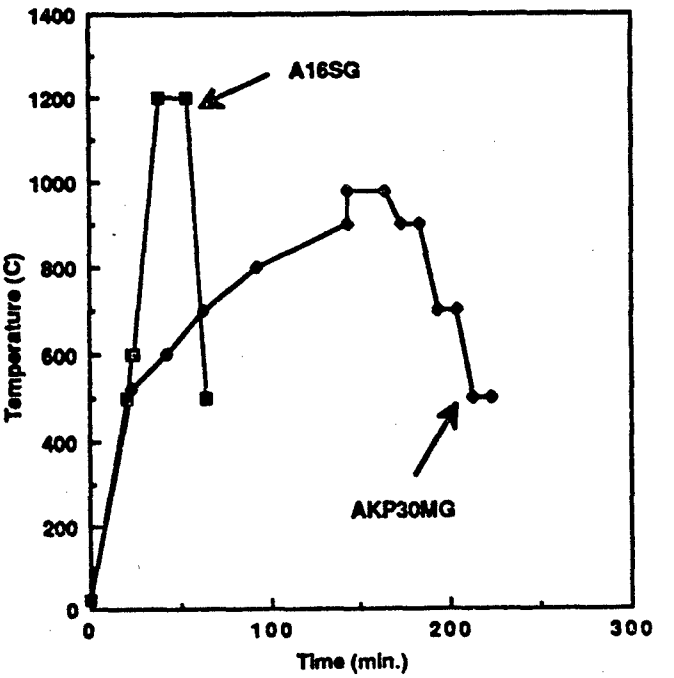


Fig. 1. Microwave sintering schedule of alumina ceramics

RESULTS AND DISCUSSIONS

Results on the microwave sintering of the alumina specimens are shown in Table 1.

Table 1 Results on various samples

S. No	Sample	Heating mode	Temperature C (Surface)	Time (hours)	% Densification
1	A16SG	Microwaves	1200	1.2	97.76
2	A16SG	Conventional	1650	17	98.68
3	AKP30MG	Microwaves	975	4	100

The density of the sample using microwave sintering was 97.76 % of the theoretical for A16SG. To get a similar density using conventional sintering we had to use a temperature of 1650 C. The conventional process took a long time (200 C/hour heating/cooling rate with 1 hour hold at 1650 C) as compared to a total 72 minutes for microwave processing. The sample AKP-30MG was sintered to theoretical density.

The microstructures of the various samples are shown in the Figs. 2-4. A slight variation in the microstructure was observed as we scanned the different regions of the sample. These variations suggest that the electric field intensity is different at the centre as compared to the edge. The difference in grain size may be due to the high electric field intensity at the centre.

Based on our observations, sintering can be potentially divided in two stages: preheating and sintering. During preheating tha samples are heated for a few minutes at a constant input power of 300-400 watts. Attempts to reach the final sintering temperature by raising the input power without preheating the sample, resulted in hot spot formation, arcing and eventual cracking of the samples.

A uniform hot zone can only be formed when the sample is properly insulated. The gradual increase in sample temperature is required to achieve uniform densificatiCn.

The thermal runaway phenomenon which is frequently observed in microwave sintering was avoided through proper insulation of the sample and by careful control of input power.

Densification of the samples was noted by the reflected power meter. As the material's absorption decreased after the densification and the minium reflected power increased.



Fig. 2. Fractured surface of the microwave sintered alumina A16SG (SEI, 5000X)

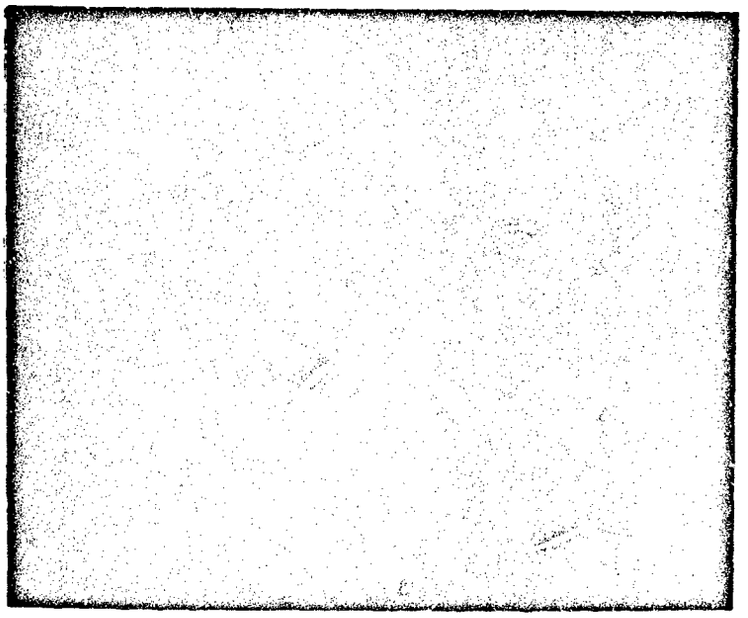


Fig. 3. Fractured surface of the conventionally sintered alumina A16SG (SEI, 5000 X)



Fig. 4. Fractured surface of microwave sintered alumina AKP30MG (SEI, 5000 X)

The observed uniform microstructure can be explained in the light of rapid heating rate. The sample passes more rapidly through the lower temperature regime where surface diffusion is relatively more dominant and the fine grained structure is raised rapidly to a high temperature where densification dominates grain growth.

CONCLUSIONS

High purity submicron Al_2O_3 powders have been densified from 60 % initial green density to near theoretical density by using a tuneable single mode applicator operating in the TM_{012} mode at 2.45 GHz. The time required to achieve similar density with conventional sintering is much higher as shown in Table 1.

Our preliminary results show the potential use of microwave energy, without any need for susceptors around the sample, to achieve full densification of fairly large (25.4 mm dia. x 25.4 mm height) alumina samples.

ACKNOWLEDGMENTS

The authors wish to thank Dr. Walter A. Johnson, Director of Institute of Materials Processing for his continuous encouragement and support. Thanks are due to Ruth Kramer for her assistance with the SEM work and students for their help. One of them (DSP) is grateful to the authorities at Bhabha Atomic Research Centre, Bombay for granting him a leave of absence.

REFERENCES

1) A. R. Von Hipple, "Dielectric Materials and Applications", M. I. T. Press, Cambridge, p. 3-46, 1954.
2) H. Puschner, "Heating with Microwaves : Fundamentals, Components and Circuit Techniques", Springer-Verlag, New York, 1966.
3) F. J. Smith, " Research and Development", January, 54 (1988).
4) C. T. Lynch, " CRC Handbook of Materials Science", vol. II, p. 360, CRC Press, Boca Raton, 1984.
5) H. D. Kimrey, T. L. White, T. S. Bigelow and P. F. Becher J. Microwave Power, Symp. Summaries, 81-82 (1986).
6) W. D. Kingery, H. K. Bowen and D. R. Uhlamann, "Introduction to Ceramics, 2nd edition, 485, John Wiley and Sons, 1976.
7) T. T. Meek, R. D. Blake and J. J. Petrovic, "Microwave sintering of Al_2O_3 and Al_2O_3-SiC whisker composites", Ceram. Engg. Sci. Proc., 8 [7-8] p.861 -871 (1987).
8) Y. L. Tian, D. L. Johnson and Morris E. Brodwin, "Ultrafine microstructure of Al_2O_3 produced by microwave sintering", Ceramic Transactions, vol. I, Ceramic Powder Science 2, part B, p. 925-932, The American Ceramic Society Inc., Westerville, Ohio, (1988)
9) J. Asmussen, H. H. Lin. B. Manring and R. Fritz, "Single mode or controlled multimode cavity applicator for precision materials processing", Rev. Sci. Instrum. 58 [8] 1477-1486 (1987).

MICROWAVE SINTERING OF ZIRCONIA-8 MOL % YTTRIA

M. A. Janney, C. L. Calhoun, and H. D. Kimrey
Oak Ridge National Laboratory
Oak Ridge, TN 37831-6087

ABSTRACT

Microwave sintering of zirconia - 8 mol % yttria in a 2.45 GHz microwave furnace is described. The nominal sintering temperature of the zirconia is 1375°C in the conventional furnace, but is only 1200°C in the microwave furnace. Difficulties were encountered in producing uncracked sintered parts in the microwave furnace because of the low thermal conductivity and rapid change in dielectric properties of the zirconia. An indirect heating method was developed to alleviate these problems and to make heating more uniform.

INTRODUCTION

This investigation was concerned with the sintering of yttria-stabilized zirconia, using microwave heating. Microwave firing has been demonstrated to reduce the temperature required for sintering of a number of ceramic materials[1-3]. Thus it was conjectured that the sintering temperatures of the zirconia could be lowered

---

Research sponsored by the U.S. Department of Energy, Fossil Energy Advanced Research and Technology Development (AR&TD) Materials Program, DOE/FE AA 15 10 10 0, under contract DE-AC05-84OR21400 with Martin Marietta Energy Systems, Inc.

MATERIALS AND METHODS

All samples in the study were prepared from TOSOH powders, either TZ3Y (3 mol % yttria) or TZ8Y (8 mol % yttria)*. A thermocouple well, 15/64 in. (6mm) diam by 1/2 in. (13mm) deep, was drilled in the microwave samples; this ensured good contact during firing between the sample and a molybdenum-sheathed, Type C thermocouple† temperature probe embedded in the part. Sample densities were determined by Archimedes principle using ethanol as the suspending fluid.

The microwave furnace used in this study was built in-house. It consisted of a water-cooled aluminum vacuum vessel, 20 in. (50 cm) diam by 24 in. (61 cm) long, with integral mode stirrer, forward and reflected power meters, microwave safety interlocks, and ports for Ar and N_2 gas feeds and thermocouple penetrations. Power was supplied by a 2.6 kW, continuously variable, 2.45 GHz microwave generator‡. The microwave power was controlled either manually, or through feedback control from a standard PID controller.

RESULTS AND DISCUSSION

Initial Sintering Studies on ZrO_2-3 mol % Y_2O_3

The initial microwave sintering experiments were conducted using a technique that was developed for our previous work on alumina[1]. The part to be sintered was buried in bulk zirconia fiber§ which was contained in an insulating crucible made of alumina fiberboard¶, Fig. 1. A 1/8 in. (0.3 cm) diam molybdenum-sheathed, Type C thermocouple embedded in the part was used to measure the temperature. The use of the zirconia bulk fiber ensured that the insulation closest to the zirconia part had microwave heating characteristics similar to those of the zirconia part being sintered. This arrangement was designed to help to reduce thermal gradients in the part being sintered. For the alumina case, this arrangement had been quite satisfactory. For zirconia fired at 2.45 GHz, additional measures were needed as will be shown below. The alumina fiberboard crucible acted as the primary thermal insulation because it was heated very little by the 2.45 GHz microwave field.

The first set of zirconia sintering experiments at 2.45 GHz was universally unsuccessful. Severe cracking of the zirconia was encountered irrespective of the thermal cycle, including rate of heating (from 0.5 to 10°C/min), intermediate temperature soaks (at 300 to 500°C), and the peak sintering temperature (from 1000 to

1300°C). "Runaway" heating conditions were routinely encountered during which the thermocouple temperature would rise rapidly, even though the microwave power into the furnace might actually be falling. Figure 2a shows a typical part after sintering. Note the "onion"-type structure that developed during firing.

The electric field distribution in the 2.45 GHz furnace that was used in this investigation is non-uniform. It was hypothesized that the non-uniform sintering which was observed in the present investigation was caused by variations in the electric field, which in turn led to thermal runaway conditions in a small volume of material. To test this hypothesis, sintering runs were made in a high-uniformity, 28 GHz microwave furnace in which the worst-case variation in the electric field strength is ± 4% of the mean value[4]. The result for a ZrO_2 - 3 mol % Y_2O_3 part is shown in Fig. 2b. The part sintered to high density (>99.9 % td) at 1150°C with no cracking or warping, even though a very high heating rate (~30°C/min) was used.

Approach to Improved Microwave Heating of Zirconia at 2.45 GHz

Based on the sintering experiments outlined above, it was concluded that control of the heating of the zirconia to a temperature of 600 - 700 °C was necessary in the 2.45 GHz microwave furnace. To accomplish this, a combination of "indirect" and "direct" microwave heating at 2.45 GHz would be required. Crack-free zirconia parts should be the result. An approach was developed that utilized a "picket fence" of SiC rods surrounding the zirconia part, which is shown in Fig. 3. The "picket fence" arrangement consists of five SiC rods (0.25 in. [0.64 cm] diam x 4 in. [10 cm] long) mounted vertically in a 4 in. [10 cm] diam circle, giving a spacing between rods of about 6 cm. Zirconia bulk fiber is placed around the part, and the entire construction is enclosed in an alumina fiber crucible. This arrangement was chosen to facilitate controlled indirect heating of the ZrO_2 at low temperatures and controlled direct microwave heating at high temperatures. At low temperatures, SiC absorbs most of the microwave power in the furnace and heats faster than the zirconia. The zirconia therefore is only heated indirectly by conduction of heat from the SiC rods at low temperatures, and the negative interactions of the zirconia with the microwaves such as hot spots and thermal runaway are avoided. As the temperature of the zirconia and SiC rods increases, the relative amount of microwave energy absorbed in the zirconia increases because its dielectric loss factor is increasing faster than that of the SiC. At the sintering temperatures of 1000 to 1250°C, all of the heating of the zirconia was provided directly by the microwaves.

The final processing factor required to produce crack-free parts was a slow heating rate. At rates of 10, 20, and 30°C/min, thermal runaway was encountered even when the "picket fence" approach was used; cracked parts were produced in all of these cases. To produce crack-free parts, a heating rate of 2°C/min was used up to 500°C and a rate of 3.5°C/min was used from 500°C to the sintering temperature. Using these techniques, excellent quality parts could be produced repeatably.

Arcing was a problem at times during the firing of zirconia using the "picket fence" approach. The problem was eliminated by introducing a small N_2 flow into the cavity.

Densification of ZrO_2 - 8 mol % Y_2O_3

The sintering study on the ZrO_2 - 8 mol % Y_2O_3 system involved a side-by-side comparison of the sintering behavior in the 2.45 GHz microwave furnace using the "picket fence" arrangement and in a conventional tube furnace. The sintering conditions were kept as close to the same as possible in the two sets of experiments. The same heating rate (3.5 °C/min), gas atmosphere (Ar - ~1% N_2), and soak times (1h at temperature) were used in both.

The sintering results summarized in Fig. 4 clearly demonstrate the presence of a "microwave effect" for the sintering of ZrO_2 - 8 mol % Y_2O_3 in the 2.45 GHz microwave furnace. Nearly full density, >99% td, was obtained at 1195°C in the microwave furnace. In contrast, to achieve the same density conventionally required a temperature of 1375°C. Not only is there a shift in the curves, but the differential in the sintering temperature increases as the sintered density increases. Similar behavior has been observed for the sintering of high-purity alumina[3]. In that system, a reduced apparent activation energy for sintering was demonstrated in the microwave case. It is hypothesized that a detailed study of the microwave sintering kinetics for zirconia would also demonstrate a reduced apparent activation energy for sintering. The shift in the sintering curves also supports our earlier hypothesis that the "picket fence" would not shield the part being sintered from the microwave field. Obviously, if the heating of the part were due only to indirect heating from the SiC rods, then the sintering curve for the "picket fence" arrangement would be identical to that for the conventional furnace.

Both microwave and conventional firing produced a microstructure that exhibited an essentially normal grain structure (i.e., soap bubble type) with most of the

residual porosity residing at grain boundaries and grain edges. The grain size of the microwave sintered zirconia was ~2.2μm (99.47% td) and of the conventionally sintered zirconia was ~3.5μm (99.35% td). This behavior is again similar to that observed for the sintering of alumina, where finer grain sizes were observed for microwave sintered material as compared to conventionally sintered material[1,3]. It is conjectured that microwave firing enhances the mechanisms that lead to densification, such as volume and grain boundary diffusion, over those that lead to coarsening of the microstructure, such as surface diffusion and evaporation/ condensation. The exact mechanism that causes the microwave field to enhance one type of diffusion over another is not known at the present time. That finer microstructures have been observed in both alumina and zirconia, however, lends support to the hypothesis.

SUMMARY AND CONCLUSIONS

Zirconia is an extremely challenging material to process in a 2.45 GHz microwave furnace. The combination of (1) dielectric properties that change rapidly with temperature and (2) very low thermal conductivity make zirconia difficult, if not impossible, to fire in a "normal" manner in the microwave furnace. A "picket fence" approach using SiC rods was developed, which combined with a slow firing rate, ~3.5°C/min, was successfully used to produce good parts in zirconia at 2.45 GHz. Sintering results using the "picket fence" showed that a "microwave effect" exists for the sintering of zirconia, whereby the sintering temperature is reduced by 100 - 150 °C as compared to conventional sintering. Microwave firing also produced a finer grain size in the final fired part.

ACKNOWLEDGEMENTS

The authors would like to acknowledge the efforts of the following people in this work: J. O. Kiggans for his laboratory skills, especially in microwave furnacing; J. R. Mayotte for metallography; and, R. L. Freeny for photography.

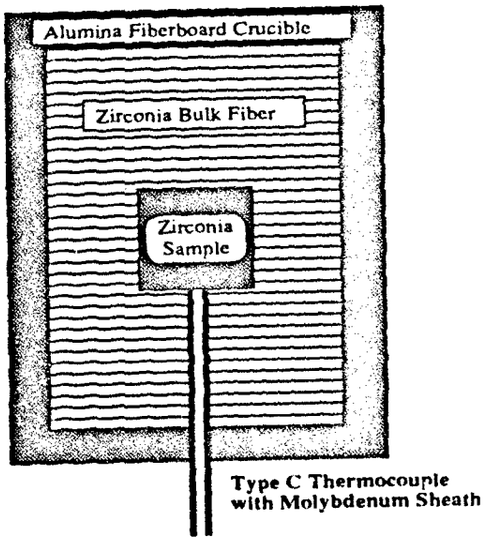
---

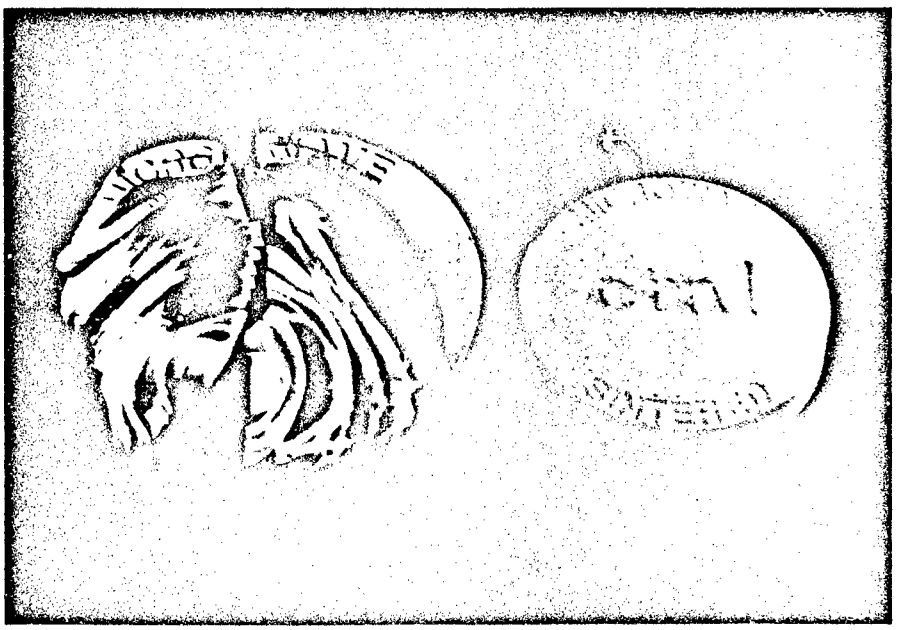
* TOSOH U.S.A., Inc., Atlanta
† Omega Engineering, Stamford, Conn.
‡ Gerling Laboratories, Modesto, Ca.
§ ZYBF, Zircar Products, Inc., Florida, N.Y.
¶ AA30, Zircar Products, Inc., Florida, N.Y.

REFERENCES

1. M. A. Janney and H. D. Kimrey, "Microwave Sintering of Alumina at 28 GHz," **Ceramic Powder Science, II**, pp 919-924, G. L. Messing, E. R. Fuller, and H. Hausner, eds., American Ceramic Society, Westerville, Ohio, 1988.
2. C. E. Holcombe, "Microwave Sintering of Non-Oxide Ceramics," presented at 91st Annual Meeting American Ceramic Society, Indianapolis, Indiana, April, 1989.
3. Y. L. Tian, D. L. Johnson, and M. E. Brodwin, "Ultrafine Microstructure of Al_2O_3 Produced by Microwave Sintering, " **Ceramic Powder Science, II**, pp 925-32, G. L. Messing, E. R. Fuller, and H. Hausner, eds., American Ceramic Society, Westerville, Ohio, 1988.
4. H. D. Kimrey and M. A. Janney, "Design Principles for High Frequency Microwave Cavities," *Proc. Mater. Res. Soc.*, Vol. 124, p.367, 1988.

Figure 1. The standard arrangement for firing ceramics in a microwave furnace requires surrounding the part with fiber insulation to contain the heat generated by the microwaves.





(a) (b)

Figure 2. Examples of zirconia samples (ZrO_2 - 3 mol % Y_2O_3) fired in (a) nonuniform and (b) highly uniform microwave furnaces.

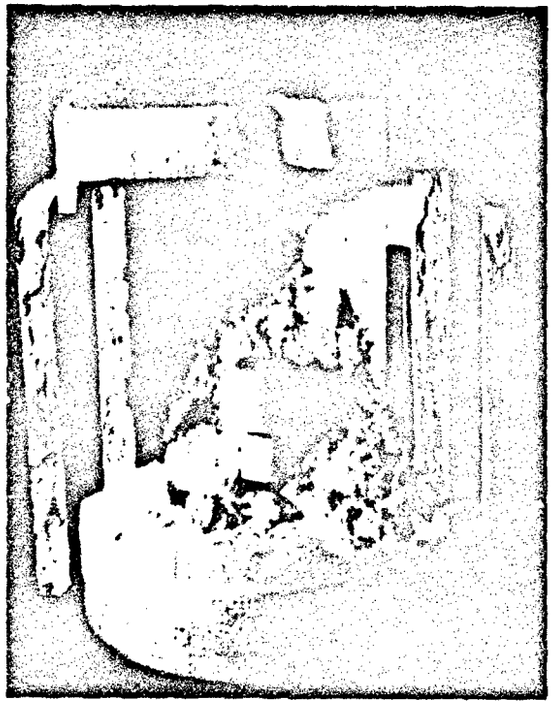


Figure 3. A "picket fence" arrangement was used to provide a combination of indirect and direct microwave heating to the zirconia samples. Shown are the zirconia samples supported on a Type C thermocouple and surrounded by zirconia bulk fiber insulation, the silicon carbide "picket fence," and the alumina fiberboard outer insulating crucible.

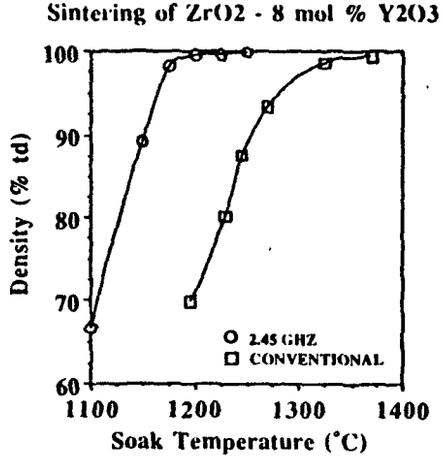


Figure 4. Microwave firing accelerated the densification of ZrO_2 - 8 mol % Y_2O_3 as compared to that for conventional firing. Microwave samples were fired using the "picket fence" arrangement.

MICROWAVE (HYBRID) HEATING OF ALUMINA AT 2.45 GHZ: I. MICROSTRUCTURAL UNIFORMITY AND HOMOGENEITY

Arindam Dé , Iftikhar Ahmad, E. Dow Whitney and David E. Clark
Dept. of Materials Science and Engineering,
University of Florida,
Gainesville, FL 32611.

Microwave (hybrid) heating (MHH) is a unique combination of microwave (MW)-material interaction and conventional radiant/conduction mechanisms that facilitates the attainment of very high heating rates in a 2.45 GHz, multimode MW cavity. Microstructural uniformity and homogeneity of dry-pressed green samples of pure, undoped alumina with (MHH) relative to conventional fast firing (CFF) has been studied. The confluence of the two heating mechanisms (with MHH) results in an improved parity in temperatures across specimen cross-sections vis-a-vis CFF and stand-alone MW (SMW) sintering. This enhanced parity in temperatures (with MHH) can be said to be responsible for the better microstructural homogeneity and improved mechanical properties relative to CFF. Sintering of larger (20 gm vs. 6 gm) samples with MHH shows evidence of a definitive mass dependance on the MHH phenomena. Larger masses show a better parity in temperatures between the surface and interior of the sample. Consequently, this results in enhancements in the homogeneity of the microstructure, and improved and more uniform mechanical properties relative to the smaller MHH and CFF samples.

INTRODUCTION

MW sintering is a technique that offers enormous potential for the fabrication of ceramics and ceramic composites with improved microstructures. Work in this area by a number of researchers [1-7] demonstrate the efficacy of MW sintering from the standpoint of lower sintering temperatures and smaller grain sizes compared to conventional sintering. This has been attributed to enhanced diffusion and a lower activation energy for sintering that is characteristic of MW energy [2-4].

In order to apply the benefits of ultra rapid heating to MW sintering, a technique that makes use of both MW-material interaction as well as conventional radiant/conduction heating mechanisms has been developed. 'Hybrid heating using MW energy' (MHH) [8-10] makes use of radiant/conduction heating to rapidly heat samples through low temperature regimes to a critical temperature above which the microwaves couple readily with the material. A heating rate of up to 750°C per minute for pure, undoped alumina in a 2.45 GHz, 6.4 KW (max.) multimode cavity, making use of less than half the peak power output, has been attained with this technique.

Microstructural homogeneity (parity in grain sizes and porosity across sample cross-sections) is difficult to achieve with conventional techniques. Although stand-alone MW (SMW) sintering has been surmised to result in more homogeneous microstructures compared to conventional techniques [2], no evidence to support that premise has been presented. Past efforts (with SMW sintering) [7] indicate non-uniformities in the form of appreciable differences in grain sizes between the surface and interior of sample cross-sections.

It is suggested that an improved parity in temperatures between the surface and the interior, that is unique to MHH is responsible for the enhancements in microstructural homogeneity and mechanical properties relative to CFF.

EXPERIMENTAL PROCEDURE

A pure, undoped, commercially available alumina was used. The alumina designated A-16* was a 99.97% pure alumina grade (as received) with an average particle size of 0.48 μm, a broad particle size distribution, and a surface area of 4.697 m^2/gm.

The experimental set-up for the MHH is illustrated in Figure 1. MHH was effected in static air in a 2.45 GHz, 6.4 KW (max) ** multimode cavity, with the sample enclosed in a silicon carbide lined susceptor. Temperature monitoring was effected by inconel shielded 'K'-type thermocouples#(for temperatures up to 1100°C) and by two color infrared pyrometry## (for temperatures above 1100°C). A peak heating rate of the order of 1500°C in 120 sec (750°C per minute) for pure undoped A-16 alumina at a power output of around 3 KW was attained.

CFF (conventional fast firing/ isothermal sintering) was effected in static air by inserting the samples into a resistance heated tube furnace+ which was preheated to the sintering temperature. The samples were stationed in alumina boats which in turn, were slowly inserted into the heat zone of the tube furnace. Temperatures were read off a 'B' type Pt-Rh thermocouple #(with digital display) which was kept in contact with the alumina boat and the walls of the alumina tube of the furnace.

In order to understand the heating mechanisms (and temperature gradients across the sample cross-sections) characteristic of MHH and CFF, experiments designed to obtain simultaneous surface and interior temperature profiles under actual conditions of heating were initiated. The experiments comprised stationing inconel shielded 'K' type thermocouples on the surface and in the interior of the samples, and heating the samples as shown in Figure 2. The samples were heated under conditions of SMW heating, MHH and CFF. Twenty five gm dry-pressed green samples, with a cavity (core) at the interior were used. For the MHH experiments, in addition to the 25 gm sample, an 8 gm dry-pressed sample was also used (to study the effect of mass on the MHH). For the CFF the specimen had to be pre-sintered to around 1000°C., for sufficient green strength, and to be able to withstand the high heating rates and thermal stresses.

In order to compare ultra rapid sintering using MHH with CFF, and study the mass dependence of the two modes of heating, 6 gm and 20 gm cylindrical pellets of A-16 alumina were cold pressed to 4000 psi. (green density~52%). These were then sintered in the MW oven under hybrid heating conditions at 1500°C, with a holding time of 30 minutes. Identical green compacts were also fired in the preheated resistance tube furnace under isothermal heating conditions at the same temperatures and holding times as the MHH samples.The samples were then scanned from the surface to the interior as shown in Figure3. The five positions from the surface to the interior and back to the surface have been designated A, B, C, D, and E, respectively.

Bulk and relative densities of the sintered samples were obtained by the Archimedes density method. The samples were then polished using standard ceramographic techniques, and thermally etched at a temperature of 1450°C for 30 min. Microstructures representative of both the surface and the interior of each sample were obtained by a scan of the transverse cross-section of the polished and etched sample section in the SEM, as shown in Figure 3. Grain intercept lengths and porosities were

---

* Aluminum Company of America (Alcoa) Inc., Pittsburgh, PA.
** Model Radarline QMP 2101B-6, The Raytheon Company, Waltham, MA.
# Omega Engineering Inc., Stamford, CT.
Ratio Scope 8, Capintec Inc., Fair Lawn, N.J.
\+ Model Sola-Basic, Lindberg, Watertown, WI.

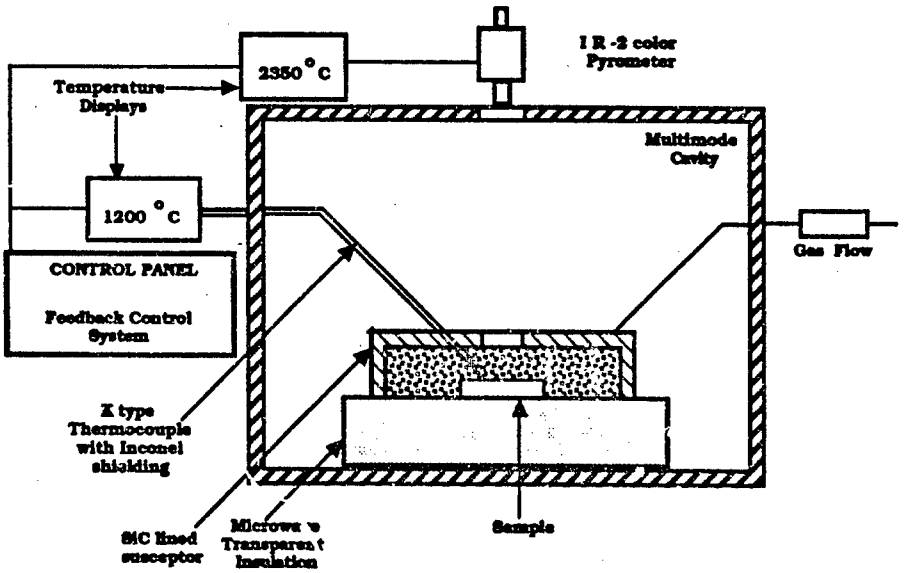


Figure 1. Schematic of multimode 2.45 GHz., 6.4 KW (max.) MW cavity.

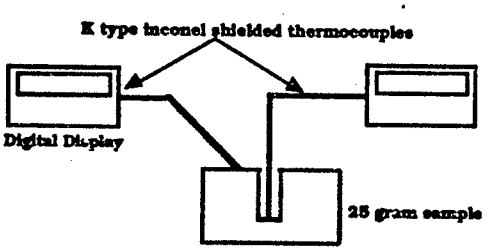


Figure 2.. Arrangement used for surface-interior temperature profile measurements.

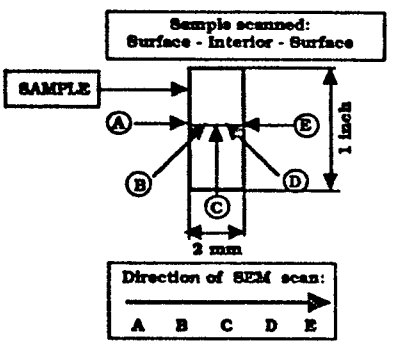


Figure 3. Sample scan in the SEM

computed from the SEM micrographs using standard quantitative stereological techniques. Average grain sizes were determined from measured average lineal grain intercept lengths according to the equation [11]

$$\text{grain size} = 1.56 \cdot \text{grain intercept length} \quad (1)$$

The resulting data were plotted, correlated and compared .

RESULTS AND DISCUSSION

Surface-Interior Temperature Profiles

Simultaneous surface-interior temperature profile measurements were carried out for samples heated by stand-alone MW heating (SMW), conventional fast firing (CFF), and MW (hybrid) heating (MHH). A uniform temperature distribution across the cross-section is vital to densification (and coarsening), and is perhaps, the single most important factor contributing to microstructural homogeneity. Twenty five gm dry pressed samples for all three techniques were employed. In addition to this, the temperature profile for an 8 gm sample heated by MHH was also obtained.

Figure 4(a) is an illustration of the temperature profile obtained for the pre-sintered 25 gm sample, heated to 1200°C by CFF. As is evident from the profiles, for the short soaking times (~ 30 minutes) employed for sintering the CFF samples, the interior of the samples, for most of the sintering time, do not experience the same thermal histories as the sample surfaces. These differences in temperature at the surface and the interior translate into microstructural inhomogeneities, as will be discussed in the following sections.

Figure 4(b) shows the surface interior temperature profile obtained for the alumina sample subjected to SMW heating. The alumina did not heat up beyond 500°C, even with power levels as high as 5 KW. However, even at the low temperatures that the sample was heated to, the interior of the sample was at a significantly higher temperature than the surface. This is a direct consequence of the inverse temperature gradients that is characteristic of SMW heating. This disparity in temperatures between the surface and the interior may be expected to increase with an increase in temperature.

Figure 4(c) is a plot of the temperatures experienced by the surface and the interior of an 8 gm sample heated by MHH.When the MW power is switched on, the SiC from the susceptor heats up quickly. This in turn, transmits heat to the surface of the alumina sample by radiation. The surface of the alumina specimen heats up and conducts heat to its interior by phonon conduction. This process continues until the entire sample heats up to a temperature of about 800°C, above which, the alumina absorbs microwaves readily. The onset of MW heating causes the interior of the sample to heat up (owing to the inverse thermal gradients characteristic of MW heating). However, the surface of the sample which receives heat from the susceptor, also conducts heat into the interior of the sample. Thus, the interior of the sample which is subjected to heat from these twin sources, heats up to a higher temperature than the surface, Besides, heat is also lost from the sample surface by dissipation, to the atmosphere, as well as the refractory bricks below. This disparity in temperatures (40-60°C at 1200°C) between the surface and the interior is reflected in Figure 4(c).

The surface-interior temperature profile for the 25 gm sample heated by MHH is illustrated in Figure 4(d).The heating process is very similar to that for the 8 gm hybrid heated sample. However, owing to the larger mass the process of heat conduction to the interior takes a longer time. Equivalent temperatures are realized at the surface and interior of the specimen throughout the sintering (soaking) time.

It is this parity in temperatures that is responsible for the more uniform and homogeneous microstructures obtained with the MHH process relative to CFF. Since the masses of the specimens used for sintering studies (6 gm and 20 gm) are very close to

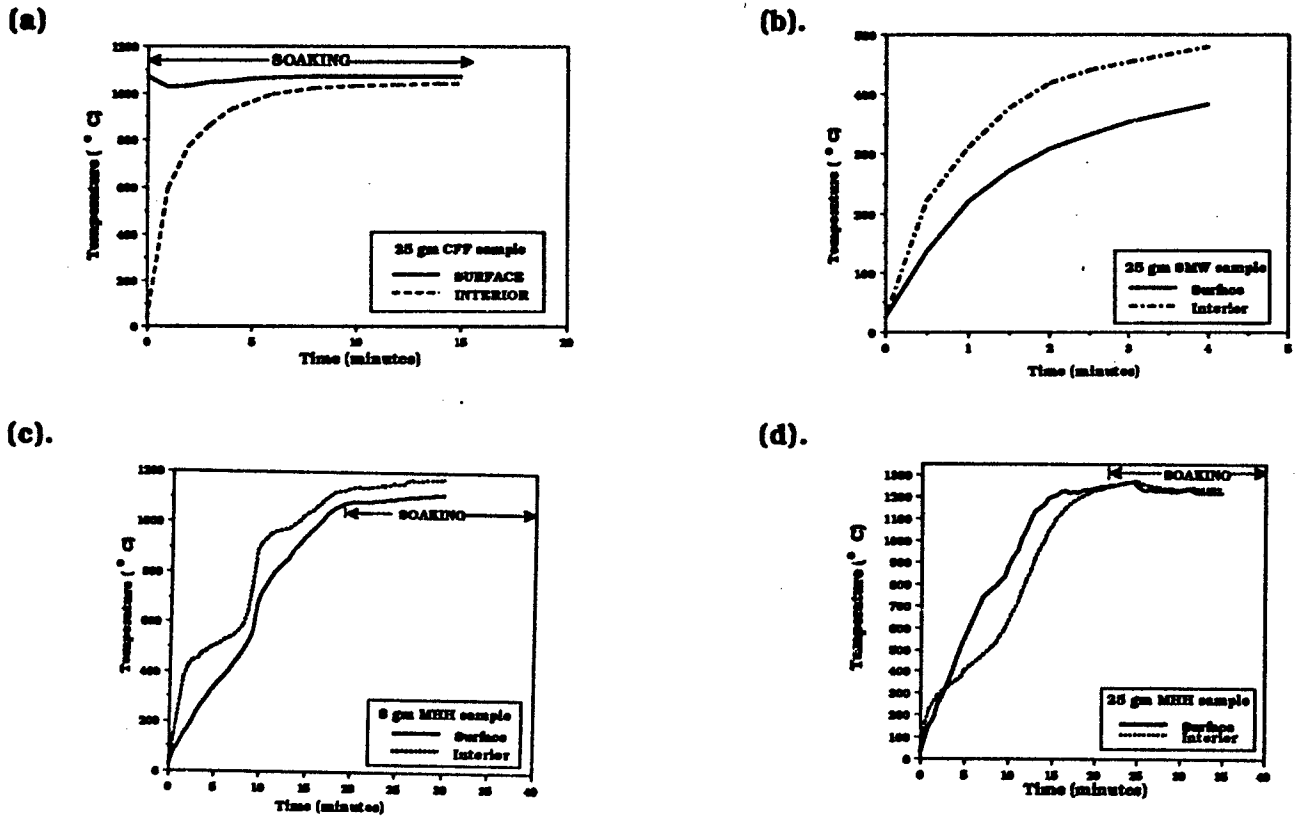


Figure 4. Surface-interior temperature profiles of: (a). 25 gm (pre-sintered) CFF sample; (b). 25 gm SMW sample; (c) 8 gm MHH sample and (d) 25 gm MHH sample.

those employed for the surface-interior temperature profiles (8 gm and 25 gm), the profiles were used to explain the differences in the sintering phenomenologies, and the consequent disparities in microstructures.

MW (Hybrid) Heating vs. Conventional Fast Firing of A-16 Alumina : Mass Dependence

In order to effect a comparison of MHH and CFF, identical 6 gm dry-pressed samples of A-16 alumina were sintered using both techniques at 1500°C, with a holding time of 30 minutes. Previous work by Dé et al. [9-11] have elucidated these results in detail. The surface-interior temperature profiles showed that a better volumetric heating and a significantly better parity in temperatures was observed with the larger samples. Subsequent efforts were therefore directed towards sintering larger (20 gm) dry-pressed samples under the same state conditions as the smaller samples (1500°C for 30 minutes) by both MHH and CFF. The 20 gm. CFF samples did not survive the excessive thermal stresses caused by the temperature gradients (thermal shock) and fractured into fragments each time.

Representative transverse cross-sections of sample portions (polished and thermally etched) were then scanned from the surface to the interior as shown in Figure 3. The results from the microstructural analysis and stereological computations for the 20 gm MHH specimen were incorporated with those from the smaller (6 gm) MHH and CFF samples, and will be discussed here.

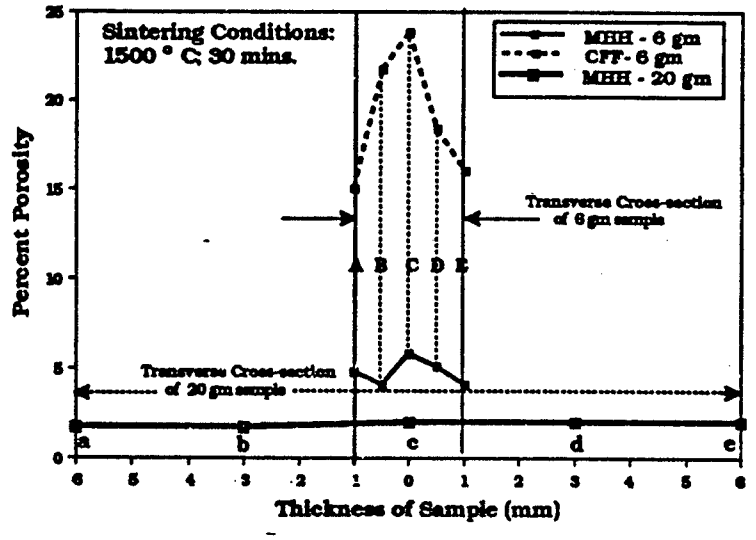
The relative densities of the 6 gm MHH and CFF samples were 96% and 87% (of the theoretical), respectively, while that of the 20 gm. MHH sample was 98% of the theoretical, sintering having been carried out under the same state conditions of time and temperature.

Figure 5(a) is a plot of the volume fraction of porosity (computed stereologically) as a function of the sample thickness. The 6 gm CFF sample showed very significant differences in porosity from the surface to the interior with a maximum porosity of around 23% at the center, whereas the porosity for the 6 gm MHH sample ranged from 4.06 to 5.8%. The porosity for the 20 gm MHH sample was only 2%.

Figure 5(b) is a plot of the ave. grain intercept size (GI) versus sample thickness for the 3 samples. The 6 gm MHH sample exhibited somewhat larger GI sizes than the CFF sample (average GI size ~1.41 μm relative to 0.70 μm for the CFF sample), with the largest grains at the center. The CFF sample (6 gm) showed an appreciable variation in the GI size distribution across the cross-section, with grains progressively increasing from surface towards the interior, and then dipping drastically in size at the interior of the specimen. The ave. GI size of the 20 gm MHH sample was 0.75 μm, with very little variance across the sample cross-section.

The enhanced microstructural uniformity and homogeneity for the bulk MHH sample (in spite of the inhomogeneities in the starting green microstructure) can be explained by the temperature distribution across the sample cross-section. As discussed earlier (Figure 4 (d)), the bulk (20 gm) MHH sample experiences nearly the same temperature (1500°C) across it's entire cross-section for the full length of the soaking time due to the confluence of the twin heating mechanisms that characterize the MHH process. This is in contrast to the temperature gradients experienced by the 6 gm CFF sample (interior significantly cooler than the surface which is at the sintering temperature) and the 6 gm MHH sample (sample interior at an appreciably higher temperature than the surface which is at the sintering temperature). It is this equanimity in temperatures between the surface and the interior of the bulk MHH sample for the entire period of sintering, that culminates in the enhanced densification (microwave enhanced diffusion) relative to the CFF specimen, and reduced grain growth as compared with the 6 gm MHH sample. Further, it is this parity in temperatures that is responsible for the dramatically improved microstructural uniformity throughout the bulk (20 gm) MHH specimen.

The microstructure-mechanical property correlation is reflected in plots of the mechanical properties (microhardness, fracture toughness) as a function of the



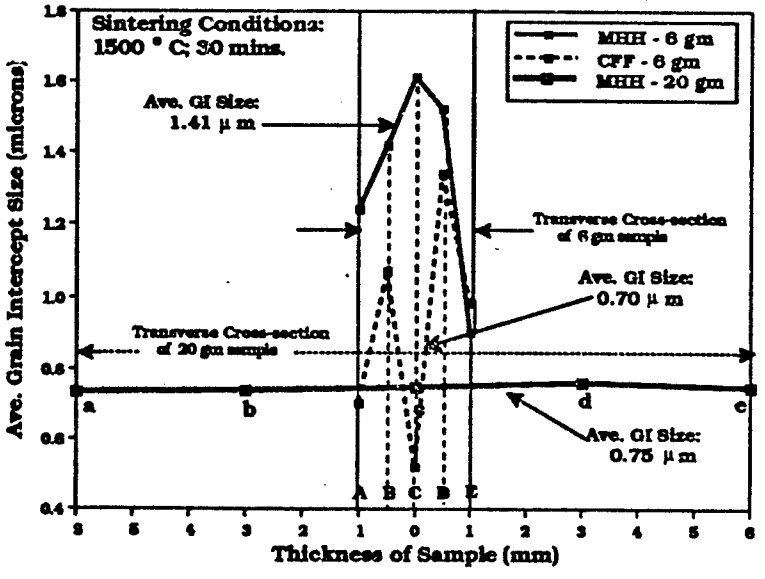


Figure 5. 6 gm (MHH and CFF) and 20 gm (MHH) samples of M-16 alumina sintered at 1500°C 30 min.
(a) Volume fraction of porosity vs. sample thickness
(b) Grain intercept sizes vs. sample thickness

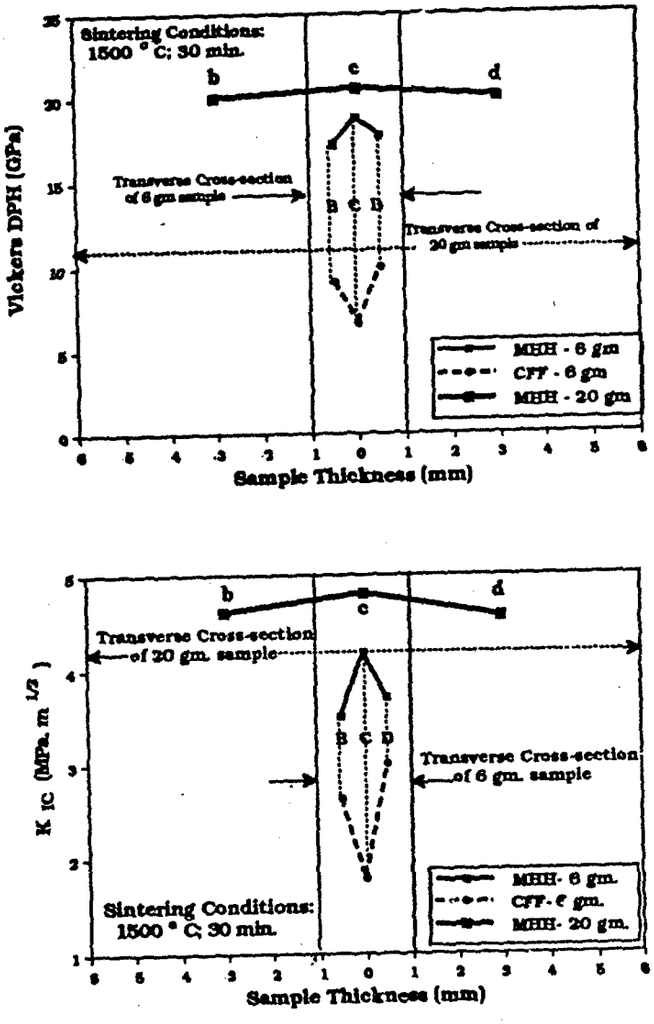


Figure 5. 6 gm (MHH and CFF) and 20 gm (MHH) samples of A-16 alumina sintered at 1500°C 30 min.
(c) Vickers DPN vs. sample thickness
(d) Fracture toughness vs. sample thickness

thickness of the 3 specimens (Figures 5(c) and 5 (d)). Figure 5(c) is a plot of the Vickers microhardness versus sample thickness. The enhanced densification, and uniform grain and pore sizes across the cross-section of the bulk MHH sample is reflected in the enhanced and uniform variation in Vickers hardness numbers (20.06 - 20.54 GPa). The hardness values for the 6 gm MHH sample ranged from 17.26-18.83 GPa, while the variation for the 6 gm CFF sample was of the order of 6.60-9.96 GPa.

Fracture toughness values were extrapolated from diamond indentations, measuring the propagated crack lengths, and computed, using the formulae suggested by Evans and Charles [12]. Trends very similar to those shown by the microhardness numbers are reflected in the fracture toughness (K_{IC}) values. The 6 gm MHH sample had appreciably higher values of fracture toughness (3.5- 4.17 MPa $m^{1/2}$) relative to the CFF sample, with the highest value at the center. The variation for the 6 gm CFF specimen was in the range of 1.8-3.0 MPa $m^{1/2}$, with the lowest values at the interior of the specimen. The 20 gm MHH sample displayed the highest and the most uniform values of the fracture toughness numbers. They ranged from 4.56 to 4.80 MPa $m^{1/2}$, with the highest values at the center of the specimen.

CONCLUSIONS

MW (hybrid) heating facilitates the attainment of perhaps the highest possible heating rates (750°C per minute) attainable with pure, undoped alumina in a 2.45 GHz, untuned, multimode MW cavity.

MHH results in more uniform microstructures and superior properties vs. CFF under the same state conditions of temperature and time. MHH of larger masses result in better volumetric heating, and consequently, an enhanced parity in temperature across the cross-section of the sample. This translates into higher densities, smaller grain sizes, better microstructural homogeneity, and improved mechanical properties. Larger masses, when subjected to CFF, fracture due to large temperature gradients and high thermal stresses across the cross-section.

Enhanced and homogeneous sintering of larger monoliths with MW (hybrid) heating in a 2.45 GHz, multimode cavity is the most significant accomplishment of this research. 'Microstructural uniformity with MW energy', appears to be vindicated with this work. This novel technique for the ultra-rapid sintering of ceramic materials using MW energy holds tremendous promise for the fabrication of advanced ceramics, composites, and bulk monoliths with uniform microstructures, and consequently, enhanced mechanical properties and reliability versus SMW sintering and CFF.

ACKNOWLEDGEMENTS

The support of the Defense Advanced Research Projects Agency (DARPA) under contract # MDA 972 -B5-J-1006 is gratefully acknowledged.

REFERENCES

1. W. H. Sutton, Amer.Ceram. Soc.Bull., 68 [2] 376 (1989).

2. M.A. Janney and H. D. Kimrey, in Sintering of Advanced Ceramics-Ceram. Trans. - Vol. 7, Edited by C. A. Handwerker, J. E. Blendall and W. A. Kaysser, Amer. Ceram. Soc., OH, 382-90, (1990).

3. M.A. Janney and H.D. Kimrey, Proceedings of the 1990 Spring Meeting of the Materials Research Society, San Francisco, CA. (1990).

4. M. A. Janney, H.D. Kimrey, M.A. Schimdt, and J.O. Kiggans, "Grain Growth in MW Annealed Alumina", Submitted to the Amer. Ceram. Soc.,(1990) (To be published).

5. T.T. Meek, J. Mat. Sci. Lett., **6**, 638 (1987).

6. T.T. Meek, R.D. Blake and J.J. Petrovic, "Ceram. Eng. and Sci. Proc., **8** , 861 (1987).

7. Y. L. Tian , D. L. Johnson and M E. Brodwin, in Ceramic Powder Science II-Ceram. Trans. - Vol. I, Edited by G. L.Messing, E.R. Fuller, jr. and H. Hausner. Amer. Ceram. Soc. OH , 925-32 (1988).

8. A. Dé, I. Ahmad, E. D. Whitney and D. E. Clark, Ceram. Eng. and Sci. Proc., **11** (1990).

9. A. Dé, I. Ahmad, E. D. Whitney and D.E. Clark, Proceedings of the 1990 Spring meeting of the Materials Research Society, San Francisco, CA. (1990).

10. D. E. Clark, I. Ahmad and A. Dé, U. S. Patent Application Serial # 07-639933, 1991.

11. D. L. Johnson in Sintering and Heterogeneous Catalysis, Edited by G. C. Kuczynski, A. E. Miller and G. A. Sargent. Plenum Publishing Corp.,New York 243-52, (1984),.

12. A. G. Evans and E. A. Charles, J. Amer. Ceram. Soc., **59** [7-8] 371, (1976).

MICROWAVE (HYBRID) HEATING OF ALUMINA AT 2.45 GHZ: II. EFFECT OF PROCESSING VARIABLES, HEATING RATES AND PARTICLE SIZE

Arindam Dé , Iftikhar Ahmad, E. Dow Whitney and David E. Clark
Dept. of Materials Science and Engineering
University of Florida
Gainesville, FL 32611

Microwave (hybrid) heating (MHH) is a novel combination of microwave (MW)-material interaction and conventional radiant/conduction mechanisms that facilitates the attainment of very high heating rates in a 2.45 GHz. multimode MW cavity. Dry-pressed green samples of pure, undoped alumina were fired under similar conditions by MHH and conventional fast firing (CFF). The effect of processing variables (temperature, time) and heating rates on MHH and CFF were investigated. The effect of particle size on the MHH phenomena was also studied. MHH has been shown to result in accelerated densification (higher densification to coarsening ratios) relative to CFF under the same conditions of temperature and time. Higher heating rates with MHH result in higher densities and smaller grain sizes. Smaller starting particle sizes with MHH also culminate in the highest densities and the largest grain sizes similar to conventional firing.

INTRODUCTION

Fast firing of ceramics and the consequent microstructural benefits in terms of higher densities and smaller grain sizes has been the subject of extensive research [1-3]. The higher densities and smaller grain sizes were attributed to a rapid transition to higher temperatures which caused a suppression of surface diffusion and other 'coarsening without densification' mechanisms that exist at lower temperatures[3]. At higher temperatures, the predominance of the mechanisms of grain boundary and lattice diffusion that cause densification, lead to rapid sintering and densification with little or no coarsening.

The use of MW energy for the sintering of ceramics, although a relatively new development, has seen a proliferation of activity in recent times. The potential of microwaves for the firing of ceramics at lower temperatures, and with smaller grain sizes compared to conventional sintering techniques, have been demonstrated unequivocally [4-8]. This has been attributed to higher diffusion and a lower activation energy for sintering that is characteristic of MW energy[4,6]. However, although the use of MW energy for sintering serves to accelerate the process, preheating the material to the critical temperature at which it starts to couple efficiently with the microwaves is still a problem, especially at the low frequency of 2.45 GHz. Longer times are spent in heating up the sample to the critical temperature range above which MW-material interaction and consequently, rapid heating occurs readily. This, as well as the higher diffusion rates that are associated with MW heating, may be the reason for the appreciably higher grain sizes (with microwaves) reported in a recent study on the 'comparison of conventionally fast fired and MW fired alumina'[9].

In order to apply the benefits of fast firing to MW sintering, a technique that makes use of both MW-material interaction as well as conventional radiant/conduction heating mechanisms has been developed. 'Hybrid heating using MW energy' [10-13] makes use of radiant/conduction heating to rapidly heat samples through low temperature regimes to a critical temperature above which the microwaves couple readily with the material. A peak heating rate of 750°C per minute for pure, undoped alumina in a 2.45 GHz, 6.4 KW(max.) multimode cavity, making use of less than half the peak power output, has been attained. Advantages of this technique over CFF, in terms of significant enhancements in the homogeneity of the microstructure and improved mechanical properties (under the same sintering conditions), have been demonstrated [10-13].

EXPERIMENTAL PROCEDURE

Two grades of pure, undoped alumina were employed. Type1(designated A-16) * was a 99.97% pure alumina grade (as received) with an average particle size of 0.48 microns, a very broad particle size distribution, and a surface area of 4.697 m^2/g. This was used for a study of the effect of processing variables (time, temperature) on specimens sintered by MHH and CFF, under the same state conditions. Type 2**(designated AKP-15, 30, 50) was a very high purity (>99.99%) undoped alumina, and comprised 3 grades of varying particle size distributions, and average particle sizes and surface areas of 0.68μ(3.5 m^2/g), 0.39μ (7.5m^2/g), and 0.23 μ (10.9 m^2/g) for AKP-15, AKP-30 and AKP-50, respectively. These were used to study the effect of particle size on the MHH phenomena.

However, for the study on the effect of heating rates on MHH, the AKP-50 grade of ultra-pure alumina powder was used after rendering it free from hard aggregates by ultrasonication and centrifugal sedimentation. The average particle size of the AKP-50 powder dropped from 0.23 μ (as-received) to 0.19 μ after processing. The hybrid heated samples were sintered under the same state conditions of temperature and time, with only a variation in the heating rates.

The experimental set-up for the MHH has been described and illustrated elsewhere [10,13]. MHH was effected in static air in a 2.45 GHz, 6.4 KW (max) *** multimode cavity, with the sample enclosed in a silicon carbide lined susceptor. Temperature monitoring was effected by inconel shielded 'K'-type thermocouples#(for temperatures up to 1100°C) and by two color infrared pyrometry## (for temperatures above 1100°C). A peak heating rate of the order of 1500°C in 120 sec (750°C per minute) for pure undoped alumina at a power output of around 3 KW was attained.

CFF (conventional fast firing/ isothermal sintering) was effected in static air by inserting the samples into a resistance heated tube furnace+ which was preheated to the sintering temperature. The samples were stationed in alumina boats which in turn, were slowly inserted into the hot zone of the tube furnace. Temperatures were read off a 'B' type Pt-Rh thermocouple #(with digital display) which was kept in contact with the alumina boat and the walls of the alumina tube of the furnace.

Bulk and relative densities of the sintered samples were obtained by the Archimedes density method. The samples were then polished using standard ceramographic techniques. Samples sintered at 1000, 1200, 1300 and 1400°C were thermally etched at 995, 1195,1290 and1390°C for 3,3,3 and 2 hours, respectively. The

---

*Aluminum Company of America (Alcoa) Inc., Pittsburgh, PA.

** Sumitomo Chemical America Inc., New York, N.Y.

*** Model Radarline QMP 2101B-6, The Raytheon Company, Waltham, MA.

Omega Engineering Inc., Stamford, CT.

Ratio Scope 8, Capintec Inc., Fair Lawn, N.J.

+ Model Sola-Basic, Lindberg, Watertown, WI.

samples sintered at 1500°C were etched at 1450°C for 1 hour. Microstructures representative of both the surface and the interior of each sample were obtained in the SEM.

Grain intercept lengths and porosities were computed from the SEM micrographs using standard quantitative stereological techniques. Average grain sizes were determined from measured average lineal grain intercept lengths according to the equation [3]

$$\text{grain size} = 1.56 * \text{grain intercept length} \quad (1)$$

The resulting data were plotted, correlated and compared .

RESULTS AND DISCUSSION:

Effect of Processing Variables on the Sintering of A-16 Alumina: Microwave (Hybrid) Heating vs. Conventional Fast Firing.

Identical green samples were sintered using MHH and CFF at 1300, 1400, 1500°C, with holding times of 15, 30 , and 60 minutes at each temperature.

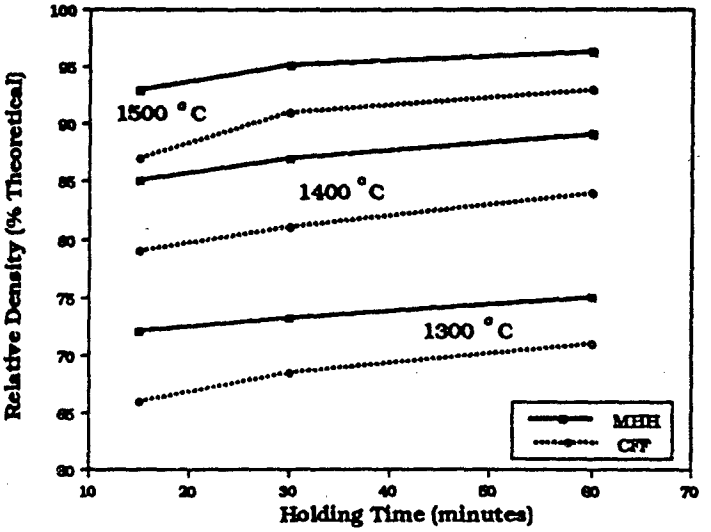
Figures 1(a) and 1(b) are plots of the relative density and densification rate against holding time, respectively. Densification rates were computed from the Fig. 1(a) by normalizing the plots with respect to the starting green density, and plotting the slopes of the 3 line segments (from each line) against time, to yield Fig. 1(b). The densification rates for MHH at each temperature and time were appreciably higher than those for the CFF. This is consistent with the results reported by Janney et al. [4,14], and Tian et al. [5], and the enhanced densification may be ascribed to the increased diffusion rates attributed to MW energy- the 'MW effect' [14]. One other factor that may be partly responsible is the higher temperature (temperatures 50-80°C in excess of the sintering temperature) experienced by the interior of the MHH samples relative to the specimens sintered by CFF [13].

Figures 1(c) and 1(d) are plots of the average grain intercept (GI) size and grain growth rate (microns per minute) as a function of the holding time, respectively. Although the MHH samples displayed somewhat larger grain sizes than the CFF samples, the disparity in grain sizes was minimal, and almost comparable. This is a significant improvement over the results reported sometime earlier in a similar study, [9] making use of MW energy alone for the sintering process. The appreciably smaller grain sizes for the MHH samples in our case may be attributed to the faster heating rates --the culmination of both MW-material interaction and conventional radiant/conduction mechanisms that contribute to the densification process. This is a pointer to the fact that there is indeed a heating rate effect on the MHH phenomena, as will be discussed in the following section. The somewhat larger grain sizes with MHH, relative to CFF can be attributed to three reasons. Recent work by by Janney et al. [14,15] has demonstrated that the activation energy for grain growth with microwave energy is about 20 % lower than that for conventional sintering (480 vs. 590 kJ/mol). Besides this, the higher temperatures at the interior of the MHH sample [13], as well as the preferential interaction of the microwaves with the porosity [7] also serve to accelerate densification as well as grain growth.

An interesting aberration in the form of a dramatically higher GI size was shown by the CFF sample that was sintered at 1500°C for 60 minutes. There was anomalous grain growth and pore coarsening at the center of the sample. The reasons for this anomaly are not well understood.

Figure 1(e) is a plot of the average grain size versus relative density, normalized with respect to the sintering temperature. From this graph, and those for the densification and grain growth rates (Figures 1(b) and 1(d)), it is evident that MHH yields significantly higher densities, with comparable or somewhat larger grain sizes (a higher densification to coarsening ratio) relative to CFF, under the same conditions of time and

1(a)



1(b)

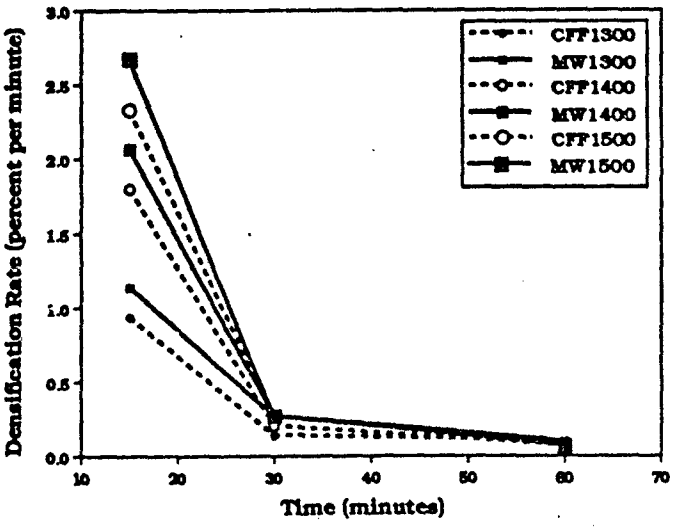
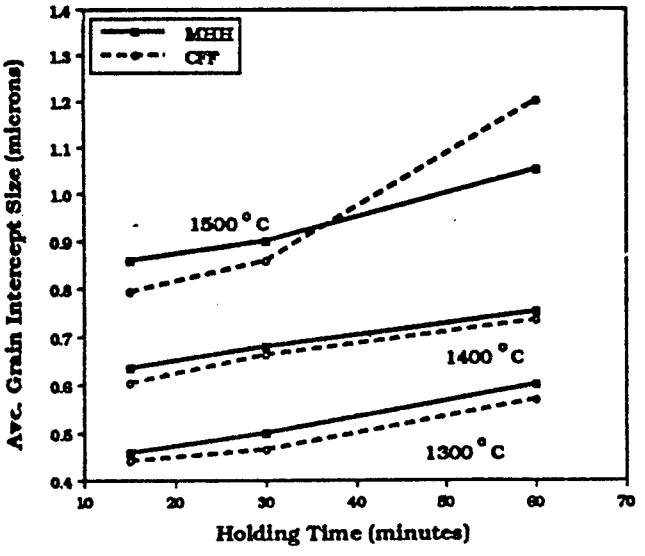


Figure 1. Effect of processing variables (temperature, time) on the sintering of A-16 alumina: MW (hybrid) heating vs. conventional fast firing.
(a) Relative Density vs. Holding Time
(b) Densification rate vs. Holding time

1(c)



1(d)

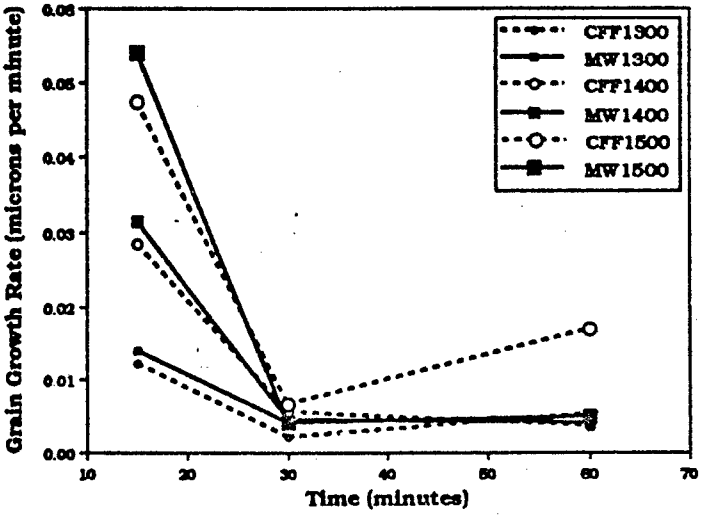


Figure 1. (Cont'd.) Effect of processing variables (temperature, time) on the sintering of A-16 alumina: MW (hybrid) heating vs. c onventional fast firing.
(c) Average Grain Intercept (GI) Size vs. Holding Time
(d) Grain Growth Rate vs. Holding Time.

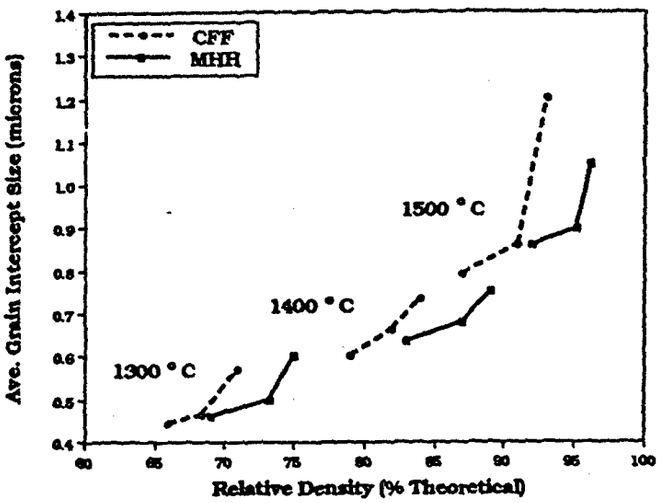


Figure 1. Effect of processing variables (temperature, time) on the sintering of (Cont'd.) A-16 alumina:: MW hybrid heating vs. conventional fast firing (e) Average Grain Intercept (GI) Size vs. Relative Density

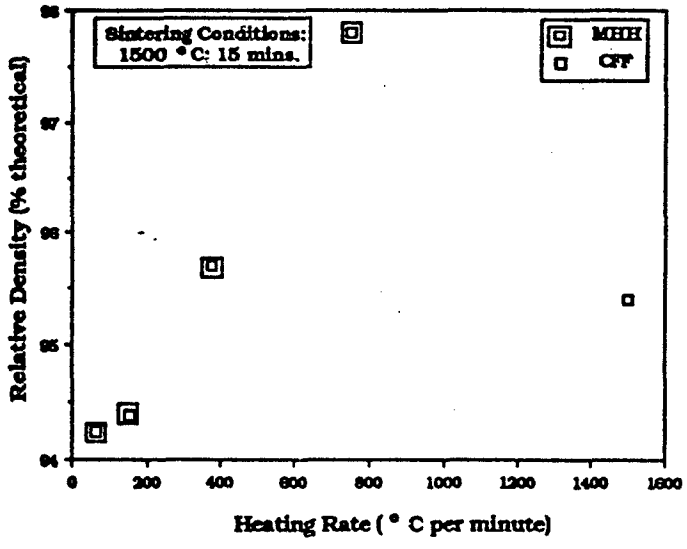
temperature. The fact that the densification rates for MHH are significantly higher than the grain growth rates relative to CFF, are consistent with results reported by Janney et al. [15], which suggest that the difference in activation energies between MW and conventional sintering for densification (160 versus 575 kJ/mol, respectively) are far higher than the difference in activation energies for grain growth (480 versus 590 kJ/mol, respectively). These results clearly show evidence of accelerated sintering and densification occurring in the MHH specimens relative to the CFF samples.

Effect of Heating Rates on the Sintering of AKP-50 Alumina: MW (Hybrid) Heating vs. Conventional Fast Firing:

For this set of experiments a more reactive (fine) powder and a better green microstructure (free of aggregates and agglomerates) was desired, so that any differences in the MHH phenomena, owing to variation in heating rates alone, would be evident. The ultrapure, ultrafine (~0.23 μ) undoped AKP-50 alumina powder was chosen. This was rendered free of hard agglomerates by ultrasonication and centrifugal sedimentation. The average particle size after processing dropped to 0.19 μ. Identical dry-pressed green samples (6 gm) were then sintered at 1500°C for 15 minutes by MHH, using heating rates of 750, 375, 150 and 62°C per min, and also by CFF (heating rate-1500°C per min).

Figures 2(a) and 2(b) are plots of the relative density and grain intercept (GI) size, respectively, versus heating rate (°C per min).The GI sizes were computed as an average of GI sizes from the surface and the interior of the specimens. Although the CFF sample was sintered using the highest heating rates (1500°C per min), the MHH samples sintered at heating rates of 375, and 750°C per min had higher densities (97.8 and 95.7 versus 95.4 for the CFF sample). Also, the GI size for the 750°C per min MHH sample was the lowest,

2(a)



2(b)

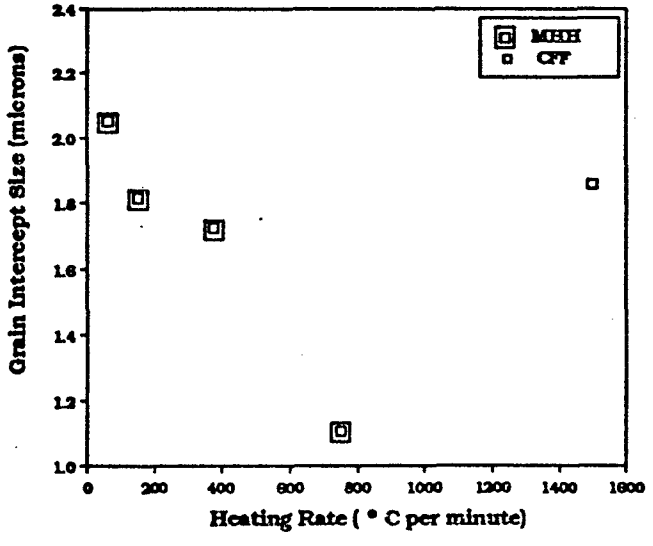


Figure 2. Effect of heating rates on the sintering of AKP-50 alumina: MW (hybrid) heating vs. conventional fast firing.
(a) Relative Density vs. Heating Rate
(b) Average Grain Intercept (GI) size vs. Heating Rate.

and that for the 62°C per min MHH sample was the highest. The CFF sample had a GI size intermediate between those of the 150°C per min and 62°C per min MHH specimens.

These results show evidence of the influence of heating rates on the MHH phenomena, relative to CFF. Although the CFF sample was sintered using the highest heating rates, the higher density and lower GI sizes for the samples sintered by MHH using appreciably lower heating rates is a pointer to the enhanced diffusion process accredited to MW energy. It can be concluded that for the samples sintered by MHH at the high heating rates of 375 and 750°C per min, densification is enhanced at the cost of coarsening, relative to the CFF sample. This is due to the fact that these specimens make a very rapid transition through the lower temperature range where surface diffusion-controlled coarsening predominates, to the higher temperatures where the densifying mechanisms of lattice and grain boundary diffusion are predominant. This results in higher densities and smaller average grain sizes (higher densification to coarsening ratios) relative to the CFF sample. For the samples sintered by MHH at the heating rates of 62 and 150°C per minute, it can be surmised that the densification to coarsening ratio is comparable or lower than that for the CFF specimen.

Effect of Particle Size on the MW (Hybrid) Heating of AKP Alumina:

The particle size distributions of the three AKP powders and the sintering cycles employed are illustrated in figures 3(a) and 3(b), respectively. Sintering was carried out at temperatures ranging from 1000° ~ 1500°C in the 2.45 GHz MW oven with a constant holding time of 30 minutes, under hybrid heating conditions.

The post sintered relative densities and resulting grain sizes are illustrated in figures 3(c) and 3(d), respectively. Grain sizes for the samples sintered at 1000°C and 1200°C could not be computed accurately owing to incomplete densification and problems encountered with thermal etching.

The trends observed for the samples sintered at 1400°C and 1500°C are pretty much analogous to those known for conventional sintering. Smaller starting particle sizes, and consequently larger surface areas result in higher densities, and larger grain sizes, owing to a higher driving force for sintering, densification, and grain growth.

CONCLUSIONS

MW (hybrid) heating facilitates the attainment of perhaps the highest possible heating rates (750°C per minute) attainable with pure, undoped alumina in a 2.45 GHz, multimode MW cavity.

MHH results in accelerated densification (higher densification to coarsening ratios) as compared to CFF, when sintered under the same state conditions of temperature and time.

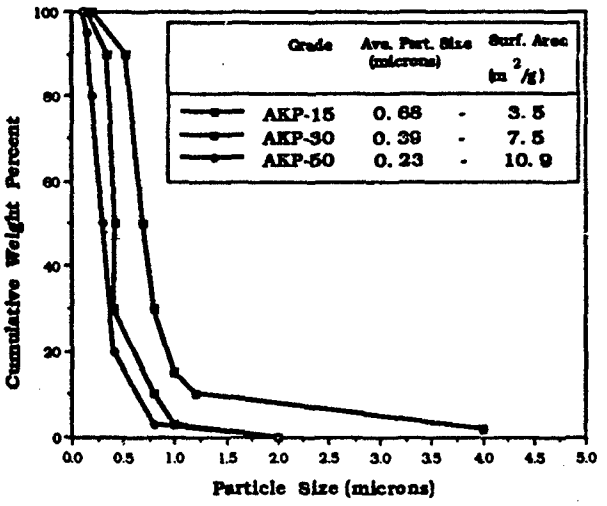
MHH is significantly influenced by heating rates, in a manner similar to conventional sintering. Higher heating rates result in higher densities and smaller grain sizes.

The influence of particle size on the MHH phenomena is analogous to conventional sintering. Smaller starting particle sizes culminate in the highest densities and largest grain sizes. This may be attributed to the higher surface area, and consequently, higher driving force for sintering.

ACKNOWLEDGEMENTS

The support of the Defense Advanced Research Projects Agency (DARPA) under contract # MDA 972 -B5-J-1006 is gratefully acknowledged.

3(a)



3(b)

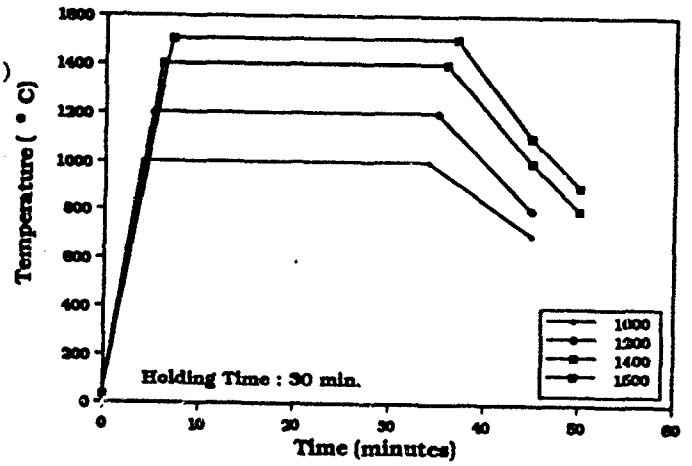
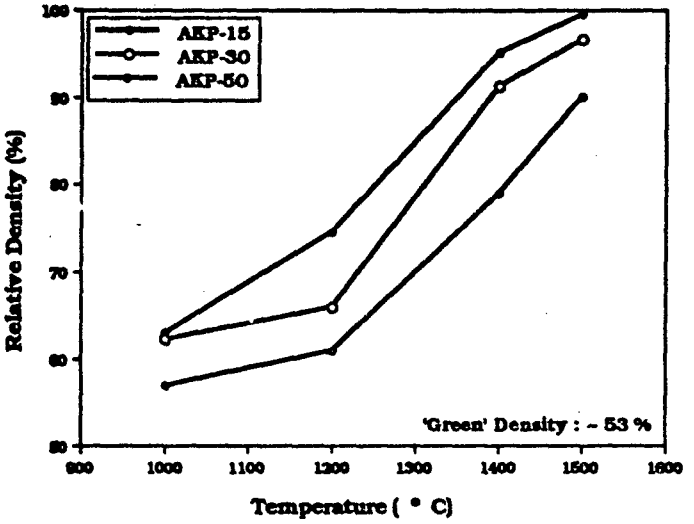


Figure 3. Effect of particle size on the MW (hybrid) heating of AKP alumina::
(a) Particle Size Distribution of AKP alumina (as-received)
(b) Temperature-Time Sintering Cycles (holding time -30 minutes)

3(c)



3(d)

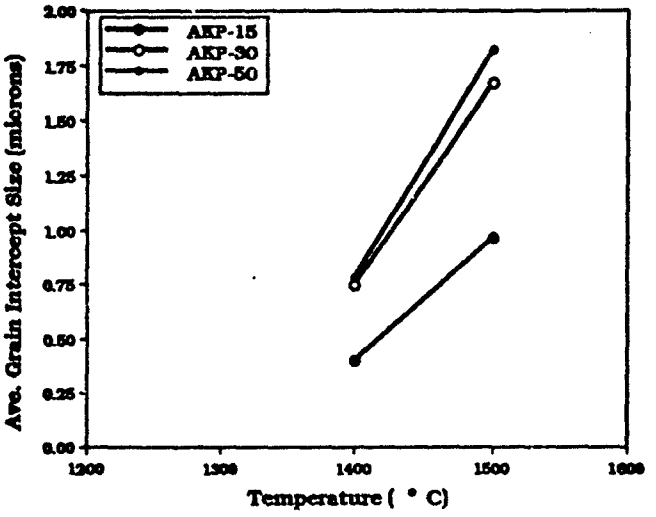


Figure 3. Effect of particle size on the MW (hybrid) heating of AKP alumina:
(c) Relative Density vs. Temperature (d)
(d) Grain Intercept (GI) Size vs. Temperature

REFERENCES

1. M.P.Harmer and R.J.Brook, J. Brit. Ceram. Soc.,80, (5),147 (1981).

2. M. Harmer, E.W. Roberts and R.J. Brook, Trans. Brit. Ceram. Soc., 78, 22 (1979).

3. D. L. Johnson in Sintering and Heterogeneous Catalysis, . Edited by G. C. Kuczynski, A. E. Miller and G. A. Sargent, Plenum Publishing Corp., N.Y., pp. 243-252(1984).

4. M. A. Janney and H .D. Kimrey, Ceram. Trans. Vol. I, Ceram. Powd. Sci., 919-24(1988).

5. Y. L. Tian , D. L. Johnson and M E. Brodwin, in Ceramic Powder Science II-Ceram. Trans. - Vol. I, Edited by G. L.Messing, E.R. Fuller, jr. and H. Hausner. Amer. Ceram. Soc. OH , 925-32 (1988).

6. M.A. Janney and H. D. Kimrey, in Sintering of Advanced Ceramics -Ceram. Trans. - Vol. 7, Edited by C. A. Handwerker, J. E. Blendall and W. A. Kaysser, Amer. Ceram. Soc., OH, 382-90, (1990).

7. T.T. Meek, J. Mat. Sci. Lett., 6, 638 ,(1987).

8. T.T. Meek, R.D. Blake and J.J. Petrovic, Ceram. Eng. and Sci. Proc., 8 861, (1987).

9. J . D. Katz and R. D. Blake, Presented at the 42nd Pacific Coast Regional Meeting of the Amer. Ceram. Soc., Anaheim,CA (1989) (unpublished).

10. A. Dé, I. Ahmad, E. D. Whitney and D. E. Clark, Ceram. Eng. and Sci. Proc., 11 (1990).

11. A. Dé, I. Ahmad, E. D. Whitney and D. E. Clark, Proceedings of the 1990 Spring meeting of the Materials Research Society, San Francisco, CA. (1990).

12. D. E. Clark, I. Ahmad and A. Dé, U. S. Patent Application Serial # 07-609933, 1991.

13. A. Dé, I. Ahmad, E. D. Whitney and D. E. Clark, Presented at the 93rd Annual Meeting of the Amer. Ceram. Soc., Cincinnati, OH, April 28-May 2, (1991).

14. M. A. Janney and H. D. Kimrey, Proceedings of the 1990 Spring Meeting of the Materials Research Society, San Francisco, CA. (1990).

15. M. A. Janney, H. D. Kimrey, M. A. Schimdt, and J. O. Kiggans, "Grain Growth in MW Annealed Alumina", Submitted to the Amer. Ceram. Soc.,(1990) (To be published).

MAGNETITE AS A SINTERING AID FOR MICROWAVE CONSOLIDATION OF SODA-LIME GLASS

Y.H. Kao and J.D. Mackenzie
Department of Materials Science & Engineering
University of California Los Angeles
Los Angeles, CA 90024

ABSTRACT

Magnetite, Fe_3O_4, is a strong absorber of microwave energy, which can be used to enhance heating in microwave transparent or low absorbing matrices. To examine the heat generation of magnetite for ultimate use in materials consolidation, magnetite was dispersed in relatively low absorbing soda-lime glass particles. The effects of magnetite weight fraction, microwave power, and sintering time on temperatures and bulk properties of the sintered specimens are presented.

INTRODUCTION

The use of microwave electromagnetic radiation is attracting increased attention as an innovative method of sintering ceramics. Strong microwave couplers such as magnetite (conductive and magnetic) are especially important as particulate additives for selective enhancement of heating in microwave transparent or low absorbing matrix [1]. Because magnetite exists naturally in iron ores, it is a cheap source of raw material for microwave consolidation and fabrication of materials [2]. This investigation examines the sintering of magnetite powders in a soda-lime glass matrix, and the properties of the consolidated materials.

EXPERIMENTAL

Industrial-grade magnetite from Alfa was dispersed in a matrix of relatively microwave transparent soda-lime glass spheres from Flex-O-Lite. Particle size distributions of the constituents were determined with a particle size analyzer[1]. The degree of nonstoichiometry of the magnetite was determined through its weight gain in O_2 using thermal gravimetric analysis (TGA) at a heating rate of 5°C/min to 950°C. An approximate assessment of the accuracy of TGA was determined by comparing theoretical weight gain with that of 99.999% Fe_3O_4 from Alfa chosen as the standard. The thermal properties of the glass were determined using differential thermal analysis (DTA) at a heating rate of 40°C/min in order to simulate a similar fast heating rate in the microwave heating of magnetite.

Thirty-gram specimens were made containing 5, 10, 15, 30, and 45 wt% magnetite. The constituents were dry-mixed until uniform, water added, pressed uniaxially to 12,000 lbs. in a 4.50

[1]Micromeritics, Norcross, GA Model # 5000D

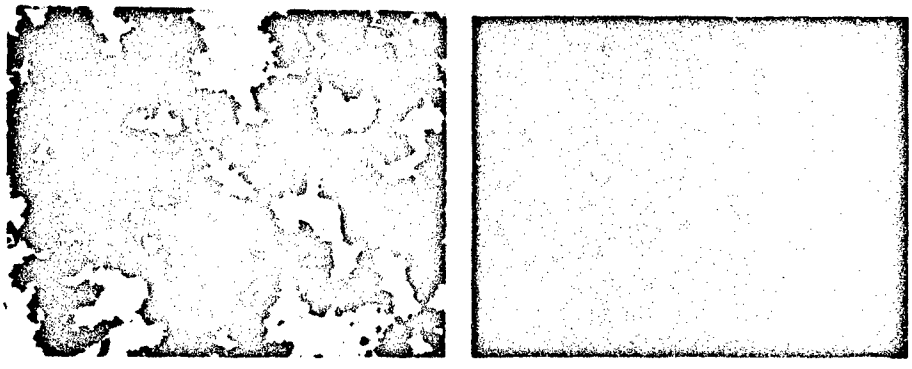
cm x 2.50 cm metal die, and air-dried. Greenbody densities were determined from the dry masses and dimensions of the specimens.

Processing was conducted at 2.45 GHz in a 900W multimode microwave applicator[2] (44 cm x 33.5 cm x 25.5 cm). In the center of the applicator was placed an insulating firebrick vessel (11.3 cm x 10.0 cm x 6 cm) and vessel cover (11.3 cm x 10 cm x 1 cm), containing a cavity (3.0 cm x 6.5 cm x 2.5 cm) for the specimen. The sintered specimen densities and porosities were determined after a 5-hour boil and a 24-hour soak, according to ASTM Standards (C373-88). Temperature measurements were made using a dual wavelength infrared pyrometer[3].

RESULTS AND DISCUSSION

Materials Characterization and Chemical Reaction

Particle sizes and shapes of the magnetite powders and the glass spheres are compared in Fig 1.



1a. Magnetite Powders (593x) 1b. Soda-lime Glass Spheres (339x)

Figure 1. Comparison of Particle Sizes and Shapes.

The irregular magnetite powders had an approximate surface area of $6 m^2/g$. Their equivalent spherical diameters ranged from 1 to 15 μm, with 50% of the cumulative mass occurring at 5 μm. (The particles shown in Fig. 1a are agglomerates.) The diameters of the solid glass spheres ranged from15-50 μm, with 50% of the cumulative mass occurring at 27 μm. Thus, the magnetite particles were approximately 5 times smaller than the glass spheres.

According to Alfa, the industrial-grade magnetite was 97% pure. Impurities included water, water-soluble salts, and traces of various elements such as Si, Mn, Mg, Na, Cr, Zn, Cu, Co, Ba, Te, and Ag. The degree of nonstoichiometry of magnetite is important, since electron hopping from Fe^{2+} to Fe^{3+} is responsible for a fraction of the dielectric susceptibility and loss [3]. The oxidation of stoichiometric Fe_3O_4 occurs between 350 and 400°C [4], and is given by

$$2\ (FeO{\cdot}Fe_2O_3) + 1/2\ O_2 \rightarrow 3\ Fe_2O_3 \qquad (1)$$

2 Litton Systems Inc., Minneapolis, MN Model # 1052

3 Mikron Instrument Co., Wyckoff, NJ Model # M77

with a theoretical weight gain of 3.455%. The TGA of 99.999% Fe_3O_4 gave an average weight gain of 3.30 wt%. This resulted in a 5% error from TGA, assuming the powder was stoichiometric. The calculations for determining the Fe^{3+}/Fe^{2+} ratio were based on these assumptions : (1) only the oxidation of Fe^{2+} contributed to the weight gain, (2) all Fe^{2+} ions were converted to Fe^{3+}, and (3) the Fe^{3+} valence did not change, since Fe_2O_3 is stable up to 1390°C [5]. With these assumptions, the general equation for the oxidation of nonstoichiometric magnetite can be written as

$$2 (x\ FeO \cdot [1-x]\ Fe_2O_3) + x/2\ O_2 \rightarrow y\ Fe_2O_3 \qquad (2)$$

where x was the amount of Fe^{2+} ions, and y was the total amount of hematite produced. Industrial-grade magnetite had an average weight gain of 1.91%, giving a Fe_2O_3/FeO mole ratio of 2.18. Thus, industrial-grade magnetite deviated significantly from stoichiometry.

Soda-lime glass had a chemical composition of 73%SiO_2 - 15%Na_2O - 7%CaO - 4%MgO - 1%Al_2O_3 by weight. The glass transition range was 550 to 610°C, softening temperature was 700°C, and crystallization temperature was 1290°C.

Microwave Processing

A specimen of just soda-lime glass spheres did not develop necking when processed at 900W for 1 hour. However, when magnetite was added, it quickly generated intense heat to consolidate the glass spheres. Figure 2 shows the generalized sintering progress for a specimen. Stages a, b and c resulted from short sintering times and/or low microwave powers. Stages d and e resulted from long sintering times and/or high powers. Stages d1 and e1 were exhibited by the lower magnetite content specimens (5, 10, and 15%) which had deformed from their greenbody shape. However, stages d2 and e2 were exhibited by the higher magnetite content specimens (30 and 45%) which did not loose their original shape.

The consolidated, glassy parts of the specimens were always found first in the central regions of the specimens shown in Stages d1 and d2. Consolidation occurs when the glass spheres at high temperatures (>700°C) lose their spherical shape and flow into the pores of the specimen. Then as temperatures increased beyond that of Stages d1 and d2, the amount of viscous glass increased from the central regions to the boundaries of the specimens shown in Stages e1 and e2. These results are particular to soda-lime glass because a temperature difference of say about 50°C around the softening point would cause the viscosity to change by about an order of magnitude ($2x10^{10}$p at 600°C; $4x10^{7}$p at 700°C; $7x10^{5}$p at 800°C [6]). Furthermore, good thermal insulation is an extremely important parameter which can reduce temperature gradients, improve the uniformity of the sintered specimens, and enhance the heating ability of magnetite. Using firebrick insulation with a cavity much larger than the specimen resulted in poor insulation, uneven heating profiles, and greater likelihood of thermal runaway.

Effects of Magnetite Content on Bulk Properties and Temperatures

Different mass fractions of magnetite resulted in different greenbody properties, because the magnetite particles were much smaller than those of glass. Green porosities were calculated from (theoretical density - greenbody density) / theoretical density x 100. The green porosities of 5, 10, 15, 30 and 45% magnetite were as follows: 40.9, 40.9, 39.1, 34.3, and 30.6%.

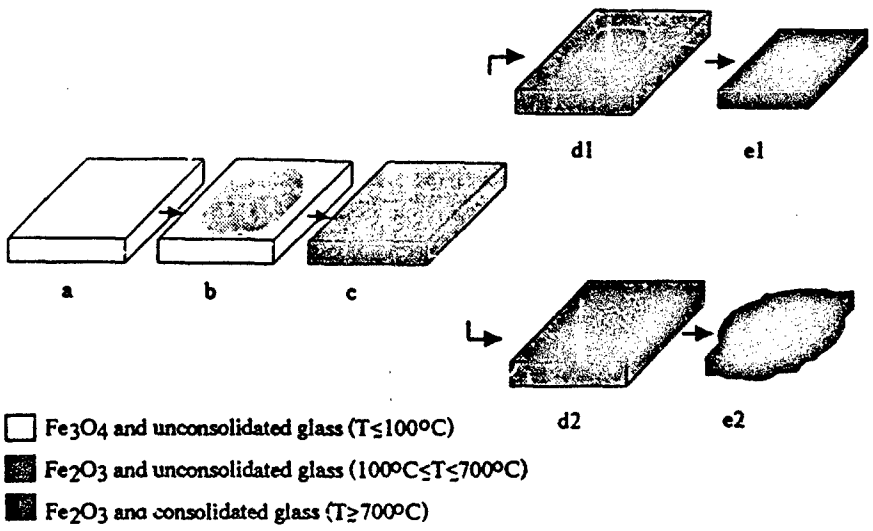


Figure 2. General Progress of Sintering.

Table 1 shows the *change* in porosity, the final porosity, and the final sintering stage for each specimen. Maximum temperatures can be estimated *roughly* based on the information in Fig. 2.

Table 1. Reductions in Porosity, Sintered Porosities, and Final Sintering Stages for Various Specimens.

Magnetite (%)	40% Power for 50 Minutes (Set A)		50% Power for 25 Minutes (Set B)	
	Porosity Reduction (%)	Final Porosity (%)	Porosity Reduction (%)	Final Porosity (%)
5	-	-	0	41 (not sintered, b)
10	30	11 (d1)	37	4 (e1)
15	15	24 (between d1 & e1)	30	9 (between d1 & e1)
30	23	11 (e2)	15	19 (e2)
45	-	-	22	9 (e2)

Compared to Set B, Set A was processed at 10% lower power for twice as long. For each magnetite content, significant differences in porosities existed between Set A and B, although different processing conditions produced roughly the same sintering stage. Set B suggests the existence of a minimum percentage of magnetite required for densification for a particular power and heating time. For the insulation system used, this minimum was between 5 and 10% magnetite. As the amount of magnetite exceeded the minimum value, a specimen exhibited the largest porosity reduction and the lowest final porosity. For both sets, as magnetite content was increased, the porosity reductions decreased and the final porosities increased. This can be attributed partly to the smaller amount of glass available for viscous flow in higher magnetite content specimens. However, for even higher content specimens, the porosity reduction increased at 30% magnetite for Set A and at 45% magnetite for Set B, while the final porosities decreased. Figure 3 shows higher surface temperatures at shorter times with increasing magnetite content.

The properties of consolidated magnetite/glass composites are the consequence of two primary densification mechanisms : viscous flow of glass and solid-state diffusion of the oxide.

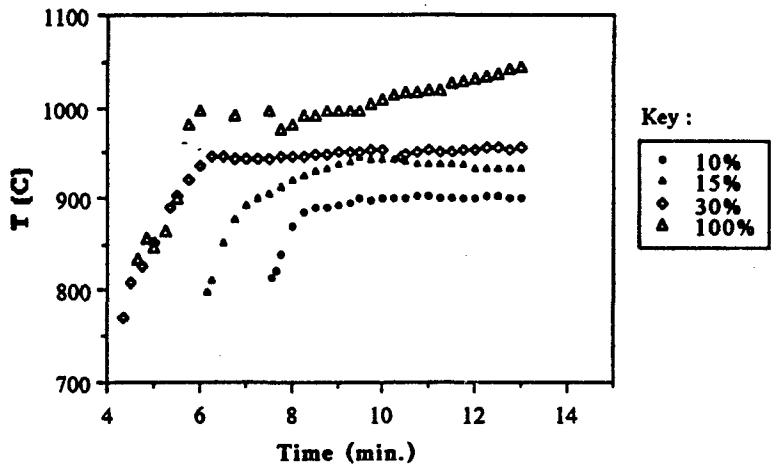


Figure 3. Surface Temperature Profiles for Various Magnetite Content (wt%) at 60% of 700W.

Effects of Microwave Power and Sintering Time on Bulk Properties

For both 30 and 45% magnetite, the reduction in porosity increased as the percentage of incident power increased from 30 to 50%, as shown in Table 2.

Table 2. Increase in Porosity Reduction With Microwave Power.

Power (%)	30% Magnetite (25 minutes)	45% Magnetite (25 minutes)
30	6	1
40	14	10
50	16	22

Porosity reduction also increased as sintering time increased, as shown in Table 3.

Table 3. Increase in Porosity Reduction With Sintering Time.

15% Magnetite, 40% Power	30% Magnetite, 40% Power	45% Magnetite, 50% Power
10 (45 min.)	14 (25 min.)	22 (25 min.)
15 (50 Min.)	24 (50 min.)	24 (35 min.)

Notice that a 15% magnetite specimen would have to be processed for much longer than 50 minutes at 40% power to reach the same porosity reduction or sintered porosity as a 30% magnetite specimen. Indeed, a 15% magnetite specimen processed at *50%* power for just 25 minutes was found to exhibit 30% porosity reduction or 9% sintered porosity. This effect was also observed with other specimens at other processing conditions.

Microstructures

In low magnetite content specimens (5, 10 and 15%), the glassy, fracture surfaces of the consolidated composite did not show glass in its original spherical shape but were extensively consolidated. An example is shown in Fig. 4. For this particular specimen, the original locations of the spheres are apparent from the positions of the small pores, which were due to the unconsolidated space between the original spheres. Thus, extensive necking (>700°C) between spheres occurred. The large pores were the products of the extensive sintering. (Optimization of the sintering conditions was not the objective of this investigation.)

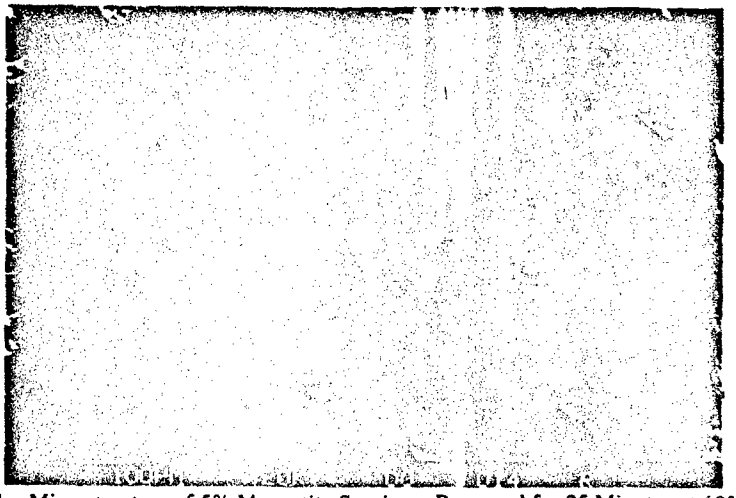


Figure 4. Microstructure of 5% Magnetite Specimen Processed for 25 Minutes at 60% Power.

The fracture surfaces of 30 and 45% magnetite specimens were also glassy, but with many spherical pores (see Fig. 5a) comparable to the sizes of the original glass spheres. Glass spheres in the greenbody did not touch but were embedded individually in the oxide. Densification involved the flow of glass into the pores of the oxide, as well as the self-sintering of the oxide. Figure 5b shows evidence of smooth fracture surfaces around the spherical pores, which indicates the presence of glass around these pores.

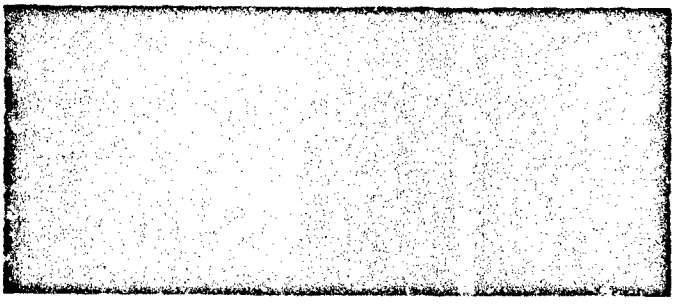


Figure 5a. Microstructure of 30% Magnetite Specimen Processed for 50 Minutes at 40% Power.

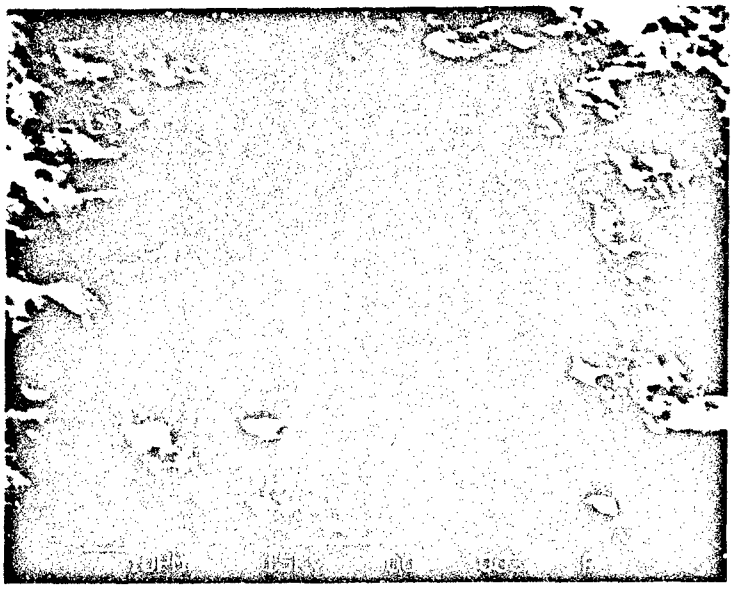


Figure 5b. Microstructure of 45% Magnetite Specimen Processed for 25 Minutes at 50% Power.

Specimens of 30 and 45% magnetite all had black cores surrounded by an outer, red oxide which was identified as hematite by XRD. However, the inner core was not identifiable. The XRD pattern of the black core was different from those of Fe_3O_4, FeO, and α-Fe_2O_3. The TGA analysis of the ground powders heated in air gave no weight gain, indicating that there were no detectable ferrous ions. The ground powders prior to TGA had a brown streak (red indicates α-Fe_2O_3 [7]), and did not turn red upon TGA heating. Since temperatures are usually higher on the inside than the outside of a specimen heated by microwaves, some reaction or solid solution between the oxide and the glass in the inner core were possible.

A *rough* estimate of the average power P_{av} generated by the oxide is determined from

$$P_{av} = 1/t \{m \int C_{poxide}(T)\, dT + m\, C_{pglass,mean}\, \Delta T\} \quad (3)$$

where t is the sintering time, m is the mass of the constituents, C_p is the heat capacity, and ΔT is the temperature increase. The microwave heating of 30% magnetite at 60% power of 700W for 6 minutes reached an approximate internal temperature of 1000°C (see Fig. 3). Based on heat capacity data for 20.4%Na_2O - 9.6%CaO - 70.0wt%SiO_2 glass [8] and for hematite [9], this specimen generated an average power of 95W. The average power supplied from the magnetron is 420W. The efficiency for the energy conversion is *roughly* 23% by microwave heating. For a typical conventional furnace operating at 1000W power and 20°C/min heating rate, the efficiency is approximately 5%. Microwave heating seems to operate more efficiently, due mainly to the high heating rate and low power necessary for heat generation in highly lossy materials.

CONCLUSIONS

Microwave heating of magnetite has been shown to enhance heating in relatively low absorbing soda-lime glass matrix. The porosities of magnetite-containing specimens decrease with increasing sintering times and increasing percentages of the on-time of the magnetron. Increasing the magnetite content increases the temperatures of the specimens. However, a minimum amount of magnetite is necessary to enhance heating. For the same power and time, the low (~5%) and high (30 and 45%) magnetite specimens produced the lowest final porosities and the highest porosity reductions. The microstructures of the consolidated areas in the low magnetite content specimens (5, 10 and 15%) did not show glass in its original spherical shape, and were well-densified. These specimens deform from their greenbody shape during processing while high magnetite content specimens (30 and 45%) retain their initial shapes. Using high magnetite content to sinter glass particles with diameters near a few tens of microns can lead to many large, closed pores in the specimens comparable to the initial sizes of the spheres, even though no spheres were left after sintering. The bulk properties of magnetite/glass composites are determined by both viscous flow of glass and solid state diffusion of the oxide. The degree and uniformity of sintering is largely influenced by the quality of thermal insulation.

ACKNOWLEDGEMENTS

The authors are grateful to the Western States Ceramic Tile Association for supporting this research through the Les Knesel Fellowship of 1989, and to the State of California through the Risk and Systems Analysis for the Control of Toxics (RSACT) Teaching Program. The assistance of Eric Bescher is greatly appreciated.

REFERENCES

1. W.H. Sutton, "Microwave Processing of Ceramic Materials", Ceramic Bulletin, Vol. 68, No. 2, pp. 376-386, (1989).
2. E.P. Bescher, Y.H. Kao, C.Y. Li and J.D. Mackenzie, "The Use of Transition Metal Oxides in Microwave Sintering of Coal Ash-derived Bricks and Tiles", Materials Research Society Symposium Proceedings, Vol. 178, pp. 279-288, (1990).
3. A.K. Jonscher, Dielectric Relaxation in Solids, Chelsea Dielectrics Press, London, p. 130, (1983).
4. D.N. Todor, Thermal Analysis of Minerals, Abacus Press, England, pp. 99-100, (1976).
5. D.R. Gaskell, Introduction to Metallurgical Thermodynamics, Scripta Publishing, p. 442, (1973).
6. N.P. Bansal and R.H. Doremus, Handbook of Glass Properties, Academic Press, Florida, p. 32-33, (1986).
7. B. Penfield, Determinative Mineralogy and Blowpipe Analysis, John Wiley & Sons, (1926).
8. N.P. Bansal and R.H. Doremus, Handbook of Glass Properties, Academic Press, Florida, p. 194, (1986).
9. G.V. Samsonov, The Oxide Handbook, Plenum, NY, Second Edition, p. 99, (1982).

RAPID SINTERING OF HYDROXYAPATITE CERAMICS BY MICROWAVE PROCESSING

Y. Fang, D.K. Agrawal, D.M. Roy and R. Roy
Materials Research Laboratory, The Pennsylvania State University, University Park, PA 16802

ABSTRACT

Completely densified hydroxyapatite ceramics were successfully sintered in a 500 W microwave oven within 5 - 10 min at sintering temperature of 1100 - 1300°C. Compared with the hydroxyapatite ceramics sintered by the conventional method, the microwave sintered hydroxyapatite ceramics have the following characteristics: denser microstructure and finer grain size, as well as the improved mechanical strength, and the process consumes a small fraction of the energy and time of conventional sintering.

INTRODUCTION

Using gels of Al_2O_3 and SiO_2, Roy, Komarneni and Yang [1,2] first showed that the extraordinary rates of temperature increase (hundreds of degrees per min) could be attained in microwave field in heating such ceramic materials. Microwave sintering, although well known [3] for ferrites and other lossy materials, is in its infancy for white or non-lossy ceramics. It has been proved to be a new, rapid and highly efficient technique in ceramic fabrication. A fundamental characteristic of the microwave sintering is that the heat is volumetrically generated right inside the material processed, instead of being transferred from outside by thermal diffusion as in a conventional sintering process. As a result, the efficiency of microwave processing depends on the properties, especially the dielectric loss factor of the material. Thermal runaway, a typical phenomenon usually encountered in microwave sintering, is noticed as an abrupt increase of temperature in the materials at temperature rates of hundreds of degrees per min. For many materials, such a high heating rate will result in destruction [4]. However, under certain circumstances, thermal runaway may just offer one a unique means to achieve new materials with novel properties.

Hydroxyapatite [$Ca_{10}(PO_4)_6(OH)_2$, HAp] is the major constituent of all mammalian's hard tissue. Hence it is obviously an important candidate material in biomedical applications, because of its excellent biocompatibility with the bones and teeth of vertebrates. The first successful microwave sintering of a HAp ceramic sample (1.4 g) was done in this lab two years ago, in a 600 W, 2.45 GHz microwave oven at its 80% power input [5]. Since then, a series of advances have been made in this area. In this paper, some results on the rapid microwave sintering of HAp ceramics are presented, and the positive contribution of thermal runaway to the high-efficiency microwave sintering is discussed.

EXPERIMENTAL PROCEDURE

Two HAp powders were used. Powder A (-325 mesh), synthesized by the hydrolysis of brushite ($CaHPO_4 \cdot 2H_2O$) followed by a "ripening" treatment with $CaCl_2$ [6], had a BET specific surface area of 47.4 m^2/g, and needle-shaped single crystallites, with an equivalent spherical particle diameter of 0.04 μm. Powder B (only slightly ground), was prepared by a precipitation method [7] followed by hydrothermal treatment in a Parr bomb at 200°C for 48 h. This powder had a BET surface area of 40.7 m^2/g, with single particles having a nearly granular morphology and an equivalent spherical particle diameter 0.047 μm. Before use, both powders were heated at 500°C to remove free and adsorbed water. With these powders, circular pellets of 1.27 cm (0.5 in) dia. were uniaxially pressed at different pressures to get various green densities.

Table 1. Processing Conditions of Microwave and Conventional Sintering of HAp Ceramics.

Batch	Starting Powder	Sintering °C,	min	Trigger Time min	Total Processing Time#, min	Density, % Green/Sintered
		I. Thermal Runaway Unsuppressed Microwave Sintering				
I-1	A	1200	10	3	15	- 51.4/- 92.1
I-2	A	1300	10	2.5	15	- 51.4/- 95.5
I-3	B	1100	5	11	20	- 60.0/- 99.7
		II. Thermal Runaway Suppressed Microwave Sintering				
II	A	1200	10	---	50	42/79.5, 47/86.5
		III. Conventional Sintering				
III-1	A	1200	120	---	360	51.4/89.4
III-2	A	1300	120	---	390	51.4/93.6

Does not include cooling time.

Two types of microwave sinterings were carried out. I. Microwave sintering with thermal runaway. This was carried out at 1100 to 1300°C in a 500 W commercial microwave oven. A porous zirconia cylinder was used for insulation around the specimens, covered with a thick Fiberfrax* cushion for further insulation. The details of the arrangements are described elsewhere [1,8]. In this type of sintering, temperature was controlled only when it nearly reached the desired sintering temperature. II. Thermal runaway suppressed microwave sintering. The sintering was carried out at 1200°C in a 1000 W microwave oven**, with silicon carbide bars of large mass as microwave absorber. The samples were placed on a platinum foil and exposed to the microwave field. In all the microwave sintering experiments, temperature near the specimens was monitored with a Pt-Pt10Rh thermocouple. For comparison, conventional sintering was carried out at 1200 and 1300°C for 2 h in a 5 kW programmable electric furnace, with a temperature rate of 5°C/min in both heating and cooling. Table 1 lists the processing conditions of all sintering experiments.

*Carborundum Co., Niagra Falls, NY Form C733-B.
**CEM Corp., Mathews, NC Model MAS-300.

The microwave sintered HAp ceramics were characterized for density, microstructure, and phase compositions. Diametral tensile strengths [9] of some samples were measured at a crosshead speed of 0.051 mm (0.002 in) per min.

RESULTS AND DISCUSSION

Microwave Sintering with Thermal Runaway (Batch I)

The thermal runaway in the current study has the features as shown in Fig. 1. In Batch I-1 and I-2, the thermal runaway took place at 3 min, and total processing took only 15 min (Table 1). Fig. 2 shows the density of the pellets in Batch I-1 and I-2, sintered for 10 min at 1200 and 1300°C, respectively. Compared with those conventionally sintered at the same temperatures, it can be seen that microwave sintering, although involving shorter period of time (only 8.3% of the conventional), resulted in higher sintered density, especially when the green density of the pellets was higher. When green density was over 43%, microwave sintering at 1200°C for 10 min achieved about the same sintered density as achieved by the conventional sintering at 1300°C for 2 h. The densities of the specimens sintered by microwave processing at 1300°C for 10 min were even higher.

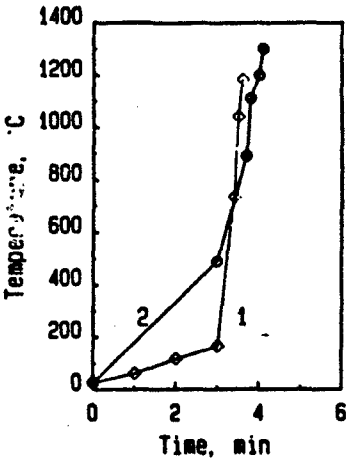


Fig. 1. Typical features of the thermal runaway in the microwave sintering (with porous zirconia as insulator and heating aid) of HAp. 1. Batch I-1. 2. Batch I-2.

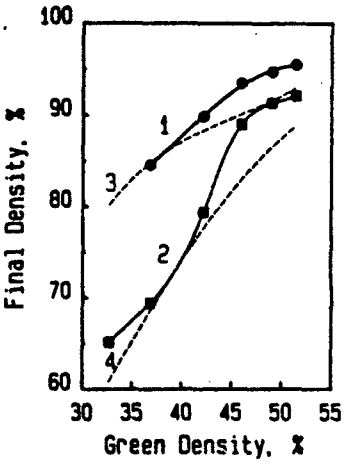


Fig. 2. Density of sintered HAp. 1. By microwave, 1300°C, 10 min. 2. By microwave, 1200°C, 10 min. 3. Conv. 1300°C, 2 h. 4. Conv. 1200°C, 2 h.

The significance of green density as related to the sintered density is further confirmed in the results of Batch I-3. The specimens in this batch had green density of 50 and 60%, respectively; when microwave processed at 1100 for 5 min, both pellets were fully densified. The average grain size of the sintered pellets was only about 0.2 μm. These sintered samples were also phase pure as determined by a careful XRD analysis on both as-sintered surface and the bulk powder of the same sintered pellets. The full densification of this batch of samples is attributed to high packing efficiency, excellent sinterability of the starting powder as well as the quick, high-efficiency

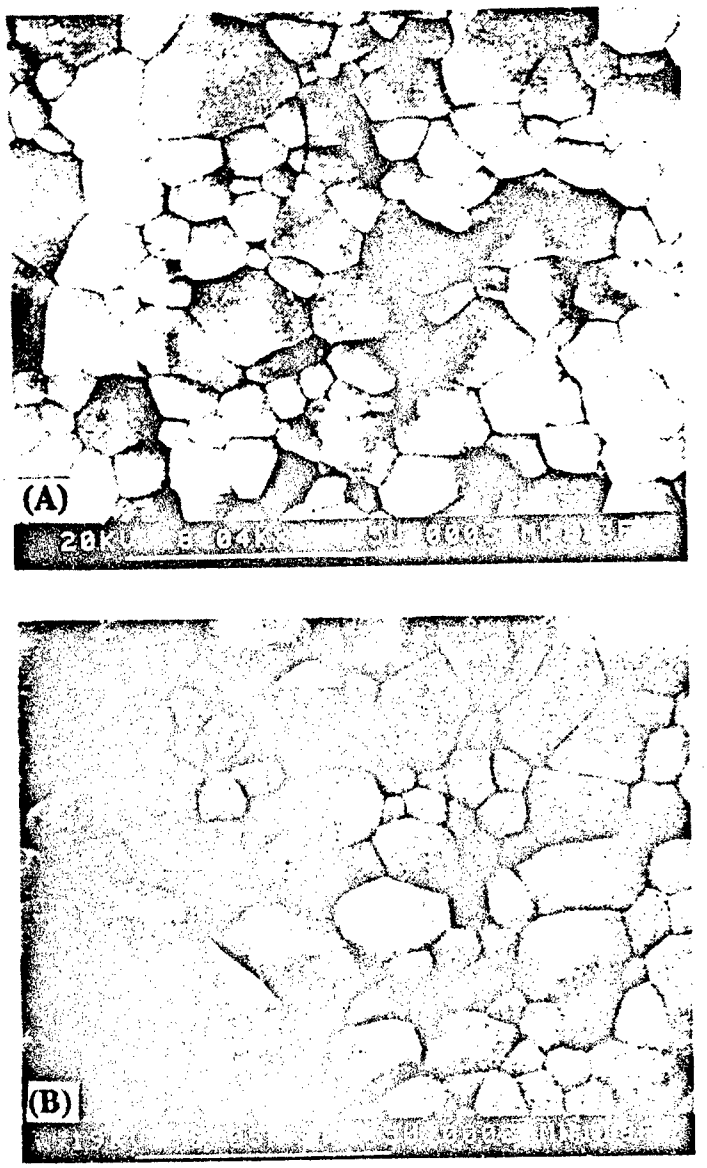


Fig. 3. A comparison of the as-sintered surface of hydroxyapatite ceramics sintered by (A), microwave processing, 1200°C, 10 min; (B), conventional method, 1200°C, 2 h.

microwave sintering. Notice that Powder B used in this batch was ultrafine, with granular morphology, which enables higher green density and better sinterability. Since the average particle size of Powder A was about the same as Powder B, it is the needle-shaped morphology of Powder A that hindered the pellets in Batch I-1 an I-2 from being further densified under the experimental conditions. Particle size distribution (not studied) might have also played an important role.

The morphology of the as-sintered pellet of microwave processing at 1200°C for 10 min (I-1) was different from that conventionally sintered at the same temperature for 2 h (Fig. 3). The microwave sintered sample showed even and uniform surface, while the conventionally sintered sample showed granular outlines. Obviously, microwave sintering, even in much shorter time (8.7% of the conventional sintering), resulted in more intensive mass diffusion. Certain secondary crystallization was noticed in the samples sintered at 1300°C by both microwave and conventional processes (Batch I-2 and III-2), but the average grain size in the microwave sintered sample was only half of that of conventionally sintered sample. This limited grain growth is attributed to the quick and efficient microwave sintering. Without applying any pressure, the sintering process of ceramics is always accompanied by densification and grain growth. Compared with the conventional sintering, while the densification process is substantially enhanced in the microwave sintering, the rate of grain growth is relatively retarded.

Thermal Runaway Suppressed Microwave Sintering (Batch II)

Two groups of samples (2 pellets each) with green density of 42 and 47% were sintered to 79.5 and 86.5% density, respectively. The corresponding results achieved in the thermal-runaway-unsuppressed microwave sintering (I-2), with the same green density and same sintering temperature, are 79.4 and 90%, respectively. In the thermal runaway suppressed microwave sintering, even though the time required to reach the sintering temperature (1200°C) was much longer (40 min vs. 4 min, Fig. 4), the density of sintered sample did not show any increase. This clearly indicates that the thermal runaway did play an important and positive role in the rapid microwave sintering of HAp ceramics.

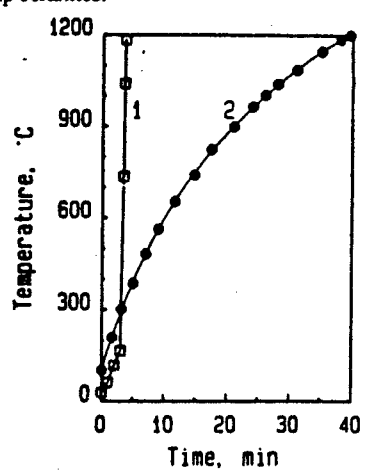


Fig. 4. A comparison of heating curves of microwave sintering of HAp ceramics. 1. With thermal runaway. 2. Thermal runaway suppressed.

It was reported that the triggering of thermal runaway is directly related to the mass of the material processed [1]. For a specific material with a reasonable loss factor, within the penetrating limit of the microwaves, the absorption of microwave energy is directly related to the area or the mass of the material irradiated. In the experiments of Batch I, however, the use of zirconia cylinder shielded the thermal runaway of the sample itself, because the mass of the samples was much less than that of the zirconia cylinder and zirconia has a high microwave absorption efficiency.

Contribution of Thermal Runaway

The high efficiency of microwave sintering involves two aspects, the high efficiency of volumetric heating without thermal gradient, and the substantial reduction of time required for the heating prior to and during sintering. In microwave sintering, thermal runaway makes it possible to reach sintering temperature within a couple of minutes which would otherwise take a few hours in a conventional sintering. In conventional sintering, the heating rate depends not only on the capacity of furnace, but also on the thermal shock resistance of the material itself. The thermal gradient at high heating rates could make the material crack or break.

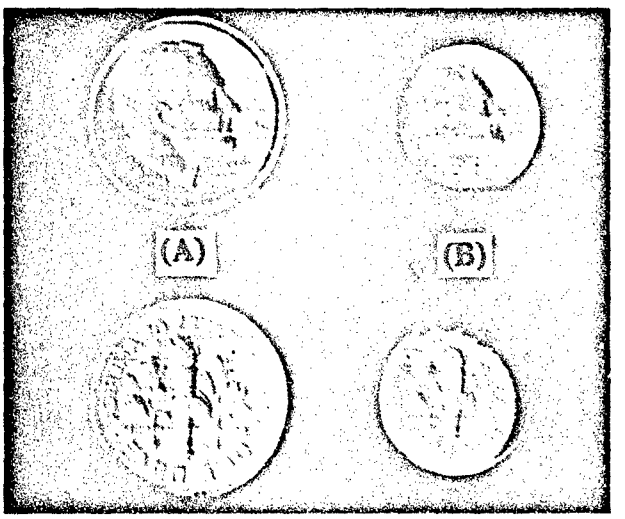


Fig. 5. Uniformity of HAp ceramics sintered by microwave processing with thermal runaway, at 1100°C for 3 min, then 1200°C for 7 min. (A). Before sintering. (B). After sintering.

The fact that the HAp specimens did not crack or break during the thermal runaway in microwave processing clearly indicates that there was no (or not significant) thermal gradient in the processed HAp specimens. The uniformity of the microwave sintered pellets is demonstrated in Fig. 5, in which imprinted samples were sintered with thermal runaway. The uniform shrinkage could not have been achieved if there were any significant thermal gradients. The following factors may explain why there is no deleterious effect on microwave sintering (Batch I):

1) Although the thermal runaway was not triggered directly by the processed material under study but mainly by the zirconia cylinder, as the runaway was triggered in the cylinder, the temperature of the sample was brought up, and according to the relation between loss factor and temperature [10], its dielectric loss factor would increase with temperature. This would make the material absorb more microwave energy and further increase the temperature, and so on. This reasoning actually indicates that the thermal runaway took place in the processed material at about the same time it occurred in the zirconia cylinder. The hysteresis between the two must not have been significant, otherwise the damage in the material would be apparent.

2) The size of the HAp sample also makes a significant difference. Since in this study the pellets processed were thin, and no doubt the thickness of these pellets was within the penetration limit of the microwaves, there was no significant thermal gradient within the sample or between the sample and the nearest surrounding of the samples during the thermal runaway or the sintering process.

From the above, it is clear that, under certain circumstances the thermal runaway condition contributes significantly to the microwave sintering of HAp ceramics. Actually, it is the thermal runaway that made the rapid sintering of HAp ceramics successful. Both dense and porous HAp ceramics with some novel properties have been successfully fabricated by microwave processing recently in this lab. The relevant results are being published elsewhere.

The diametral tensile strength data of the microwave sintered HAp ceramics and some of the conventionally sintered samples are plotted in Fig. 6. The data from both sources seem to follow the same density-strength relation. This indicates that microwave sintering substantially improves the sintering efficiency but does not bring about any change in the structure. As shown previously, with the HAp specimens of the same green density, microwave sintering results a higher sintered density than conventional sintering. So that the enhanced mechanical strength of the microwave sintered samples is attributed to the denser microstructure of the sintered bodies.

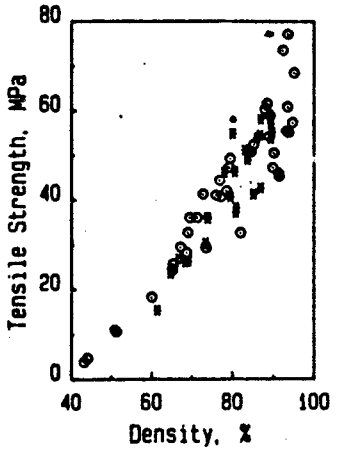


Fig. 6. Diametral tensile strength of HAp ceramics. (*) Conventionally sintered. (o) Microwave sintered.

CONCLUSIONS

HAp ceramics have been fabricated by microwave processing with a porous zirconia cylinder as insulator and a heating aid. Thermal runaway positively contributes to the highly efficient microwave sintering, and results in a substantial reduction in the processing time and energy. At the same time, the grain growth can be significantly suppressed while achieving full or nearly full densification. Sinterability, thermal stability, and the dehydration of the starting material are important factors for successful microwave sintering.

ACKNOWLEGEMENT

This research was supported by NSF Research Grant 8 812 824.

REFERENCES

1. R. Roy, S. Komarneni, and L.J. Yang, "Controlled Microwave Heating and Melting of Gels", J. Am. Ceram. Soc., 68 [7] 392-95 (1985).
2. S. Komarneni and R. Roy, "Anomalous Microwave Melting of Zeolites", Materials Letters, 4 [2] 107-110 (1986).
3. W.H. Sutton , "Microwave Processing of Ceramic Materials", Am. Ceram. Soc. Bull., 68[2] 376-86 (1989).
4. R.W. Bruce, "New Frontiers in the Use of Microwave Energy: Power and Metrology", Microwave Processing of Materials, MRS Symp. Proc., vol. 124, edited by W.H. Sutton, M.H. Brooks and I.J. Chabinsky, MRS, Pittsburgh, pp3-15 (1988).
5. Y. Fang, D.K. Agrawal, D.M. Roy, and R. Roy, "Preparation and Microwave Sintering of Hydroxyapatite", presented at 92nd Am. Ceram. Soc. Annual Meeting, No. 31-T-90, Dallas, Texas, April 22-26, 1990.
6. H. Monma and T. Kamiya, "Preparation of Hydroxyapatite by the Hydrolysis of Brushite", J. Mat. Sci., 22 4247-50 (1987).
7. M. Jarcho, C.H. Bolen, M.B. Thomas, J. Bobick, J.F. Kay and R.H. Doremus, "Hydroxylapatite Synthesis and Characterization in Dense Polycrystalline Form", J. Mat. Sci., 11, 2027-35 (1976).
8. Y. Fang, D.K. Agrawal, D.M. Roy and R. Roy, "Microwave Sintering of Hydroxyapatite Ceramics", submitted to J. Am. Ceram. Soc., manuscript No.196,932, Feb., 1991.
9. A. Rudanick, A.R. Hunter, and F.C. Holden, "An Analysis of the Diametral-Compression Test", Materials Research Standards, pp. 283-89, April, 1963.
10. M.G. Hamlyn and A.L. Bowden, "Microwave Processing of Earthware Ceramics", Am. Ceram.Soc. Bull., 69 [3], 368-72 (1990).

MICROSTRUCTURAL EVOLUTION OF $YBa_2Cu_3O_{7-x}$ USING MICROWAVE ENERGY

A.D. Cozzi, D.K. Jones, Z. Fathi, and D.E. Clark, Dept. of Mat. Sci. & Eng., Univ. of Florida, Gainesville, FL 32611-2066

ABSTRACT

Discs of $YBa_2Cu_3O_{7-x}$ were sintered at 2.45 GHz in a Raytheon model QMP2101B-6 microwave oven using hybrid heating. Heating $YBa_2Cu_3O_{7-x}$ solely by microwaves is feasible, but a silicon carbide susceptor was used to insulate the discs and provide a more uniform thermal environment. In order to begin with a uniform green microstructure, the discs were slip-cast from a non-aqueous dispersion containing fine $YBa_2Cu_3O_{7-x}$ powder. The effects of varying times and temperatures on the microstructural uniformity, densification, and grain growth were investigated using optical and quantitative microscopy.

INTRODUCTION

The discovery of superconductivity in oxide systems by Bednorz and Müller[1] attracted many scientists to the field of superconductivity. The subsequent findings of Wu, Chu, and coworkers[2] of a relatively easy to fabricate ceramic superconductor with a critical temperature above that of liquid nitrogen prompted many researchers to investigate the properties of these new materials.

Microwave interactions with materials have proven to be a valuable tool in the characterization of superconductors and other materials. Information such as the critical temperature, T_c[3], the real and imaginary parts of the dielectric constant, ε' and ε'',[4] and the power absorbed by the material[5] can be obtained using microwaves. The zero resistance property of superconductors has also been used for the fabrication of microwave cavities.[6,7] However, most of the research performed in the microwave/superconductor system has been at temperatures near or below the critical temperature of the superconductor.

Baghurst and Mingos[8] determined that copper oxide (CuO) strongly absorbs microwaves at a frequency of 2.45 GHz at ambient temperature. $YBa_2Cu_3O_{7-x}$ was later synthesized from precursor materials using microwave energy.[9,10] Chandler et al[11] used microwaves to provide energy for the tetragonal to orthorhombic phase transformation in oxygen on samples sintered conventionally. They reported a superconducting fraction in the microwave annealed samples twice that of the samples conventionally annealed. Cozzi[12] sintered superconducting $YBa_2Cu_3O_{7-x}$ pellets to low densities using microwaves at 2.45 GHz and 800 watts.

EXPERIMENTAL PROCEDURE

$YBa_2Cu_3O_{7-x}$ powder was produced by a solid-state synthesis reaction from

Y_2O_3,* CuO,** and $BaCO_3$,*** powders with a nominal purity of 99.9 %. The powders were weighed to achieve a Y:Ba:Cu ratio of 1:2:3 and mixed with an equal volume of deionized water to homogenize the powders. The slurry was dried and calcined in an alumina boat at 970 °C for eighteen hours in a box furnace. The loosely sintered block of $YBa_2Cu_3O_{7-x}$ was removed from the boat and ground into a < 300 micron powder in a Diamonite mortar and pestle. The powder was calcined again at 945 °C for four hours in a tube furnace with an oxygen flow of 100 ml/hr. This was followed by a slow cool to 600 °C and a four hour hold before furnace cooling to room temperature. Hueberger[13] reported this process to yield single phase $YBa_2Cu_3O_x$. The $YBa_2Cu_3O_{7-x}$ powder was ground to < 125 microns and milled with zirconia media with ethanol in a polypropylene jar for five hours. Wu[14] reported that this process in not detrimental to the phase purity of the powder. The powder/ethanol mixture was then diluted with ethanol to approximately ten volume percent solids and allowed to settle for fifteen minutes. The ethanol and fines were decanted with samples of the settled powder and fines retained for x-ray analysis. Wu[15] has shown that this removes any minor-phase particles of smaller size and lower density. The remaining ethanol was evaporated and the agglomerated mass was crushed into powder.

A suspension of fifty volume percent $YBa_2Cu_3O_{7-x}$ powder in ethanol was prepared with a one weight percent addition of suspending agent, PVP K-30.**** The suspension was deagglomerated by ultrasonication for thirty minutes. The suspension was then aged overnight on a rolling mill to allow the viscosity to stabilize.

Sample discs twenty millimeters across and five millimeters high were slip-cast using the suspension. The shapes were formed using polypropylene molds on plaster bats. A 0.22 micron nylon filter was used as a barrier to prevent the fine powders from hindering the casting. Binder removal of the samples was achieved by heating the discs at 1 °C/mir. in air to 500 °C and holding for one hour.

The discs were sintered in a Raytheon Model QMP 2101B-6 6.4 kW, 2.45 GHz microwave oven using the configuration in figure 1. The nickel foil barrier was used to prevent arcing between the thermocouple and sample. Peng[16] concluded that small substitutions of nickel does not significantly effect the superconducting properties of $YBa_2Cu_3O_{7-x}$. The discs were sintered in air using the times and temperature listed in Table I. The heating rate used was 50 °C/min and was accomplished with one 800 watt magnetron tube operating at 2.45 GHz. The setpoint during the heat up and hold was maintained by altering the duty cycle of the microwave tube as necessary.

The bulk density of the specimens was determined using the Archimedes technique with ethanol as the liquid medium. The total porosity was calculated from the bulk density and a theoretical density of 6.38 g/cm^3 for $YBa_2Cu_3O_7$.

Phase determinations were performed on the initial $YBa_2Cu_3O_{7-x}$ powder, the supernatent from the settling process, and the three samples sintered for ninety minutes using x-ray diffraction analysis.

---

*Johnson Matthey Electronics, Y_2O_3 # 1900

**Fisher Scientific Company, Cupric Oxide # C-472

***Johnson Matthey Electronics, $BaCO_3$ #14341

**** GAF Chemicals Corporation, PVP K-30 polyvinlypyrrolidone

Micrographs were taken using a scanning electron microscope* across the thickness of the sample discs. Standard quantitative microscopy techniques were used to determine the average grain size and porosity with respect to position in the sample.

RESULTS AND DISCUSSION

The bulk density of the specimens increased with temperature for all of the sintering times evaluated. There was minimal densification noted in the sample sintered at 750 °C for sixty minutes and only a small increase in bulk density measured for the sample sintered at 750 °C for ninety minutes. Similarly,the sample sintered at 800 °C for ninety minutes exhibited only a small measurable increase in bulk density. The first appreciable increase in bulk density was achieved by sintering at 850 °C for 90 minutes. At 875 °C, significant densification was noted at sintering times of fifteen minutes. The bulk density gradually increased with time at 875 °C to 5.32 g/cm^3, 83.9 percent the theoretical density of $YBa_2Cu_3O_7$. Figure 2 plots the bulk density versus time for the specimens at the different temperatures examined.

The x-ray diffraction pattern of the $YBa_2Cu_3O_{7-x}$ starting powder contained some peaks that were not associated with $YBa_2Cu_3O_7$. Traces of $YBa_2Cu_3O_6$ and $BaCO_3$ were included in the sample. The analysis on the supernatant showed that it consisted primarily of $BaCO_3$ and Y_2BaCuO_5 with some traces of $YBa_2Cu_3O_{7-x}$. The diffraction patterns for the three sample sintered at 875 °C were almost exclusively $YBa_2Cu_3O_{7-x}$, however, the sample sintered for ninety minutes also contained Y_2BaCuO_5. This may have been caused by localized melting within the sample as the microwave field is not perfectly uniform.

Micrographs of the sample sintered for ninety minutes at 875 °C are shown in figure 3. Quantitative microscopy performed on the specimens show that the porosity is slightly higher in the center of the samples sintered for short times. All of the samples sintered at 875 °C had a much lower porosity than the unsintered sample. This suggests that significant sintering occurs at 8765 °C even at times as short as fifteen minutes. Figure 4 is the porosity of the specimens sintered at 875 °C for various times with respect to position across the sample. Similar methods were used to calculate the mean grain size of the same samples. Figure 5 plots the grain size of the samples sintered at 875 °C for various times with respect to position across the sample. The grain size appeared relatively uniform across each of the samples and increased with increasing sintering times. Again, comparing these results to the unsintered sample, there was appreciable grain growth even at the shortest times examined.

CONCLUSIONS

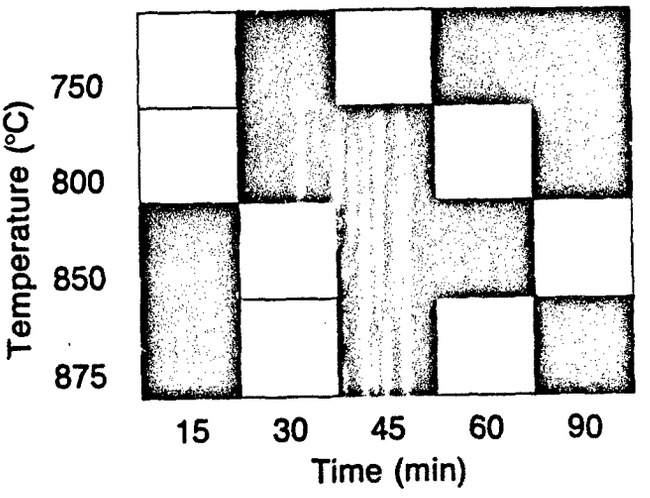
$YBa_2Cu_3O_{7-x}$ superconductors can be densified significantly at a temperature of 875 °C. In the ranges examined, temperature has a greater affect on the densification of the samples than the sintering times. Uniform grain size and porosity can be obtained using microwave sintering for specimens up to five millimeters in thickness.

ACKNOWLEDGEMENTS

The authors would like to thank the Florida High-Tech Industry Council and the Space Research institute for their support during this study.

*JOEL JEM 35C

Table 1. Matrix of Samples Tested.



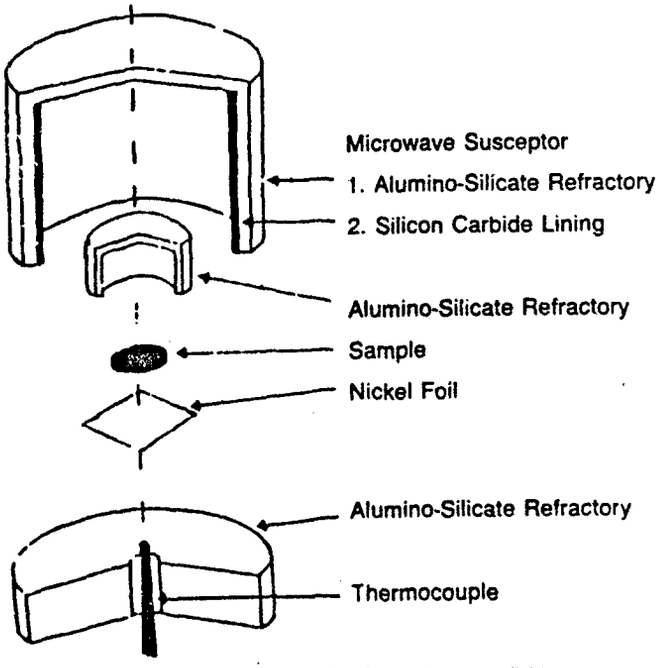


Figure 1. Setup used to sinter $YBa_2Cu_4O_{7-x}$ in a microwave field.

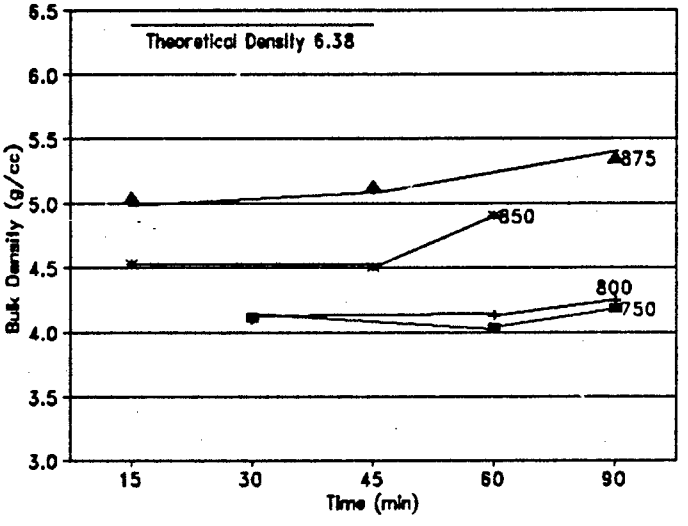


Figure 2. Bulk Density versus time for samples sintered at various temperatures.

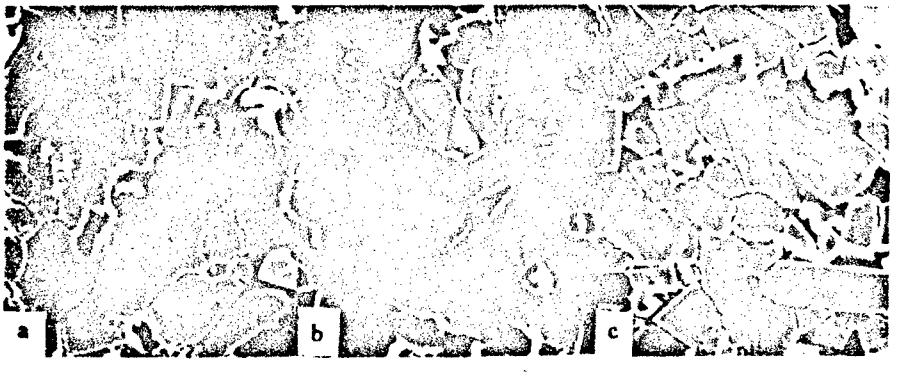


Figure 3. SEM's taken through the thickness of the sample sintered at 875 •C for 90 minutes. a) edge, b) center, c) edge.

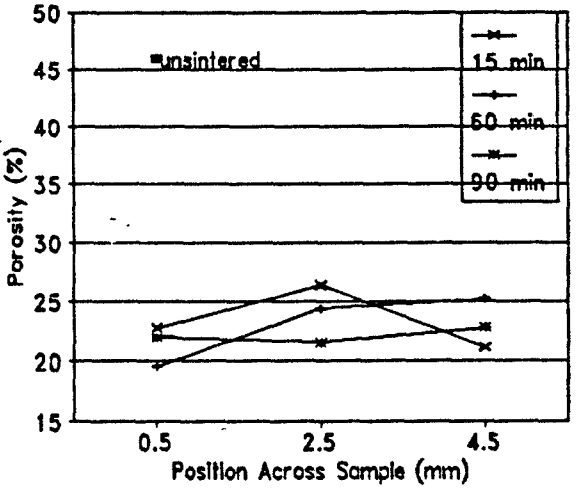


Figure 4. Porosity with respect to position across sample sintered at 875 • C.

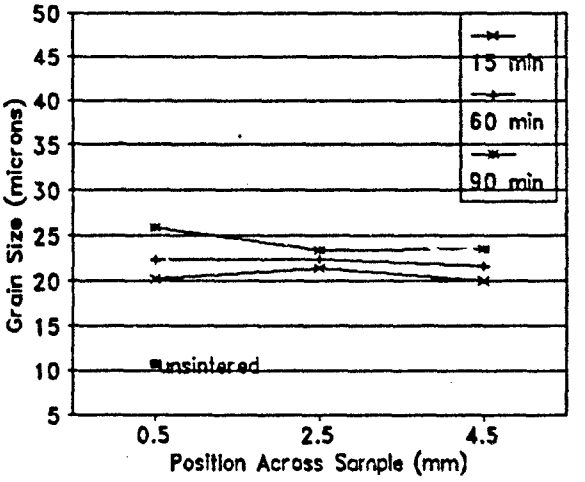


Figure 5. Grain size with respect to position across sample sintered at 875 • C.

1. J.G. Bednorz and K.A. Müller, "Possible High T_c Superconductivity in the Ba-La-Cu-O System," Z. Phys. B - Condensed Matter, Vol.64, pp. 189-193, (1986).

2. M.K. Wu, J.R. Ashburn, C.J. Torng, P.H. Hor, R.L. Meng, L. Gao, Z.J. Huang, Y.Q. Wang and C.W. Chu, "Superconductivity at 93 K in a new MIxeed-Phase Y-Ba-Cu-O Compound System at Ambient Pressure," Phys. Rev. Let., Vol. 58 No. 9, pp. 908-910, (1987).

3. V.F. Gantmakher, V.I. Kulakov, G.I. Leviev, R.K. Nikolaev, A.V. Polisskii, N.S. Sidorov, and M.R. Trunin, "High-Frequency Resistance of the Y-Ba-Cu-O Ceramics," Physica C, Vol. 162-164, pp. 1539-1540, (1989).

4. Z. Trybula, J. Stankowski and J. Baszynski, "Dielectric Study of $YBa_2Cu_3O_{7-\delta}$ Ceramic in a Microwave Electric Field," Physica C, Vol. 156, pp. 485-488, (1988).

5. E.M. Jackson, S.B.Liao, J. Silvas, A.H. Swihart, S.M. Bhagat, R. Crittenden, R.E. Glover III, and M.A. Manheimer, "Initial Susceptibility and Microwave Absorption in Powder Samples of $Y_1Ba_2Cu_3O_{6.9}$," Physica C, Vol. 152, pp. 125-129, (1988).

6. E. Minehara, R. Nagai and M. Takeuchi, "The TM_{010} Microwave Cavity Made of $YBa_2Cu_3O_{7-d}$," Jap. J. Appl. Phys., Vol. 28 No. 1, pp. L100-L101, (1989).

7. W.J. Radcliffe, J.C. Gallup, C.D. Langham, M. Gee, and M. Stewart, "Microwave Cavity Made From YBaCuO," IEEE Trans. on Mag., Vol. 25 No. 2, pp. 990-992, (1989).

8. D.R. Baghurst and D.M.P. Mingos, J. Chem. Soc.

9. D.E. Clark, I. Ahmad and G.Chandler, "Processing of Superconducting Ceramics Using Microwave Energy," Patent 07/177,774, pending (1988).

10. D.R. Baghurst, A.M. Chippendale and D.M.P. Mingos, "Microwave Synthesis for Superconducting Ceramics," Nature, Vol. 332, p. 311, (1988).

11. I. Ahmad, G.T. Chandler and D.E. Clark, "Processing of Superconducting Ceramics Using Microwave Energy," Mat. Res. Soc. Symp. Proc., Vol. 124, pp. 239-246, (1988).

12. A.D. Cozzi, I. Ahmad, D.C. Folz, and D.E. CLark, "Microwave Processing of $YBa_2Cu_3O_{7-x}$ Ceramic Superconductors," Proc. 2nd Ann. Conf. on Micro. and Mat., pp. 149-151, (1990).

13. M. Hueberger, A. Bhargava and R.L. Snyder, "The Reproducible Production of Pure Superconducting $Ba_2YCu_3O_x$," Mat. Lett., Vol. 5 No. 11-12, pp. 489-494, (1987).

14. N.L. Wu, E. Ruckenstein and S. Narain, "The Effects of Wet Processing on the Superconducting Properties of $YBa_2Cu_3O_{7-x}$ Powders," Supercond. Sci. Technol., Vol. 1, pp. 276-279, (1989).

15. N.L. Wu, S. Narain and E. Ruckenstein, "Purity Improvement of the High-Temperature

Superconducting Powders by Sedimentation," Mat. Lett., Vol. 6 No. 10, pp. 321-326, (1988).

16. N. Peng, J. Yuan, D. Zheng, and W.Y. Liang, "On the Effect of Ni Substitution in Superconducting $YBa_2Cu_3O_{7-\delta}$," Supercond. Sci. technol., Vol. 4, pp. S313-S315, (1991).

MICROWAVE PLASMA SINTERING OF ALUMINA

Mary P. Sweeney* and D. Lynn Johnson
Northwestern University
Department of Materials Science and Engineering
Evanston, IL 60208-3108

ABSTRACT

A tunable single mode (TM_{012}) microwave cavity was designed to initiate and sustain a plasma for sintering ceramic materials. Almost 100% of the incoming microwave energy could be coupled to the plasma under optimal tuning conditions. An optical fiber thermometer was used to continuously monitor the temperature of alumina specimens during plasma sintering. The sintering temperature and resulting density of the specimens were dependent on gas content at constant net power absorption.

INTRODUCTION

The history of plasma sintering dates back to 1968, when Bennett *et.al.* first reported developing a 2.45 GHz microwave-induced plasma heat source for sintering ceramics.[1] Alumina compacts were found to sinter more rapidly in a plasma and had higher densities, greater strengths and finer grain sizes than conventionally sintered specimens. Evidence of enhanced densification in a plasma also was observed.[2] Specimens that were partially sintered in a discharge showed a negligible increase in densification upon further heating in a conventional furnace at the same temperature. However, densification would continue when the same specimen was reimmersed in the plasma, and its final density would be equivalent to that of specimens that were plasma sintered continuously for the same amount of time. These results suggest that a plasma sintering environment may be more than a simple heat source.

---

*Now at Raytheon Co., 50 Apple Hill Drive, Tewksbury, MA 01876

Extensive work in the field of plasma sintering has been conducted for over ten years at Northwestern University. Microwave applicators and RF and DC hollow cathode plasma devices have been used to generate plasma discharges. Rapid densification rates and anomalous heating characteristics were reported.[3-5] Knowlton first showed that the final densities of RF plasma sintered specimens were strongly related to the amount of dopant gas present during sintering, whether directly added to the plasma or injected into the plasma by desorption from the surface of the ceramic powder particles.[6] Chen further quantified these results and reported that outgassed alumina specimens did not show any significant amount of shrinkage in a 100% argon plasma, but could be heated to sintering temperatures when small amounts of polyatomic gases such as N_2, O_2, H_2 and H_2O were added to the argon.[7] The net power consumption of the plasma could not be accurately determined for these experiments.

The present work was undertaken to further investigate the effects of plasma composition on microwave induced plasma heating of alumina. A tunable single mode (TM_{012}) resonant cavity that had on-line power monitoring and tuning capabilities was designed and implemented for the microwave plasma sintering studies. It has been noticed that a microwave discharge takes on a shape related to the filled pattern of its electromagnetic mode.[8] The TM_{012} mode was chosen because the electric field lines run parallel to the coaxial plasma tube.[9]

EXPERIMENTAL

The single mode (TM_{012}) tunable cylindrical resonant cavity used as the microwave plasma sintering apparatus was designed in accordance with the descriptions published by Asmussen.[8] A schematic representation is shown in Figure 1. The adjustable movable plate short of the cavity served two purposes: tuning the TM_{012} mode and improving impedance matching with the plasma. A coaxial launch probe assembly was used to transmit 2.45 GHz microwave power into the cavity. Both the insertion depth of the probe into the cavity and the position of its short circuit could be individually adjusted to optimize tuning of the system. The 40 mm I.D. fused quartz plasma tube was cooled by compressed air and the outer brass walls were water cooled. A microwave power directional detector was used to continuously monitor power absorption into the cavity.

The alumina specimen configurations were used in this study were 4 mm diameter x 150 mm rods and thimble shaped specimens, 8 mm ID, 11 mm OD and 10 mm high. All specimens (30 m^2/g alumina* with 3% polyvinyl butyral binder) were isostatically pressed and pre-sintered at 650°C in air to burn out the binder. Both types of specimens were held stationary in the cavity, with the rods extending

* Baikowski CR30, Baikowski International Corp., Charlotte, NC 28210

along most of the length of the cavity and the thimbles rested inverted in the center of the plasma on the end of a single crystal sapphire tube*. An optical fiber thermometer** (OFT) lightpipe sensor was inserted into the interior of the thimble to provide temperature readings.

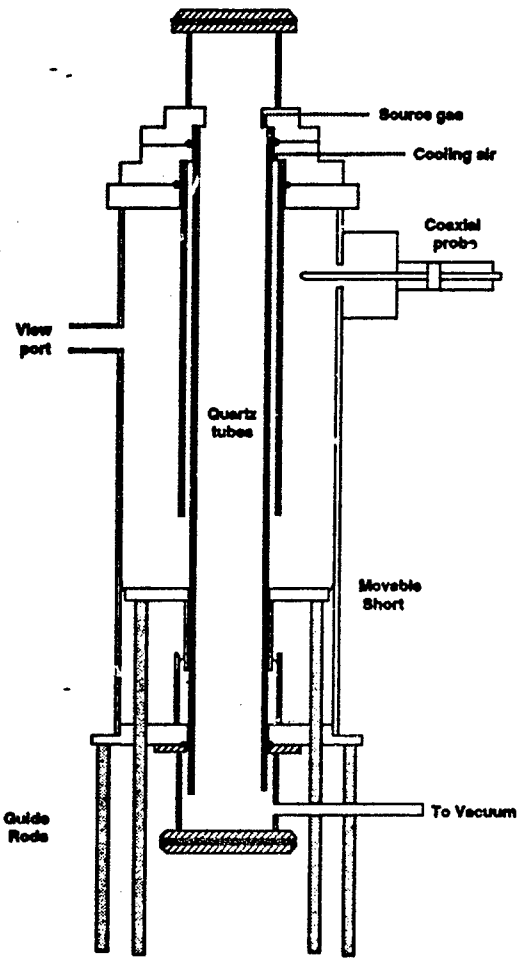


Fig. 1. Schematic cross section of the TM_{012} plasma sintering cavity.

* Kindly supplied by R.D. Bagley, Corning Glass Works, Corning, NY 14830

** Accufiber, Inc., Vancouver, WA 98661

The sintering runs for all specimens began by subjecting them to a low power argon plasma to drive off adsorbed gases from the powder particle surfaces without causing sintering. Gas composition and flow rates were adjusted and the power and pressure were brought up to their working levels to initiate sintering.

The alumina rods were plasma sintered with varying amounts of nitrogen or oxygen in argon. The sintering conditions, which were constant for all runs, were 475 W net power absorbed, 14 kPa total pressure, 10 ml/min STP total gas flow rate, and 5 minute soak. The diameters of the rod specimens were measured before and after sintering as a function of position in the cavity. Using the OFT, the same time/temperature profile was reproduced under different plasma gas conditions for the thimble experiments. Here the flow rate was fixed at 2.5 ml/min STP at a pressure of 15 kPa. The final densities of the specimens were determined by Archimedes' method.

RESULTS AND DISCUSSION

Initial experiments showed that under optimal tuning conditions essentially 100% of the forward power could be coupled to the plasma. Certain plasma operating conditions resulted in the melting of quartz and alumina after tuning.

The normalized final shrinkage of plasma sintered alumina rods as a function of position in the cavity is shown in Figures 2 and 3. Rods sintered in a 100% argon plasma showed no evidence of densification with the same net power that caused shrinkage with diatomic molecules present. As the overall content of diatomic gas in the source gas was raised, the shrinkage of the rods increased. The length of the plasma hot zone was approximately constant regardless of diatomic gas content. The enhanced heating effects may be attributed to the additional heating modes of diatomic gases (atomic recombination). The maximum temperature (maximum shrinkage) position was located in line with the coaxial probe, rather than at the center of the cavity as expected for the undistorted TM_{012} mode.

Figures 4 and 5 show the relative density and normalized shrinkage of the sintered rods as a function of diatomic gas content. At low percentages, oxygen provided greater densities and shrinkage rates than nitrogen for the same volume content and same net power. At higher levels the densification effects of both gases converged.

Figures 6 and 7 show the time-temperature profiles of thimble specimens sintered in a variety of plasmas. A summary of the operating conditions and resulting thimble densities can be found in Table 1. As expected, more net power was required to bring the lower diatomic gas levels to the same temperatures as for the higher quantities. Plasma source gases doped with nitrogen required greater overall net power levels to reach the same temperature as those doped with oxygen. A significant increase in density was seen with the 50% nitrogen sintered thimbles.

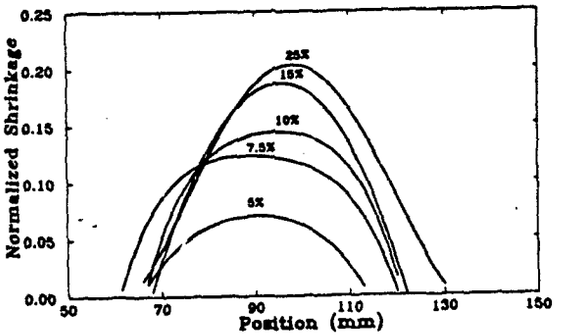


Fig. 2. Normalized diametral shrinkage as a function of distance from the top of the cavity. Indicated are volume percent levels of oxygen in an argon carrier gas.

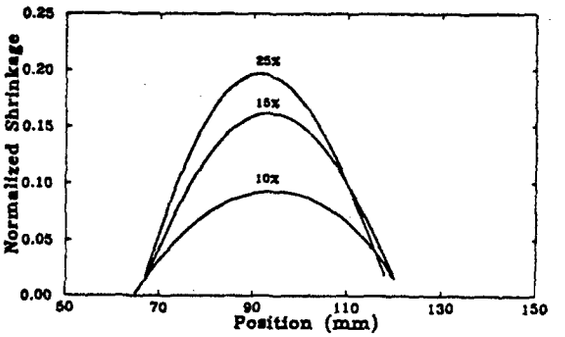


Fig. 3. Normalized diametral shrinkage of plasma sintered alumina rods as a function of distance from the [illegible] the cavity. Indicated are volume percent levels of nitrogen in an argon carrier gas.

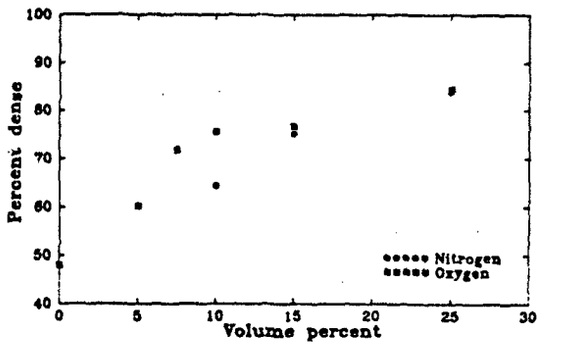


Fig. 4. Maximum density of alumina rods sintered in the plasma as a function of diatomic gas content. Data of Figures 2 and 3.

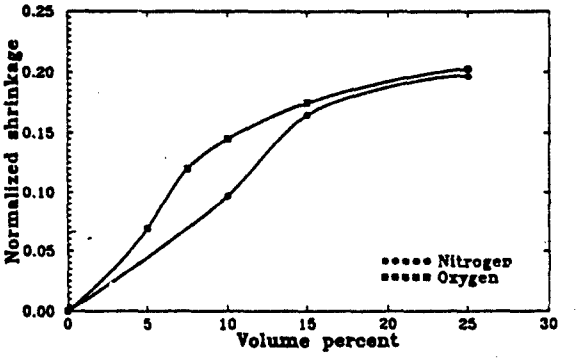


Fig. 5. Normalized maximum diametral shrinkage of plasma sintered alumina rods as a function of diatomic gas content.

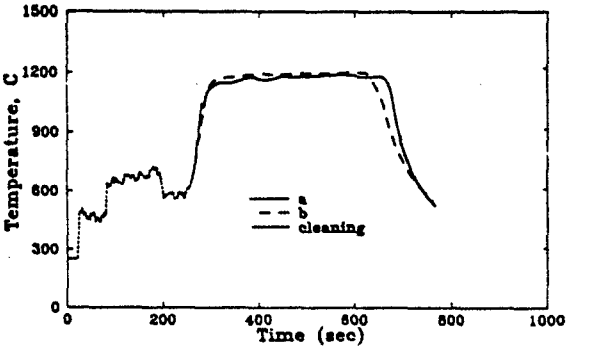


Fig. 6. Indicated temperature-time profiles of alumina thimble specimens sintered under different oxygen gas contents. Label letters refer to Table 1. Low power was applied first to remove adsorbed gases from the specimen.

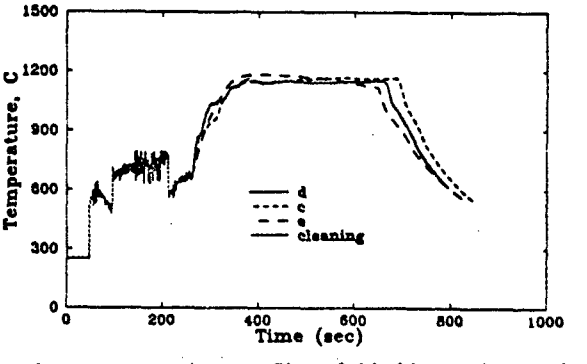


Fig. 7. Indicated temperature-time profiles of thimble specimens sintered under different nitrogen gas contents. Label letters refer to Table 1.

Table 1. Time-Temperature Thimble Runs

Run ID	Volume percent of Additive Gas	Net Power (watts)	Relative Density
a	50% O_2	600	79.1%
b	10% O_2	880	84.2%
c	50% N_2	870	94.9%
d	50% N_2	820	93.8%
e	10% N_2	1180	83.8%

After the present work was completed, Hansen observed that the OFT reads a temperature that is biased to significantly lower values because of translucency of the thimble specimens at the wavelength of radiation sampled by the OFT.[10] While the temperatures shown in Figures 6 and 7 are substantially below the true temperatures, it is reasonable to suppose that the error is approximately the same for all specimens since they do not differ greatly in density (and therefore translucency).

CONCLUSIONS

The single mode (TM_{012}) tunable resonant cavity was shown to be a viable means for microwave-induced plasma sintering. Advantages of this system include real-time monitoring of the net power absorbed by the plasma and tuning capabilities to optimize power coupling. Sintering studies with alumina showed that the previously recognized enhanced sintering characteristics in diatomic gases were not a function of power absorbed by the plasma, but rather depended upon the chemical composition of the plasma.

ACKNOWLEDGEMENTS

This work was supported by the National Science Foundation Grant DMR-8719077, and made use of Central Facilities supported by the National Science Foundation through the Northwestern University Materials Research Center, Grants Nos. DMR 85-20280 and 88-21571. The contributions of Prof. M.E. Brodwin, Department of Electrical Engineering and Computer Science, particularly the design of the launch probe, are gratefully acknowledged.

REFERENCES

1. C.E.G. Bennett, N. A. McKinnon, and L. S. Williams, "Sintering in Gas Discharges," Nature, 217, 1287-88 (1968).

2. C.E.G. Bennett and N. A. McKinnon, "Glow Discharge Sintering of Alumina," in Kinetics of Reactions in Ionic Systems, Edited by T. J. Gray and V. D. Frechette, Plenum Press, New York, 1969; pp.-408-12.

3. Joung Soo Kim and D. Lynn Johnson, "Plasma Sintering of Alumina," Am. Ceram. Soc. Bull., 62 [5] 620-22 (1983).

4. D. L. Johnson, V. A. Kramb, and D. C. Lynch, "Plasma Sintering of Ceramics," in Emergent Process Methods for High-Technology Ceramics, Vol. 17, Edited by R. F. Davis, H. Palmour III, and R. L. Porter, Plenum Publ. Corp., 1984; pp. 207-211.

5. E. L. Kemer and D. L. Johnson, "Microwave Plasma Sintering of Alumina," Am. Ceram. Soc. Bull., 64 [8] 1132-36 (1985).

6. J. M. Knowlton, "Radio Frequency Plasma Sintering of Alpha-Alumina Doped with Various Oxides," MS Thesis, Northwestern University, 1985.

7. M. Y. Chen and D. Lynn Johnson, "Effects of Additive Gases on Radio Frequency Plasma Sintering of Alumina," J. Mat. Sci., accepted for publication.

8. J. Asmussen, Jr., R. Mallavarpu, J. R. Hamann, and H. C. Park, "The Design of a Microwave Plasma Cavity," Proceedings of the IEEE 1, 109-117 (1974).

9. J. Asmussen and R. Garard, "Precision Microwave Applicators and Systems for Plasma and Materials Processing," in Materials Research Society Symposium, Vol. 124, (Materials Research Society, 1988), pp. 347-352.

10. J. D. Hansen, private communication, 1991.

Section VI. Microwave Processing of Nonoxides

"ULTRA" HIGH-TEMPERATURE MICROWAVE SINTERING

C. E. Holcombe and N. L. Dykes

Oak Ridge Y-12 Plant,* P.O. Box 2009, Oak Ridge, Tennessee 37831, USA

ABSTRACT

"Ultra" high-temperature microwave processing, utilizing temperatures over 1900°C, is addressed. Primary areas of concentration involve titanium diboride (TiB_2 - 3 wt% CrB_2) and boron carbide (B_4C -2.5 wt% C). Using 2.45 GHz radiation, high-density, crack-free specimens can be produced. The importance of "casketing" and coverings along with material interactions is discussed. Comparison of microwaving with conventional sintering or hot-pressing indicates that microwaving may be advantageous.

INTRODUCTION

If the area of "ultra" high-temperature microwave processing is defined as ≥1900°C, then only a few materials are expected to require such temperatures for sintering. Oxides and nitrides do not need such high processing temperatures. However, several borides, carbides, and refractory metals require such conditions. Examples are B_4C, TiB_2, ZrB_2, HfB_2, AlB_{12}, LaB_6, SiB_6, SiC, SiB_4C, TaC, TiC, WC, W, and Ta. The primary areas of this investigation have been TiB_2 and B_4C. These nonoxides have attractive properties, including high hardnesses, high melting points (2300° to 3000°C), and electrical conductivity. Additionally, TiB_2 and B_4C have interesting commercial uses as cutting tools, armor, wear components, liners, nozzles, electrodes, and evaporation boats. Therefore, these microwave processing investigations utilizing "ultra" high temperatures have evolved from sintering studies of these nonoxides.

The primary considerations of "ultra" high-temperature processing of nonoxides are (1) equipment (applicator cavity with 2.45 GHz capability and appropriate variable power level, with inert gas and/or vacuum capability), (2) "casketing" or insulation arrangement (an area that has been discussed in detail elsewhere[1] but which cannot be overstated in importance and will be mentioned throughout this report), (3) material interactions with each other and with the applied microwave field, and (4) the characteristics of the material being sintered (surface impurities, degree of agglomeration, overall purity, etc.).

---

*Managed by Martin Marietta Energy Systems, Inc., for the United States Department of Energy.

DISCUSSION

The equipment used for this study is the third generation of microwave furnace that has evolved and is shown in Figure 1. Figure 1 (a) shows the front view with two Cober Electronics Co. 2.45 GHz microwave generators with adjustable 6 kW power output, thus totaling 12 kW capability; high-vacuum equipment can also be seen. Figure 1(b) shows the door to the applicator cavity along with the waveguide entrances on either side of the cavity and the mode stirrer.

Figure 2 shows the sequence of processing where the "casket" is readied, the optical pyrometer is used for temperature measurements, the 2200° C specimen is observed through the viewport (protected with a grid to prevent microwave leakage), and the "casket" exterior becomes hot after 20 minutes at 2200° C. The point at which the exterior becomes over red (over 800° C) heat generally determines the run time, since additional power or time heats the "casket" more than the sample.

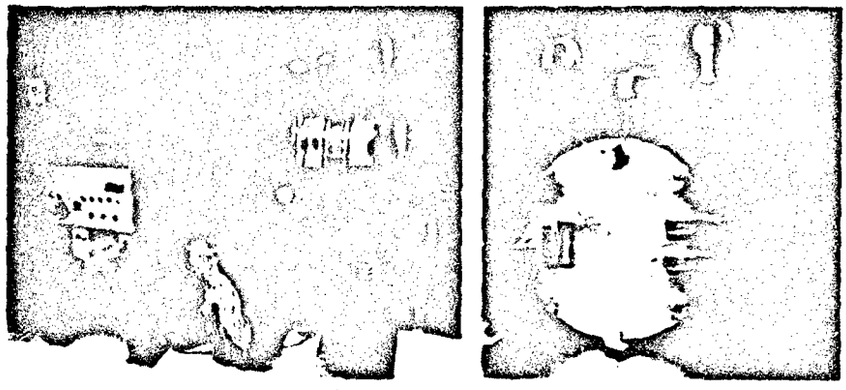


Figure 1. Microwave equipment: (a) front view, (b) door to applicator cavity.

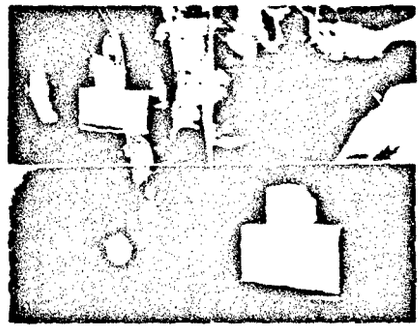


Figure 2. Processing sequence.

Figure 3 shows an assortment of shapes of TiB_2 - 3 wt% CrB_2 specimens that were microwave sintered. The work with this material has been presented in detail elsewhere.[2] The interesting observation was that the material actually contained ≤8 wt% yttrium-titanium oxide when contained in an yttria grit "casket" and processed at 1900 to 2100°C to yield ≥95% dense specimens.

A "casketing" scheme of special coverings was devised[3] to eliminate the yttria infiltration so that a comparison could be made with conventional processing of TiB_2 - 3 wt% CrB_2. The densities achieved are shown in Figure 4. A "microwave effect"[4] of enhanced sintering occurs with this material since the covered (yttria-free) specimen sintered to 94% of theoretical density at 1900 C. Higher temperatures only lead to grain growth with microwaving whereas with conventional sintering still leads to increased density specimens. Physical properties of these materials are shown in Table 1. Microwaving lead to higher densities with reduced fracture toughness when no yttria was present. However, the yttria contamination that occurs when samples are not covered is beneficial[5] in yielding reduced grain size, higher hardnesses, higher densities, and somewhat higher fracture toughnesses as compared to yttria-free microwaved or conventionally sintered material.

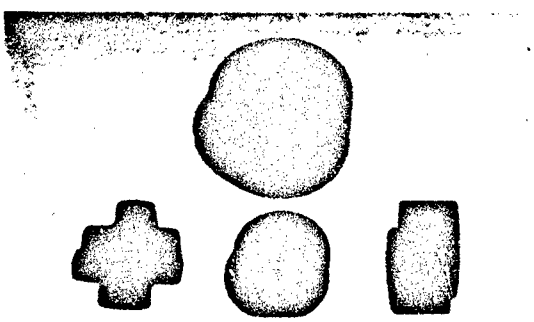


Figure 3. TiB_2 - 3 wt% CrB_2 specimens microwave sintered.

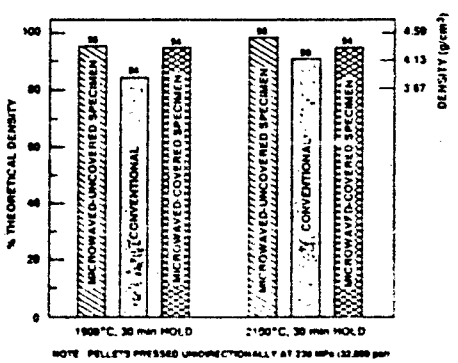


Figure 4. Comparison of microwave and conventional sintering of titanium diboride - 3% Chromium Diboride.

This study of boron carbide microwave sintering arose from early work[6,7] on its microwave absorption. Pressureless sintering of B_4C, conventionally and with microwaves, has been reported.[8-11] Initially, our study involved two powders (Grades D and E), with the material characterization given in Table 2, reported previously.[12] Both grades of B_4C consisted of spherical agglomerates (approximately 100 micrometer spheres, mostly comprised of 1-3 micrometer particulates).

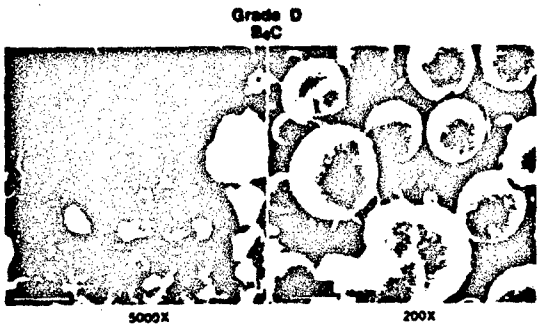
An initial sintering study with small pellets involved comparing the B_4C powders with different additives and with a boiling water treatment, whereby powders were contacted with boiling water for 3 hours followed by drying and then blending under rapid agitation with methyl alcohol followed by filtering. The addition of 3% carbon derived from "Varcum"* furan resin was accomplished by dissolving the resin in acetone, slurry-coating the powder, drying, pressing into a pellet, curing in air to 200°C, and then heating to 1000 to 1100°C in argon to thoroughly outgas the pellets before sintering. The carbon yield of the "Varcum" was 31.1%.

Table 1. Physical properties of TiB_2- 3% CrB_2 specimens

	1900 °C, 30 min			2100 °C, 30 min		
	μwaved Uncovered**	Conv Sintered	μwaved Covered	μwaved Uncovered**	Conv Sintered	μwaved Covered
Fracture Toughness* (MPa • m1/2)	6.2	5.7	5.2	6.1	6.1	5.3
Vickers Hardness (GPa, using 8.3 Kg Load)	16	9	15	16	11	14
Average Grain Size (μm)	4	4	6	4	12	8
Theoretical Density (%)	95	84	94	98	90	94

*Using E = 535 GPa
**Contains 5.6 wt % Yttrium-Titanium Oxide

Table 2. Starting material characterization boron carbide



		GRADE D	GRADE E
Surface Area (m^2/g)		5.3	9.5
Av. Particle Size (μm)		0.4–3	0.2–1
Chemical Analyses (%)			
B_4C			
(78.3)	B	75.7	75.8
(21.7)	C	20.9	21.4
	O	1.63	1.70
	N	0.24	0.14
Impurities over 50 wppm (wppm)			
	Li	<200	<200
	Si	30	300
	Ca	250	100
	Ti	25	110
	Fe	100	160

*Produced by BTL Specialty Resins Corp., Niagara Falls, NY.

The effect of the additives is shown in Figure 5. Note that Grade D powder consistently yielded smaller grain sizes. The 3% carbon and boiling water treatment were most effective for sintering the B_4C. Although Table 2 shows that fluorine was below 50 wppm and thus not reported, surface examination of both Grades D and E powders revealed fluorine species. Electron spectroscopy for chemical analyses (ESCA) determined that the boiling water treatment removed much of the fluorine contamination, leaving a surface of mostly carbide and some nitride.

All the pellets of B_4C, except those with the carbon additive, cracked somewhat during processing. Therefore, the further studies utilized boiling-water-treated, Grade D B_4C with carbon additive.

Tests were conducted to determine if coatings or coverings could prevent the contamination of B_4C pellets fro m the "casketing" material while microwaving. Combinations of painted coatings utilizing a polyvinyl acetate/chloride solution, 9.5% PVAC in methylethylketone (MEK) carrier, as a binder were studied.

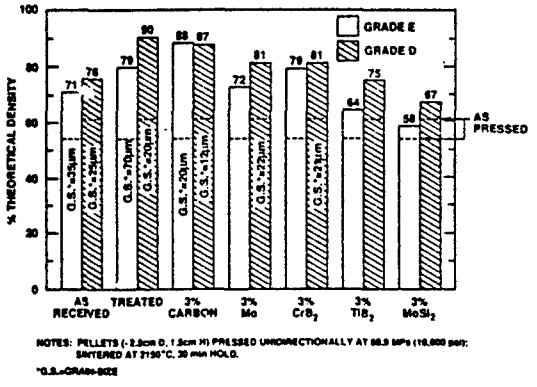


Figure 5. Effect of treatment and additives on the microwave densification of boron carbide.

The best system utilized a covering of Grafoil* glued onto a pressed pellet with the PVAC/MEK binder. Paints using boron nitride (25 g per 75 g of binder), tungsten (100 g per 25 g of binder), or niobium (50 g per 10 g of binder) were used in various combinations. The layers of Grafoil were peculiar in their effect on the B_4C heatability. Figure 6 compares the heatup of the yttria grit insulation alone with a pellet of B_4C that was coated with Grafoil only, and a pellet of B_4C coated with a combination of Grafoil and a tungsten outer layer. The latter covering system produces the highest temperature and allows it to be maintained for considerable time.

Further testing with layering/coatings lead to the system[3] shown in Figure 7. This system consistently allowed the high temperatures to be attained and maintained while preventing contamination of the B_4C by the yttria insulation "casket."

*Produced by Union Carbide Corp., Lakewood, OH.

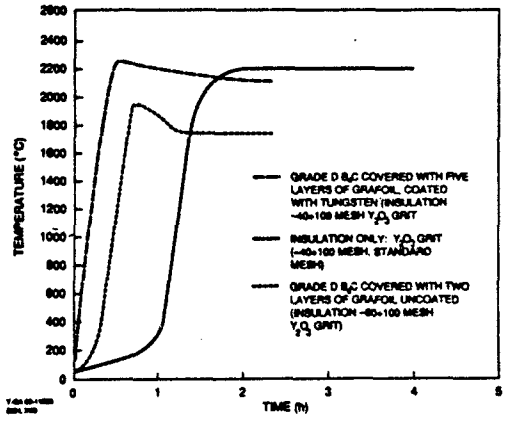


Figure 6. Tests with "Caskets for Higher Microwave Temperatures and Specimen Purity."

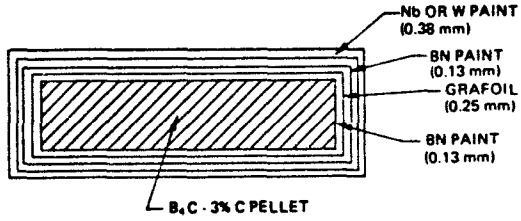


Figure 7. Layering system for microwaving boron carbide that prevents reaction with yttria grit insulation and yet allows microwave transmission.

There is always some question regarding temperature measurements in high-temperature processing experiments. With "ultra" high-temperature microwaving utilizing a multilayered covering, there is additional concern as to the temperature uniformity and to the actual temperature reached by the specimen. Thus, a "casket" was arranged for a "Hole Experiment" utilizing the multilayered coverings shown in Figure 7. The "casket" setup is shown in Figure 8, whereby the temperatures of individual layers and of the interior of the pellet can be monitored.

The temperature versus time thermal profile for a small B_4C - 2.5 wt% C (derived from 8 wt% "Varcum") pellet is shown in Figure 9. The outer tungsten layer initially heats up considerably faster than does the B_4C - 2.5 wt% C pellet. The Grafoil heats up rapidly also, trailed by the B_4C - 2.5 wt% C pellet. After a few minutes above 1900°C, the B_4C - 2.5 wt% C pellet heats up preferentially over the encapsulating materials. At the end of this run, the power level was rapidly increased to see the effect: the exterior layers increased in temperature rapidly but the interior of the B_4C - 2.5 wt% C pellet only slightly increased.

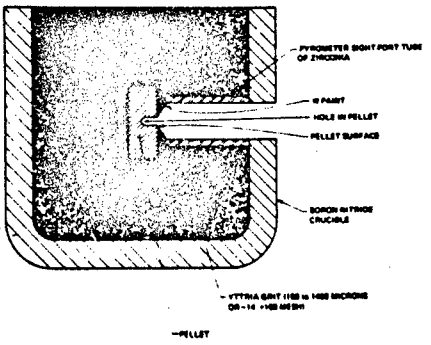


Figure 8. "Casket" arrangement for sintering B_4C-2.5% C for "Hole Experiment."

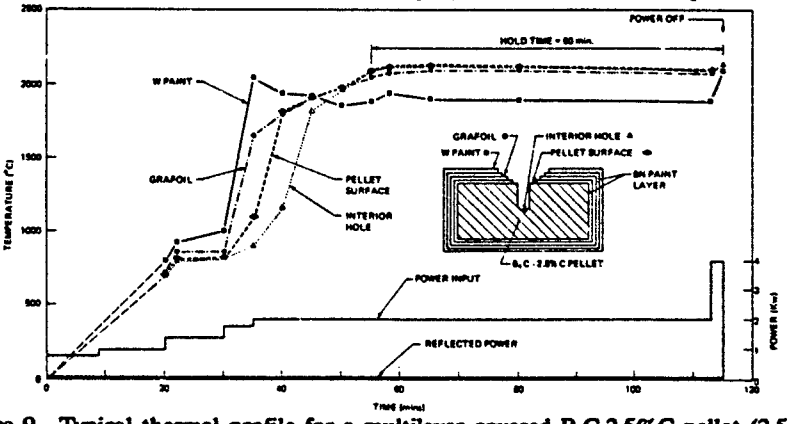


Figure 9. Typical thermal profile for a multilayer covered B_4C-2.5%C pellet (2.54 cm diameter, 1.27 cm height initially, 12.0g.) while microwaving.

Further "Hole Experiments" utilizing a niobium outer layer showed the B_4C - 2.5 wt% C pellet to reach 2200°C while the outside was approximately 2120°C. The outside temperature of the niobium has never reached 2200°C with several tests, nor has the B_4C - 2.5 wt% C pellet temperature ever exceeded 2230°C. Therefore, there appears to be an upper limit on the B_4C - 2.5 wt% C pellet temperatures achievable with 2.45 C Hz radiation.

A comparison of B_4C - 2.5% C processed by microwave sintering, hot-pressing, and conventional sintering was initiated. Large pellets (approximately 6.4 cm D x 1.3 cm H or 2.5 in. D x 0.5 in. H) were unidirectionally pressed at 28.1 MPa or 4075 psi, leading to pressed densities of approximately 50% of theoretical density. All pellets were encapsulated in a multilayered wrapping and sintered at 2200°C for 1 hour in argon. Hot-pressing utilized 13.8 MPa (2000 psi) and the pellet was pressed in a carbon pack.

The thermal profile for the microwaved large B_4C - 2.5 wt% C pellet is shown in Figure 10. The niobium outer coating reached 2200°C. The actual pellet temperature is unknown, since a "hole" for reading the temperature would have badly contaminated the specimen.

However, the actual pellet temperature is expected to be approximately 2200 to 2230°C, since those are the highest temperatures observed with "Hole Experiments." Figure 11 shows the large microwave-sintered B_4C - 2.5 wt% C pellet before and after processing.

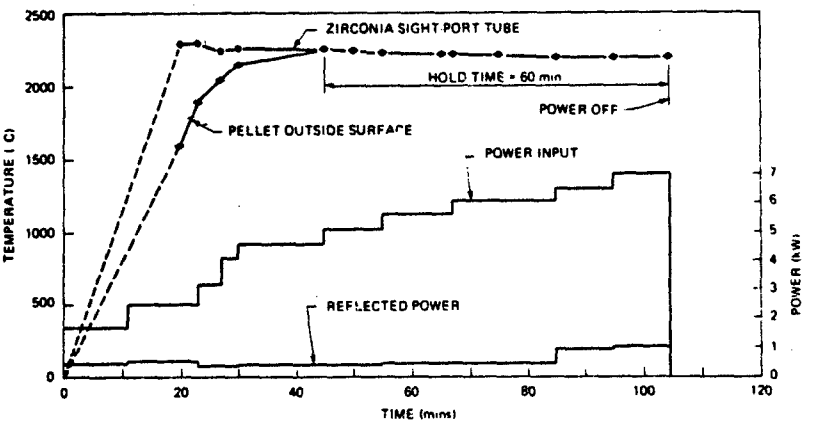


Figure 10. Temperature versus time for large multi-layer covered (niobium outer layer) B_4C-2.5%C pellet (6.35 cm diameter, 1.4 cm height initially, 59.1 g).

All the pellets were analyzed for impurities. Yttrium levels were 175, 130, and 70 wppm respectively for microwaving, hot-pressing, and conventional-sintering: contamination during milling of the carbon additive is expected as the yttrium source since all three methods lead to the low-level contamination, still considerable when compared to the <1 wppm of the Grade D starting material. The average niobium levels were all below 50 wppm. Other minor impurities (up to around 50 wppm) of calcium, titanium, iron, and hafnium occurred. The overall purity, boron plus carbon, of the three pellets prepared by microwaving, hot-pressing, or conventional sintering was >99.95 wt%.

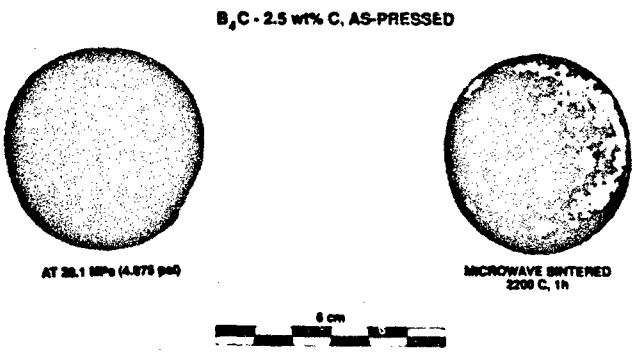


Figure 11. Large pellet before and after processing.

The microstructures of the three specimens are illustrated in Figure 12 (utilizing the etch technique of Katz et al.).[9] The average particle sizes were much larger for microwaved material than for conventionally sintered or hot-pressed material; otherwise, the structures are very similar. A comparison of the three specimens by scanning electron microscopy of fracture surfaces (Figure 13) again shows the similarity of the structures except for density and particle size.

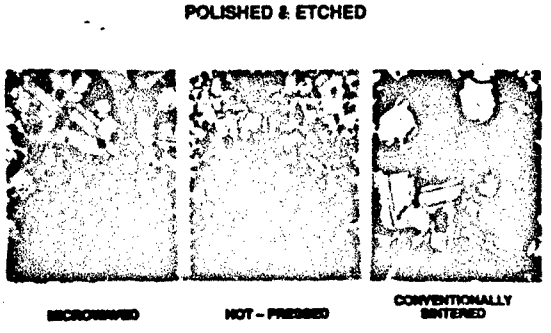


Figure 12. Microstructure of specimens processed with different techniques.

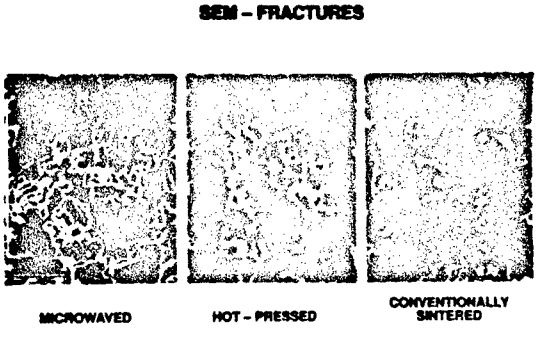


Figure 13. Fracture surfaces of specimens processed with different techniques.

Physical-chemical properties of the large-sized B_4C - 2.5 wt% C specimens prepared by microwaving, hot-pressing, and conventional sintering are shown in Table 3. Acoustic property measurements[13] were used to determine Young's modulus and Poisson's ratio. Micro-indentation hardness and fracture toughness measurements were determined on polished, unetched specimens, using the method described by Evans.[14] Chemical purity was determined by spark source mass spectrometry (SSMS). Average grain size was derived from counting techniques, and percent theoretical density was determined from mercury porosimetry results.

Table 3. Properties of boron carbide–2.5% carbon specimens (2200 C, 1 h, argon)

	MICROWAVED	HOT-PRESSED	CONVENTIONALLY SINTERED
		(σ' 13.8 MPa or 2 ksi)	
YOUNG'S MODULUS (GPa)	221	361	140
POISSON'S RATIO	0.22	0.23	0.20
FRACTURE TOUGHNESS (MPa* m1/2)	4.2	3.3	---
VICKER'S HARDNESS (GPa, USING 6.8 Kg LOAD)	5	17	4
AVERAGE GRAIN SIZE (MICRONS)	17	4	8
% THEORETICAL DENSITY	83	93	70
SSMS ANALYSES			
Y, wppm	175	130	70
Nb, wppm	10	15	40
TOTAL PURITY (%)	99.95	99.96	99.97

Sonic moduli and Poisson's ratios were highest for hot-pressed specimens followed by microwaved and then conventionally furnaced specimens. Comparison of microwave-sintered and hot-pressed B_4C - 2.5 wt% C specimens using indentation fracture toughness measurements indicates a 25% greater toughness for the microwaved material. The mechanical properties determined for the hot-pressed B_4C - 2.5 wt% C (i.e., Young's modulus and fracture toughness) compare very closely to values recently reported[8] for similar density, pressureless-sintered specimens of the same composition. Further work is necessary with denser microwaved specimens to substantiate the observed apparent increase in fracture toughness.

Microwaving at 2.45 GHz and other recent work[11] indicates that temperatures over 2200° C are necessary to achieve densities over 90% of theoretical with boron carbide. Higher-density microwaved specimens of boron carbide may be achieved by producing higher temperatures through layering or "casketing" schemes, by vacuum microwaving (since vacuum conventional-sintering yields improved densification),[10] by use of low-level additives such as silicon carbide,[8] by particle deagglomeration or oxygen scrubbing to change surface properties or to activate the particle surfaces, or by varying the microwave frequency. One experiment using 28 GHz radiation (with "casketing" as used with 2.45 GHz radiation) has indicated the possibility of improved densification of boron carbide. Additionally, a variable-frequency (4-8 GHz with a 2 kW capability) microwave applicator is currently being assembled for testing with several refractory materials including boron carbide.

How high a temperature can one achieve with microwaving? Figure 14 shows a boron nitride crucible that contained molten yttria (mp = 2410° C): the boron carbide pellet floated up and the Grafoil coverings separated and floated. There may be ways to achieve even higher temperatures, and more work is needed in this area.

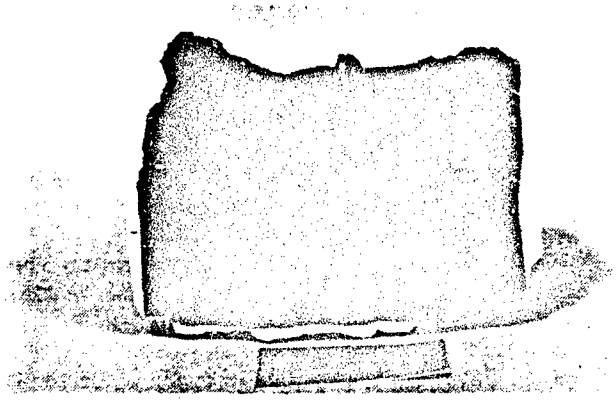


Figure 14. Melted yttria grit inside a boron nitride crucible containing a boron carbide specimen.

CONCLUSION

"Ultra" high-temperature microwave sintering at temperatures over 1900°C can be accomplished through appropriate "casketing" and addressing materials interactions. For titanium diboride and boron carbide, microwave sintering appears to offer advantages over conventional sintering or hot-pressing—including fabrication speed and possibly superior properties. Additional work is required to further define advantages of microwaving and to consistently produce higher density and larger specimens.

REFERENCES

1. C. E. Holcombe, and N. L. Dykes, "Importance of 'Casketing' for Microwave Sintering of Materials," *J. Matls. Sci. Letters, 9*, 425-428 (1990).

2. C. E. Holcombe and N. L. Dykes, "Microwave Sintering of Titanium Diboride," *J. Matls. Sci., 26*, in publication (1991).

3. C. E. Holcombe and N. L. Dykes, "A Method of Sintering Ceramic Materials," U.S. Patent Application in Progress (1990).

4. W. H. Sutton, "Microwave Processing of Ceramic Materials," *American Ceramic Society Bulletin*, *68* (2), 376-386 (1989).

5. C. E. Holcombe and N. L. Dykes, "A Titanium Diboride - Chromium Diboride - Yttria Ceramic Composition and a Process for Making Same," U.S. Patent Application in Progress (1990).

6. C. E. Holcombe, "Microwave Coupler and Method," U.S. Patent 4,559,429, issued December 17, 1985.

7. C. E. Holcombe, "New Microwave Coupling Material," *American Ceramic Society Bulletin*, *62* (12), 1388 (1983).

8. F. Thevenot, "Sintering of Boron Carbide and Boron Carbide - Silicon Carbide Two-Phase Materials and Their Properties," *J. Nucl. Matls.*, *152*, 154-162 (1988).

9. J. D. Katz, R. D. Blake, J. J. Petrovic and H. Sheinberg, "Microwave Sintering of Boron Carbide," *Microwave Processing of Materials*, Vol. 124 (Eds.: W. H. Sutton, M. H. Brooks, and I. J. Chabinsky), pp. 219-226 (1988).

10. K. A. Schwetz and G. Vogt, "Process for the Production of Dense Sintered Shaped Articles of Polycrystalline Boron Carbide by Pressureless Sintering," U.S. Patent 4,195,066, issued March 25, 1980.

11. S. L. Dole, S. Prochazka, and R. H. Doremus, "Microstructural Coarsening During Sintering of Boron Carbide," *Journal of American Ceramic Society*, *72*, 958-966 (1989).

12. C. E. Holcombe and N. L. Dykes, "High-Temperature Microwave Sintering of Nonoxide Ceramics," presented at The Am. Ceram. Soc. 91st Annual Meeting, Indianapolis, Indiana, April, 1989.

13. M. W. Moyer and J. P. Hammond, *Ultrasonic Measurements of Elastic Constants at Temperatures from 20 to 1100°C*, U.S. Energy Research and Development Report Y-2047, Union Carbide Corporation, Nuclear Division, Oak Ridge Y-12 Plant, Oak Ridge, Tennessee 37830 (1976).

14. A. G. Evans, "Fracture Toughness: The Role of Indentation Techniques," *Proc. of 11th National Symposium on Fracture Mechanics*, Pt. II, ASTM Special Publication 678, pp. 112-135 (1978).

MICROWAVE SYNTHESIS OF METAL CARBIDES

Hiromitsu Kozuka* and John D. Mackenzie
Department of Materials Science and Engineering
University of California, Los Angeles, Los Angeles, CA 90024

Microwave heating of metal oxide / graphite or glassy carbon powder mixtures was carried out in Ar, utilizing a commercial microwave oven operated at 2.45 GHz and 700 W. Temperatures of up to 1400 - 1500 °C could be obtained within 13 min, and SiC, TiC, NbC and TaC were formed within 20 min. This method was also shown to offer a new process for producing SiC whiskers. Not only the amount of carbon but also the compactness of the starting powders was found to be essential for heating efficiency.

INTRODUCTION

Many metal carbides have promise as high temperature structural materials because of their extremely high mechanical strengths, melting points and corrosion resistance. Metal carbides have been prepared by carbothermal reduction of metal oxides, direct reaction between metal elements and carbon, and gas phase reaction of metal halides and appropriate hydrocarbons[1]. On an industrial scale, carbothermal reduction of metal oxides is the most promising route due to the low raw materials cost. However, reaction temperatures for this route are generally high. Temperatures as high as 2200 - 2600 °C are needed for production of SiC and 1700 - 2100 °C for TiC[2]. If energies consumed in furnace operation are too high, development of new technologies for saving energy might be a very important issue for the industrial production of carbides. Another essential topic is a processing of carbide whiskers, which are used to toughen ceramic composites. There have been several methods used to prepare SiC whiskers, such as vaporization and deposition of SiC at high temperatures under reduced pressure[3], reductive decomposition of methylchlorosilane[4], thermal decomposition of rice hulls[5,6], and vapor-liquid-solid (VLS) process where silica is reduced and reacted with methane in contact with iron powders[7].

Recently the use of microwave energy has been attracting significant attention as a way of processing ceramic materials. One of the most important reasons for this is significant reductions in manufacturing costs due to energy savings and shorter processing times[8]. Heating by microwave takes place through transformation of the electromagnetic energy into thermal energy via absorption of microwave by microwave-susceptible components. This is particularly important because microwaves can penetrate powders instantaneously whereas in conventional heating, heat transfer is very slow for powder compacts. Hence internal and volumetric heating of the materials is possible and the energy conversion effeciency is thought to be higher than that through conventional furnace heating.

In the present study, the authors attempted to synthesize metal carbides from

* Present address: Institute for Chemical Research, Kyoto University, Uji, Kyoto-Fu 611 Japan.

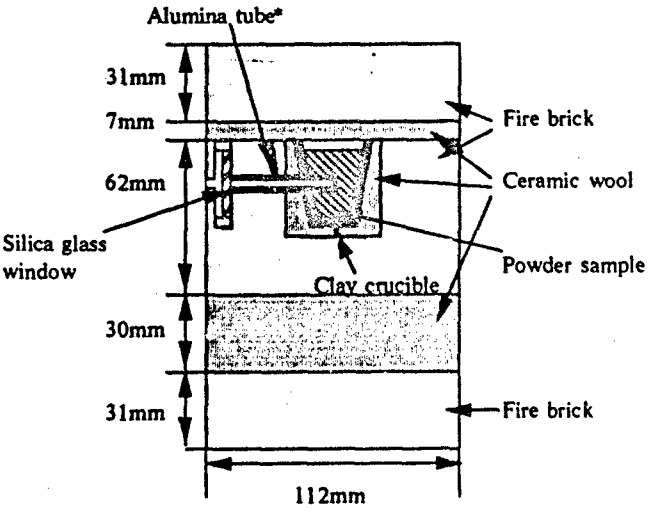
metal oxide / carbon powder mixtures using a commercial microwave oven, in order to evaluate the possibility of carbide production by microwave processing.

EXPERIMENTAL

For the C/SiO_2 mixtures, reagent grade quartz powders (-325 mesh) or silica gel powders (60-200 mesh), and graphite powders (-300 mesh) or spherical glassy carbon granules (3-12 μm in diameter) were used. For the C/TiO_2, C/Nb_2O_5 and C/Ta_2O_5 mixtures, graphite powders and reagent grade of TiO_2, Nb_2O_5 and Ta_2O_5 powders were used. Mole ratios of carbon to metal oxides, batch weight and volume, and batch carbon content are shown in Table 1. The powder mixtures

Table 1 Powder mixtures used in the present microwave processing.

Metal oxide	Carbon	Mole ratio	Weight (g)	Volume (cm^3)	Carbon content (g)
For C/SiO_2					
Quartz	Graphite	C/SiO_2	10.0	11.0 - 13.5	1.2-4.4
		= 0.7 - 4	15.0	11.0 - 13.5	1.9-6.7
Quartz	Glassy carbon	C/SiO_2 = 3	10.0	12.5	3.7
Silica gel	Glassy carbon	C/SiO_2 = 3	8.0	12.5	3.0
For C/TiO_2, C/Nb_2O_5 and C/Ta_2O_5					
TiO_2	Graphite	C/TiO_2 = 3	8.2	16.5	2.6
Nb_2O_5	Graphite	C/Nb_2O_5 = 7	13.0	16.5	3.1
Ta_2O_5	Graphite	C/Ta_2O_5 = 7	15.0	16.5	2.4



* The end of the tube inserted in the sample is closed with alumina powder compact.

Figure 1 Sample holder and insulator for the microwave heating.

were put in a clay crucible of 25 mm in bottom diameter, 41 mm in top diameter, 43 mm in height and 3 mm in thickness, which was placed in an insulator made of fire bricks and ceramic wool and having a window for observation at the center of the powder for temperature measurement by optical pyrometery as illustrated in Fig. 1. This was then placed in a plastic bell jar, in which Ar was passed, and put in the cavity of a commercial microwave oven (General Electric Co. Model JE 1453H) operated at 2.45 GHz and 700W. Temperature was measured using Mikron M77S 2-color optical pyrometer. Phases in the products were identified by powder X-ray diffraction measurement using Cu Kα radiation.

RESULTS

Formation of silicon carbide

Formation of SiC from the mixtures of quartz / graphite, quartz / glassy carbon and silica gel / glassy carbon was observed within 15 min of microwave

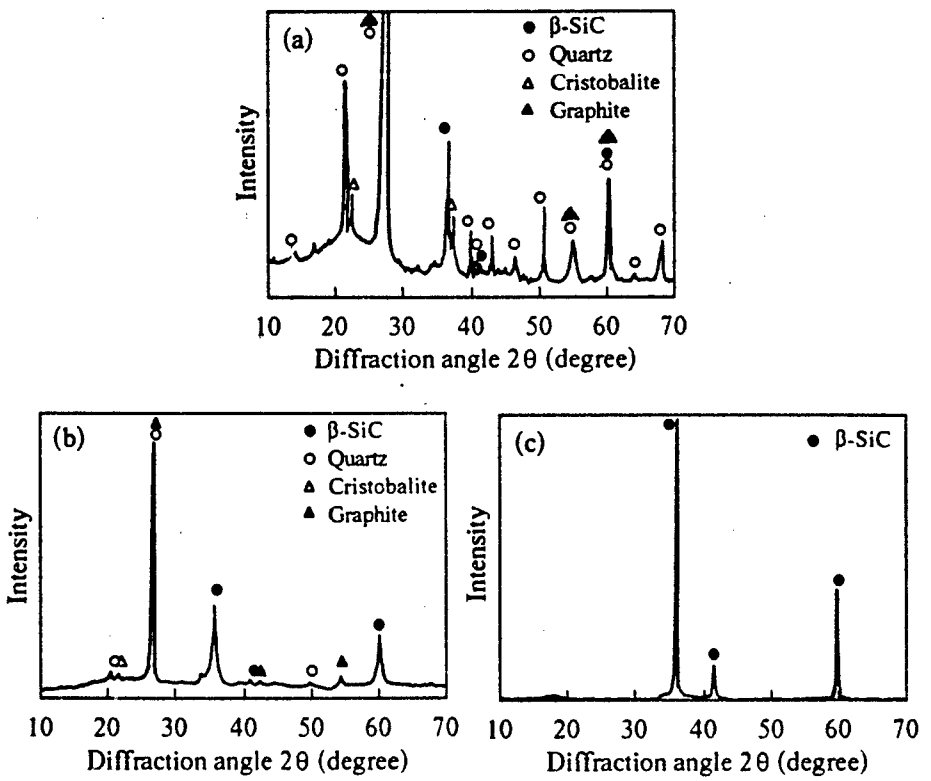


Figure 2 XRD patterns of the products from the C/SiO2 mixtures of R = 3 heated for 15 min. The whole (a) and the central part (b) of the 10 g quartz / graphite mixtures, and the central part of the 8 g silica gel / glassy carbon mixture (c).

exposure. Diamond powder was tested in place of graphite or glassy carbon but no heat generation was found. X-ray diffraction (XRD) patterns (Fig. 2) of the products from the 10 g quartz / graphite mixtrue of C/SiO_2 mole ratio R = 3 heated for 15 min have SiC peaks of higher intensity for the inner part than the outer part of the sample. The inner portion of the sample was lightly green in color whereas the outer portion was black, gray or white. The main SiC phase formed was β-SiC. The green-colored inner part of the product obtained from the silica gel / glassy carbon mixture had dominant SiC XRD peaks.

The 10 g powder mixtures of quartz / graphite of R = 3 and 4 showed rapid temperature increase up to 1400 - 1500 °C within 4 min as shown in Fig. 3 (a). Temperature drops observed at about 1400 °C are thought to be due to the endothermic reaction of $SiO_2 + 3C \rightarrow SiC + 2CO$. Heating ability of the mixtures is reduced with decrease in the graphite content, which can be seen in the time - temperature curves for the powders of R = 0.85 and 1.

Graphite content dependence of the heating ability changes, however, when the starting powder mixture is pressed to give denser packing. The 15 g powders pressed to the same volume as the 10 g powders had time - temperature curves as shown in Fig. 3 (b). The 15 g pressed powder mixture of R = 0.7, which could not be heated within 15 min for 10 g unpressed state, reached 1500 °C in 15 min, and that of R = 1 reached 1500 °C in 7 min. As seen in the curves for R = 3 and 4, however, lower heating rates were observed. There was no SiC formation for the pressed samples of R = 3 or 4.

Scanning electron micrographs reveal the formation of SiC whiskers of thickness around 0.2 μm from quartz / graphite mixtures as shown in Fig. 4 (a). Whisker formation was also observed for the products from the quartz / glassy carbon mixtures. When silica gel was used as the Si source, however, micrometer-sized SiC crystals were formed instead of whiskers as shown in Fig. 4 (b).

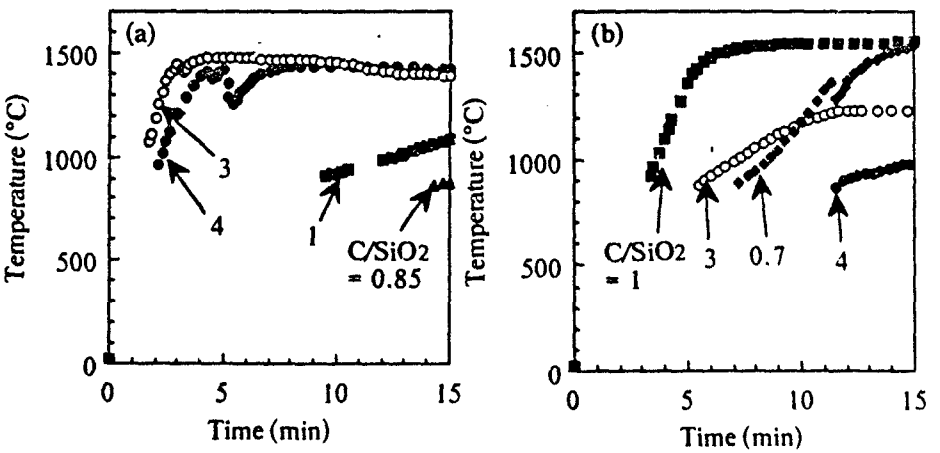


Figure 3 Time -temperature curves of the 10 g unpressed (a) and 15 g pressed (b) quartz / graphite mixtures.

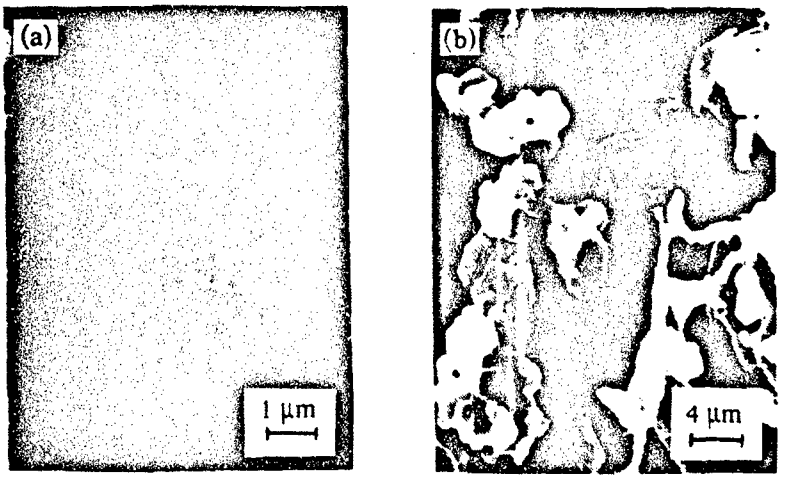


Figure 4 SEM pictures of the heated products from the quartz / graphite (a) and silica gel / glassy carbon (b) mixtures.

Formation of titanium carbide, niobium carbide and tantalum carbide

Figure 5 shows XRD patterns for the products obtained by heating the mixtures of graphite and TiO_2, Nb_2O_5 and Ta_2C for 20 min. Formation of TiC, NbC and TaC is seen in the XRD patterns. Compared with the XRD pattern of the heated product from the quartz / graphite mixture shown in the top of Fig. 2, relatively higher yield of the carbides, especially for NbC and TaC, is found for these metal carbides. Time - temperature curves for these mixtures shown in Fig. 6 reveal that temperature goes up to 1400 °C within 7 - 13 min and the maximum temperature they had was 1400 - 1500 °C.

DISCUSSION

Factors affecting the microwave heating of oxide / carbon powder mixtures

Heating of carbon particles takes place via the Joule effect caused by microwave-induced electrical current in the particles[9]. Therefore it is reasonable to find no heating for non-conducting diamond powder. Heat generated in the carbon particles is transferred through oxide particles and pores, but because of the low thermal conductivity of the oxide particles and pores, the heat can be trapped at the interface of the carbon / oxide or carbon / pore interface. In order to have sufficient heat generation, however, a minimum amount of carbon powders is required in the batch, which is shown in the time - temperature curves of the 10 g quartz / graphite mixture of R = 3 (Fig. 3 (a)).

Skin effect should also be taken into account. Conductive materials have penetration depth d, defined as the depth at which electromagnetic field strength decays to 1/e of that at their surface, and d is given by

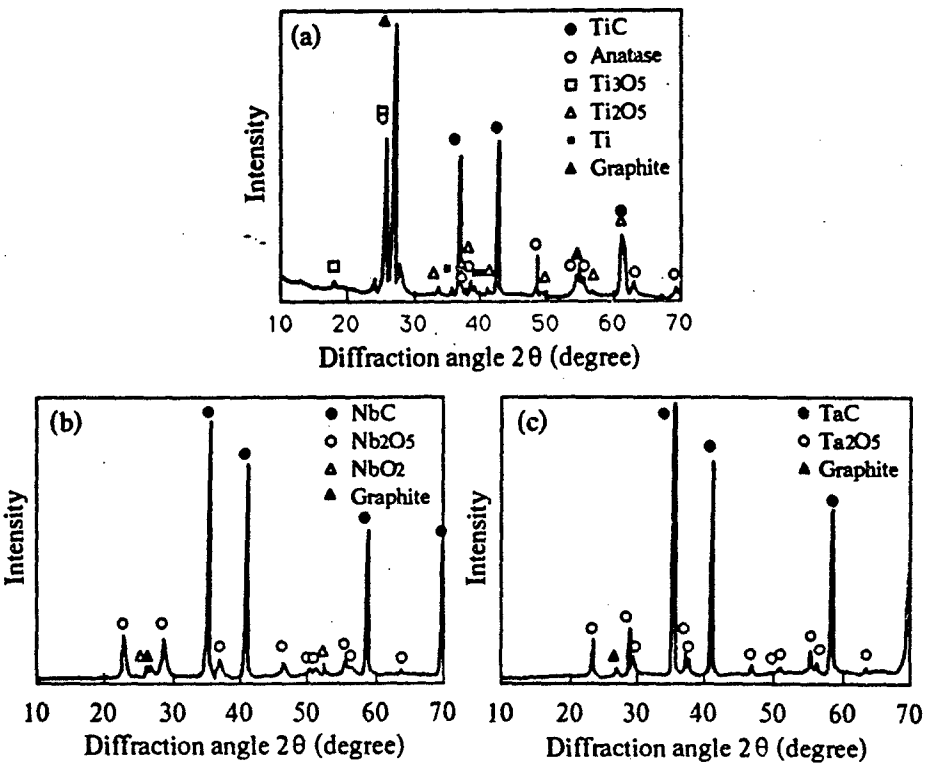


Figure 5 XRD patterns of the products from the C/TiO2 (a), C/Nb2O5 (b) and C/Ta2O5 (c) mixtures heated for 20 min.

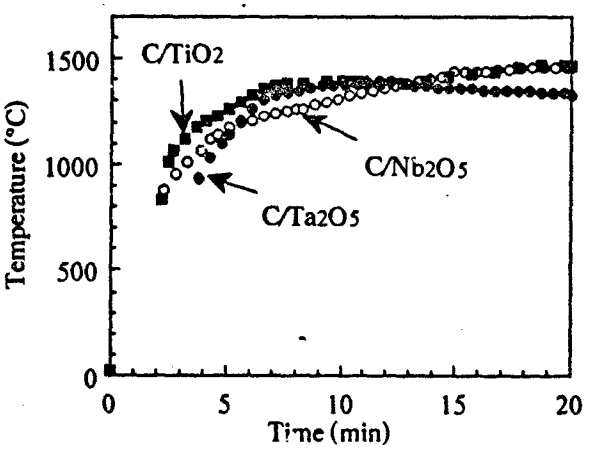


Figure 6 Time - temperature curves of the C/TiO2, C/Nb2O5 and C/Ta2O5 mixtures.

$$d = (\pi f \mu \sigma)^{-1/2} \quad (1)$$

where f is the frequency of the electromagnetic field, σ is the conductivity and μ is the permeability of the material[9]. Conductivity of $10^3\ \Omega^{-1}cm^{-1}$, which is the case with graphite at room temperature, results in d = 30 μm for 2.45 GHz microwave, which is almost the same order as the size of the graphite powders used here. For the pressed powder mixtures as the 15 g quartz / graphite mixture of R = 3, it is possible that some of the graphite particles were in contact with each other to form larger agglomerates, and since the specific surface area of the agglomerates is smaller than that of non-agglomerated particles, the volume of the skin per unit weight of graphite would be smaller. This effect is more evident for mixtures of higher graphite content. As a matter of fact, a dense graphite piece cannot be heated in the microwave oven and it just reflects the microwave to cause arcing. This is the reason for the decrease in heating capability for the 15 g quartz / graphite mixtures of higher graphite content. Similar experimental phenomena were observed in copper / alumina and chromium / alumina mixtures, where copper or chromium particles generate heat under microwave exposure[10].

Formation of silicon carbide whiskers

The microwave method presented here is a new process for preparing SiC whiskers. The whiskers are thought to be formed through vapor phase reaction, since formation of droplets on the tip of the whiskers, which is the evidence of vapor-liquid-solid process[11], could not be found. On the other hand, whiskers were not found in the product from the silica gel / glassy carbon mixture. Formation of glass and glass melt during heating, which does not happen for quartz crystals below melting point, might have some influence on the final microstructure of the product from the gel / carbon mixture.

Thermodynamic consideration on the metal carbide formation

Free energy change ΔG at various temperatures for the conversion of oxide / graphite mixtures into carbide / carbon monoxide mixtures was calculated on the basis of the published data of free energy of each component[12], and the temperatures where ΔG becomes 0 were evaluated (Table 2). It can be seen that

Table 2 Chemical reactions for the formation of carbides and temperatures where free energy change ΔG becomes 0.

Products	Reaction formula	Temperature of ΔG = 0 (°C)
β-SiC	$SiO_2 + 3C \rightarrow SiC + 2CO$	1520
TiC	$TiO_2 + 3C \rightarrow TiC + 2CO$	1270
TaC	$Ta_2O_5 + 7C \rightarrow 2TaC + 5CO$	1110
$NbC_{0.98}$*	$Nb_2O_5 + 6.96\ C \rightarrow 2NbC_{0.98} + 5CO$	950

*Free energy data of NbC was not available in the literature.

formation of NbC and TaC is possible at much lower temperature than SiC. That must be the reason for the observation of the higher relative intensity of the XRD peaks for NbC and TaC. Better insulation and higher power of microwave, which enables higher temperature achievement, should improve the yield of SiC.

CONCLUSION

SiC, TiC, NbC and TaC could be produced from metal oxide / carbon mixtures under microwave exposure, and SiC whiskers were found to be formed from quartz / carbon mixtures. For the mixtures of higher carbon content, compactness of the powders was shown to decrease the heating ability.

References

[1] R.H. Smoak, T.M. Korzekwa, S.M. Kunz and E.D. Howell, "Carbides"; pp. 476-535 in *Kirk-Othmer Encyclopedia of Chemical Technology*, 3rd Edition, Vol. 3. Edited by M. Grayson, D. Eckroth, M. Bickford, G.J. Bushey, L. Campbell, A. Klingsberg and L. van Nes, John Wiley, NY, 1978.

[2] J.W. Tereskko, "Carbides"; pp. 130-139 in *Encyclopedia of Industrial Chemical Analysis*, Vol. 8. Edited by F.D. Snell and L.S. Ettre, Interscience Publishers, NY, 1969.

[3] W.F. Knippenberg and G. Verspui, "Growth Mechanisms of Silicon Carbide in Vapor Deposition II"; pp. 108-122 in *Silicon Carbide - 1973.* Edited by R.C. Marshall, J.W. Faust Jr. and C.E. Ryan, University of South Carolina Press, Columbia, South Carolina, 1973.

[4] C.E. Ryan, I. Berman, R.C. Marshal, D.P. Considine and J.J. Hawky, "Vapor - Liquid - Solid and Melt Growth of Silicon Carbide," *J. Crystal Growth*, 1, 255-262 (1967).

[5] J.-G. Lee and I.B. Cutler, "Formation of Silicon Carbide from Rice Hulls," *Ceram. Bull.*, 54, 195-198 (1975).

[6] N.K. Sharma and W.S. Williams, "Formation and Structure of Silicon Carbide Whiskers from Rice Hulls," *J. Am. Ceram. Soc.*, 67, 715-720 (1984).

[7] J.V. Milewski, F.D. Gac, J.J. Petrovic and S.R. Skaggs, "Growth of Beta-Silicon Carbide Whiskers by the VLS Process," *J. Mater. Sci.*, 20, 1160-1166 (1985).

[8] W.H. Sutton, "Microwave Processing of Cermic Materials," *Ceram. Bull.*, 68, 376-386 (1989).

[9] A.R. Von Hippel, *Dielectrics and Waves*; pp. 61. John Wiley, NY, 1954.

[10] E. Bescher and J.D. Mackenzie, "Microwave Processing of Cermets"; included in this volume.

[11] R.S. Wagner and W.C. Ellis, "Vapor - Liquid - Solid Mechanism of Single Crystal Growth," *Appl. Phys. Lett.*, 4, 89-90 (1964).

[12] JANAF Thermochemical Tables 3rd Edition. Edited by M.W. Chase Jr., C.A. Davies, J.R. Downey Jr., D.J. Frurip, R.A. MacDonald and A.N. Syverud, American Chemical Society and American Institute of Physics for the National Bureau of Standards, NY, 1986.

PRODUCTION OF ULTRA-FINE SILICON CARBIDE BY FAST FIRING IN MICROWAVE AND RESISTANCE FURNACES

S.N. Kumar*, A. Pant*, R.R. Sood*, J. Ng-Yelim** and R.T. Holt***
* Ceramics Kingston Inc., Box 655, Kingston, Ontario K7L 4X1, Canada
** Metals Technology Laboratories, CANMET, Ottawa K1A 0G1, Canada
***Institute for Aerospace Research, National Research Council, Ottawa Ontario K1A 0R6, Canada

ABSTRACT

Ultra-fine SiC powder has been synthesized by the carbothermal reduction of silica by microwave and conventional firing techniques. Analysis of these powders by transmission electron microscopy, Auger electron spectroscopy and X-ray diffraction has shown the formation of β-SiC. The crystallite size of β-SiC produced by the microwave and conventional firing techniques range from 30-200 nm and 50-450 nm respectively. The product obtained from conventional firing also revealed stacking faults over a number of crystallites.

INTRODUCTION

Nanophase materials have recently attracted increasing interest in the fabrication of dense advanced ceramics. They are known to possess a variety of novel and useful properties [1-4], which are often superior to those of their coarser grained counterparts. Using nanophase SiC particles in conjunction with boron and carbon as sintering aids, nearly dense bodies of SiC have been obtained by pressureless sintering [4]. Froes et. al.[5] and Karch et. al. [6] have shown that ultra-fine grained TiO_2 and CaF_2 do not possess the inherent brittleness of their conventional counterparts. Beside the known improvements in the mechanical properties offered by nanophase ceramics, the possibility of easily doping them with impurities at relatively low temperatures through their dense grain-boundary network (with only a few atomic jumps separating their grain-boundaries) also allows an efficient introduction of impurity levels into their band gaps. This would offer a good possibility of controlling their electrical and optical properties.

The use of microwaves in ceramic processing is gaining importance owing to the inherent advantages of microwave heating. Since microwave energy can continuously couple to a material and is not limited by the thermal diffusion process, a material can be heated, at least theoretically, to any desired temperature. The main advantages of microwave processing over conventional processing are: (1) high heating rates, (2) instantaneous application or removal of energy thereby lending the possibility of controlled temporal heating profiles [7], (3) improved thermal diffusion (4) limited grain growth (however, the time and temperature dependency would be critical), (5) high energy transfer efficiency, (6) localized energy deposition and (7) more uniform and better chemical properties.

Technological benefits would include the possibility of higher production throughput and a lower capital cost. Thus, Katz et. al. [8] have observed that sintering of boron carbide could be accomplished with microwaves at a temperature of 1900 - 2000 °C, whereas conventional heating required a temperature of 2150 - 2200 °C. The cost of microwave equipment was $ 35,000 versus $ 120,000 to 200,000 for the conventional equipment, and the sintering times for the microwave and conventional heating were reported to be 12 min and 1-2 hr respectively.

The high hardness, high thermal conductivity, high-temperature resistance and chemical stability make ultra-fine SiC a potentially interesting material both in fundamental research and technological use. There are two principal routes to produce submicron silicon carbide: (a) carbothermal reduction of silica or compounds containing silica, and (b) pyrolysis of silane compounds. The production of β-silicon carbide from silicious material and the Acheson process of making α-silicon carbide belong to the first category, whereas the synthesis of SiC through decomposition of silanes belongs to the second category. The objective of the present work was to investigate the concept of microwave fast firing technologies developed at Ceramics Kingston Inc., and to compare the powder thus obtained with that produced by conventional firing techniques. This paper gives only a preliminary account of the study initiated. A detailed investigation of the kinetics of the reactions involved and the structural characterization of the product formed (by using X-ray photoelectron spectroscopy and Fourier transform infrared spectroscopy) is underway to fully understand and improve the quality and yield of the product obtained.

EXPERIMENTAL

Conventional Heating

Sample loads of amorphous silica and carbon (up to 3 g) were heated in graphite crucibles (2.5 cm diameter) in a pulsed resistance heated vacuum furnace (CKC model JB-1). The thermocouple was located in the reactant material. In all cases the samples were evacuated at room temperature and the furnace temperature ramped to approximately 1000 - 1200 °C in 2 hours. After a soak period at the intermediate temperature the furnace was pulsed to final temperature (> 1500 °C) in about one minute. Soak period at this temperature was up to 11 minutes. The samples were cooled to the ambient with the furnace power off.

Microwave Heating

Precursor samples of amorphous silica and carbon (a total charge of up to 3 g) were placed in a single mode microwave cavity and heated using microwave power. The power source was a CKC model WK - 10 - 800 W variable power unit. Power was coupled via a slide screw tuner to the cavity. The cavity was pumped down using a Edwards model EM2 - 28 rotary vacuum pump. Base pressure for all the tests was 0.4 m bar. The forward power for all the tests was 750 - 800 W. Reflected power was varied between 100 and 200 W. Temperature measurements made at the beginning of the run using a retractable thermocouple (temperature measurements taken with the power off) indicated that the initial ramp rate was significantly higher than 10 °C/min. The samples were soaked at the final

temperature for a period of up to 11 min. In some cases plasma formation was observed.

Optical pyrometer measurements at the elevated temperatures were confounded by the fact that the outer surface of the sample remained cold while the inner regions appeared to be hot. Visual observations suggested that the actual inner temperature of the sample was considerably higher than the measured temperature of 1300 °C, but this cannot be confirmed with any accuracy. Post facto product analysis indeed confirmed that the temperature exceeded that required for reaction initiation, but the actual temperature achieved remains unknown. In our experience fiber optic probes probably give the least spurious temperature measurements in a microwave environment and further tests are planned using these probes. Typical microwave power and absorption curves are shown in Fig. 1.

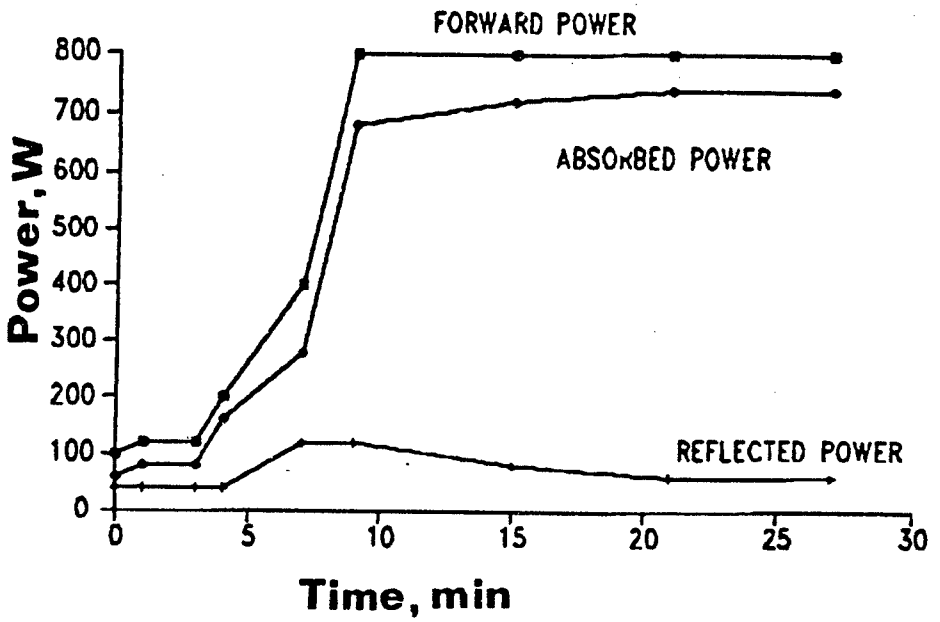


Fig. 1. Typical microwave power and absorption curves.

Sample Analysis

After completion of the reaction (by either of the above two methods), the product was scrapped off the furnace and analyzed. For examination by transmission electron microscopy (TEM), the powders were collected on holey carbon films supported on copper grids. They were then examined in a Philips 400 TEM/STEM to determine particle size, distribution and morphology. The compositions of the powders were determined by energy dispersive X-ray analysis (EDAX) and electron energy loss spectroscopy (EELS). The crystalline structures

were determined by convergent beam microdiffraction (CBMD). The X-ray diffraction measurements were performed on a Siemens type F diffractometer using monochromated Cu Kα radiation and a Si (Li) detector. Auger analysis was performed using a PHI 600 model Auger spectrometer. The powder samples were loosely pressed over a thin indium foil and analyzed with a 10 kV beam at currents of 0.05 - 1.8 μA. Argon ion sputtering was performed with a 2 kV beam, rastered over a 4 mm^2 area. The powder samples are submicron particles, therefore individual particles were not analyzed. Generally a 20x20 μm area was analyzed giving an average analysis.

RESULTS

TEM Data:

Figure 2 (a) shows a typical TEM micrograph and CBMD pattern of the stoichiometric microwave processed SiC powder.

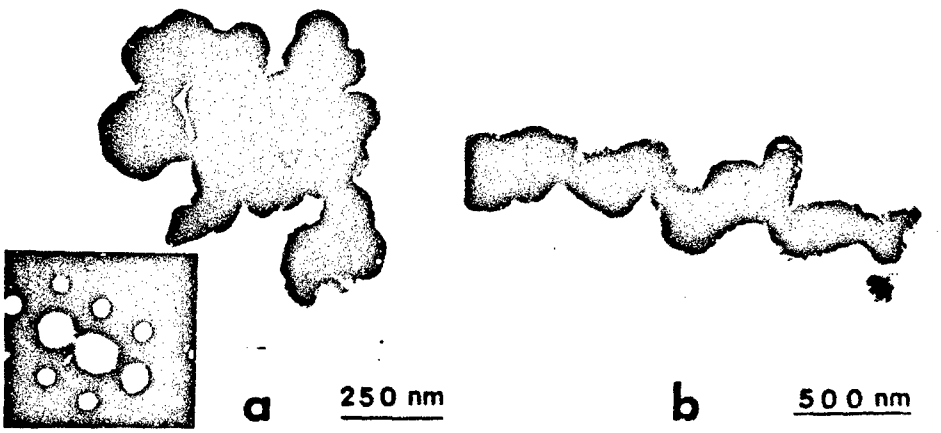


Fig. 2 Micrographs of (a) microwave annealed and (b) conventionally fired SiC samples with stoichiometric amounts of reactants. The inset in (a) shows a CBMD pattern with [0 $\bar{1}$ 1] zone axis.

The SiC particles are plate-like and some are hexagonal shaped. They range in size from 30 - 200 nm. The CBMD pattern (shown in the inset) with a [0 $\bar{1}$ 1] zone axis confirms the crystal structure of the SiC powder to be face centered cubic with a = 0.43589 nm. Figure 2(b) shows a TEM micrograph of a conventionally fired sample with stoichiometric quantities of precursor materials. These SiC particles are mainly plate-like, ranging in size from 100 nm to 450 nm. Stacking faults are observed in many of these particles. The chain-like agglomeration observed in this conventionally fired material is of interest. At present the nature and strength of the interparticle bond is not known, but such agglomerations will certainly be

detrimental for the successful densification of the powders if their bonds cannot be broken.

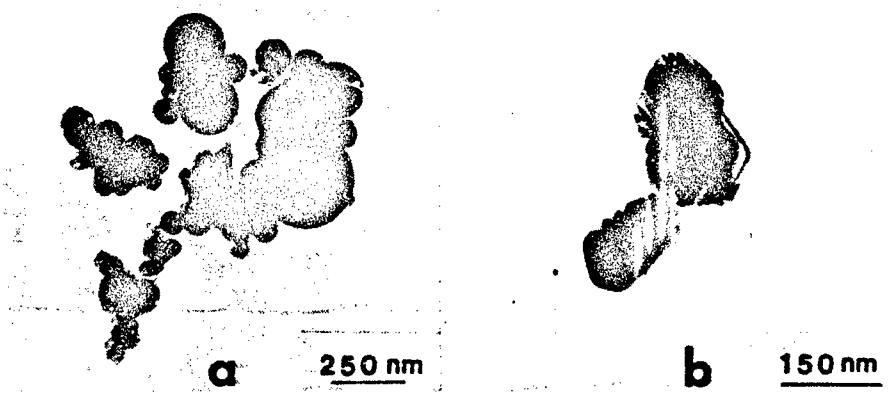


Fig. 3(a) TEM of microwave annealed SiC with 2.5 mol% excess carbon, (b) TEM of conventionally fired sample with 2.5 mol% excess carbon.

One of the objectives of the present experiments was to study the effect of small batch-to-batch variations in the silica and carbon contents that may result during large scale production operations. For this purpose, carbothermic reduction was carried out in both the conventional and microwave furnaces with 1-5 mol % excess of carbon over stoichiometric quantities. Figure 3(a) shows electron micrographs of microwave annealed samples obtained from 2.5 mol % excess of carbon in the reactant precursor. A significant amount of spherical shaped unreacted material is observed. This unreacted material was amorphous. The micrograph of the conventionally fired precursors with 2.5 mol % excess carbon is shown in Fig. 3(b). Here again the plate-like nature of the SiC particles are observed. The crystalline particles range in size from 50 - 250 nm and stacking faults are observed in some of them.

XRD Data:

Figure 4 shows the X-ray diffraction patterns of the microwave and conventionally fired samples with the stoichiometric quantities of the reactants. The pattern of the microwave heated sample shows β SiC [(SiC)-8H] structure in which the characteristic peaks are observed at $2\theta = 35.7$, 41.47, 60.15, and 71.92°. The β-(cubic) structure is preferred for structural ceramics applications. The pattern involves small peaks due to C [(C) 12H] at $2\theta = 63.47°$ and SiO_2. Figure 5 shows the XRD patterns of the microwave and conventionally fired samples with 2.5 % excess of carbon over the stoichiometric quantities of the reactants. These also show predominantly the β-SiC phase in both the samples. The peak at $2\theta = 35.13°$ is due to the unreacted SiO_2 while those at 120.87, 132.54 and 142.56° are likely due to C.

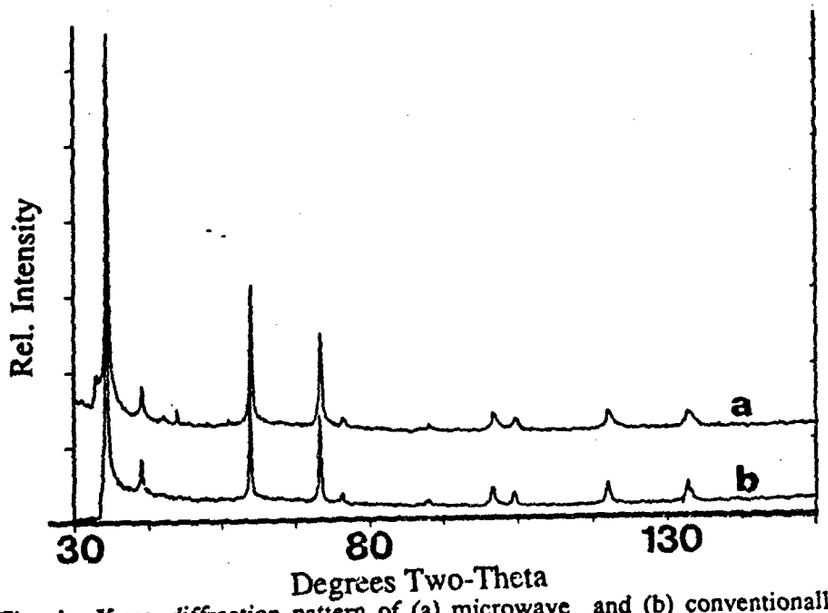


Fig. 4. X-ray diffraction pattern of (a) microwave and (b) conventionally processed SiC with stoichiometric amounts of reactants.

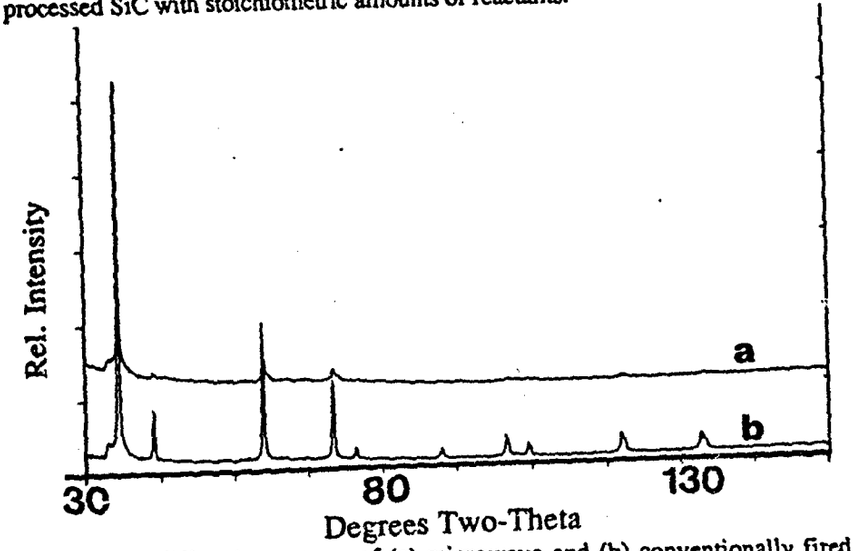


Fig. 5. X-ray diffraction pattern of (a) microwave and (b) conventionally fired samples with 2.5 mol% excess carbon added during firing.

DISCUSSION AND CONCLUDING REMARKS:

The overall reaction of formation of SiC through carbothermal reduction of silica can be represented as:

$$SiO_2 + 3\,C \text{ ----------> } SiC + 2\,CO_{(g)} \quad (1)$$

$$\Delta G^\circ_T = 609.023 - 0.351\,T \text{ (kJ/mol)}$$

where ΔG°_T is the standard free energy change for the reaction, and T is the temperature in Kelvins. The reaction is highly endothermic and proceeds above 1500 °C for a partial pressure of CO below 0.1 MPa. The standard free energy of reaction (1) was calculated by the usual estimation : $\Delta G^\circ_T = \Delta H^\circ_{298} - T\Delta S^\circ_{298}$.

Reaction (1) can be viewed as proceeding in the following steps:

$$SiO_2 \text{ ----------> } SiO_{(g)} + O \quad (2)$$

$$O + C \text{ ----------> } CO_{(g)} \quad (3)$$

$$SiO_{(g)} + 2\,C \text{ ----------> } SiC + CO_{(g)} \quad (4)$$

It has been reported by Bluementhal et. al. [9] that an increase in the reaction rate with increasing interface area between reactants occurs as the particle size of silica was decreased. They concluded that the formation of gaseous SiO occured in all the mixtures of silica and carbon with the C : SiO_2 molar ratio from 0.86 to 3.0. Klinger et. al. [10] have studied reactions between silica and graphite from 1445 to 1765 °C. They observed that the particle size of the SiC reaction product was close to that of the original graphite particles and that the measured weight loss data could be explained only by assuming the dissociation of silica into oxygen and gaseous SiO (reaction 2), which subsequently reacted with graphite to form SiC. From their investigation of reactions of rice hulls (containing 10 to 15 wt. % silica and cellulose), Lee and Cutler [11] concluded that the rate controlling step for the SiC formation was the formation of SiO. An increase in the rate of reaction (1) was observed as the surface area of the catalyst was increased. The formation of gaseous SiO thus seems to be an important rate determining step in the overall yield of SiC formation. The equilibrium partial pressure of SiO over solid SiO and carbon is 0.1 kPa at 1430 °C, 0.2 kPa at 1530 °C and 5.1 kPa at 1630 °C [10]; therefore, retention of gaseous SiO and removal of CO gas, as the reaction proceeds, are essential to shift the overall reaction (1) in the favourable direction of high yield for SiC.

The AES data of the microwave and conventionally annealed samples (with the Auger sensitivity factor calibration done using a single crystal of SiC) have shown that the total Si/C ratio for both these samples were close to 0.6. Such a high concentration of carbon was also seen in the other two microwave and conventionally fired samples, with 2.5 mol % excess carbon over the stoichiometric quantities. This ratio was not markedly changed even after a depth profiling of ~ 6000 Å. In all the samples, the surface carbon peak shape clearly showed the presence of graphitic carbon and the carbon of carbide. Thus, about 40 at %

excess carbon (with the valid assumption that the carbon contamination from the AES system would be equal in both the standard SiC crystal and the fired samples) seems to be present in both of them. Such a large excess carbon was not noticed in the XRD data. Therefore, most of the carbon seen in the elemental form remains amorphous. This was also noticed in the TEM micrographs where a relatively large number of clusters of unreacted spherical microreactors were observed at many places with their diffraction pattern showing an amorphous nature. Comparison of the X-ray diffraction peak integrated intensities of crystalline SiC versus crystalline silica for the microwave and conventionally annealed samples shows that about 40 at % and 30 at % respectively of crystalline silica remain in these samples. These data suggest that out of a total of 60 at % Si (as SiC and SiO_2), about 40 at % or 30 at % are bound with SiO_2 in the microwave and conventionally annealed samples respectively. Consequently, the remaining amount of only 20 at. % or 30 at. % is actually consumed in the formation of SiC. Further the high amount of about 40 at. % of unreacted carbon present in both these samples, as shown by AES, also corroborates with these results. Since only 30 at. % (as compared with 40 at. % for the case of microwave annealed sample) is crystalline in the conventionally fired sample, the remaining 10 at. % of SiO_2 seems to remain unchanged from the original amorphous form.

In conclusion, the work done to date indicates that microwave heating is a feasible technique for the production of ultra-fine silicon carbide. A small excess of C (1 - 5 mol %) does not seem to change the crystallite size of the product formed.The crystallite size of β-SiC produced by the microwave and conventional firing techniques range from 30-200 nm and 50-450 nm respectively. A preliminary comparison with conventional fast firing tentatively indicates that both firing techniques are very similar in terms of the product yield. Further comparative experiments are underway.

ACKNOWLEDGEMENTS: The skilful assistance of Dr. L. Dignard in the AES and E. Cousineau and P. Fryzuk in the XRD analyses is gratefully acknowledged.

REFERENCES:

[1] C.G. Granqvist and R.A. Buhrman, J. Appl. Phys., **47**, 2200 (1976)
[2] K. Kimoto, Y. Kamiya, M. Nonoyama and R. Uyeda, Jpn. J. Appl. Phys., **2**, 702 (1963).
[3] R.W. Siegel and J.A. Eastman, Mater. Res. Soc. Symp. Proc., **132**, 3 (1989).
[4] T. Hase and H. Suzuki, Yogyo-Kyokai-Shi, **88**, 258-264 (1980).
[5] F.H. Froes and C. Suryanarayana, J. Metals, **41**, (6), 12 (1989).
[6] J. Karch, R. Birringer and H. Gleiter, Nature, **330**, 556 (1987).
[7] W.R. Tinga, Presented at the 1988 MRS Spring Meeting, Reno, NV (1988) (unpublished).
[8] J.D. Katz, R.D. Blake, J.J. Petrovic and H. Shenberg, ibid.
[9] J.L. Bluementhal, M.J. Santy and E.A. Burns, AIAA J., **4**, 1053 (1966).
[10] N. Klinger, E.L. Strauss and K.L. Komarek, J. Am. Ceram. Soc., **49**, 369 (1966).
[11] J.G. Lee and I.B. Cutler, Am. Ceram. Soc. Bull., **54**, 195 (1975).

CHARACTERIZATION OF SILICON NITRIDE SYNTHESIZED BY MICROWAVE HEATING

J. O. Kiggans, C. R. Hubbard, R. R. Steele, H. D. Kimrey,
C. E. Holcombe, and T. N. Tiegs - Oak Ridge National Laboratory,
P.O. Box 2008, Oak Ridge, TN 37831-6087

ABSTRACT

Recently, a new procedure was developed for the nitridation of high purity silicon via microwave heating. Silicon samples were processed to various stages of nitridation utilizing microwave heating and then analyzed by X-ray diffraction and by scanning electron microscopy. These data were compared to that obtained from samples nitrided by conventional heating methods.

INTRODUCTION

Reaction-bonded silicon nitride (RBSN) is a leading candidate for several ceramic components for high temperature fuel combustion. A great body of research has been devoted to conventional heating methods to produce RBSN materials. Researchers have shown this process to most likely have two steps--a low temperature process (1200 to 1300°C) in which SiO (gas) combines with nitrogen to produce predominantly α-Si_3N_4 and a later high-temperature process (1300 to 1400°C) in which silicon metal and nitrogen react in a liquid-phase process to produce β-Si_3N_4 [1,2]. The overall combined reaction is an exothermic or self-propagating high-temperature synthesis type reaction [3].

However, the actual process of producing RBSN products has been plagued by several problems: (1) the need to utilize silicon particulates with high iron content, (2) high temperature gradients generated by the exothermic reaction itself, and (3) poor penetration of nitrogen into silicon bodies as nitridation proceeds [1].

In recent years, microwave energy has been introduced as a possible avenue to achieve superior processing of ceramics [4]. By direct coupling, microwaves can "volumetrically" heat materials with favorable dielectric properties. This is very different from conventional heating processes, which rely on external radiant energy to heat materials. Microwave heating also appears to enhance diffusion of certain chemical species in ceramics and accelerates certain processes [5].

Holcombe and coworkers [6] discovered that high-purity silicon metal compacts were heated quiet efficiently by microwave energy at 2.45 GHz. This paper presents results obtained from a comparison of the nitridation of high-purity silicon utilizing microwave and conventional heating. Since our ultimate goal is the sintering of RBSN materials, we have also included some results on the nitridation of RBSN containing sintering additives.

EXPERIMENTAL PROCEDURE

Samples were prepared by two methods: (1) ~100 g quantities of unprocessed silicon powder* were isopressed at 137 MPa (20 ksi), (2) silicon plus other additives such as silicon nitride,† aluminum oxide,** or yttrium oxide†† were milled together in isopropanol for 2 to 6 h and dried. The powder was then isopressed as above. Samples, and the silicon nitride powder which some of the samples were ultimately packed in, were heated a minimum of 3 h at 140°C prior to furnace runs to remove any absorbed water.

The insulation arrangement used in the microwave heating experiments has been previously discussed [7]. A Type "C" thermocouple was inserted into a 0.25 in. hole drilled to the center of the sample for measurement purpose and for control feedback to a microwave power controller. In addition to the control thermocouple, other thermocouples were used to measure the temperature of the surface of the sample and of the insulating materials. In some cases, an alumina sight tube was inserted into a hole drilled adjacent to the control thermocouple and to the center of the sample. This sight tube was used for infrared pyrometer measurements.

Prior to runs in the microwave furnace, the cavity was pumped down to 600 millitorr and then backfilled with nitrogen . Experiments were performed with flowing nitrogen.

Comparison heating experiments were performed in a graphite element furnace. In the initial heating experiments, samples were packed in silicon nitride powder as in the microwave runs. However, this approach was discarded when it was found that the early exothermic reaction of the nitridation process resulted in premature melting of the test sample. Results presented in this paper are for the set-up in which samples were placed in an alumina dish with no surrounding powder. In these experiments, the furnace temperature was measured and controlled by a Type "C" molybdenum sheathed thermocouple which was inserted into the furnace cavity at a point near the sample.

---

*Elchem Corp., Buffalo, NY, Grade HQ, <10 μm.
†Ube Corp., Japan; Grade E-10.
**Ceralox Corp., Tucson, AZ; Grade HPA.
††Molycorp. Louviers, CO; Grade 5600, >99.99%.

The furnace was purged with nitrogen and experiments were performed with flowing nitrogen.

Samples were weighed before and after heating cycles to determine the percent weight gain and nitridation. A weight gain of 66.5% is considered 100% nitridation. Following the heating cycle, samples were sectioned near the center of the sample into a 140-mm thick slab. A 30-mm x 15-mm rectangle was sectioned from the slab for x-ray diffraction studies. A small fragment was also broken from the slab for scanning electron microscopy (SEM) analysis.

EXPERIMENTAL RESULTS

One important and critical aspect of these heating experiments is temperature measurements. Figure 1 shows the temperature measurements taken during a typical nitridation experiment in the microwave furnace. The thermocouples at the center and surface of the sample differ during the ramp up, but come together at 1200°C. Likewise, although the pyrometer measurement is around 100°C higher than the control thermocouple at 600°C, the temperatures converge near 1200°C. As previously noted, the sample temperature in the conventional furnace is assumed to be the same as the thermocouple adjacent to the sample.

In Table 1 are shown the percent nitridation for temperatures from 1150°C to 1300°C and dwell times of 60 and 300 minutes for silicon nitrided during conventional or microwave heating. The most important result is that the nitridation of silicon by microwave heating begins at approximately 1200°C; whereas, the nitridation of the silicon processed by conventional heating begins near 1250°C. As seen in Figure 2, the percent of nitridation in the microwave-heated samples was higher. Table 1 results indicate that increasing the hold time for a given temperature led to greater increases in nitridation for the microwave-heated silicon than the silicon heated by conventional methods. These results indicate that microwave heating enhances some processes in the nitridation reaction. An attempt was made to carry out the experiments at higher temperatures; however, the strong exothermic heating of the sample hindered reliable and repeatable results, particularly in the microwave system. It should be noted, however, that when α-Si_3N_4 and sintering aids were added to silicon, the microwave heating experiments were controllable and near 100% nitridation could be achieved.

As noted in the experimental procedures, sectioned samples were also analyzed by x-ray diffraction and SEM. Figure 3 shows two x-ray diffraction patterns obtained from silicon heated to 1250°C for 1 h by conventional and microwave heating. Data were collected on the peak intensities of two α-Si_3N_4 peaks $\alpha(102)$ and $\alpha(210)$ and two β-Si_3N_4 peaks designated $\beta(101)$ and $\beta(210)$. A formula developed by Devlin et al. [8] was used to calculate the α/β ratio. Note in Table 1 that the α/β ratio of the conventionally-heated sample is much lower than that of the microwave-heated sample at 1250°C, but it is very similar to α/β ratio of the microwave-heated sample at 1200°C. At 1300°C, both the conventional- and microwave-heated samples had nearly identical α/β ratios and similar profiles. The higher β-Si_3N_4 in the conventional (1250°C) and microwave (1200°C) samples at the onset of

Table 1. Percent Nitridation and α/β Si_3N_4 Ratios for Silicon Heated by Conventional and Microwave Furnaces

Heating Source	Temperature (°C)	Time (Min.)	Percent Nitridation	α/ß Ratio
Microwave	1150	60	1.0	-
Conventional	1200	60	0.5	-
Microwave	1200	60	8.9	6.8
Conventional	1250	60	9.1	4.0
Microwave	1250	60	12.6	11.6
Conventional	1250	300	10.0	-
Microwave	1250	300	17.7	12.8
Conventional	1300	60	9.7	9.2
Microwave	1300	60	13.3	9.2
Conventional	1300	300	11.9	-
Microwave	1300	300	18.0	9.2

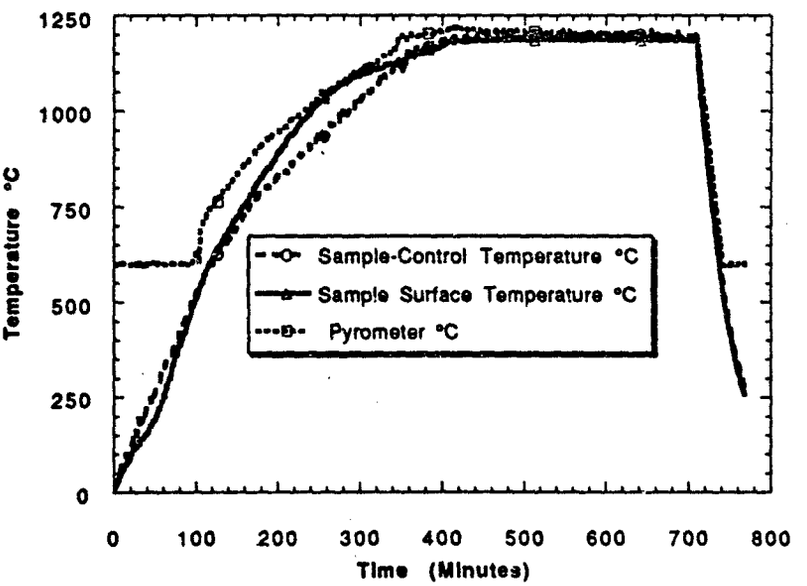


Figure 1 Heating profile of silicon nitrided by microwave heating.

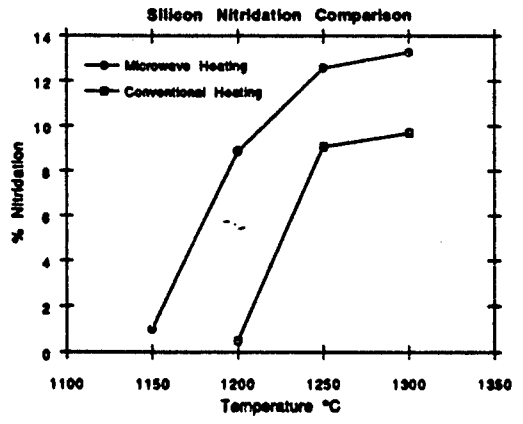
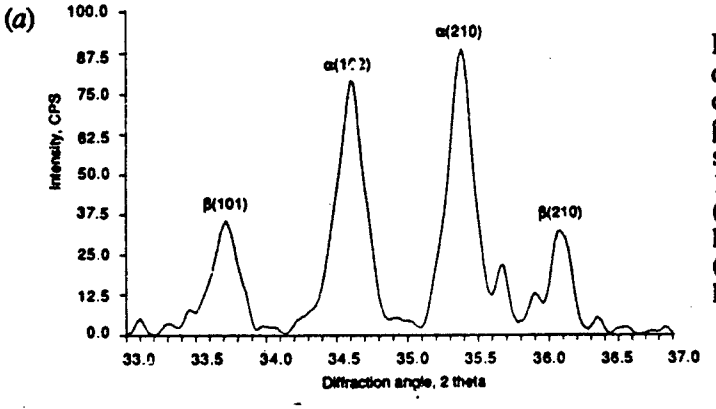


Figure 2 Early phase of nitridation of silicon by conventional and microwave heating.



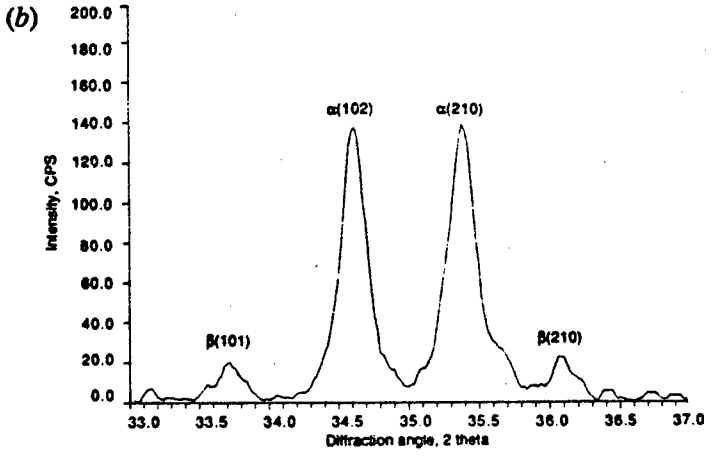


Figure 3 X-ray diffraction patterns of selected α- and β-Si_3N_4 peaks for silicon nitrided for 1 h at 1250°C by (*a*) conventional heating or (*b*) microwave heating.

nitridation may be some oxynitride form. These results indicate that the reaction products of both nitridation processes are similar but are present in different amounts.

As noted in the procedures, we also heated silicon plus sintering aids . X-ray diffraction analysis was performed on some of these samples. Figure 4 is a pattern of silicon plus 10% Si_3N_4, 2% Al_2O_3, and 6% Y_2O_3 heated to 1330°C in the microwave furnace. Note that there is an enhanced amount of the β-Si_3N_4 peaks. These β-Si_3N_4 peaks probably are sialon products. This result is comparable to what has been reported for similar samples heated by conventional methods.

Besides calculating the α/β Si_3N_4 ratios, we also used another formula adapted from Gazzara et al. [9] to calculate the percent of free silicon left in some of our samples. These results were compared to our weight-gain results. For example, silicon heated at 1250°C with a 60 min dwell yielded a nitridation of 9.1%. When the x-ray peak intensities are plugged into the Gazzara formula, we obtained 7.3% nitridation. This is good agreement for these type of experiments.

SEM analysis was performed on some of the microwave and conventional nitrided silicon samples. Figure 5 shows a 10,000X photomicrograph of silicon heated in the conventional furnace to 1250°C for 1 h and in the microwave to 1200°C for 1 h. One can see the α-Si_3N_4 whiskers in both as well as a surface film of Si_3N_4 . Figure 6 shows the same two samples at higher magnification. The lumpy-rippled growth pattern of silicon nitride on the surface of the silicon is apparent in both cases.

CONCLUSIONS

A comparative study of the low-temperature nitridation phase of high-purity silicon in nitrogen has been conducted using microwave- and conventional-heating sources. Nitridation of the 99.95% pure silicon begins at ~1200°C by microwave heating versus 1250°C for conventional heating. Early nitridation levels are higher in microwave heated silicon. Following the initial burst of nitridation at 1200 to 1250°C, there is a decrease in the rate of nitridation in both cases. However, the microwave-heated samples continued to react at an appreciable rate (as measured by weight gain) indicating continued diffusion and reaction of the silicon.

A comparison of the x-ray diffraction patterns indicate a higher level of α-Si_3N_4 in the microwave-heated samples at the initiation of nitridation. However at 1300°C, the α/β Si_3N_4 ratios were nearly identical for both cases. The x-ray diffraction pattern for silicon plus Al_2O_3 and Y_2O_3 heated to 1330°C shows an enhanced amount of the β phase. This finding correlated well with findings in conventional nitridation studies.

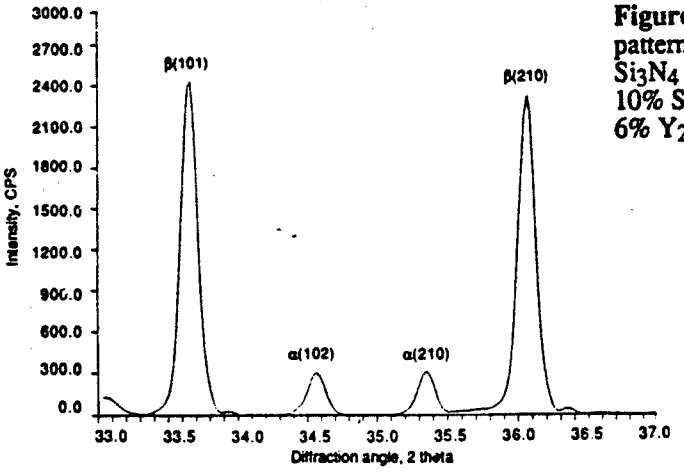


Figure 4 X-ray diffraction pattern for selected α–and-ß Si_3N_4 peaks of silicon plus 10% Si_3N_4, 2% Al_2O_3, and 6% Y_2O_3.

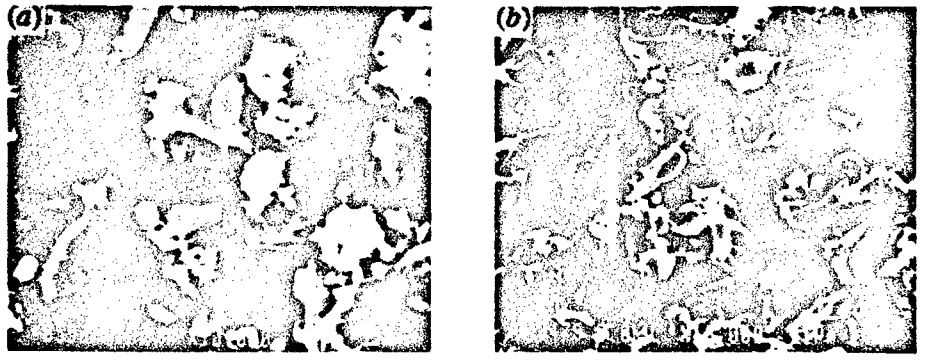


Figure 5 SEM 10,000X photographs of silicon nitrided by (*a*) conventional heating at 1250°C for 1 h and (*b*) micro-wave heating at 1200°C for 1 h.

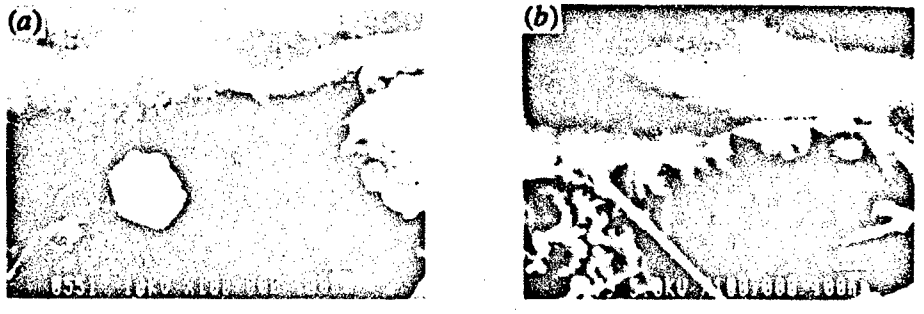


Figure 6 SEM 100,000X photographs of silicon nitrided by (*a*) conventional heating at 1250°C for 1 h and (*b*) micro-wave heating at 1200°C for 1 h.

Calculation of percent nitridation by weight gain and by calculations from x-ray diffraction peaks correlated very well. SEM analysis of conventional- and microwave-heated and nitrided silicon show the expected early whisker growth as well as coarse Si_3N_4 growth on the silicon surfaces.

ACKNOWLEDGEMENT

Research sponsored by the U.S. Department of Energy, Assistant Secretary for Conservation and Renewable Energy, Office of Transportation Systems, as part of the Ceramic Technology for Advanced Heat Engines Project of the Advanced Materials Development Program, under contract DE-AC05-84OR21400 with Martin Marietta Energy Systems, Inc.

REFERENCES

1. A. J. Moulson, "Reaction-bonded Silicon Nitride: Its Formation and Properties," J. Mater. Sci., Vol. 14, pp. 1017-51 (1979).

2. M. Barsoum, P. Kangutar, and M. J. Koczak, "Nitridation Mechanisms of Silicon Powder Compacts," Ceram. Eng. Sci. Proc., Vol. 10, No. 7-8, pp. 794-806 (1989).

3. F. L. Riley, "Nitridation and Reaction Bonding", pp. 265-288 in Nitrogen Ceramics, F.L. Riley (ed.), Noordhoff, Netherlands (1977)

4. W. H. Sutton," Microwave Processing of Ceramic Materials," Am. Ceram. Soc. Bull., Vol. 68, No. 2, pp. 376-86 (1989).

5. M. A. Janney and H. D. Kimrey, "Microwave Sintering of Alumina at 28 GHz, pp. 919-24 in Ceramic Transactions, Ceramic Powder Science, II, B., ed G. L. Messing, E. R. Fuller, Jr., and H. Hausner, American Ceramic Society, Westerville, OH (1988).

6. C. E. Holcombe, Martin Marietta Energy Systems, Inc., Oak Ridge, TN, unpublished results (1988).

7. J. O. Kiggans, Jr., T. N. Tiegs, H. D. Kimrey, "Microwave Sintering of Silicon Nitride," MRS Proc., unpublished (1990).

8. D. J. Devlin and K. E. Amin, "A Method for Quantitative Phase Analysis of Silicon Nitride to X-ray Diffraction," Powder Diffraction, Vol. 5, No. 3, pp. 121-24 (1990).

9. C. P. Gazzara and D. R. Messier, "Determination of Phase Content of Si_3N_4 by X-ray Diffraction Analysis," Am. Ceram. Soc. Bull., Vol. 56, No. 9, pp. 777-81(1977).

MICROSTRUCTURE DEVELOPMENT DURING MICROWAVE ANNEALING OF DENSE SILICON NITRIDE*

T. N. Tiegs, M. K. Ferber, J. O. Kiggans, K. L. More, C. M. Hubbard, and D. W. Coffey, Oak Ridge National Laboratory, Oak Ridge, TN 37831-6069

ABSTRACT

Microwave annealing of dense silicon nitride-based ceramics can result in substantial SiO volatilization from the grain boundary phases and compositional changes of those phases. It also results in further α-to-ß Si_3N_4 transformation accompanied by grain growth. These changes occur at bulk temperatures well below comparable observations in conventional heating. The differences are believed due to enhanced diffusion within the intergranular phases.

INTRODUCTION

Microwave heating is of interest for thermal processing of ceramics as reviewed by Sutton [1]. Current applications include drying, clinkering, sintering, melting, joining, and fiber drawing. Other researchers have reported increased diffusion rates and enhanced sintering during microwave heating in oxide-based ceramic systems [2-5].

Silicon nitride ceramics are the leading candidate materials for high-temperature structural applications because of their combination of excellent strength, fracture toughness, wear resistance, thermal shock tolerance and high-temperature properties. Si_3N_4 cannot be sintered by solid state diffusion, but must use liquid phase sintering techniques. Typically, additives, such as Y_2O_3 and Al_2O_3, are utilized to create liquid phases to aid in densification. Microstructural development and densification occurs by both particle rearrangement and solution-reprecipitation processes [6]. Precipitation of ß-Si_3N_4 grains occurs from a liquid phase, and because of differences in growth kinetics, the ß-Si_3N_4 grains grow with elongated

* Research sponsored by the U. S. Department of Energy, Assistant Secretary for Conservation and Renewable Energy, Office of Transportation Technologies, as part of the Ceramic Technology for Advanced Heat Engines Project of the Advanced Materials Development Program, under contract DE-AC05-840R21400 with Martin Marietta Energy Systems, Inc.

morphologies. It has been long recognized that silicon nitride gets many of its superior properties from the interlocking structure of the elongated ß-Si_3N_4 grains developed during densification at high temperature. Diffusion through the liquid phase determines the densification behavior, the resulting grain sizes, the aspect ratio of the ß-Si_3N_4 grains and the extent of the α-to-ß conversion [6]. The final microstructure consists of ß-Si_3N_4 grains (and possibly residual α-Si_3N_4 particles) surrounded by an oxide-based grain boundary phase with a composition dependent upon on the initial sintering additives used. Further heating of the silicon nitride under nitrogen can affect the microstructure in several different ways depending on whether it is done above or below the intergranular eutectic temperature.

If the materials are annealed above the intergranular eutectic temperature, diffusion continues in the intergranular liquid. This results in completion of the α-to-ß conversion, grain growth and coarsening of the ß-phase with a decrease in aspect ratio and an increase in the average diameter. The rate of coarsening is apparently dependent on the viscosity of the grain boundary liquid phase and the diffusion rate. In conventional heating, significant coarsening in representative processing times (≤ 20 h) is observed at temperatures >1800°C [7].

Heating below the intergranular phase eutectic temperature is commonly performed on silicon nitride ceramics to crystallize the grain boundary phases. This is because that while the liquid phase aids densification, after sintering it can be retained as an intergranular glass phase degrades the mechanical properties at elevated temperatures. Crystallization of these intergranular phases has been demonstrated to improve the high temperature mechanical properties, such as strength and creep resistance [8]. Conventionally, crystallization is done at temperatures of 1000 to 1400°C depending on the chemistry of the intergranular phase. At these temperatures α/ß ratios and grain size are not affected.

Microwave heating of silicon nitride-based materials has been shown to occur by coupling to the grain boundary phases [9,10]. Previous results showed that microwave annealing of silicon nitride ceramics resulted in significant grain growth and improved high-temperature mechanical properties [10,11]. In the present research, further examination of the materials from the annealing process was done to study the microstructure development with attention to the α-to-ß transformation, and crystallization of the grain boundary phases.

EXPERIMENTAL

Appropriate amounts of Si_3N_4,* Y_2O_3,# and Al_2O_3† were milled together in isopropanol for 2 h and then dried with constant stirring. Discs of material approximately 5 mm (0.2 in.) thick and 6.4-cm (2.5 in.) diameter were hot-pressed with 24 MPa pressure in BN-coated graphite dies under 0.1 MPa nitrogen for

* Ube, Japan; Grade E-10.
# Molycorp, White Plains, NY; Grade 5600.
† Reynolds, Malakoff, TX; Grade RC-HP DBM.

60 min. The Si_3N_4-4 wt % Y_2O_3 samples were done at 1775°C and the Si_3N_4-6 wt % Y_2O_3-2 wt % Al_2O_3 at 1725°C. Densities were determined by the Archimedes method. The surfaces of the discs were diamond ground prior to annealing and then machined into bars with nominal dimensions of 3 by 4 by 50 mm after annealing. In a few selected cases, the samples were annealed as bars.

Microwave annealing was performed in a 2.45-GHz furnace with the materials packed in Si_3N_4** powder (with 2 wt % Y_2O_3) in an insulation package previously described [10]. Temperatures were monitored by a thermocouple surrounded by the specimens. Temperatures of selected samples were also verified by an optical pyrometer, and the two readings were generally within 20°C of each other. Conventional heating was done in a graphite element furnace with the specimens packed in the same powder mixture as the microwave heated materials. All annealing was at 0.1 MPa (1 atm) nitrogen.

RESULTS

The hot-pressing produced materials that were high density: 3.20 g/cc (98.8%) for the Si_3N_4-4% Y_2O_3 and 3.25 g/cc (99.4%) for the Si_3N_4-6% Y_2O_3-2% Al_2O_3. Examination of the materials after annealing revealed significant weight losses had occurred as a function of the microwave thermal treatment conditions as summarized in Fig. 1. The conventional heated specimens showed losses <0.1% for comparable times and temperatures. The surfaces of the microwave-heated specimens with high weight losses had a "white" reaction layer ≤0.25-mm (0.01 in.) thick indicating that the weight losses were predominantly associated with the external surfaces. Prior to further testing of these materials, the surfaces were ground to remove the "white" surface coating. To keep comparisons on an equal basis, an equal amount of surface material was also removed from the conventionally-heated specimens. No decreases in immersion density were observed even for the Si_3N_4-6% Y_2O_3-2% Al_2O_3 material that exhibited a loss of ~8 wt %. Since SiO volatilization is the main cause for weight loss, a second set of annealing tests were run where the packing powder was oxidized at 800°C prior to being used. Those results, also summarized in Fig. 1, show that the weight losses can be effectively reduced by a protective powder bed, but not eliminated at the higher temperatures for the less refractory composition. Powder beds are typically used during sintering of silicon nitrides where the temperatures are >1700°C.

Microstructural changes occurring during the annealing were also significant depending on the intergranular phase composition and the annealing conditions. Comparisons made by scanning electron microscopy showed minor differences between the microstructures of the materials containing 4% Y_2O_3 (Fig. 2). However, the microwave annealed specimens with 6% Y_2O_3-2% Al_2O_3 experienced enhanced grain growth during heat treatment as shown in Fig. 3.

** Elkem, Buffalo, NY; Grade Silicon Nitride HQ.

Accompanying the grain growth was a change in the phase composition of the materials. Interestingly, the microwave annealing, in most cases, resulted in further α-to-ß Si_3N_4 phase transformation as indicated in Fig. 4.

Transmission electron microscopy (TEM) was used to examine the nature of the grain boundary phases in selected samples. Minor differences of the intergranular phases were observed between the conventional- and microwave-annealed samples (1400°C for 20 h) containing 4% Y_2O_3. The as-fabricated samples and those conventionally heated-contained two crystalline grain boundary phases: $Y_2Si_2O_7$ and a yttrium-silicon-oxynitride phase. The microwave-annealed sample contained only the yttrium-silicon-oxynitride as a grain-boundary phase (Fig. 5).

Examination of the Si_3N_4-6% Y_2O_3-2% Al_2O_3 materials by TEM showed the intergranular phases in the as-fabricated samples to be amorphous, as expected. During conventional annealing at 1400°C for 10 h, large grain boundary pockets of $Y_2Si_2O_7$ crystallized with the aluminum existing predominantly in small amorphous pockets, which is also typical for this material composition. When the material was microwave annealed for 10 h at 1400°C, there was a significant improvement in crystallization and, in fact, no amorphous phases were found in this sample. As noted in the sample conventionally heated under the same conditions, when there is some residual amorphous phases present, it is due to the aluminum segregating into discrete areas as the $Y_2Si_2O_7$ or other Y-Si-O-N phases crystallize. In this case, however, the aluminum was found in solid solution within the crystalline grain boundary pockets in a high Y-containing silicate (but not $Y_2Si_2O_7$) as shown in Fig. 6.

TEM was also performed on samples microwave annealed at 1200°C for 20 h. These conditions resulted in an inhomogeneous distribution of phases: in some areas, the majority of the grain boundary pockets had fully crystallized as a high Y-containing phase with no aluminum; whereas, in other relatively large regions adjacent to these areas, there were no crystalline pockets, only residual amorphous pockets. These regions ranged in size from ~1 to 10 μm.

DISCUSSION

Microwave heating of silicon nitride-based materials occurs predominantly via power absorption by the intergranular phases. Because of the high thermal conductivity of the silicon nitride and the small intergranular distances, the temperatures are expected to be relatively uniform throughout the specimens, especially with the long hold times in the present study. However, a number of factors indicate that either (1) the bulk temperature measurements are too low, (2) the intergranular temperatures are higher than the bulk, or (3) diffusion within the intergranular phases is significantly increased. These factors include the observed weight losses, the changes in the intergranular phase compositions, the further α-to-ß transformation and the enhanced grain growth.

As stated before, the temperatures were monitored during every anneal with a thermocouple surrounded by the samples. Temperatures were also checked in a

few cases with an optical pyrometer and the two measurements were generally within 20°C. During heat-up, it is conceivable that the temperatures of the samples could have been higher due to large thermal gradients from the samples through the packing powder. However, in other tests, we have found that the gradients diminish quickly (<1 h) as the entire insulation package heats up. Unfortunately, no optical measurements were taken during heat-up of the present samples. Since the anneal times for the present study were all ≥10 h, the majority of the anneal time was spent with small thermal gradients in the insulation package and thus the thermocouple readings were accurate.

Johnson has recently examined the potential for thermal gradients with grain boundary heating in polycrystalline ceramics [13]. Heat flow calculations indicated that temperature differences between grains and grain boundaries would be negligible. In the present study with near theoretically dense materials, there is little difference between the grains and the intergranular phases.

Weight losses are not significant in dense materials heated conventionally until temperatures >1700°C are used, but in the microwave-heated materials, we observed considerable losses at ~1400°C. SiO volatilization from the intergranular phases would result in compositional shifts favoring high Y-containing phases. Thus, the appearance of high Y-containing silicates and the disappearance of $Y_2Si_2O_7$ in the microwave-annealed specimens are consistent with such a mechanism. Enhanced diffusion of Si-O species would result in increased weight losses.

The α-to-ß Si_3N_4 transformation is known to transpire only by solution-reprecipitation through a liquid or by vaporization-condensation through a gas [6]. Grain growth is associated with the transformation in the presence of a liquid. In the present study, the intergranular eutectic liquid temperatures are ~1500°C for the Si-Y-O-N system and ~1280°C for the Si-Al-Y-O-N system. Conventionally, diffusion within these liquids is very low at temperatures just above the eutectic because of extremely high viscosities, and temperatures >1750°C are normally required to observe changes in reasonable times. In both material compositions in the present study, substantial transformation took place at temperatures below the eutectic: in 20 h anneals at 1400°C for the Si_3N_4-4% Y_2O_3 and 1200°C for the Si_3N_4-6% Y_2O_3-2% Al_2O_3. The Si_3N_4-4% Y_2O_3 material microwave annealed at 1400°C for 10 h did not show any further α-to-ß Si_3N_4 transformation, but this sample also exhibited no weight loss and the high-temperature creep properties were similar to the as-fabricated material indicating it may be an anomaly [11]. In any event, comparable observations of α-to-ß transformation and grain growth in conventionally annealed silicon nitrides requires temperatures ≥300°C higher than those observed in the microwave. Thus, since the bulk temperature measurements are not off by that magnitude and the intergranular phase temperatures are not substantially different from the bulk, the observations must be attributable to enhanced diffusion within the intergranular phases.

CONCLUSIONS

Microwave annealing of dense silicon nitride-based ceramics can result in substantial SiO volatilization from the grain boundary phases and compositional changes of those phases. Further α-to-ß Si_3N_4 transformation is accompanied by grain growth. Even considering errors in the temperature measurements, comparable observations in conventionally annealed silicon nitrides take place at temperatures ≥300°C higher than in the microwave. These observations indicate enhanced diffusion in the intergranular phases by microwave heating.

REFERENCES

1. W. H. Sutton, "Microwave Processing of Ceramic Materials," Am. Ceram. Soc. Bull. Vol. 68, No. 2, pp. 376-86 (1989).

2. M. A. Janney and H. D. Kimrey, "Microstructure Evolution in Microwave Sintered Alumina," pp. 382-390 in *Ceramic Transactions, Sintering of Advanced Ceramics, Vol. 7*, ed. by C. A. Handwerker, J. E. Blendell and W. A. Kaysser, Am. Ceram. Soc., Westerville, OH (1990).

3. Y.-L. Tian, H. S. Dewan, M. E. Brodwin, and D. L. Johnson, "Microwave Sintering Behavior of Alumina Ceramics," pp. 391-401 in *Ceramic Transactions, Sintering of Advanced Ceramics, Vol. 7*, ed. C. A. Handwerker, J. E. Blendell and W. A. Kaysser, Am. Ceram. Soc., Westerville, OH (1990).

4. T. T. Meek, R. D. Blake, and J. J. Petrovic, "Microwave Sintering of Al_2O_3 and Al_2O_3-SiC-Whisker Composites," Ceram. Eng. Proc., Vol. 8, No. 7-8, pp. 861-71(1987).

5. M. A. Janney and H. D. Kimrey, "Diffusion-Controlled Processes in Microwave-Fired Oxide Ceramics," in *Microwave Processing of Materials-II, Vol. 189*, ed. W. B. Snyder, W. H. Sutton, D. L. Johnson, and M. F. Iskander, Materials Research Soc., Pittsburgh, PA (1991).

6. M. H. Lewis, G. Leng-Ward. and C. Jasper, "Sintering Additive Chemistry in Controlling Properties of Nitride Ceramics," pp. 1019-1033 in *Ceramic Transactions, Ceramic Powder Science, II, B.*, ed. G. L. Messing, E. R. Fuller, Jr., and H. Hausner,.American Ceramic Society, Westerville, OH (1988).

7. G. Wotting, B. Kanka, and G. Ziegler, "Microstructural Development, Microstructural Characterization and Relation to Mechanical Properties of Dense Silicon Nitride," pp. 83-96 in *Non-Oxide Technical and Engineering Ceramics*, ed. S. Hampshire, Elsevier Applied Science, London (1986).

8. A. Tsuge, K. Nishida, and M. Komatsu, "Effect of Crystallizing the Grain Boundary Phase on the High-Temperature Strength Hot-Pressed Si_3N_4 Containing Y_2O_3," J. Am. Ceram. Soc., Vol. 58, Nos. 7-8, pp. 323-26 (1975).

9. W. W. Ho, "High-Temperature Dielectri Properties of Polycrystalline Ceramics," pp. 137-148 in *Microwave Processing of Materials, Vol. 124*, eds. W. H. Sutton, M. H. Brooks, and I. J. Chabinsky, Materials Research Society, Pittsburgh, PA (1988).

10. T. N. Tiegs, J. O. Kiggans, and H. D. Kimrey, "Microwave Processing of Silicon Nitride," in *Microwave Processing of Materials-II, Vol. 189*, eds. W. B. Snyder, W. H. Sutton, D. L. Johnson, and M. F. Iskander, Materials Research Soc., Pittsburgh, PA (1991).

11. M. K. Ferber, T. N. Tiegs, and M. G. Jenkins, "Effect of Post-Sintering Microwave Treatments Upon the Mechanical Performance of Silicon Nitride," to be published in Ceram. Eng. Proc., Vol. 9-10 (1991).

12. F. F. Lange, "Volatilization Associated with the Sintering of Polyphase Si_3N_4 Materials," J. Am. Ceram. Soc., Vol. 65, No. 8, pp. C-120-C-121 (1982).

13. D. L. Johnson, "Microwave Heating of Grain Boundaries in Ceramics," J. Am. Ceram. Soc., Vol. 74, No. 4, pp. 849-850 (1991).

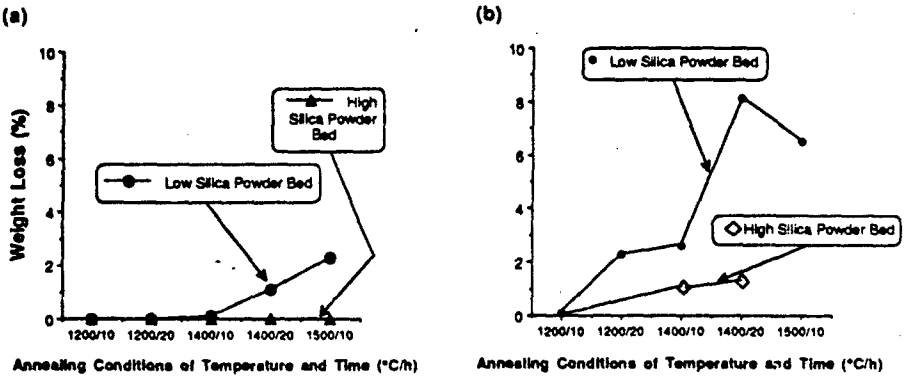


Fig. 1 - Summary of weight losses by silicon nitride materials during microwave annealing. Use of a powder bed with high silica content reduces SiO volatilization. (a) Si_3N_4-4% Y_2O_3, (b) Si_3N_4-6% Y_2O_3-2% Al_2O_3. Samples annealed in powder beds with high silica in form of bars.

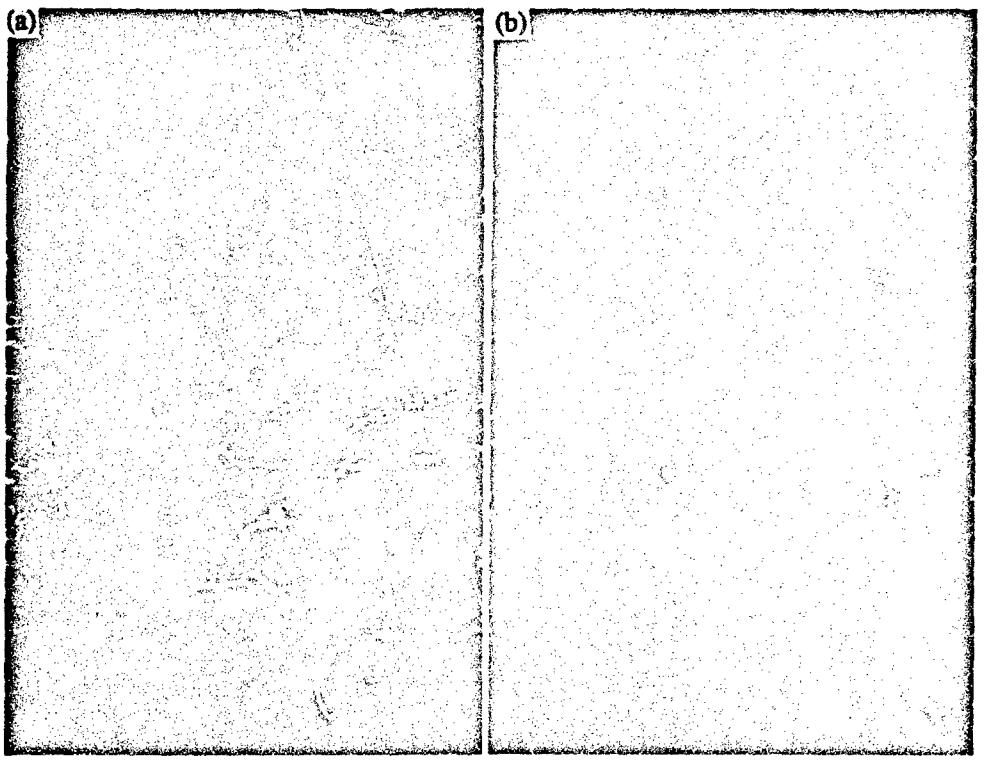


Fig. 2 - Fracture surface of Si_3N_4-4% Y_2O_3 material annealed for 20 h at 1400°C. (a) conventional heating, (b) microwave heating.

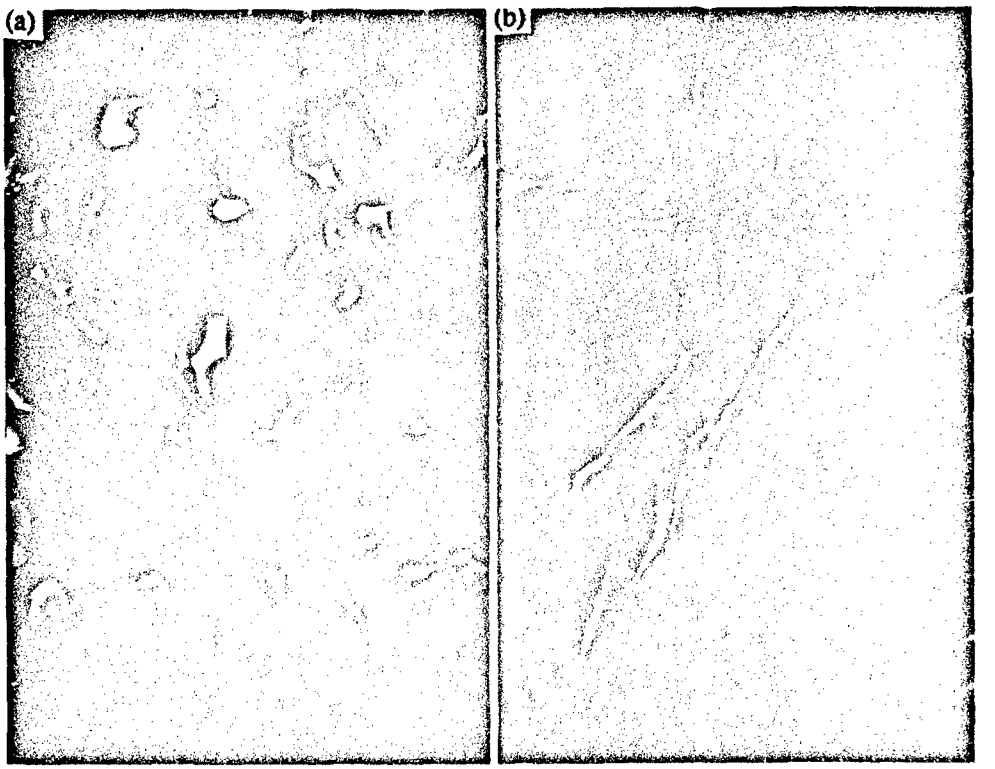


Fig. 3 - Fracture surface of Si_3N_4-6% Y_2O_3-2% Al_2O_3 material annealed for 10 h at 1400°C. (a) conventional heating, (b) microwave heating.

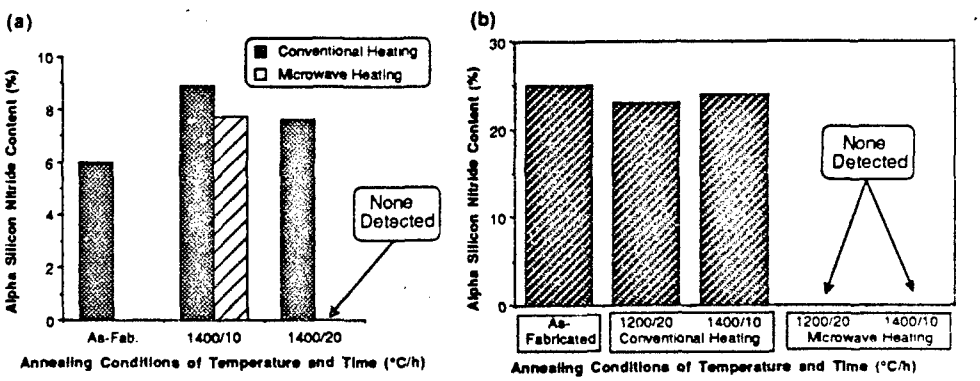


Fig. 4 - Alpha phase silicon nitride content as a function of the annealing conditions. Microwave annealing can result in substantial α-to-ß transformation at relatively low temperatures. (a) Si_3N_4-4% Y_2O_3, (b) Si_3N_4-6% Y_2O_3-2% Al_2O_3.

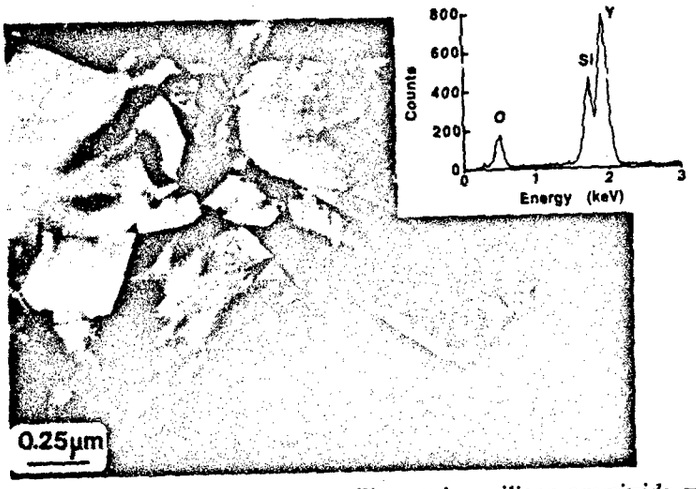


Fig. 5 - TEM micrograph showing crystalline yttrium-silicon-oxynitride grain boundary pockets in microwave annealed Si_3N_4-4% Y_2O_3. Microwave annealing conditions were 1400°C for 20

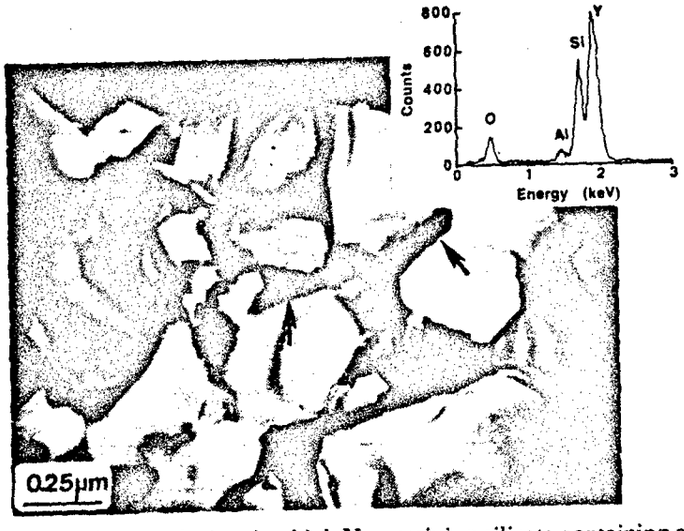


Fig. 6 - TEM micrograph showing high Y-containing silicate containing aluminum phases in microwave annealed Si_3N_4-6% Y_2O_3-2% Al_2O_3. Microwave annealing conditions were 1400°C for 10 h.

SYNTHESIS OF NONOXIDE CERAMIC POWDERS BY NONTHERMAL MICROWAVE PLASMA

A. K. Singh*, P. Mehta and A. I. Kingon.
Department of Mat. Sci. and Eng. NCSU, Raleigh, NC 27695-7919.
*On study leave from Physics Department, Banaras Hindu University, VARANASI-221005 INDIA.

ABSTRACT

We report the synthesis of nonoxide ceramic powders of aluminum nitride, silicon carbide and silicon nitride by nonthermal microwave plasma of precursor gases under conditions of laminar flow. The precursor gases used were trimethylaluminum and nitrogen for aluminum nitride, silane and acetylene for silicon carbide, and silane and nitrogen for silicon nitride. The argon gas was used as the diluent/carrier gas in all the cases. The effect of flow rate of the gases and hence the effect of concentration and residence time of the activated species in the plasma is discussed. The microwave energy in the plasma was (50-100) Watts. The product particles were characterized by transmission electron microscopy, Auger electron spectroscopy and X-ray photoelectron spectroscopy.

The synthesized material was found to be ultrafine (~5nm) and crystalline. Aluminum nitride stabilized in either hexagonal or cubic phases depending on the nitrogen concentration.

The silicon carbide formed was mostly cubic-3C accompanied with several hexagonal and rhombohedral polytypic modifications. The implications of the occurrence of polytypes in particles of nanometer size are discussed in terms of the existing theories.

The silicon nitride was formed in the α phase modification.

INTRODUCTION

Aluminum nitride, silicon carbide and silicon nitride are well known ceramics which can stand high temperature and offer high strength and resistance to corrosion. They are being used to replace metals with an advantage of being of lower density (1-6). Also they are being applied to the microelectronic devices in thin film form (7,8).

The high temperature processing of these ceramics introduces a variety of defects, consequently the properties of the ceramics are greatly limited. Particularly, in silicon carbide the abundance of polytypes and phase transformations amongst them develop an additional complication. These phase transformations often result in undesirable changes in microstructure including exaggerated grain growth (9). The defects compromise the mechanical strength and thermal properties of the materials. Many of the defects originate from the milling (Acheson process for silicon carbide), presence of hard agglomerates and post firing machining. As a result, several groups have embarked upon gas phase synthesis (10) using thermal plasma torches and lasers (11-14) to produce nanoscale particles. However, the former method has generally been unsatisfactory, primarily because of large temperature and velocity gradients in the plasma. The resulting material has been highly agglomerated, chemically inhomogeneous and difficult to densify.

The objective of this investigation is to synthesize crystalline aluminum nitride, silicon carbide and silicon nitride ultrafine powders via gas phase synthesis using contained nonthermal microwave plasma under laminar flow conditions of the precursor gases.

Aluminum nitride and silicon carbide exhibited polytypism. The phenomenon of polytypism (15-17) refers to the ability of a solid to crystallize into more than one crystallographic modification with the same chemical composition but differing in number and/or manner of stacking of layers in the unit cell. The implications of the occurrence of polytypism in nanometer sized particles will be discussed.

EXPERIMENTAL

Reactor System and Gas Flow

The experimental apparatus (Fig.1) consisted of a long (2.1m) fused quartz tube (O.D=38 mm, I.D =35 mm) which was inserted into a circular applicator of a microwave source (S-1500 Astex) capable of 1.5 kWatts. This tube was connected to the mass flow controllers on one end and the vacuum pump fitted with automatic throttle valve pressure controller on the other. A teflan filter (pore size-10 micron) was placed down stream to collect the powder. The system could be purged with argon and/or nitrogen and similarly the exhaust gases diluted.

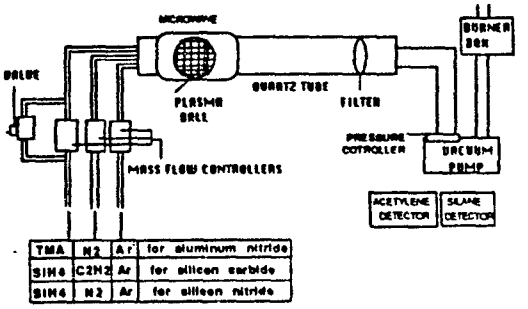


Fig.1. Schematic diagram of the apparatus

The synthesis was accomplished by triggering the microwave plasma in the mixture of precursor gases and the diluent gas argon. The flow rate was limited to result in a laminar flow to minimise particle-particle collision.

The aluminum nitride was synthesized by triggering the microwave plasma in the mixture of trimethylaluminum (TMA), nitrogen and argon. An excess nitrogen was necessary to make hexagonal aluminum nitride. The actual flow rate to synthesize hexagonal aluminum nitride was found to be 20 standard cubic centimetre per minute (sccm) of nitrogen, 5 sccm of TMA and 50 sccm of argon. A lower concentration of nitrogen, 15 sccm of nitrogen with the same flow rates of TMA and argon resulted in the formation of cubic aluminum nitride. A still lower concentration of nitrogen (10 sccm) resulted in a mixture of cubic aluminum nitride and aluminum.

The silicon carbide was synthesized by triggering the microwave plasma (50-100 Watts) in a laminar flow of acetylene, silane and argon. The optimum flow rates were determined to be 10 sccm of silane, 4 sccm of acetylene, and 160 sccm of argon to form silicon carbide, and 3 sccm of silane, 15 sccm of nitrogen, and 50 sccm of

argon in case of silicon nitride. Laminar flow is maintained at these flow rates. It should be noted that these rates do not quite correspond to thermodynamic stoichiometric ratios. We deduce that this is due to more difficult excitation of silane compared to that of acetylene.

The optimum flow ratio was determined by compositional analysis performed by Auger electron spectroscopy of the collected particles. Higher acetylene flow rates resulted in excess carbon.

The Langmuir probe was used to characterize the plasma. The details regarding this are described elsewhere (18).

The particles synthesized in the plasma ball were ultrafine (~ 5nm) which were suspended in the argon stream and were collected on the filter placed in the quartz tube. The efficiencies as determined by the total amount of particles formed were found to be 5%, 20% and 15% for aluminum nitride, silicon carbide and silicon nitride respectively.

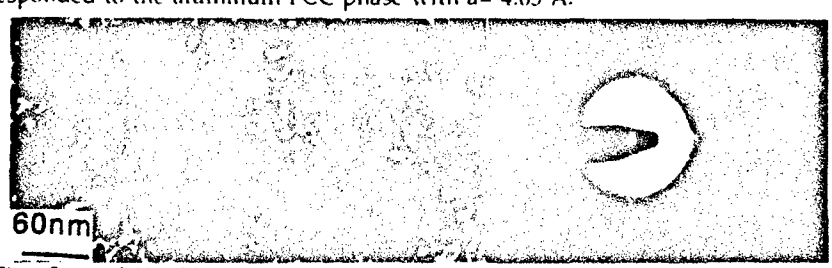
The powders collected were characterized crystallographically by electron diffraction and chemically by Auger electron spectroscopy and X-ray photoelectron spectroscopy.

The electron microscope samples were prepared by transferring the powder particles on the holey carbon grid either directly or by putting drops of the particles suspended in acetone on the grid.

RESULTS AND DISCUSSION

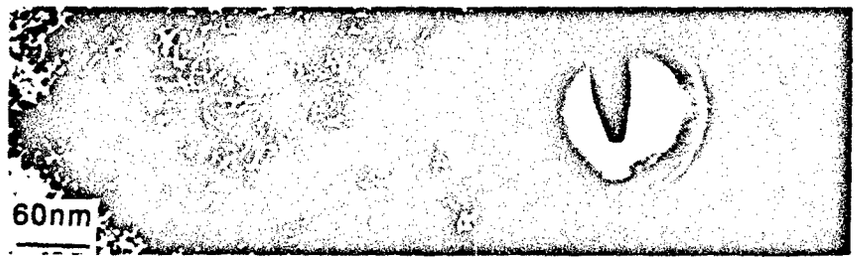
The electron microscopic observations of the aluminum nitride formed with different concentrations of the nitrogen, TMA, and argon is described below:

A mixture of 5 sccm of nitrogen, 5 sccm of TMA and 100 sccm of argon resulted in aluminum powder. The electron micrograph and the electron diffraction from these powders are shown in Figs.2a. and 2b. respectively. The diffraction pattern corresponded to the aluminum FCC phase with a= 4.05 Å.



Figs. 2a. and 2b., Electron micrograph and diffraction from the powders (see text).

These observations suggest the lack of active nitrogen for the nitridation of aluminum resulting from TMA. We therefore increased the nitrogen concentration which resulted in the formation of cubic aluminum nitride (a= 4.12 Å), and aluminum. Figs.3a. and 3b. show the electron micrograph and the electron diffraction, respectively, from the powder resulting from the mixture of 10 sccm of nitrogen and 5 sccm of TMA with 50 sccm of argon. Fig.3b. corresponds to the mixed pattern of cubic aluminum nitride and cubic aluminum. The broadening of the rings is attributed to the closeness of the lattice parameters of aluminum and aluminum nitride and the lack of resolution.



Figs. 3a. and b., Electron micrograph and diffraction pattern from the powder (see text).

A further increase of nitrogen concentration to 15 sccm with 5 sccm of TMA and 50 sccm of argon resulted in the cubic aluminum nitride powder. The electron diffraction pattern exhibited from such powder is shown in Fig.4.

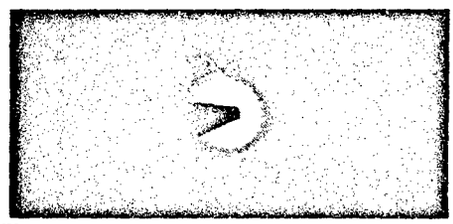
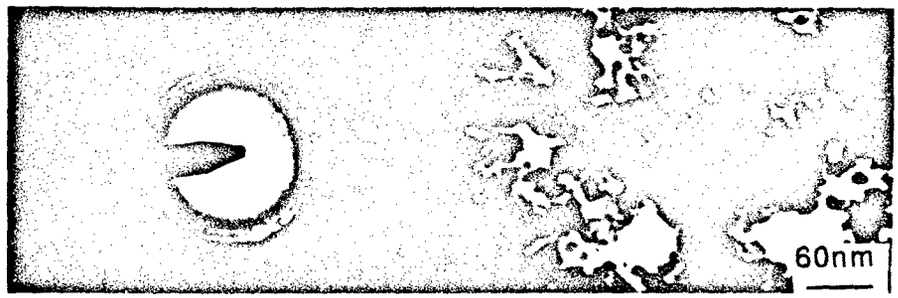


Fig.4. Electron diffraction from cubic aluminum nitride.

Finally, a still further increase of nitrogen concentration to 20 sccm with the same flow rates of TMA and argon resulted in hexagonal aluminum nitride. Figs.5a. and 5b. show electron diffraction and electron micrograph from such powder. The diffraction pattern could be indexed on the basis of hexagonal aluminum nitride phase with a=3.11Å and c=4.98Å.



Figs.5a. and 5b., Electron diffraction pattern and micrograph from aluminum nitride

Fig.6. shows the electron diffraction pattern exhibiting spots corresponding to the c-periodicity double that of the ususal c-periodicity without any change in the a-periodicity. This is evidence of the occurrence of polytypism in aluminum nitride.

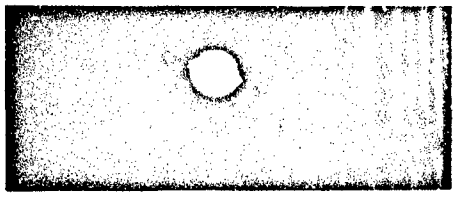
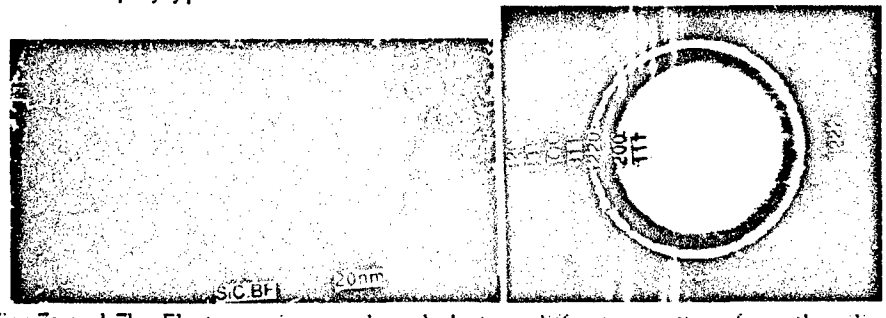


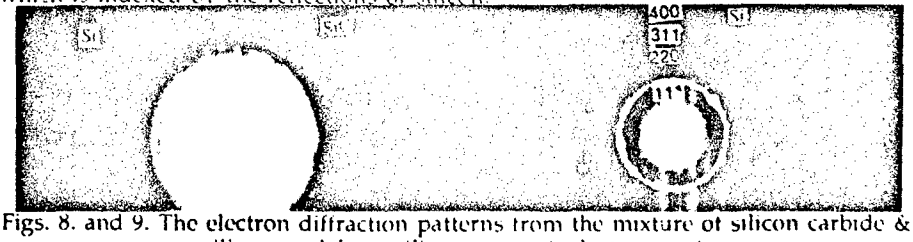
Fig. 6., Electron diffraction pattern showing double c-periodicity (polytypism).

The general appearance of the particles of silicon carbide in TEM is shown in Fig.7a. The powder electron diffraction pattern (Fig.7b.) from the particles collected on the filter corresponds to 3C modification with a = 4.36 Å. The flow rates used in this was 10 sccm of silane, 4 sccm of acetylene and 160 sccm of argon. An extensive investigation of a large number of isolated particles led to the discovery of different polytypic modifications (18)



Figs.7a.and 7b., Electron micrograph and electron diffraction pattern from the silicon carbide powder

When the flow rates for silane and acetylene were increased to 25 sccm of silane and 10 sccm of acetylene, respectively, the resulting particles were a mixture of silicon and silicon carbide, indicating that increased flow rates (decreased residence time in the plasma) is not favorable for synthesizing silicon carbide. Fig.8. shows the powder diffraction pattern which was indexed by reflections for silicon and silicon carbide with a mixture of 21R and 3C. Noticeably, all the rings for silicon are spotty. This implies that the number of silicon particles are small relative to the number of silicon carbide particles. A further increase in the flow rates to 50 sccm of silane and 20 sccm of acetylene of the precursor gases resulted in the particles rich in silicon. The electron diffraction from these is shown in Fig.9. which is indexed by the reflections of silicon.



Figs. 8. and 9. The electron diffraction patterns from the mixture of silicon carbide & silicon, and from silicon respectively (see text).

The silicon nitride was formed with flow rates of 3 sccm of silane, 15 sccm of nitrogen and 50 sccm of argon (18).

The size of the particles was determined by taking a dark field image partially enclosing the rings in the objective aperture. Figs.10a. and 10b. show the bright field and dark field images from aluminum nitride powder. The inset in Fig.10b. shows the rings partially enclosed in the aperture.

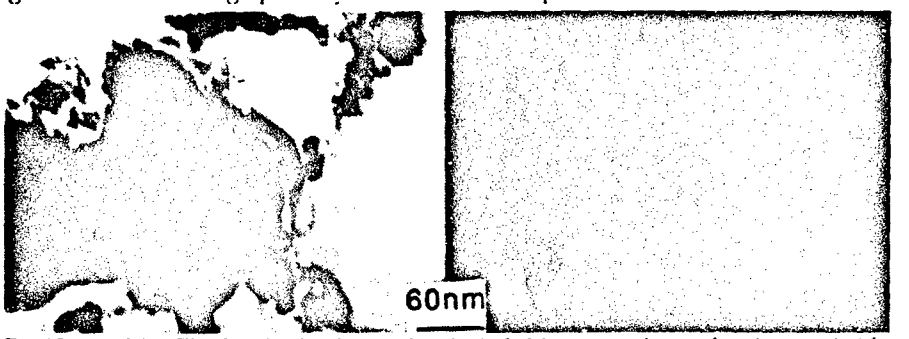


Fig.10a. and b., The bright field and the dark field images from aluminum nitride powder. The inset in Fig. 10b. shows the partial rings enclosed in the aperture.

Fig.11 shows the AES for the aluminum nitride powder. The oxygen peak is presumably due to absorption of oxygen by the fine particles during their transfer to the Auger electron microprobe.

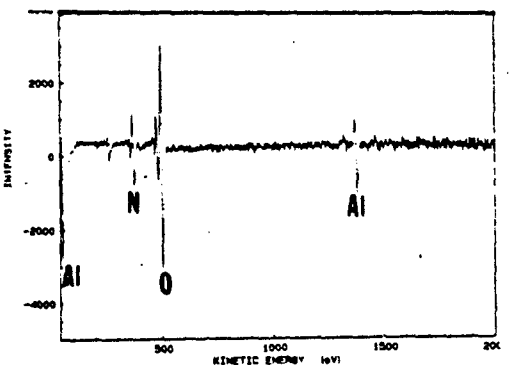


Fig. 11., AES spectrum for aluminum nitride powder.

Fig.12. shows the XPS data from the silicon carbide particles. The particles were cleaned by argon ions before recording the spectrum. The peak positions for the silicon carbide in XPS is clearly observed.

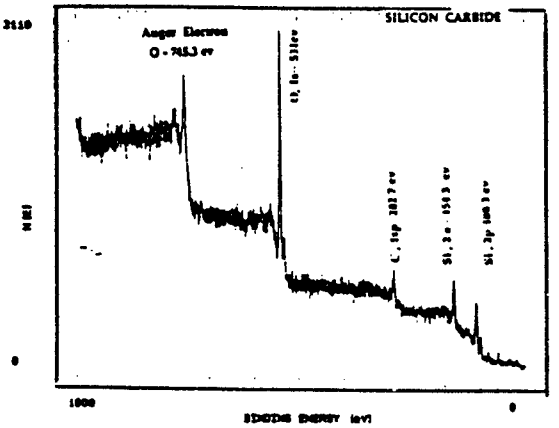
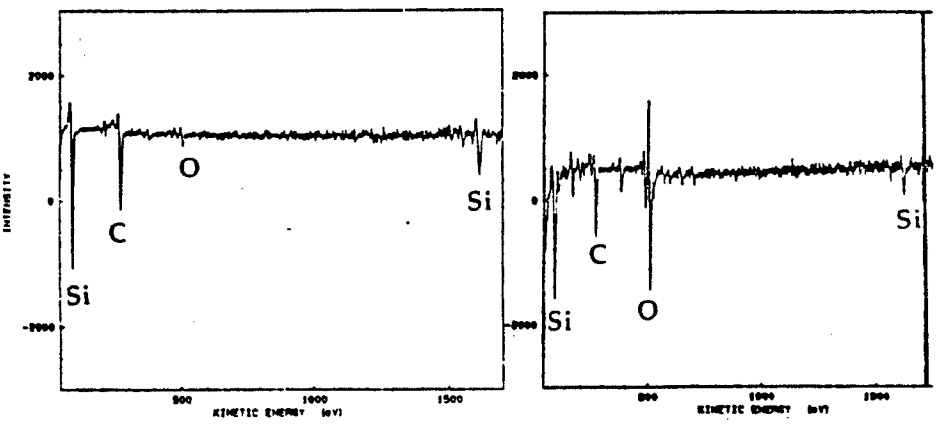


Fig.12., XPS spectrum from silicon carbide powder

Figs. 13a. and 13b. show the AES for standard silicon carbide and the siliconcarbide particles, respectively. It can be noticed that the signals for silicon and carbon in the two spectrums are tallying reasonably. The oxygen peak observed in the particles spectrum was expected due to the fact that particles were supported on magnesium oxide and due to absorption of oxygen by fine particles during their transfer to Auger electron microprobe.



Figs. 13a. and13b., AES data from standard and synthesized silicon carbide powder.

The observations provide evidence that crystalline aluminum nitride, silicon carbide and silicon nitride can be synthesized in a non-thermal microwave plasma of a gas mixture of precursor gases (TMA and nitrogen for aluminum nitride, silane and acetylene for silicon carbide, and silane and nitrogen for silicon nitride) and diluent and/or carrier gas argon. These particles are ultrafine (~5 nm).

The flow rates of the precursor gases decide the concentration and the residence time in the plasma ball and hence play an important role in the synthesis. Larger concentration of nitrogen was required to synthesise aluminum nitride. Presumably this increases the active nitrogen concentration. Lower concentration (lower flow rate) of nitrogen resulted in cubic aluminum nitride. An

evidence for the occurrence of polytypism in aluminum nitride has been encountered too.

The observations regarding synthesis of silicon carbide revealed that silicon forms at higher flow rates, (50 sccm of silane) . At medium (15 sccm) flow rates a mixture of silicon carbide and silicon is formed. At lower flow rates (4 sccm) only silicon carbide is synthesized. These observations support the idea that silicon carbide is formed by carborizing the silicon nuclei generated by microwave ionization of the silane. We have separately investigated effect of flow rates on the crystallinity of silicon resulting from triggering the microwave plasma in the laminar flow of the mixture of silane and argon. Varied flow rates (and hence the varied concentration) of silane were used: 5,10 and 20 sccm with 50 sccm of argon. The crystallinity as interpreted from the width of the x-ray diffraction peak was found to be the best for the intermediate flow rate viz.10 sccm. The crystallinity corresponding to 20 sccm of silane was slightly worse than that for 10 sccm of silane, and the crystallinity for 5 sccm of silane was the worst. It is remarkable to note that the flow rates of silane for the best formation of silicon carbide and the best crystallinity of silicon is the same, namely 10 sccm.

The aluminum nitride and the silicon carbide formed exhibited polytypism. The occurrence of polytypism in the nanometer sized particles suggests that the polytypes are formed during nucleation (Jagodginskie's theory) and not during growth (screw dislocation theory) (Ref.16 and references therein).

Silicon nitride could be formed within a narrow range of flow conditions.

The Auger electron spectroscopic analysis revealed the presence of oxygen on the surface. This is expected in view of particles being ultrafine and exposed to the atmosphere before the Auger spectrum analysis.

4. CONCLUSIONS

- The nonthermal synthesis of crystalline nanoparticles of aluminum nitride, silicon carbide and silicon nitride is possible.
- Aluminum nitride can be synthesized in either cubic or hexagonal modification depending on the synthesis parameters.
- Aluminum nitride and the silicon carbide powders exhibited polytypism.
- The occurrence of polytypism in ultrafine powder suggests that the polytypes are formed at the nucleation.

ACKNOWLEDGEMENT

Authors gratefully acknowledge the financial support from Army Research Office under Project Nos. DAAL03-89-K-0131 and DAAL03-88-G-0055 (Equipment).

REFERENCES:

1. K. Komeya, "Development of Nitrogen Ceramics", Ceram. Bull. 63(9), 1158-1159 and 1164 [1984].
2. "Aluminum Nitride Powders Predicted to Grow Through 1995". , Ceram. Ind., News, 134, 14, [1990].
3. Clifford F Lewis , "Silicon Carbide; The Hot One", M. E., May, 39-41[1989]
4. Neil N . Ault and John. T. Crowe. " Silicon Carbide"; Ceram. Bull.", 68[5] 1062-1063.[1989].
5. Clifford F. Lewis, "Silicon Nitride; The Rock Solid Performer," M. E. May, 30-33[1989].

6. Neil N. Ault and John T, Crowe." Silicon Nitride ; Ceram. Bull.;" 68[5] 1063-1064.[1989].
7. R. F. Davis, "Recent Advances Regarding the Definition of the Atomic Environment, Film Growth and Microelectronic Device Development in Silicon Carbide", in "The Physics and Chemistry of Carbides, Nitrides and Borides", Applied Sciences, Series E, Kluwer Acad. Pub. Co., 185, 589-623, [1989].
8. Ibid," Current Status of the Research on III-V Mononitride Thin Films for Electronic and Optoelectronic Applications", pp. 653-669.
9. W. Rafaniello, W. M. R. Plichta, and A. V. Virkor, "Investigation of Phase Stability in the System SiC AlN," J. Am. Ceram. Soc., 66[4] 272- 76 [1983].
10. S. Motojima and M. Hasegawa ,"Chemical Vapour Deposition of SiC. Layers from a Gas Mixture of CH_3 $SiCl_3$ +H_2 [+Ar], and Effects of the Linear Velocity and Ar Addition."J. Vac. Sci. Technol. A815, 3763-68,Sep/Oct. (1990)
11. W .R . Cannon, S. C. Danforth, J. H. Flint, J.S. Haggerty, and R. A .Marra, "Sintrable Ceramic Powders from Laser Driven Reactions; I Process Descriptions and Modelling." J. Am. Ceram. Soc., 65[7] 324 -30 [1982].
12. W. R. Cannon, S. C. Danforth, J. S. Haggerty, and R. A. Marra, "Sintrable Powder from Laser Driven Reactions: II Powder Characteristics and Process Variables," J. Am. Ceram. Soc. 65[7] 330 -35[1982].
13. K. Sawano, J. S. Haggerty and H. K. Bowen," Formation of SiC Powder from Laser-Heated Vapour Phase Reactions," J.Ceram Soc. Jpn 95[1] 64-69 [1987].
14. W. Symons and S.C. Danforth," Synthesis Characteristics of Laser Synthesized Silicon Nitride Powder," pp. 249-56 in Advances in Ceramics Vol. 21, Ceramic Powder Science, Edited by G. L. Messing, K. S. Mazdiyasni, J. W. McCanley and R. A. Haber. American Ceramic Society, Westerville,OH, [1987].
15. A.R. Verma and P. Krishna , " Polymorphism and Polytypism in Crystals", John Wiley & sons Inc. (1966)
16. G.C Trigunayat and A.R.Verma, " Polytypism and Stacking Fault", in Crystals with Layer Structure," pp 269-340. Vol.2, Edited by, F. Levy. D. Reidel publishing Co.[1976].
17. "Crystal Growth and Characterisation of Polytype Structures", Edited by, P. Krishna, Pergomon Press Ltd. [1983]
18. A. K. Singh and A. I. Kingon, "Syntesis of SiC Clusters in a Microwave Plasma" pp551-556. Vol.206, in " Cluster and Cluster Assembled Materials", (1990, MRS Fall Meeting, Boston MA). Edited by, R. S. Averback, D. L. Nelson and J. Bernholc.

Section VII. Microwave Applications in Waste Management

THE USE OF "SELF HEATING" CERAMICS AS CRUCIBLES FOR MICROWAVE MELTING METALS AND NUCLEAR WASTE GLASS

E. F. Sturcken
Building 773-A, Room C-160
Westinghouse Savannah River Company
Aiken, South Carolina, 29808-0001

ABSTRACT

Silicon carbide (SiC) crucibles were used to melt aluminum and copper in conventional and tuned microwave cavities at a microwave frequency of 2450 MHz. SiC crucibles were also used to vitrify and homogenize mixtures of nuclear waste and glass frit.

BACKGROUND

Microwave heating offers a number of advantages over conventional electric furnace heating in radioactive environments. Heating is faster and cooling is faster since, when the microwaves are switched off, no insulated heating coils are present to delay cooling. The sample is contained in microwave transparent insulation and the magnetron is isolated from the cavity so contamination incidents are more easily controlled. The microwave unit can easily be remoted, [1], so that the electric and electronic components are located outside the radiation cell, thereby simplifying operation and reducing maintenance.

A number of materials can be heated by applying energy to them in the form of high frequency electromagnetic waves, [2]. The mechanism of heating depends on the nature of the material, i.e., its electronic, molecular and crystalline structure and its microstructure and impurity content.

Note: This paper also appears in Ceramic Transactions Vol. 23: Nuclear Waste Management IV.

Dielectric heating has its origin in the ability of the applied high frequency electric field to polarize the charges in the material and the inability of this polarization to remain in phase with the extremely rapid reversals of the field. There can also be heating due to relaxation and resonance processes under the influence of the alternating magnetic field. In addition conduction type heating occurs due to charge particles forming conducting paths under the influence of the applied field.

The first application of microwave heating to ceramics was due to M. L. Levinson, [3,4] , who patented a "Microwave Kiln" in 1969 and "Methods of Firing Ceramic Articles Utilizing Microwave Energy" in 1971.

A furnace with more uniform heating and requiring less microwave power was patented, [5] , in 1981 by S. Maeda, Y. Minowa and H. Komura. The unit employs ZrO_2 and ZnO as heating materials.

A microwave muffle furnace employing SiC components was described by E. D. Neas and M. J.Collins, [6] . The heating elements for the furnaces are housed in microwave transparent refractory insulators and the furnaces fit into conventional size microwave ovens.

Materials that have high absorption factors for microwaves are described as "lossy" and heat rapidly, even in conventional microwave units with nominal powers, e.g.,600 watts. Some examples of lossy ceramics are SiC, ZrO_2, ZnO, UO_2, U_3O_8, and PuO_2 (see other papers in this book).

The crucible material for the present studies was SiC. The first microwave application of SiC was its use as a high efficiency "dummy load" to absorb radar and prevent its escape during tuning of radar transmitters for military application, where secrecy of location was important to the security of the device.

MELTING NUCLEAR WASTE GLASS

SiC crucibles and a muffle furnace, [6] , constructed of SiC components, were both used to vitrify and homogenize mixtures of simulated nuclear waste and glass frit. The SiC for the crucibles and the muffle furnace was housed in microwave transparent fused quartz foam insulation.

The microwave systems used for melting the nuclear waste glasses were 850 watt multimode commercial units with furnace temperature controls of +/- 5 oC.

In the Floyd microwave system, an Al_2O_3 crucible containing the mixture of simulated nuclear waste and glass frit, was contained in an SiC crucible which was mounted in a block of fused quartz foam insulation. The insulation block was split in two with cylindrical holes in the top and bottom so that the SiC crucible fit snugly into the holes.

The CEM Corporation microwave system and muffle furnace* arrangement is shown in Fig. 1. Heating was more rapid and required less power with the SiC crucible than the SiC muffle furnace since the heat source was more insulated and closer to the sample.

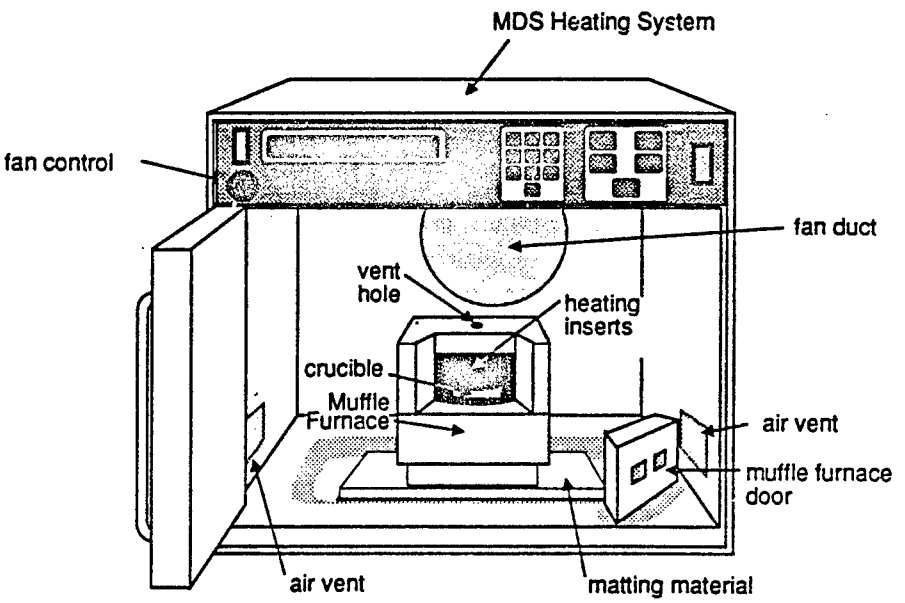


Figure 1. Muffle Furnace Arrangement For Melting Glass.

* Model MDS-205, CEM Corporation, Matthews, N.C. 28105

The Floyd, Inc., microwave system* is more suitable for the Defense Waste Processing Facility (DWPF) since it is already remoted for operation in environments that are either corrosive or contain a high level of nuclear radiation that is harmful to personnel and deteriorate the physical, mechanical and electronic properties of the instrument.

The dimensions of the SiC crucibles** were .044 m (1.75 in.) O D X .038 m (1.50 in.) I.D. by .089 m (3.50 in.) length. The length was reduced to .051 m (2.00 in.) for these experiments.

To localize the heating and preserve the SiC crucible for further melts, the material to be melted was placed in a Pt, MgO, Al_2O_3 or BN crucible which was in turn placed in the SiC crucible.

Platinum and other metals do not arc when enclosed in SiC crucibles or furnaces in the microwave cavity because the "lossy" SiC absorbs nearly 100% of the microwaves, heats rapidly and in turn heats the metal. The SiC muffle furnace reached a temperature of 1100 ° C in about 15 minutes and the SiC crucibles in about 10 minutes due to their smaller mass.

Mixtures of 3 to15 grams of simulated nuclear waste and glass frit were melted and homogenized in platinum and Al_2O_3 crucibles in less than 10 minutes. These nuclear waste glasses are discussed by C.M. Jantzen in the next paper of this book, "Characterization of Radioactive Waste Melter Feed Vitrified by Microwave Energy".

The molten liquid glass was observed to be extremely mobile during microwave melting; displaying a wave like and sometimes bubbling motion. This natural agitation is probably due to the high thermal and field intensity gradients inherent in microwave heating and considerably enhances homogenization and diffusion in the molten liquid.

* Model RMS-150, Floyd Inc., Lake Wylie, S. C. 29710

** Cryston, type CN-137, Si_3N_4 bonded SiC, Norton Company, Worcester, MA., 01615

MELTING METALS

Metals can be heated, melted or reacted with other materials in a microwave cavity by placing the metal in a SiC crucible or other ceramic crucible which has a high absorption factor for microwaves.

The SiC crucible rapidly heats by absorbing nearly 100 percent of the microwaves then transfers the heat to the metal. The caveat of metal melting is oxidation; hence all melting must be performed in an inert atmosphere or under vacuum.

Copper was melted using a 2 kilowatt, resonant cavity microwave system*, Fig. 2. The "tuned" single mode cavity provided a higher microwave field intensity through direct coupling of the microwave energy with the SiC crucible and the metal sample.

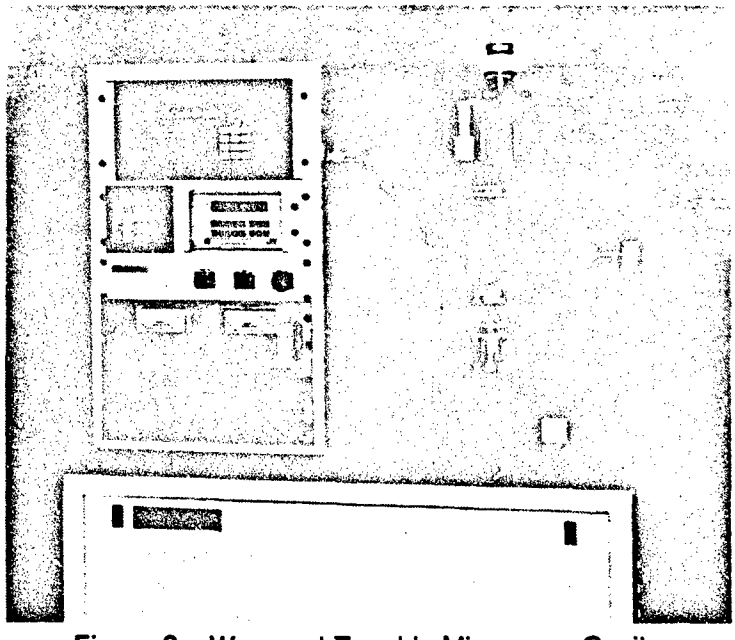


Figure 2. Wavemat Tunable Microwave Cavity.

* Model MCR-1300, Wavemat, Inc., Plymouth, MI., 4817

In these experiments, the cavity dimensions were continuously adjusted , i.e., "tuned", to maximize microwave absorption as it changed with increasing temperature. The copper was completely melted (m.p. = 1085 ° C) in less than 20 minutes using a net power of 575 watts.

The dimensions of the cavity, Fig. 2, were changed with the vernier controlled sliding "short" at the top of the cavity and the adjustable microwave "launch" probe in the wall cavity on the right side. The sample mounting stage is shown at the bottom in the open position. The inlet and outlet for gas are located on the top and bottom of the cavity. The cavity is water cooled.

The temperature is sensed through the front glass port by an optical fiber thermometer system attached to the right side of the instrument panel. The microwave cavity was designed so that an inert gas could continuously flow over the sample.

Argon and nitrogen gases were employed in the present experiments; however nitrogen caused a black oxide to form over the melt. An open port is available in the top of the cavity to observe or video tape the appearance of the sample as it heats. After melting, the copper was observed to bubble profusely throughout the crucible until the microwave power was turned off.

As suggested in the case of the glass, the bubbling is believed to be due to the field intensity and associated thermal gradients inherent in the microwave heating process. The stirring action provided by bubbling should enhance diffusion and homogenization and eliminate the need for mechanical stirrers required for carrying out some sluggish chemical reactions,e.g., molten salt reductions of metal oxides.

To preserve the SiC crucible for further melts the copper cylinder, .016 m (0.625 in.) diameter X .038 m (1.5 in.) length,was inserted in an MgO crucible, .032 m (1.25 in.) OD X .025 m (1.00 in.) ID X .064 m (2.5 in.) length. The MgO crucible was in turn inserted in the SiC crucible whose dimensions were .064 m (1.8 in.) OD X .038 m (1.5 in.) ID X .064 m (2.5 in.) length. The MgO crucible was relatively transparent to the microwave radiation.

Metals may also be melted with the multimode units discussed above as long as an inert gas or vacuum environment is provided .

For all of these units, the mass of the "lossy" material, i.e., the SiC crucible, or the argon pressure must be adjusted to prevent breakdown of the argon into a plasma by the microwaves.

CONCLUSIONS

SiC crucibles heated by microwaves were used as secondary containers to melt and homogenize mixtures of nuclear waste and glass frit and to melt metals.

The microwave heating system is more flexible and efficient since the mass and geometry of the crucible or muffle furnace can be designed to provide the required power and be located closer to the sample than in conventional furnaces.

During microwave melting the molten liquid is agitated by bubbling and wave like motion; hence reaction rates and homogenization are enhanced.

ACKNOWLEDGMENTS

The information contained in this article was developed during the course of work under contract number DE-AC09-89SR18035 with the U.S. Department of Energy. The author wishes to express his appreciation to Dan F. Steedly and James R. Cadieux, Jr. of WSRC for their assistance with the experiments.

REFERENCES

1. E. F. Sturcken, T. S. Floyd, D. P. Manchester, Chapter 9, "Remote Operation of Microwave Systems", pp. 188-202, "Introduction to Microwave Sample Preparation", H.M. Kingston, L.B.Jassie, ACS Professional Reference Book, American Chemical Society, Washington, D. C., 1988.
2. R. C. Metaxas, R.J. Meredith, "Industrial Microwave Heating", Peter Peregrinus Ltd., London, UK., 1983.
3. M. L. Levinson, "A Microwave Kiln", U.S. Patent # 3,469,053, 1969.
4. M. L. Levinson, "Methods of Firing Ceramic Articles Utilizing Microwave Energy", U.S. Patent # 3,585,258, 1971.
5. S. Maeda, Y. Minowa, H. Komura, "Microwave Heating Oven" , U.S. Patent # 4,307,277, 1981.
6. E. D. Neas, M. J. Collins, Chapter 2, "Microwave Heating", pp. 28,30, "Introduction to Microwave Sample Preparation", H.M. Kingston, L.B. Jassie, ACS Professional Reference Book, American Chemical Society, Washington, D. C., 1988.

CHARACTERIZATION OF RADIOACTIVE WASTE MELTER FEED VITRIFIED BY MICROWAVE ENERGY

Carol M. Jantzen and James R. Cadieux
Westinghouse Savannah River Co.
Savannah River Laboratory
Aiken, SC 29808

ABSTRACT

Liquid high-level nuclear waste will be immobilized at the Savannah River Site (SRS) by vitrification in borosilicate glass. The glass will be processed in the Defense Waste Processing Facility (DWPF) and poured into stainless steel canisters for eventual disposal in a geologic repository. Vitrification of melter feed samples is necessary for DWPF process and product control. Microwave fusion of melter feed at ~1200°C for 10 minutes has been shown to yield homogeneous glasses comparable to those melted in a conventional furnace for 4 hours. Microwave fusion at lower temperatures for longer times was found to crystallize $NiFe_2O_4$ spinel. The use of higher temperatures was determined to cause significant volatilization and recrystallization of the glass. Redox measurements indicated that microwave vitrification of melter slurries may also yield more representative measures of glass $Fe^{2+}/\Sigma Fe$ ratio of the glass which is important to melter processing of the glass.

INTRODUCTION

Liquid high-level nuclear waste will be immobilized at the Savannah River Site (SRS) by vitrification into borosilicate glass at the Defense Waste Processing Facility (DWPF). In this facility, control of the oxidation/reduction (redox) equilibrium in the glass melter is critical for processing of the nuclear waste. The glass needs to be somewhat reducing to minimize foaming[1] of the melt and devitrification of the glass.[2] However, overly reducing conditions may cause metallic species to form in the melt. The metallic species can agglomerate, settle to the floor of the melter, and potentially short the electrodes in the joule-heated melter.[3-6] As part of the DWPF process control strategy, the glass redox expected in the melter will be determined by measuring the ratio of $Fe^{2+}/\Sigma Fe$ in vitrified slurry from the Slurry Mix Evaporator, SME (Figure 1).[7,8] Chemical analysis of the vitrified SME feed will be used to ensure that other process control constraints are satisfied.[9] These constraints are related to glass viscosity, liquidus, and waste component solubility.[10] The vitrified SME product must meet these

Note: This paper also appears in Ceramic Transactions Vol. 23: Nuclear Waste Management IV.

constraints before the feed can be sent to the Melter Feed Tank (MFT) and subsequently to the DWPF melter (Figure 1).

The glass melted in the DWPF will be poured into stainless steel canisters for eventual disposal in a geologic repository. The canistered borosilicate waste glass must comply with the Waste Acceptance Preliminary Specifications (WAPS) established by the DOE Office of Civilian Radioactive Waste Management.[11] Specification 1.1.2 requires the elemental composition of the glass waste form be reported for all elements present in concentrations greater than 0.5 percent by weight. According to current plans for the DWPF analytical facility, elemental analyses will be performed on the vitrified melter feed from the MFT.[9]

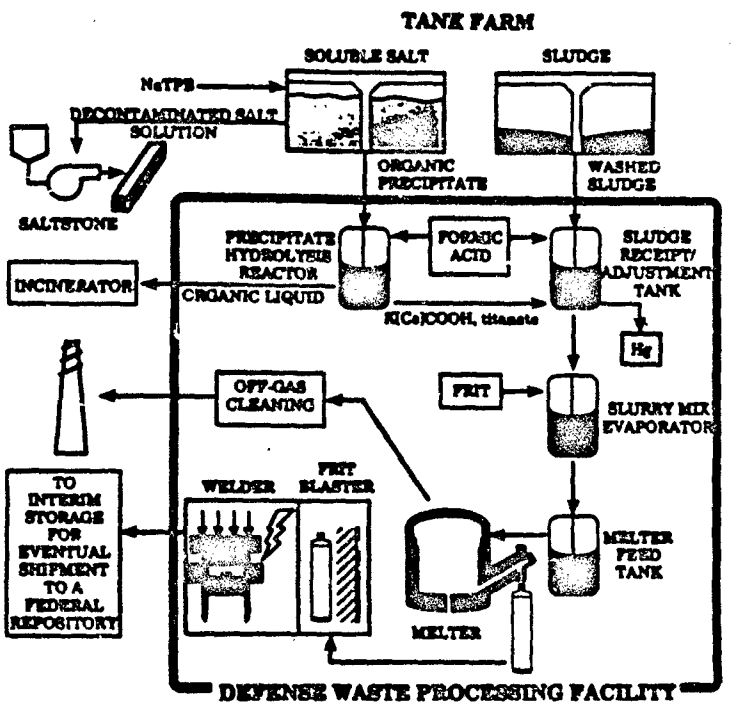


Figure 1. Schematic of the glass melting process in the Defense Waste Processing Facility (DWPF).

Melter feed slurries contain many anionic components other than oxygen, making an oxide basis calculation difficult. Moreover, the slurries contain considerable amounts of organics, formic acid and tetraphenylborate. After vitrification, however, oxygen can be assumed to be the only anion present in the waste glass, and the vitrified glass can be analyzed simultaneously with NIST (National Institute of Standards and Testing) standard glasses for greater precision and accuracy.[9]

Conventional vitrification of SME/MFT slurries takes 4 hours at the DWPF melt temperature of 1150°C. The fusions are carried out in sealed crucibles so that the carbon volatilizing from organics controls the oxygen fugacity, fO_2, of the atmosphere in the crucible.[7,8] The oxygen fugacity, in turn, controls the equilibrium between the oxidized Mn_2O_3 and Fe_2O_3 and the reduced MnO and FeO species in the glass.

Microwave fusions of crushed rock with $Li_2B_4O_7$ added as a flux have been shown to produce very homogeneous glass in 24 minutes,[12] presumably due to the rapid convection in the crucible. This technology has now been applied[13] to the vitrification of simulated nuclear waste slurries. Microwave slurry vitrification has been shown to significantly reduce the time required to vitrify slurry samples.[13] In this study, the homogeneity and redox ratio of microwave vitrified slurries were examined. The redox ratio was determined from the $Fe^{2+}/\Sigma Fe$ equilibrium in the glass produced. This enabled the optimum time and temperature for microwave vitrification of melter slurries to be determined.

EXPERIMENTAL

In the preliminary experiments, a wide range of variables and conditions were tested at the vendor's establishment. Small amounts of sample were used and the usage of Al_2O_3 crucibles, used in conventional vitrification, was not examined. The sample size ranged from 1-10 grams. Simulated SME slurry was dried in a conventional oven while other portions were dried in the microwave furnace at 10% power for 20 minutes (Table I). In these tests open porcelain, silica, and platinum crucibles were used and microwave furnaces of different wattage were tested.[13] The microwave fusions were carried out at varying times and temperatures (Table I). Each vitrified sample was submitted for x-ray diffraction (XRD) analysis so that the homogeneity of the resulting glass could be determined. For glasses which were not homogeneous, the crystalline phase content was determined by XRD. There was sufficient material to analyze the $Fe^{2+}/\Sigma Fe$ ratio of two of the samples in duplicate. Conventional vitrification of the same slurry was carried out in duplicate in closed crucibles at 1150°C for periods of 1 hour and 4 hours. The comparative $Fe^{2+}/\Sigma Fe$ redox ratios were determined.

In a second set of experiments, the DWPF reference sample size and temperature were used (Table II). The tests were carried out at the Savannah River Laboratory with a CEM Corporation microwave. The performance of Al_2O_3 and Pt crucibles were compared. The reference sample size was 40 to 60 mL of well characterized synthetic SME slurries. The

Table I. Characterization of Preliminary Microwave Vitrified Melter Slurries

Run No.	Starting Material	Temp (°C)	Total Time (min)	Type of Crucible	Crystal Phases Present
1	dried slurry	1100	45	porcelain	$NiFe_2O_4$ spinel
2	dried slurry	1100	240	porcelain	$NiFe_2O_4$ spinel & Al_2O_3
4*	dried slurry	~1500	20	porcelain	Fe_3O_4 spinel & $MgSiO_3$ (enstatite) & $2SiO_2 \cdot 3Al_2O_3$ (mullite) & Al_2O_3
5*	micro-wave dried slurry	~1500	5	porcelain	$Mn_{1.5}Cr_{1.5}O_4$ & $NiFe_2O_4$ spinel & $2SiO_2 \cdot 3Al_2O_3$ (mullite) & Al_2O_3
7*	micro-wave dried slurry	1200	10	porcelain	None
8*	dried slurry	1200	10	Pt	None
9*	dried slurry + 165 black frit	1200	10	SiO_2	None

* Vitrified in 1000-watt CEM Model MDS-205 oven; Runs 1 and 2 were vitrified in a 600-watt CEM Model MDS-81D microwave dissolution oven that was not designed as a higher temperature oven.

Table II. Characterization of DWPF Reference Slurries Vitrified by Microwave

Run No.	Starting Material	Amount (mL)	Temp (°C)	Total Time (min)	Crucible	Crystal Phases Present
1	microwave dried slurry	60	1150	15	Al_2O_3	None
2	IR dried slurry	60	1150	15	Pt	None
3	microwave dried slurry	60	1150	15	Al_2O_3	None
4	microwave dried slurry	60	1150	15	Pt	None
5	microwave dried slurry	40	1153	19	Al_2O_3	None
6	DWPF startup frit (dry)	20g	1150	15	Pt	None
7*	microwave dried slurry	40	1150	15	Pt	SiO_2
8[t]	slurry	60	1150	4 hrs	Al_2O_3	None
9*[t]	slurry	60	1150	4 hrs	Al_2O_3	SiO_2

* SiO_2 due to additions of excess frit to these slurries

t Melted in a conventional oven for 4 hours for comparison

slurries were dried in the CEM Corporation microwave furnace at 10 to 20% power. Because of the large slurry volumes the evaporation took ~ 3 hours. Vitrifications were carried out in covered Pt and alumina crucibles at ~1150°C for 15 minutes (Table II). The 1150°C temperature was used in these experiments because it is the temperature that will be used to melt nuclear waste glass in the DWPF. Each vitrified sample was submitted for XRD analysis so that the homogeneity of the resulting glass could be determined. For glasses which were not homogeneous, the crystalline phase content was determined by XRD. Elemental composition and redox determinations of these samples will be performed in the future.

The 1000-watt CEM microwave furnace, model CEM MDS-205, was used for some of the preliminary experiments and for all of the DWPF reference set of experiments. This furnace has silicon carbide heating elements of 1/2"-thick disk and bars in a 2" thick refractory shell, which surrounds the 60 mL crucibles of slurry. The shell has a removable top to allow insertion and removal of the sample crucible. During sample drying, the microwave was operated at 10-20% power with the top removed. A high forced air flow, used to keep the interior of the microwave cool, aided the evaporation. The rate of drying was limited by splattering of the viscous slurry. After evaporation to a thick, nonflowing consistency, the top was replaced and the samples were heated at full power to 1150°C. The refractory, silicon carbide, and crucible took about 35 minutes to reach 1150°C. Temperature was monitored by a thermocouple penetrating the refractory/ to within 1/4" of the crucible and controlled to within ±5°C. After 15 minutes, the refractory block containing the crucible could be taken from the microwave. The top half of the refractory was removed and the crucible lifted out to cool.

RESULTS AND DISCUSSION

X-ray diffraction analysis of the dried SME slurries from the preliminary experiments indicated that the 1200°C heat treatment for 10 minutes produced totally amorphous and homogeneous glass regardless of whether the crucible was porcelain, Pt, or SiO_2 (Table I). This is the test temperature that most closely represents the DWPF reference melt temperature of 1150°C.

Slurries which had been dried and then heated at 1100°C, ~50°C below the 1150°C melt temperature, for 3/4 to 2 hours formed $NiFe_2O_4$ spinel and Al_2O_3 (Table I). The presence of Al_2O_3 indicates that reaction of the glass with the porcelain crucible had occurred. The presence of spinel indicate that the heat treatment temperature was below the glass liquidus which caused the glass to crystallize.

Slurries which had been dried and then vitrified at 1500°C for 5 and 20 minutes formed several crystalline phases due to the decomposition of the glass (Table I). This decomposition was caused by a combination of alkali vaporization and decomposition of the porcelain crucibles, which only tolerate maximum temperatures of ~1250°C. The crystalline phases observed included various spinels, mullite ($2SiO_2 \cdot 3Al_2O_3$), and some magnesium or magnesium-iron silicate (enstatite or magnesioferrite solid solution in the pyroxene family).

The $Fe^{2+}/\Sigma Fe$ ratio was only measured on the homogeneous glasses formed during Runs 8 and 9 because there was insufficient samples for the other runs (Table I). Run 8 was fabricated from dried slurry and Run 9 was fabricated from 1/4 dried slurry and 3/4 simulated nuclear waste glass 165, which had been purchased from a vendor as a "black" frit-like glass making material. The redox values measured varied from 0.12 to 0.15, which is less than the 0.33 $Fe^{2+}/\Sigma Fe$ ratio specified for DWPF operation.[7] Conventional vitrification of the same SME slurry for 1 hour and 4 hours indicated that the $Fe^{2+}/\Sigma Fe$ ratio was very oxidizing with values ranging between 0.004-0.017. This indicates that the use of open crucibles during microwave fusion of DWPF slurries may give a conservative (overly reduced) $Fe^{2+}/\Sigma Fe$ ratio due to the rapidity of the reactions.

During the DWPF reference experiments, directed heating of the area immediately around the sample with microwave energy was found to be very effective and to allow rapid cycling of samples. Customizing the shape of the refractory heating block provided the optimum geometry for the experiments. Using the microwave to both dry and vitrify 40-60 mL of slurry has significant advantages for processing radioactive material where space in contained and shielded areas is limited and remote handling of sample transfers is difficult.

It was also determined that the vitrified glass samples could be removed more easily from the Pt crucibles than from the alumina crucibles. This was achieved by thermally shocking the bottom of a warm Pt crucible containing the glass on a cold surface and then mechanically flexing the sides of the crucible. The glass usually "popped" out cleanly in one or two large chucks leaving little or no residue on the inside of the Pt crucible. The alumina crucibles usually cracked or shattered on cooling with much if not most of the glass firmly embedded on the alumina shell. The use of Pt crucibles will, therefore, eliminate the need to dispose of contaminated alumina crucibles in DWPF.

Nearly all of the glasses vitrified in the CEM MDS-205 at 1150°C for 15 minutes were homogeneous (Table II). Only one sample, Run 7, contained crystalline SiO_2. Samples were also melted in a conventional furnace for 4 hours for comparison (Run 8 and 9, Table II). One of these samples also contained crystalline SiO_2 since some excess glass forming frit had been added to this slurry.

CONCLUSIONS

Microwave vitrification has been shown to be an acceptable process for fabricating homogeneous glass samples for DWPF process control and WAPS reporting. A 1000-watt CEM MDS-205 microwave with a ceramic susceptor block in which the crucible was placed was found to give the most rapid and reproducible temperature response. The glasses fused for 10-15 minutes at 1150-1200°C yielded the most homogeneous glasses. Longer times and lower temperatures cause the formation of spinel while higher temperatures and shorter times cause significant volatilization of alkali and recrystallization of the glass. Pt crucibles were found to be completely reusable. Use of Pt crucibles in DWPF would eliminate the disposal problems

associated with the usage of alumina crucibles, which become contaminated during the slurry vitrification.

Microwave vitrification appeared to form more homogeneous glass than conventional vitrification. This may be attributed to the rapid thermal convection currents set up in the crucible during the intense microwave treatment as noted in glasses fabricated from crushed rock with $Li_2B_4O_7$.[12]

Drying of small amounts of slurry before vitrification, can be achieved in the microwave at 10% power in 20 minutes. Larger volumes of slurry can take up to 3 hours. Since vitrification takes only 10 minutes the entire DWPF glass fabrication procedure can be reduced from the current 4-hour duration to 30 minutes if small amounts of slurry are used. This is actually a larger reduction in time since ~2 hours drying is also necessary for conventional vitrification.

Comparison of $Fe^{+2}/\Sigma Fe$ ratios from the 1200°C/10-minute microwave vitrification in open crucibles demonstrated that these glasses were more reduced than those vitrified in a conventional oven at 1150°C for 1 and 4 hours. The microwave vitrification may, therefore, yield a more conservative measure of glass redox than conventional vitrification. The reproducibility of the redox measurement is currently under investigation.

ACKNOWLEDGEMENT

This paper was prepared in connection with work done under Contract No. DE-AC09-89SR18035 with the U.S. Department of Energy.

REFERENCES

1. M. J. Plodinec, "Factors Affecting the Iron Oxidation State and Foaming in SRP Waste Glass," Proceedings of the Symposium on High Temperature Materials Chemistry, D. D. Cubicciotti and D. L. Hildebrand (Eds.), The Electrochemical Society, Pennington, New Jersey, 201-209 (1982).

2. C. M. Jantzen, D. F. Bickford and D. G. Karraker, "Time-Temperature-Transformation Kinetics in SRL Waste Glass," Advances in Ceramics, V. 8, G. G. Wicks and W. A. Ross (Eds.), 30-38 (1984).

3. D. F. Bickford and R. B. Diemer, Jr., "Redox Control of Electric Melters with Complex Feed Compositions, Part I. Analytical Methods and Models," J. Non-Cryst. Solids, 84, 276-284 (1986).

4. D. F. Bickford and R. B. Diemer, Jr., D. C. Iverson "Redox Control of Electric Melters with Complex Feed Compositions, Part II. Preliminary Limits for Radioactive Waste Melters," J. Non-Cryst. Solids, 84, 285-291 (1986).

5. D. F. Bickford, R. C. Probst, and M. J. Plodinec, "Control of Radioactive Waste Glass Melters: Part III. Glass Electrical Stability," Advances in the Fusion of Glass, D. F. Bickford, et. al. (Eds.), The American Ceramic Society, Westerville, OH, 19.1-19.17 (1988).

6. L. R. Bunnell, "Laboratory Work in Support of West Valley Glass Development," USDOE Report PNL-6539, Battelle Pacific Northwest Laboratory, Richland, WA (May, 1988).

7. C.M. Jantzen and M.J. Plodinec, "Composition and Control of Waste Glasses: Recommendation for Process Control Limit," USDOE Report DPST-86-773, E.I. duPont deNemours & Co., Aiken, SC (November, 1986).

8. C.M. Jantzen, "Verification and Standardization of Glass Redox Measurement for DWPF," USDOE Report DPST-89-222, E.I. duPont deNemours & Co., Aiken, SC (January, 1989).

9. C.M. Jantzen, "Verification of Glass Composition and Strategy for SGM and DWPF Glass Composition Determination," USDOE Report DPST-86-708, E.I. duPont deNemours & Co., Aiken, SC (March 30, 1987).

10. D.F. Bickford, A.A. Ramsey, C. M. Jantzen, and K.G. Brown, Control of Radioactive Waste Glass Melters: I. Preliminary General Limits at Savannah River," J. Am. Ceram. Soc., 73[10], 2896-2902 (1990).

11. Waste Form Compliance Plan for the Defense Waste Processing Facility," USDOE Report WSRC-SW4-6, Rev. 0, Westinghouse Savannah River Co., Aiken, SC (March, 1990).

12. S.A. Matthes, "Guidelines for Developing Microwave Dissolution Methods for Geological and Metallurgical Samples," in Introduction to Microwave Sample Preparation, Theory and Practice, H.M. Kingston and L.B. Jassie (Eds.), American Chemical Society, Washington, DC, 33-52 (1988).

13. C.M. Jantzen, "Characterization of Melter Slurries Vitrified by Microwave," USDOE Report WSRC-TR-90-204, Rev. 1, Westinghouse Savannah River Co., Aiken, SC (April, 1991).

MICROWAVE PROCESSING OF SIMULATED NUCLEAR WASTE GLASS

R.L. Schulz, Z. Fathi, D.E. Clark
Department of Materials Science and Engineering
University of Florida
Gainesville, FL 32611

G.G. Wicks
Westinghouse Savannah River Co.
Aiken, SC 29808

ABSTRACT

The objective of this study was to determine the effect of microwave processing on nuclear waste glass properties. Several experiments were carried out using microwave heating techniques using borosilicate glass frit containing simulated nuclear waste material and borosilicate glass frit without waste products. A time study was conducted to determine whether or not microwave processing can produce a homogeneous glass melt (in less time) when compared with conventional heating methods. Surface analysis techniques such as FTIRRS and SEM were conducted to determine the quality of the glasses. Some preliminary short-term leaching experiments were run to begin determination of the durability of waste glasses processed using microwave heating.

INTRODUCTION

In the United States today there are approximately 100 million gallons of high level radioactive waste [1]. The current strategy for storage of this waste is in underground steel tanks. Most of these tanks were constructed in the late 1940's and early 1950's and are approaching the end of their projected lifespans. Because of this and the need to find a safe long-term disposal method, researchers are investigating several proposed systems of waste encapsulation.

Most countries including the United States, who have made a choice, have selected vitrification in a borosilicate matrix for long-term disposal of their waste. One result of this extensive research and selection process is the Defense Waste Processing Facility at Savannah River. This facility which is 95-99% complete will process over 1.5 tons of glass/waste per day when fully operational.

There is precedence for the use of microwave energy for drying, sintering and joining ceramic materials [2-6]. The preliminary work presented in this paper proposes perhaps the next iteration for a radioactive waste processing facility. The objective of the study was to determine whether or not simulated nuclear waste glass frits could be successfully melted using microwave

Note: This paper also appears in Ceramic Transactions Vol. 23: Nuclear Waste Management IV.

energy [2], and if so, what period of time would be required to achieve a homogeneous melt, and finally, would the chemical durability of the glass be retained. The experimental procedure for this application is described below.

EXPERIMENTAL

Equipment/Materials

The microwave energy source used in all experiments was a RadarLine[1] microwave operating at 2.45GHz. K-type thermocouples[2] were used to determine the temperature of the sample and a Fisher X-Y recorder was connected to the thermocouple to record sample temperature versus time. Alumina crucibles were used to contain the melt. Borosilicate glass frits (SRL-165 and SRL-165/29.8wt% TDS) were obtained from Westinghouse Savannah River Co.

Procedure

The compositions of the glass frits are shown in Table I and were used as received with the exception of the mixed frit samples. In the heating rate experiment, 20 gram samples were weighed out for the SRL-165, the SRL-165/29.8wt% TDS and a mixture of the two frits containing 15wt% TDS. The mixed frit sample was milled for 24 hours prior to melting to assure complete mixing of the two frits. The samples were placed in fused silica crucibles and set inside a SiC lined zirconia susceptor. A thermocouple was then inserted into the sample. The duty cycle was set at 70% and the power was adjusted by activating two of the magnetrons (800 watts each). The microwave and X-Y recorder were turned on simultaneously. The glass samples ramped up to the accepted melting point for these compositions (1150°C) in approximately 17 minutes and were held at that temperature for 10 minutes. In order to maintain the melt temperature it was necessary to decrease the duty cycle to an average of 43% ± 5%. Upon completion of the run the samples were placed in an annealing oven for one hour at 500°C.

Similar procedures were carried out for the two homogeneity studies with the exception of using alumina crucibles and 30 gram samples. The decision to switch to alumina crucibles was made after it was observed that the samples fractured upon annealing. This was thought to be due to differences in thermal expansion coefficients between the fused silica and borosilicate glass samples. This problem did not occur after the change to alumina crucibles was made. Sample weights were also increased at this time in order to fully fill the crucibles and to insure that there would be sufficient glass product for sample analysis.

---

[1] Raytheon Co. Waltham, MA Model# QMP-2101B-6

[2] Omega Engineering, Inc., Stamford, CT 06906

Table 1. Borosilicate Frit Compositions

COMPONENT	SRL-165 (wt%)	SRL-165/29.8wt% TDS (Ferro AX-581875)
SiO_2	68.0	54.1
B_2O_3	10.0	6.8
Na_2O	13.0	10.3
MgO	1.0	0.8
ZrO_2	1.0	1.2
Fe_2O_3	--	12.3
Li_2O	--	4.7
MnO_2	--	2.9
Al_2O_3	--	4.1
NiO	--	0.9
CaO	--	1.5
Cl	--	0.05
Pb	--	0.05
F	--	0.06

RESULTS

Heating Rate Experiment

The results of the heating rate experiment are summarized in Figure 1. It is clear from these results that the use of microwave hybrid heating allows the glass frits to couple with the microwaves and that melting does not occur solely from heat supplied by the susceptor [7,8]. This is evidenced by the rapid increase in temperature between 400-500°C. It was also expected that SRL-165/29.8wt% TDS and mixed frit compositions would heat at somewhat faster rates than the SRL-165 frit due to the increased amounts of iron and other metallic compounds contained in the simulated waste product interacting with the microwaves [9].

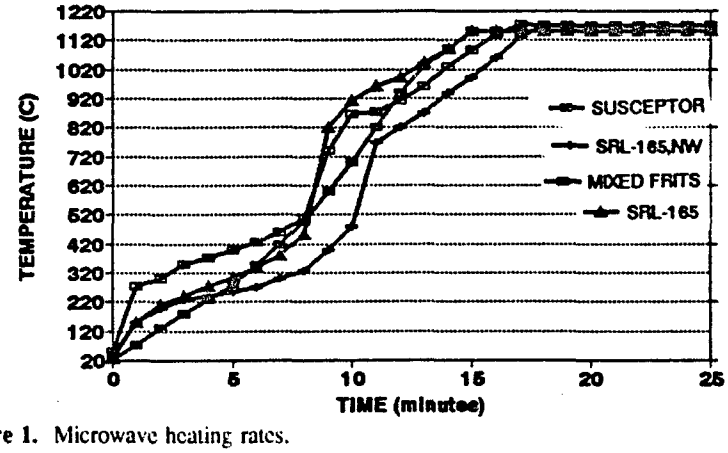


Figure 1. Microwave heating rates.

Homogeneity Studies

One of the important quality assurance parameters in glass production is homogeneity. In order to test this parameter in our melts, 30 gram samples of the mixed frit were ramped up to 1150°C and held for different periods of time. While Fourier transform infrared reflection spectroscopy (FTIRRS) results showed very little variation in peak number between the samples (Figure 2), it was clear from visual observation of the samples that as soak time increased, the number of seeds and voids visible in samples decreased. It was also noted that the samples held for the shorter periods of time were more prone to fracture during polishing operations.

In a second homogeneity study, the two glass frits were layered one on top of the other in the alumina crucible, each layer weighing 15 grams. This was done to see if mixing was occurring during the melt. As seen in Figure 3 some mixing of the two frits does occur, however, complete homogeneity is not achieved. It was noted that increasing the length of time of the melt or changing the positions of the two frits did not have an effect on the outcome of the study. From FTIRRS results shown in Figure 3, peak position data for scans taken from the bottom of the crucible can be related to the SRL-165/29.8wt% TDS, in the middle of the crucible spectra obtained correspond to mixed frit peak positions, and at the edges of the top of the crucible peak position data indicates a composition closer to that of the SRL-165 without waste products. It is unclear why the SRL-165 without waste rises to the top of the melt. However, this phenomena occurs is thought to be due to density differences between the two frits.

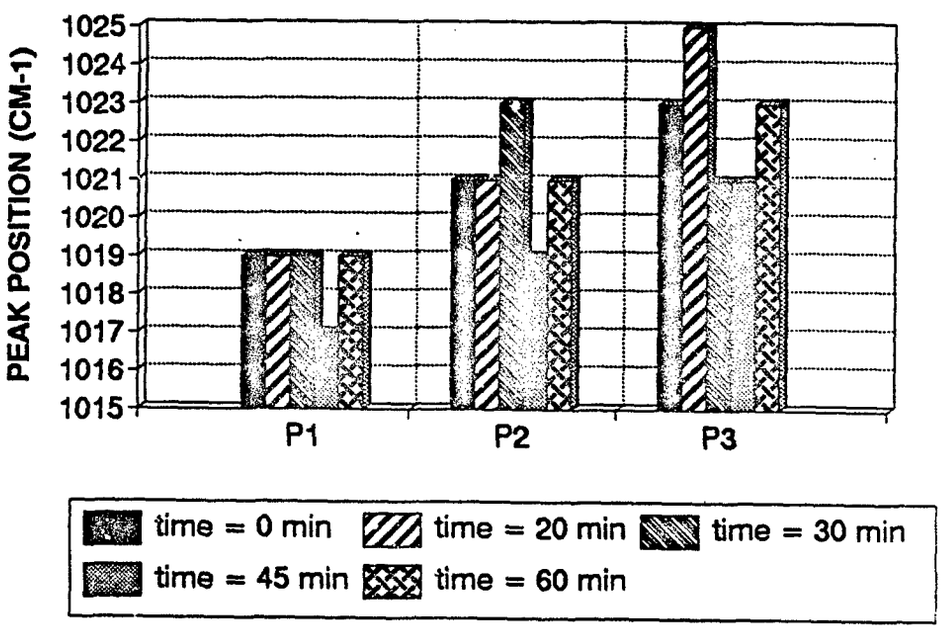


Figure 2. Mixed frits FTIRRS peak position data. P1, P2 and P3 refer to areas on the disk shaped samples where IR scans were run (ie, one on the outer edge, center and opposite edge).

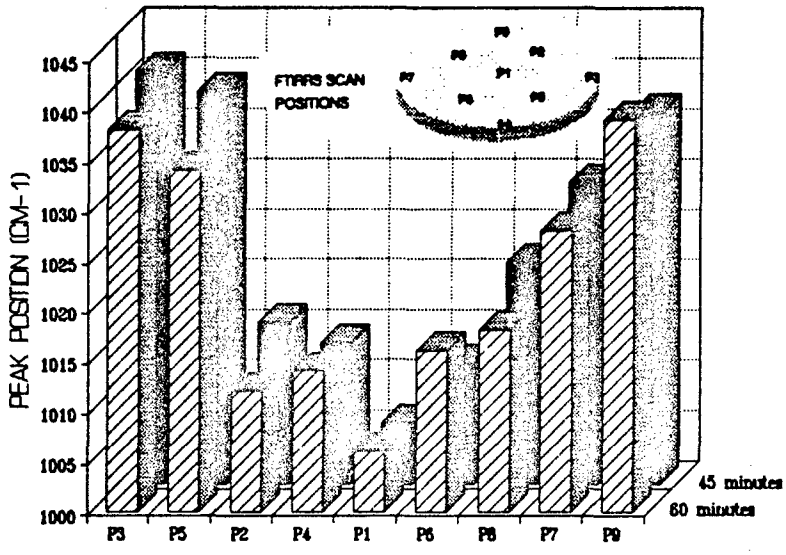


Figure 3. FTIRRS peak position data for the layered frits. P1-P9 indicates areas on the samples where IR spectra were gathered, see inset.

Leaching Experiment

A chemically durable wasteform was one of the primary objectives of this study. Most research in the area long-term disposal matrices centers around the materials' chemical durability and more specifically, leaching studies, whether in field tests or laboratory studies. In order to ascertain whether we were achieving a sound material with the shorter microwave processing times a short (7 days) leaching experiment was conducted in deionized water at 90°C. The results are shown in Figure 4 and Table 2. A 60 and 10 minute microwave sample, along with a conventionally prepared sample (conventional heating, held for 24 hours at 1150°C) were weighed and placed in a Teflon® leaching vessel. Deionized water was added to achieve a surface area to volume ratio (SA/V) of 0.03cm^{-1}, the containers were sealed and placed in a controlled temperature cabinet at 90°C, and held at that temperature for 7 days. Upon removal, the samples were dried, weighed, and then cleaned in an ultrasonicator and ethanol for 5 minutes and then re-weighed. FTIRRS showed no significant differences between the samples other than the fact that the 10 minute sample exhibited negative peak shifts (what is commonly observed after leaching is a shift to higher wavenumbers due to loss of alkali ions). It must be emphasized that this is only a preliminary leaching study and much more work will need to be conducted before any firm conclusions can be drawn.

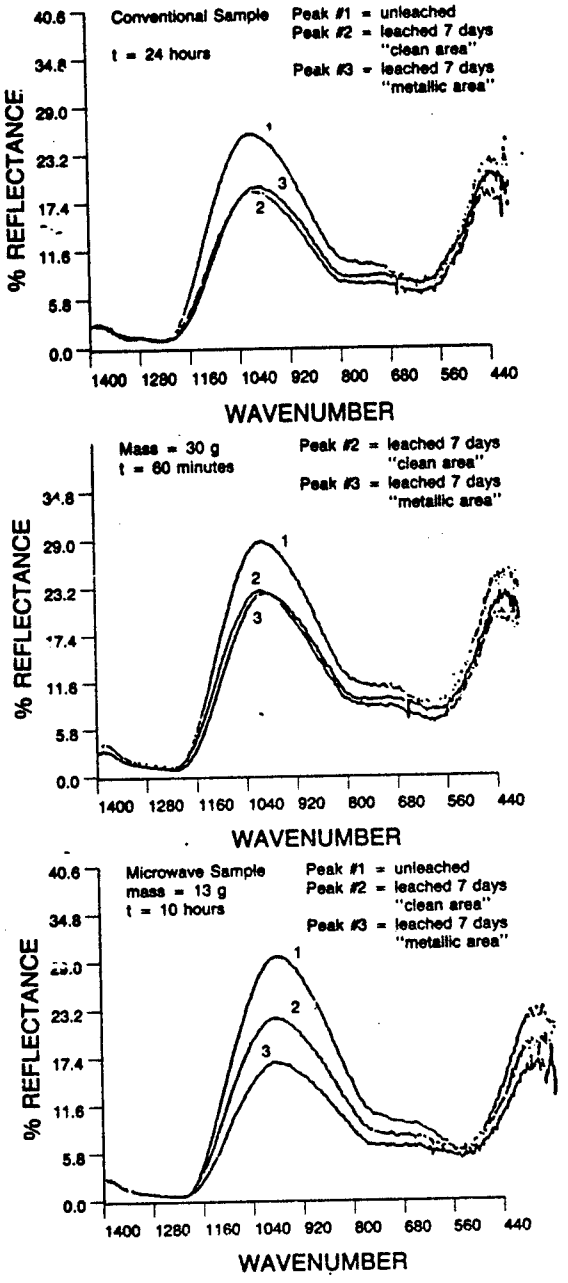


Figure 4. FTIRRS spectra for the microwave and conventional samples before and after leaching.

Table 2. Weight Loss Data for Conventional and Microwave Samples

SAMPLE	Pre-Leach Weight (g)	Post-Leach Weight (g)	Weight Past Cleaning (g)	Total Weight Lost (g)
Conv. Prepared (t=24 hr)	1.2383	1.2360	1.2356	0.0027
Microwave (t=1 hr)	1.0690	1.0677	1.0675	0.0015
Microwave (t=10 min)	0.7243	0.7227	0.7224	0.0019

CONCLUSIONS

- Melting and homogenization of borosilicate glass frits is possible with microwave hybrid heating.
- For the mixed frits, longer soak times appear to improve the quality of the glass.
- For the layered frits, it appears that some mixing does occur during the melt, however there is a distinct separation of the two frits even after 120 minutes of microwave heating. This may be due to density or a weight effect.
- There are no significant differences in the short term leaching behavior between the microwave samples and the conventionally prepared glass.
- Microwave heating has potential as a processing form for the vitrification of high level nuclear waste.

FUTURE WORK

This is clearly a preliminary study. More work needs to be done in order to understand how the microwave couples with the glass along with more work in the area of optimizing the soak times as well as a more extensive studies into leaching behavior (see Jantzen, this volume).

ACKNOWLEDGEMENTS

The authors wish to thank Westinghouse Savannah River Co. for financial support during this study and for providing sample material.

REFERENCES

1. G.G. Wicks, in **Corrosion of Glass, Ceramics and Ceramic Superconductors,** (D.E.

Clark and B.K. Zoitos, eds.) Noyes Publications, NJ, to be published 1991.
2. I.J. Chabinsky, and E.E. Eves III, **The Applications of Microwave Energy in Drying Calcining and Firing of Ceramics,** presented at the AGM of the American Ceramic Society, Chicago, 1985.
3. R.J. Brook, *Mat. Sci. and Eng.*, 71:305 (1985).
4. H. Mostagachi, and R.J. Brook, *Trans. J. Br. Ceram. Soc.*, 82:167 (1983).
5. J.D. Katz, R.D. Blake, J.J. Petrovic, and H. Sheinberg, in: **Microwave Processing of Materials**, 24:209-216 (W.H. Sutton, M.H. Brooks, and I.J. Chabinsky, eds.) Materials Research Society (1988).
6. Y. Hassler, L. Johansen, in: **Microwave Processing of Materials**, 24:273-78 (W.H. Sutton, M.H. Brooks, and I.J. Chabinsky, eds.) Materials Research Society (1988).
7. A.S. De, I. Ahmad, E.D. Whitney, and D.E. Clark, **Effect of Green Microstructure on Microwave Processing of Alumina,** Presented at the 14th Annual Conference on Composites and Advanced Ceramics, January, 1990. Proceedings to be published
8. Z. Fathi, I. Ahmad, and D.E. Clark, in: **Better Ceramics Through Chemistry IV**, Materials Research Society Symp. Proc. (B.J.J. Zelinski, C.J. Brinker, D.E. Clark, D.R. Uirich, eds.) 180:401-406 (1990).
9. W.H. Sutton, *Ceram. Bull.* 68:2, p. 376 (1989).

APPLICATION OF MICROWAVE HEATING TECHNIQUES TO THE DETOXIFICATION OF CONTAMINATED SOILS

Clifford E. George, Inchul Jun, and Jiayi Fan
Department of Chemical Engineering
Mississippi State University
P. O. Drawer CN, MS State, MS 39762

ABSTRACT

Soils contaminated with toluene and p-xylene are readily decontaminated at low temperature without combustion when heated with microwave energy under vacuum conditions. Findings indicated that the solvent removal rate was increased several times if the soil samples contain moisture in the form of 3.00 wt.% water. The combination of moisture and vacuum yielded the best results. This observation can be attributed to the enhancement of microwave absorption by the water molecule and by partial pressure effects of the water vapor which is generated upon heating.

INTRODUCTION

Toluene and xylene are extensively used as organic solvents and reactants for many organic synthesis processes in various industrial applications. However, such simple aromatic hydrocarbons appear as primary contaminants in volatile organic compounds of concern affecting the soil and groundwater[1,2]. It has been identified that aromatic chemicals in contaminated soil can cause symptoms of central nervous system depression in human body. Also, possibilities of photochemical transformation in the presence of NO_2 with UV radiation may result in other toxic byproducts such as nitrotoluene and phenyl nitromethane[3,4].

The most popular conventional methods of contaminated soil treatment include incineration and landfill disposal. Both of these methods have serious drawbacks due mostly to public and governmental objections to such practices. It is believed that if the organic compounds could be removed from the soil for offsite disposal, most of the objections will be satisfied.

A study was made to see if microwave energy could be effective in a thermal process to detoxify soils contaminated with organic solvents. It was desired to take advantage of the internal heating mechanism of microwaves and the fact that microwave energy can be utilized in subatmospheric conditions. Since toluene and xylene are known as nonpolar aromatic compounds with very small dielectric loss factors ($\epsilon'' \approx 0.1$ to 0.01), it was not known how

Note: This paper also appears in Ceramic Transactions Vol. 23: Nuclear Waste Management IV.

effective microwave heating for contaminate removal would be.

In addition, it was not known what effects the electric field intensity, E, of the equation (1) power dissipation

$$P_{diss} = 2\pi f \epsilon_o \epsilon'' E^2 \ (W/m^3) \qquad (1)$$

Where P_{diss} : Power dissipation
f : frequency
ϵ_o : dielectric constant of vacuum
ϵ'' : dielectric loss factor
E : magnitude of electric field
W : watts
m : length, meters

would have on the volatilization of the organic compounds. Also, behavior of the contaminants in reduced pressure conditions could have a drastic effect on the effectiveness of the proposed thermal treatment process.

Toluene and xylene have very low water solubility. However, water is found soaked or mixed in contaminated soils over a wide range of concentrations. The water molecule possesses a permanent dipole moment and has the advantage that it generates considerable heat on exposure to microwave radiation. This fact encouraged a further study of the enhancement of added water to the volatilization rate of the organic chemicals when exposed to microwave energy as first reported by Dauerman and Windgasse[5].

It is well known that the boiling point of an organic compound is reduced if the partial pressure of that compound is reduced. Both the reduction of total system pressure and the presence of water vapor in the system reduce the partial pressures of the organic compounds present.

The volatilization behavior in different soil grain size was also studied since dielectric properties of the soil may differ depending on porosity[6]. Also, since sandy soil and clay soil were known to have different physical and dielectric properties, it was expected that the different soil types would exhibit variations in organic diffusion processes.

MATERIALS AND METHODS

The sandy and clay soils samples were air-dried, sieved (<1 mm), and spiked with toluene or p-xylene in a concentration of 13,700 or 136,700 ppm. Water was added over a range of 0.75 to 8.00 wt.%. Each sample was placed inside a Teflon vessel (100ml volume), and incubated for a set time period. When clay soil was exposed to high vacuum during microwave drying, a filter was placed under the vessel and this prevented fine dust in the soil from flowing outward.

Vacuum levels in a range of 60 to 160 Torr were provided via a mechanical vacuum pump. A vacuum trap with ice water bath was installed between microwave vacuum chamber and vacuum

pump to collect the organic vapors evolved during microwave heating (see Figure 1). A 2.45 GHz laboratory oven* was used for the testing program. Due to the difficulties of measuring the temperature of samples with thermocouples in a microwave cavity, temperature measurements were not made for this work.

Treated soils were weighed, and the mass balance of the contaminant was determined. Gas chromatographic analysis was also carried on the residue to verify the results (see Table 1).

Figure 1. Experimental Design of Microwave Vacuum Processing for Detoxification of Contaminated Soil

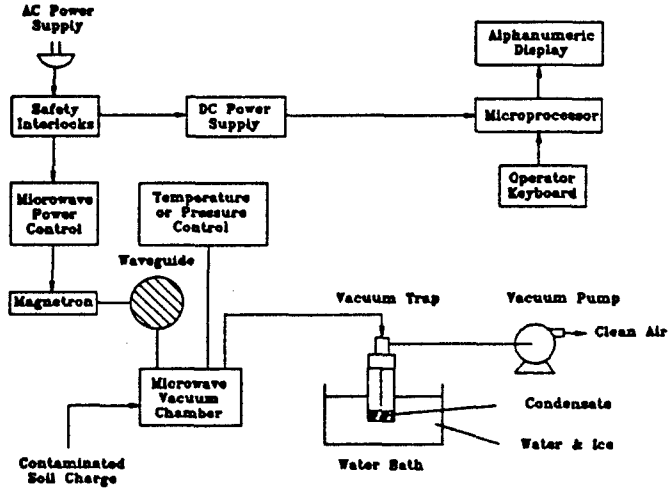


Table 1. Removal of p-Xylene from Wet and Dry Contaminated Soils at Constant Vacuum of 60 Torr in Vessel

Soil Type	Water Content (wt. %)	Drying Time (min.)	P-xylene Removal (%)
Sand	0.00	40	99.999
Sand	3.00	15	99.756
Clay	0.00	13	96.993
Clay	1.50	8	99.629

Initial Content of
p-Xylene in Soil (ppm) :13,700
Soil Particle dia. (mm) :0.80

* Model MDS-81D, CEM Corp., Matthew, NC

Figure 2. Effect of Microwave Energy (Variable Power) on Volatilization of Toluene in Soil (Sand) under Vacuum of 60 Torr

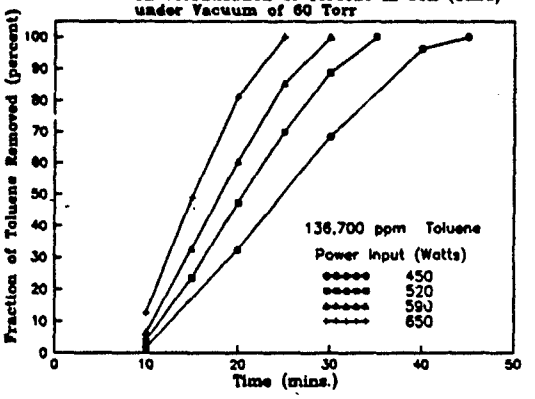


Figure 3. Effect of Microwave Energy (Variable Power) on Volatilization of p-Xylene in Soil (Clay) under Vacuum of 80 Torr

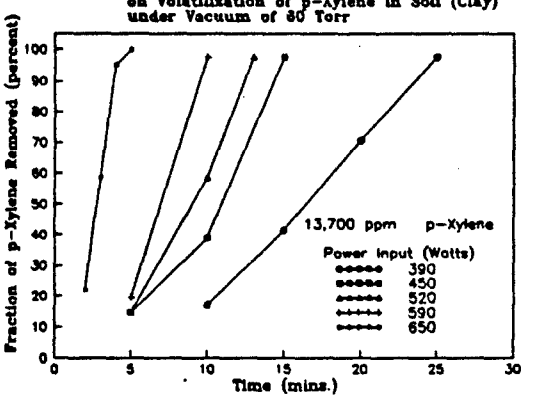


Figure 4. Effect of Variable Vacuum on Volatilization of p-Xylene in Soil (Sand) by Microwave Energy

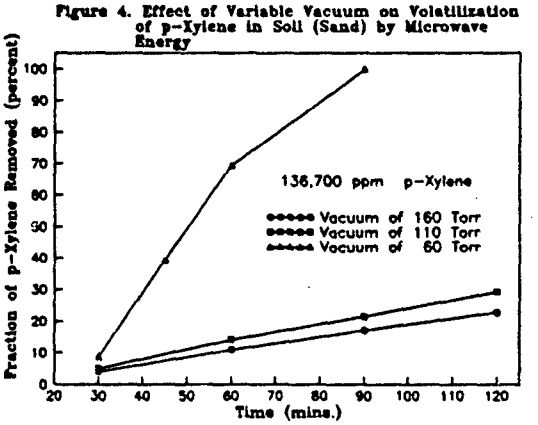


Figure 6. Volatilization of Variable Content of p-Xylene in Soil (Sand) by Microwave Energy under Vacuum of 60 Torr

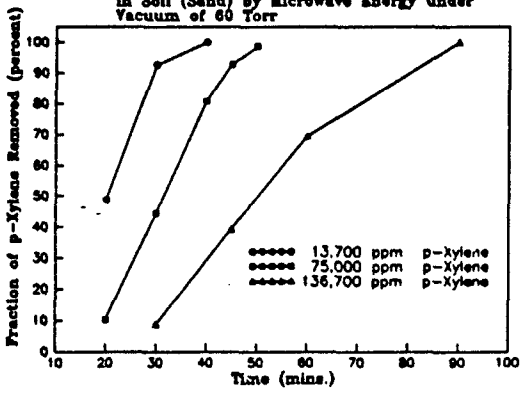


Figure 8. Comparision of Volatilization of Toluene in Dry and Wet Soil (Sand) by Microwave Energy under Vacuum of 60 Torr

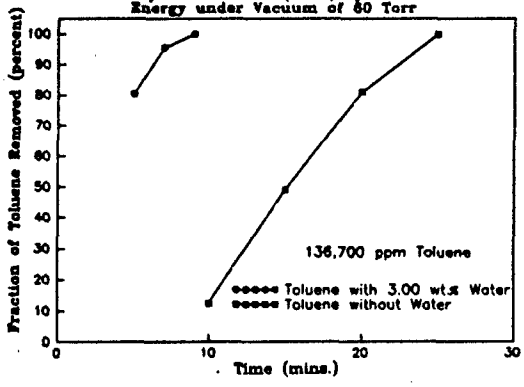


Figure 7. Comparision of Volatilization of p-Xylene in Dry and Wet Soil (Sand) by Microwave Energy under Vacuum of 60 Torr

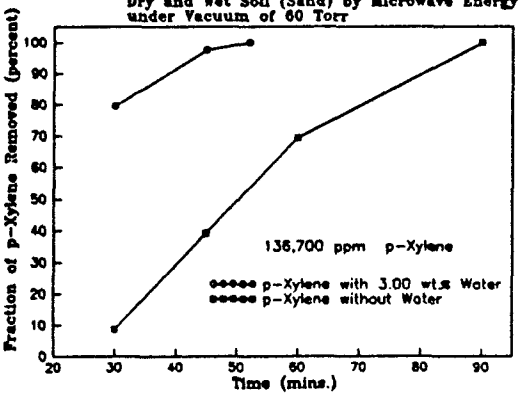


Figure 8. Effect of Variable Water Content on Volatilization of p-Xylene in Soil (Sand) by Microwave Energy under Vacuum of 60 Torr

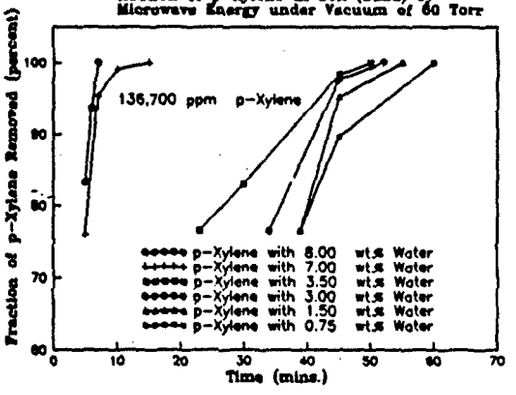


Figure 9. Comparision of Volatilization of p-Xylene in Wet Soil (Sand) of Different Grain Size by Microwave Energy under Vacuum of 60 Torr

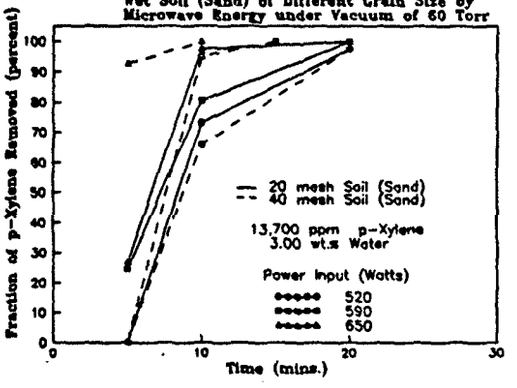
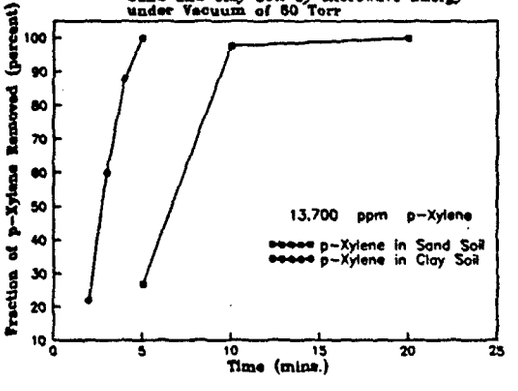


Figure 10. Comparision of Volatilization of p-Xylene in Sand and Clay Soil by Microwave Energy under Vacuum of 60 Torr



RESULTS

The data for the various conditions are given in graphical form and can be summarized as follows:

1. The rate of toluene and p-xylene removal from soils was progressively increased with increasing power level (Figure 2 and 3).
2. The higher vacuum (lower absolute pressure) significantly enhanced the rates of p-xylene removal (Figure 4).
3. P-xylene removal was effective at high and low levels of the contamination (Figure 5).
4. The presence of water in the contaminated soil significantly accelerated the rate of removal of the solvent from soil and increasing the moisture to the soil greatly reduced the required exposure time (Figures 6 to 8).
5. Soils of small grain size promoted the rate of removal of P-xylene (Figure 9).
6. The rate of p-xylene removal from the clay soils was higher than that from the sandy soils (Figure 10).

CONCLUSIONS

The soils are readily decontaminated at low temperature without combustion when heated with increasing microwave energy under vacuum conditions. The higher vacuum significantly reduces the exposure time and intensity of the microwave radiation required to remove the hydrocarbon. Furthermore, it was found that the solvent removal rate was increased several times if the soil samples contain moisture in the form of 3.00 wt.% water. The combination of moisture and vacuum yielded the best results. This observation can be attributed to strong interaction between water and microwave radiation, rapid heat generation due to increased energy absorption rate, and reduction in boiling point of the volatile organic due to a reduction in partial pressure.

In sandy soil, the soil texture (grain size) alters the dielectric properties of the wet soil in a manner that is not fully understood. This in turn modifies the rate of volatilization of the organic contaminant. Also, clay soil appears to be more sensitive to microwave radiation than sandy soil thus yielding faster organic extraction rates.

ACKNOWLEDGEMENTS

This project has been funded in part with Federal Funds as part of the program of the Gulf Coast Hazardous Substance Research Center which is supported under cooperative agreement R 815197 with the United States Environmental Protection Agency and in part with funds from Mississippi Power and Light Company. The contents do not necessarily reflect the views and policies of the U.S. EPA or MP&L nor does the mention of trade names or commercial product constitute endorsement or recommendation for use.

REFERENCES

1. Y. Jin and G. A. O'Conner, "Behavior of Toluene added to sludge-amended Soils," J.

Environ. Qual., 19(3), pp 573-9 (1990)

2. R. N. Smith, "Small Scale Recovery of Hydrocarbons in Groundwater: a case study," EPA/ET AL Northwestern Groundwater Issues Conf., Portland (1986)

3. M. N. Marunyak, N. N. Sirotkina, and L. N. Denisenko, "Photochemical transformation of simple aromatic hydrocarbons in the soil," Vin. Sil's'kogosospod. Nauki, (12), pp 82-4(1986)

4. N. I. Sax and R. J. Lewis, "Hazardous chemicals Desk Reference," Van Nostrand Reinhold Company, New York (1987)

5. L. Dauerman and G. Windgasse, "Microwave Treatment of Hazardous Waste," Proceedings of the International Conference on High Frequency/Microwave Processing and Heating, p 6-6-1, Arnhem, The Netherlands, (1989)

6. P. Hoekstra and A. Delaney, "Dielectric Properties of Soils at UHF and Microwave Frequencies," J. Geophys. Res. Vol.79, No.11, (1974)

OXIDATIVE DEGRADATION OF TRICHLOROETHYLENE ADSORBED ON ACTIVE CARBONS: USE OF MICROWAVE ENERGY•

R. Varma and S. P. Nandi ••
Los Alamos National Laboratory
Los Alamos, New Mexico 87545

INTRODUCTION

Chlorinated hydrocarbon compounds (CHCl), such as chlorinated alkanes/alkenes, benzene and biphenyl etc,represent an important fraction of the industrial hazardous wastes produced. Trichloroethylene (TCE) can be removed from waste streams by adsorption on active carbons. Among the various methods of active carbon regeneration[1] only the high temperature (~1000°C) steam activation serves the dual purpose of carbon regeneration and combustion of adsorbed species. A carbon bed loaded with halocarbons (TCE for example) may contain as much as 20% of chlorine by weight. The product gases will produce severe corrosion in the furnace system.

The primary objective of the present work was to study the detoxification in air-stream of TCE adsorbed on different types of active carbons using *in situ* microwave heating. A secondary objective was to examine the regeneration of used carbons from the effects of repeated cyclic operations (adsorption-detoxification).

A number of Japanese patents[2-5] claim that active carbons loaded with halocarbons can be decontaminated (regenerated) using microwave radiation in the frequency range from 0.9 to 4.5 GHz. The prevailing temperature is reported to be in the range of 450 to 550°C. The fate of the adsorbed organics in the processes has not been clearly indicated.

Major advantages of microwave heating over thermal heating are: (a) it provides uniform *in situ* rapid heating, (b) the container vessel can remain at room temperature while the material in it is heated, and (c) chemical processes can usually be conducted at lower temperature.

Thermal decomposition (pyrolysis) of TCE was studied by Goodall and Howelett.[6] It decomposes in the temperature range 385-445°C, the final reaction products are hydrogenchloride and hexachlorobenzene. The reaction is a degenerate branched chain process, the initiator being chlorine atoms produced directly or indirectly. Similar thermal decomposition characteristics has been observed for tetrachloroethylene[7] and methylene chloride.[8]

•Work performed at Argonne National Laboratory, Argonne, Illinois 60439

••Present address: Washington Street, Downers Grove, Illinois 60515

Note: This paper also appears in Ceramic Transactions Vol. 23: Nuclear Waste Management IV.

Experimental

A microwave oven (CEM Model MDS-81 with 600 Watts CW output at 2.45 GHz) was modified to energize a flow-through reactor. Reagent grade trichloroethylene was used without further purification. Three samples of active carbon obtained from Calgon Corporation were used. One sample of carbon contained Cu and Cr which are expected to serve as oxidation catalysts. The characteristics of the carbons are described in Table I.

Table I. Characteristics of Active Carbons Used in Experiments

Name	BET Surface Area (m^2/g dry)	Ash	Composition, wt% Cr_2O_3	CuO	C	H	N
Base Carbon	1050	8.6	- - -	- - -	90.3	0.65	0.55
FCA Calgon	950	20.1	3.8	9.7	78.4	0.83	0.67
PCB Calgon	1100	3.2	- - -	- - -	- - -	- - -	- - -

The experimental set up for investigating the oxidative decomposition (detoxification) of TCE is shown in Figure 1.

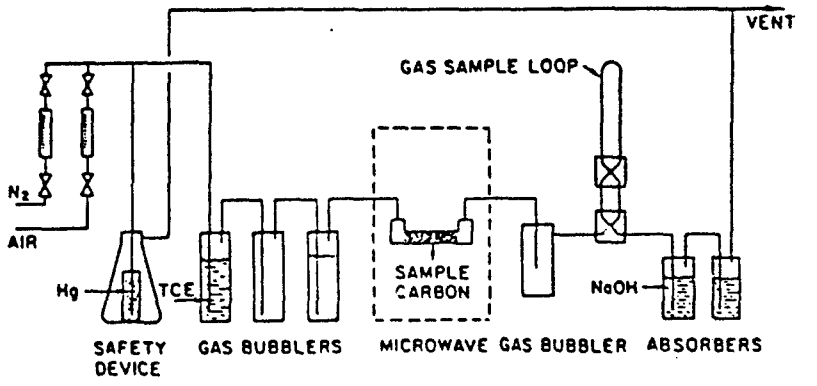


Fig. 1 Experimental Set Up for TCE Adsorption/Detoxification using Microwave Energy

A known weight of active carbon (6 to 10 g) was placed in the 12-mm ID quartz sample tube-reactor which was placed in the microwave oven. The tube was detachable and could be weighed when needed. The active carbon was dried using microwave heating and the dry weight of the carbon was noted. Nitrogen gas stream carried vapors of TCE onto the active carbon at ambient (21-22°C) temperature. After the adsorption step, the sample tube was weighed, the weight of TCE adsorbed was noted, and the tube was placed back in the cavity. The flow of air was then started through the carbon bed; the oven was energized at the same time. As will be outlined later, the major products of reaction from microwave heating of active carbon (with or without catalyst), with pre-adsorbed TCE, in air streams were identified by mass spectral analyses to be HCl, CO_2, CO, $C_2H_2Cl_2$, etc. The evolved gases were passed through an ice trap (to remove any high boiling product), a gas sampling loop, and one bubbler containing 1N NaOH solution; finally, they were passed to a laboratory vent. Periodic gas samples were quantitatively determined by mass spectroscopic analysis. Hydrochloric acid produced in an experimental run from degradation of the TCE was also absorbed in NaOH-solution as NaCl. The chloride was precipitated as AgCl and determined quantitatively. This step provided an independent estimate of total HCl produced during an experimental run.

Accurate temperature measurement is difficult during microwave heating. Temperature of the carbon bed was measured using an extrapolation technique. The temperature of the carbon bed was measured after 5-min. continuous microwave irradiation while gas flow through the bed was maintained. At the end of the 5-min. period, microwave power was switched off, a thermocouple was quickly inserted, and the temperature was read every 40 seconds. An extrapolation of the temperature-time plot gave the value of temperature of the bed.

Results

The catalyst-containing carbon was shown to have a slightly higher capacity for TCE adsorption than did the coconut-shell carbon. The linear nature of the sorption isotherm observed indicates that the bed did not attain adsorption equilibrium in the time allowed for these measurements.

Trichloroethylene does not form explosive mixture with air at any concentration. Possibility of temperature overrun in passing air through carbon bed can be minimized by controlling the the mass flow rate of air. As will be seen from the exit gas analysis of TCE detoxification runs, free oxygen was not present in the exit gases.

Oxidative Degradation of TCE

In one run (No. 107), TCE vapor mixed with moist air was passed through a bed of carbon particulates containing a catalyst while the bed was irradiated with microwave radiation. The exit gas analysis for the run show that there was no decomposition of

Detoxification Runs with Used Carbon and Carbon Regeneration

The results in Table II indicate that considerable amounts of chlorine is retained by the carbon after a detoxification run. The volume percent of HCl in the effluent gas generated during detoxification at different time (microwave irradiation period) for carbon with different initial chlorine content is shown in **Figure 2** . It is seen that the detoxification efficiency decreases markedly with the increase in the initial amount of chlorine in the carbon.

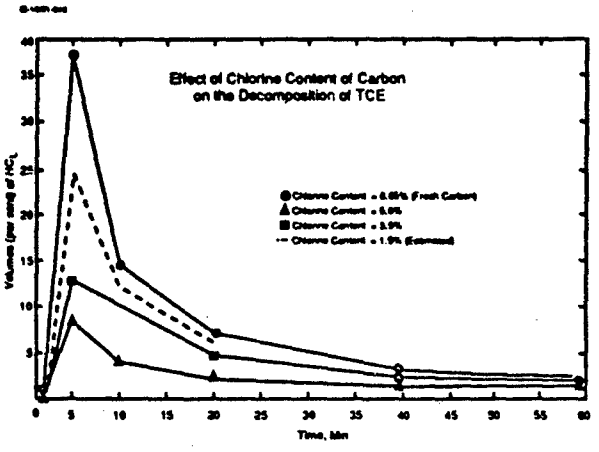


Fig. 2 TCE Detoxification as a Function of Chlorine Content of the Carbons

Some attempts were made to remove the chlorine from the used carbon to determine if a process for regenerating an active form of this carbon for further use in TCE detoxification can be developed. Passing low concentration water vapor (nitrogen gas saturated with water at 25°C) through the used carbon bed under microwave irradiation could remove only ~1/3 of chlorine. Using higher concentration of water is expected to remove more chlorine from the bed. Washing the used carbon with hot (90°C) water reduced the chlorine content from 6.2 to 1.5 wt %. If we pass a higher concentration of water vapor (i.e. steam + air) through a used carbon bed which is heated by microwave, we anticipate regeneration of carbon to be more successful. The results of this study indicate that, under in situ heating by microwave radiation, TCE and the detoxification products are more readily desorbed from a catalyst-free bed than from one containing catalyst.

TCE. It was evident from observation that no evolution of HCl took place. It is therefore concluded that TCE does not undergo decomposition or oxidation if it is not preadsorbed on active carbon. The residence time for the case of horizontal reactor was too-short for any surface-enhanced reaction to occur.

The remaining experiments were done with TCE preadsorbed on active carbon at room temperature (22°C). After the adsorption step flow of dry or moist (air saturated with moisture by bubbling house air through a water bubbler at 25°C) air is then started. The bed is heated by microwave radiation in all cases at the 20% power level. The total reaction time is 30 min. The carbon bed is weighed again after reaction, and the used carbon is analyzed for chlorine. Gas samples collected from the product gas stream were analyzed by mass spectroscopy. A graphical integration of HCl gas profile vs. time gave an estimate of total HCl formed in any particular reaction. The chloride formed in the NOH-absorber in each run was determined as AgCl to provide yet another estimate of total HCl produced.

The data obtained from all detoxification experiments were analyzed in terms of (a) initial TCE loading in the carbon bed, (b) calculated chlorine loading in carbon bed, (c) percent of original chlorine loading retained in the bed after reaction (from chlorine analysis of the carbon bed), and (d) percent of original chlorine in gas phase as HCl, $C_2H_2Cl_2$, and C_2HCl_3 from mass spectroscopic analysis and HCl analysis from AgCl recovered. The experimental data obtained for a large number of runs for the case of dry (house) or moist air were analyzed in this manner. The results of material balance, in terms of chlorine, is reported in Table II.

Table II. Chlorine Mass Balance Between Reactant and Products of Reaction from TCE Oxidation Experiments Conducted with Microwave Heating at 20% Power Level, Air Flow at 100 mL/min, and Reaction Time of 60 Minutes

			Adsorption		Desorption/Detoxification					
						Chlorine in Gas Phase,[b] wt%				
Run No.	Fresh Carbon (Unused)	Air Flow	TCE[a] Loading (g/g) in Carbon	Calc. Cl Loading (g/g) in Carbon	Cl in[b] Carbon Bed (% of Original Cl Loading)	Cl as HCl (from AgCl)	Cl as HCl (Gas. Anal.)	Cl as $C_2H_2Cl_2$ (Gas Anal.)	Cl as C_2HCl_3 (Gas Anal.)	Chlorine Accounted For %
101	FCA	dry	0.217	0.176	37.3	41.3	45.5	4.1	3.9	90.8
106	FCA	dry	0.284	0.230	36.0	32.9	37.6	5.2	12.1	90.9
105	Base Carbon	moist	0.107	0.159	12.5	36.2	42.0	2.2	32.6	89.3
127	PCB	moist	0.180	0.146	8.2	36.5	41.8	5.1	29.2	84.3
102	FCA	moist	0.215	0.174	28.7	52.6	48.7	2.9	3.6	83.9
114	FCA	moist	0.268	0.217	29.2	30.9	37.5	6.1	10.6	84.3
119	FCA	moist	0.168	0.136	35.1	37.6	43.2	3.5	6.2	88

[a]As TCE initially preadsorbed on carbon bed.
[b]Chlorine retained in the bed after reaction and as HCl, $C_2H_2Cl_2$, and C_2HCl_3 species in gas stream.

Discussion

The temperature range of thermal decomposition of TCE has been reported to be 385-445°C(6). It is also reported that oxidation of chloroalkanes can proceed at an appreciable rate at temperature ~50°C lower than that for pyrolysis. The temperature attained in the carbon bed in the present work was in the range from 355 to 425°C. Two reaction conditions were used: (a) adsorbed TCE on active carbon reacted with dry air flow and (b) adsorbed TCE on active carbon reacted with moist air flow. It is expected that under (a), the reaction products will be CO, C_2, HCl and Cl_2 and stable intermediates of TCE decomposition. The following reactions should be considered:

$$C_2HCl_3 + O_2 \rightarrow 2CO + HCl + Cl_2 \quad (1)$$

$$H_2O + Cl_2 \rightarrow 2HCl + 1/2\,O_2 \quad (2)$$

The reaction (2) as written is endotheronic. The amount of chlorine converted to HCl under our reaction conditions was difficult to estimate. However, the cumulative amount of HCl was higher in case of moist air runs compared to that for dry air runs indicating that the reaction (2) contributed to some extent towards the higher production of HCl. The effluent gas samples in all runs did not contain any free chlorine. It is assumed that free chlorine generated was completely adsorbed by the active carbon bed. Chlorine is expected to be held more strongly by active carbon compared to hydrochloric acid. Selection of pure trichloroethylene for oxidative degradation over active carbon was unfortunate because production of free chlorine can not be avoided. If trichloroethylene is mixed with other less chlorinated hydrocarbons (e.g. CH_4) and the resultant mixture contained enough internal hydrogen then the production of free chlorine could be avoided.

The product gases contains both CO and CO_2. However, the carbon oxides derived from TCE decomposition could not be separated from that produced from the active carbon bed. It has been indicated that comparatively lower CO is present in the effluent gas when active carbon with catalyst was used for detoxification.

The fraction of TCE converted from oxidative degradation in air streams can be estimated. Since the original TCE is converted into HCl + Cl_2 and most of the Cl_2 is absorbed in carbon, the measure of the TCE converted may be derived from the sum of the original chlorine loadings retained in the carbon and those which appears in the gas phase (these appear as HCl and $C_2H_2Cl_2$ in Table II). The total single pass conversion of TCE into degradation products, on this basis, turns out to be greater than 80% in all cases. The oxidative degradation of TCE observed was highest with FCA carbon (i.e., catalyst-loaded active carbon) and with moist air.

Conclusions

The experimental study has shown that trichloroethylene adsorbed on active carbon can be oxidatively degradated in presence of microwave radiation. Energy can be transferred efficiently to the reaction sites without losing heat to the surrounding vessel. One of the decomposition product of trichloroethylene is free chlorine which is held very strongly active carbon. Hydrochloric acid on the other hand seems to be less strongly held and appears in large concentration in the exit gas. Production of free chlorine can be avoided by using chlorohydrocarbon mixed with sufficient internal hydrogen. This is also expected to minimize the problem of carbon regeneration encountered in this study. The results obtained from studies on the oxidative degradation of TCE under microwave radiation are promising in a number of respects: (1) the detoxification of TCE adsorbed on active carbon can be conducted at moderate (<400°C) temperatures, and (2) the used carbon bed can be regenerated. A patent on the process has been issued.[9]

References

1. Kiang, Y-H., "Hazardous Waste Processing Technology," Ann Arbor Science, Ann Arbor, 1982.

2. Katsuta, A., "Regeneration of Activated Carbon by Microwave Irradiation," Japan. Kokai, 7627893, March 9, 176 (CA 87:70374v).

3. Mashida, T., and Matsushita, S., "Regeneration of Activated Carbon," Japan. Kokai, 76145491 Dec. 14, 1976 (CA 87:8041f).

4. Tanaka, M., Ikeda, A., Kobayashi, H., and Takenda, Y., "Regeneration of Activated Carbon in Presence of Steam," Japan. Kokai, 7643395, Apr. 14, 1976 (CA 85:166188x).

5. Iriguchi, N., Iwaisako, T., Watanabe, S., and Ohkuni, Y., "Regeneration of Spent Activated Carbon," Japan. Kokai, 7671894 (CA 85:162542K).

6. Goodal, A. M., and Howellte, K. E., J. Chem. Soc., 76, 2599-2603 (1954).

7. Barton, D. H. R., and Howellte, K. E., J. Chem. Soc., 73, 2033-2038 (1951).

8. Hoare, M. R., Norrish, R. G. W., and Whittingham, G., Proc. Roy. Soc. (London) A250, 197-211 (1959).

9. "Microwave Enhanced Chemical Processes," US Patent 4,935,114 Issued to Department of Energy, 1990; Inventor: Ravi Varma.

MICROWAVE REACTIVATION OF CIP SPENT CARBON

I.S. Balbaa and S.J. Oda
Ontario Hydro Research Division, 800 Kipling Ave, Toronto, Ontario M8Z 5S4
K.E. Haque, P.D. Kondos and R.J.C. MacDonald
CANMET, Mineral Sciences Labs, 555 Booth St, Ottawa, Ontario K1A 0G1

ABSTRACT

Spent carbon from the carbon-in-pulp (CIP) process was reactivated using 2450 and 915 MHz microwave energy. Dry and wet carbon was used in the tests. Reactivation temperature and dwell periods were varied to determine optimum reactivation and energy consumption. The results indicate that the important properties of microwave-reactivated carbon are superior to those of conventionally reactivated carbon. Microwave heating at 915 MHz is preferred for this application because of its higher electrical efficiency and greater penetration depth compared to 2450 MHz.

INTRODUCTION

The carbon-in-pulp process is a proven technology for gold recovery from gold leach pulps. During gold stripping all the chemical species adsorbed are not completely removed from the carbon, and consequently the activity of the spent carbon is always lower than that of the fresh carbon. In order to reactivate spent carbon it needs to be thoroughly acid-washed and heated in the range of 650°C to 850°C in a rotary kiln. The thermal activation process removes all the moisture, carbonizes the organic matter and enlarges the pore size. However, inadequate power input, and poor heat transfer often result in insufficient residence time and lower activation.

Industrial microwave heating at allocated 915 MHz and 2450 MHz frequencies is finding increased application for processing products including: foods, rubber, and ceramics. Up to the present time, research work to investigate the use of microwave heating for reactivating carbon has been limited and additional experimental testing was recommended (1). On this basis, an investigation was initiated to confirm the feasibility of microwave reactivation of spent carbon and determine the energy requirements.

Note: This paper also appears in Ceramic Transactions Vol. 23 Nuclear Waste Management IV

EXPERIMENTAL

Samples examined for reactivation were either wet (80% moisture, dry-basis) or dry. In the first set of microwave heating tests dry carbon samples weighed 100 g. Wet samples weighed 180 g. Tests were performed at the two allocated microwave frequencies of 2450 MHz and 915 MHz. The results obtained from these tests were used to estimate experimental conditions for the larger batches (ie, 1.5 kg dry-basis). All samples were contained in fused quartz crucibles. Each crucible was covered with a high temperature insulating block (microwave-transparent) which had two access holes, one for the temperature probe and one for the nitrogen gas inlet. All tests were undertaken in a continuous flow of nitrogen gas to minimize oxidation and possible ignition of the carbon.

The basic experimental apparatus consisted of three main components: a microwave generator, an applicator (oven) and a temperature/power monitoring system. Figure 1 shows a schematic of the experimental arrangement.

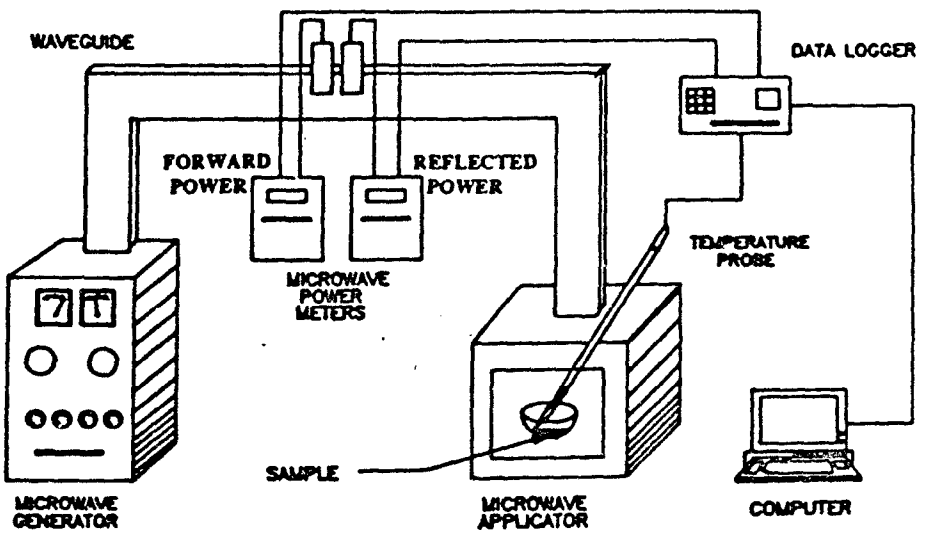


Figure 1. Schematic of experimental arrangement.

Two microwave generators were used in these tests. The first was a 2450 MHz generator with a maximum microwave output power of 6 kW and an estimated efficiency of 50% (ie, 50% of the electrical input is converted into usable microwave energy). The second wass a 915 MHz generator with a maximum microwave power output of 30 kW and an efficiency of 70%. Microwave power entering the applicator (forward power) as well as the unused microwave power (reflected) were measured by power meters which were connected to a computer for data storage.

The dimensions of the multimode applicator used in all of the 2450 MHz tests were 50 cm wide by 46 cm high by 64 cm deep. The 915 MHz variable mode applicator was cylindrical in shape with a diameter of 40 cm and a height of 80 cm. Both applicators contained several openings/ports for viewing, exhaust, temperature measurement and nitrogen gas inlet.

A high-temperature optical-fibre probe*, connected to a computer for data storage and display, was used to continuously record temperature. The optical-fibre probe was used to record temperatures above 300°C. Temperature control was manual but effective. Following the microwave exposure, the sample was allowed to cool to about 400°C and then quenched in distilled water for subsequent examination and analysis. These tests included the determination of the gold adsorption rate, adsorption capacity, surface area, attrition weight, apparent density, ash weight and iodine value.

RESULTS AND DISCUSSION

The best reactivation results on the 100 g samples were obtained when the samples were heated to a maximum temperature between 700 and 750°C with an optimum residence time of about 4 minutes. Figures 2 and 3 show typical heating curves for the wet and dry carbon using microwave energy at 2450 and 915 MHz. Table 1 summarizes some of the relevant parameters and results at each frequency.

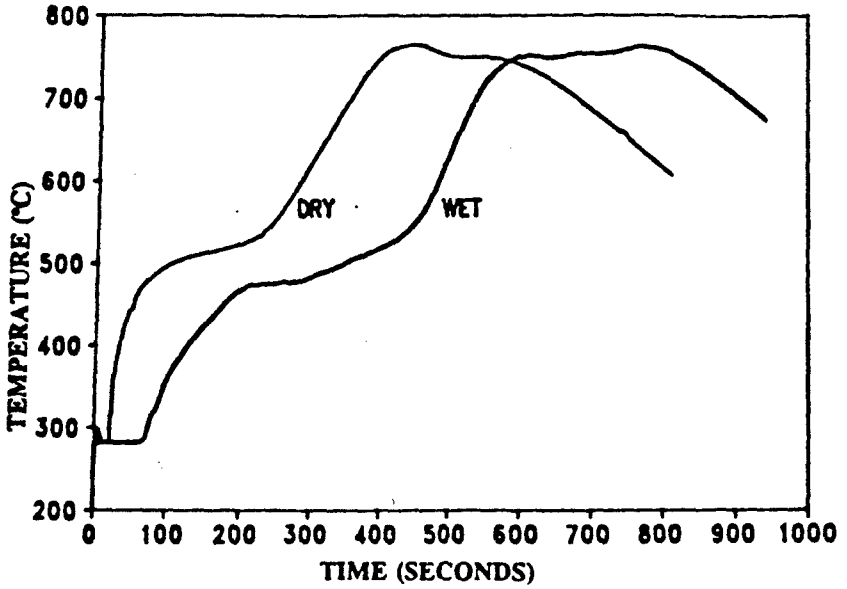


Figure 2. Microwave heating curves for 100g samples (2450 MHz).

* Accufiber Model 100, Accufiber Inc., Beaverton, Oregon, U.S.A.

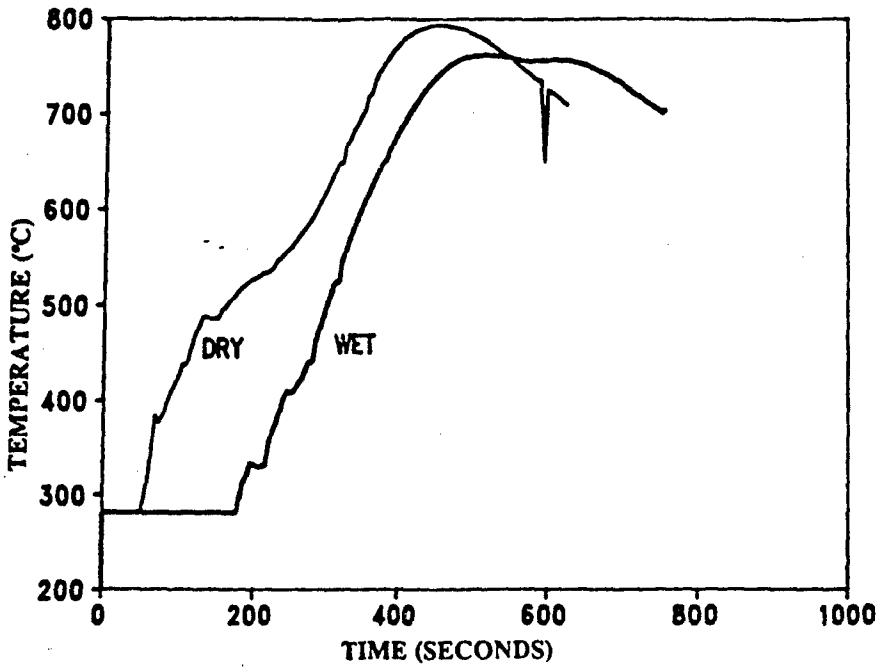


Figure 3. Microwave heating curves for 100g samples (915 MHz).

The forward and reflected microwave powers were not constant throughout a test. The microwave energy was therefore determined by integrating the power over 5-second intervals. The amount of microwave energy absorbed (ie, forward minus reflected energy) was very similar for both dry and wet tests at both 2450 MHz and 915 MHz. As expected, the dry samples required less energy and were heated at a faster rate compared to the wet samples. The average amount of microwave energy required for carbon reactivation was 0.181 kWh/100 g dry carbon and 0.232 kwh/100 g wet carbon.

Table 1. Parameters Used For Microwave Reactivation Of 100 g Carbon Samples.

FREQUENCY	CARBON CONDIT'N	AVG. M.W. POWER FORWARD/REFLECT	ABSORBED M.W. ENERGY	HEATING RATE TO 700°C AVG./NORMALIZED
2450 MHz	DRY	1.7 / 0.44 kW	0.194 kWh	105°C.min^{-1} / 83°C.min^{-1}.kW^{-1}
	WET	1.6 / 0.41 kW	0.251 kWh	73°C.min^{-1} / 61°C.min^{-1}.kW^{-1}
915 MHz	DRY	1.8 / 0.39 kW	0.176 kWh	114°C.min^{-1} / 81°C.min^{-1}kW^{-1}
	WET	1.7 / 0.38 kW	0.227 kWh	91°C.min^{-1} / 69°C.min^{-1}.kW^{-1}

Heating rates at both microwave frequencies (ie, 915 MHz and 2450 MHz) were also quite similar. On average, the normalized heating rate** for 100 g carbon samples was 82°C/min/kW (dry) and 65°C/min/kW (wet). Heating rates were normalized with respect to the average microwave power absorbed (ie, average forward power minus average reflected power).

Heating tests on larger 1.5 kg (carbon) batches were also undertaken at 2450 MHz and 915 MHz. Figures 4 and 5 show typical temperature profiles for the dry and wet batches at both frequencies while Table 2 summarizes the important results. Heating rates at 915 MHz and 2450 MHz were very similar for the dry carbon; however, heating of wet carbon was faster at 915 MHz than at 2450 MHz by 2.4°C/min/kW. This enhanced heating rate is partly due to the greater penetration depth in water provided by the lower microwave frequency (at 60°C, microwave penetration depth in water is about 3 cm for 2450 MHz and 30 cm for 915 MHz (2)). For the smaller 100 g samples, the effect of the difference in the penetration depth for the two frequencies would be negligible.

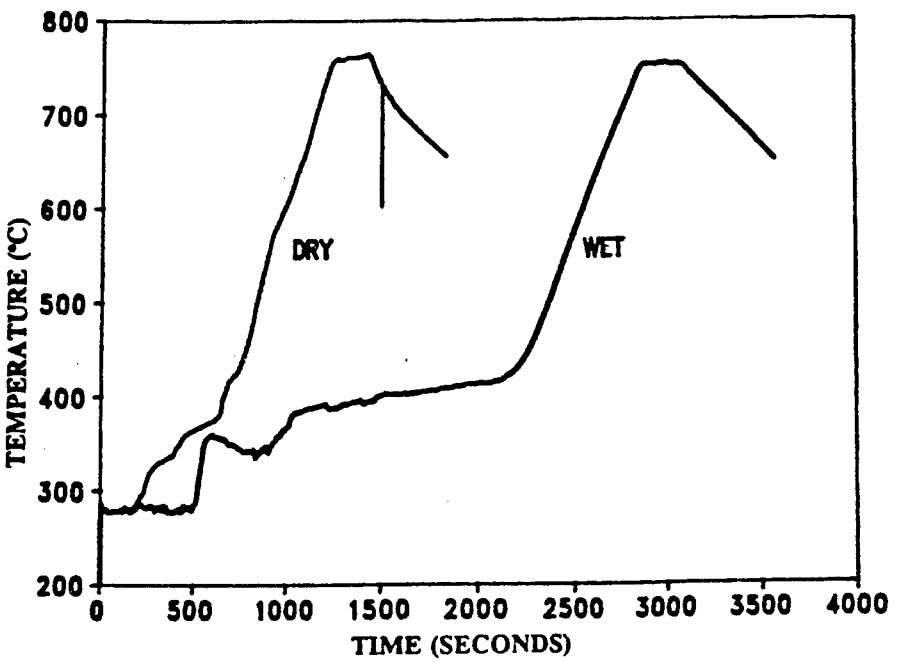


Figure 4. Microwave heating curves for 1.5 kg carbon (2450 MHz).

** normalized heating rates were obtained by dividing the average heating rate by the absorbed microwave power (ie, absorbed power equals average forward power minus average reflected power).

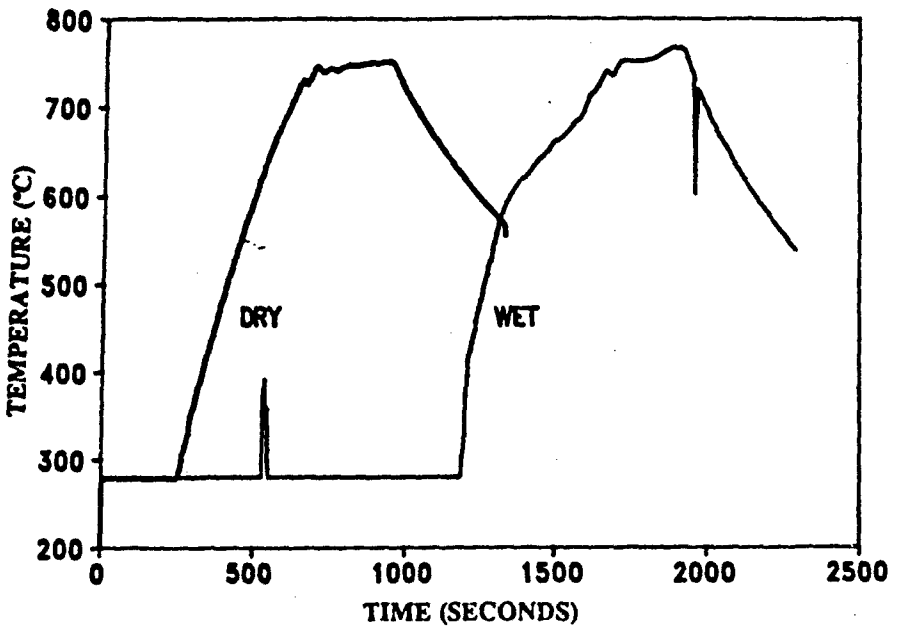


Figure 5. Microwave heating curves for 1.5 kg carbon (915 MHz).

Table 2. Parameters For Microwave Reactivation Of 1.5 kg Carbon Samples

FREQUENCY	CARBON CONDIT'N	AVG. M.W. POWER FORWARD/REFLECT	ABSORBED M.W. ENERGY	HEATING RATE TO 700°C AVG./NORMALIZED
2450 MHz	DRY	3.9 / 0.23 kW	1.468 kWh	33°C.min^{-1} / 9.0°C.min^{-1}.kW^{-1}
	WET	4.6 / 0.04 kW	3.876 kWh	14°C.min^{-1} / 3.1°C.min^{-1}.kW^{-1}
915 MHz	DRY	7.5 / 0.71 kW	1.765 kWh	58°C.min^{-1} / 8.6°C.min^{-1}kW^{-1}
	WET	5.1 / 0.61 kW	2.208 kWh	25°C.min^{-1} / 5.5°C.min^{-1}.kW^{-1}

For simplicity, test results for the 1.5 kg batches were normalized with respect to a 1 kg batch. These results are shown in Table 3. From the results for 100 g (Table 1) and 1 kg (Table 3) batches, the absorbed microwave energy per unit mass decreases with sample size. This effect is a characteristic of microwave heating and is usually attributed to the 'filling factor' (ie, microwave absorption by a material increases by increasing its volume in the applicator) (3).

In order to compare different reactivation techniques and assess the quality of reactivated carbon, a number of different parameters was measured. Among the more important

Table 3. Energy Consumption And Heating Rates Normalized To 1 kg Batch.

MICROWAVE FREQUENCY	CARBON CONDITION	ABSORBED MICROWAVE ENERGY	HEATING RATE
2450 MHz	DRY	1.0 kWh	13.5°C.min^{-1}.kW^{-1}
	WET	2.6 kWh	4.7°C.min^{-1}.kW^{-1}
915 MHz	DRY	1.2 kWh	13°C.min^{-1}.kW^{-1}
	WET	1.5 kWh	8.3°C.min^{-1}.kW^{-1}

parameters are the physical properties of reactivated carbon (eg. apparent density and ash content), as well as the adsorption capacity and rate. Table 4 gives typical results from the analysis of the microwave-reactivated carbon. For comparative purposes, the properties of fresh carbon and conventionally reactivated carbon are also provided. Other properties that were considered and measured were the iodine number, surface area and attrition loss. Measurement of these properties indicated consistency with the results in Table 4.

The applied frequency did not appear to affect the properties of reactivated carbon; therefore, carbon reactivated at either 2450 MHz or 915 MHz is simply termed as 'microwave-reactivated'. Conventional reactivation generally increases the apparent density of the carbon due to shrinkage and structural compaction. In all tests, the density of the microwave-reactivated carbon was even higher than conventional reactivation, including the tests performed at 550°C (with a residence time of 2 minutes) and 700°C (with a residence time of 30 seconds). Comparing the results of the other parameters suggests that the higher density value did not affect the other properties.

The ash present in the carbon is an indication of the amount of inorganic residue remaining after complete combustion of organic material in the carbon. Clearly, ash content in microwave-reactivated carbon is less than half the content present in either fresh or conventionally activated carbon.

The gold adsorption capacity is a measure of the amount of gold adsorbed on a unit mass of carbon. As a reference, fresh carbon has an adsorption capacity of about 26 kg Au/tonne Carbon. Therefore, carbon reactivated by microwaves has an adsorption capacity of 80 - 90% that of fresh carbon. Conventionally reactivated carbon has an adsorption capacity of only 58% of fresh carbon (ie, microwave-reactivated carbon adsorbs at least 38% more gold than conventionally reactivated carbon). A second advantage of microwave-reactivated carbon over conventionally reactivated carbon is the higher gold adsorption rate. As shown in Table 4, adsorption rates from microwave-reactivated carbon were even higher than that of fresh carbon. This result has been reported elsewhere (4). Therefore, in the actual adsorption process in a gold mine, microwave-reactivated carbon can be expected to adsorb more gold than conventionally

Table 4. Properties Of Microwave-Reactivated Carbon.

CARBON REACTIVATION TECHNIQUE	ADSORPTION CAPACITY kg Au/tonne C	ADSORPTION RATE (kg Au/tonne C)/min	ASH CONTENT WEIGHT %	APPARENT DENSITY g/ml
microwave heating (2450 MHz)	21.0	0.34	0.38	0.67
microwave heating (915 Mhz)	23.4	0.43	0.42	0.69
conventional heating	15	0.10	1.0	0.51
fresh carbon	26	0.33	1.0	0.48

reactivated carbon and undertake this adsorption process at a faster rate. These two factors will result in energy savings as well as increased throughput.

The total electrical energy required to activate 1 kg carbon at 2450 MHz and 950 MHz is shown in Table 5. The results are based on 50 and 70% efficiencies for the 2450 and 915 MHz frequencies, respectively. It is clear that microwave reactivation at 915 MHz is more efficient than at 2450 MHz. Another advantage for using 915 MHz versus 2450 MHz is the size of generators. The maximum generator size at 915 MHz is 60 kW compared to 5 kW at 2450 MHz. By using the 915 MHz frequency the number of generators required for the process would be fewer, and therefore the control and reliability of the equipment would be simpler. Therefore, from the standpoint of a practical industrial application, carbon reactivation at 915 MHz appears to be more attractive.

Table 5. Electrical Energy Consumption For Reactivating 1 kg Carbon.

MICROWAVE FREQUENCY	CARBON CONDITION	TOTAL ELECTRICAL ENERGY*
2450 MHz	DRY	2 kWh
	WET	5.2 kWh
915 MHz	DRY	1.7 kWh
	WET	2.2 kWh

* Total electrical energy is calculated by dividing the microwave energy required by the efficiency of the microwave generator, ie, 50% for 2450 MHz and 70% for 915 MHz.

At the present time, the cost of energy for reactivating carbon using conventional electrical heating is approximately $0.083/kg (dry) carbon, based on an electricity cost of $0.0387/kWh (5). Using microwave heating at 915 MHz and allowing for an additional 10% in losses (for reflected microwave energy), the total energy cost using microwaves (2.42 kWh x $0.0387) will be $0.094/kg carbon. However, based on adsorption capacity results presented in Table 4, 0.65 kg of microwave-reactivated carbon will adsorb the same amount of gold as 1 kg of conventionally reactivated carbon. Considering this difference in adsorption capacities, the energy cost for microwave reactivation of carbon at 915 MHz ($0.061/kg) is about 75% of the energy cost of conventional reactivation.

CONCLUSIONS

The tests confirmed the technical feasibility of applying microwave heating in an inert atmosphere to reactivate spent carbon from the CIP process. In general, it appears that the properties of microwave-reactivated carbon are superior to conventionally reactivated carbon (eg, higher gold adsorption capacity). Testing of the two industrial heating frequencies indicated that microwave heating at 915 MHz is preferred for this application because of its higher electrical efficiency and greater penetration depth compared to 2450 MHz. The associated energy cost for microwave reactivation of carbon is estimated to be about 25% lower than the cost of conventional reactivation.

ACKNOWLEDGEMENTS

The authors wish to thank Mr. R.A. Solczyk (Ontario Hydro Research Division) for his invaluable contributions made to this study, and Mr. D. Laforest (EMR CANMET) for his technical assistance and analysis of reactivated carbon

REFERENCES

1. J.T. Woodcock, G.J. Sparrow and D.H. Bradhurst; "Possibilities For Using Microwave Energy In The Extraction Of Gold"; Proceedings of the First Australian Symposium on Microwave Power Applications; p. 139 - 154; Wollongong, Australia; February 1989.

2. T. Ohlsson, N.E. Bengtsson and P.O. Risman; "The Frequency And Temperature Dependence Of Dielectric Food Data As determined By A Cavity Perturbation Technique"; J. Microwave Power 9(2), p. 129, 1974.

3. R.C. Metaxas and R.J. Meredeth; 'Industrial Microwave Heating"; p. 139 - 143; Peter Peregrinus Ltd; London, England; 1983.

4. K.E. Haque, P. Kondos, R.J.C. MacDonald and D. Laforest; "Microwave Activation Of Carbon", paper presented at the International Microwave Power Institute Symposium, August 20-23, 1989, Stamford, Connecticut, U.S.A. (to be published in the proceedings).

5. K.E. Haque, Private Communications.

Section VIII. Joining/Composite Fabrication with Microwave Energy

INVESTIGATION OF INTERLAYER MATERIALS FOR THE MICROWAVE JOINING OF SiC

Richard Silberglitt and David Palaith
Technology Assessment and Transfer, Inc.
Annapolis, MD 21401

W. Murray Black and H. S. Sa'adaldin
Department of Electrical and Computer Engineering
George Mason University
Fairfax, VA 22030

Joel D. Katz and Rodger D. Blake
Los Alamos National Laboratory
Los Alamos, NM 87545

Microwave joining of SiC to SiC was accomplished with interlayer materials composed of Si, C and Ti. The width of joints using Si as the interlayer material varied from 3-50 micrometers, depending upon the method of application of the interlayer material. A joint made from a SiC disk plasma-sprayed with Si had an interlayer width less than 5 micrometers. There was no substantial variation in Knoop hardness across this joint interface. Joints were also made via combustion synthesis of Ti and C powders in situ.

INTRODUCTION

Microwave joining of ceramics has the potential for increased speed and convenience [1,2]. Joints have been made in

alumina, mullite and silicon nitride with flexure strength approaching, and in some cases exceeding, that of the as received material in a fraction of the time that is customarily required with conventional techniques [3,4]. This paper describes the initial results of investigations aimed at applying microwave joining to SiC and other carbide ceramics.

RATIONALE FOR THE JOINING APPROACH

Microstructural, mechanical and X-ray data reported in Refs. 3 and 4 suggest that microwave joining occurs through the filling of pores in the interfacial region by intergranular glassy phases. This mechanism is further supported by conventional joining experiments in silicon nitride, in which the joining material is an oxynitride glass very similar to the silicon nitride intergranular phase [5,6]. These results suggest the following general approach to microwave joining: first investigate joining without interlayer materials, using the intergranular phases present in the material to be joined; if direct joining is not possible, then use as a joining interlayer a material that closely approximates the intergranular phases.

To implement this approach for SiC joining, two different avenues were followed. First, metallic braze joints were made using Si as the primary interlayer material. Second, attempts were made to initiate a combustion synthesis reaction [7] in the interfacial region to form a composite interlayer containing SiC or TiC.

PREPARATION OF SPECIMENS TO BE JOINED

The SiC specimens used for joining were disks of Carborundum Hexoloy^{TM} approximately 0.952 cm in diameter and 0.635 cm in height, rough cut with a wafering saw, with no polishing.

Four different methods were used to prepare and apply interlayer materials. Three of these methods used blended powders of Si, C and Ti. The first method consisted of simply

placing the powder mixture on top of one SiC disk and then pressing the second disk in place. In the second method, the powder was mixed with Nye[1] watch oil to form a slurry, which was applied to the top of the lower disk. In the third method, a cold pressed disk of the powder was made, using 1-Eicosene as a binder, and this disk was inserted in between the two SiC disks. In the fourth method, a thin layer of Si was plasma-sprayed onto one of the SiC disks.

EXPERIMENTAL PROCEDURE

These microwave joining experiments, with the one exception noted below, were carried out using the apparatus described in Ref. 3. The samples were placed in the center of a TE_{103} rectangular microwave cavity and oriented with the electric field parallel to the disk axis. Coupling of microwave power from the 2.45 GHz magnetron was accomplished with a resonant rectangular iris. The dimensions of the iris were determined experimentally by requiring nearly critical coupling between the input waveguide and the cavity when the sample was within the desired joining temperature range.

The power incident on and reflected from the cavity was monitored with voltage probes inserted in appropriate positions through the broad wall of the waveguide. The temperature of the sample was measured through a shielded hole cut in the narrow wall of the cavity using a two-color IR pyrometer[2].

The SiC samples and interlayer materials were held in place for joining by two low loss alumina rods of 0.952 cm diameter. This sandwich of alumina-SiC-interlayer material-SiC-alumina was inserted through openings in the broad wall of the cavity, positioned so that the interlayer material was at the geometrical center of the cavity, and clamped in place with a

---

[1]William F. Nye, Inc., New Bedford, MA 02742
[2]Capintec, Inc., Ramsey, NJ 07446 Model # ROS-10

PAGES 490 + 491

ARE

MISSING

IN

ORIGINAL

DOCUMENT



Figure 3 SEM micrograph of SiC joint made with plasma-sprayed Si coating.

As a prelude to joining experiments attempting to utilize combustion synthesis in the interfacial region, we used the multi-mode cavity to react cold pressed disks equal in size to the joining samples. A disk made from Si and C powders in stoichiometric ratio was heated first. X-ray diffraction data showed only Si and C peaks, indicating that no combustion synthesis reaction took place. Since the Ti-C reaction is much more energetically favorable than the Si-C reaction (Ref. 7), we then heated a cold pressed disk composed of 2% Ti and 98% stoichiometric Si:C powders. The X-ray diffraction data obtained from this disk clearly indicated the presence of SiC.

Based upon the above results, joints were attempted using powder mixtures of 4% and 10% Ti, with the balance being stoichiometric Si:C. No combustion reaction was observed during the heating of these materials.

An additional joining attempt was made using a cold pressed disk of about 1 mm in height made from a stoichiometric powder mixture of Ti and C, in an Eicosene binder. The assembly of SiC disk-Ti:C cold pressed disk-SiC disk was heated

using the single mode cavity method. The Eicosene binder was first observed to vaporize; then as the power was increased a flame was observed to be ignited at the joining interface. When this flame extinguished, the temperature of the SiC disks rose rapidly to 1500°C and stabilized. This temperature was held for several minutes, and then the samples were cooled by gradually reducing the microwave power, over a period of approximately 15 minutes. Figures 4 and 5 are SEM micrographs of the sectioned joined specimens. Fig. 4 was

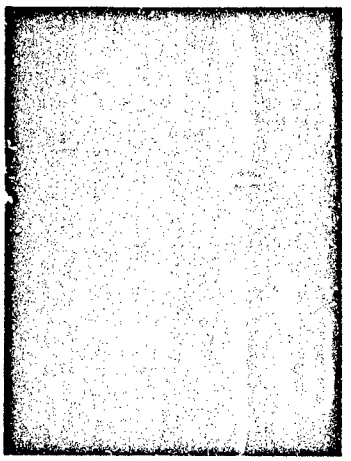


Figure 4 SEM micrograph of SiC joint made with cold pressed disk of Ti:C (outer edge).

taken at the outer edge of the specimen. Fig. 5 was taken in the interior of the sectioned specimen. The interlayer material in Fig. 4 is orange-white, while the interlayer material in Fig. 5 is dark gray. X-ray diffraction data clearly indicated TiC, TiO_2 and Ti_3O_5, as well as SiC, in the joined samples.

CONCLUSION

Microwave joining of SiC has been accomplished using both a single mode and a multi-mode joining apparatus at 2.45 GHz. Homogeneous joints were made using Si as the interlayer material, applied directly as powder, in an oil-based slurry, or



Figure 5 SEM micrograph of SiC joint made with cold pressed disk of Ti:C (interior of sectioned specimen).

plasma-sprayed onto the surface of one of the specimens to be joined. The plasma-spray technique yielded the thinnest interlayers, and for these Knoop hardness did not vary substantially across the sectioned joint interface. Microwave-induced combustion synthesis was achieved in a cold pressed disk of Si:C:Ti to produce SiC, using the multi-mode cavity. Microwave-induced combustion synthesis of a cold pressed disk of Ti:C placed at the interface was used to join SiC to SiC.

ACKNOWLEDGEMENTS

The authors are grateful to: Dr. Robert Cozzens and Ms. Marsha Goodell of the GMU Chemistry Department for several helpful discussions and for preparing the cold pressed disks for joining; Mr. Michael Mauro of LANL for preparing the plasma-sprayed SiC disks for joining; Mr. Andrew Green of TA&T for performing the SEM and microhardness measurements; and Mrs. Joyce Hunter of LANL for performing the X-ray measurements.

This work was sponsored by the U.S. Department of Energy Advanced Industrial Concepts Materials Program, through

Subcontract 9-XG1-U0554 with LANL. Work at GMU was performed under contract to TA&T, with additional funding provided by the Virginia Center for Innovative Technology.

REFERENCES

1. T. T. Meek and R. D. Blake, "Ceramic-Glass-Ceramic Seal by Microwave Heating," U.S. Pat. No. 4,529,857, July 16, 1985.
2. D. Palaith, R. Silberglitt, C. C. M. Wu, R. Kleiner and E. L. Libelo, "Microwave Joining of Ceramics," pp. 255-266 and H. Fukushima, T. Yamanaka and M. Matsui, "Microwave Heating of Ceramics and its Application to Joining," pp. 267-272, in Materials Research Society Proceedings, Vol. 124, Materials Research Society, Pittsburgh, PA (1988).
3. D. Palaith and R. Silbergiitt, "Microwave Joining of Ceramics," American Ceramic Society Bulletin, Vol. 68, No. 9, pp. 1601-1606 (1989).
4. H. Fukushima, T. Yamanaka and M. Matsui, "Microwave Heating of Ceramics and its Application to Joining," Journal of Materials Research, Vol. 5, No. 2, pp. 397-405 (1990).
5. R. E. Loehman, M. L. Mecartney and E. J. Rowcliffe, "Silicon Nitride Joining," USAF Report No. AFOSR-TR-82-0304 (February 8, 1982).
6. R. M. Neilson, Jr. and D. N. Coon, "Strength of Silicon Nitride-Silicon Nitride Joints Bonded With Oxynitride Glass," ACerS Forum Paper No. 40-FII-87, 89th Annual ACerS Meeting, Pittsburgh, PA (1987).
7. R. C. Dalton, I. Ahmad and D. E. Clark, "Combustion Synthesis Using Microwave Energy," Ceramic Engineering and Science Proceedings, Vol. 11, Nos. 9-10, pp. 1729-1742 (1990).
8. J. D. Katz, "Microwave Sintering of Boron Carbide," Materials Research Society Proceedings, Vol. 124, pp. 219-226 (1988).

APPLICATION OF MICROWAVE PROCESSING TO SIMULTANEOUS SINTERING AND JOINING OF CERAMICS

X.D. Yu, V.V.Varadan and V.K.Varadan
227 Hammond Building
Research Center for the Engineering of Electronic and Acoustic Material &
Department of Engineering Science and Mechanics
The Pennsylvania State University
University Park, PA 16802

ABSTRACT

Simultaneous sintering and joining of ceramics, often referred to as green state joining, is used in producing structural and electronic composites as well as complex-shaped ceramic components. In this paper, a novel idea of using microwave energy to simultaneously sinter and join ceramics is proposed. Alumina green samples are fired and joined in a single mode microwave heating device. Scanning Electron Microscope and Scanning Acoustic Microscope are used to evaluate joining interface. Experimental results show that, because microwaves offer rapid and uniform heating, fast densification and excellent joining can be achieved.

INTRODUCTION

Microwave heating is a volumetric process. It provides rapid and uniform heating so that temperature gradients which are observed in conventional rapid heating can be avoided. Its application in material processing has produced many interesting results [1]. Microwave processing of ceramics is especially encouraging. Using microwaves to sinter alumina , Tian et al [2] has shown that rapid densification and ultra-fine microstructures can be obtained. Janney et al. [3] has shown that ceramics begin to densify at a lower temperatures with microwave heating than with conventional heating. The joining of ceramics by microwave heating has been studied by Fukushima et al. [4]. Their study has shown that the dielectric loss factor, which is the determining factor for absorbing microwave energy, rapidly increase with temperature and the value at 1800°C is two orders of magnitude larger than that at room temperature. Results prove that thermal runway effect occurs even in the microwave region, thus allowing the microwave heating and joining of ceramics. As a result, ceramics can be joined and higher joining strength will be obtained.

BACKGROUND

Simultaneous sintering and joining, often referred to as green state joining, is used in producing structural and electronic ceramic composites as well as complex-shaped ceramic components. In this joining process, the parts to be joined are green samples rather than densified ceramics. Green state joining can be used in producing structural composite materials to increase material fracture toughness. In a study by Boch et al. [5], an Al_2O_3/ZrO_2 laminated composite was made. In that process, ceramic layers to be laminated were first fabricated by the tape casting method. The tapes were then stacked and thermocompressed. After burning out the organic components, the green composite was densified and joined. Test results showed that greater fracture toughness was achieved even with Al_2O_3/Al_2O_3 composite. In this production process, excellent densification and joining are needed to increase material toughness. Green state joining can also be used in the production of multilayer capacitors and smart materials [6]. In which, tape casted electroceramic layers that have same or different materials are co-densified. Electrodes for each layer are screen printed before firing in the conventional method. In a so-called fugitive method, a fugitive layer is placed between electroceramic layers and electrode metals are squeezed into the fugitive cavity in the later process. Lower firing temperature and shorter firing time are desirable so that deleterious chemical reaction between electroceramic phases can be avoided and inexpensive electrode materials can be used to minimize the production cost. The joining has to be designed so that the electrode material can be squeezed to form good electrodes. Green state joining also finds application in producing complex ceramic parts. Advanced ceramic materials have the potential to be used for precision engine components. However, the use of ceramic materials have been inhibited by the difficulty and cost of manufacturing complex-shaped components. Methods such as injection molding, slip casting and pressure casting can be used in producing complex-shaped ceramic components. But difficulties with defects, removal of binder/lubricants, control of warpage , lengthy drying cycle, mold release and drying shrinkage crack limit fast throughput. Those can be overcome by joining small parts together to form a complex shaped aggregate. Studies conducted by Bates et al. [7] show that simultaneous sintering and joining is applicable in producing some non-oxide ceramics for high temperature application. In all the applications of simultaneously sintering and joining mentioned above, fast densification, short firing time and excellent joining are always desired. Microwave processing has the potential to reach these goals.

In this research work, an effort was made to integrate the microwave sintering and microwave joining to form a simultaneous process so that the joining and sintering of ceramics can be accomplished at the same time. In doing so, the tedious tasks of grinding and polishing which are necessary for joining densified ceramics can be eliminated. The metal and glass interlayers that are often used in ceramic joining, resulting in lower high temperature strength of the joined components, are not necessary for joining of ceramics. More importantly, fast production rate and excellent joining may be achieved with the microwave heating method.

INSTRUMENT DESCRIPTION

A single mode high power microwave heating device which operates at 2.45 GHz is used in this experiment. It is displayed in figure 1. The magnetron and associated control system can generate a maximum of 3kW microwave power in a continuous or pulsed form. A circulator follows the magnetron to divert the reflected microwave to the dummy load to protect the magnetron. A section of quarter wavelength waveguide, which is equipped with two directional couplers for measuring forward and reflected power, is connected to the system next to the circulator. The impedance analyzer, which has four detectors with fixed phase relationship, is used to monitor the working condition of the system through obtaining the reflection coefficient of the cavity. A 4-stub tuner is also placed before the microwave resonator for the fine tuning of the system.The microwave resonator is formed by an iris, a section of waveguide and a variable short-circuted waveguide. The sample is placed at the position where the electric field has the maximum value. The diagnostic system has two main components, HP9826 PC and HP3497A data acquisition system. They collect and process the signal from the impedance analyzer for calculating the reflection coefficient as well as from the temperature controller connected to a pyrometer for recording temperature history. The sample to be sintered, being small, is placed in a quartz sample holder and surrounded by the insulating material. A small hole is made in the insulating material to allow the pyrometer to monitor the temperature variation. Upon turning on microwave generator, the variable short is adjusted so that the microwaves will resonant inside cavity and microwave energy can be absorbed by the ceramics efficiently.

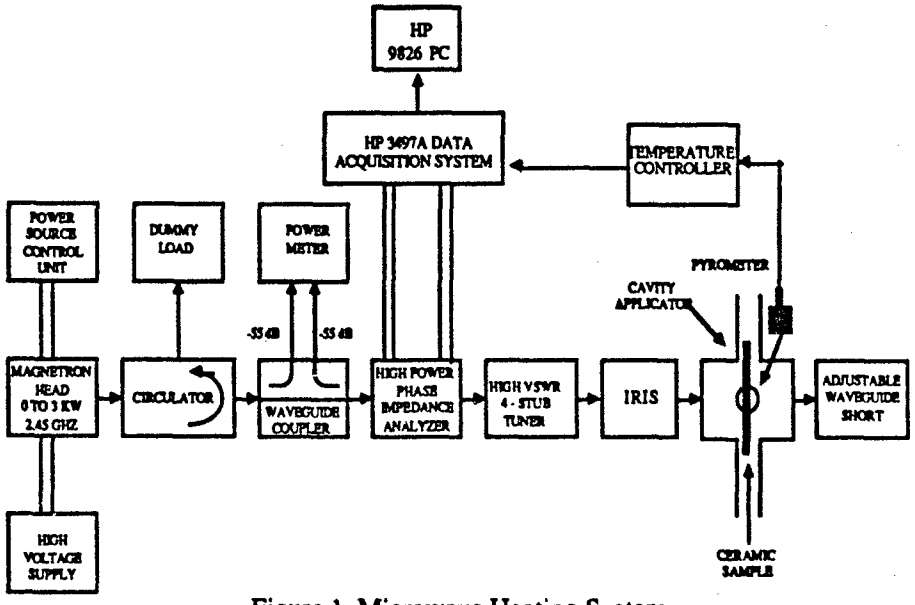


Figure 1. Microwave Heating System.

EXPERIMENT

The Bailobax[1] alumina powder having an average particle size 3μm was used in this study. Alumina powder doped with 0.3% (wt) magnesium and 3% (wt) PVA was ball milled in the methanol for two hours. The addition of magnesium was to inhibit grain growth and to promote diffusion. The mixed powder was dried in the furnace at 80°C to evaporate the alcohol. The parts to be joined were green pellets obtained by dry pressing at a pressure of 2800 MPa. Since the surfaces to be joined were not perfectly flat, a slip interlayer of the same material mixed with PVA is placed in between parts to be joined. The two green pellets and the slip interlayer formed a whole body by isostatic pressing with a pressure 150 MPa. The slip, being viscous, conforms to the asperities of the green surface, so that minor defects can be filled. The whole joining body was then prefired at 600°C for two hours. Finally, the sample was sintered in the high power microwave heating system. By adjusting the variable short plate, the resonance was achieved inside the single mode cavity. To uniformly radiate the sample, the sample holder is rotated 10 revolutions/minute. Figure 2. gives the microwave sintering history. The microwave power used here was 600W. The sample heated to 1400°C with heating rate of 100°/min. The temperature was held at 1400° for 14 minutes and the power was then lowered to zero in 3.5 minutes. The whole sintering and joining time was about 28 minutes. Figure 3 shows the conventional sintering and joining history.

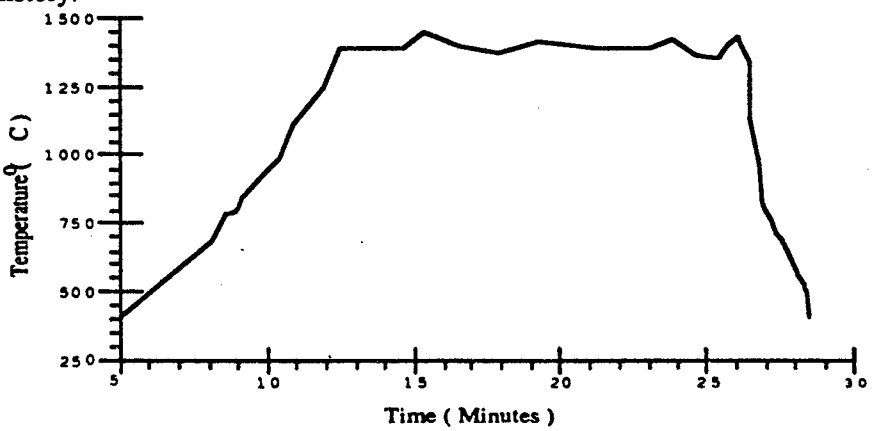


Figure 2. Microwave Sintering and Joining History

By using the above stated processing method, the green aggregates are sintered and joined by using the microwave heating as well as the conventional heating method with or without a pressure 0.283MPa applied at the interface of the joining. A total of 4 samples are researched for each condition. The relative density was obtained by using Archimedes' principle.

---

[1]Bailobax Co., Charlotte, N.C. Bailobax-CR-30

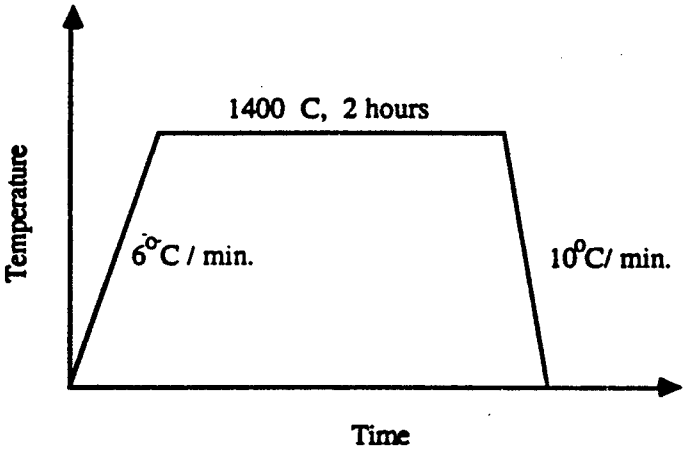


Figure 3. Conventional Sintering and Joining History

RESULTS AND DISCUSSION

Scanning Electron Microscope Study Joining Interface

To examine the joining result, the joined sample was sectioned with a diamond saw and subsequently polished with a 600 grit sand paper. The joint boundary was then examined by the Scanning Electron Microscope.

Figure 4 is the micrograph of the joined boundary of the sample formed by a pressure of 0.238 MPa at the interface during microwave sintering and joining. This figure shows that excellent joining was obtained. Defects at the interface have similar dimension to those in the sintered bulk body. The bulk density is measured to be 94%. The joint boundary was invisible to the eye. Figure 5 gives the microstructure of the sample which is microwave sintered and joined at 1400°C for 35 minutes. A complete densification was realized with an average grain size 2μm. Figure 6 is the micrograph of the join boundary of the sample which was formed with no pressure at interface during microwave sintering and joining. It shows that only half of the boundary was joined. The bulk density is also 94%. Large voids can be readily seen from SEM picture. These large defects may be formed due to the non-uniform shrinkage between interlayer and bulk body during fast densification. However, such large voids can be eliminated by applying proper pressure at the interface during sintering and joining, which has been demonstrated by the figure 4. Hence, proper pressure is needed at interface during microwave sintering and joining. The magnitude of the pressure should be selected such that excess deformation in the bulk body will not be induced and the voids which might appeared at interface could be eliminated. The pressure 0.283MPa used here is based on the several experimental results of the microwave sintering and joining of green samples. To avoid any excess deformation in the bulk body, the isostatic pressure may be used. Since the pressure needed is small, isostatic pressure can be readily realized.

Figure 7 is the micrograph of the joined boundary of the sample formed with

0.283MPa at the interface during conventional sintering and joining. The picture shows that because of low densification , the joined boundary can be clearly seen and different densities were also observed in the joining interface and bulk body. Figure 8 is the micrograph of the join boundary of the sample which formed with no pressure at the interface in the conventional sintering and joining. Because there is no pressure applied at the interface during sintering and joining, the joining boundary was not dense and some of the sections can be damaged during the polishing process.

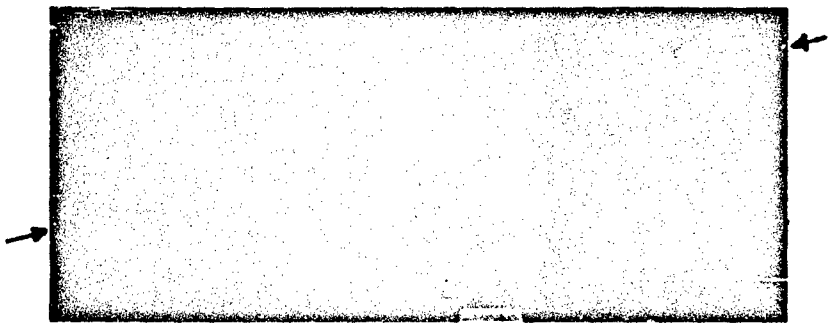


Figure 4. SEM Micrograph of Microwave Sintered and Joined at 1400°C for 14 minutes with 0.283MPa pressure, Bulk Density 94%

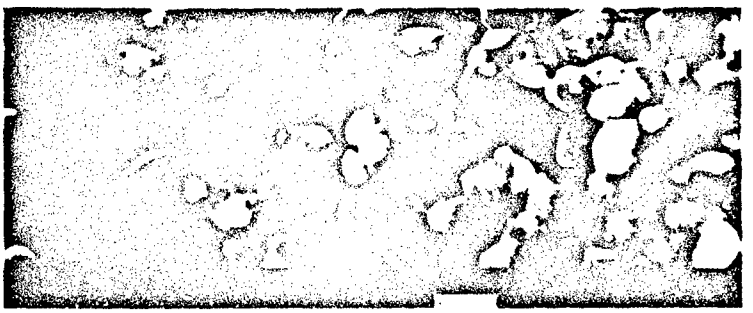


Figure 5. SEM Micrograph of Microwave Sintered and Joined at 1400°C for 35 minutes with 0.283MPa pressure, Bulk Density 99%



Figure 6. SEM Micrograph of Microwave Sintered and Joined at 1400°C for 14 minutes with no pressure, Bulk Density 94%

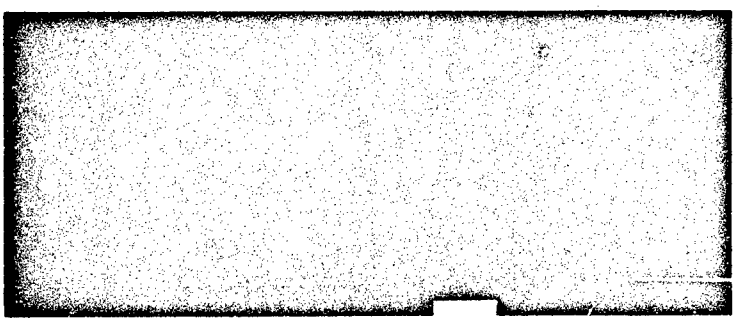


Figure 7. SEM Micrograph of Conventional Sintered and Joined at 1400°C for 2 hours with 0.283MPa pressure, Bulk Density 80%

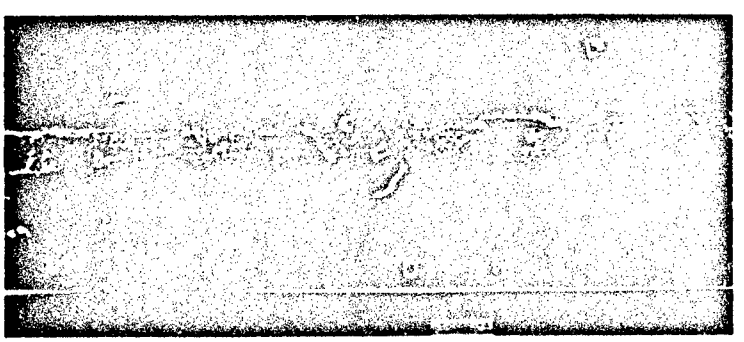


Figure 8. SEM Micrograph of Microwave Sintered and Joined at 1400°C for 14 minutes with no pressure, Bulk Density 80%

Scanning Acoustic Microscope Study Joining Interface

The scanning acoustic microscope (SAM) is a high precision instrument which focuses acoustic waves to a point on or below the surface of a specimen. The intensities of the reflected waves are analyzed and compiled to give detailed images of the specimen at the prescribed depth. This non-destructive technique is extensively useful in determining the material properties inside of a sample. Some relative information about Scanning Acoustic Microscope can be found in [8,9].

The SAM used here was to evaluate the joining interface, and thus determine the effectiveness of the microwave sintering and joining process. The sample was polished so that the surface was parallel to the interface. By doing so, the interface could be evaluated. The distance between the surface and the interface was less than 41.9μm. The sample was then mounted on a glass slide for use with the SAM.

From scanning electron micrographs of the edges of the interface for the sample which was microwave sintered and joined with no pressure at the interface, it was seen that voids existed on the order of 10-20μm in diameter. It follows that a lens with a resolution of at least 10μm is needed. The 400MHz lens was chosen which has a resolution of 9.26μm and a maximum penetration depth of 41.9μm. The objective was positioned so that the focal point could be placed above, below, or on the interface. SAM micrograph images were taken at all three of these depths.

Figure 9 shows the black and white images of $1mm^2$ of the sample at the interface. The contrast is the result of voids in the sample which cause acoustic impedance mismatch and strong reflection. The darker regions tell where the voids exist. From this micrograph, we can clearly see that there are few voids located at the interface which has a dimension similar to the defects shown on the SEM picture. For the surface below and above the interface, the SAM images did not show any voids. A 1000MHz lens which has higher resolution and lower penetration capability will be used in the future to evaluate other joined specimen.

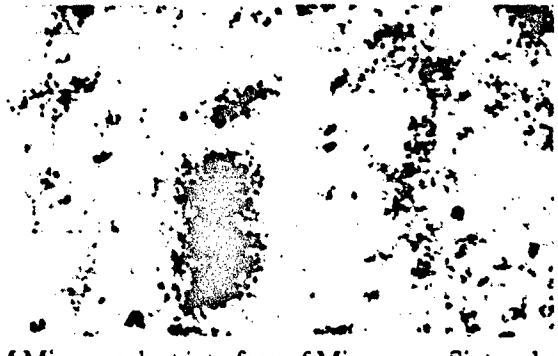


Figure 9. SAM Micrograph at interface of Microwave Sintered and Joined at 1400°C for 14 minutes with no pressure, 100×

CONCLUSION

The experimental results show that simultaneous sintering and joining using

microwave heating is feasible. This method can be used to produce complex ceramic components. Its usefulness can also be applied to the production of multilayer capacitor where several tape casted layers are stacked together. In the case where joining strength is not strictly required, the pressure applied during sintering and joining may not be necessary. Further research should be conducted to examine the strength of sintering and joining of larger samples.

Acknowledgement

The authors would like to thank Dr. B. Tittmann at the Penn. State Ultrasonic Laboratory for helping use the Scanning Acoustic Microscope.

REFERENCES

1. W.H. Sutton, M. H. Brooks, and I.J. Chabinsky. Microwave Processing of Materials, Symposium Proceedings, Vol. 124., Material Research Society, Pittsburgh, PA, 1988.
2. Y.L. Tian, D. Lynn Johnson, and M.E.Browin, " Ultra Microstructure of Al_2O_3 by Microwave Processing", in Ceramic Powder Science II (Ceramic Transaction Vol. 1). Eds. G.L.Messing, E.R. Fuller, Jr., and H. Hausner, American Ceramic Society, Inc., Vol.124, pp. 925-32, 1987 .
3. M.A. Janney and H.D. Kimmrey, " Microwave Sintering of Alumina at 28 GHz", in Ceramic Powder Science II (Ceramic Transaction Vol. 1). Eds. G.L.Messing, E.R. Fuller, Jr., and H. Hausner, American Ceramic Society, Inc., pp. 919-24, 1987.
4. H. Fukushima, T.Yamanaka and M.Matsui, "Microwave Heating Of Ceramics and its Application to Joining", pp.267-72 in Microwave Processing of Materials, Symposium proceedings, Vol.124. Edited by W.H. Sutton, M.H. Brooks, and I.J. Chjabinsky. Material Research Society, Pittsburgh, PA , 1988.
5.P. Boch, T. Charter, and M. Huttepain, " Tape Casting of Al_2O_3 /ZrO_2 laminated Composites", J.Am. Ceram. Soc., 69 [8] C-191-C-192 ,1986.
6.R.E. Newnham and G. R. Ruschau, " Smart Electroceramics", J. Am. Ceram. Soc., 74 [3] 463-80 , 1991.
7.C. H. Bates, M. R. Foley, G. A. Rossi, G. J.Sunderberg, and F. J. Wu, " Joining of Non-Oxide Ceramics for High Temperature Applications", Ceramic Bulletin. , Vol. 69, No.3, pp.350-56, 1990.
8. M.Issouckis. " The Scanning Acoustic Microscope-principles and applications", Metals & Materials, 5, (2), pp.63-67, Feb. 1989.
9. G.C. Smith, " The Scanning Acoustic Microscope-a New Tool for the Materials Scientist", Material Science & Technology, 2, (9), pp.881-87, Sept. 1986.

MICROWAVE JOINING OF Si-SiC/Al/Si-SiC

T. Y. Yiin, V. V. Varadan, V. K. Varadan, and J. C. Conway
Center for the Engineering of Electronic and Acoustic Materials
The Pennsylvania State University, University Park, PA 16802

ABSTRACT

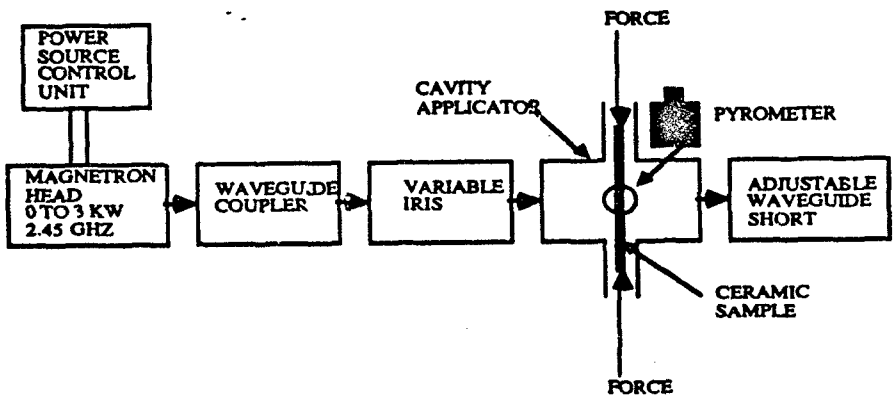
Microwave energy is used to join high dielectric loss Si-SiC to Si-SiC with Al foil as an interlayer. Rapid heating with moderate applied pressure has led to excellent bond strength in a short time. The joining was successfully achieved in about 5 minutes at 1250°C and 1.2 MPa axial pressure in a single mode microwave cavity without damaging the samples. The joined specimen interfaces were examined using optical microscopy and scanning electron microscopy. The diffusion paths of Al were also detected with electron microprobe image mapping. Average fracture strength of the joined specimen was shown to be comparable to the original material strength using the four point bending fracture test. Comparison of Weibull plots for original and joined Si-SiC has also verified the high strength at the Si-SiC/Al/Si-SiC interface.

INTRODUCTION

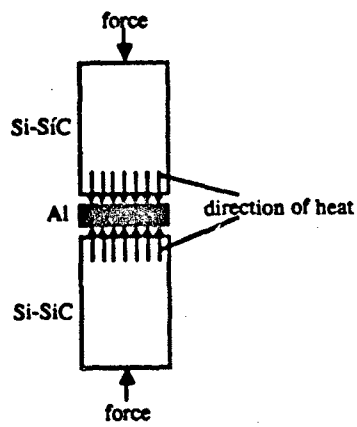
For more than a decade, research has been performed on joining ceramic to metal for electrical and engineering applications. In the 1980's, microwave energy has been successfully used to join similar ceramics with or without an adhesive ceramic, [1,2,3]. The possibility for this kind of joining is to heat up the low dielectric loss ceramic. As the ceramic heats up, the loss tangent will increase exponentially with temperature. Because the energy absorbed by the ceramic is proportional to the square of the loss tangent, it can be heated up to very high temperatures and joined in a short time. However, some ceramics do not readily reach this temperature without adding microwave coupling agents. Furthermore, once the ceramic is heated to the thermal runaway region, a thermal breakdown effect for local heating can be induced which could badly damage the microstructure of the ceramic.

In this study, we join ceramic to ceramic with microwave heating. We wish to take advantage of the positive features of microwave heating and eliminate the negative aspects. Some ceramics, like silicon carbide, have a high dielectric loss tangent at room temperature and a high thermal conductivity. Therefore, silicon carbide is very easy to heat up with microwave power to some temperatures, but not to the thermal runaway region. This is because the high thermal conductivity of silicon carbide could conduct the heat to the surfaces where it can escape and thus eliminates "hot spots". We try to use these properties to join samples of SiC together in a single mode microwave cavity with aluminum as the adhesive. Aluminum metal has been chosen as a candidate material to join structural ceramics for its low melting temperature and possible chemical reaction with ceramics in a conventional furnace as heating sources, [4].

In microwave heating, although Al metal cannot absorb microwave energy, the heat generated from the silicon carbide can heat up the Al by conduction. Figure 1 shows the set-up and the directions of heat conducted to Al metal with microwave power inside the cavity. In Si-SiC/Al/Si-SiC joining, the highest temperature was around 1250° C which could be reached quickly in a single mode microwave cavity without damage to the silicon carbide.



(a)



(b)

Figure 1 Schematic diagram of Si-SiC/Al/Si-SiC joining with microwave power (a) single mode cavity (b) heat generated from Si-SiC.

MATERIALS

Commercial reaction sintered silicon carbide (Si-SiC) samples* were used in this work. The Si-SiC exhibits a bi-modal microstructure of SiC grains; the small grains range from 2 to 5 μm and large grains range 100 to 150 μm. This material contains 11% by volume free silicon, and the bulk density was 3.1 gcm^{-3}. Si-SiC appears to contain no porosity, indicating a perfect bonding and infiltration between the silicon and the SiC grains. The Si-SiC blocks to be joined were cut in the dimensions $15 \times 10 \times 10$ mm^3. and all the surfaces are polished with a 15 μm grit diamond wheel. The two-surfaces were made parallel to each other to avoid any mismatch between them. The Al foil** surface roughness was around 1 μm and the thickness was 16 μm before joining. To minimize the oxidation on the Al surface and avoid contamination on all the surfaces, the samples thus prepared were used immediately after cleaning in the ultrasonic cleaner.

EXPERIMENTAL PROCEDURE

In preparation for microwave joining, Al foil was sandwiched between a pair of Si-SiC blocks. The specimen was then placed inside the center of a single mode copper cavity (5" × 4" × 2") with 500 watts microwave power supplied. The power was coupled to the cavity through a variable iris and tuned to resonate at 2.45 GHz by an adjustable short. By placing through-tube quartz bars on the top and bottom of the joining Si-SiC, pressure was applied to the specimen from outside the cavity through tubes on the broad sides of the cavity. These tubes are designed to provide access to the cavity and are designed to support only modes below the cut off frequency of the resonant cavity. The whole process was conducted in an air atmosphere during heating.The heating history was recorded on the joining interface by a pyrometer.
After joining, the specimen was gradually polished to 0.25 μm around the Si-SiC/Al/Si-SiC interface for optical microscopy , scanning electron microscopy (SEM) , and electron microprobe analysis. Original Si-SiC's without microwave joining and joined Si-SiC's were then cut into rectangular bars of dimension $1.5 \times 2.0 \times 30$ mm^3 for the four-point bend and three-point bend tests. The tensile surfaces were polished and edges were beveled to remove any surface crack flaws caused by machining for all the testing bars. Ten original Si-SiC bars and ten joined Si-SiC bars were fractured separately using an INSTRON in air atmosphere at a cross head speed of 0.5 mm./min as shown in figure 2. The two parameter Weibull modulus plot was used for statistically analyzing the fracture strengths of original and joined Si-SiC's. Three joined specimens were indented on the interfaces for three-point bend test. In the three-point bend test, we try to estimate the direction of fracture flows.

RESULTS AND DISCUSSION

For joining Si-SiC/Al/Si-SiC, the total microwave processing time was around 5 minutes as shown in figure 3.The maximum surface temperature was 1250° C recorded in the heating history. After the temperature stayed for one minute at 1250° C, the power was turned off to let the joined specimen cool down to the room temperature.

---

* Norton Co., Worcester, Mass.

** 98.5 vol% Al, 0.5 vol% Fe and 1.0 vol% Si, Reynolds Metals Co., Richmond, Va.

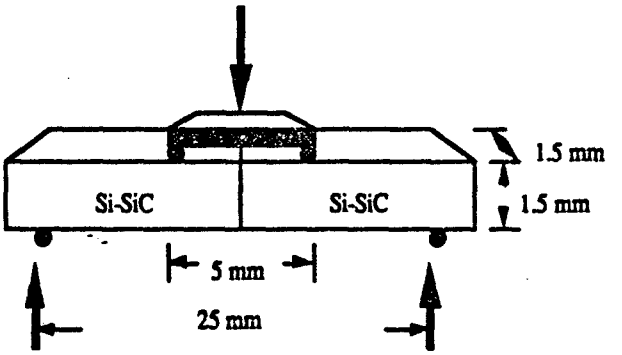


Figure 2 Schematic diagram of four-point bending test.

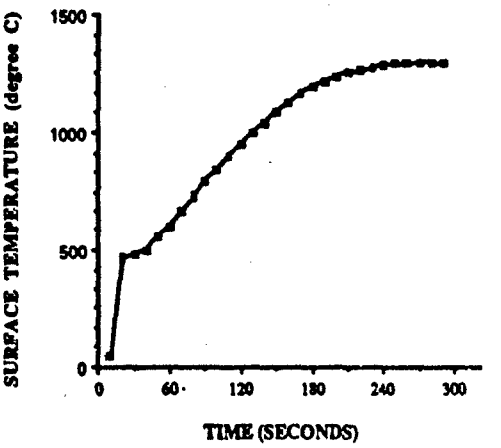


Figure 3 Heating history of Si-SiC/Al/Si-SiC joining with microwave power. Maximum temperature was around 1250° C.

Figure 4 shows the typical optical micrographs of the joined Si-SiC/Al/Si-SiC interface. Since the highest joining temperature was around 1250° C which could melt the Al metal and the applied forces on the specimen could accelerate the distribution of melted metal into the pores on the surfaces of the Si-SiC's, a uniform interface without any cracks was observed at the interface. Residual stress problems caused by the thermal expansion mismatch between ceramic and metal could be relieved in the molten metal also.The thickness of the Al foil was reduced from 16 μm to 5 μm due to the force applied in the joining process. Some of the Al is squeezed out from the interface and some Al diffuses into the Si-SiC once Al has been melted. Figure 5 shows the SEM and electron microprobe photographs. From the variation of Al composition across the joint, Al diffuses into Si but not the SiC grains. It is possible that chemical reaction between Al and Si might occur to form the strong bonding.

Typical fracture paths of the four-point bend and three-point bend tests are shown in figure 6. For the four point-bend test, the joined Si-SiC fractured away from the interface. Furthermore, the three-point bend test specimen was notched on the interface, but the fracture path still flowed into the base material. These indicate that the joined specimen has higher bond strength in the Si-SiC/Al/Si-SiC interface than the Si-SiC base material.

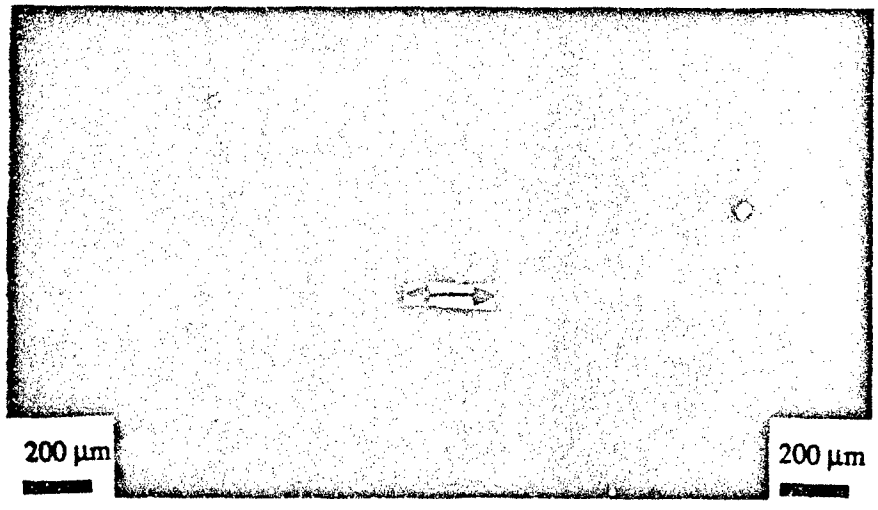


Figure 6 Fracture paths of (a) four-point bend and (b) three-point bend tests. Arrows indicate the joined interface.

Results from the two parameter Weibull statistical approach are shown in figure 7 and Table 1. As predicted, the joined specimen has higher fracture strength than the original ceramic. These data prove that the interface has at least as strong and perhaps stronger than the Si-SiC. The higher fracture strength in microwave joining has also been reported separately by Palith *et al.*[2] and Fukushina *et al.* [3] for joining similar ceramics without adhesives.

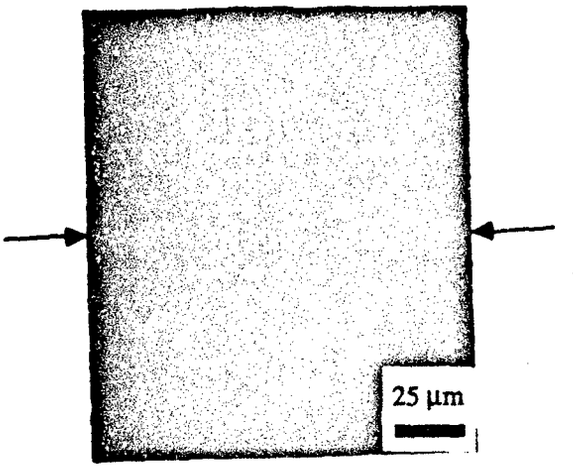
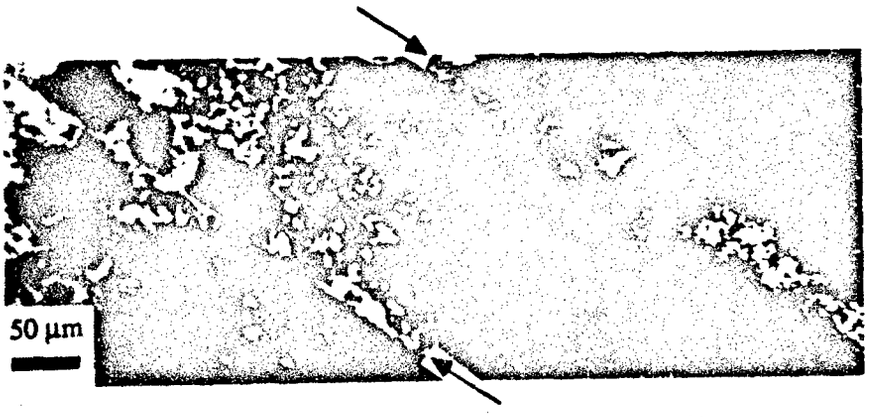


Figure 4 Optical micrograph of the polished Si-SiC/Al/Si-SiC interface showing uniform joining. Arrow indicates the joined interface.



(a) (b)

Figure 5 Photographs of Si-SiC/Al/Si-SiC interface on the same position by (a) SEM (dark phases shows the SiC grains) (b) electron microprobe image of Al on the interface (Al diffuses into the Si but not the SiC grains). Arrow indicates the joined interface.

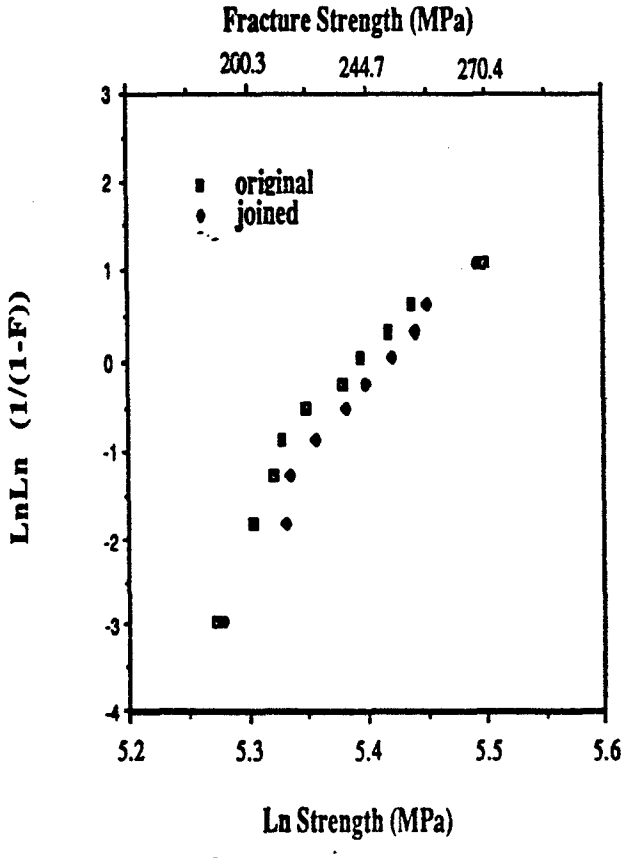


Figure 7 Weibull plots of four-point bend strength of original and joined Si-SiC fracture strengths.

Table 1. Comparison of Original and Joined Si-SiC Mechanical Properties

Specimen Configuration	Average Strength (MPa)	Standard Dev.	Weibull Modulus (m)	Characteristic Strength (σ_0)
Original	215.4	15.1	17	222.2
Joined	219.4	14.2	18	225.6

CONCLUSION

High dielectric loss ceramic to ceramic joining using a metal interlayer with microwave power has been successfully applied to a Si-SiC/Al/Si-SiC system in a short joining time. Microwave heating enhanced the diffusion of Al into Si is the key point for high joined fracture strength. As is evident from the experimental results, ceramic/metal/ceramic joining is also achievable with microwave heating.

ACKNOWLEDGEMENT

This research was partially supported by U. S. Army CECOM under contract # DAAB07-90-A033 to the Pennsylvania State University.

REFERENCES

1. T. T. Meek, R. D. Blake, "Ceramic-ceramic Seals by Microwave Heating", pp.270-274, J. Mater. Sci. Lett. 5, 270 (1986)

2. D. Palaith, R. Silberglitt, C. C. M. Wu, R. Kleiner, and E. L. Libelo, "Microwave joining of ceramics", pp. 255-66 in Microwave Processing of Materials, Symposium Processing, Vol. 124. Edited by W. H. Sutton, M. H. Brooks, and I. J. Chabinsky. Materials Research Society, Pittsburgh, PA, 1988.

3. H. Fukushima, T. Yamanaka, and M. Matsui, "Microwave Heating of Ceramics and Its Application to Joining", pp.267-72 in Microwave Processing of Materials, Symposium Processing, Vol. 124. Edited by W. H. Sutton, M. H. Brooks, and I. J. Chabinsky. Materials Research Society, Pittsburgh, PA, 1988.

4. T. Iseki, T. Kameda, T. Maruyama, "Interfacial reactions between SiC and aluminum during joining", pp.1692-1698 J. Mater. Sci. 19(1984)

MICROWAVE JOINING OF CERAMICS

Salwan Al-Assafi, Iftikhar Ahmad, Zakarye Fathi,
and David E. Clark
Department of Materials Science and Engineering
University of Florida
Gainesville, FL 32611

ABSTRACT

AlOOH gel was used as a bonding layer for alumina samples to be joined. Microwave radiation was used as a source of energy in a multi-mode cavity. The gel was brushed on the surfaces of the substrates to be joined and by applying pressure of 0.6-2 MPa, while heated with microwave energy, joints of different strengths were produced. The maximum strength was achieved at 1650°C and it was approximately 93 % of the original strength. It was found that the use of AlOOH gel improves the joint quality for samples joined at relatively low temperature. Our results suggest that bonding occurred due to a diffusion process at the interface.

INTRODUCTION

Sol-gel processing is of particular interest in the ceramic industry due to the unique properties achieved in terms of particle size. Sol is a dispersion of colloidal particles in a liquid. Colloids are solid particles with diameters of 1-100 nm [1]. A gel is an interconnected, rigid network with pores of submicrometer dimensions and polymeric chains whose average length is greater than a micrometer. The gel is obtained by heating the sol for a specified temperature and time, or by any other means that reduce the liquid between the colloids.

The subject of joining of ceramics has attracted a great deal of attention recently as a result of the increasing demand for ceramics in the high-tech industry. The importance of ceramic joining arises from the fact that ceramics are difficult to machine. Since large and complex shapes are often necessary, a satisfactory joining process is desired.

One of the newest techniques in joining of ceramics is microwave joining. Meek and Blake [2] were the first to report fabrication of ceramic-glass-ceramic seals using microwave energy. They succeeded in sealing alumina substrates using a home-type (700 Watt) microwave oven. The joining temperature was in the range of 700-800°C and the processing time was 99 minutes. They reported that the predominant bonding mechanism was diffusion bonding.

Microwave joining of ceramics in a single mode cavity has also been carried out. Fukushima, Yamanaka, and Matsui [3] have reported joint strength equal to the original strength for low purity alumina ceramics joined directly (without intermediate layer) using a single mode cavity. The joining time was 3 minutes and the applied pressure was 0.6 MPa. Joining of high purity alumina was also carried out using a lower purity interlayer, but the joint strength in this

purity alumina was also carried out using a lower purity interlayer, but the joint strength in this case, was between 70 % and 90 % of the base ceramics. The maximum strength was achieved for samples joined at temperatures of 1750°C or higher. Palaith and Silberglitt [4] have used almost the same approach to join Si_3N_4, Al_2O_3, and mullite. However, in their experiments, the joining process was monitored by using an acoustic NDE system. With this system, different stages of the joining process can be monitored by analyzing the echoes from the joint interface.

This paper describes a joining process for alumina substrates using a new technique in which AlOOH gel is the interlayer and the microwave energy generated in a multi-mode cavity is the heating source.

EXPERIMENTAL PROCEDURE

Sample Preparation

Alumina substrates[1] (94 % purity) were used in this study. These substrates contain 3 wt% SiO_2 and 2 wt% MgO. The substrates were cut into 0.45-1 cm^2 specimens using a diamond saw. The AlOOH sol was obtained by a process described by Clark and Lanutti [5]:

$$Al(OC_4H_9)_3 + H_2O \xrightarrow{90°C} Al(OC_4H_9)_2(OH) + C_4H_9OH$$

$$Al(OC_4H_9)_2(OH) + 2H_2O \xrightarrow[Acid]{} 2C_4H_9OH + \underset{(Sol)}{AlOOH} + H_2O$$

$$\underset{(Sol)}{AlOOH} \xrightarrow[\text{liquid}]{\text{reduce}} \underset{(Gel)}{AlOOH}$$

$$\underset{(Gel)}{AlOOH} \xrightarrow{1300°C} \alpha\text{-}Al_2O_3 + H_2O$$

The sol was then heated until gelation state were achieved.

Since alumina does not couple with 2.45 GHz microwaves at low temperatures, a susceptor was manufactured to increase the temperature to the coupling temperature at which alumina begins to absorb microwave radiation. The susceptor consists of a zirconia cylinder lined with SiC as a coupling material.

[1]AlSiMag Technical Ceramics, Inc., Laurens, SC 29360

The Joining Process

Gel was brushed on both surfaces of the samples to be joined. These samples were placed inside the susceptor and the entire assembly was placed inside the microwave cavity which contains eight-2.45 GHz magnirons each with 800 W of power. After applying pressure of 0.6-2 MPa, 3-4 of the 8 magnirons were turned on. Different joining temperatures were attempted from 1450°C to 1650°C. Also, different processing times were attempted (ramp time = 11.3-35 min, soak time = 10-33 min) to achieve maximum joint strength. At a temperature of 1300°C, the AlOOH gel transforms into α-Al_2O_3 colloids [5]. After the joining process, the specimens were allowed to cool in air to room temperature.

Characterization

Bending strength measurements for the joined specimens were obtained from three-point bending test. After cutting the joined specimens in a direction normal to the joint, scanning electron micrographs and x-ray micrographs of the joint area were obtained, using a wave length dispersive electron microprobe.

RESULTS

Indicating the importance of the use of the gel, our results show that at a joining temperature of 1520°C, pressure of 0.6 MPa, and soak time of 10 min, the joining did not occur when gel was not present at the interface. However, under the same conditions, and when the gel was used, joining did occur. Furthermore, the joining occurred in both cases, with and without gel, for joining temperatures greater than 1520°C.

The effect of joining temperature on joint quality is shown in Figures 1, 2 and 3. Figure 1 shows SEM micrographs for samples joined at 1520°C, 1600°C, and 1650°C with gel as a bonding layer. As shown in this figure, it is possible to discern the joint in the sample joined at 1520°C, while it is impossible to discern the joint in the sample heated at 1650°C. Figure 2 shows x-ray maps for Si of specimens joined at 1520°C and 1650°C. In (a), fields depleted of Si can be observed along the joint, while in (b), a homogeneous distribution of Si is observed. Figure 3 represents the results of the bending strength test of the joined samples compared to the strength of the original material (as-received material) and the strength of two substrates with no joining. The maximum strength was achieved at 1650°C and was approximately 93% of the original strength. Another way to estimate the joint quality was to examine the fracture surface to observe any deviation in the course of the fracture. As shown in Fig. 4, for the specimen joined at 1600°C, there is a slight deviation in the course of the fracture at the joint, while, for the 1650°C specimen, there is no change in the fracture course at the joint.

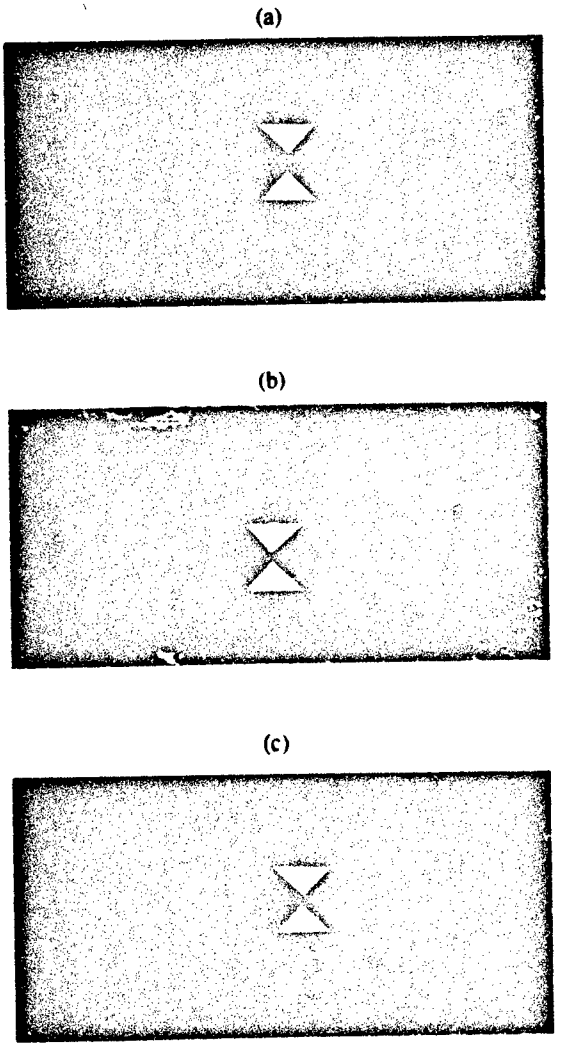


Figure 1. SEM micrographs of the joint area for (a) sample joined at 1520°C,(b) sample joined at 1600°C, and (c) sample joined at 1650°C.



(a) (b)

Figure 2. X-ray maps for Si of (a) sample joined at 1520°C and (b) sample joined at 1650°C.

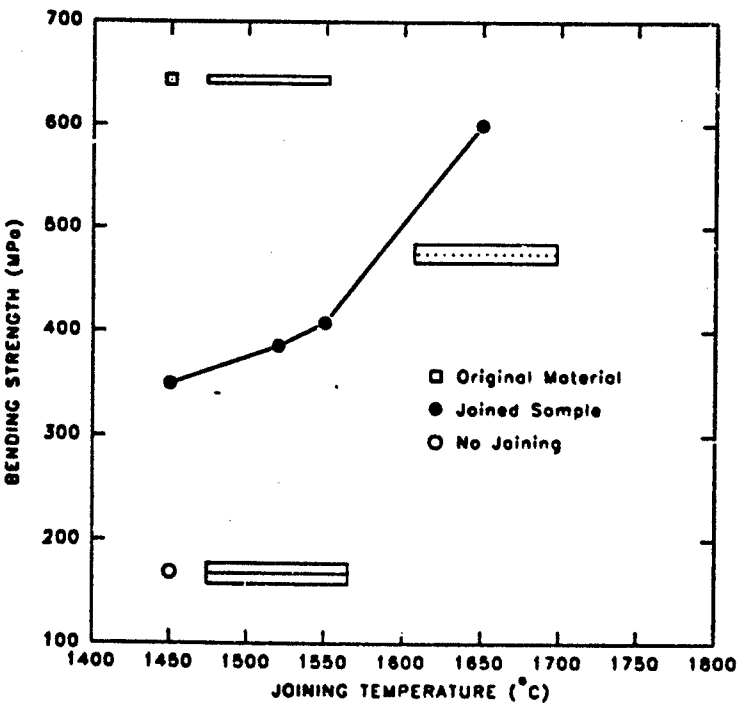
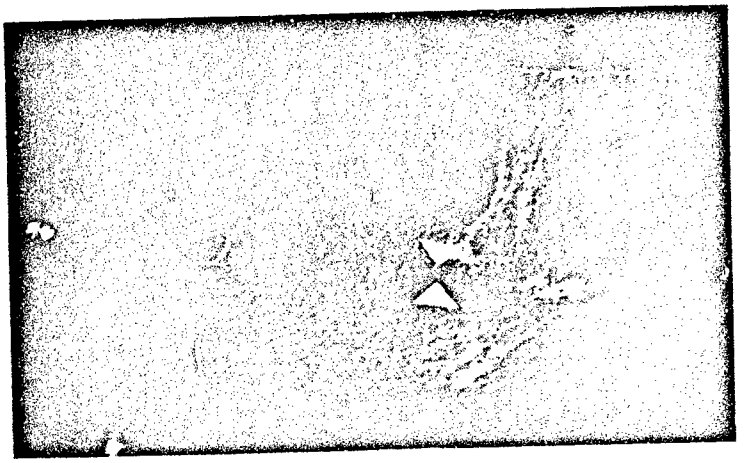


Figure 3. Bending strength of samples joined at different temperatures.

(a)



(b)

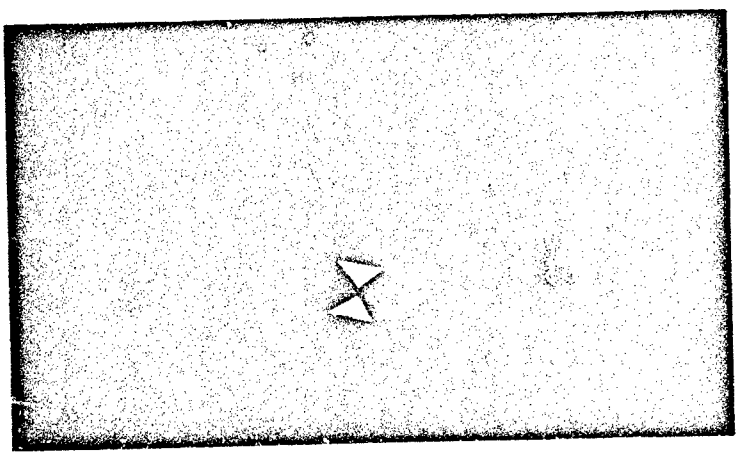


Figure 4. Fracture surfaces of (a) sample joined at 1600°C and (b) sample joined at 1650°C.

DISCUSSION

As indicated earlier, AlOOH gel transforms into Al_2O_3 colloids at a temperature of 1300°C. Since all joining temperatures investigated exceeded this temperature, the gel which fills the voids at the interface helps in reducing voids at the joint and, as a result, helps in improving the joint strength.

The other effect of the gel arises from the standpoint of the sintering rates of colloids. Since the sintering rate is inversely proportional to the particle size [6], Al_2O_3 colloids, which are very small (1-100 nm), will have a high sintering rate. This may explain the improvement in joints obtained at low temperatures when the gel was used. Another advantage in using the gel is the behavior of the gel as an adhesive at room temperature. This means that there is no need for any

additional means, such as binders, to hold pieces together before or during the joining process. In addition, the use of AlOOH gel provides consistency in the properties across the joint as the gel transforms during the joining process to α-Al_2O_3 which is the bulk material itself.

The use of the microwave energy has also several advantages from the standpoints of processing time and power. In addition, it is suggested that the use of the microwave energy has more than a thermal effect. Microwave energy may have an effect in improving the diffusion of atomic species across the interface, and this results in strong, hard to discern, and consistent joints at specified joining temperatures.

CONCLUSION

The use of AlOOH gel in microwave joining of alumina is a useful way to produce strong alumina-alumina joints. The advantages in using the gel are:

* Reduction in joining time, joining temperature, and as a result, required power.
* The use of AlOOH gel, instead of other materials, as a bonding layer is more favorable since AlOOH gel transforms into α-Al_2O_3 during the process and this provides a consistency in the properties across the interface.
* The gel acts as an adhesive at room temperature, this would help in holding the samples together without using additional binders.

The use of the microwave energy in joining of ceramics indicates that this method is an efficient way to join ceramics considering processing time, processing power, and the possible non-thermal effects of microwave energy.

ACKNOWLEDGMENT

The authors would like to thank AlSiMag Technical Ceramics Inc. for providing materials necessary for this project.

REFERENCES

1. L. L. Hench and J. K. West, The sol-gel process, *Chem. Rev.*, 90 (1990) 33-72.
2. T. T. Meek and R. D. Blake, Ceramic-glass-ceramic seal by microwave heating, *U.S. Pat. No. 4 529 857*, July 16, 1985.
3. H. Fukushima, T. Yamanaka, and M. Matsui, Microwave heating of ceramics and its application to joining, *Mat. Res. Soc. Symp. Proc.*, 124 (1988) 267.
4. D. Palaith and R. Silberglitt, Microwave joining of ceramics, *Ceramic Bulletin*, 68 (1989) 1601.
5. D. E. Clark and J. J. Lannutti, Phase transformations in sol-gel derived aluminas, in *Ultrastructure Processing of Ceramics, Glasses, and Composites*, Edited by L. L. Hench and D. R. Ulrich, John Wiley & Sons, 126-41 (1984).
6. W. D. Kingery, H. K. Bowen, and D. R. Uhlmann; pp. 477 in *Introduction to Ceramics*, 2nd ed. Wiley & sons, 1975.

ENHANCED MICROWAVE ABSORPTION IN CHIRAL COMPOSITE MATERIALS

Y. Ma, V. K. Varadan, and V. V. Varadan
Research Center for the Engineering of Electronic and Acoustic Materials
Department of Engineering Science and Mechanics
The Pennsylvania State University
University Park, PA 16802

ABSTRACT

In microwave joining of composite materials as well as in high frequency dielectric heating for processing of polymeric materials, proper loss factors in the joining adhesives and in the sensitizers are essential. A composite material can be tailored through its chiral microstructure to attain a desired absorption mechanism. For surface heating as well as in microwave joining, a fairly high loss factor is produced in chiral composite materials. For volumetric heating, a preferred loss factor can be obtained using chiral composites to optimize the dielectric processing.

INTRODUCTION

Novel chiral materials and their composites have recently drawn lots of attention from the research community as well as from various application groups in the industry. In less than five years, the interest originally focusing on the academic research has been directed towards the manufacturing of chiral materials. In order to tailor such novel materials, dependable equations in predicting their performance as well as the material properties when they are used in, for example, microwave joining and processing of materials, are indispensable.

A chiral material is characterized by either a left-handedness or a right-handedness in its microstructure. As a result, in a chiral material left circularly polarized (LCP) and right circularly polarized (RCP) fields propagate with different phase velocities. Because the specific attribute of chirality is the geometry of the material microstructure. Therefore, it can be brought into the design and manufacture of artificially chiral materials or chiral composites which would exhibit similar effects like optical activity but at much lower frequencies, for example, microwave frequencies [1].

An incident LCP or RCP field will give both scattered LCP and RCP fields in a chiral composite medium due to its interaction with chiral microstructures. However, this phenomenon will not occur if microstructures are made of lossy dielectric materials. A dispersion equation can be obtained for either an LCP or an RCP incidence which is suitable for frequency dependent analysis.

Numerical results for absorption of a chiral layer using the current formalism are also presented and compared with measurements made in the microwave laboratory of the Center for the Engineering of Electronic and Acoustic Materials at Pennsylvania State University. Comparison of attenuations among different microwave absorbing composites shows the excellent performance from chiral composite materials.

CONSTITUTIVE AND WAVE EQUATIONS FOR A CHIRAL MEDIUM

Consider a region V occupied by an isotropic chiral medium in which the constitutive relations

$$\mathbf{D} = \epsilon_c \mathbf{E} + \beta_c \epsilon_c \nabla \times \mathbf{E}, \quad \mathbf{B} = \mu_c \mathbf{H} + \beta_c \mu_c \nabla \times \mathbf{H} \tag{1}$$

hold. The properties associated with subscript c represent those of the isotropic chiral medium. The em field can be transformed to [1]

$$\begin{bmatrix} \mathbf{E} \\ \mathbf{H} \end{bmatrix} = [A_c] \begin{bmatrix} Q_L \\ Q_R \end{bmatrix} \tag{2}$$

where the left- (LCP) and the right- (RCP) circularly polarized fields, Q_L and Q_R, respectively, must satisfy the conditions

$$(\nabla^2 + k_L^2)\, Q_L = 0; \qquad (\nabla^2 + k_R^2)\, Q_R = 0, \tag{3}$$

In the above equations, the matrix

$$[A_c] = \begin{bmatrix} 1 & a_R \\ a_L & 1 \end{bmatrix} \tag{4}$$

while,

$$k_L = k_c / (1 - k_c \beta_c); \qquad a_L = -i\,(\epsilon_c/\mu_c)^{1/2}$$

and

$$k_R = k_c / (1 + k_c \beta_c); \qquad a_R = -i\,(\epsilon_c/\mu_c)^{-1/2}.$$

MULTIPLE SCATTERING FORMULATION

It is well known that when a wave propagates through a medium containing dispersed particles, the entrained energy (intensity) is redistributed in various directions by scattering and absorbed by intrinsic absorption mechanisms. By appropriately controlling the host and inclusion properties, as well as the geometry and distribution of the inclusion phase, it is possible to increase the absorption of energy in a composite medium.

Because chirality of the inclusion phase can enhance the absorption of electromagnetic waves, a novel microwave adhesive may be made of a lossy dielectric material (host phase) containing randomly distributed microballoons made of a chiral material. The absorption of the electromagnetic energy of such a composite can be investigated by studying the propagation of an electromagnetic wave through such a chiral composite material.

We consider N($N \to \infty$) chiral scatterers randomly distributed in a nonchiral medium of volume V($V \to \infty$) so that the number of particles per unit volume $n_0 = N/V$ is finite. The incident field can be either an LCP or an RCP one. Here, We consider an incident LCP field, however, the formulation holds for an incident RCP field as well. For the scattering of waves by those scatterers located at $r_1, r_2, \ldots, r_N$, the total field and the exciting fields outside the scatterer can be expressed by

$$U(r) = Q^{o}_{L}(r) + \Sigma\, Q^{s}_{L}{}^{i}(r - r_i) + \Sigma\, Q^{s}_{R}{}^{i}(r - r_i). \tag{5}$$

$$Q^{e}_{L}{}^{j}(r) = Q^{o}_{L}(r) + \Sigma\, Q^{s}_{L}{}^{i}(r - r_i) \tag{6}$$

$$Q^{e}_{R}{}^{j}(r) = \Sigma\, Q^{s}_{R}{}^{i}(r - r_i) \tag{7}$$

where Q^{o}_{L} is the incident LCP field and $Q^{s}_{L}{}^{i}$ and $Q^{s}_{R}{}^{i}$ are, respectively, the scattered LCP and RCP fields from the i-th scatterer. The exciting LCP and RCP fields at the j-th scatterer are expressed as $Q^{e}_{L}{}^{j}$ and $Q^{e}_{R}{}^{j}$ respectively. All the fields in Eqs. (5) - (7) can be expanded using the basis functions as follows

$$Q^{o}_{L}(r) = \Sigma\, a_{\tau}{}^{i}\, \mathrm{Re}\, L_{\tau}(r - r_i) \tag{8}$$

$$Q^{e}_{L}{}^{i}(r) = \Sigma\, C_{\tau}{}^{i}\, \mathrm{Re}\, L_{\tau}(r - r_i) \tag{9}$$

$$Q^{s}_{L}{}^{i}(r) = \Sigma\, F_{\tau}{}^{i}\, \mathrm{Ou}\, L_{\tau}(r - r_i) \tag{10}$$

$$Q^{e}_{R}{}^{i}(r) = \Sigma\, D_{\tau}{}^{i}\, \mathrm{Re}\, R_{\tau}(r - r_i) \tag{11}$$

$$Q^{s}_{R}{}^{i}(r) = \Sigma\, G_{\tau}{}^{i}\, \mathrm{Ou}\, R_{\tau}(r - r_i) \tag{12}$$

In Eqs. (8) - (12), the vector circular functions L and R represent the left- and right- circularly polarized fields which can propagate in a chiral medium. The relationships between L and R and the commonly used vector basis functions M and N [2] are through $L = M + N$ and $R = M - N$. The qualifiers Re and Ou are associated with the regular (incident and exciting) and outgoing (scattered) fields. For a time harmonic incident plane field, all the fields have implicit time dependence $e^{-i\omega t}$. The expansion coefficients, except the incident field $a_{\tau}{}^{i}$, the exciting and scattered ones, i.e., C, F, D, and G are all unknown which need to be determined using the boundary conditions.

After substituting Eqs. (8) - (12) in Eqs. (6) and (7) and applying the translation-addition theorem as well as the orthogonality conditions for the vector basis functions, we have the following equations for the exciting LCP and RCP field coefficients C and D.

$$C_{\tau}{}^{i} = a_{\tau}i + \Sigma\,\Sigma\,\Sigma\, F_{\tau}{}^{j}\,[\alpha_q(r_{ij})] \tag{13}$$

$$D_\tau^i = \Sigma\Sigma\Sigma G_\tau^j [\beta_q(r_{ij})] \tag{14}$$

In the above equations, $[\alpha_q]$ and $[\beta_q]$ are the translation matrices whose details can be worked out in terms of the 3-j or 6-j symbols depending upon the orientation of the scatterers.

Equations (13) and (14) can be reexpressed in terms of only C_τ and D_τ if the T-matrix [3] is invoked. For a chiral scatterer, the scattered LCP and RCP field coefficients are related to the exciting LCP and RCP field coefficients through the following matrix equation:

$$\begin{bmatrix} F \\ G \end{bmatrix} = \begin{bmatrix} T^{LL} & T^{LR} \\ T^{RL} & T^{RR} \end{bmatrix} \begin{bmatrix} C \\ D \end{bmatrix} \tag{15}$$

where T^{LL}, T^{LR}, T^{RL}, and T^{RR} are the T-matrix elements of the chiral scatterer. The superscripts denote the mode conversion. For example, "LR" represents the scattered LCP field due to an exciting RCP field. The mode conversion will vanish for a spherical scatterer without chirality and also in this case T^{LL} is equal to T^{RR}. Eqs. (13) and (14) can thus be converted to the following

$$C_\tau^i = a_\tau i + \Sigma\Sigma\Sigma\Sigma (T^{LL} C_\tau^j + T^{LR} D_\tau^j) [\alpha_q(r_{ij})] \tag{16}$$

$$D_\tau^i = \Sigma\Sigma\Sigma\Sigma (T^{RL} C_\tau^j + T^{RR} D_\tau^j) [\beta_q(r_{ij})] \tag{17}$$

Because the chiral particles are randomly dispersed in a matrix medium, a configuration or ensemble average needs to be performed over all possible arrangements over the positions of the particles in order to obtain the average field which is meaningful in describing the random medium. Following our previous derivations in multiple scattering analysis [3,4,5,] when this operation is done on Eqs. (16) and (17), we have

$$\langle C_\tau^i \rangle_i = a_\tau i + n_0 \Sigma\Sigma\Sigma \int (T^{LL} \langle C_\tau^j \rangle_j + T^{LR} \langle D_\tau^j \rangle_j) G(r_{ij}) [\alpha_q(r_{ij})] dr_j \tag{18}$$

$$\langle D_\tau^i \rangle_i = n_0 \Sigma\Sigma\Sigma \int (T^{RL} \langle C_\tau^j \rangle_j + T^{RR} \langle D_\tau^j \rangle_j) G(r_{ij}) [\beta_q(r_{ij})] dr_j \tag{19}$$

where the angle bracket represents the configuration or ensemble average. The subscript associated with it is for the conditional configuration average, i.e. the position of a given particle is not random anymore but conditional. G( ) is the joint probability distribution function which gives the probability of joint occurrence of two particles separated by a position vector r_{ij}. Eqs. (18) and (19) actually restrict the physical properties of the particles so that all particles are the same except their orientations and positions which are random. Without repetition, details of these can all be found in our previous publications [3,4,5].

Equations (18) and (19) can be used to solve the effective propagation constant k_L for an incident LCP field as those work done in finding the complex effective wavenumber of an effective medium. Similarly, if an incident RCP field is considered, the same procedure can be used to find k_R. The subscripts L and R tell the nature of the effective propagation constant which is either

LCP or RCP. The reason is that if the composite medium becomes effectively chiral, the effective propagation constant should bear the same polarization of the incident field which in this paper is either LCP or RCP.

The effective wave number $\langle k \rangle = \langle k_1 \rangle + i \langle k_2 \rangle$ can be solved from the above equations as a function of the frequency via k, the size and properties of the scatterer via the T-matrix. The real part $\langle k_1 \rangle$ describes the phase velocity while the imaginary part $\langle k_2 \rangle$ gives the attenuation of the amplitude of the average wave in the effective medium. For a nonmagnetic composite material, the effective loss factor $\langle \varepsilon'' \rangle$ is related to the effective wavenumber K through the following

$$\langle \varepsilon'' \rangle = \mathrm{Im}[(\langle k \rangle / k)^2 \varepsilon] \qquad (20)$$

where ε is the relative permittivity of the matrix material. Im[ ] denotes the imaginary part of [ ].

Although Eqs. (18) and (19) are symbolically simple and clear, in practice, they are fairly complicated to solve. The degree of the numerical hardship increases with the increasing frequency. In one of our papers, some numerical results have been obtained when the composite medium is considered to be nonchiral [5]. Even for this case, the contribution of chirality towards the attenuation of the chiral composite medium is considerable. In addition, the dynamic response in attenuation shows quite a broad bandwidth.

RESULTS AND DISCUSSION

In the microwave laboratory at Penn State, we have made several chiral samples of dispersing different volume fractions of metal helices in an epoxy resin (eccogel 1365-90 from Emerson and Cuming, Inc., Canton, MA). A free space microwave testing facility has been used to measure the reflection and transmission coefficients of these samples. Details on the measurement setup, calibration, as well as on the data conversion can be found in [6,7]. The experimental procedure employed to obtain the data reported here is well described in an article in this issue by Ro et al. [6]. Comparison of the calculated results with those measured are presented in Table 1.

Table 1. Attenuations Calculated and from the Transmission Measurements.

Type of Chiral Sample - Right-handed and left-handed metal springs of 0.8% volume fraction in eccogel
Sample Thickness = 1.17 cm

Frequency (GHz)	Loss in dB (Computed) Right (Left)	Loss in dB(Measured) Right (Left)	$\langle k_2 \rangle$ (in m^{-1}) (Computed) Right (Left)
13	- 3.71 (- 3.63)	- 3.41 (- 3.27)	36.6 (35.9)
14	- 3.60 (- 3.42)	- 3.14 (- 2.93)	35.5 (33.8)
15	- 3.30 (- 3.24)	- 2.91 (- 2.77)	32.5 (32.0)
16	- 3.14 (- 3.31)	- 2.90 (- 2.97)	31.0 (32.8)
17	- 3.09 (- 3.72)	- 3.13 (- 3.48)	30.4 (36.8)
18	- 3.07 (- 3.75)	- 3.41 (- 3.69)	30.2 (37.1)

Three microwave composite materials are compared based on their absorbing capabilities. Because the imaginary part $\langle k_2 \rangle$ of the effective wavenumber $\langle k \rangle$ is proportional to the attenuation of such composites, calculated results for those materials are presented for $\langle k_2 \rangle$ only. The conversion of $\langle k_2 \rangle$ to the physical dB scale is quite straightforward if the thickness of the material is given. Table 2 presents computed $\langle k_2 \rangle$ for, ferrite powders, lossy dielectric powders, and metal helices, all in eccogel with three different volume fractions. Although the frequency is 13 GHz, because the sizes of the dispersions are all considered to be much smaller than the wavelength, the results are for the response in the Rayleigh region. Because of low mass loading of the composites, the reflection loss for the current situation is minimized which is also verified by the experiments done on the composites with metal helices. The scattering loss has been counted for and it is much smaller than the absorption loss in the Rayleigh region for this case. From the magnitudes of $\langle k_2 \rangle$, one can tell that the chiral composite material has the superior absorbing ability compared to the other two commonly used microwave absorbing composite materials in which the particles are assumed to be spherical in shape.

Table 2. Comparison of Calculated Attenuations among Different Microwave Composites.

Matrix material : eccogel ($\varepsilon = 2.72 + 0.067\,i$; $\mu = 1 + 0\,i$)
Frequency : 13 GHz

Type of Dispersions	Ferrite Powders	Lossy Dielectric Powders	Metal Helices
Volume Fraction	$\langle k_2 \rangle$ (in m^{-1})	$\langle k_2 \rangle$ (in m^{-1})	$\langle k_2 \rangle$ (in m^{-1})
0.8%	5.52	5.88	36.6
1.6%	5.52	6.23	75.6
3.2%	5.50	6.93	172

In addition, we consider a composite material having three different property combinations and show the enhanced absorption due to the chiral microstructure. In all the cases, the volume fraction of the microstructure is taken to be 0.05. From Table 3, it is obvious that chirality in addition to the lossy dielectric property gives the largest absorption which could be as high as three thousand times that of lossy dielectric spheres at 1.5 GHz. This fact indicates that for given microwave composites embedded with chiral microballoons the frequency can be tuned in order to achieve a maximum absorption like the principle used in the design of microwave oven. We clearly elucidated the effect of enhanced absorption loss using a step by step approach. First, lossy dielectric spheres introduce the absorption loss. Next, the lossy chiral spheres increased dramatically the absorption loss compared to that of lossy nonchiral spheres beyond 1 GHz. The last case considers lossy chiral microballoons in a lossy matrix whose intrinsic loss factor is 0.2 and such a chiral composite turns out to provide a much larger absorption. The excess absorption is mainly from the enhanced absorption due to chirality.

In Table 3 the effective loss factor $\langle \varepsilon'' \rangle$ is obtained using Eq. (20) in which $\langle k_2 \rangle$ is implicit in the expression of $\mathrm{Im}[\langle k \rangle / k]$. The effective wavenumber $\langle k \rangle$ is calculated through a multiple scattering computer code developed at our research center using the dispersion relation (5].

Table 3. Effective Loss Factors $< \varepsilon'' >$ in Different Composites with Lossy Microballoons with/without Chirality. (The Relative Permittivity of the Matrix Material is $2.5 + \varepsilon_m''$ i and That of the Microballoon is $20 + \varepsilon_s''$ i. The Radius b of the Microballoon is 9.5 mm)

Frequency (GHz)	Case 1. $\varepsilon_m'' = 0$, $\varepsilon_s'' = 0.2$, $\beta = 0$ $< \varepsilon'' >$	Case 2. $\varepsilon_m'' = 0$, $\varepsilon_s'' = 0.2$, $\beta = 1.0 \times 10^{-4}$ m $< \varepsilon'' >$	Case 3. $\varepsilon_m'' = 0.1$, $\varepsilon_s'' = 0.2$, $\beta = 1.0 \times 10^{-4}$ m $< \varepsilon'' >$
0.5	0.1372×10^{-2}	0.1419×10^{-2}	0.1090
1.0	0.4207×10^{-2}	0.5619×10^{-2}	0.1157
1.5	0.1280×10^{-1}	0.9269	1.006
2.0	0.3290×10^{-1}	0.2712	0.3677
2.5	0.7606×10^{-1}	0.2126	0.3111

CONCLUSIONS

From the results presented, chiral composite material proves to be one of the best candidates for microwave absorbers. In addition, when a chiral absorber is considered, a tunable frequency (or a desired operating frequency) is available by tailoring the size of its microstructure.

REFERENCES

1. A. Lakhtakia, V.K. Varadan, and V.V. Varadan, *Time-Harmonic Electromagnetic Fields in Chiral Media*, Lecture Notes in Physics 335, Springer-Verlag, New York (1989).
2. P.M. Morse and H. Feshbach, *Methods of Theoretical Physics*, Vol. 2, McGraw-Hill, New York, 1953.
3. V.K. Varadan and V.V. Varadan, eds., *Acoustic, Electromagnetic and Elastic Wave Scattering-Focus on the T-matrix Approach*, Pergamon Press, New York, 1980.
4. V.K. Varadan, Y. Ma, and V.V. Varadan, "Coherent electromagnetic wave propagation through randomly distributed and oriented pair-correlated dielectric scatterers," *Radio Science* 19, 1445, 1984.
5. V.V. Varadan, Y. Ma, and V.K. Varadan, "Effects of chiral microstructures on em wave propagation in a lossy dielectric composite material," *Radio Science* 24, 785, 1989.
6. R. Ro, V.V. Varadan, and V.K. Varadan, "Parametric experimental study on chiral composites," this issue, 1991.
7. D.K. Ghodgaonkar, V.V. Varadan, and V.K. Varadan, "A free-space method for measurement of dielectric constants and loss tangents at microwave frequencies," IEEE Trans. Instrum. Meas. IM-38, 789, 1989.

PARAMETRIC EXPERIMENTAL STUDY OF MICROWAVE ABSORPTION IN CHIRAL COMPOSITES

Ruyen Ro, Vasundara V. Varadan and Vijay K. Varadan
Center for the Engineering of Electronic and Acoustic Materials &
Department of Engineering Science and Mechanics
The Pennsylvania State University
University Park, PA 16802

ABSTRACT

Theoretical and experimental studies have shown that chiral composites constructed by embedding chiral inclusions in an otherwise achiral lossy medium enhance power absorption in the microwave frequency range. Chiral composites can hence be used as microwave absorbers to achieve rapid heating during microwave processing of ceramics, glass, and composites. Power absorption bands of chiral composites are discussed and the corresponding ratio of the one turn length of the chiral inclusion to the wavelength in the medium L/λ_c are reported. This ratio can be used to optimize absorption at different operating frequencies. Experimental studies on chiral composites having different sizes of chiral inclusions are also included.

INTRODUCTION

In recent years, the exploitation of microwave energy in thermal processing of materials has caused great interest [1]. The prevalent applications of microwave power have been seen in the dehydration of various materials and in the processing of ceramics, glass and composites [2, 3, 4]. The major advantages of the microwave heating are: 1) high heating rates can be obtained because of microwave absorption inside the material 2) energy can be applied or removed instantly and 3) the heating is volumetric rather than surface heating. The fundamental principle of applying microwave powers in materials processing is due to loss mechanisms (dielectric and magnetic) in the material during the interaction of electromagnetic waves. Since many ceramics are difficult to heat using microwave power due to their low dielectric loss tangent at room temperature, the microwave processing of ceramics is limited to those which have a high dielectric loss tangent. However, with the help of a sealing agent or interlayer which exhibits microwave absorption properties, microwave sealing or joining of ceramics is possible. For example,

coupling agents such as SiC and Si_3N_4 whiskers have been used to couple electromagnetic waves for microwave sintering of the matrix materials Al_2O_3-SiC and ZrO_2-Si_3N_4, which are transparent to microwave energy [5]. Recently, the research group at Penn State has discovered theoretically and experimentally that chiral composites can enhance microwave absorption [6, 7, 8, 9]. Due to recent progress in the construction of artificial composites and synthesis of polymers, it is feasible to design artificial chiral composite materials consisting of specified materials. Lately, we have developed a method for determining the electromagnetic properties of chiral composite materials in the frequency range 8-40 GHz [10]. It is also important to investigate the power absorption bands of chiral composites not only for confirming the "Cotton effect" phenomenon [11] but also for designing chiral composites as microwave absorbers. From electromagnetic properties of chiral composites, the ratio of the one turn length of the chiral inclusion to the wavelength in the chiral medium which maximizes power absorption can be calculated and will be examined in this study.

Optical activity and chirality have been observed for almost two centuries. The twin phenomena, optical rotation dispersion (ORD) and circular dichroism (CD), are the special features of optically active media. They can be explained by directly substituting new constitutive relations, e.g., $\mathbf{D} = \varepsilon\mathbf{E} + \beta\varepsilon\,\nabla \times \mathbf{E}$ and $\mathbf{B} = \mu\mathbf{H} + \beta\mu\,\nabla \times \mathbf{H}$, into Maxwell's equations [8, 12]. Here, ε and μ are the complex permittivity and permeability, respectively, while β is the complex chirality parameter which results from any chirality (handedness) in the microstructure of the medium. For a normally incident, linearly polarized wave, the transmitted wave traveling through the chiral medium is not only rotated but becomes elliptically polarized due to the existence of the chirality parameter [8, 10]. This results from the different phase velocities and different absorption for the left- and right-circularly polarized waves. The reflected wave, however, is linearly polarized for a normally incident, linearly polarized wave. Hence, one reflection and two transmission measurements are needed to fully characterize the chiral composite [10].

The planar chiral composites characterized in this study were constructed by embedding chiral inclusions (helices) into an otherwise achiral host medium (Eccogel). Samples made in this research have the dimensions 15 cm × 15 cm × 1.2 cm. For detailed information on how the samples are made, refer to Guire *et al.* [9]. A free-space measurement setup was employed to measured the reflection and transmission characteristics of the chiral composites. The calibration technique and time domain gating for enhancing measurement accuracy, as well as the measurement procedure for the free-space measurement system are referred to Ghodgaonkar *et al.* [13].

ABSORPTION BANDS OF CHIRAL COMPOSITES

The time-averaged Poynting vector denoted by <P> represents the amount of power crossing a unit area in the direction perpendicular to both **E** and **H** fields and is defined by

$$\langle \mathbf{P} \rangle = \frac{1}{2}\mathrm{Re}\,(\mathbf{E} \times \mathbf{H}^*) \qquad (1)$$

where Re means the 'real part of' and the asterisk denotes the complex conjugate. The electromagnetic fields (E and H) in free-space can be expressed in terms of LCP (left-circularly polarized) and RCP (right-circularly polarized) waves Q_L and Q_R as

$$\mathbf{E} = Q_L + Q_R \tag{2a}$$

$$\mathbf{H} = \frac{i}{\eta_0}(-Q_L + Q_R) \tag{2b}$$

Substituting Eqs. (2a) and (2b) into Eq. (1), one can obtain

$$\langle \mathbf{P} \rangle = \frac{1}{2}\mathrm{Re}\left\{\frac{1}{\eta_0}(Q_L \times Q_L^* - Q_R \times Q_R^*)\right\} \tag{3a}$$

and

$$P = |\langle \mathbf{P} \rangle| = \frac{C^2}{4\eta_0}\{S_L S_L^* + S_R S_R^*\} \tag{3b}$$

where C is the magnitude of the incident field E_{inc} and η_0 is the free-space impedance. S_L and S_R are either the reflection or transmission coefficients for the LCP and RCP waves, respectively. The reflection and transmission characteristics for the normally incident, circularly polarized waves can be obtained from the measured reflection and transmission characteristics for a normally incident, linearly polarized wave as

$$S_{11L} = S_{11R} = S_{11co} \tag{4a}$$

$$S_{21L} = S_{21co} - iS_{21cross} \tag{4b}$$

$$S_{21R} = S_{21co} + iS_{21cross} \tag{4c}$$

and

$$S_{21cross} = \frac{S_{21\alpha} - S_{21co}\cos\alpha}{\sin\alpha} \tag{4d}$$

where S_{11co} is the measured reflection coefficient and S_{21co} and $S_{21\alpha}$ are the measured transmission coefficients at co-polarization position and angle α from co-polarization position, respectively [10].

The power reflection ratio $R = P_{ref}/P_{inc}$ and power transmission ratio $T = P_{tra}/P_{inc}$ then can be calculated by

$$R = \frac{P_{ref}}{P_{inc}} = \frac{1}{2}\{S_{11L}S_{11L}^* + S_{11R}S_{11R}^*\} = S_{11co}S_{11co}^* \tag{5a}$$

and

$$T = \frac{P_{ref}}{P_{inc}} = \frac{1}{2}\{S_{21L}S_{21L}^{*} + S_{21R}S_{21R}^{*}\} = S_{21co}S_{21co}^{*} + S_{21cross}S_{21cross}^{*} \quad (5b)$$

Computations of the power absorption coefficient of the chiral composite

$$A = \frac{P_{inc} - P_{ref} - P_{tra}}{P_{inc}} = 1 - R - T \quad (6)$$

can therefore be made.

The chiral inclusions used for determination of the properties have the dimensions diameter D = 0.11684 cm, pitch P = 0.0529 cm and one turn length L = 0.371 cm. From the reflection and transmission measurements S_{11co}, S_{21co}, and $S_{21\alpha}$, the electromagnetic properties of chiral composites ϵ, μ, and β can be calculated [10]. The wavenumbers for the LCP and RCP waves, k_L and k_R, as well as the wavelengths for the LCP and RCP waves, λ_L and λ_R, can then be obtained from these properties [8,10]. The ratios of the one turn length of the chiral inclusion to the wavelengths in the chiral medium, L/λ_L and L/λ_R, at each frequency for each sample then can be calculated. Table 1 shows peak values of power absorption coefficients, A, and the corresponding frequencies as well the corresponding ratios, L/λ_L and L/λ_R, for the chiral composites.

Table 1. Peak values of power absorption coefficients, A, and the corresponding frequencies as well as the corresponding ratios, L/λ_L and L/λ_R, of power absorption coefficients for the chiral composites.

Sample	Peak value	Frequency (GHz)	L/λ_L	L/λ_R
0.8% left	0.7626	28.86	0.596	0.610
0.8% right	0.7135	28.19	0.5933	0.578
0.8% racemic	0.7853	28.19	0.589	0.589
1.6% left	0.8516	26.84	0.556	0.588
1.6% right	0.9263	26.50	0.565	0.562
1.6% racemic	0.8491	27.51	0.585	0.585
3.2% left	0.9281	28.19	0.609	0.672
3.2% right	0.9881	31.23	0.742	0.693
3.2% racemic	0.9657	30.55	0.693	0.693

It can be seen in Table 1 that the peak frequencies for the same volume concentration samples are very close. For the 0.8% samples, the averaged peak frequency is 28.41 ± 0.446 GHz. While for the 1.6% and 3.2% samples, the averaged peak frequencies are 26.95 ± 0.56 GHz and 29.99 ± 1.24 GHz, respectively. The peak values of the power absorption coefficients are also very close for the same volume concentration samples, but vary as the volume concentrations change. The values are 0.7538 ± 0.0403, 0.876 ± 0.0503, and 0.9606 ± 0.0325 for the 0.8%, 1.6%, and 3.2% samples, respectively.

It also can be seen that the ratios L/λ_L and L/λ_R are different for handed (left- or right-) samples but are the same for the racemic samples. This is because LCP waves travel faster than RCP waves inside the left-handed medium, and *vice versa*, while both LCP and RCP propagate with the same speed inside the racemic samples [8]. Since the difference between L/λ_L and L/λ_R is less than 5% for every sample, one can use the average value of L/λ_L and L/λ_R as the ratio L/λ_c with an error of less than 3%. The ratio L/λ_c varies as the volume concentration changes. The values are 0.5926 ± 0.01, 0.5735 ± 0.0115, and 0.6837 ± 0.04 for the 0.8%, 1.6%, and 3.2% samples, respectively.

Table 2. 95% and 90% power absorption bandwidths.

Sample	95% peak value bandwidth (GHz)	90% peak value bandwidth (GHz)	Frequency (GHz)
0.8% left	26.50 ~ 31.56 5.06	25.23 ~ 32.58 7.35	28.86
0.8% right	25.01 ~ 30.55 5.54	24.59 ~ 31.56 6.97	28.19
0.8% racemic	25.65 ~ 29.54 3.89	23.31 ~ 30.55 7.24	28.19
1.6% left	22.46 ~ 31.23 8.77	21.82 ~ 32.24 10.42	26.84
1.6% right	25.01 ~ 29.88 4.87	22.04 ~ 32.24 10.20	26.50
1.6% racemic	25.23 ~ 31.23 6.0	22.25 ~ 32.58 10.33	27.51
3.2% left	26.29 ~ 32.91 6.62	25.01 ~ 35.61 10.60	28.19
3.2% right	26.29 ~ 37.30 11.01	25.23 ~	31.23
3.2% racemic	26.50 ~ 36.96 10.46	25.23 ~	30.55

Based upon the data shown in Table 1, the average value and standard deviation of the ratio L/λ_c are 0.6038 and 0.051, while for the peak frequency they are 28.45 and 1.4828 GHz. The variances of the peak frequency and the ratio L/λ_c among the same volume concentration chiral samples may be due to sample variations and post-calibration errors. Thus $L/\lambda_c = 0.6038$ can be used as a design criterion to obtain an absorption peak at a desired operating frequency.

It is also interesting to study the bandwidths of the power absorption coefficients. Table 2 shows the 95% and 90% peak values power absorption bandwidths for the chiral samples. The average bandwidths of 95% and 90% power absorption coefficients are 6.92 and 10.29 GHz, respectively. The smallest bandwidths for the 95% and 90% power absorption are 3.89 and 6.97 GHz, respectively. The corresponding changes for the ratios L/λ_c are 0.08 and 0.143, respectively. From this data, one can clearly see that the average values of the peak frequency 28.45 GHz and the ratio L/λ_c 0.6038 are within the 95% power absorption bandwidths region for each chiral sample. Hence, for this special kind of helix embedded into an epoxy host medium (Eccogel), it is appropriate to use the average values of the peak frequencies and the ratio L/λ_c of these nine chiral composites to represent the characteristic peak frequency 28.45 GHz and the ratio ratio L/λ_c 0.6038.

PARAMETRIC EFFECTS OF CHIRAL COMPOSITES

In addition to the one kind of helix as discussed above, three different geometrical dimensions of helices have been selected to examine the parametric effects of chiral inclusions. Four additional 3.2% left-handed samples have been made. One of them contains all four different geometrical sizes of chiral inclusions, which have been mixed well. The other three samples have only one kind of helix. Detailed description of the samples and the dimensions of helices are shown in Table 3.

The reflection and transmission characteristics for these samples may be measured in the frequency range 8-40 GHz by employing the free-space measurement system. The transmission coefficients of some samples, especially for samples C, D, and E, are less than – 40 dB at certain frequencies. This is very close to the dynamic range of the free-space measurement system, hence, it is improper to use these values to determine the properties of samples.

However, the power absorption of samples can also be seen from the reflection coefficients with metal backing. Fig. 1 shows the measured reflection coefficients with metal backing for each sample. It can be seen that the reflection coefficient for sample D has the largest value over the whole frequency range, probably due to the big impedance mismatch caused by variations of sample preparations. The reflection coefficient of sample E has not only the smallest value in the frequency range of 12-37 GHz but also the widest power absorption bandwidth. Since each kind of helix may have its power absorption peak frequency and bandwidth separately, e.g., 28.45 GHz peak frequency and 6.92 GHz 95% power absorption bandwidth for sample A, then combinations of different kinds of helices may cause the power absorption bandwidth to increase. The increase in the power absorption for sample E may be due to the impedance match for the free-space or the interaction between each different kind of helix. However, no conclusion should

be made until more is known about the effects of the dimensions of the helix and the host material.

Table 3. Description of the samples and the dimensions of helices.

Name	Dimensions of the helix (cm)			
	Diameter D	Pitch P	One turn length L	No. of turns
Sample A	0.11684	0.0529	0.371	3
Sample B	0.11684	0.0794	0.3755	3
Sample C	0.18288	0.0529	0.577	3
Sample D	0.11176	0.254	0.433	3
Sample E	Mixed			

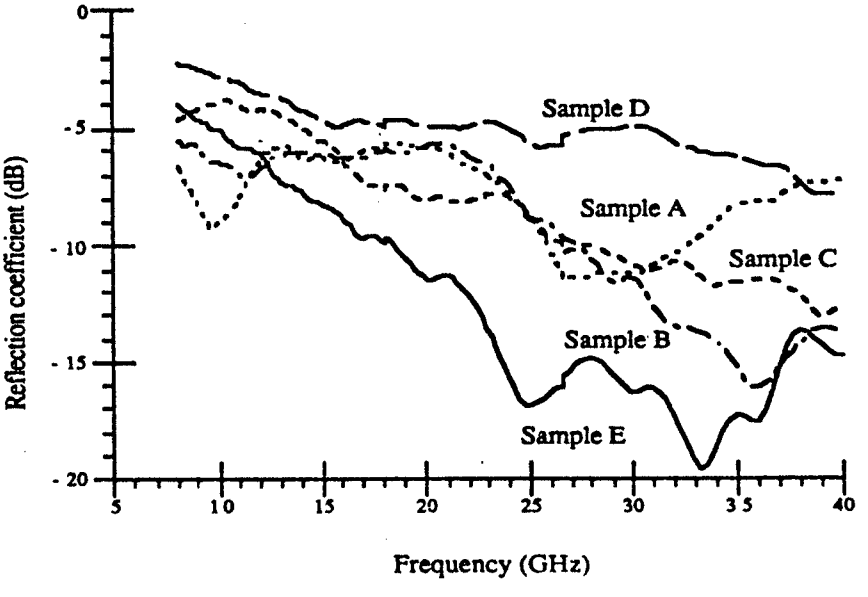


Fig. 1. The reflection coefficient with metal backing for each sample.

CONCLUSION

The power absorption bandwidths and the corresponding ratios L/λ_c of the one turn length of the chiral inclusion to the wavelength in chiral media have been examined. We have discovered that it is appropriate to use the averaged power absorption peak frequency and the corresponding ratio L/λ_c of different handed and different volume concentrations chiral samples to represent the characteristic peak frequency and the corresponding ratio L/λ_c of each chiral sample. Also, both the power absorption peak value and its bandwidth increase for the mixed sample compared with the samples which consist of only one kind of chiral inclusion. Thus the bandwidth of the absorption peak can be increased by considering inclusions with appropriate L/λ_c values at the frequencies in the band of interest. Such absorbers can then be used as the interlayer or heating catalyst in the joining and processing respectively of ceramics.

REFERENCES

[1]. W. H. Sutton, M.H. Brooks, and I.J. Chabinsky (Eds.), *Microwave processing of materials*, Materials Research Society Symposium Proceedings, Vol. 124, Pittsburgh, Material Research Society, 1988.

[2]. W.R. Tinga and W.A.G. Voss, *Microwave power engineering*, Academic Press, New York, 1968.

[3]. M.P. Borom and M. Lee, *Adv. Cerem. Mater.* **1**, 335, 1986.

[4]. T.T. Meek, *J. Mater. Sci.* **6**, 638, 1984.

[5]. Blake, R.D. and Meek, T.T., *Chapman and Hall Ltd.*, 1097-1098, 1986.

[6]. A. Lakhtakia, V.V. Varadan, and V.K. Varadan, *IEEE Trans. EMC.*, Vol. **28**, No. 2, 90-95, 1986.

[7]. V.K. Varadan, V.V. Varadan, and A. Lakhtakia, *J. Wave-Material Interaction*, Vol. **2**, No. 1, 71-81, 1987.

[8]. A. Lakhtakia, V.K. Varadan, and V.V. Varadan, *Time-harmonic electromagnetic fields in chiral media*, Springer-Verlag, Vol. 335, New York, 1989.

[9]. T. Guire, V.V. Varadan, and V.K. Varadan, *IEEE Trans. EMC.*, Vol. **32**, 300-304, 1990.

[10]. V.V. Varadan, V.K., Varadan, R. Ro, and M. Umari, presented at the 1990 URSI Radio Science Meeting, Paper No. 36-1, Dallas, Texas, MAy 7-11, 1990.

[11]. P. Crabbe and S.A. Syntex, *Optical rotatory dispersion and circular dichroism in organic chemistry*, Holden-day, San Francisco, 1965.

[12]. C.F. Bohren, *Chemical Physics Letters*, Vol. **29**, 458-462, 1974.

[13]. D.K. Ghodgaonkar, V.V. Varadan, and V.K. Varadan, *IEEE Trans. IM.*, Vol. **39**, 387-394, 1990.

MICROWAVE HEATING FOR FIBER-PLACEMENT MANUFACTURING OF CARBON-FIBER COMPOSITES

Arthur C. Lind
McDonnell Douglas Research Laboratories
St. Louis, MO 63166

Frederick C. Wear, James E. Kurz
McDonnell Aircraft Company
St. Louis, MO 63166

The electrical impedance of cross-ply carbon-fiber composites at 2.45 GHz is about 0.6 Ω. Since the impedance of free space is 377 Ω, 99.3% of the microwave energy incident on the composite is reflected and little heating occurs. Our applicator, which overcomes this problem, rapidly and efficiently heats thermoplastic-impregnated carbon fibers to fabricate well-consolidated composite structures. This applicator is suited to an automated fiber-placement manufacturing process in which composite structures are built up one layer at a time.

INTRODUCTION

Usually, carbon-fiber/polymeric composite parts have been assembled manually and cured using autoclave techniques. To reduce labor costs and to enable the manufacture of composite parts larger than available autoclaves, an automated fiber-placement process is being developed. In this process composite parts are fabricated one layer at a time from polymer-impregnated carbon fibers in tapes of various widths. As the fibers come into contact with the part, heat and pressure are applied to consolidate the fibers with the part, as shown in Fig. 1.

To achieve low cost the fiber-placement process must be rapid, requiring rapid heating of the polymer-impregnated fibers and the surface to which it will be consolidated. Microwaves have been investigated for rapid heating and curing of polymeric composite materials in numerous studies over the past decade.[1-4] Successful results were obtained if the reinforcing fibers were not electrically conducting, such as glass and Kevlar. However, if the fibers were electrically conducting, such as carbon, it was difficult to couple microwave power into the composite efficiently and reliably.[2,4] In addition, previous microwave ovens and cavities were not suitable for fiber-placement processing of large parts because they needed to surround the carbon-fiber composite part. Therefore, we have invented[5] and are patenting a novel microwave applicator for heating carbon-fiber composites external to the applicator. Microwave

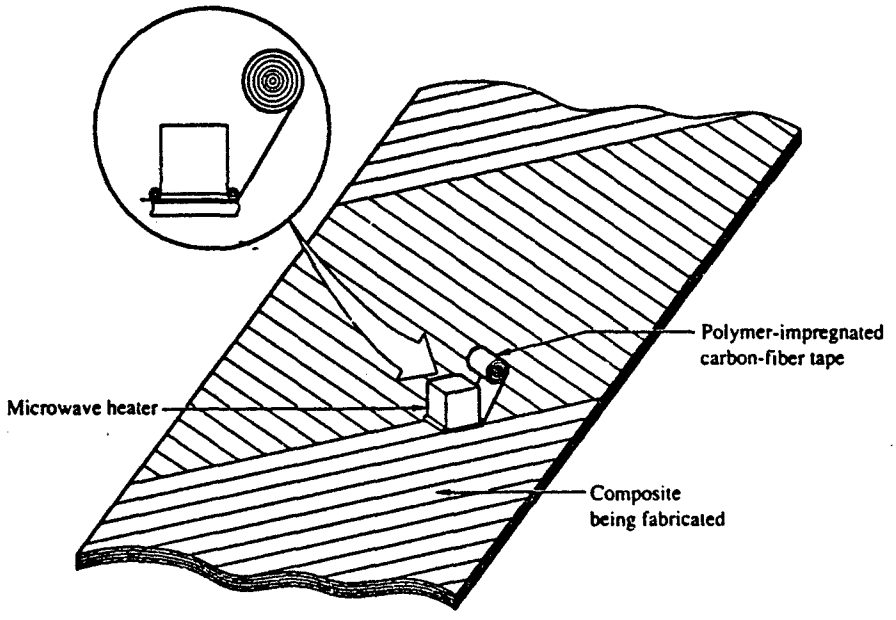


Figure 1. Schematic of fiber-placement process in which large composite parts are fabricated one layer at a time. Microwaves are shown here as a heating source.

heating is confined to a distance of the order of the thickness of one ply at the surface of the carbon-fiber composite. This is ideal for the tape-placement process because the consolidation region can be adequately heated without unnecessarily heating the composite previously consolidated.

INTERACTION OF MICROWAVES WITH CARBON-FIBER COMPOSITES

The electrical conductivity along the length of continuous carbon fibers is large, but the electrical conductivity perpendicular to their length is smaller because of the many poor electrical contacts between adjacent fibers. Thus, the electrical conductivity of a carbon-fiber composite depends upon its construction and the direction in which the conductivity is measured.

Measurements of the effective electrical conductivities have been made at frequencies between 45 and 300 MHz for well-consolidated carbon-fiber composites in which the fiber orientation alternates between 0° and 90° in adjacent plies.[6] The effective electrical conductivity in a direction parallel to the plies, $\sigma_{\parallel}$, is about 25,000 S/m. A simple approximation[6] can be used to calculate $\sigma_{\parallel}$ from the conductivity of the fibers and their orientation in the composite. The effective electrical conductivity perpendicular to the plies, $\sigma_{\perp}$ is about 100 S/m.[6] A simple approximation cannot be used to calculate $\sigma_{\perp}$ because it is very dependent upon the degree of consolidation. Before consolidation $\sigma_{\perp}$ can be as small as 3 S/m.[7]

An effective electrical conductivity is used in inhomogeneous materials which requires that the amplitude and phase of the electromagnetic fields do not change significantly within the scale of the inhomogeneity. In the case of carbon-fiber composites the scale of the inhomogeneity depends upon the polarization and the direction of propagation of the microwaves. For propagation normal to the plies, the scale of the inhomogeneity is equal to the repeat distance of the ply orientation stacking sequence. Since the thickness of a single ply is about equal to 0.13 mm, the scale of inhomogeneity is about 0.26 mm in a composite having a repeating 0°, 90° stacking sequence. As will be seen, this approximation is not always rigorous at 2450 MHz, a common microwave heating frequency, but it is useful for estimates.

When microwaves are incident normal to the surface of a multi-layer carbon-fiber composite, the electric field is parallel to the plies and the electric field interacts with a material whose conductivity is σ_l. When the microwaves are incident normal to an exposed edge of a multi-layer carbon-fiber composite, the electric field can be chosen to be parallel, perpendicular or intermediate to the plies. Thus, depending upon the relative orientation, the electric field interacts with a material whose conductivity lies between $\sigma_\perp$ and σ_l.

The fraction of the power that is absorbed when microwaves are incident upon the surface of a conductor is given by[8]

$$P/P_0 = 1 - [(Z - Z_0)/(Z + Z_0)]^2, \tag{1}$$

where P is the absorbed power density (w/m^2), P_0 is the incident power density, Z_0 is the impedance of free space (377 Ω) and Z is the impedance of the conductor. The impedance Z of the conductor is given by[8]

$$Z = (\pi f \mu/\sigma)^{1/2}, \tag{2}$$

where f is the microwave frequency (Hz) and μ is the permeability of the composite, usually equal to that of free space, $\mu_0 = 4\pi \times 10^{-7}$ H/m.

The microwaves that are absorbed at the surface propagate into a good electrical conductor normal to the surface and the power density decays exponentially with increasing distance, d, as[8]

$$P(d) = [H_s \exp(-d/\delta)]^2 Z, \tag{3}$$

where H_s is the magnetic intensity (A/m) at the surface (d=0) and δ is the skin depth. The skin depth, δ, is given by[8]

$$\delta = (1/\pi f \mu \sigma)^{1/2}. \tag{4}$$

Table 1 presents numerical values of the quantities given in Equations (1)-(4) for 2450 MHz microwaves entering the face and edge of a carbon-fiber composite having a 0°, 90° stacking sequence. The wide range of composite properties shown in Table 1, depending upon the microwave propagation direction and the degree of consolidation, explains why previous investigators experienced different and unreliable

Table 1. Properties of 0°,90° Carbon-Fiber Composite at 2450 MHz.

Direction of Incident Microwaves	Impedance Z (Ω)	Fractional Absorbed Power P/P_0	Skin Depth δ (mm)	Surface Current, H_s, for Absorbed Power Density of 1000 w/cm^2 (A/cm)
Into Edge[7] $\sigma=\sigma_\perp=3$ S/m, before consolidation	56.8	0.455	5.87	4.20
Into Edge[6] $\sigma=\sigma_\perp=100$ S/m	9.84	0.099	1.02	10.1
Into Face[6] $\sigma=\sigma_\parallel=25000$ S/m	0.62	0.007	0.06	40.1

results. Before consolidation, for propagation into the edges of the a composite, heating occurs to a depth of about 6 mm. However, as the composite becomes consolidated, the microwave heating occurs only to depth of about 1 mm.

For microwaves entering the composite through the face of the plies, as shown in Fig. 1, the skin depth is only 0.064 mm. This skin depth is less than the 0.26 mm repeat distance of the ply stacking sequence, so our analysis, which uses an effective electrical conductivity, is not strictly valid. These results, nevertheless, indicate that the microwave heating is confined to a distance of the order of the thickness of one ply at the surface of the composite. This is ideal for the tape-placement process because the consolidation region can be adequately heated without unnecessarily heating the composite previously consolidated.

Table 1 shows that when microwaves are incident into the face of the composite, as shown in Fig. 1, the fractional absorbed power is only 0.007; hence, 99.3% is reflected. Our microwave applicator repeatedly redirects this reflected power back to the composite surface to increase the absorbed power.

Heating power densities up to 1000 w/cm^2 may be needed for fiber-placement speeds of 50 cm/s. Such large power densities produce surface currents of 40 A/cm, which would normally require good electrical contact between the microwave heater and the surface of the composite to prevent arcing. Our microwave applicator suppresses this possibility for arcing.

OPEN-ENDED TE_{011} MODE MICROWAVE CAVITY

Our microwave applicator is an open-ended resonant cavity based on the TE_{01} circular waveguide mode. In this mode the electric field is maximum along a circular path whose diameter is about one-half the diameter of the circular waveguide. Hence,

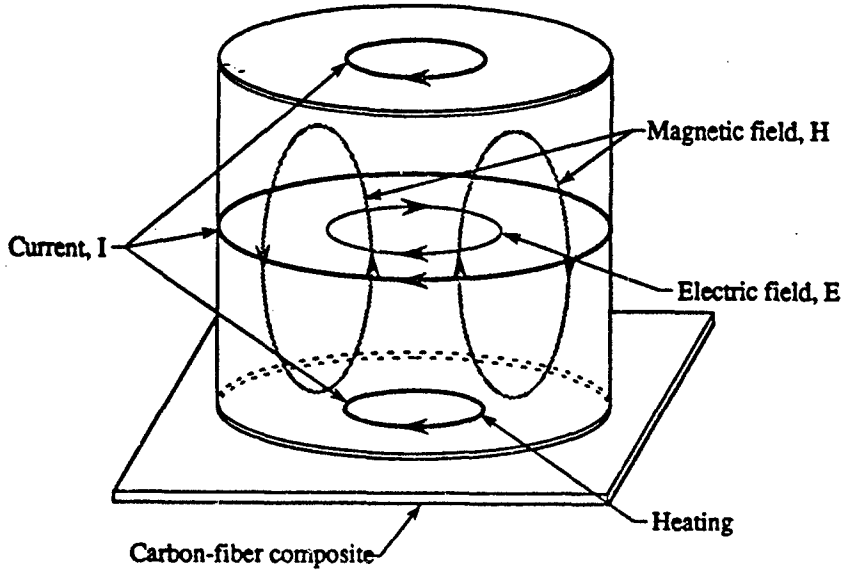


Figure 2. Schematic of open-ended circular TE_{011} mode cavity. The carbon-fiber composite serves as a cavity end wall which is heated by the surface currents.

a TE_{011} mode cavity with an open end placed against a carbon-fiber composite material induces large surface currents which flow in circles confined to the composite, as shown in Fig. 2. Because the currents need not flow between the cavity and the composite, the heating is not limited by the normally high contact resistance between the cavity and the composite. Thus, the problem of poor electrical contact and arcing between the microwave heater and the surface of the composite is eliminated.

The design criteria and the electric and magnetic fields of the TE_{011} mode cavity are well known.[9] The length, ℓ, of the cavity at resonance satisfies the following equation.

$$\ell = \lambda/2\,[\varepsilon - (3.8317\,\lambda/2\pi a)^2]^{-1/2}, \tag{5}$$

where ε is the dielectric constant of the interior of the cavity (ε=1 for air), λ is the free-space wavelength of the microwaves, and a is the inside radius of the cavity.

The magnetic fields at the circular end walls are parallel to the end walls and radially directed. For a cylinder of radius a, the radially directed magnetic field on the

surface of an end wall at a distance r from its center is proportional to the derivative of the zeroth order Bessel function. These magnetic fields induced surface currents which flow in concentric circles, producing a radial power density profile given by

$$P(r) = P_t\,[J_0'(3.8317r/a)/J_0(3.8317)]^2/\pi a^2$$

$$= 1.96\,P_t\,[J_1(3.8317r/a)]^2/a^2, \qquad (6)$$

where P_t is the total power delivered to the surface by the cavity. Fig. 3 shows a contour plot of the radial power density on the surface of a composite produced by a stationary cavity. No heating occurs in the center or perimeter of the cavity; heating is primarily in an annular region. In the fiber-placement process the cavity moves relative to the composite and the path along which the cavity moves is heated. The time-average heating contour on the path of the cavity as it moves relative to the composite is also shown in Fig. 3. The heating contour for the moving cavity shows that the heating at the center is about 80% of that near the edges, desirable for offsetting the conductive heat losses away from the edges.

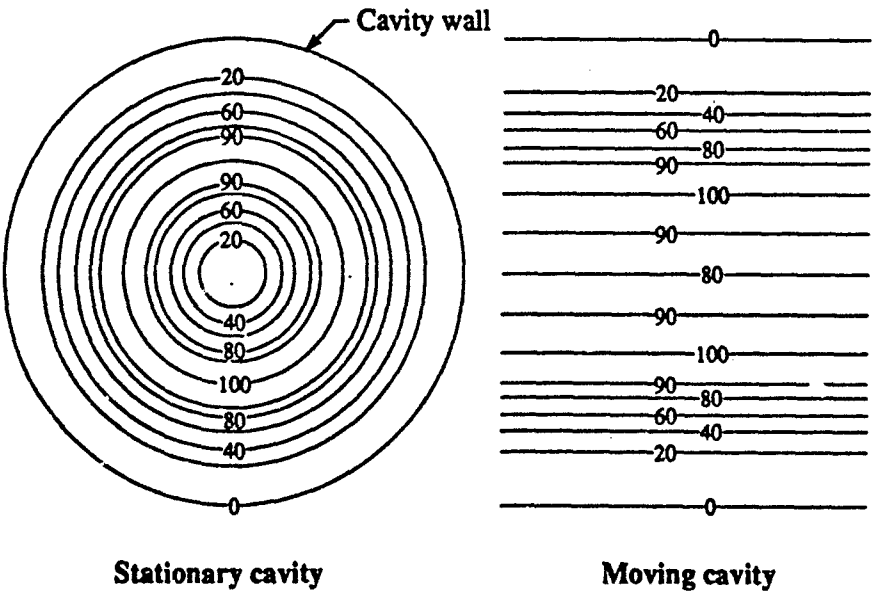


Figure 3. Power deposition contours for stationary and moving circular TE_{011} mode cavity.

The TE_{011} mode cavity can be moved away from the surface of the composite without adversely affecting its heating profile or efficiency, although its operating frequency changes predictably according to Equation (5). The efficiency, η, of the TE_{011} mode cavity heater can be estimated by comparing the measured or calculated[10] Q's of the cavity when placed on the composite, Q_c, and when placed on a low-loss metal surface, Q_m. The Q is the power stored in the cavity divided by the power lost per cycle. Thus, the reciprocal of the Q is proportional to the total loss which is the sum of the losses of the parts of the cavity, e.g., top, sides and bottom. Assuming the loss in the metal bottom is small compared to the loss in the composite part, the efficiency is given by

$$\eta \approx 1 - Q_c/Q_m. \tag{7}$$

EXPERIMENTAL RESULTS AND CONCLUSIONS

A cavity 17.8 cm in diameter and about 11 cm long was constructed from copper sheet metal. The axial position of the top end plate could be changed to tune the cavity to resonance. Microwave power was fed into the cavity via a waveguide into the side of the cavity through an aperture whose size was chosen to match the cavity to the waveguide. A capacitive screw in the waveguide next to the aperture was used to fine-tune the aperture for different composite materials. During use on a particular type of composite material the matching screw required no adjustment, but the end plate required adjustment to maintain resonance if the distance between the cavity and the composite changed.

The measured unloaded Q_m of the cavity with an aluminum metal bottom was 10,400 and the measured unloaded Q_c of the cavity with a cross-ply carbon-fiber composite bottom was 4,500. Using these Q's in Equation (7) the efficiency of our cavity was calculated to be 57%. Theoretical calculations[10] for a copper ($\sigma = 5.7 \times 10^7$ S/m) cavity show that Q_m should be 56,900 and Q_c should be 5,100, leading to an expected efficiency of 91%. Thus, we anticipate that the efficiency of our cavity could be improved by taking greater care in its construction.

Actual measurements show that Q_c does not decrease measurably when the cavity is moved 1 cm away from the composite surface or if the composite surface has a 30 cm concave or convex radius of curvature. This indicates that the microwaves do not leak from the gap between the cavity and the surface being heated, assuring personnel safety and efficient operation even when the heater is used to manufacture parts having complex curved surfaces.

A high-power heating experiment in which a single ply of carbon-fiber/PEEK prepreg was bonded to the surface of a carbon-fiber cross-ply laminate confirmed that the efficiency of the TE_{011} mode cavity applicator is greater than 50%. The power reflection during heating remained minimal and no arcing occurred between the cavity and the cross-ply laminate. The heating pattern was annular, with inside diameter of 6.4 cm and an outside diameter of 11.4 cm, as in Fig. 2.

The microwave applicator has been used in a stationary mode to fabricate carbon-fiber/PEEK 15-ply laminates about 18 cm in diameter. During the fabrication of these laminates they were vacuum bagged to provide a consolidation pressure of about 0.1

MPa. In these experiments low-power (~1 kW) microwave heating was used to prevent burning the surface during the five minutes required for the heat to diffuse through the 15 plies. The interlaminar shear strength of these laminates was 100 MPa (14.5 ksi), almost equal to the 103 MPa obtained using an autoclave. The results of these tests indicate very good consolidation. In fact, higher consolidation pressures exceeding 0.3 MPa and longer consolidation times at 399° C (750° F) are usually required in press or autoclave processing to achieve these good results.

These results strongly encourage the application of the TE_{011} mode microwave cavity as a heating source for fiber-placement. Microwave heating could be used as the primary energy source or as a supplementary source. Since power can be applied in pulses or continuously as desired, this type of heating lends itself to real-time control.

ACKNOWLEDGEMENTS

This work was supported by DARPA and administered by Charles Y.-C. Lee of the Wright Laboratories under Contract No. F33615-88-C-5420, Adtech Subcontract Nos. 704-T6 and 704-T10, Electromagnetic Energy Consolidation of Composites.

REFERENCES

1. J. Jow, M. C. Hawley, M. Finzel, J. Asmussen Jr., H.-H. Lin, and B. Manring, "Microwave Processing and Diagnosis of Chemically Reacting Materials in a Single-Mode Cavity Applicator," IEEE Trans. Microwave Theory Tech., Vol. 35, No. 12, pp 1435-1443, (1987).
2. Y.-F. Chen and C. Y.-C. Lee, "Coupling of Microwave Energy with Carbon Reinforced Composites," Polym. Mater. Sci. Eng., Vol. 60, pp. 680-684, (1989).
3. J. C. Hedrick, D. A. Lewis, G. D. Lyle, S. D. Wu, T. C. Ward, and J. E. McGrath, "Microwave Processing of Functionalized Poly(Arylene Ether Ketones)," Polym. Mater. Sci. Eng., Vol. 60, pp. 438-442, (1989).
4. W. I. Lee and G. S. Springer, "Interaction of Electromagnetic Radiation with Organic Matrix Composites," J. Comp. Matl, Vol. 18, No. 4, pp. 357-386 (1984).
5. A. C. Lind, L. N. Medgyesi-Mitschang, J. E. Kurz, H. F. McKinney, and F. C. Wear, "Microwave Heating for Manufacturing Carbon-Fiber Thermoplastics," in *Microwave Processing of Materials II*, edited by W. B. Snyder, W. H. Sutton, D. L. Johnson, and M. F. Iskander (Mater. Res. Soc. Symp. Proc. Vol. 189, Pittsburgh, PA, 1990).
6. A. C. Lind, C. G. Fry, and C. H. Sotak, "Measured Electrical Conductivities of Carbon-Fiber composite Materials: Effects on Nuclear Magnetic Resonance Imaging," J. Appl. Phys., Volume 68, No. 7, pp. 3518-3528, (1990).
7. A. C. Lind, unreported measurements between 0.5 and 100 MHz.
8. R. F. Harrington, *Time-Harmonic Electromagnetic Fields*, pp. 48-56, (McGraw-Hill, New York, 1961).
9. Charles P. Poole Jr., *Electron Spin Resonance*, pp. 270-290, (Interscience Publishers, New York, 1967).
10. H. Soga, J., "A New Microwave Thickness Gauge," Microwave Power, Vol. 8, No. 3, pp. 253-266, (1973).

DISTRIBUTION OF DISSIPATED POWER IN A GRAPHITE FIBER REINFORCED EPOXY COMPOSITE HEATED IN A MICROWAVE CAVITY

R. Fritz and J. Asmussen, Jr.
Michigan State University
Department of Electrical Engineering
East Lansing, Michigan 48824

ABSTRACT

Temperature profiles of a carbon fiber epoxy composite disk heated in a single mode/controlled multimode cylindrical resonant cavity with 2.45 GHz microwave energy indicate that microwave energy is limited in its penetration into the disk, from the top and the perimeter (a skin effect). Initial heating profiles allow an approximate determination of the penetration depth. In the steady state, the temperature gradients indicate that the heat flow was primarily by thermal conduction from the perimeter of the disk, toward the center and out the upper and lower surfaces.

INTRODUCTION

Microwave radiation is among the alternative ways of processing composite materials. Microwave processing requires an understanding of the interaction of radiation and materials. As an example, heating of nylon and wet wood rods and silicon wafers in a resonant cavity has been investigated by Asmussen et. al. [1], and glass- and graphite-fiber epoxy composites in a rectangular waveguide have been examined by Li and Springer [2].

Four significant advantages of microwave materials processing are worth noting. One is in the area of process control: the temperature excursion of an exothermic reaction of an uncured material can be reduced or eliminated by appropriate power control. Secondly energy consumption is reduced since most of the input energy is coupled directly into the sample, and not used to heat the air in the oven (resulting also in a lower oven temperature). A third advantage is the ability to monitor the cure of the composite sample by on-line measurement of the dielectric constant, as determined by

cavity parameter measurements (swept frequency, power coupling or field measurements at the wall of the applicator). Fourth, smaller ovens of different geometries can be used, possibly reducing capital outlay.

The experiments described here employed a cured thick-section graphite-fiber epoxy composite in a tunable single mode or controlled-multimode cylindrical cavity applicator, excited at 2.45 GHz. Temperatures were monitored with optical fiber temperature probes positioned at various depths near the vertical axis of the disk, and at various radii in the midplane of the disk.

EXPERIMENTAL APPARATUS AND PROCEDURE

The experimental circuit is shown in Figure 1. The energy source is a variable (0-100 W) microwave power source (Model MPG 4M from Opthos Instruments, Rockville, MD). Incident power is measured by the first directional coupler, attenuator, and power meter. The

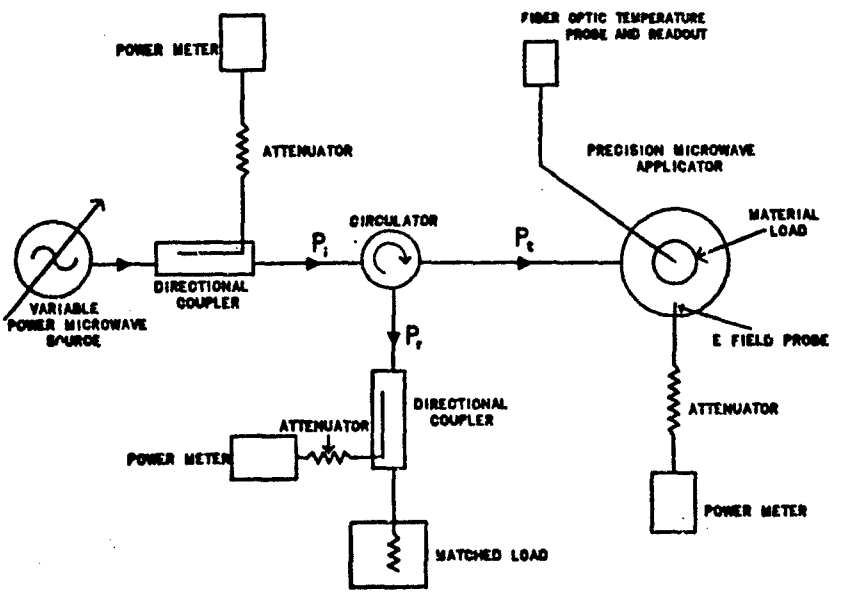


Figure 1. Schematic of the microwave processing system.

energy passes through the circulator to the applicator, which is a 7-inch diameter cylindrical resonator with one movable end plate (sliding short) and variable length input probe. Reflected power is directed by the circulator to the second directional coupler, where it is measured by the power meter and dissipated in the matched load.

An optical fiber temperature measurement system (Model 750 from Luxtron, Mountain View, CA) was used with four probes. Three measurements were taken for each reading, with an update interval of 15 seconds during initial heating. The probes were located for radial temperature profiles as indicated in Figure 2. For the axial profiles, all four were in the center (at 1) at the surface, 1/4, 1/2 and 3/4 of the thickness of the disk (Figure 4a inset).

A half-inch styrofoam support was used to elevate the disk above the bottom of the cavity (Figure 2) to couple energy more uniformly into the disk. The composite was previously convection cured in an oven, thus eliminating exothermic heating that would be present in reacting epoxy, and isolating the microwave heating pattern and material heat conduction phenomena.

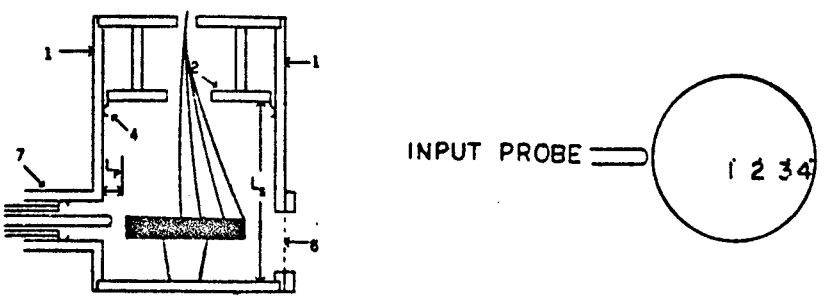


Figure 2. (a) Cross-section of the cavity applicator, showing the supported process material and location of temperature probes. (b) Configuration of microwave input probe and composite disk of 6.4 cm radius and 2.5 cm thickness. The probes are about 2 cm apart, in the midplane of the disk.

RESULTS

The composite disk was heated at three different power levels—18, 35 and 70 watts. Several modes were examined. The mode which resulted in the highest initial heating rate for the described cavity-sample

configuration and probe locations was investigated in more detail. The electric field (not included here) exhibited a dipolar pattern, with an axial variation similar to a half-wave cosine. More field measurements are needed to determine if the mode is TE, TM or a combination, since the cavity had a significant material load. In all cases, the loaded applicator could be impedance matched by adjusting the cavity short length and input probe to reduce the measured reflected power to zero, so that all of the input power was absorbed by the load and applicator walls. It is assumed that the power absorbed by the applicator was negligible compared to that absorbed by the composite.

Figure 3a shows the radial heating profile for 18 watts of input power. The higher curve corresponds to the outside probe so it is

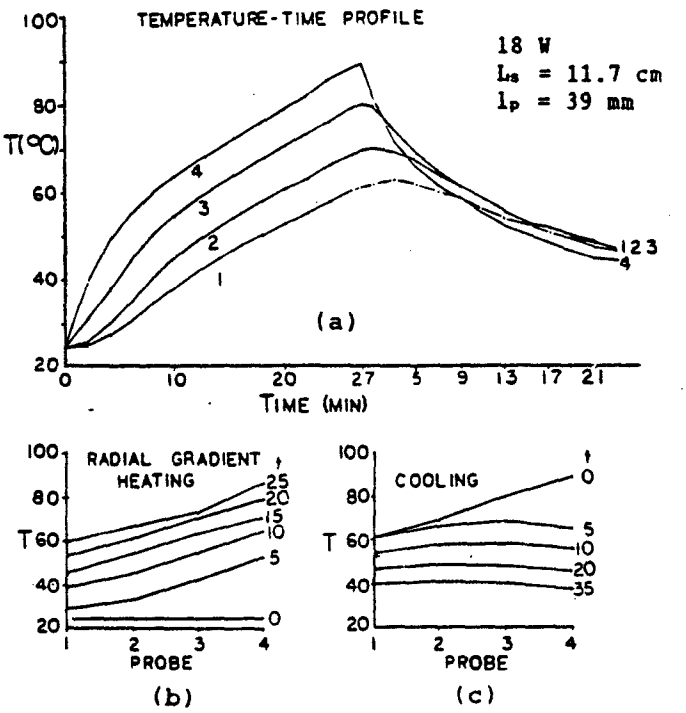


Figure 3. Radial temperature profiles for 18 W. Figure a illustrates the temporal variation (heated for 27 minutes), figures b and c the gradients for heating and cooling, respectively. The numbers to the right of the plots indicate elapsed time in minutes.

obvious that the microwave energy is absorbed at the perimeter of the disk as evidenced by the more rapid temperature rise, while very little microwave energy reaches the center of the disk.

Figure 3b shows the gradient of the radial heating profile. Since the heat flow is in the direction of -grad(T), one can see that it is from the perimeter toward the center. The addition of the cooling curve shown in Figure 3c demonstrates the heat flow due to conduction in the interior and convection at the surface, when the microwave power was turned off. Note that a high value of thermal conductivity is indicated by the near uniformity of the temperature for probes 1, 2 and 3 after about 14 minutes of cooling.

Figures 4a, 4b and 4c show the axial temperature profiles for heating at 35 and 70 watts, applied for 90 to 100 minutes. Note that in this figure, the probes are located along the vertical axis of the disk, on the surface and at depths of .6, 1.2, and 1.8 cm. As might be expected, the surface temperature (probe 1) exhibited the highest rate of increase for initial heating, but the lowest steady state temperature—due to convection (and radiation) heat losses. A cross-over can be seen from the gradient plot at around 8 to 10 minutes when the interior temperatures are about the same as the surface temperature and then surpass it. As the steady state is approached, the interior of the disk is at a higher temperature than the surface (a reversal of the temperature gradient).

The overall heat conduction for the disk is illustrated by Figure 5. During initial heating surface temperatures are higher than interior temperatures, so that heat flow is inward from the surfaces, primarily by conduction, except for a surface layer of electromagnetic heating. Around the cross-over time, t_c, heat continues to flow inward from the perimeter of the disk toward the center, but there is little heat flow in from the top or bottom surface, near the axis. In the steady state, t_{ss}, the axial temperature gradient has reversed, so that the heat flow is from the perimeter toward the axis, and from there toward the top (and bottom) faces.

ANALYSIS

During initial heating, the temperature difference between the material and the surrounding air is small, as is grad T, and can be ignored, yielding

$$P_t e^{-2\alpha r} = \rho c \frac{\partial T}{\partial t} \qquad (1)$$

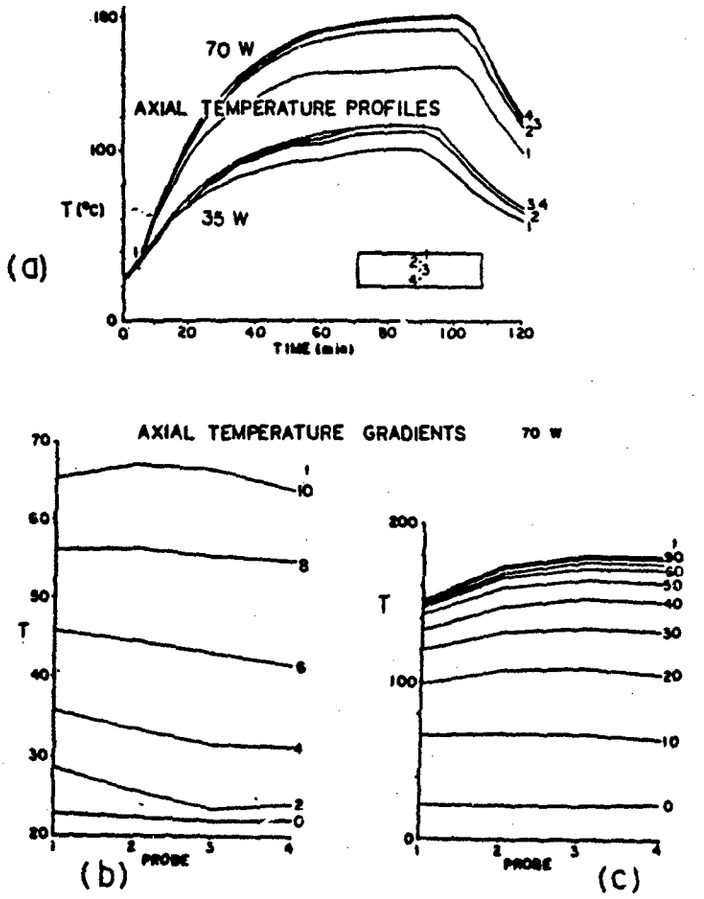


Figure 4. Axial temperature profiles. Figure a illustrates the temporal variation, and figure b shows the heating gradient for 70 W. The numbers to the right of the plots indicate elapsed time in minutes.

or

$$\frac{\partial T}{\partial t} = \frac{P_t}{\rho c} e^{-2\alpha r} \qquad (2)$$

P_t is the power transmitted into the sample at the interface, α is the material electromagnetic attenuation coefficient, r is the depth

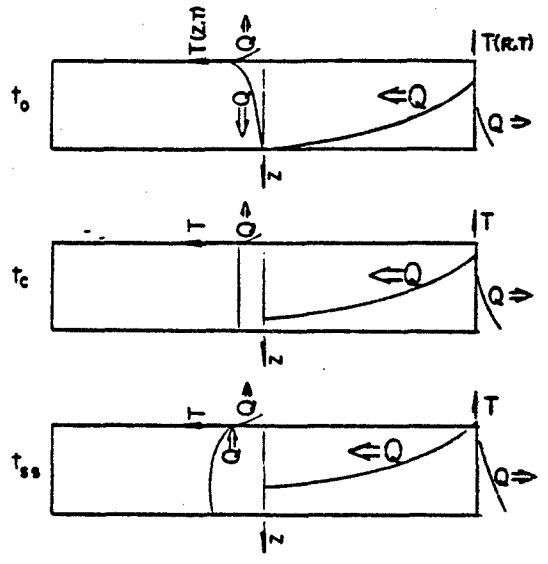


Figure 5. Heat flow in the sample during initial heating, t_o, cross-over, t_c, and steady state, t_{ss}, based on the measured temperature gradients.

of the point under consideration, ρ is the material density, c is its specific heat capacity, and $\partial T/\partial t$ is the rate of temperature increase (or decrease).

From equation (2), the ratio of the temperature increase for the same time intervals at adjacent positions (along the radius or axis) allows a determination of the attenuation coefficient (or penetration depth) in that direction:

$$\frac{\partial T(r_2)}{\partial T(r_1)} = e^{-2\alpha(r_2 - r_1)} \qquad (3)$$

or

$$\alpha = \frac{\ln\left(\frac{\partial T_{n+1}}{\partial T_n}\right)}{2\,(r_n - r_{n+1})} \qquad (4)$$

and the penetration depth is $1/\alpha$.

In Figure 6 the "skin" effect (attenuated propagation of the radiation into the material) is apparent from the curvature of the plots connecting probes 1, 2 and 3. The skin depth can be calculated from the reciprocal of the attenuation constant, which is given by equation (4), in terms of the measured temperature increments at adjacent probe positions. Figure 7 illustrates the calculated penetration of microwave energy into the composite from the axial and radial directions based on the calculated attenuation constant. It is important that the time of measurement be taken as close to the initiation of heating as possible to be able to neglect the heat transfer terms.

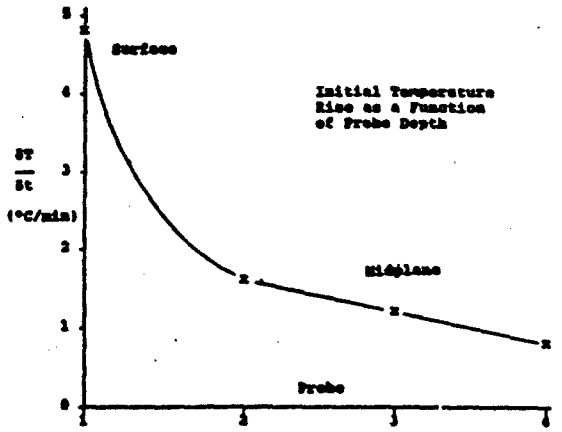


Figure 6. Initial rate of temperature rise as a function of the temperature probe depth (vertical) for an axial heating profile. The low heating rate at probe 4 (0.6 cm from the bottom) indicates that microwave heating from the lower face was less than that from the upper face.

Choosing time intervals that indicate the greatest temperature rise at the surface, the attenuation constant between the probe at the surface and the one below it is 0.87 /cm at 70 W and 2.13 /cm at 35 W. The reciprocals yield penetration depths of 1.15 cm and 0.47 cm, respectively. The effective value is assumed to lie between these two. Propagation of microwaves into the sample has been calculated

and illustrated in Figure 7, comparing propagation parallel (radial) and normal (axial) to the graphite fibers. One can see that radial penetration for a relative transmitted power of 5 to 10 % is about 3 times longer than for axial penetration.

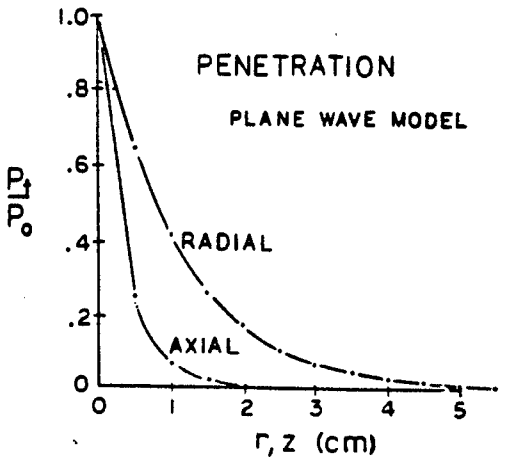


Figure 7. Attenuated transmission of microwave energy into the sample based on calculated attenuation coefficients in the radial and axial directions.

CONCLUSIONS

Clearly there is a skin effect for microwave heating in a resonant cavity applicator along the center axis of the disk, and this penetration depth is of the order of about 1 cm or less, based on attenuation values of 1-2 /cm. It is also clear that the interior of the disk can be heated by thermal conduction when the surface is heated by microwave energy. Most of the heating is by thermal conduction from the perimeter of the disk.

Internal temperature gradients could be controlled by heating at an appropriate input power or pulsing the input power (manually or electronically) when monitored points reach predetermined reference temperatures.

Finally, the depth of penetration and therefore uniformity of heating may be influenced by judicious selection of power source frequency (eg. 2450, 915 or 400 MHz) and appropriate "oven" design (size and geometry), as well as by the chemistry of a reacting sample.

References:

1. Asmussen, J. A., Lin, H., Manring, E. B., Fritz, R., Single Mode or Controlled Multimode Microwave Cavity Applicators for Precision Materials Processing, Review of Scientific Instruments, vol. 58, no. 8, August 1987, pp. 1477-1486.

2. Lee, W. I., and Springer, G. S., Microwave Curing of Composites, J. of Composite Materials, vol. 18, July 1984, pp. 387-409.

3. Watters, D. G., Brodwin, M. E., Kriegsman, Dynamic Temperature Profiles for a Uniformly Illuminated Planar Surface, Materials Research Society Symposium Proceedings, vol. 124, pp. 129-134, Materials Research Society, Pittsburgh, PA, 1988.

4. Jow, J., Hawley, M., Finzel, M., Asmussen, J. A., Lin, H., Manring., E. B., Microwave Processing and Diagnosis of Chemically Reacting Materials in a Single Mode Cavity Applicator, IEEE Transactions on Microwave Theory and Techniques, vol. MTT-35, no. 12, December 1987, pp. 1435-1442.

MICROWAVE HEATING OF CERMETS

Eric Bescher and John D. Mackenzie
Department of Materials Science and Engineering
University of California Los Angeles, Los Angeles, CA 90024

Metals are microwave reflectors. However, it is possible to produce heat by microwave irradiation in metal-insulator powder mixtures. Copper-alumina and chromium-alumina mixtures have been exposed to 2.45 GHz radiation in a 700W multimode cavity. Temperatures ranging from 1000°C to 1400°C have been obtained. Heating rates were found to be dependent on the weight fraction of metallic filler. Some of the parameters involved in the microwave processing of metal-ceramic composites are presented.

INTRODUCTION

Metals are known to reflect microwaves. For an electromagnetic wave at normal incidence on an ideal conducting surface, there is total reflection of the incident wave, and the electric field E is zero at the surface. In practice, however, no conductor is perfect, i.e. it has a finite conductivity σ. This imperfectness of the conductor leads to a fraction of the incident energy entering the conductor and dissipating as heat. Therefore, it is possible to exploit the microwave losses in metals for the fabrication of metal-based composites by microwaves. An obvious method is the use of metal powder particles dispersed in a ceramic material. The aim of this paper is to explore some of the parameters involved in the use of metals for the microwave heating of ceramic-metal composites or cermets. Cermets can be of two kinds, oxide- and carbide-based, and can be developed in a wide number of compositions [1]. They combine the useful properties of ceramic and metal materials into one system. In the present work, examples of microwave heating of chromium-alumina and copper-alumina mixtures are presented.

EXPERIMENTAL

Microwave processing experiments were carried out in a 700 Watt 1.3 cubic feet microwave oven*, operating at 2.45 GHz. The microwave oven was placed in a glove box in which industrial grade dry nitrogen was circulated. The oxygen concentration was kept at 25 ppm to prevent oxidation of the metals during processing. The surface temperature of the samples was monitored by a two-color infrared pyrometer** with a working temperature range from 650°C to 1700°C. The powder samples to be processed were placed in alumina crucibles from Coors. A 3-inch thick microwave transparent ceramic fiber was used as thermal insulation. The surface temperature of the samples was read through a $5mm^2$ hole in this insulation. For the experiments involving compacted powders, the green bodies were fabricated in a 1" by 2" steel die under 17 000 psi of uniaxial pressure. The alumina powder was reagent grade -325 mesh from Johnson Matthey. The copper and chromium powders were -325, -200 and -100 mesh, 99+% purity from Aldrich Chemical.

*Model JE1453H002, General Electric, Louiville, KY.
**Model M77S, Mikron Instruments Inc., Wyckoff, NJ.

The shape of the particles was irregular when observed under an optical microscope. Mixtures were prepared in 10 weight percent increments of metallic powder. Typically, a 60% copper-40% alumina mixture had a porosity of 61 % when loosely packed, and 30% when cold-pressed.

RESULTS AND DISCUSSION

Loosely packed powder mixtures

Alumina-chromium and alumina-copper unpacked powder mixtures, when exposed to microwaves, reached temperatures in excess of 1000°C (Figures 1 and 2). In the case of the chromium mixtures below 60 weight percent of chromium, no temperature above 650°C was recorded after 90 minutes of exposure. In all the other samples, after reaching a maximum, the temperature slowly decreased, typically at a rate of 1 to 2°C per minute.

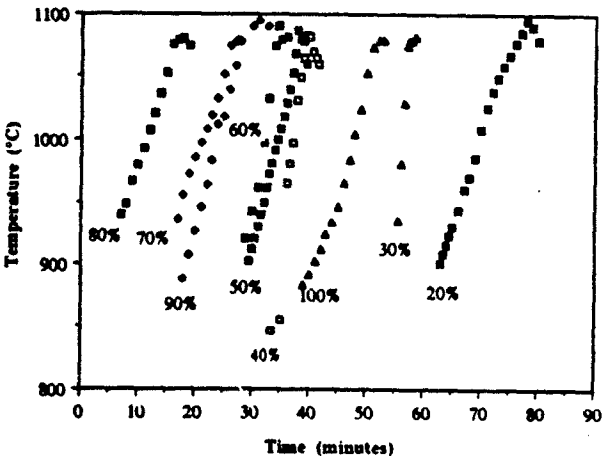


Figure 1. Heating of copper-alumina powder mixtures as a function of metal weight fraction.

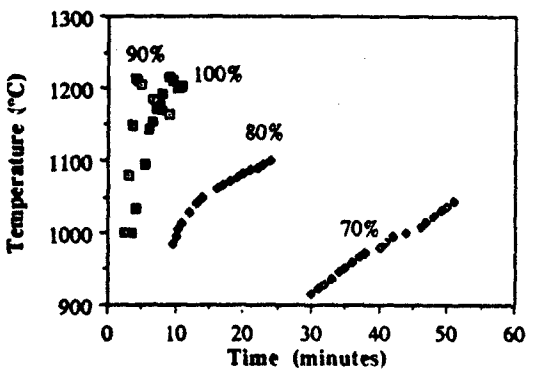


Figure 2. Heating of chromium-alumina powder mixtures as a function of metal weight fraction

As seen in Figures 1 and 2, microwave absorption did not vary linearly with weight percent of metal additions. Microwave absorption initially increased with increasing metallic weight fraction, but then decreased after reaching a maximum for mixtures containing 80 to 90 weight percent metal.

This effect is more clearly seen in a plot of the overall heating rate (time to reach 1000°C from room temperature) versus weight fraction. In Figure 3, this heating rate increases with increasing weight fraction of metal, reaches a maximum for 80% and decreases. It is more difficult to heat up a predominantly metallic powder mixture. Additionally, in high metal compositions, intense arcing was noticeable in the microwave cavity at the beginning of the experiment. This effect was attributed to high reflections from the sample; it diminished during processing and disappeared as the temperature increased in the sample.

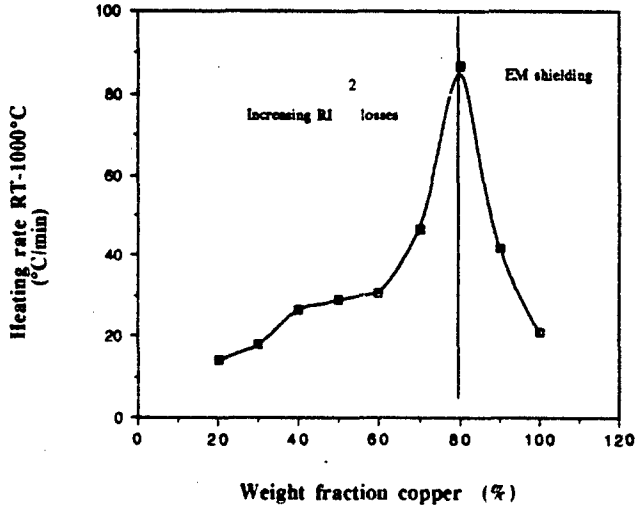


Figure 3. Heating rate of copper-alumina composites

Compacted powders

Experiments were also carried out with compacted green samples of the same compositions as above. The effect of compacting the powders on the heating rate was studied. The peak of the curve described above (Figure 3) shifted towards the lower weight fractions of metals. A 70 weight percent chromium mixture, difficult to heat up when loosely packed, became extremely absorptive when compacted. Concurrently, an absorbing loosely packed 90% weight fraction mixture became poorly absorbing when compacted. A typical shift is presented in Figure 4, in the case of chromium mixtures.

In this case, the best absorbing mixture shifts from a 90% metallic fraction to 70% metallic fraction when compacted.

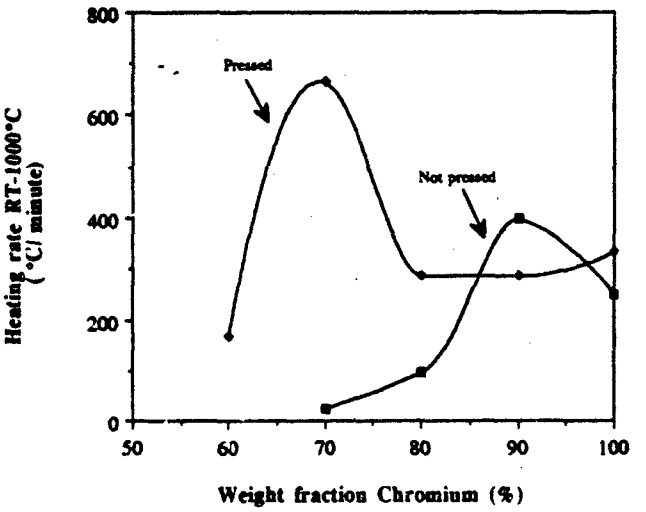


Figure 4. Heating rates of loosely packed and compacted chromium-alumina composites.

The combination of these results seems to be consistent with a phenomenon in which heat would be dissipated primarily on the exposed surface of the metal.

Skin depth and particle size

In order to investigate the effect of particle size on the heating rate, identical masses of metallic powders alone were exposed to microwaves. The heating rate decreased with increasing particle size (Figure 5). The temperature of the metal powder increased up to the melting point of copper (1086°C) and then stabilized, as the surface area of the powder decreased and the metal melted. This behavior confirms the importance of the surface effect.
Microwaves penetrate a metal to a depth known as skin depth δ, where the electric field falls to 1/e of its value at the surface. A simplified expression is [2]

$$\delta = 2.9\ 10^{-2} (\rho\lambda)^{1/2} \qquad (1)$$

where ρ is the resistivity of the metal in ohm.meter and λ the wavelength of the radiation.

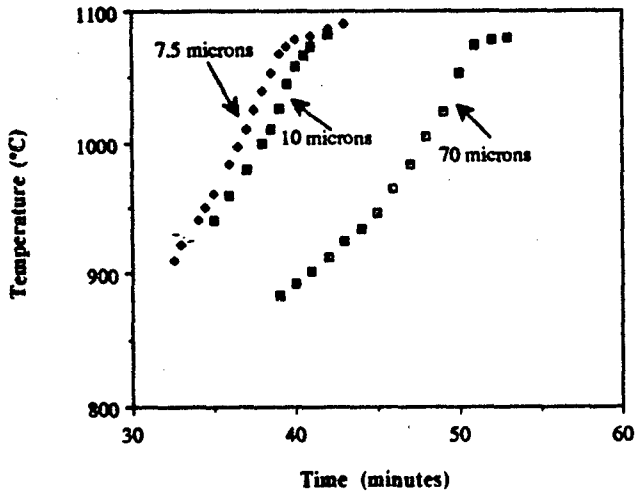


Figure 5. Influence of particle size on the heating of copper powder.

Table 1. Resistivity and skin depth at 2.45 GHz for Cu and Cr

	ρ (μm)	δ (um)
Cr	12.9	3.61
Cu	1.67	1.34

The more conducting of two metals will have a smaller skin depth. Surface currents within this skin depth are responsible for the heating mechanism by Joule effect [2]. The particle size effect can be explained by considering two mixtures containing the same amount of metal, say copper, but with two different particle sizes. Table 2 shows that for 10-gram copper powder samples containing particles of different radii, the one with a particle radius closer to the skin depth is more effected by the surface currents. At equal volume fraction of metal in a composite, the total exposed surface area of a sample containing small particles is larger than that of a sample containing large particles. The volume of conducting medium affected by skin currents is therefore larger for the small metal particles mixture and the Joule heating is consequently more important.

Table 2. Influence of the particle size on volume affected by the surface currents

Particle radius (μm)	Volume affected by surface currents (cm^3)
10	0.27
1000	0.003

As the volume fraction of metallic filler increases, the heating rate increases. This is in accordance with various models explaining dielectric losses of mixtures [3]. As the metal particles come closer to each other and the probability of contact increases, the area exposed to microwaves diminishes -clusters of metallic particles are equivalent to bigger particles with lower surface area, and microwave losses decrease. The mixture then reaches a composition ϕ_c known as the percolation limit [4,5] for the onset of dc conductivity. A similar effect is obtained by applying a pressure on a powder: as the probability of contact between adjacent particles increases, the dc conductivity of the composite increases [6] (an increasing fraction of the inside of the composite is shielded from the microwaves). Good electromagnetic shielding is usually obtained for metallic volume fractions close to twice the critical volume fraction [7]. Our results, showing that is is more difficult to heat compacted metal-insulator mixtures, are consistent with this observation. This phenomenon is also being reported at the present meeting in the papers on processing of carbides from silicon carbide [8].

Figure 6 shows a cold-pressed alumina-chromium sample fired at 1200°C for 20 minutes. The 80 % chromium-20% alumina sample exhibited a Vickers hardness of 550 VHN and a density of 71% of theoretical density. A sample containing 90% chromium sintered to 85% of the theoretical density. The mechanical properties of microwave cermets are the subject of an upcoming publication.

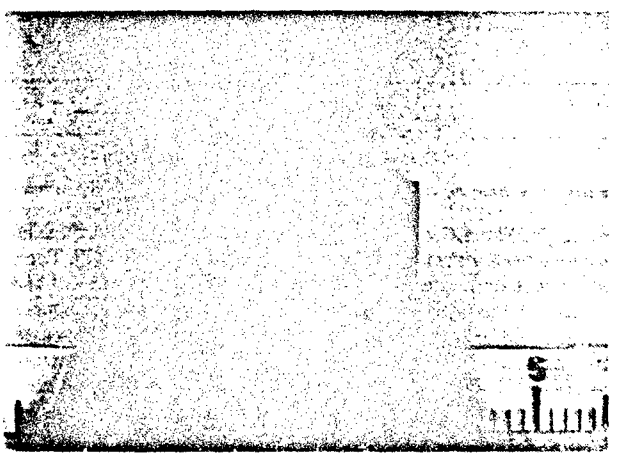


Figure 6. Photograph of a microwave-derived Chromium- Alumina (80-20 wt%) composite fired for 15 minutes.

CONCLUSIONS

We have demonstrated that metallic powders can be used for the generation of heat in ceramic-metal mixtures at microwave frequencies. Some of the most essential processing parameters are metallic volume fraction, particle size and packing density. The microwave absorption of such mixtures is not linear with increasing metallic fraction but decreases by shielding effect at higher metal contents. Microwave processing can therefore, with some limitations inherent to the reflective characteristics of metals, be applied to the fabrication of cermets.

ACKNOWLEDGEMENTS

The authors wish to acknowledge the support of the State of California through the Risk and Systems Analysis for the Control of Toxics (RSACT) Teaching Program.

REFERENCES

1. Cermets, J.R. Tinklepaugh and W.B. Crandall eds., Reinhold Publishing Corporation, New York, 1960.
2. Dielectrics and Waves, A.R. Von Hippel, John Wiley ed., New York, 1954.
David S. McLahan et al, Electrical Resistivity of Composites, J. Am. Ceram. Soc., 73, [8] 2187-2203 (1990)
3. Wayne W. Tinga, Fundamentals of Microwave-Material Interactions and Sintering, Mat. Res. Soc. Symp., Vol.124, 1988
4. B.W. Licznerski et al, Conductivity Model of Cermets treated as Critical Percolative Systems, Phys. Stat. Sol, 104, 891 (1987)
5. D.Bergman and Y. Imry, Critical Behavior of the Complex Dielectric Constant near the Percolation Threshold of a Heterogeneous Material, Physical Review Letters, 39, 17,1222-1225 (1977).
6. N. Deprez and D. S. McLachlan, The Analysis of the Electrical Conductivity of Graphite Powders during Compaction, J. Phys., 21, 101-107 (1988).
7. S.Reich, Percolation and Eddy Current in Random Close Packed Metal Polymer Composites, Journal of Materials Science, 22,3391-3394 (1987)
8. H. Kozuka and J.D. Mackenzie, Microwave Processing of Carbides, presented at the Annual Meeting of the American Ceramic Society, Cincinnatti, OH.
9. C.Béraud, M.Courbière et al, Study of copper-alumina bonding, Journal of Materials Science, 24,4545-4554 (1989].
10. W. Schott, Gefügeuntersuchungen an Sinterkörpern aus Tonerde und Chrom, Silikattechnik, 195

MICROWAVE SINTERING OF Al_2O_3:ZrO_2 CERAMICS

D. S. Patil*+, B. C. Mutsuddy+
Institute of Materials Processing
Michigan Technological University
Houghton, Michigan 49931

James Gavulic, M. Dahimene
Wavemat Inc., Plymouth, Michigan 48170

ABSTRACT

It is well established that the transformation toughening in alumina-zirconia (Al_2O_3:ZrO_2) ceramics depends critically on the ultimate size of the ZrO_2 particles in the sintered body. Microwave sintering offers the possibility of rapid densification, thereby avoiding the excessive grain growth.

In this study, sintering of Al_2O_3:ZrO_2 ceramics was performed in a cylindrical cavity applicator operating at 2.45 GHz in the TM_{012} mode. Different types of Al_2O_3:ZrO_2 powders were sintered to densities close to theoretical using microwave energy. The resulting microstructures were compared with the materials conventionally sintered.

INTRODUCTION

Microwave sintering of ceramics is a growing area of interest. It offers greater flexibility in thermal treatment and allows better control of microstructure development.

Heat is generated when microwave energy interacts with ceramic materials. Absorption of the electromagnetic energy inside the material is direct when the material couples with the microwaves. This particular kind of heating system has a low thermal inertia, therefore, it provides high heating rates. Rapid heating is limited by several factors such as some materials are transparent to the microwaves at room temperature and consequently do not absorb sufficient microwave energy for heating to occur.

Microwave and radio frequency dielectric heating is easy in a material which is polarizable and which efficiently converts the energy absorbed from the

* Permanant Address : Laser and Plasma Technology Division
Bhabha Atomic Research Centre, Trombay, Bombay 400 085, INDIA.
+ Member, American Ceramic Society.

oscillating electric field into the thermal energy in the lattice [1,2]. The power dissipated by a dielectric in an electric field is given by :

$$P = 2\pi f \varepsilon (E^2/2) \tan \partial \qquad (1)$$

where
P = power absorbed in the material
ε = dielectric permittivity
f = frequency of the incident radiation
E = electric field strength
$\tan \partial$ = loss tangent of the material

Temperature and impurities can have a profound effect on the energy losses in ceramics. Conduction losses are typically found to be predominant at higher temperatures. As the losses go up the depth of wave penetration decreases, opposing the goal of uniform sintering. While any decrease in the thermal conductivity of the material with temperature minimizes the heat loss and provides a better control on the heating profile. In some cases, introduction of impurities can be used to increase the conductivity and loss factor to the desired level.

The rate of heating increases with temperature for ceramics like Al_2O_3 and ZrO_2. It is therefore necessary to control the power available to the process to prevent thermal runaway. To induce the absorption of the microwave energy in the materials it is necessary to preheat the material before it really starts to couple to the microwaves [3]. Sintering aids which might couple at low temperature and burn off at higher temperature may be an alternative to the preheating.

Rapid heating and sintering of materials minimizes segregation of the impurities to the grain boundaries while a decrease in sintering time reduces grain growth [3]. In conventional heating temperature gradient causes greater pore elimination at the surface [4]. On the other hand microwave heating creates higher internal temperatures keeping the surface relatively cool and allows more uniform pore elimination. Good uniformity from microwave sintering is not an easy objective to achieve. It requires a knowledge of the material's high temperature microwave properties as well as the ability to modify and control them.

The difficulties encountered in efficient microwave heating of the ceramics can be reduced by the use of a tunable resonant cavity. Power absorbed by the material being proportional to the square of the electric field strength (equation 1), allows more power absorption in materials even with low dielectric loss. Single mode resonant systems can be designed to yield controlled and very high field strength which in turn results into high heating rates. This increase is due to the high quality factor "Q" of the cavity.

Toughness is one of the most important parameters in improving the mechanical properties of ceramics and composites. One way to improve the fracture toughness of these ceramics is to take advantage of the phenomenon of transformation toughning, which is associated with the zirconia containing ceramics. The ceramics containing zirconia have relatively high fracture toughness, and this has been attributed to a number of different mechanisms such as crack deflection and stress induced tetragonal-monoclinic martensitic transformation [5, 6].

In the zirconia toughned ceramics, retention of > 10 volume % metastable, tetragonal ZrO_2 in the matrix is the key to obtaining the increased fracture toughness. However, to retain the metastable, tetragonal ZrO_2 it is essential that ZrO_2 grain size be less than some critical size which is reported to be in the range of 0.5 to 0.8 μm [7-9]. This small ZrO_2 particle size in the matrix is important for achieving the advantages of transformation toughening. Above this critical size ZrO_2 grains transform to the monoclinic form. Due to the higher temperatures required for the densification of the ZrO_2, significant grain growth above this critical size occurs and therefore retaining desired volume fraction becomes difficult in the matrix.

To avoid excessive grain growth, hot pressing is frequently being used. Microwave sintering offers an alternative to hot pressing or pressureless sintering. Since microwaves provide heating rates higher than achievable by conventional processing methods, samples pass more rapidly through the lower temperature regime where surface diffusion is relatively more important and the small grained microstructure is raised to high temperature where grain boundary and lattice diffusion dominate over surface diffusion. Consequently, the grain growth is significantly supressed.

Microwave sintering of Al_2O_3:ZrO_2 has been investigated by a number of investigators [10]. To the best of our knowledge successful sintering of reasonable size samples of Al_2O_3:ZrO_2 using a single mode applicator has not been reported. The objective of this study is to show the feasibility of using a single mode applicator for sintering of Al_2O_3:ZrO_2 samples. The samples prepared from three different types of Al_2O_3:ZrO_2 powders, have been chosen to investigate microwave sintering characteristics. The objective of this study is also to avoid the external use of a susceptor and/or a binder.

EXPERIMENTAL SET UP

The experimental system consists of variable power-CW microwave power supply 3 KW-operating at 2.45 GHz, 2 circulators and matched dummy loads, power meters (that measures the incident power P_i and the reflected power P_r), a coaxial input coupling system, Wavemat's cavity CMPR-250 and Accufibre temperature measurement system+. The details of the applicator are discussed in another paper by the same authors in this volume.

+ Model 100 C, Accufiber, Inc., Beaverton, OR 97005.

SAMPLE PREPARATION AND EXPERIMENT

Three different types of Al_2O_3:ZrO_2 powders were used for this study to give the parametric variations in the sintering characteristics.
Three different types are : AlZr-J, AlZr-P and AlZr-C.

Starting material for AlZr-J is a commercial grade ZF alundum abrasive*. The chemical analysis (as provided by the vendor) is : Al_2O_3-75 %, ZrO_2-23 %, TiO_2-0.4 %, SiO_2-0.3 %, Fe_2O_3-0.3 %, Na_2O-0.08 %, CaO-0.10 %, MgO-0.03 %, S-0.06 %. Average crystal size is 17 μm.

The as received abrasive was sieved and the fraction collected between 200 and 500 mesh size was collected for this study. The fraction collected was wet milled using isopropyl alcohol and zirconia grinding balls to reduce the zirconia particle size below 1 μm. The slurry was dried under an infra-red lamp and the powder was sieved through a100 mesh screen. The zirconia particle size in the milled powder was examined under scanning electron microscope (JEOL+, JSM-820).

The second lot of powder (AlZr-P) was made by mixing alcoa A16SG alumina** and Cerac ZrO2 (monoclinic) L-1041*** to get 15 volume % ZrO_2 in the mix. The mixture was rolled with ZrO_2 grinding balls in isopropyl alcohol. The slurry was dried under an infra-red lamp and the powder was sieved through 100 mesh screen. The zirconia particle size in the milled powder was examined under the SEM and was below 0.2 μm.

The third lot of powder (AlZr-C) was prepared by chemical dispersion of ZrO_2 particles in an alumina matrix. For the sake of comparision the volume fraction of zirconia was kept the same as AlZr-P. Sumitomo alumina (AKP30-MG) # was used as the matrix. The following procedure was used in dispersing ZrO_2 in the Al_2O_3 matrix. An appropriate amount of $ZrOCl_2.8H_2O$++ was weigned and dissolved in the deionized water till a clear solution is obtained. The AKP30-MG alumina powder was added to this solution. The resulting slurry was dried slowly and thoroughly. It was then calcined at 1100 C for 2 hours at a heating/cooling rate of 6 C/min. The calcined powder was washed with deionized water till it was free of Cl^- radicals. The washed powder was dried under an IR lamp and milled using ZrO_2 grinding balls and isopropyl alcohol. The slurry was then dried and the powder was sieved through the 100 mesh screen. The ZrO_2 particle size was below 0.3 μm as seen by SEM.

All three grades of powder mixtures were cold isostatically pressed into approximately 25.4 mm. dia. x 25.4 mm. long pellets at 276 MPa. No binder was added. To remove any residual moisture the pellets were held in an oven at 100 C for 12 hours. As pressed pellets were around 60 % of theoretical density.

---

* Norton Company, Worcester, MA 01615.
+ JEOL, USA, Inc., Peabody, MA 01960.
** Alcoa, Aliminium Company of America, Pittsburgh, PA.
*** Cerac, Inc., Milwaukee, WI 53201.
# Sumitomo Chemical Company, Ltd., Osaka, Japan.
++ Johnson Matthey, Alfa Products, Ward Hill, MA 01835.

For microwave sintering each pellet was wrapped with a small amount of fiber insulation to minimize surface radiation. The insulated pellet was placed at the center of the cavity base plate.The incident microwave power was coupled through an adjustable coupling probe. Tuning of the particular mode TM_{012} was accomplished by adjusting the position of a sliding short and the coupling probe. A hole approximately of 3 mm diameter was made through the insulation to view the sample surface by the Accufiber optical pyrometer system through a non-radiating opening on the wall of the cylindrical cavity.

Accuracy of temperature measurement was limited by three factors. First, a thermocouple was tried but the metallic leads acted as surface wave conduction paths in the cavity high field region, introducing measurement uncertainties. Second, errors in sample temperature measurement were due to the interference from luminous fiber insulation at high temperature. Third, the emissivity of the sample which is also temperature dependent varies during sintering due to morphological changes.

Despite these limitations, the recorded temperature did provide some relative information on the thermal history of different samples. Efforts are now being directed to get a true estimate of the temperature. With some more modifications we will be able to measure the actual temperature of the sample to a reasonably good accuracy.

The samples were processed in the cavity according to the schedule shown in figure I.

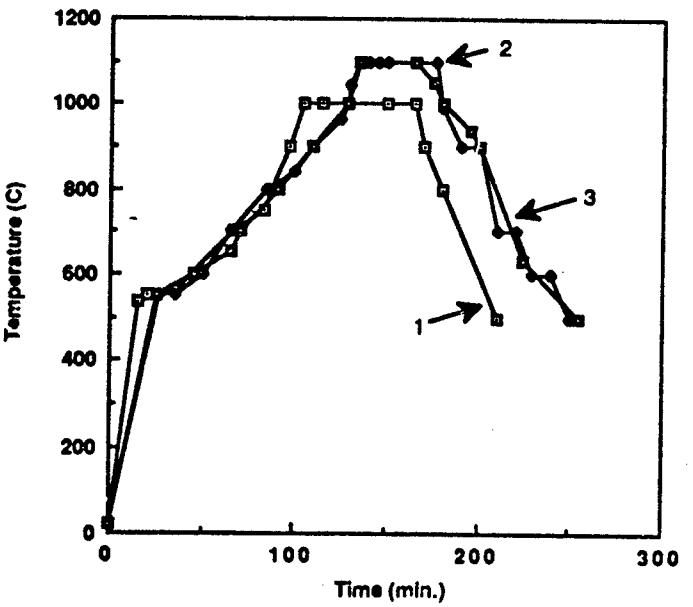


Fig. 1. Microwave sintering schedule of the various samples (1: AlZr-J, 2: AlZr-P, 3: AlZr-C)

The densities of the samples were measured by the Archimedes method. The specimens were cut from the sintered samples and were polished to a 0.25 μm finish with diamond paste and the samples were chemically etched to reveal the microstructure. The polished and fractured surfaces were examined under the SEM.

To compare the results of the microwave processing with the conventional sintering, similar samples of AlZr-J and AlZr-P were sintered conventionally at 1600 C for 10 hours and 1450 C for 1.5 hours (followed by high pressure sintering in Argon gas, 10.35 MPa, at 1450 C for 2 hours).

RESULTS AND DISCUSSIONS

Results of the miocrowave sintering of the alumina-zirconia specimens are shown in Table I

Table I Densification results on various samples

S.No	Sample	Sintering mode	Time (hours)	% Densification
1	AlZr-J	microwaves	3.67	95.79
2	AlZr-J	conventional	36.00	94.6
3	AlZr-P	microwaves	4.50	99.72
4	AlZr-P	conventional	26.50	100
5	AlZr-C	microwaves	4.42	100

The microstructures of the microwave sintered and conventionally sintered material are shown in the figure nos 2-8.

The sintering can be described in two stages: preheating stage where samples are heated for a few minutes at a constant input power of 300-400 W, and sintering where the power input is steadily raised. Attempts to reach the final sintering temperature without preheating gave rise to hot spots, arcing and eventual cracking of the samples.

The uniform hot zone can only be maintained when the sample is properly insulated. The gradual increase in sample temperature is essential to achieve crack-free and uniformly dense samples. The thermal runaway which is frequently observed in microwave sintering has been avoided.

The progress in densification through controlled increase in sample temperature can be monitored by noting a steady increase in minium reflected power as the material's absorption decreases. AlZr-J sample showed some interesting features. Being impure, it coupled very well with the microwaves initially but due to decrease in the depth of penetration the sample failed to couple well at highe. temperatures and resulted in an increase in the reflected power. Nonetheless, this material was successfully sintered to 95.79 % density, which was higher than that obtained by conventional sintering at 1600 C for 10 hours followed by sintering under high pressure of Argon gas.



Fig. 2. Fractured surface of conventionally sintered AlZr-P (SEI, 5000 X)



Fig. 3. Fractured surface of microwave sintered AlZr-P (SEI, 5000 X)

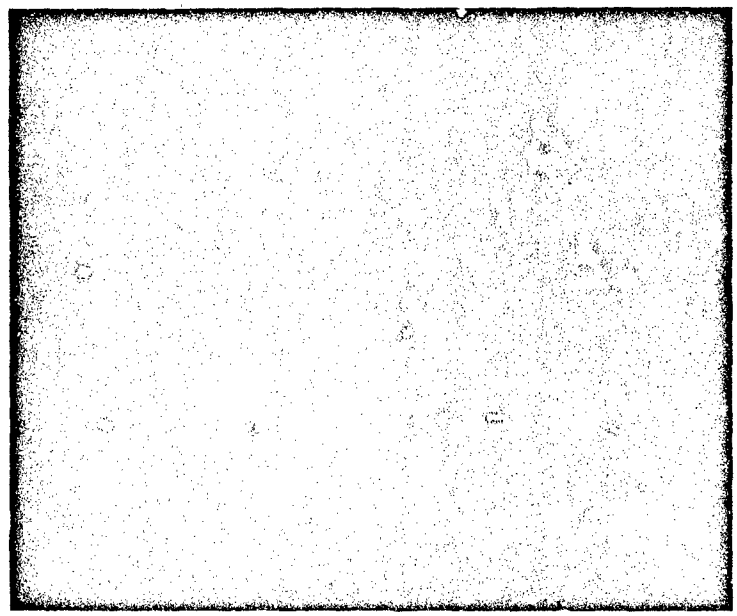


Fig. 4. Polished section of conventionally sintered AlZr-P (BEI, 5000 X)



Fig. 5. Polished section of microwave sintered AlZr-P (BEi, 5000 X)



Fig. 6. Polished section of conventionally sintered AlZr-J (SEI, 5000 X)



Fig. 7. Polished section of microwave sintered AlZr-J (SEI, 5000X)

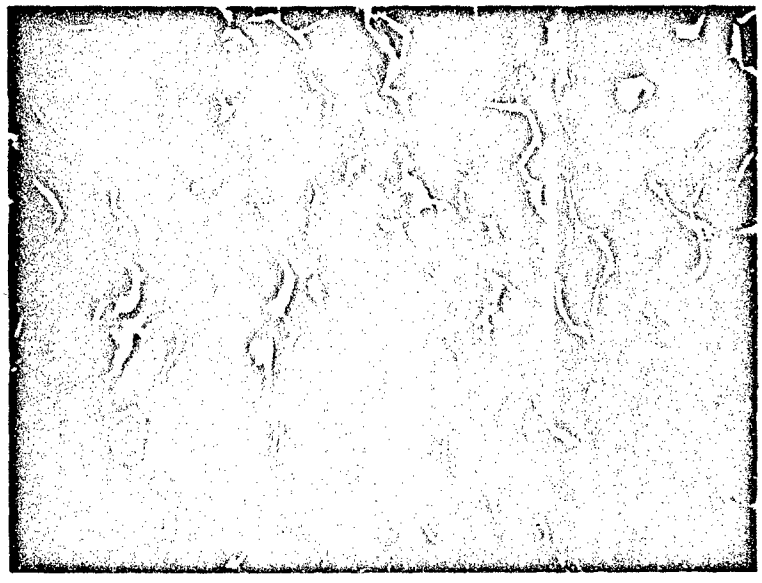


Fig. 8. Fractured surface of microwave sintered AlZr-C (SEI, 5000 X)

The grain size of zirconia is smaller in microwave sintered samples as compared to the conventionally sintered samples and is evident from figures 4-7.

The fine microstructure can be explained in the light of higher heating rates with microwaves. The sample passes more rapidly through the lower temperature regime where surface diffision is likely to be more dominant and a rapid raise to high temperature allows grain boundary and lattice diffusion to enhance densification and retard grain growth.

CONCLUSIONS

Al_2O_3:ZrO_2 samples of various kinds were successfully densified from 60 % initial green density to a high density by using a tunable single mode applicator operating in the TM_{012} mode at 2.45 GHz. The times required for conventional sintering for achieving similar densities were very high.

To the best of our knowledge this is the first successful experiment where practical sized Al_2O_3:ZrO_2 samples have been microwave sintered to high density without the need for susceptors around the samples. High density and ultrafine microstructures in Al_2O_3:ZrO_2 can be achieved by rapid sintering with microwave heating. The ability to control zirconia grain size by ultra-rapid sintering is critical in achieving the advantages of transformation toughening in zirconia containing ceramics. Microwave sintering offers a major advantage over conventional sintering of zirconia based ceramics.

ACKNOWLEDGMENTS

The authors wish to thank Dr. Walter A. Johnson, Director of Institute of Materials Processing for his continuous encouragement and support. Thanks are due to Ruth Kramer for her assistance with the SEM work and students for their help. One of the authors (DSP) is grateful to the authorities at Bhabha Atomic Research Centre, Bombay for granting him a leave of absence.

REFERENCES

1) A. R. Von Hipple, "Dielectric Materials and Applications", M. I. T. Press, Cambridge, p. 3-46, 1954.
2) H. Puschner, "Heating with Microwaves : Fundamentals, Components and Circuit Techniques", Springer-Verlag, New York, 1966.
3) H. D. Kimrey, T. L. White, T. S. Bigelow and P. F. Becher J. Microwave Power, Symp. Summaries, 81-82 (1986).
4) W. D. Kingery, H. K. Bowen and D. R. Uhlamann, "Introduction to Ceramics, 2nd edition, 485, John Wiley and Sons, 1976.
5) M. Ruhle, A. H. Heuer and N. Claussen, "Transformation and Microcrack Toughening as Complementary Processes in ZrO_2 Toughened Al_2O_3", J. Am. Ceram. Soc. 69 [3] 195-197 (1986).
6) F. F. Lange, "Transformation Toughening Part 2 : Contribution to Fracture Toughness", J. Mater. Sci. 17 [2] 235-39 (1982).
7) D. J. Green, "Critical Microstructures for Microcracking in Al_2O_3 -ZrO_2 Composites", J. Am. Ceram. Soc. 65 [12] 610-14 (1982).
8) F. F. Lange, "Transformation Toughening Part 1 : Size Effects Associated with the thermodynamics of constrained transformations", J. Mater. Sci. 17, 225-234 (1982).
9) F. F. Lange and D. J. Green "Effects of Inclusion Size on the Retention of Tetragonal ZrO_2 : Theory and Experiments", pp. 217 -25 in Advances in Ceramics, vol. 3, Edited by A. H. Heuer and L. W. Hobbs, The Am. Ceram. Soc., Columbus, OH, 1981.
10) H. D. Kimery, M. A. Janney and J. O. Kiggans, "Microwave Sintering of Zirconia Toughened Alumina ceramics", Paper presented at the MRS symposium on "Microwave Processing of Materials at San Francisco, CA, April 17-20 (1990).

MICROWAVE SINTERING OF Y_2O_3(3%)-ZrO_2(TZP)

Yong-Lai Tian, Bao-Shun Li, Jian-Lin Shi, Yao-Ping Xu, Jing-Kun Guo and Dong-Sun Yen
Shanghai Institute of Ceramics, Chinese Academy of Sciences, Shanghai, China, 200050.

ABSTRCT

Microwave sintering of Y(3%)-TZP has been performed in a TE_{10n} single mode rectangular applicator. Ultra-fine grain sizes of 0.2-0.35 μm and high densities of 98-99.5%(TD) were achieved as the sintering temperatures ranged from 1250 to 1600° C. The problem of phase transformation induced cracking may be solved by raising the presintering temperature to remove the residual monoclinic phase in green samples.

INTRODUCTION

In recent years it has been of considerable interest for materials scientists to develop fine grained Y-TZP (Y_2O_3 stabilized tetragonal ZrO_2 polycrystals) at submicron and nanosize scales because of its high fracture toughness and exceptional superplasticity. Microwave sintering has been demonstrated to be very promising in developing ultra-fine microstructure for some ceramics such as Al_2O_3 and Al_2O_3-TiC composites due to its high heating and densification rates[1,2]. The present study was undertaken to explore the feasibility of producing fine grain sizes in Y-TZP by microwave sintering.

Prior studies indicated two major problems encountered in microwave sintering of Y-TZP[3,4]: (1) It was difficult to heat up Y-TZP samples from room temperature to high sintering temperatures in a single mode cavity. (2) Y-TZP samples cracked frequently at high heating rates. The reasons and possible solutions for these problems will be

discussed in this article.

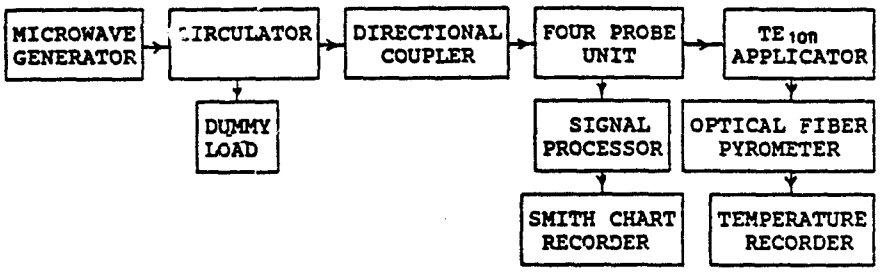


Fig.1 Diagram of Microwave Sintering System.

EXPERIMENTAL PROCEDURE

The commercial TZ-3Y powder of Y_2O_3(3 mol%)-TZP* was used in this sintering study. The average particle size and the specific surface area of this powder were measured as 0.065 μm and 16.5 m^2/g, respectively. The green samples were isostatically pressed at 294 MPa as 4 mm diameter rods. The samples were presintered in air at 1150° C for 1 hour.

The 2.45 GHz microwave sintering system is shown schematically in Fig.1. Sintering tests of Y-TZP samples were performed in a high Q rectangular TE_{10n} single mode applicator. The structure and components of this applicator have been well designed for the purpose of sintering various ceramics[5]. Optimal coupling and tuning were accomplished by adjusting the position of a moving plunger and the size of an adjustable iris. Surface temperatures were measured by an optical fiber pyrometer and controlled by varying input power. Sintering temperatures varied from 1250° C to 1600° C. Polished specimens were thermally etched in air at 1200° C for 4 hours to reveal the microstructure. Grain size was measured on SEM micrographs by stereological methods. Densities were measured by the Archimedes method.

---

* Tosoh corporation, Japen.

RESULTS AND DISCUSSION

Wilson and Kunz reported that they were unable to heat up Y-TZP green samples in their rectangular cavity because of its low microwave absorption at ambient temperature[3]. It was noted that although a movable reflector was used for tuning, the lack of optimal coupling, as no iris shown in the diagram of their cavity, seems to be the reason for their failure of heating up Y-TZP samples.

In this study, a set of circular plate iris and a high Q adjustable iris were used to investigate the effects of coupling conditions on heating Y-TZP samples. The usefulness of high Q adjustable iris in heating ceramics with low loss factors was discussed elsewhere[5]. It was possible to heat up Y-TZP samples from room temperature to 1000-1200° C with the small plate iris of 27.5 mm and 37.5 mm diameters but was impossible to do so with the large plate iris of 42.5 mm and 50 mm diameters. However, the maximum temperatures reached with full input power (800W) were limited to below 1250° C and 1000° C with 37.5 mm and 27.5 mm iris, respectively. Sintering tests were unable to be performed at these low temperatures.

Y-TZP samples were heated up very rapidly from room temperature to 1600° C or higher with the high Q adjustable iris. During the heating process, the size of the adjustable iris was continuously adjusted from 24 mm at room temperature to 109 mm at above 1400° C (fully opened). This maintained the applicator in optimal coupling states of more than 95% energy efficiency at all times. The wide change of iris size with temperature indicated that the dielectric properties of Y-TZP changes dramatically with temperature. A small iris size was required for critical coupling at room temperature due to the low dielectric loss. At sintering temperatures, its loss became very high and a big iris must be used for optimal coupling. The variation of temperature with input power for different iris was plotted in Fig.2. It is seen that using an adjustable iris instead of a plate iris improved energy efficiency significantly.

It was also reported previously that Y-TZP green samples cracked frequently during rapid sintering[3,4]. We had the same problem with cracking when the green samples were presintered at 800° C. The onset of cracking was observed

to be prior to the commencement of shrinkage. Further tests with varying the presintering temperatures revealed that there was a critical presintering temperature of 1150° C beyond which the cracking of green sample could be eliminated. X-ray analysis of the original powder and the green samples identified the existence of 6% and 3.5% monoclinic phases in the original Y-TZP powder and in the green sample presintered at 1100° C, respectively, but no monoclinic phase was detected from the green samples presintered at the temperatures above 1150° C. Fig.3 shows the x-ray diffraction pattern of the 1100° C presintered green sample. It is known that there is 9% volume change when ZrO_2 transforms from monoclinic phase to tetragonal phase[6]. Therefore, it is reasonable to believe that the cracking was induced by the high stresses from the large volume changes associated with this phase transformation during microwave sintering. In order to avoid the cracking problem, a presintering temperature of 1150° C is necessary for eliminating the residual monoclinic phase.

All the green samples were presintered at 1150° C in air for 1 hour. The sintering tests were performed at different temperatures using the adjustable iris for coupling. Y-TZP green samples were rapidly heated up to 1100° C with a small hot zone initially appeared at the center of the applicator. A slow heating was followed between 1100-1200° C to reduce the chance of cracking. Once the temperature passed through 1200° C without sample cracking, a stable sintering temperature can be maintained with constant power supply. Shrinkage commenced at temperatures between 1200-1300° C. The samples were smoothly translated through the cavity at 1 cm/min and sintered to a high density. As the temperature increase, a uniform hot zone grew rapidly over the sample due to the rapid increase of the thermal conductivity with temperature. It is significant to note that thermal runaway phenomena frequently encountered in the sintering of ceramics was not observed in the sintering of Y-TZP which may be attributed to the fact that Y-TZP has a high melting point and a high thermal conductivity at sintering temperatures. The temperature dependence of the density and the grain size as a function of density are plotted in Fig.4 and Fig.5, respectively. It is seen that fine grain sizes of 0.2-0.3 μm and high densities of 98-99.5% TD were achieved with sintering temperatures of 1200-1600° C. A typical microstructure of a microwave sintered Y-TZP sample is

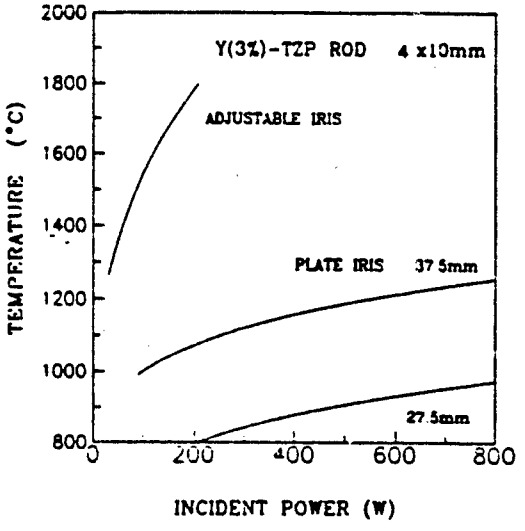


Fig.2 Variation of Temperature with Incident Power for Different Iris.

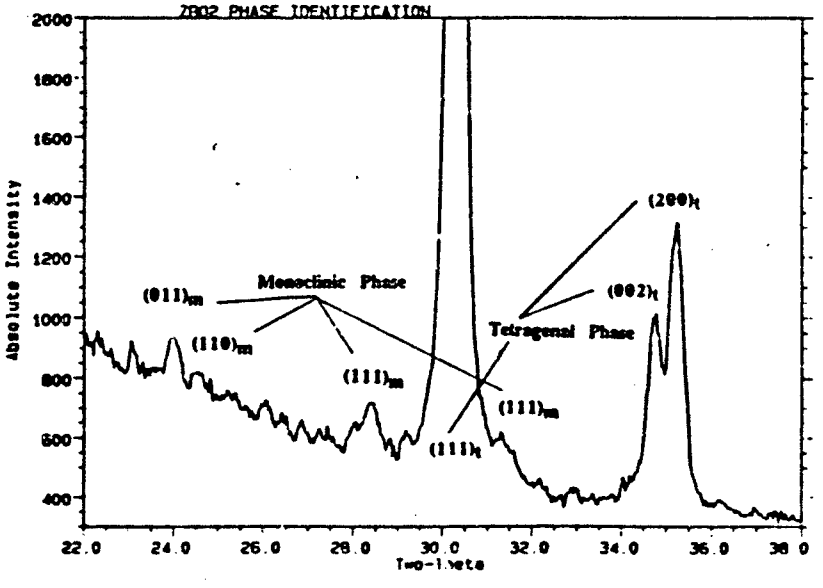


Fig.3 X-Ray Diffraction Pattern of Y-TZP Green Sample Presintered at 1100° C.

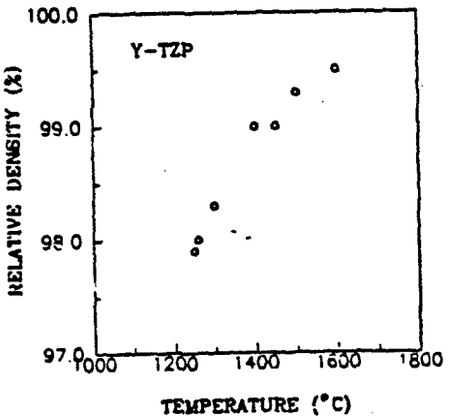


Fig.4 Density of Y-TZP Sample as a Function of Sintering Temperature.

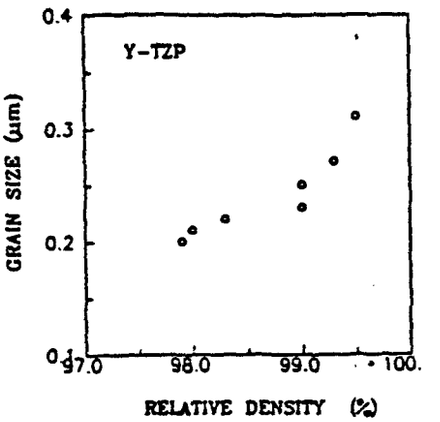


Fig.5 Grain Size vs Density of Microwave Sintered Y-TZP.

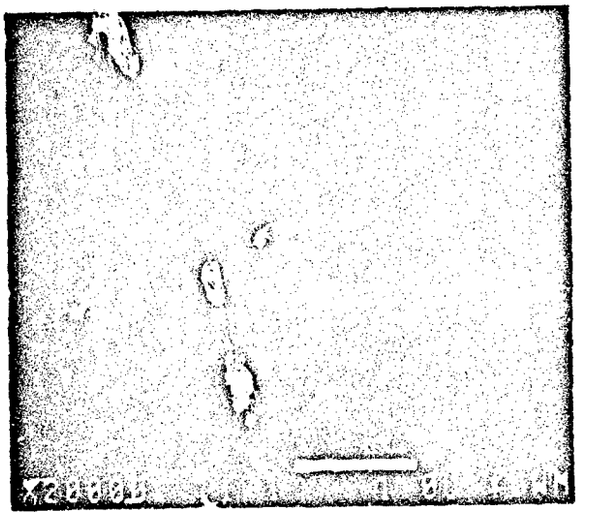


Fig.6 Microstructure of Microwave Sintered Y-TZP. Sintering Temperature: 1250 C; Density: 98% TD; Grain Size: 0.2 μm.

illustrated in Fig.6. These results indicate that ultra-fine low submicron grained Y-TZP is readily achieved by microwave sintering. However, further decreases of the grain size to nanosizes seem to be difficult because of the pre-growth of the particles at the high presintering temperature of 1150° C. If pure Y-TZP powder without residual monoclinic phase becomes available, presintering temperature can thus be reduced and microwave sintering may have the potential to produce the nanosize microstructure.

SUMMARY

Rapid sinterting of Y-TZP has been achieved in a single mode applicator by microwave heating. Critical coupling and tuning is essential for direct heating of Y-TZP from room temperature to sintering temperatures. Ultra-fine grain sizes of 0.2-0.3 μm and high densities of 98-99%TD can be achieved by microwave sintering of Y-TZP. The problem of phase transformation induced cracking during rapid sintering of Y-TZP may be solved by raising the presintering temperature to remove the residual nonoclinic phase in green samples. Microwave sintering has the potential to produce nanosize microstructure if pure Y-TZP powder without monoclinic phase becomes available.

ACKNOWLEDGEMENTS

This work is being supported by National Natural Science Foundation of China under grant No. 58972097.

REFERENCES

1. Y.L. Tian, D.L. Johnson and M.E. Brodwin, "Ultrafine Microstructure of Al_2O_3 Produced by Microwave Sintering", Ceramic Powder Science II, p.925-932, 1987.

2. Y.L. Tian, D.L. Johnson and M.E. Brodwin, "Microwave Sintering of Al_2O_3-TiC Composites", ibid, p933-938, 1987.

3. J. Wilson and S.M. Kunz, "Microwave Sintering of Partially Stabilized Zirconia", J. Am. Ceram. Soc., 71 [1] C-40-C-41, 1988.

4. D.L. Johnson and M.E. Brodwin, "Microwave Sintering of Ceramics", U.S. Army Research Office, Grant No.DAAG

29-80-K-0031, 1984.

5. Y.L. Tian, B.S. Li, J.K. Guo and D.S. Yen, " A microwave Processing System for ceramics with Improved Energy Efficiency and Processing Control", Proceedings of the 25th IMPI Microwave Power Symposium, p13-14, 1990.

6. T.K. Gupta, J.H. Bechtold, R.C. Kuznicki, L.H. Cadoff and B.R. Rossing, "Stabilization of Tetragonal Phase in Polycrystalline Zirconia", J. Materials Science, Vol.12, p2421-2426, 1977.

Section IX. Novel Applications of Microwave Energy

MICROWAVE PROCESSING OF POLYESTER AND POLYESTER/GLASS COMPOSITES.

Ursula Hottong, Jianghua Wei, Ramakrishna Dhulipala, and Martin C. Hawley
Department of Chemical Engineering, Michigan State University, East Lansing, MI 48824

ABSTRACT

Keywords:microwave processing; polyester; polyester/glass composite; extent of cure; dielectric measurement; mode switching

Polyester resins and polyester/glass composites were processed using 2.45GHz microwave radiation in single mode resonant cavities. An alkyl phthalate polyester resin (diluted with vinyltoluene) and a unidirectional glass fiber/polyester (diallyl phthalate) prepreg were examined. In the study of polymerization kinetics, a 6 inch diameter resonant cavity and a thin film technique were used to cure neat resin samples. Thermal curing was carried out for comparison. The extents of cure of the samples were determined using Fourier Transform Infrared Spectrophotometry (FTIR). Faster reaction rates were observed during microwave cure compared with those of thermal cure. In addition, microwave curing initiated the reaction at a lower bulk temperature in a shorter time. The complex dielectric permittivity of the cured and uncured resins at room temperature were measured using a swept frequency method in a TM_{012} mode. Fully cured samples were microwave heated in various resonant modes in the 7 inch cavity and temperature distributions for each mode were measured. These measurements were used to determine which combinations of modes could be used to produce uniform heating of uncured samples in a mode switching technique. It was shown that a relatively uniform temperature distribution can be achieved in both fresh and fully cured composites using a mode switching technique.

INTRODUCTION

Microwave processing has been investigated as an alternative to conventional

thermal processing of polymers and composite materials. Single-mode, cylindrical microwave resonant cavities have been developed at Michigan State University to process polymers and composites with controlled heating cycles. These microwave methods offer potentially faster and more controllable cures than conventional thermal methods. Enhanced properties have been obtained for epoxies and graphite/epoxy composites processed in microwave cavities.[1,2,3,4]

Polyester resins are often used as matrix material for composites because of their comparatively low cost and easy molding at low temperatures. In addition, they have excellent electrical properties, good mechanical properties, and require short cure cycles. Typical applications in manufacturing processes are Sheet Molding Compounds (SMC), Pultrusion, and Filament Winding.

The goal of the research is to demonstrate the feasibility of processing polyesters and polyester/glass composites using microwave technology.

EXPERIMENTS

The details of microwave processing and diagnostic system have been described previously [5]. There are four major units in the system. They are microwave generating circuit, cylindrical tunable resonant cavity, fluoroptic temperature sensing system*, and closed-loop, feedback control and data acquisition unit. The essential part of closed-loop, feedback control is a coaxial switch which turns the microwave power on and off to maintain isothermal conditions. This switch was regulated by a dc power supply that was controlled by an I/O interface board in the data acquisition system. Actuation of the on/off switch was automated with a computer in response to temperature feedback from the fluoroptic temperature sensing system.

Microwave processing experiments of both neat polyester resin and polyester/glass composites were conducted. An n-alkyl phthalate polyester was chosen for the neat resin studies. Vinyltoluene(30 wt%) was used as the crosslinking monomer for this study. Benzoylperoxide(1%) was added as a catalyst. Glass fiber (70 wt%) composites with a diallyl phthalate polyester as matrix material were used in the composites study. The prepreg was a 1.6cm wide x 0.3cm thick tape.

In the neat resin study, both reaction kinetics and dielectric properties were studied. A thin film technique was used in the reaction kinetics study to avoid

---

* Fluoroptic temperature sensing Model 750, LUXTRON, Mountain View, CA

large temperature gradients. The extent of cure was determined using Fourier Transform Infrared Spectroscopy**. In the preparation of the thin film polyester samples, about 4 mg of the resin mixture was evenly distributed on a potassium bromide (KBr) disk (13 mm in diameter, 1 mm in thickness). Another disk, with a hole in the center for insertion of the temperature probe, was placed on the top of the resin. KBr was chosen because of its transparency to infrared and microwave radiation. Fresh thin film samples were scanned in the FTIR before cure. Samples were isothermally microwave cured at 85, 100, and 115°C for various times employing the TE_{111} mode in a 6" dia microwave cavity. The sample was placed in the center of the cavity where the E-field is the strongest. The cavity was manually adjusted to maintain the resonance during the microwave cure. Thermal cure experiments were carried out for comparison. All samples were quenched in dry ice at specified times and scanned in the FTIR. The extent of cure of the processed polyester was calculated using the following formula.

$$\alpha = 1 - \frac{\left[\frac{A_{900}}{A_{1600}}\right]_{cured}}{\left[\frac{A_{900}}{A_{1600}}\right]_{uncured}} \qquad (1)$$

where A_{900} is the area under the analytic absorbance peak of the reacting alkyl group and A_{1600} is the area under the reference absorbance double peak of the nonreacting ortho disubstituted benzene ring. The reference peak is used to compensate for possible changes in the film thickness during cure.

In the measurement of the complex permittivity of polymer materials, swept frequency methods were developed based on a TM_{012} mode and the cavity-material perturbation theory. The detailed experimental procedures were reported previously [5].

In the microwave study of polyester/glass composites, a 7 inch dia cavity was used with constant input power of 60 watts. The composite sample was 3 inch by 3 inch and was made from the prepreg tape. There were two parts in this study. The first part was a single mode study with focus on the microwave heating characteristics of a fully cured sample in various resonant modes. This part enabled us to find the combination of modes which could achieve a uniform temperature distribution in a cured sample. Second was mode-

** FTIR Model 1850, Perkin Elmer, Norwalk, CT

switching study in which fresh polyester/glass composites were processed using a combination of the modes found in the first part. Several midplane temperatures and/or surface temperatures were measured during both parts of the study. In the single mode study, the sample was heated until one of the temperatures reached 180 °C or the time limit of 20 minutes was exceeded. The uncured sample was placed inside a vacuum bag, covered with a nonporous release film and the temperatures measured on top of the film.

RESULTS AND DISCUSSION

Figures 1, 2 and 3 show the extent of cure versus time profiles for thermal and microwave processed thin film samples. Higher reaction rates were observed in microwave curing as compared to thermal curing. At lower cure temperatures, such as 85 °C, the ultimate extent of cure is higher in microwave cure than in thermal cure as shown in Figure 1.

Figure 4 shows the temperature-time profiles in microwave cure at constant power, and thermal cure at constant oven temperature. The sample in the microwave environment reached the intended temperature faster, and with a lower peak exotherm temperature than the sample in the oven. Microwave heating initiated the reaction at a lower bulk temperature than thermal heating.

The dielectric constant ϵ', and the loss factor ϵ'' of the uncured and the cured samples measured using the swept frequency method at room temperature are:

$\epsilon' = 3.2 \pm 0.2$ and $\epsilon'' = 0.051 \pm 0.003$ for the uncured polyester and
$\epsilon' = 3.4 \pm 0.3$ and $\epsilon'' = 0.033 \pm 0.002$ for the cured polyester.

Table 1 contains a summary of results for the single mode heating experiments. Lc and Lp in the second column represent cavity length and coupling probe length for the single mode heating. Columns 3 and 4 are listings of maximum temperature differences in the interior and overall, respectively, at the end of each run. All heating with single modes exhibited poor temperature uniformity. Runs #2, #3 and #4 had the best heating efficiencies. Due to their high heating rates, these runs reached the control temperature of 180 °C within 7 minutes. The overall temperature difference ranged from 140 °C to 57 °C. The interior temperatures were most uniform (ΔT = 26 °C) for run #5. The nonuniformities were due to two factors, 1) the nonuniform E-field and 2) the low thermal conductivity of the matrix and the fibers. Column 5 shows the relative values of the four interior temperatures at each location. Numbers of 1 to 4 were used to represent the location of the lowest to the highest temperature. This information was used to develop the mode switching technique to process composites using modes with complementary heating patterns. Runs 1 and 2

were nearly complementary and were used for mode switching processing.

Table 1 Summary of Experimental Results

run #	L_c/L_p [cm/mm]	ΔT inside	ΔT all	#T-profile high - low	heat rate
1	6.403/18.15	84 °C	90 °C	4 2 3 1	medium
2	8.427/14.31	72 °C	72 °C	1 3 4 2	high
3	11.50/15.44	68 °C	104 °C	1 2 3 4	high
4	11.51/20.75	112 °C	140 °C	4 1 2 3	high
5	11.67/20.27	26 °C	57 °C	1 2 3 4	medium
6	13.17/16.19	71 °C	93 °C	4 2 3 1	low
7	14.93/12.38	44 °C	44 °C	4 2 1 3	very low

Figures 5 and 6 show the temperature time profiles for microwave heating of the cured and uncured sample, respectively, using the mode switching technique. The temperature profiles are relatively uniform compared to the individual single modes and are controllable by mode switching. The temperature distribution is within 20 celsius for fresh samples. These experiments demonstrate the promise of mode switching for temperature control during curing of composites. Additional benefits may be derived from variations in power or frequency switching.

CONCLUSIONS

A neat polyester resin(alkyl phthalate diluted with vinyltoluene) was cured using 2.45 GHz microwave radiation and a thin film technique. Microwave cure kinetics were compared to those of thermal cure. Faster reaction rate was observed in microwave curing as compared to that of thermal curing. Higher ultimate extents of cure were observed in microwave curing than in thermal curing at low cure temperatures. Microwave heating initiated the reaction at a lower bulk temperature than thermal heating. Microwave heating characteristics of a fully cured polyester/glass composite were studied using a 7" diameter

cavity and 2.45 GHz microwave radiation. Heating rates and temperature uniformity were strong functions of the resonant modes. No single resonant mode could produce a uniform temperature profile due to the nonuniform E-field and low thermal conductivity of the glass/polyester composites. A mode-switching technique using modes with complementary heating patterns was employed to obtain a uniform temperature profiles during microwave heating of both cured and uncured polyester/glass composites.

REFERENCES

1. J. Wei, J.D. Delong, and M.C. Hawley, Proceeding of the American Society for Composites, 5th Tech. Conf., 239, June,1990.

2. R. Agrawal, and L.T. Drazl, J. Adhesion, 29, 63, 1989.

3. J. Wei, Y. Chang, B. Thomas, and M.C. Hawley, ICCM/VIII Conf., Honolulu, Hawaii, July 1991.

4. J.D. Delong, J. Jow, and M.C. Hawley, 2nd Topical Conf. on Emerg. Tech. in Mat., Am. Inst. of Chem. Eng., San Francisco, CA, 1989, paper 220c.

5. J. Jow, Michigan State University, Ph.D Thesis 1987.

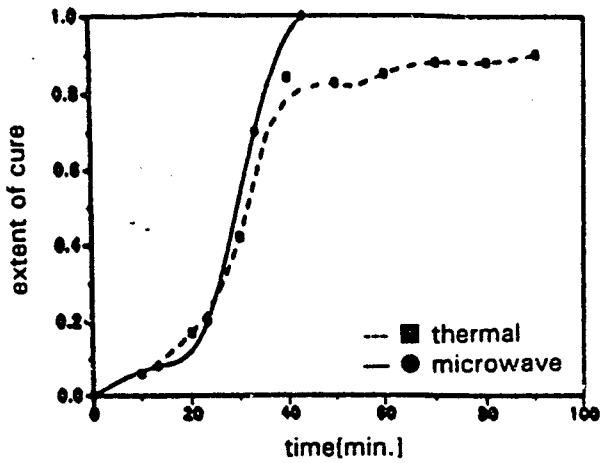


Figure 1. Extent of cure Versus time profile for thin film polyester samples at cure temperature of 85°C

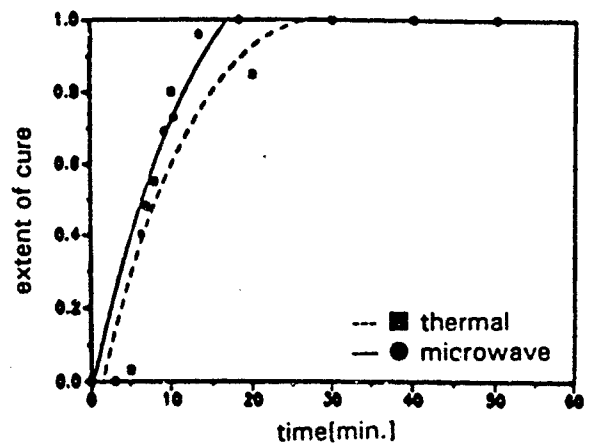


Figure 2. Extent of cure Versus time profile for thin film polyester samples at cure temperature of 100°C

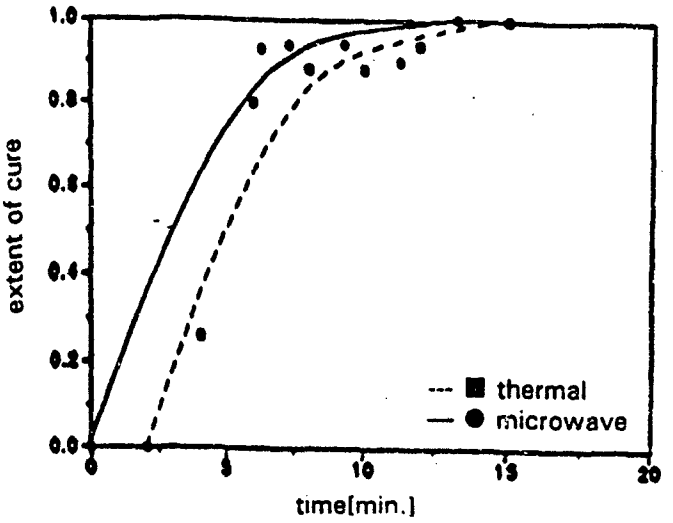


Figure 3. Extent of cure versus time profile for thin film polyester resins at cure temperature of 115°C

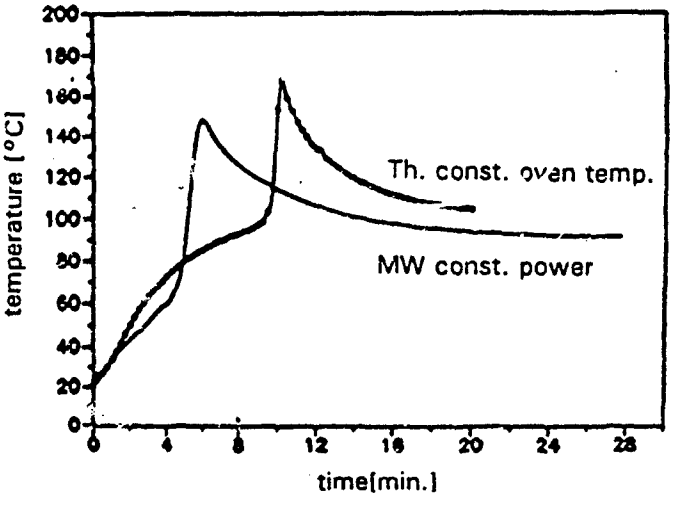


Figure 4 Temperature profiles during microwave and thermal processing of polyester resins

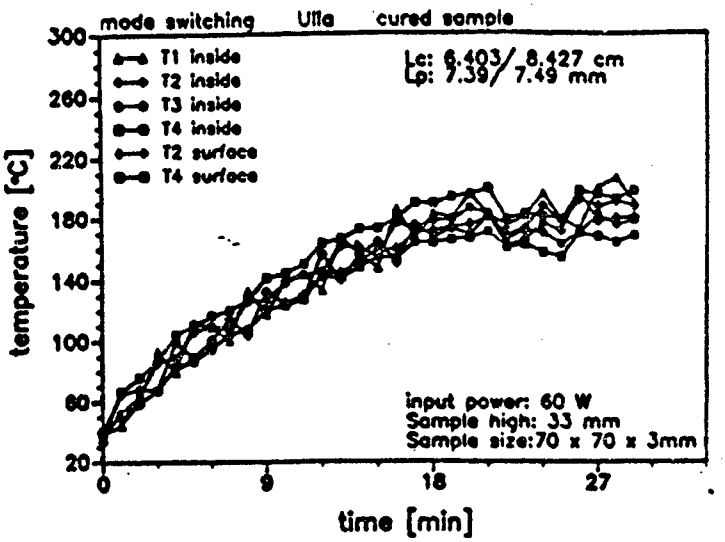


Figure 5 Temperature profiles during microwave heating of cured glass/polyester composite using mode switching technique

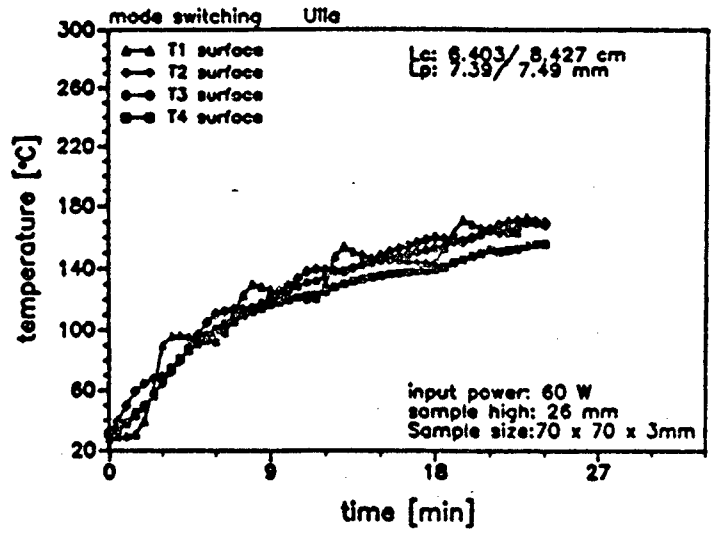


Figure 6 Temperature profiles during microwave processing of uncured glass/polyester composite using mode switching technique

USE OF A TM_{010} MICROWAVE CAVITY AT 2.45 GHz FOR AEROSOL AND FILAMENT DRYING

D. E. Christiansen and W. P. Unruh
Los Alamos National Laboratory
Los Alamos, NM 87545

ABSTRACT

As part of the development of a generic spray-drying process for aerosol preparation of homogeneous powders of complex metal oxide systems, we have investigated the use of 2.45 GHz power in a high-Q single-mode TM_{010} cavity coupled directly to aerosols of aqueous solutions. Partial success was attained with a concentrated solution of ferric nitrate. Although all particulates showed drying, only a few percent of the particles were fully dried prior to collection. The cavity operated at a power level just below that sufficient to cause electric field breakdown in the carrier gas (dry nitrogen). The large inherent dielectric shielding of the spherical droplets makes it difficult to couple enough power into an aerosol at 2.45 GHz to overcome the heat loss from individual droplets to the surrounding gas and achieve full particulate drying. The calculated and measured dielectric shielding of a thin cylinder of water aligned with the cavity electric field is very much smaller. We have produced heating rates in water ~600 times more rapid than could be achieved with aerosols. This suggests using 2.45 GHz microwave power for drying extruded filaments and then calcining those dried filaments to ceramic fiber.

INTRODUCTION

The use of microwave power to dry fine sprays of solutions of oxide systems has several attractive aspects. The solutions may be formulated to produce complex oxide powders directly as the droplets are evaporated. The evaporation rates may be adjusted over a wide range, and even controlled in a feedback system, to produce particular product characteristics. Controlling the nozzle itself to yield an aerosol of uniformly-sized droplets would result in particulates which are quite monodisperse, and would allow powder production in any convenient size, down to nanoparticulates, by adjusting the droplet diameter and solution concentrations appropriately. Furthermore, after the droplet stream has been dried, additional thermal processing in the same (or a spatially related) microwave field may be attained. Thus, it seems possible to design a highly-efficient integrated system to spray, dry and process complex metal solutions to quality powders in a controlled manner using microwaves.

Initial experiments have been completed using a 3 kW commercially-available 2.45 GHz microwave source coupled to a single-mode TM_{010} cavity. The resulting axially-uniform microwave electric field has been coupled to two different aerosol generators.

THE EXPERIMENTAL SYSTEM

I. The Microwave Supply and Cavity System.

The microwave supply and cavity system is shown in Figure 1. The 3 kW power generator* is designed for low ripple and stable frequency and power output. The transmission and coupling system is designed to isolate the magnetron source from the high-Q cavity, through careful matching, to prevent phase-shifted cavity reflections from disturbing the operating frequency of the magnetron. This provides a spectral purity of less than 300 kHz, narrow enough to match over 95% of the power into the cavity. A variable-stub tuner provides power level adjustment up to a maximum of 2.2 kW (reduced from 3 kW by system losses) incident on the cavity coupling iris and allows operation of the magnetron at constant power and frequency. Essentially all of the incident microwave power is dissipated in the cavity walls, which are cooled at a temperature above ambient (~30° C) to prevent condensation. A system of cavity coupling irises, of the beyond-cutoff type, allows us to externally reduce the operating Q of the cavity from a maximum of ~9600 and to critically couple microwave power from the source into the cavity.

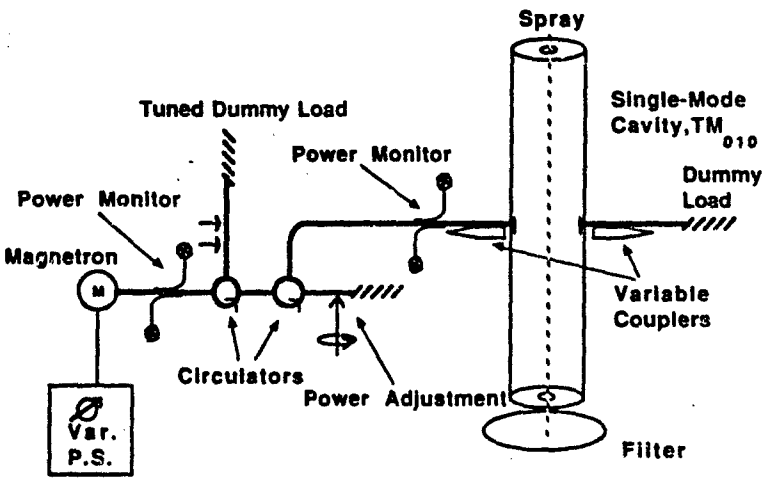


Figure 1. Functional diagram of the microwave and cavity system.

*Gerling Laboratories, Modesto, CA, Model GL119.

This flexible system makes it possible to fully couple any power level into the cavity and thus achieve any microwave electric field up to, and including, breakdown in dry nitrogen. Directional couplers allow us to measure the power bled from the cavity (in adjusting its Q) and to measure incident and reflected power, thus providing accountability of all power in the sytem. The high isolation between the microwave power source and the cavity-coupling system provides great flexibility in setting up the appropriate parameters. We can attain the electric field intensity desired with a high degree of control and stability of the system. After a few minutes warm up, the magnetron source can be run open loop, without feedback control, maintaining its tuning on the cavity resonant frequency for long periods of time without adjustment.

II. THE AEROSOL GENERATORS AND GAS FLOW SYSTEM

Two droplet generators have been used in these studies. The first, a commercial unit*, consists of an ultrasonically-driven nozzle which produces a polydisperse conical spray (half angle of ~40 degrees). It is capable of a liquid throughput of $\sim 2 \times 10^{-8}$ $m^3 s^{-1}$ (1-2 ml/min). The conical spray does not conform well to the axial microwave electric field in the cavity. A significant fraction of the droplets are able to migrate to the cavity walls and are deposited there in a region where the electric field is near zero. They eventually accumulate a layer of fluid and/or dried solute which must be removed mechanically.

The second design, while more difficult to maintain, has been more satisfactory from the viewpoint of producing sprays which are better characterized and more convenient to use in the microwave system. A reservoir holding the solution is pressurized at ~30 psi and delivered through a filter to a nozzle whose diameter is ~1/2 the desired droplet diameter. This fine nozzle is mounted in a piezoelectric transducer which produces an oscillatory disturbance in the laminar stream of fluid leaving the nozzle. The resulting coherent disturbance (typically excited at ~250 kHz) forces the growing instabilities in the detached stream to be equally spaced along the flow, so that the droplets generated are uniform in both spacing and diameter. An example of the droplet stream obtained is shown in Figure 2.

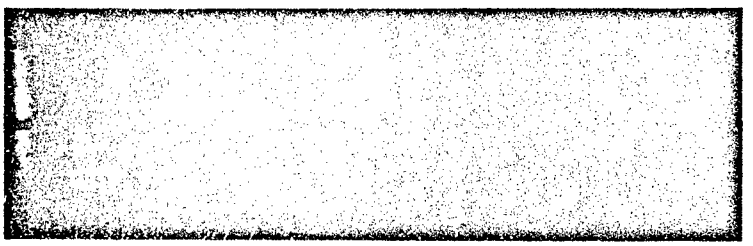


Figure 2. The droplet stream produced by the coherent generator. Final diameter is approximately 30μm. This time exposure (~200 sec.) shows the exact coherence of the stream.

*Sono-Tech Corp., Poughkeepsie, NY, Model 8700-120MS.

This stream is directed axially into the microwave electric field in such a way that only detached spherical droplets enter the cavity. The interior volume of the cavity is filled with a carrier gas (dry nitrogen) which is introduced into the cavity through a seive of fine holes in the top cover of the cavity. The droplets are injected into this flow. Because of their small diameter, the droplets are immediately decelerated as they enter the cavity and are transported through the cavity at rest with respect to the carrier gas, moving at about 0.05 m/sec. Most of the particulates are deposited on a filter just below the mesh screen which forms part of the bottom end cap of the cavity. A mild underpressure is applied to the filter by means of a small vacuum pump at the exit of this system to enhance the flow, as desired, and make particulate collection on the filter more complete. However, the cavity itself is always maintained at ambient (or slightly higher) pressure during the processing.

With the microwave power being stably coupled into the cavity and the carrier gas flow established, the droplet generator is started and mounted on the cavity while running, so only the desired droplet distribution is introduced into the operating cavity. After a few seconds (enough time to collect particulates on the filter), the droplet generator is removed and microwave power turned off. Collected particulates are recovered from the filter for microscopic examination.

OBSERVATIONS

It is observed that drying is very slow at 2.45 GHz . Dried particles are shown in Figure 3. Only a few were dried fully (as judged from their morphology) by the microwaves. This result is consistent with the observation that introduction of droplets into the cavity disturbs the cavity frequency and Q only slightly, showing that the microwave electric field is only very weakly coupled into the droplets at this frequency.

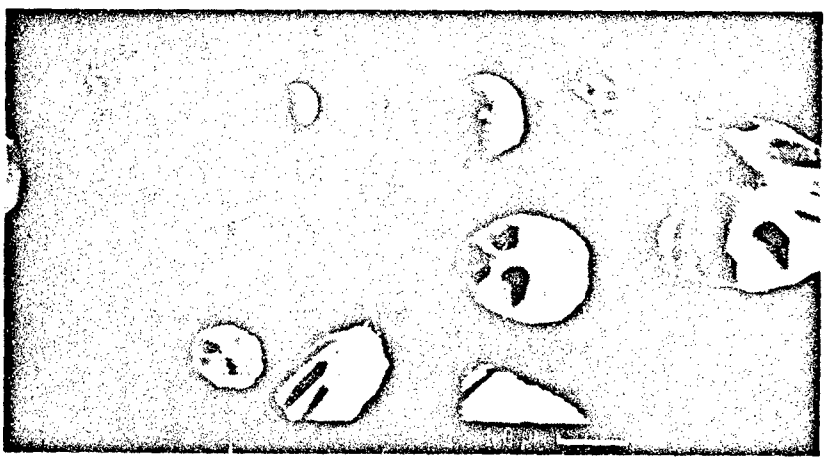


Figure 3. A sample of the particles collected from the cavity. Those with well-developed spherical shells are presumed to have been dried within the cavity by the microwaves.

In contrast, a very thin, unbroken cylindrical stream of water couples well to the cavity at this frequency, as evidenced by the much larger shifts of resonance frequency and Q. This greater coupling results in much stronger microwave heating of such a stream than of droplets. We estimate volumetric heating rates as much as ~600 times larger with this geometry. We have produced continuous boiling and pressurization to 6.9×10^5 Pa (100 psi) of a 300μm dia. stream of water confined in a small teflon tube, with negligible disturbance during operation of the frequency and Q of the microwave cavity. That is, boiling and superheating took place so rapidly, with so little extraction of the available microwave power, that the fluid stream penetrated the cavity only a short distance (perhaps 0.01-0.02 m) before being converted to steam at ~6.9×10^5 Pa.

Both results are to be expected from the basic electromagnetic boundary conditions governing interaction of the applied microwave electric field with the water solution. The microwave energy dissipation within the droplet is given by

$$(dq/dt)_\mu = (55.63 \times 10^{-12}) k''(E_{int})^2 \omega_0 \text{ W/m}^3, \qquad (1)$$

where E_{int} is the rms microwave electric field at angular frequency ω_0 in the interior of the solution and k" is the relative imaginary dielectric constant of the solution. For water the relative real dielectric constant at 27°C is k' ~80. In spherical droplets a standard calculation using the electromagnetic boundary conditions shows that the internal electric field is reduced by the factor 3/(k'+2), which decreases the microwave energy dissipation by ~750. On the other hand, because the tangential electric field is continuous across a dielectric boundary, the internal field in a long thin dielectric oriented parallel to the applied microwave electric field is approximately equal to the applied field in the cavity. Thus volumetric heating of filaments and fibers, suitably oriented to be parallel to the applied microwave electric field, will be much more effective than attempts to heat small spherical droplets directly.

Because of the large ratio of surface area to volume for small droplets, this direct method of volumetric heating cannot significantly raise the interior temperature of individual droplets if a frequency of 2.45 GHz is used. In effect, the thermal conduction through the droplet surface to the surrounding gas can remove the energy deposited volumetrically by the microwave field nearly as fast as it is deposited. This limitation holds up to and including applied microwave electric fields as high as breakdown in air, approximately 1 MV/m at 2.45 GHz.

One can respond to this constrast in behavior between droplets and filaments in two ways. First, because water solutions are polar, exhibiting Debye-like relaxation, increasing the applied microwave frequency will make the process of coupling to individual small droplets more efficient. This improvement results from both the increase in frequency (which drives the relaxation/dissipation cycle faster) and the two relaxation-coupled changes in the relative dielectric constants. With increasing microwave frequency, the relative real part, k', decreases, allowing better penetration of the applied microwave electric field, while the relative imaginary part, k", increases, resulting in more volumetric dissipation in the

droplet. Second, the relatively strong coupling to oriented fibers and filaments, even at 2.45 GHz, provides new and novel processing opportunities which can be exploited at the more conventional processing frequencies now authorized for use. These two points are discussed briefly in the following sections.

MICROWAVE-DROPLET INTERACTIONS

We have developed a preliminary numerical model of the evaporation and condensation of spherical droplets by sequentially solving and propagating in time the equations of heat conduction and mass transport at the droplet surface. This numerical simulation has been used to provide a qualitative understanding of the behavior of small droplets and to provide numerical scaling of heating effects at higher microwave frequencies.

The first-order differential equations[1,2] describing heat balance in the droplet and mass transport were used directly. Because the internally-heated droplet is not at equilibrium, no subsidiary equilibrium conditions are invoked. It is assumed that mass transport is driven by the difference in saturated vapor pressure at the droplet surface and the partial pressure of the vapor in the gas[2]. The latent heat of vaporization is used to compute, for each time step, the thermal loss due to evaporation, which is then added to the energy inputs from microwave losses and conductivity across the droplet boundary from the gas. The temperature dependences of k' and k"[3], the latent heat[2], the saturated vapor pressure of water[2], and the thermal diffusion and mass transport constants[2] were included in the computation. Higher-order contributions due to radial flow, 2nd-order conductivity corrections, surface tension, or relative velocity between droplet and gas were neglected, in the spirit of investigating the main effect of volumetrically depositing significant thermal energy within small droplets which are at rest in the ambient gas. In any case, these several corrections make only a few percent difference in the results[1], and can readily be included in the computations. The numerical results, displayed graphically, reproduce both evaporation and condensation phenomena (in the absence of an applied microwave electric field) in nominal agreement with published data, including the so-called b^2-law (mass loss/gain proportional to surface area)[1] known to be applicable to droplets larger than ~100μm dia. Significant deviations from this surface-area proportional evaporation rate are obtained at smaller diameters, in agreement with observations.

Introducing the volumetric energy deposition driven by an applied 2.45 GHz microwave electric field produces the following qualitative changes in modeled droplet behavior. 1) For larger diameters, the initial evaporation rate is greatly increased, greatly decreasing the total time to evaporation, as a consequence of the initial elevated droplet temperature allowed by a large volume/surface ratio. 2) As droplet diameter rapidly decreases under external heating, below ~ 50μm dia. the volumetric heating becomes progressively ineffective compared to conduction loss to the gas, allowing the internal temperature of the droplet to rapidly approach the dew point in the carrier gas, effectively slowing evaporation. If one starts with small droplets (say, smaller than ~30μm dia.), as would be used in the production of nanoparticulates, the microwave heating is essentially ineffective at 2.45 GHz.

Figure 4 compares the evolution in time of droplet temperature and radius for a 40μm dia. droplet with and without microwave heating.

As expected, increasing the applied microwave frequency, to take advantage of the more favorable dielectric parameters, makes a dramatic improvement in the calculated evaporation rates of very small droplets. Our computations indicate that it is possible to effectively heat and evaporate quite small droplets at frequencies of

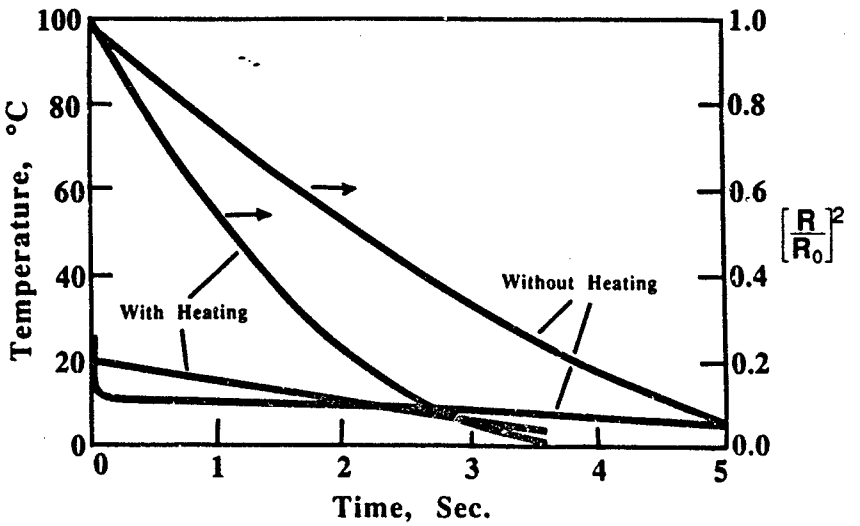


Figure 4. Droplet size and temperature evolution with and without microwave heating (2.45 GHz, 750,000 V/m), for an initial diameter 40μm at rest in 27°C nitrogen having a dew point of ~2°C.

10 GHz and above, at microwave electric fields substantially below breakdown in air.

MICROWAVE-FILAMENT INTERACTIONS

Because the internal microwave electric field in a long, thin cylindrical dielectric oriented parallel to an applied field is equal to the applied field, microwave heating rates can be achieved which are very much larger than in droplets. As indicated above, for water at 27° C the heating rate is ~ 750x higher in filaments than in droplets. This overwhelming increase in energy deposition, verified in our experiments on heating a cylindrical stream of water, makes possible a wide range of processing capabilities for fibrous and filamentary material, provided the orientation in the material can be maintained parallel to an applied microwave field during the processing stages.

DIELECTRIC CONSTANT MEASUREMENTS

The design of a microwave apparatus suitable for efficient drying of small droplets requires an understanding of the dielectric constants and cavity interaction

parameters of typical solutions of mixed oxides or nitrates at higher microwave frequency. We expect to demonstrate that the measured microwave interaction with droplets of such solutions can be well understood from published data and our own measurements. Because the major loss mechanism in our solutions is due to Debye-like relaxation of the water molecules, only a weak dependence on solution ionic conductivity is expected. A first step is to make comparative measurements using both coherent droplet streams and unconstrained cylindrical fluid flows of water and weak oxide or nitrate solutions. We are presently making these measurements, by means of cavity perturbation techniques, at 10 GHz and at 20 GHz. Because spherical droplets couple so weakly to an applied electric field, the use of coherent droplet streams in such measurements may provide a convenient way to obtain the dielectric parameters of lossy fluids at high microwave frequencies, where such measurements are quite difficult to make reliably.

CONCLUSIONS

Two conclusions result from this study. First, because of the unfavorable dielectric properties of water in conjunction with spherical geometry, coupling of 2.45 GHz microwave power to micron-sized aqueous droplets becomes comparable to the rate at which thermal energy is conducted to the surroundings, even for microwave electric fields approaching breakdown. Second, because of the much more favorable geometry, cylindrical aqueous streams are easily heated to evaporation with more modest microwave electric fields. Thus rapid microwave drying of aqueous sprays at 2.45 GHz may be difficult to achieve, while processing of filamentary aqueous materials should be very easy. Because of a favorable shift in dielectric properties, both processes would be more effective at higher frequencies.

ACKNOWLEDGEMENTS

Support for this work was provided by the DOE-CE/OIT Advanced Industrial Materials Program. We gratefully acknowledge discussions with and the technical assistance of Joel Katz, Frank Gac, Gerald Vogt, Brian Rusnak and James Kennedy.

REFERENCES

(1) N. A. Fuchs, "Evaporation And Droplet Growth In Gaseous Media," Pergamon Press (New York) 1959 (Translated From Russian).

(2) K. Masters, "Spray Drying Handbook," Wiley (New York) 1985, pp302, 667, 88.

(3) A. von Hippel, "Dielectric Materials And Applications," Wiley (New York) 1954, p.361.

EFFECT OF MICROWAVE HEATING ON SOLID STATE REACTIONS OF CERAMICS

Iftikhar Ahmad and David E. Clark
Department of Materials Science and Engineering
University of Florida
Gainesville, FL 32611

ABSTRACT

Solid state reaction studies were conducted on a zinc oxide-alumina system. Previous studies indicate the reaction kinetics of this system are diffusion controlled. Powder mixtures of similar particle sizes of reactants do not satisfy kinetic models either by conventional or microwave heating. With larger particle sizes of alumina, where reaction is limited by diffusion of zinc oxide through the product layer, microwave heating appears to enhance the reaction rate. An increase in compaction pressure results in an increase in the amount of product formed by conventional heating but shows a decrease in product formation with microwave heating.

INTRODUCTION

Microwave processing of ceramics appears to be an attractive alternative to conventional processing. The emphasis has been mainly in sintering of numerous ceramics and composites [1]. The reduction in processing time and temperature indicate higher sintering rates which are believed to be because of higher diffusion rates induced by the microwave field [2].

Although calcination and reactions between solids are important in ceramic processing only a few references, using microwave energy, are available in the literature [3,4]. Solid state reactions are usually carried out by intimately mixing fine ceramic powders and subjecting them to high temperatures. Under isothermal conditions, the rate of formation of the product may depend on the rate of diffusion [5]. Solid state reactions have also been studied by forming diffusion couples of polycrystalline as well as single crystal ceramics [6]. This investigation concerns the solid state reaction between zinc oxide and aluminum oxide powders to form zinc aluminate spinel (the product).

The reaction of ZnO and Al_2O_3 forming a stable compound, $ZnAl_2O_4$, is an interesting system and has been used extensively for the solid state reactions studies [6-11]. This reaction occurs at moderately high temperatures (800° C and higher). It has been demonstrated that the reaction is diffusion controlled and it proceeds only on the alumina particle by one-way transfer of zinc oxide through the product layer [7-10]. Zinc oxide vaporizes at higher temperatures

[12], so the reaction may be contemplated to proceed by the simultaneous action of solid state and evaporation-condensation mechanisms [9]. However, the vaporization of ZnO may not be considered as the rate controlling step in the formation of $ZnAl_2O_4$ [11].

Since the above reaction is diffusion controlled, if microwave heating results in enhanced diffusion, it should alter the reaction rates as well. The objective of this study was to observe whether microwave heating enhances the reaction of zinc oxide and alumina.

MATERIALS AND METHODS

High purity (>99.9%) alumina powders [a] were used in this study. These powders have mean particle sizes of 0.18μ m, 0.4μ m and 0.68μ m, respectively. Chemically pure (99.9%) laboratory grade zinc oxide [b] used had an average particle size of 0.3μ m.

Equimolar mixtures of alumina and zinc oxide were prepared by wet mixing in deionized water for 30 minutes. Small zirconia milling media was used to ensure proper mixing of the powders. The mixture was then dried in a conventional furnace [c]. The powder mixture was weighed in a fused quartz crucible and placed either in the microwave oven or the conventional furnace for reacting isothermally in the temperature range of 600 - 1100° C. Specimens weighing 4 grams were pressed [d] to pressures ranging from 2000 psi to 8000 psi to see the effect of compaction on the solid state reaction of zinc oxide and alumina.

For conventional heating of the specimens the furnace was preheated to the desired temperature and the reactant mixture was placed in the furnace. At the end of the reaction period, samples were removed from the furnace and allowed to cool in air. In case of the pressed samples, the sample was placed on another similar pressed sample of the same composition to avoid any contamination on the base of the sample.

Microwave heating was carried out in an industrial microwave oven [e] operating at 2.45 GHz capable of delivering a maximum power of 6.4 KW. However, only 1.6 KW were used for these experiments. Temperature was monitored with a thermocouple and controlled [f] by pulsing the output power. Since alumina and zinc oxide do not couple very well at room temperature, a susceptor was used to assist the powder mixture to attain higher temperatures, where it couples efficiently with microwave energy. With the susceptor around the sample one gets uniform

---

[a] AKP-50, AKP-30, AKP-15, Sumitomo Chemical Company, Ltd.

[b] Aldrich Chemical Company.

[c] Blue M Stabil-Therm.

[d] Carver Laboratory Press.

[e] Raytheon Radarline Microwave Oven Model QMP 2101A-6.

[f] Inconel shielded K-type thermocouple and Process Controller Series CN8600 from Omega.

heating with almost no temperature gradient within the sample. This has been established in our laboratory on ultra-rapid sintering of alumina, with what we refer to as, microwave hybrid heating [13,14].

Quantitative x-ray analysis [9] was used to ascertain the extent of reaction by determining the amount of spinel formed. A unified matrix-flushing method for quantitative multicomponent analysis reported by Frank H. Chung [15-18] was used. In this method the calibration curve procedure is shunted and all components can be determined. The weight fraction of any component in a multicomponent system is expressed in terms of the intensity ratios I_i/I_j and k-ratios ($k_i/k_j = I_i/I_j$). The use of the intensity ratio makes it immune to many sources of errors [15]. This method was verified to give experimental values within 2 percent of the synthesized values. The intensities of the 002 plane, 104 plane and 311 planes were used, respectively, for zinc oxide, aluminum oxide and zinc aluminate spinel.

RESULTS AND DISCUSSION

Homogeneous mixtures of zinc oxide and aluminum oxide were heated either in the microwave oven or the conventional furnace for reaction in the temperature range of 600° C-1100° C. No zinc aluminate (spinel) formation was observed below 800° C, which is in agreement with the results reported in the literature [7,8]. Hence, in most of the cases only the results for temperatures 800° C and above are presented.

Since this reaction is reported to be diffusion controlled, an attempt has been made to try to fit the data obtained to the diffusion controlled Valensi-Carter model [7] given by

$$K_{VC}\,t = \{\Delta - [1+(\Delta-1)x]^{2/3} - (\Delta-1)(1-x)^{2/3}\}/(\Delta-1) = f(x) \qquad (1)$$

where x is the extent of reaction and Δ is the change in volume between reactants and product. If f(x) is plotted against the time t, a straight line of slope K_{VC} should be obtained which defines the reaction rate constant. In order for the model to hold the straight line should pass through the origin.

Microwave Heated Samples

The data obtained by heating the mixture of alumina (AKP-50, average particle size 0.18 μm) and zinc oxide (average particle size 0.3 μm) in the microwave oven are shown in Figure 1. They show the weight percent spinel formed versus reaction time for temperatures ranging from 800 - 1100° C. Figure 2 shows an attempt to fit the data to Valensi-Carter model. For temperatures of 800, 850 and 900° C the straight lines pass through the origin indicating that for these temperatures the data satisfies the diffusion controlled Valensi-Carter model. However, above 900° C straight lines are obtained with almost the same slope with increasing temperatures and do not pass through the origin. This indicates that at these temperatures either the reaction is not diffusion controlled or the model does not hold for reaction with microwave heating. Since it has been shown that this model is valid [7] for conventional

[9] Philips Automated Powder Diffractometer System Model APD-3720.

heating, one might wishfully think that reactions in the microwave heating are not limited by diffusion.

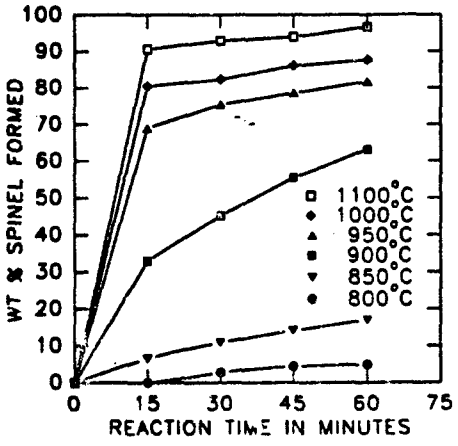


Figure 1. Microwave heating of the mixture of alumina AKP-50 and zinc oxide at different temperatures. The spinel formation with increasing heating time is shown for each temperature.

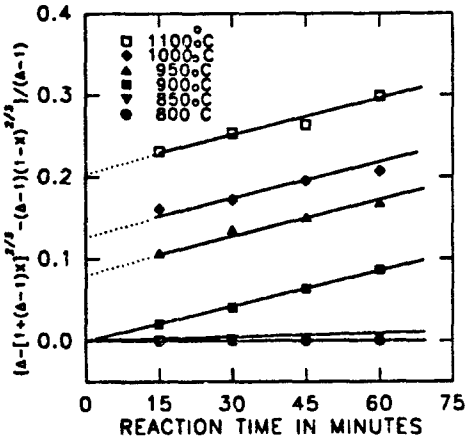


Figure 2. Microwave heating of mixture of alumina and zinc oxide. Attempt to fit the experimental data to Valensi-Carter model.

Conventionally Heated Samples

Since this reaction by conventional heating should satisfy the Valensi-Carter model [7], it seemed essential to repeat the reactions of the same powders by conventional heating. Figure 3 shows the weight percent of spinel formed as a function of reaction time for various temperatures. The data for conventional heating used in Valensi-Carter model is shown in Figure 4.

Comparison and Discussion

In the case of conventional heating of the mixtures, the spinel formation data does not satisfy the Valensi-Carter model for temperatures above 900° C, but certainly differs from that for microwave heating. The straight lines for the 1000° C and 1100° C appear to pass through a common point on the y-axis, which is not observed in the microwave heating case.

For temperatures up to 900° C, reactions both in microwave heating and conventional heating appear to be diffusion controlled. Above 900° C there is a abrupt increase in reaction until the first data point at 15 minutes and then the reaction rate decrease for the subsequent times. This can be understood by the fact that zinc oxide vaporizes at higher temperatures [12]. Below 900° C the reaction proceeds because of the contacts of the powder particles of zinc oxide and

alumina. The zinc oxide has to diffuse through the spinel formed at the points of contact to allow further reaction and the process is, therefore, diffusion controlled. As the temperature

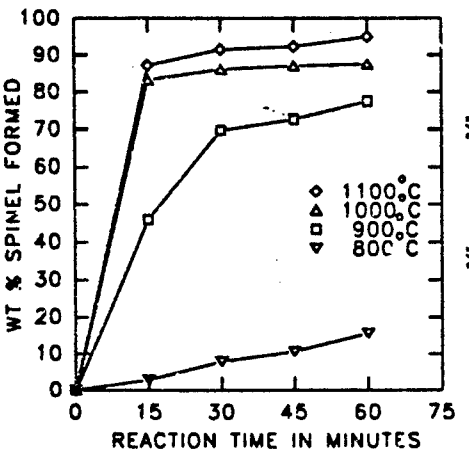


Figure 3. Conventional heating of the mixture of alumina AKP-50 and zinc oxide at different temperatures. The spinel formation with increasing heating time is shown for each temperature.

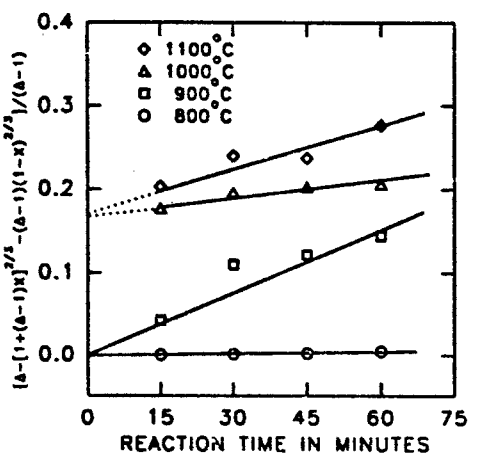


Figure 4. Conventional heating of mixture of alumina and zinc oxide. Attempt to fit the experimental data to Valensi-Carter model.

is increased the zinc oxide vaporizes and condenses on the alumina particles. This increases the interface area between the alumina powder particles and the zinc oxide vapors and results in much higher zinc aluminate spinel formation at the early stage of the reaction. As the reaction proceeds the reaction rate appears to slow down. This change in mechanism possibly explains the abrupt increase in reaction above 900° C.

Although there are differences in reaction rate data for the conventional and microwave heating cases, the main concern is that even the conventionally heating of mixtures does not satisfy the diffusion controlled models. This can be explained in terms of "coefficient of surrounding" which is defined as the fraction of the solid angle occupied by the small particle on the larger particle. If the ratio of the dimensions of the smaller particle to that of the larger particle ($d_{small} << d_{large}$) is very small the coefficient of surrounding has a maximum value, that is, larger particles are properly covered by smaller particles and in such cases the conventional kinetic models can be applied. When the ratio d_{small}/d_{large} gets larger the geometric factors are more important and models of kinetic powder reactions should take them into account. In ceramics, solid state reactions are usually carried out by using fine powders in order to profit from their higher reactivity. Nevertheless, care must be taken in using fine powders of similar grain size in which reaction rapidly concentrates the product formed on portions of the host grain leading to difficulties in obtaining complete reaction [9,10].

The powders used so far had the average particle size of 0.18μm for alumina and 0.3μm for zinc oxide thus giving a large value of d_{small}/d_{large} ratio, where obviously the conventional kinetic models are going to have problems.

Effect of the Particle Size on the Reaction Rate

Having seen the limitation of the smaller and similar particle size, the next step was to see how the larger particle size would affect the reaction rate. The larger particle size of alumina were AKP-30 (average particle size of 0.4μm) and AKP-15 (average particle size of 0.68μm). Ramachandran [8] reports that the percent spinel formed increases with the decrease in particle size of aluminum oxide. However, the particle size of alumina used was much larger, that is 84 μm as compared to 2 μm for zinc oxide. Figure 5 shows our results for 30 minutes of microwave and conventional heating of the mixture. At 900° C, the spinel formation decreases for both microwave and conventional heating, as the particle size increases. This can be understood in terms of the decrease in surface area and the contact of particles of zinc oxide and alumina. At 1000° C, the spinel formed by conventional heating appears to increase slightly with the increase in the particle size. It is especially interesting to note that although the spinel formation with microwave heating was comparable or less for the smallest particle size, as the particle size increases the weight percent spinel formed increases significantly and exceeds the values for conventional heating. The reaction reached completion with larger particle size of alumina (AKP-15), by both microwave (30 minutes of heating at 1000° C) and conventional heating (30 minutes at 1100° C, not shown). However, with smaller particle size of alumina (AKP-50) the reaction did not reach completion even after 60 minutes of microwave (Figure 1) and conventional heating (Figure 3) at 1100° C. The increase in the spinel formation with increase in particle size for both the conventional and microwave heating can be understood by the above mentioned reasons [9]. The higher values of spinel formation with microwave heating of larger particle sizes of alumina suggest that microwave heating is more efficient than conventional heating for the conversion of the reactants into spinel. When the particle size becomes large enough so that the reaction is limited by diffusion of zinc oxide through the product layer, microwave heating is beneficial and this can most likely be accounted for on the basis of enhanced diffusion with microwave heating. To confirm this, the experiment was repeated a number (five) of times and the values were averaged (error bars in Figure 5) only for the largest particle size. This observation was further verified with polycrystalline and single crystal alumina heated in zinc oxide. The microwave heated specimens showed larger penetration depth of zinc as compared to conventional heating. These results will be presented later in a separate paper.

Effect of compaction pressure on reaction rate

It has been reported [8] that the percent conversion of the reactants to spinel increases with the increase in compaction pressure. This trend is observed in the conventional heating of alumina AKP-15 and zinc oxide, as shown is Figure 6. However, the trend is exactly the opposite for microwave heating. The weight percent spinel formed decreases as the compaction pressure increases. This result seems rather unusual for someone used to thinking in terms of the phenomenon occurring in conventional heating. But microwave heating, unlike conventional heating, is dependent on various microstructural properties including the initial porosity of the sample. A somewhat analogous result has been reported by Varadan [19] where the rate of

microwave heating of strontium titanate and alumina decrease as the initial porosity decreases.

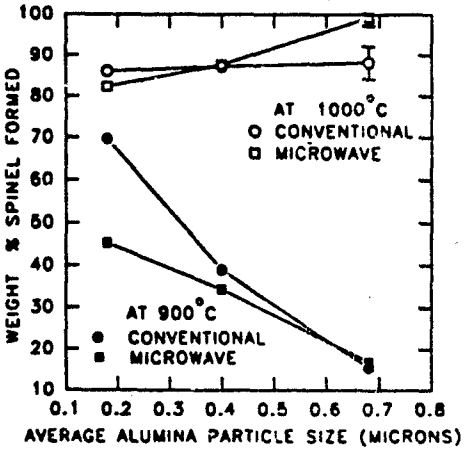


Figure 5. Weight percent zinc aluminate spinel formation as function of particle size of alumina at 900°C and 1000°C for 30 minutes of conventional and microwave heating.

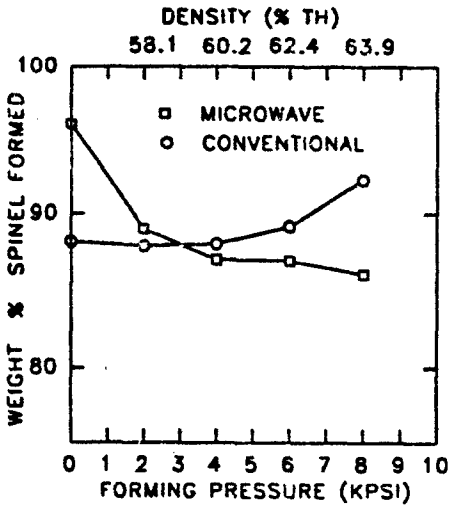


Figure 6. Weight percent spinel formation as a function of compaction pressure for both conventional and microwave heating at 1000°C for 30 minutes.

CONCLUSIONS

The reactions between fine powders of similar particle sizes of aluminum oxide and zinc oxide do not satisfy the Valensi-Carter kinetic model by conventional or microwave heating. Smaller particle sizes of both reactants may not always be beneficial in acheiving rapid or complete reactions. With larger particle sizes of alumina where reaction is limited by diffusion of zinc oxide through the product layer, microwave heating apparently forms more product. The increase in reaction rates suggests the enhanced diffusion with microwave heating.

ACKNOWLEDGEMENTS

The authors acknowledge the financial support from Defense Advanced Research Project Agency and Florida High Technology and Industry Council for this research work.

References.

1. W.H. Sutton, Microwave Processing of Ceramics, Ceramic Bulletin, Vol. 68, No. 2, 376 (1989).
2. M.A. Janney and H.D. Kimery, Diffusive Processes and the Development of Microstructure in Microwave Processed Oxide Ceramics, Proceedings of Spring Meeting of the Materials Research Society, San Francisco, CA (1990).

3. I. Ahmad, G.T. Chandler and D.E. Clark, Processing of Superconducting Ceramics using Microwave Energy, p. 239, in Microwave Processing of Materials, Vol. 124, Eds. Sutton, W.H., Brooks, M.H. and Chabinsky, I.J., Materials Research Society, Pittsburgh, Penn. (1988).
4. W.B. Harrison, M.R.B. Hanson and B.G. Koepke, Microwave Processing and Sintering of PZT and PLZT Ceramics, p. 279, in Microwave Processing of Materials, Vol. 124, Eds. Sutton, W.H., Brooks, M.H. and Chabinsky, I.J., Materials Research Society, Pittsburgh, Penn. (1988).
5. W.D. Kingery, H.K. Bowen and D.R. Uhlmann, Introduction to Ceramics, 2nd Ed., John Wiley & Sons, (1976).
6. G. Yamaguchi and T. Tokuda, Some Aspects of Solid State Reactions between Oxides, Bulletin of the Chemical Society of Japan, Vol. 40, 843 (1967).
7. D.L. Branson, Kinetics and Mechanism of the Reaction Between Zinc Oxide and Aluminum Oxide, Journal of the American Ceramic Society, Vol. 48, No. 11, 591-95 (1965).
8. S. Ramachandran, A. Baradarajan and M. Satyanarayana, Kinetic Studies of Mixed Powder Compact System Between Zinc Oxide and Aluminium Oxide, Materials Science and Engineering, 20, 63-70 (1975).
9. M.R. Anseau, F. Cambier and C. Leblud, Some comments on ceramic solid-state reaction kinetics using results obtained on the ZnO-Al_2O_3 system, Journal of Materials Science, 16, 1121 (1981).
10. C. Leblud, M.R. Anseau, E. Di Rupo, F. Cambier and P. Fierens, Reaction Sintering of ZnO-Al_2O_3 mixture, Journal of Materials Science, 16, 539 (1981).
11. H. Okada, H. Kawakami, M. Hashiba, E. Miura, Y. Nurishi and T. Hibino, Effect of Physical Nature of Powders and Firing Atmosphere on $ZnAl_2O_4$ Formation, Journal of the American Ceramic Society, Vol. 68, No. 2, 58 (1985).
12. J.L. Margave, The Characterization of High-Temperature Vapors, John Wiley & Sons, Inc. p 497, (1967).
13. A.S. Dᵃ, I. Ahmad, E.D. Whitney and D.E. Clark, Effect of Green Microstructure on the Microwave Processing of Alumina: Effect of Particle Size, Ceram. Eng. and Sci. Proc., 11 (1990).
14. A.S. Dᵃ, I. Ahmad, E.D. Whitney and D.E. Clark, Effect of Green Microstructure and Processing Variables on the Microwave Sintering of Alumina, Proceedings of the Spring Meeting of Materials Research Society, San Francisco, CA (1990).
15. F.H. Chung, A New X-ray Diffraction Method for Quantitative Multicomponent Analysis, Advanced X-Ray Analysis, 17, 106 (1974).
16. F.H. Chung, Quantitative Interpretation of X-ray Diffraction Patterns of Mixtures. I. Matrix-Flushing Method for Quantitative Mutlicomponent Analysis, J. Appl. Cryst. 7, 519 (1974).
17. F.H. Chung, Quantitative Interpretation of X-ray Diffraction Patterns of Mixtures. II. Adiabatic Principle of X-ray Diffraction Analysis of Mixtures, J. Appl. Cryst. 7, 526 (1974).
18. F.H. Chung, Quantitative Interpretation of X-ray Diffraction Patterns of Mixtures. III. Simultaneous Determination of a Set of Reference Intensities, J. Appl. Cryst. 8, 17 (1975).
19. V.K. Varadan, Y. Ma, A. Lakhtakia and V.V. Varadan, Microwave Sintering of Ceramics, in Microwave Processing of Materials, Vol. 124, Eds. Sutton, W.H., Brooks, M.H. and Chabinsky, I.J., Materials Research Society, Pittsburgh, Penn. (1988).

APPLICATIONS OF MICROWAVES IN HIGH TEMPERATURE SUPERCONDUCTOR MATERIALS AND DEVICES

P. J. Gielisse, H. Niculescu, B. Roy
Florida A & M University / Florida State University
College of Engineering
Tallahassee, Fl 32316

P. Pernambuco - Wise, J. E. Crow
MARTECH Center for Materials Research and Technology
Florida State University
Tallahassee. Fl 32306

G. Sykora, R. Wahlers
Electro-Science Laboratories Inc.
King of Prussia, Pennsylvania

ABSTRACT

Direct and indirect microwave processing of bulk and thick film type sensors has a significant influence on performance, such as sensitivity and noise level, in flux modulated magnetometer devices, developed in our laboratory. Microwave processing effects the material structures and thus device characteristics. Our present results represent the first steps in attempts to configure resistors, capacitors and sensors into a complete functional circuit by one processing means.

INTRODUCTION

The generation of high quality thick films from high temperature superconductors holds promise for high volume applications in magnetic coils, power transmission lines, high field magnets, passive microwave devices, magnetic shielding, interconnects and perhaps most importantly in the new multichip hybrid microelectronic circuits and sensors which are intended to be operated at high power levels and at frequencies in the GHz range.

The advantages of thick films include the conventional ones of flexibility, reliability, performance and cost effectiveness. The ability to configure resistors, capacitors and other circuit elements, such as sensors and detectors, into a complete functional circuit for insertion into electronic control systems is one of the most desirable objectives.
Although thick films can and have been made by a variety of techniques [1-3] such as plasma spraying, doctor blading and various spinning, dipping and spraying methods, our efforts have exclusively involved the silk screening process. It is felt that, particularly in the case of electronic and microelectronic applications, such parameters as thickness, line width and via control, can be held with greater accuracy than with any other method.

PARAMETERS RELEVANT TO MW PROCESSING

In spite of the fact that $YBa_2Cu_3O_7$ has been found to couple reasonably well with 2450 MHz microwaves [4,5] and that most of the present substrate materials do not, at least at lower temperatures, is not sufficient knowledge for the efficient processing of intricate microcircuitry. A brief overview of the significant aspects and parameters follows.
Electromagnetic theory, as applied to dielectric materials [6], defines the complex dielectric permittivity as

$$\epsilon^* = \epsilon' - j\epsilon'' = \epsilon_0(\epsilon_r' - j\epsilon_r'') \tag{1}$$

where, ϵ_0 = permittivity of free space ($8.86 \times 10^{-12}\ F/m$),
ϵ_r' = relative dielectric constant of the material,
ϵ_r'' = relative loss factor
A variety of polarization mechanisms – dipolar, electronic, atomic and Maxwell-Wagner – give rise to and determine the value of the dielectric constant and loss factor for any one material. Both parameters behave as a function of frequency and temperature. The absorbed power of the microwave energy which is a measure of how well the heating process will proceed, is given by,

$$P = \omega\epsilon_0\epsilon_r''|E_i|^2 \tag{2}$$

where ω= radian frequency and E_i the internal electric field. E_i and ϵ_r'' are the primary variables of interest.
Applying the commonly used term loss tangent, $\tan\delta$, defined as

$$\tan\delta = \frac{\epsilon_r''}{\epsilon_r} \tag{3}$$

yields loss factor = loss tangent × dielectric constant. We can define the absorbed power as

$$P = \omega\epsilon_r\epsilon_0 \tan\delta|E_i|^2 \tag{4}$$

It will be noted that an increase by a factor of two in the internal field strength quadruples the power absorbed. Efficient microwave heating thus requires a high loss tangent or a high loss factor.
To be efficient, the microwaves must penetrate the material. The penetration depth D, at which fields are reduced by a factor of 1/e, can be expressed as,

$$D = \frac{0.225\lambda}{\sqrt{\epsilon_r}\sqrt{\sqrt{1+\tan^2\delta}-1}} \tag{5}$$

which for $\tan\delta \ll 1$, i.e., low loss materials reduces to,

$$D \simeq \frac{0.318\lambda}{\sqrt{\epsilon_r}\tan\delta} \tag{6}$$

A very important parameter in the power expression is that of the internal field, E_i. It relates to the external field as,

$$|E_i/E_0| = \omega\epsilon_0/\sigma \tag{7}$$

where σ = conductivity so that if $\sigma \gg \omega\epsilon_0$ (at lower frequencies) we may, in spite of higher penetration, have $E_i \ll E_0$, and thus inefficient heating.

THICK FILM SUPERCONDUCTOR SENSORS

The non-linear response of a superconducting thick film to an alternating magnetic field, can be used to measure an external dc field with great sensitivity in the nano-tesla range. We have reported the initial device details elsewhere [7]. In principle the ac field can be applied through an excitation coil or by direct current injection into the sensor. A pick up coil and ancillary electronics measure the second harmonic of the excitation frequency as the dc field related signal.
We have developed these sensors from the earlier reported bulk type $YBa_2Cu_3O_7$ sensors [8], into co-deposited multilayer thick film devices, incorporating the sensing element, excitation means, pick-up coil and contact pads onto a single substrate. The ability to process, oxidize and package such devices in one manufacturing operation would clearly be advantageous. It is from this and other aspects, that appropriate microwave processing is seen to be of benefit.
In contrast to the extended period of time required for sintering and densification in resistive heating, microwave heating takes place throughout the entire sample volume and, in homogenous materials, leads to substantially shortened processing times and suppression of grain growth. The latter point is important from both the mechanical and device physical properties point of view. Furthermore, shrinkage is reduced and sintering at lower temperatures, preventing e.g. liquid phase formation,

is possible. The latter point has not yet been fully substantiated from a device development point of view.

Differences in thermal expansion at the film substrate interface, often leads to cracking in conventional processing. This has not occurred in MW heating under the right energy conditions. Sintering of the active material, at lower temperatures and without substrate heating, will suppresses the reaction at the interface and the in-migration of substrate elements into the superconductor. It is well known that substitution in $YBa_2Cu_3O_7$ is detrimental. In the case of Al_2O_3, aluminum will substitute for yttrium and copper and lower the temperature of transition. Shorter sintering times and lower temperatures also reduced outdiffusion of the superconductor into the substrate and into other device components and helps in producing sharp, non-diffuse, line detail. We have started to see the benefits of in-situ texturing, grain boundary modification and the advantages inherent in hybrid heating. Many of the advantages will come about as MW processing is coupled with much needed improvement in process control, which is a must for MW applications in device fabrication as distinct from MW heating or processing only.

STRUCTURE OF THICK FILM DEVICES

Our thick films were screen-printed on 25 mm × 25 mm Al_2O_3 or ZrO_2 substrates from ternary metal oxide ceramics powders of $YBa_2Cu_3O_7$ mixed with printing vehicles and thinners as available on a commercial basis. Two starting grain sizes 1-3μm and approximately 35μm were used to make up the inks.

The structures that resulted from the as-fired thick films at 930 and 980^{0}C are shown in the SEM photomicrographs of Figs. 1, 2 and 3. At 930^{0}C the film consists of particles approximately 1.5–3 μm in size which have formed from the sintering of 1–1.5 μm grains, the morphology of which is still visible. The remnant structure, whereas continuous, remains very porous. Necks have formed along the contact regions and particles have coalesced, but the structure is remniscent of the early stages of sintering. The intergranular porosity is multi faceted with contacts of five or six grains quite common. There appears to be no evidence (up to 15,000X) of liquid phase formation at the grain boundaries, which are essentially structural. There is, furthermore, no intragranular porosity or internal cracking which is quite common in structures sintered at > 930°C. There is evidence of parting (0.1μm thick) with orientation roughly parallel to the surface. X-ray diffraction shows the material as monophasic $YBa_2Cu_3O_7$. There is no evidence of the 211 phase.

In contrast, the thick films sintered at 980^{0}C show a denser structure consisting of 30–40 μm fused areas. From these areas grow lenticular particles, normally 10–20 μm in length, with aspect ratios of 10:1. This morphology is characteristic of sintering phenomena in the presence of a

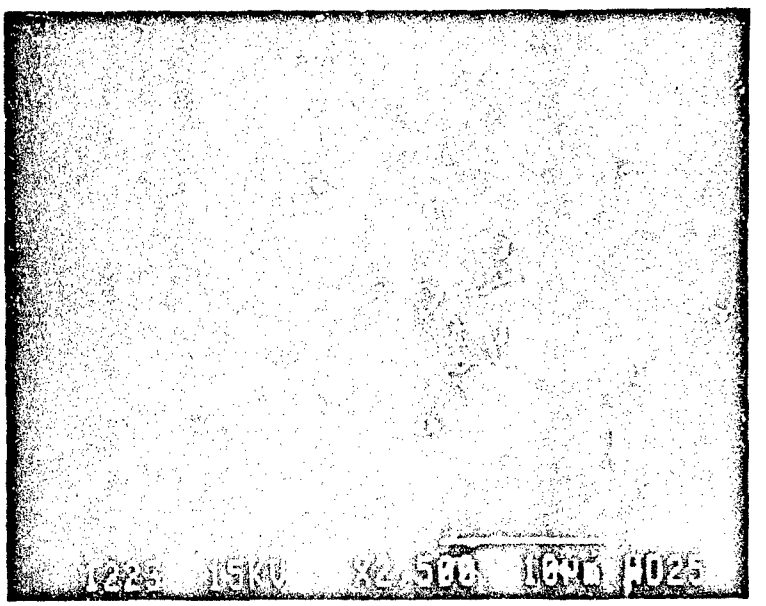


Fig. 1. $YBa_2Cu_3O_7$ thick film sintered at 930° C



Fig. 2. $YBa_2Cu_3O_7$ thick film sintered at 930° C, magnified view of center of Fig. 1.

liquid phase. These features have also been observed in our single crystal growth experiments, in which aspect ratios of 50:1 have not been uncommon. Cross granular cracking is abundant. X-ray analysis shows ample evidence of the development of the 211 phase which is characteristic of sintering above the peritectic temperature of 930^0 C.
When the 980^0 C sintered material is further processed through hybrid or direct microwave heating (2450 MHz) the structure takes on the appearance of stacked platelets (Fig. 4) which seem to have developed as a result of broadening of the lath like particles in the a-b crystallographic plane. A more advanced stage of sintering has developed. The material has been textured. The structure is criss-crossed by cracks which can be considered primary. The platelets are oriented parallel to the surface, perpendicular to the slower growth C-axis direction. The 211 phase is still present.

DEVICE SENSITIVE PARAMETERS

The signal in flux modulated HTS sensors relates to the two component applied field,

$$H_a(t) = H_{ac}\cos(2\pi ft) + H_{dc} \tag{8}$$

in which the terms refer to the ac and dc contributions and f is frequency. The signal will linearly depend on the applied frequency. The total time dependent coil voltage depends not only on the physical aspects but also on sensor device parameters, such as the number of turns in the pick-up coil (N), the total effective or active sensor area (A) and a constant (k) for each design, reflecting the efficiency with which the sensor field is coupled to the pick-up coil,

$$V_t = kNA(dH_a(t)/dt) \tag{9}$$

Numerical Fourier analysis then shows that the second harmonic signal can be expressed as,

$$V(2f) \simeq 2fH_{ac}NA \tag{10}$$

Thick film techniques can easily cope with increases in the effective sensor area, if desired. The number of turns in the co-deposited sensing coil will depend on the line width limitations. HTS thick films have already been found to be applicable in high frequency microwave applications, and are thus likely to perform well in the present technology. Microwave processing should aid in the fabrication of the required high resolution microstructures.



Fig. 3. $YBa_2Cu_3O_7$ thick film sintered at 980°C



Fig. 4. $YBa_2Cu_3O_7$ thick film sintered at 930°C and processed by microwave heating (2450 MHz) to 800°C.

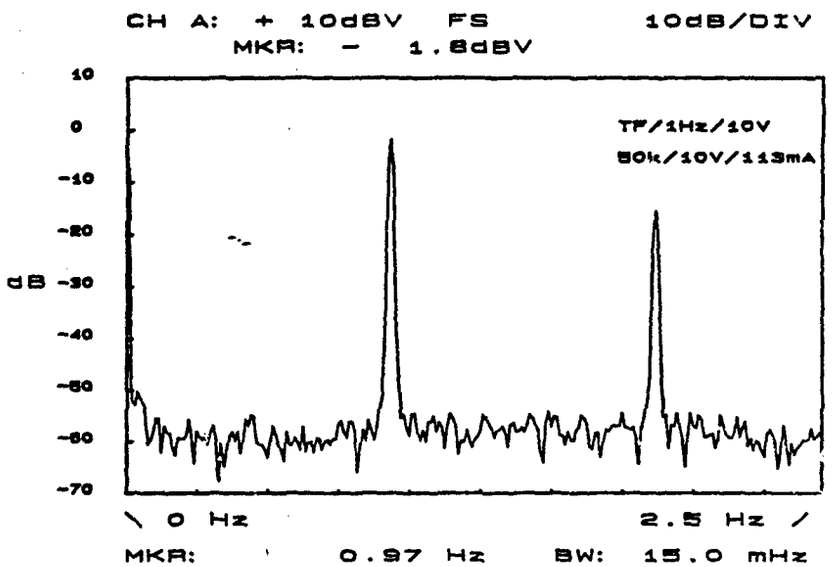


Fig. 5. Typical thick film superconducting magnetometer response spectrum.

The actual sensor response will critically depend on the thick film microstructure which in turn is determined by processing. The influence of this microstructural detail is presently being investigated. A typical response spectrum for devices of the type discussed here, is shown in Fig. 5.

CONCLUSIONS

Although our microwave processing of thick film superconductor sensors and detector structures is only in its preliminary experimental phases, some observations can be made. Microwaves do couple directly to thick film structures of $YBa_2Cu_3O_7$ in both sintering and oxygenation purposes. Under the right energy conditions MW processing does not lead to sensor surface cracking as often observed in conventional heating. There is little or no reaction of the superconductor with the substrate and a sharp sensor delineation without diffusion into the substrate is maintained. In situ texturing is possible. The effect of this on device performance is yet to be determined.

ACKNOWLEDGMENTS

Part of this work was supported by the Defense Advanced Research Project Agency, contract MDA 972-88-j-1006 and the Department of the Army-Strategic Defense Command, contract DASG60-90-C-D138. We acknowledge support and assistance through their monitors.

REFERENCES

1. Y. Tzeng, "High Temperature Oxide Superconductor Thick Films," in: High Temperature Superconductor Materials, W. E. Hatfield and J. H. Miller, Eds., Univ. N. Carolina, Marcel Dekker Inc., New York, pp. 159-165 (1988).
2. M. Levinson, S. S. P. Shah, and D. Y. Wang, "Large Zone Melted Bi-Sr-Ca-O Thick Films," Appl. Phys. Lett. vol. 55, No. 16, pp. 1683-1685 (1989).
3. K. Tachikawa, I. Watanabe, and S. Kosuge, "High Tc Superconducting Films by Low Pressure Plasma Spraying," Mat. Res. Soc. Symp., vol. 99, pp. 63-66, (1988).
4. I. Ahmad, G.T. Chandler and D.E. Clark, "Processing of Superconducting Ceramics Using MW Energy", Mat. Res. Symposium on MW Processing of Materials, Reno, Nevada, vol. 124, pp.239-246 (1988).
5. A.D. Cozzi, D.K. Jones, Z. Fatai and D.E. Clark, "Microwave Evolution of $YBa_2Cu_3O_{7-x}$ Using Microwave Energy", ibid. (1991).
6. J. M. Osepchuk, "A History of Microwave Heating Applications," IEEE Transactions on Microwave Theory and Techniques, vol. 32, No. 9, pp. 1200-1224(1984).
7. P. J. Gielisse, H. Niculescu, B. Roy, and H. Shin, "High Tc Thin Film Fluxgate Magnetometer and Gradiometer," Final report, Contract No. N 61331-89-D-0021, Naval Coastal Systems Center, Panama City, Florida, Nov., (1990).
8. H. Niculescu, P. J. Gielisse, Y. S. Hascicek, and L. R. Testardi, "Superconducting and Mechanical Properties of $YBa_2Cu_3O_7$/Silver Granular Solids," Mat. Res. Soc. Symp. Proc. vol. 195, pp. 341-346 (1991).

SURFACE MODIFICATION OF SODIUM ALUMINOSILICATE GLASSES USING MICROWAVE ENERGY

Z. Fathi, I. Ahmad, J.H. Simmons and D.E. Clark
Department of Materials Science & Engineering
University of Florida
Gainesville, FL 32611

A.R. Lodding
Chalmers University of Technology
Gothenburg, SWEDEN

ABSTRACT

Microwave energy has been used in ion exchange reactions for four sodium-aluminosilicate compositions. The exchangeable cation in the glass (Na^+) was replaced at the surface by a larger atomic radii cation (K^+). Secondary ion mass spectroscopy (SIMS), electron microprobe analysis (EMP) and x-ray mapping were used to evaluate the effect of microwave heating on the extent and rate of ion exchange in comparison to conventional heating.

INTRODUCTION

Glasses have been known to man for thousands of years, and their applications have gone from rudimentary purposes to top-of-the-line technology. Today's world has broadened the use of oxide glasses in diverse and far-ranging fields such as telecommunication, electronics and aerospace. The intrinsic brittle behavior of oxide glasses and their catastrophic failure have been major drawbacks to their use in applications which require mechanical strength and durability.

In general, brittle materials fail to exceed more than a fraction of their theoretical strength. This characteristic behavior has triggered extensive research aimed at developing higher strength bodies. The desired strength can be achieved by various methods that can be split into two broad categories; bulk and surface techniques. The surface techniques aim at developing a compressive stress distribution on the glass surface. The resulting strength becomes the original strength of the glass plus the strength added by surface compression. These surface modification techniques can be summarized as the following: thermal strengthening, chemical strengthening, surface crystallization, thin coating, cladding, etching and related techniques[1].

Strengths greater than those obtained by thermal toughening can be reached by chemical strengthening. However, any significant strengthening is unlikely to be achieved within times compatible with the modern production rates[2], due to the slow reactions involved in the ion exchange process. For this reason, chemical strengthening techniques are applied where safety predominates over economics.

Within our microwave processing center at the University of Florida, we have been investigating techniques that could enhance ion exchange reactions. Processes by which deeper penetration of a selected ionic species into a glass matrix can be achieved when compared to the conventional techniques.

The present study was undertaken to evaluate the effect of microwave radiation on the ion exchange reactions of K^+ for Na^+ in four different compositions of sodium aluminosilicate glass. For the four chosen glass compositions, we are reporting the penetration depth and the relative concentration of the alkali ions achieved after processing. A comparison is made of the penetration depths accomplished by microwave processing and those achieved by conventional processing for each of the sodium aluminosilicate compositions.

The sodium aluminosilicate system was found to be the system of choice for surface modification using microwave energy. Indeed, this system exhibits major structural changes accompanied with significant dielectric properties differences when the ratio of alumina to alkali ion is taken as a variable.

THEORETICAL BASIS

Ion Exchange Process

Ion exchange reactions in oxide glasses are limited substantially to alkali ions[3]. Ion exchange is a process by which at least two ionic species exchange with each other, as shown by

$$Na^+_{(g)}+K^+_{(s)}\rightarrow Na^+_{(s)}+K^+_{(g)} \quad (1)$$

Where the subscripts represent glass and molten salt solution, respectively. The driving force for the reactions is a concentration gradient which is the natural phenomenon of mixing. A constructive approach to this phenomenon is to partially replace an ionic species pre-existing within a given glass matrix by another with a larger radius. The exchanged glass layer tries to expand. It cannot, due to restraint from the underlying bulk glass. The surface is thus put under compression.

The process mentioned above is diffusion controlled. The concentration of the selected species and its penetration depth are of primary importance and are related directly to the rate of exchange. The objective was to evaluate the effect of microwave heating on the extent and rate of ion exchange in comparison to conventional heating.

Microwave Processing

It is reported in the literature that an array of ceramic products have been heat treated in the presence of microwave radiation. Characterization of these materials revealed major microstructural differences when compared to those conventionally processed. It is our belief that the addition of activations other than those of a thermal nature, namely electrical and magnetic, account for the observed property differences.

Microwave heating is intrinsically different from conventional heating. It is a volumetric heating in which the sample itself generates heat due to the ability of the electric and magnetic fields to polarize molecules and the inability of the molecules to keep up with the rapid reversal of the fields [4]. The resulting dielectric losses account for the volumetric heating. Microwave radiation falls within a range of frequencies at which the orientation polarization is the predominant polarization mechanism. There are losses from the other polarization mechanisms due to the extended tails of the loss curves which are different for each given system.

In glasses, the ionic dipole motions can be split into two categories: (1) deformation

polarization in which permanent dipoles oscillate under an applied electric field and (2) defect associated dipoles which oscillate between several equilibrium positions. The temperature of glass plays an important role because, at high enough temperatures, the conductivity of the glass is such that a discharge of the induced dipoles occurs.

EXPERIMENTAL

The selected compositions in the sodium aluminosilicate system are shown in Table 1. The glasses that were studied had a constant concentration of alkali ions (15mol% of Na_2O). The molar ratio of alumina to sodium oxide, defined as Γ, was taken as a variable and was equal to 0.2, 0.5, 1.0 and 1.1.

The glasses were melted in alumina crucibles at 1500°C for 24 hours and annealed at 600°C for 5 hours. The alumina crucibles were cut to provide workable samples. Care was taken to disregard the glass areas that were in contact with the crucible walls. The faces that were to be ion exchanged were polished to a 1μm finish. The samples were coated with a potassium containing medium[1].

Electron microprobe analysis was used to evaluate the penetration depths involved in the ion exchange reactions. The change of x-ray intensity of the alkali species was found, by several investigators, to be related to time and to be proportional to the electron beam current, specimen temperature and bulk composition of the glass [5].

In the present study, we avoided the use of a stationary electron beam and conducted the analysis using a scanning beam sweeping a 100μm by 1.5μm area. The samples edges to be analyzed were polished to a 1μm finish.

The ion exchange reactions were performed in a multimode microwave oven[2] (2.45 GHz) using hybrid heating [6,7]. The samples were placed in an insulating material lined with a microwave susceptor which, in turn, heated the sample. The reactions temperatures were controlled with an error of ±6°C using an Inconel-shielded K-type thermocouple.

Table 1. Compositions of the Glasses Investigated.

Components	Γ=0.2	Γ=0.5	Γ=1.0	Γ=1.1
Na_2O	15.0	15.0	15.0	15.0
Al_2O_3	3.0	7.5	15.0	16.5
SiO_2	82.0	77.5	70.0	68.5

RESULTS AND DISCUSSION

The results for the interdiffusion of $Na^+ \leftrightarrow K^+$ at 400°C for 30 min are shown in Figure 1. The

[1] Ceramicoat, G-C International Corp., Scottsdale, AZ 85260

[2] Radarline Model QMP-2101B-6, Raytheon Co., Waltham, MA.

general trend is an increasing potassium penetration in the different glass compositions as Γ increases from 0.2 and 0.5 to 1.0. As Γ goes above 1.0, interdiffusion appears to decrease.

If we define P^i_m and P^i_c as the respective penetration depths of microwaved and conventionally prepared samples, and $\Delta P^i_{m,c}$ as the difference between these penetrations for the (i) compositions. We found that P^i_m, P^i_c and $\Delta P^i_{c,m}$ all reach a maximum in the Γ=1.0 composition.

Initially, as Al_2O_3 is introduced into a binary alkali-silicate glass, only AlO_6^- is formed [8]. As Γ increases, there is more formation of AlO_6^- along with AlO_4^-. The ratio AlO_6^-/AlO_4^- decreases with further increase of Γ. The AlO_6^- concentration goes through a maximum, the point

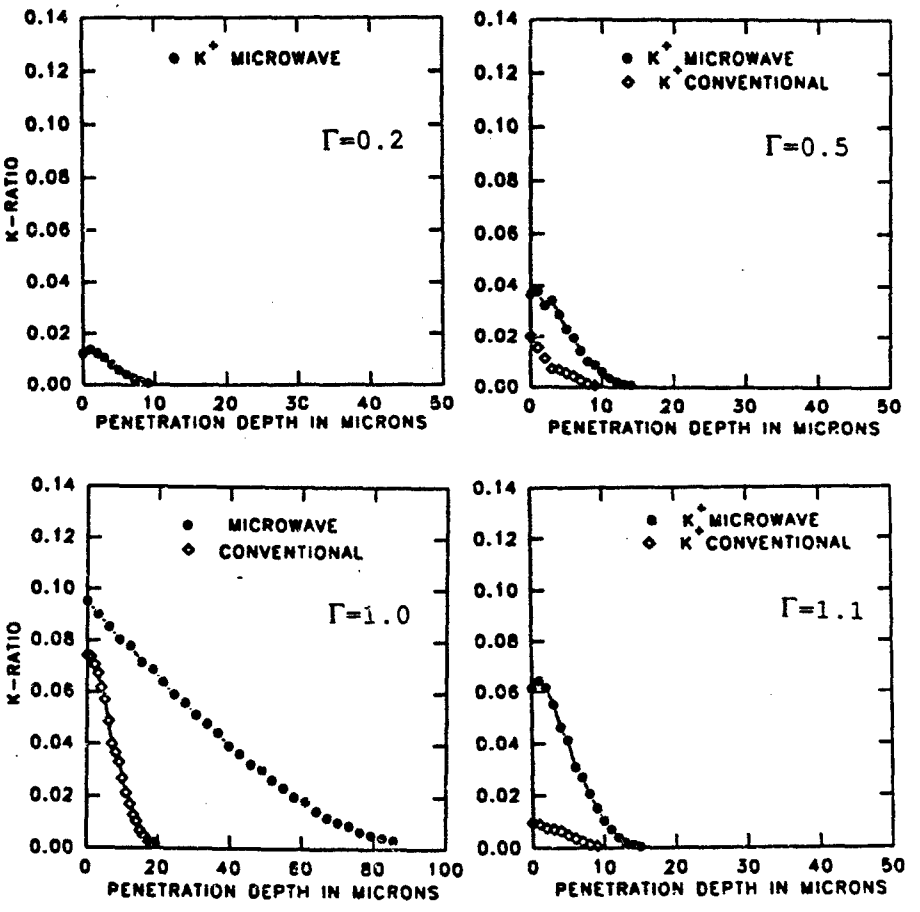


Figure 1. Penetration depths(in μm) of potassium into the glass compositions. K-ratios are relative to tugtupite for sodium and biolite for potassium.

where the activation energy for alkali diffusion is at a maximum. With further increasing values of Γ, mainly AlO_4^- groups will be formed [9], and both the electrical and steric interactions of the alkali ion with the glass network decrease. This is reflected by a rise in the alkali ion diffusion coefficients. Increasing the amount of alumina in the alkali silicate glass reduces the number of oxygens which are only bound to one network former, either Si^{4+}or Al^{3+}. The number of non-bridging oxygen ions decreases to a minimum for Γ=1.0 in which all the alkali ions are positioned to the negative charge of the AlO_4^- groups [10]. The activation energy for diffusion reaches a minimum for Γ=1.0. For compositions having Γ>1.0, the alumina can no longer be present only as AlO_4 tetrahedra because of the absence of compensating positive charges. Thus, $AlO_{4,cl}$ triclusters groups will form. The increasing packing density makes it more difficult for the alkali ion to move out of or through the triclusters. This translates into a small diffusion coefficient [10]. This trend of interdiffusion is retorted by the conventional curves in Figure 1.

The dielectric properties of sodium aluminosilicate glasses at microwave frequencies exhibit changes when the compositional factor, Γ, is taken as a variable [11]. It was found that the temperature-dependent losses were due to the broad tail of the migration loss mechanisms. The temperature-independent losses are due to the deformation losses and are not associated with the concentration of the non-bridging oxygens. Those losses were attributed to resonance with vibrational modes involving large atomic grouping.

The dielectric losses followed the structural model and were found to increase with increasing values of Γ up to Γ=1.0 at which the dielectric losses exhibit maximum values. When compared to conventionally heat treated samples, P_m' can be correlated to the loss tangent of each of the glass compositions [11].

Two characterization techniques were used to verify the findings of the electron microprobe analysis. Figures 2 and 3 correspond to x-ray mapping and SIMS depth profiling of the Γ=1.0 composition for microwaved and conventionally processed samples. As shown, there were higher surface concentrations and deeper penetration of the K^+ into the Γ=1.0 glass composition that were heat treated in the presence of microwave radiation.

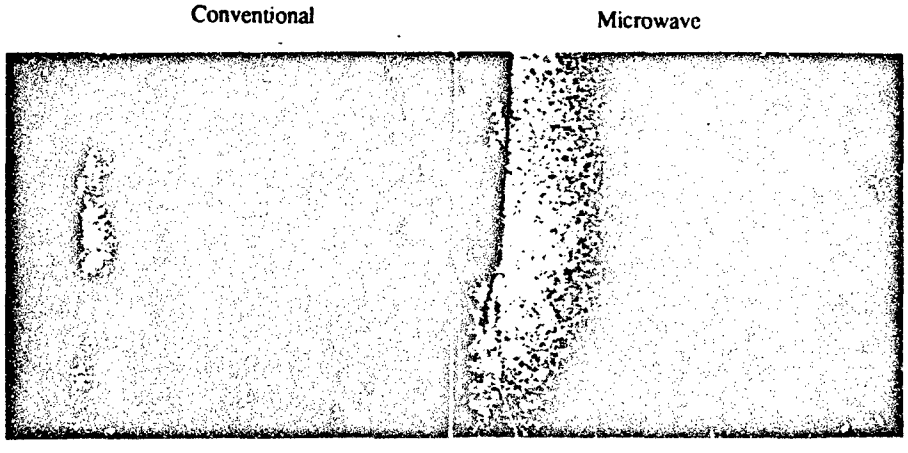


Figure 2. X-Ray mapping of potassium in the Γ=1.0 composition

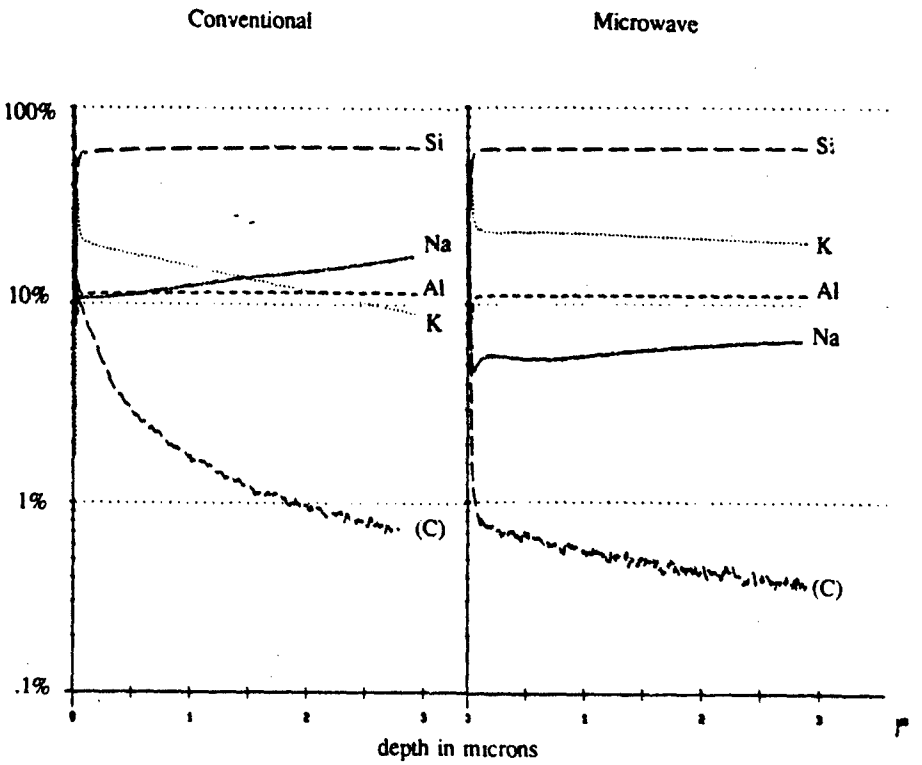


Figure 3. SIMS depth profiling on Γ=1.0 composition

CONCLUSIONS

It is premature to give definite reasons for the high interdiffusion in the case of microwave heating. We believe that the vibrational frequency of an ion within a potential well is increased due to the electric field of the microwave radiation. The rapid reversal of the electric field might be increasing the local temperature of the ion, thus making the ionic jump out of the well easier. More work needs to be done in order to understand fully how microwave radiation affects interdiffusion.

The ion exchange process using microwave energy provides a means by which deeper penetration and higher surface concentrations can be achieved, as compared to conventionally ion exchanged glass. The sodium aluminosilicate compositions having Γ=1.0 exhibited the deepest penetration of K^+, as compared to the compositions Γ=0.2, 0.5 and 1.1. A correlation can be drawn between the dielectric losses of the different compositions and their corresponding K^+ depths of penetration.

ACKNOWLEDGEMENTS

The authors gratefully acknowledge support from the Space Research Institute,Florida High Technology and Industry Council (FHTIC) and the Defense Advanced Research Project Agency (DARPA).

The authors acknowledge W.A. Acree and the Major Analytical Instrumentation Center (MAIC) at the University of Florida for the electron microprobe analysis.

Special acknowledgement for H. Odelius and A. Lodding in the SIMS-laboratory at Chalmers University of Technology for their SIMS depth profiling.

REFERENCES

1. Donald, I.W, *J. of Materials Science*, 24 (1989) 4177-4208.
2. Doyle, P.J., **Glass Making Today,** Portcullis Press, Redhill.
3. Metaxas, A.C. and Meredith, R.J., **Industrial Microwave Heating**, Peter Peregrinius, Ltd. (1983).
4. Terai, R. and Hayami, R., *J. of Non-Cryst. Solids*, 18:217-264 (1975).
5. Clark, D.E., Hench, L.L. and Acree, W.A., *J. Am. Cer. Soc.*, 58:11-12, Nov-Dec., (1975).
6. De, A.S., Ahmad, I., Whitney, E.D. and Clark, D.E., **Effect of Green Microstructure on Microwave Processing of Alumina**, Presented at the 14th Annual Conference on Composites and Advanced Ceramics, January 14-17, 1990, Cocoa Beach, FL. Proceedings, 11[9-10] pp. 1743-1753 (1990).
7. Fathi, Z., Ahmad, I. and Clark, D.E. **Mat. Res. Soc. Symp. Proc.**, Vol. 180, 401-406, (1990).
8. Day, E. and Rindone, G.E., *J. Am. Cer. Soc.*, 45:579 (1962).
9. Day, E. and Rindone, G.E., *J. Am. Cer. Soc.*, 45:489-496 (1962).
10. Isard, J.O., *J. Soc. Glass Tech.*, 43, 113T-123T, (1959).
11. Topping, J.A., Isard, J.O., *Physics and Chemistry of Glasses*, Vol. 12, No. 6, Dec. (1971).

METALLORGANIC AND MICROWAVE-PROCESSING OF CERAMIC POWDERS AND COMPACTS

M.A. Willert-Porada, S. Vodegel; University of Dortmund, Dept. of Chem. Eng., P.O.Box 500500, D-4600 Dortmund 50

ABSTRACT

Metallalcoholates as ceramic precursors were infiltrated into porous ceramic matrices and decomposed to sinteractive powders. Fully crystalline powders with cluster-like morphology were obtained by microwave heating (2.45 GHz) of the precursor whereas amorphous powders were obtained by conventional heating. After sintering the mechanical properties of the infiltrated ceramic are improved as compared to the matrix material. Microstructure modelling of Al_2O_3 ceramics towards "self strenghtened" materials by metallorganic infiltration and decomposition and by microwave heating is proposed.

INTRODUCTION

Flaw control and toughening are currently the most promising approaches on the way to structural ceramics with increased reliability (1). However, an intrinsic separation of these two approaches exists, in part due to different processing routes necessary to achieve high strength or enhanced toughness (2). Addition of fibers or particles to increase toughness often generates larger processing flaws in the composite compared to the pure matrix material (2). Microstructure modelling by varying sintering profiles and employing sintering aids is possible too (3) but limited because of the strong coupling between grain growth and density (4). Toughening due to phase transformations is by now possible in a few ceramic materials only (1,3).
In case of monolithic materials with no polymorphism, e.g. Al_2O_3, which exhibit R-curve behavior due to a coarse grained microstructure (5), the development of alternative processing routes is of particular interest. To beneficially combine strength and crack resistance behavior of high alumina ceramics, a simultaneous "flaw control" and "toughening" processing route is necessary

in order to balance the amount and size of a coarse grained region within a fine grained matrix without decreases in density (5,6). A combined metallorganic infiltration and microwave heating (MW) apprcach should for two reasons be capable of unifying "flaw"control with "toughening":

- infiltration is pore-size selective, therefore reducing the flaw size by filling the largest pores first
- heating by MW offers the opportunity for local thermal gradients and therefore for selective grain growth.

The infiltration/decomposition sequence is, in the case of monolithic materials, comparable with the carbon-fiber-composite (CFC) - technology (7), for polyphasic materials with the work done by Marple and Green on Mullite/Al_2O_3 composites (8,9). Powder preparation by microwave processing has recently been reported by Kladnig and Horn (10). To our knowledge the direct decomposition of metallorganic compounds as well as the " in situ " generation of a powder by MW-heating is not described in literature yet. Using this approach a microwave-absorbing metallorganic compound can be decomposed to a second ceramic powder within a MW-transparent matrix, e.g. $Al(OR)_3$ or $Zr(OR)_4$ in a - Al_2O_3-matrix (6,11) as well as a non absorbing ceramic precursor within a MW-absorbing matrix, e.g. SiC/ polysilane (12). In cases with both matrix and metallorganic compound being MW-active, e.g. SiC/$Al(OR)_3$ or $Zr(OR)_4$ (11,12) selective heating occurs on the more lossy material. To study the influence of infiltration and MW-heating on the microstructure development and mechanical properties of alumina ceramic, the "monolithic" mixture $Al(OR)_3$/- Al_2O_3 is used as model system. In this paper preliminary results are reported.

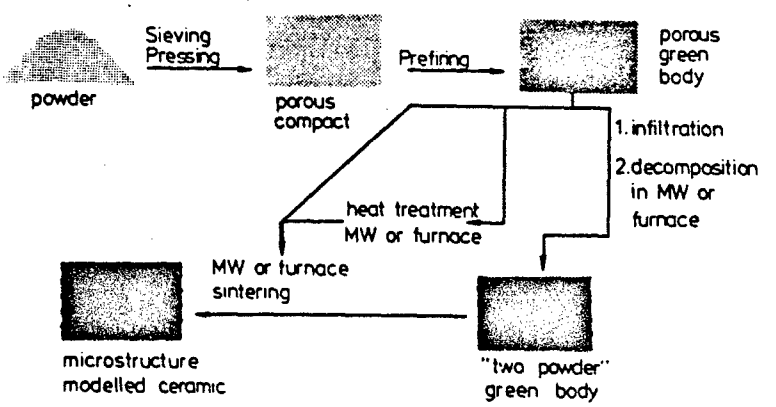


Figure 1: General processing scheme

Table 1 . Characteristic properties of the powders.

	CT 8000 SG	ATIP/furnace	ATIP/MW
Composition (%)			
Al_2O_3	99.6	not estimated	
Na_2O	0.10	"	
SiO_2	0.07*	"	
MgO	0.02	"**	
grain size (µm)	0.10	d ≥ 0.05	
spec. area ($m^2 g^{-1}$)			
293 K	19	35-20	230-98
1073 K/3h	-	16	104-98
1273 K/3h	8	-	70
1473 K/3h	-	-	7
% Phase			
293 K	99α	amorphous	crist.unkn.
1273 K/3h	"	-	γ (XRD)
1473 K/3h	"	-	α + γ (XRD)
Source	Alcoa	ATIP : Fluka	

* 0.1 % added, ** no MgO addition, ATIP distilled prior to use

Table 2 . Processing details and characterisation of the compacts.

Matrix	Processing	density ($g\ cm^{-3}$)	porosity (%)	spez. surface ($m^2\ g^{-1}$)
CT 8000	Standard *	1.6+/-0.05	58	9 - 10
CT 8000	infiltrated & MW-decomp.	max. 1.76	max. 58	max. 50

*: sieving 500 µm, dry-pressing 60 MPa isostat., prefiring 1273 K/3h

Table 3 . Processing routes for CT 8000-matrix ceramics.

Symbol	Description
A	firing in a furnace, 1700°C/2h, 100°C/h heating rate
B	firing in a furnace, 1700°C/2h, 1200°C/h heating rate
C	infiltration of prefired body with ATIP, MW-decomposition
D	heat treatment in a furnace, 1450°C/ t (minutes), firing A
E	heat treatment in MW-oven*, 1450°C/ t (minutes), firing A
F	MW-sintering*, 1665°C/2h, 2000°C/h heating rate
F_1	as F with post firing A
G^1	furnace sintering 1665°C/2h, 2000°C/h heating rate
G_1	as G with post firing A

* : SiC is used to preheat the Al_2O_3 (MW-hybrid heating)

RESULTS

The general procedure is shown in Figure 1. Experimental details of the processing steps are given in Tables 1, 2 and 3.

Infiltration and Decomposition

The prefired green bodies were infiltrated with molten aluminium-tri-isopropanolate, (ATIP). The spatial distribution of the infiltrated ATIP depends directly upon the different agglomeration and packing behavior of the matrix-powder (6). The infiltration depth depends upon the temperature and viscosity of the melt as well as upon the infiltration time (6). Decomposition of the infiltrated ATIP to Al_2O_3, C_nH_{2n} and H_2O can be achieved by heating in a furnace as well as using microwave radiation (2.45 GHz). In MW-heating without ATIP for the same amount of Al_2O_3 in the same configuration (isolation, power level etc.) a decreased steady-state temperature is reached. When a 100g sample of Al_2O_3 is heated with 195 watts MW-power a steady-state is reached after 60 minutes with a temperature of 100°C. The same porous sample infiltrated with 30 g ATIP reaches 120°C after 60 min and a maximum temperature of 200°C after 180 minutes, corresponding to 75% decomposition of the ATIP to Al_2O_3. To achieve the same degree of decomposition in a conventional furnace a temperature gradient of 200-230°C in 90 minutes is necessary. At 200°C in a furnace only 40% decomposition can be achieved within 210 minutes. The powders and compacts from both decomposition routes were characterized microscopicaly and by surface area and density measurements. The coarsening behavior has been qualitatively investigated by subsequent heat treatment. As shown in Table 1 and Figure 2a the morphology and coarsening behavior of the powders generated from ATIP differ significantly upon the ATIP-decomposition route. MW-heating yields a fully crystalline powder with the smallest particle size fraction of 50 nm and rather a high specific area. A XRD-pattern could not be obtained from this powder. Subsequent heating experiments and XRD-analysis indicated the presence of γ-Al_2O_3 up to 1200°C. TEM revealed a "cluster" morphology typical for hard agglomerates or sintered particles. Furnace decomposition yields a fine powder of globular morphology with a medium surface area. The morphology of the infiltrated compacts depends also upon the decomposition route as shown in Figure 2b. The MW-decomposed sample exhibits a smoother fractured surface compare to the furnace decomposed one.

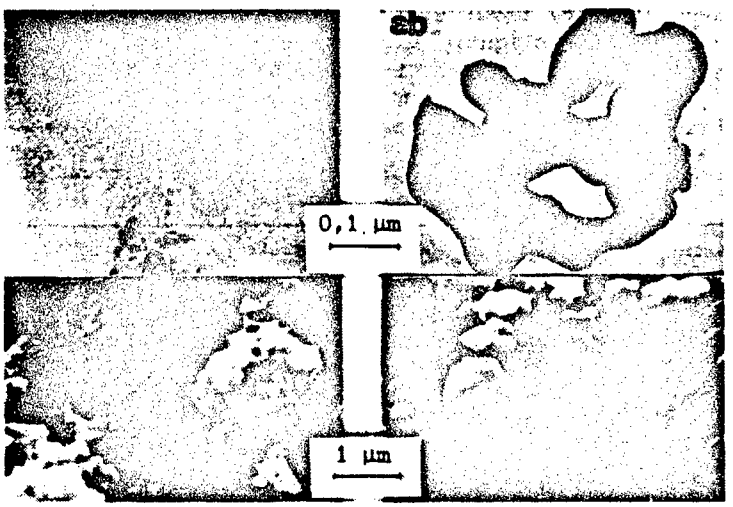


Figure 2: a) TEM-micrographs of Al_2O_3-powders from decomposition of ATIP in aa) a furnace ab) MW-oven
b) SEM-micrographs of infiltrated CT8000 green bodies after decomposition in ba) a furnace bb) a MW-oven

Firing

Sintering and heating conditions are given in Table 3. The final densities and qualitative grain size analysis results are given in Table 4. Compared to not infiltrated samples, a decrease in the total amount and a better spatial distribution of the coarse grains is achieved for the infiltrated CT 8000 SG matrix material. A "bimodal" microstructure with a fine grained matrix is obtained. A similar morphology but a lower final density is achieved by "fast" sintering of a non infiltrated sample. The influence of MW-radiation on the microstructure has been investigated by varying the heating profile in the temperature region below 1600°C. Two samples of the same origin reveal differences in the microstructure when heated by MW compare to the same sintering profiles in a furnace. The MW-samples exhibit a grain coarsening not observed at the same temperature and time for samples fired in a furnace. This difference is preserved upon final sintering at 1700°C/2h as shown in Table 4.

Mechanical properties

The Young's modulus (resonance method), crack resistance parameters R_o (starting value) and R_p (plateau value) of single edge notched bending test bars (SENB) [5] as well as strength measure-

ment (3-point bend) results are collected in Table 5. Infiltrated samples exhibit a slightly higher Young's modulus and beginning R-curve behavior compared to the non infiltrated material. However, strength measurements show an increased scattering, indicating the presence of larger flaws in some of the samples.

Table 4 . Microstructure and density (g cm^{-3}) versus processing route for CT 8000 matrix ceramics.

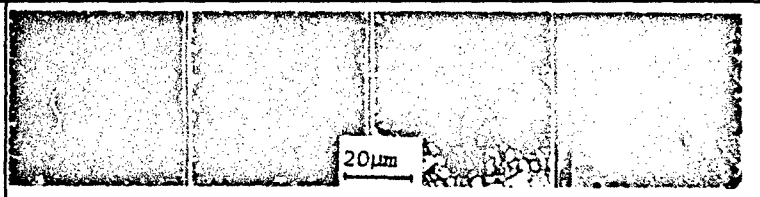
Processing route	Microstructure			
	bimodal		homogeneous	
	coarse	fine	fine	coarse
				
A	3.74	-	-	-
B	-	3.78	-	-
C	-	3.99	-	-
$D_{t=240}$	-	-	3.91	-
$D_{t=120}$	-	-	3.93	-
$D_{t=40}$	-	3.77	-	-
$E_{t=240}$	3.94	-	-	-
$E_{t=120}$	3.96	-	-	-
$E_{t=40}$	3.95	-	-	-
F	-	-	3.86	-
F_1	-	-	-	3.93
G	-	-	3.90	-
G_1	-	-	-	3.95
	final density (gcm^{-3})			

Table 5. Mechanical properties of the materials A and C with CT 8000 matrix.

		A	C
Young's-modulus E (GPa)		350 +/- 10	375 +/- 10
strength σ_b (MPa)		225 - 275	200 - 300
R-curve R_0, R_p (Jm^{-2})	R_0^*	27 (H_2O)	23 (H_2O)
		25 (air)	30 (air)
	R_p^*	30 (H_2O)	43 (H_2O)
		35 (air)	50 (air)

DISCUSSION

The crucial step in the processing route is the ATIP decomposition which gives a large quantity of gaseous products. At this processing step new flaws can be generated. The scattering in σ_b-values indicates the need for further optimization of the decomposition procedure. In particular, a continuous adjustment of the MW-power level is necessary as well as a better isolation and lower heating/cooling rates in order to avoid temperature gradients due to the cold MW-oven interior.

The effect of infiltration on the microstructure depends upon the packing and agglomeration properties of the matrix powders, as described in more detail elsewhere (6). For CT 8000 SG matrix material the main effect is preservation of a bimodal microstructure as well as reduction of excessive grain growth. Furthermore, depending upon the degree of infiltration an increased densification is observed (6). However, this effect may depend upon the powder properties of the "in situ" generated powder. Due to the large difference between furnace- and MW-powders a more detailed analysis of coarsening and densification kinetics upon infiltration/decomposition is necessary.

The influence of MW-radiation on the coarsening behavior of non-infiltrated alumina bodies also needs further investigation. As suggested by Brook (13) and Johnson (14) for sintering of alumina MW-radiation could selectively influence one diffusion path, depending upon the heating profile used. In previous work MW-heating has been used for "fast" sintering of alumina. A fine grained material has been obtained (14). The material sintered at 1665°C by MW-hybrid heating using SiC exhibits no differences in density and morphology compared to a material prepared with the same heating rate in a furnace, as shown in Table 3 and 4. However, a moderate heating rate was used. On the other hand, annealing the same material at temperatures below the sintering temperature reveals more coarsening in the microwave heated samples. A contamination of the material by SiC or SiO_2 has not been found. In MW-experiments the temperature was measured by a pyrometer. The pyrometer readings were adjusted to the actual emissivity of Al_2O_3 as estimated on furnace heated samples in the same configuration as the MW-oven one. Therefore, no extreme difference in the temperature profile of the furnace and MW-oven heating is expected. The uniform microstructure within the MW-heated samples indicates little, if any thermal gradients between the sample interior and the surface. However, the coarsening in the MW-heated samples could indicate an enhanced surface diffusion. In this case certain sintering/annealing profiles using MW-heating would be capable of further modifying the amount

and morphology of coarse grains within a ceramic material. Combined with the metallorganic infiltration process coarsening and density of a ceramic could be varied over a very broad range, not accessible by any of the single processing routes.

CONCLUSION

It has been demonstrated that R-curve behavior of a fine grained matrix alumina ceramic can be induced by using a metallorganic infiltration and microwave decomposition process. In addition the amount of coarse grains within a fine grained matrix can be increased compared to conventionally processed materials with microwave hybrid-heating. Combination of both processing routes could provide ceramic materials with a diversity of grain size distributions and morphology thereby preserving a high density.

ACKNOWLEDGMENT

The authors wish to acknowledge the financial support of the Land NRW, contract IV 6-214 501 89.

REFERENCES

(1) A.G. Evans, "Perspective on the Development of High-Toughness Ceramics",J.Am.Ceram.Soc.73,187-206,(1990)
(2) F.F. Lange, "Powder Processing Science and Technology for Increased Reliability",J.Am.Ceram.Soc.72,3-15(1989)
(3) N. McN. Alford, J.D. Birchall, K. Kendall, "Engineering ceramics - the process problem", Mat. Sci. & Techn. Vol. 2, 329-336, (1986)
(4) F.F. Lange, "Sinterability of Agglomerated Powders" J. Amer. Ceram. Soc. 67, 83-89, (1984)
(5) R. Knehans, R. Steinbrech, "Effect of Grain Size on the Crack Resistance Curves of Al_2O_3 Bend Specimens", Science of Ceram. 12, 613-619, (1983)
(6) M. Willert-Porada, F. Schmidt, W. Schaarwächter, "Effect of Metallorganic Aluminium Compounds on Microstructure and Mechanical Properties of Alumina Ceramic", Proc.Ann. Meeting of the DKG, Nürnberg 1990, 12-14
(7) K.J. Hüttinger, "Carbon-The Material of the Next Century", Ber.F&E Nr. 41, (1989), Symposium Schunk Werkstoffe, 2-18
(8) B.R. Marple, D.J. Green, "Mullite/Alumina Particulate Composites by Infiltration Processing", J. Am. Ceram. Soc. 72, 2043-2048, (1989)
(9) B.R. Marple, D.J. Green, Part 2, ibid.73, 3611-3617, (1990),
(10) W.F. Kladnig, J.E. Horn, "Submicron Oxide Powder Preparation by Microwave Processing, Ceram.Int.16, 99-106, (1990)
(11) M. Willert-Porada, T. Gerdes, unpublished work
(12) M. Willert-Porada, T. Krummel, unpublished work
(13) R. J. Brook, Symposium on Microwave Application in Ceramic Processing, Bayreuth, October 1990 (14)
(14) Y. L. Tian, D. L. Johnson, M. E. Brodwin, "Ultrafine Microstructure of Al_2O_3 Produced by Microwave Sintering", Cer. Trans., 1, 925-932, (1988)

Section X. Microwave Equipment Design

ACCURATE HIGH TEMPERATURE MEASUREMENTS IN MICROWAVE ENVIRONMENTS

Jason Mershon
Applications Engineer, Luxtron Corporation/Accufiber Division
9550 SW Nimbus Avenue Beaverton, OR 97005

ABSTRACT

The paper will explore the use of Optical Fiber Thermometry (OFT) in applications where coupling of microwave energy is the form of heating. These include sintering of ceramic materials, brazing, analytical work and other applications ranging from 200°C to 4000°C. OFT includes both contact and non-contact temperature measurement based on Aluminum Oxide (Sapphire) optical sensors.

Proper methods of application, heat transfer solutions and expected results will be explored. Recent developments resulting in total immunity of the sensor technology to electromagnetic interference will be explained.

INTRODUCTION

The use of microwave energy as a heating method is rapidly increasing. This technology brings improved productivity and better quality to many processes. Microwave heating also causes new issues to arise. Most important of these is temperature. Temperature measurements in a microwave field are not always a simple matter. The thermocouple is a device not well suited to microwave applications due to electromagnetic interference (EMI). The methods that show best results universally are optical measurements. Optical fiber thermometry, its advantages, and primarily its applications will be discussed in this paper.

DISCUSSION

A brief description of Optical Fiber Thermometry should begin with the basic principle upon which it is founded. The energy radiated by any object at a particular wavelength is a strongly dependent function of absolute temperature. Planck's equation describes this phenomenon. (See Figure 1). A measurement of emitted radiation from a target at certain defined wavelengths allows one to make a calculation of absolute temperature. Typically, an optical filter is chosen that limits the radiation collected by the detector to a certain selected range of wavelengths. This allows tailoring the measurement for the characteristics of the detector and surface properties of the target material.

$$E_b(\lambda,T) = \frac{C_1 * \lambda^{-5}}{e^{\frac{C_2}{\lambda * T}} - 1}$$

Where: $E_b(\lambda, T)$ = Energy emitted by a blackbody cavity per unit area per unit wavelength, at temperature T and wavelength λ. $\left(\frac{W}{m^2 * \mu m}\right)$

λ = Wavelength (μm).

T = The Absolute Temperature (K).

C_1 = Constant: $3.743 * 10^8$ ($(W * \mu m^4) / m^2$)

C_2 = Constant: $1.4387 * 10^4$ ($\mu m * K$)

Figure 1. Plancks Equation

In Optical Fiber Thermometry or OFT, the radiant energy from a heated object is gathered by sensors of three general types: Blackbodies, Lightpipes and Pyrometers. Each has its own strengths and weaknesses but all produce the same type of signal; a simple light flux. The amplitude of this signal at each wavelength is important as this is what uniquely allows determination of the target's actual temperature. The light is then conducted via an optical fiber, to a calibrated radiometer, where the temperature is calculated from Plancks equation knowing the wavelength at which the measurement is made.

For measurements made in which the sensor establishes thermal contact with the target, the blackbody sensor is used. It consists of a single crystal rod of Al_2O_3 (Sapphire) capped (on the sensing end) with a thin film of noble metal. This metal film forms a cavity on the surface when viewed from inside, which becomes hot and emits radiation, according to Planck's Law, into a sapphire lightpipe. It couples only weakly to the microwave field, tolerates temperature up to 1900°C, and is easily configured for difficult access to a process.

Non-contact measurements are made with the lightpipe or pyrometer sensors. The first of these, the lightpipe sensor, is also a rod of sapphire. It however, has no metal cavity. Instead it gathers light in a cone of approximately 52° from the sensing end which has been optically polished. It does not couple with the microwave energy, tolerates 1900°C and above, averages temperature over a larger area, and provides ease of access to a process. The lightpipe sensor can be bent to a wide variety of custom configurations.

The pyrometer sensor is essentially a small telescope. It is designed to gather light from an incandescent target at greater distances and with finer spacial resolution. Major advantages also include simplicity of installation, greater ease of high temperature measurement, and again, no microwave interference in the measurement.

The advantages of OFT in a microwave environment are several. OFT can be totally immune to EMI. Its signal/noise ratio is much greater than other methods and it offers phenomenal response speed. Microprocessor control contributes to its adaptability and

flexibility. More conventional means of temperature measurement such as thermocouples and Resistive Temperature Detectors (RTDs) have problems with this sort of environment. The thermocouple and RTD sensors conduct and couple with the E field. The sensor becomes self heated, possibly more so than the material being processed, leading to significant measurement errors, changes in local heating, and often sensor failure. High temperatures, found in many microwave applications, can frequently exceed the service temperature of the thermocouple or RTD itself. With the use of OFT in the non-contact mode, measurement temperature is virtually unbounded at the high end. Measurements of 3000°C are commonly done with optical fiber technology. Contact measurements can be made as high as 1900°C with the sapphire sensors.

OFT technology allows response of 10kHz over a wide range of temperatures. In production applications where temperature control is important, the equipment makes temperature measurements at up to 50/sec. This gives the Proportional Integral Derivative, or PID, controller more continuous data on which to base its adjustments to process power. Microwave processes tend to be subject to thermal runaway. Typically this occurs when absorption characteristics of the material improve as temperature increases. Fast controller response in such situations is critical. Heating rates up to 700°C/sec for various ceramic materials have been observed in relatively low power cavities.* OFT has demonstrated control better
than ± 1°C at ramp rates to 1500°C/sec.

The first application is a simple single mode resonant cavity, (See Fig 2) used in an experiment done at JPL in Pasadena, California in November, 1989. The objective was twofold. Observation of the heating characteristics of a ceramic material called Wangite©, and demonstration of the capabilities of the standard blackbody sensor. Wangite© is used as a blackbody cavity in certain high temperature or harsh environments.

The results were as expected. The ceramic material was strongly self heating. In other words, it coupled well with the microwaves. With the input power at 26 watts, frequency at 4.62 GHz, in the TM 010 mode a temperature of 680°C was reached in 12 minutes. An interesting effect was that as heating progressed, the peak absorption shifted in frequency, leading to a temperature plateau. After the cavity was retuned to minimize reflected power each time, a new higher plateau temperature was reached. This confirmed the materials unsuitability as a sensor material for most microwave applications.

The second objective involved use of the conventional metal cavity blackbody sensor. It was equally successful. Introducing the bare sensor into the cavity did cause a slight perturbation in tuning but the probe was not noticeably self heating. The lower temperature detection threshold with the equipment used was 400°C. A simultaneous measurement of the probe top with a sensitive pyroelectric detector detected a small temperature rise from ambient of 5° ± 2°C.

---

* W.R. TINGA*, B.Q. TIAN* AND W.A.G. VOSS*

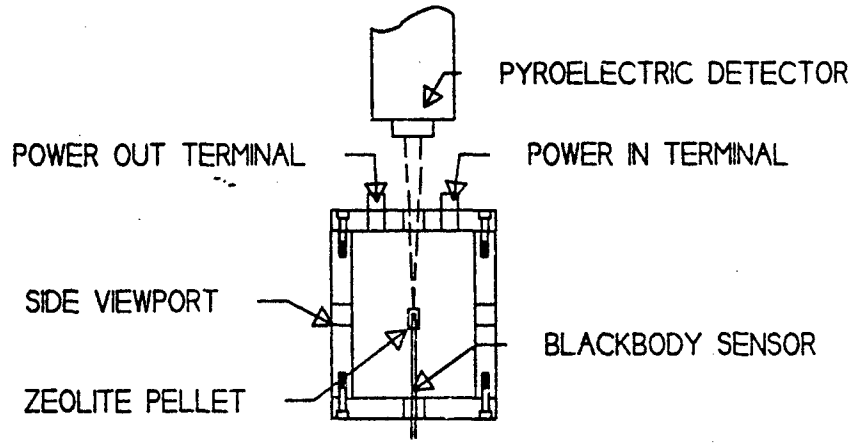


Figure 2

This small change will be further reduced if the probe is in contact with a solid to which heat will rapidly transfer. At higher temperatures, the effect of radiative heat transfer will further reduce the phenomenon.

Using the probe as a support, a small (3.5mm x 6mm) zeolite pellet with a cavity in it was heated in the chamber. The blackbody sensor made a measurement of true bulk temperature. This allowed for an effective emissivity calibration of the pyroelectric detector. Use of the word "effective" is key here. The effects of convective cooling will always act to lower the outer temperature of an internally heated body. For optically opaque or thick materials, a lightpipe sensor inserted into the material will serve the same function, and have absolutely no coupling to the microwave field itself. The concept however, was well proven; that an effective emissivity or heat transfer correction can be developed to allow a process controller to track true bulk temperature accurately and repeatably with an optical fiber sensor input.

Optical Fiber Thermometry has been utilized as the only practical means of temperature measurement in some very demanding applications where all else have failed. One example to be discussed is a high temperature fluidized bed used in the nuclear materials processing field.

The fluidized bed is contained within a double wall reactor at a process temperature around 1500°C. The environment was 40% hydrogen, strongly reducing, so the blackbody sensors in sapphire sheaths are protected by boron nitride outer sheaths.

Before installation and use of the Accufiber OFT system, temperature fluctuations in

the uncontrolled bed would approach 2500°C, destroying product and process components simultaneously. Tungsten/rhenium thermocouples failed to measure the temperatures of this harsh environment. The thermocouples gave no meaningful results until the microwave field was turned off, making control impossible. With the Optical Fiber Thermometry system in place, temperature in the bed is controllable with eight separate sensors and the 2500°C hotspots are an anomaly of the past.

Results have shown that high resolution OFT technology leads to better temperature control--even when using existing control equipment. The OFT signal is practically noise free and control circuits can be adjusted to respond to much smaller temperature changes. The ability to measure very small, real changes in furnace temperature enables a control circuit to respond to the onset of temperature change and rapidly adjust furnace power before the change becomes excessive. Figure 3 shows an example of this type of control using the Accufiber Model 100 in a production furnace.

The Figure 3 data was obtained from a 15-year-old microwave component brazing furnace with an analog control. The OFT signal was converted to a type R thermocouple output signal and fed directly to the existing control circuit. The Figure 3 data shows that the furnace was controlled within ± 0.5 °C at 1500°C. Moreover, the user found that product quality improved and remained stable over the first year of operation. The low drift and high

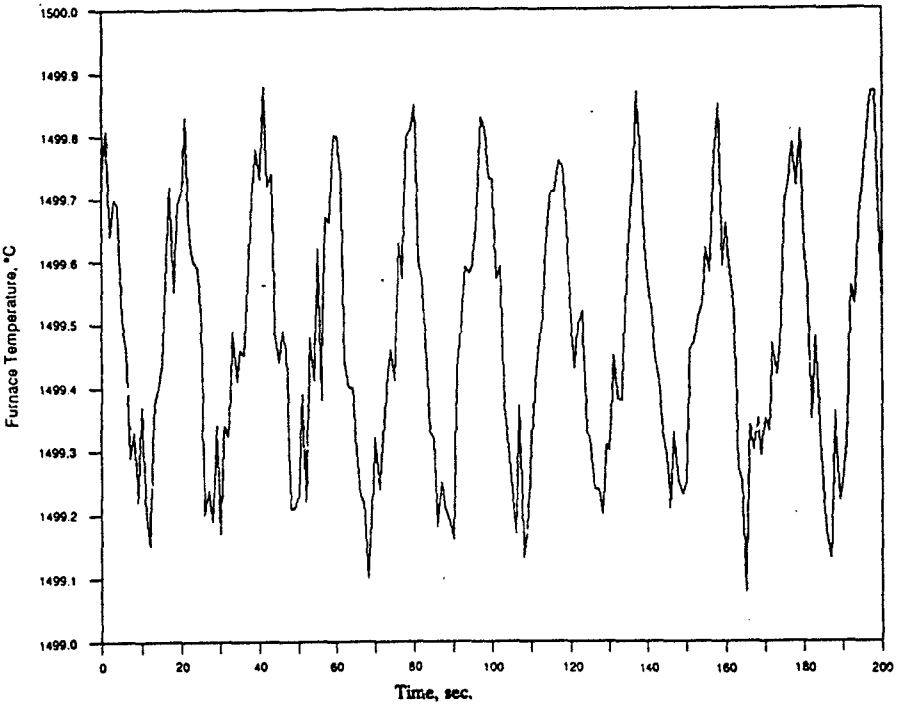


Figure 3

resolution of the OFT sensor provided significant durability and repeatability improvements over previous thermocouple performance.

The customer has now installed eight channels of OFT instrumentation for production control.

Many microwave plasma applications are also well within the realm of OFT. These techniques are being demonstrated and used daily in applications from 200°C to over 2000°C. The E.M.I. immunity and non-intrusive nature of this technology make it a natural choice of temperature measurement for this environment. Diamond film deposition, plasma etch and deposition, and microwave heated MBE are all good applications for optical fiber technology.

Optical Fiber Thermometry has been proven in ceramic sintering operations of several types. The repeatability, resolution, and accuracy make possible the process control necessary in a highly sensitive, temperature dependant system.

Advantages to sintering in a microwave chamber are many: smaller microstructure, greater densification, higher product strength, energy efficiency, and lower process time. In order to fully realize these advantages, a microwave compatible temperature measurement and control system must be implemented.

OFT serves as the controlling measurement means on the Wavemat model MCR 2200 Microwave Ceramic Processing System, a system created exactly with the above attributes in mind. The chamber itself is approximately 0.15 meters in diameter and twice as long. The system is microprocessor controlled in all process parameters including the closed loop temperature control. A pyrometer sensor is chosen to obtain complete remote sensing in the measurement and to facilitate maintenance of the controlled environment inside the chamber. The pyrometer views its target, the part being sintered, through a quartz window in the side of the chamber. A polynomial emissivity correlation vs temperature for any particular material can be developed and entered into the microprocessor controlled OFT temperature controller if necessary.

Benefits to materials processing from microwave processing serve to make it an attractive technology. These benefits are often only fully realized when OFT Technology is used to gain complete process measurement and control. Marriage between microwave processing and Optical Fiber Thermometry technologies is a symbiotic one not unlike the application of microwave energy to ceramic sintering. The best temperature measurement possible in a microwave environment comes from optical fiber technology.

REFERENCES

1 W.R. Tinga*, B.Q. Tian* and W.A.G. Voss*, "New High Temperature Multipurpose Applicator", Presented at Spring (April) 1990, Materials Research Society. *Electrical Engineering Dept., University of Alberta, Edmonton, Alberta, Canada, T6G 2G7.

A WIDE RANGE TUNABLE AND MATCHABLE HIGH TEMPERATURE APPLICATOR

B. Q. Tian* and W. R. Tinga*
* Dept. of Electrical Eng., Univ. of Alberta, Edmonton, Alberta, Canada, T6G 2G7

ABSTRACT

Tuning and matching is vital for a resonant microwave material processing applicator. A wide range tunable and matchable, resonant, high temperature, microwave applicator is proposed consisting of a coaxial cavity with a gap cutting its center conductor. It can be tuned and matched for different gap loads, ranging from air to water, by adjusting two non-contact short circuit plungers. This scheme varies the internal impedance or energy storage in contrast to using external tuning reactances.

A simple, analytic, lumped parameter circuit is obtained for an arbitrarily positioned gap in the center conductor using an artificial electric wall concept. Based on this, an equivalent circuit model is built to characterize the internal tuning and matching mechanism. As an application example, 3 mm and 5 mm diameter mullite rods were joined successfully, without an intermediary, using less than 60 W of microwave power at 915 MHz for 10 minutes.

INTRODUCTION

Recently, interest in high temperature microwave material processing has been growing rapidly. These new applications of microwave energy impose new requirements upon microwave applicators. A crucial one is the applicator's tuning and matching ability. Most materials exhibit a temperature dependence resulting in an unstable applicator input impedance. For this reason, an applicator tunable and matchable over a wide range of dielectric properties is desirable.

In this paper, a new, high temperature, microwave resonant applicator capable of internal tuning and matching to different dielectric loads is presented. Moreover, an artificial electric wall concept is introduced to build an equivalent circuit model and to characterize the applicator's tuning and matching performance.

Subsequently, as an application example, mullite rods of 3 mm and 5 mm in diameter are joined with less than 60 W of power at 915 MHz.

APPLICATOR DESCRIPTION

Our applicator consists of a coaxial cavity with a gap cutting its hollow center conductor and two movable circuit plungers, as shown in figure 1. The material to be processed is held in the gap and in the adjacent hole region. A coupling loop is mounted on one of the short circuit plungers. The two holes on the side wall are for inspection and temperature measurement.

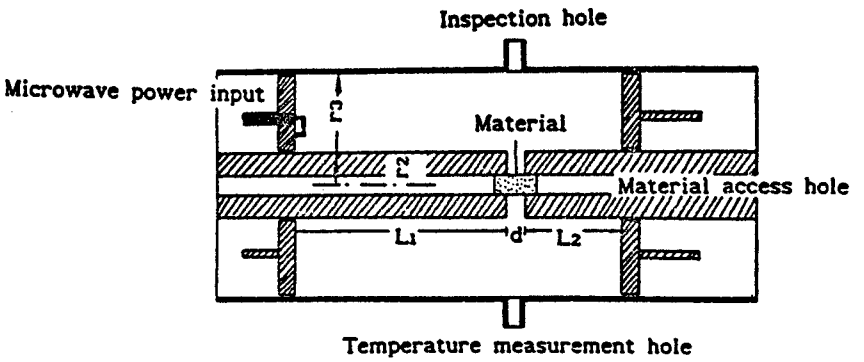


Figure 1. Schematic of the wide range tunable and matchable high temperature microwave applicator.

The present applicator was developed from a coaxial high temperature applicator proposed by Tinga,et in 1990.[1] Instead of using a disk-screw tuner in the former case, two movable short circuit plungers are used for tuning and matching the applicator to overcome the limited tuning and matching capability of the previous design.

THEORETICAL ANALYSIS

This applicator, loaded in the gap, is electromagnetically a complex problem to solve. There are, in the literature, no simple analytic formula of lumped circuit parameters for a gap positioned arbitrarily on a center conductor. However, lumped capacitance formula for a gap at the end of a coaxial cavity are available.[2] Interestingly, we found that once an artificial wall concept was established, this formula could be adapted to a gap at an arbitrary position on the center conductor. Thus an equivalent circuit model can be developed based on this procedure.

Artificial Electric Wall

As shown in figure 2, the position of an electric wall in the gap

is designated by d_1 and d_2. To determine d_1 and d_2, two special cases can be considered. First, if $L_2=0$, that is, the gap is positioned at the end of the cavity, the electric wall is simply the end plate itself, thus $d_2=0$ and $d_1=d$. Secondly, if $L_1=L_2$, i.e. the gap is located at the midplane of the cavity and the electric wall at the midplane of the gap, $d_1=d_2=d/2$, due to symmetry. This fact suggests that an artificial electric wall may move from the midplane of the cavity to the end of the cavity as the gap moves from the midplane to the end. For simplicity, we assume d_1 and d_2 vary with L_1 and L_2, approximately, in a linear fashion, that is

$$d_1=\frac{d(L_1+L_2)}{3L_2+L_1}, \quad \text{and} \quad d_2=d-d_1 \qquad (1)$$

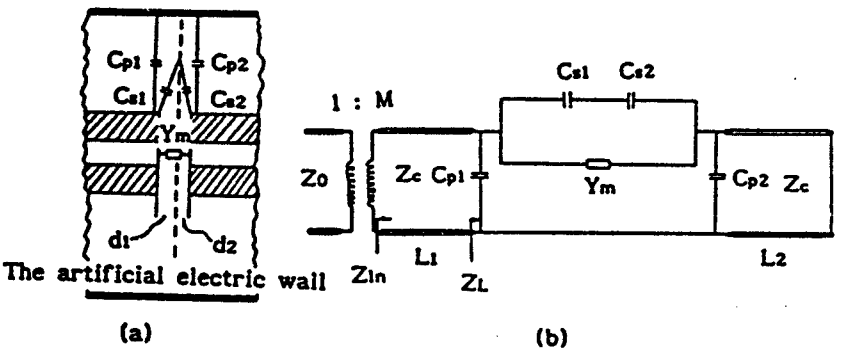


Figure 2. The artificial electric wall (a) and the equivalent circuit (b) of a coaxial cavity with a gap on its center conductor.

Lumped Circuit Parameters

Based on the imaginary electric wall, the gap discontinuity can be represented by the following lumped parameters as shown in figure 2 : two series capacitances, C_{s1} and C_{s2}, two shunt capacitances, C_{p1} and C_{p2}, and an admittance of Y_m, which accounts for the effects of the sample and the hole present in the gap. Using the formula in reference [2], the series gap capacitances can be written as[2]

$$C_{s1}=4r_2\varepsilon_0\ln\left(\frac{r_3-r_2}{d_1}\right)+\frac{\varepsilon_0\pi r_2^2}{d_1} \qquad (2)$$

$$C_{s2}=4r_2\varepsilon_0\ln\left(\frac{r_3-r_2}{d_2}\right)+\frac{\varepsilon_0\pi r_2^2}{d_2} \qquad (3)$$

The shunt capacitances of C_{p1} and C_{p2} are 100 times less than C_{s1}

and C_{s2} for a narrow gap.[3] Therefore, only $Y_m=G_m+jB_m$, determined by the hole and the material's electromagnetic properties, remains unknown.

Resonant and Matching Equation

Based on the equivalent circuit representation in figure 2, the input impedance is given by

$$Z_{in}=Z_c\frac{Z_L+jZ_c\tan(\frac{2\pi}{\lambda}L_1)}{Z_c+jZ_L\tan(\frac{2\pi}{\lambda}L_1)} \qquad (4)$$

where Z_L, a function of L_2, G_m and B_m is readily obtained using the equivalent circuit in figure 2.

Finally, resonance is established when the input reactance

$$Im(Z_{in})=0 \qquad (5)$$

and a matching condition is obtained when we make

$$M^2Re(Z_{in})=Z_0 \qquad (6)$$

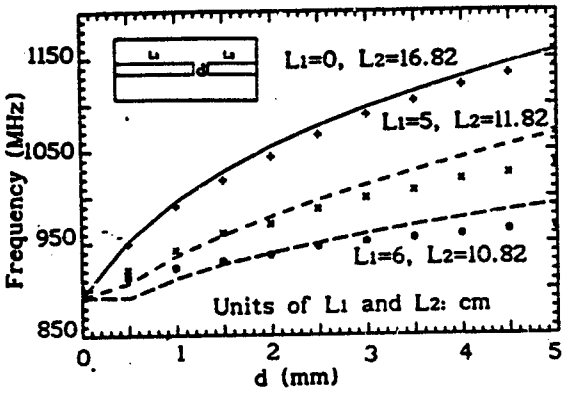
where M is the coupling loop's transformer ratio.

EXPERIMENTAL VERIFICATION OF THE CIRCUIT MODEL

In order to verify the theoretical model, we compared calculated values to measurement results in the L-band. The resonant frequency versus gap width for three different gap positions is depicted in figure 3 and indicates agreement to better than 3.1% for the gap width over 0-5 mm. Figure 4 shows the resonant frequency versus L_1 for three commonly used gap widths of 1 mm, 2 mm and 3 mm, and the maximum discrepancy is 2.1%. Verification for the tuning characteristics predicted by the model is demonstrated in figure 5. L_1 and L_2 are adjusted to tune the cavity to 915 MHz, and the discrepancy between theory and experiment is less than 3.5%. These three figures prove the validity of the artificial electrical wall concept used to develop the equivalent circuit.

TUNING AND MATCHING CHARACTERISTICS

During heating, property variation of the material in the gap invariably leads to detuning and mismatching. For this reason, two adjustable variables related to resonant frequency, f and reflection coefficient amplitude, $|\Gamma|$, are required to keep f and $|\Gamma|$ at their optimal values, namely f=source frequency and $|\Gamma|=0$. Theoretically, the two independent variables L_1 and L_2 can satisfy the equations (5)



Fiure 3. Resonant frequency vs. gap width, d, for different gap position, L_1 and L_2. Lines are theoretical results and dots experimental data.

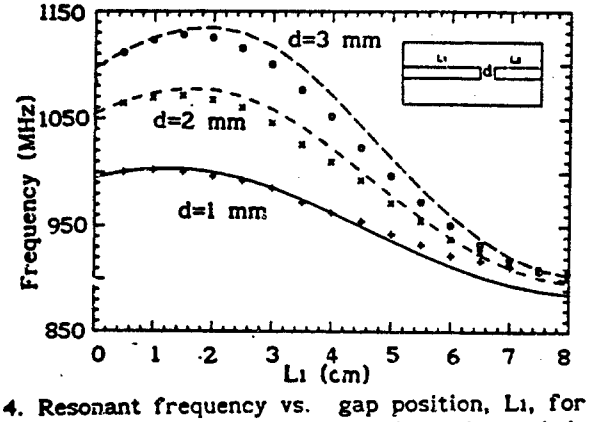


Figure 4. Resonant frequency vs. gap position, L_1, for different gap widths, d. Lines are theoretical results and dots are experimental data.

and (6) simultaneously. Physically, the gap field strength may vary from nearly zero to a maximum for different combinations of L_1 and L_2. Therefore, resonance and matching can be retained regardless of the material property variation in the gap. As a result, this applicator is capable of being tuned and matched internally, eliminating the energy loss problems associated with external tuners.

The tuning curve at 915 MHz is depicted in figure 5. Figures 6 and 7 exhibit the matching characteristics at 915 MHz for different susceptance and conductance in the gap, showing that matching points will shift towards the middle of the cavity as the susceptance or the conductance in the gap increases. Besides, our experiment also showed that perfect matching can be achieved for loads from air to water.

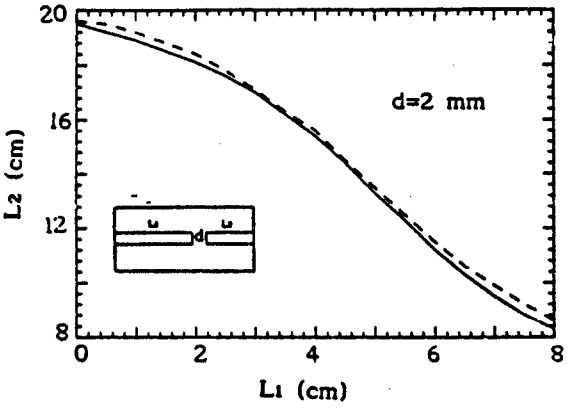


Figure 5. Tuning curves at MHz in terms of L1 and L2. Solid lines are theoretical results and broken lines are experimental ones.

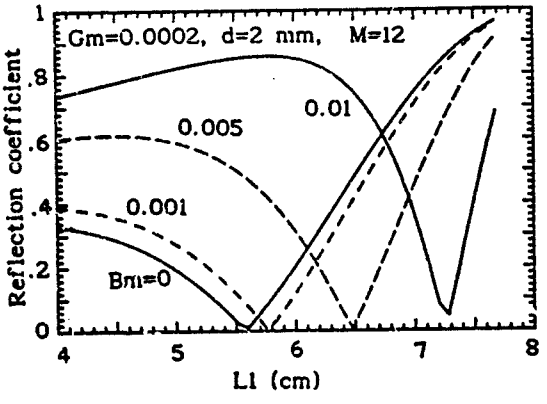


Figure 6. Reflection coefficient vs. gap position, L1, and varying gap load susceptance, Bm.

CERAMIC JOINING EXPERIMENT

As an application example of this applicator, a ceramic rod joining experiment was conducted at 915 MHz. The joining system is shown in figure 8. Microwave power is transmitted into the applicator from a solid-state 915 MHz power source with a maximum 60 W output. Between them is a reflectometer to monitor the tuning and matching. Adjusting the positions of the two plungers we can tune the cavity to 915 MHz and minimize reflected power. The joining surface of the ceramic rods is located in the middle of the gap, where the electric field is focused.

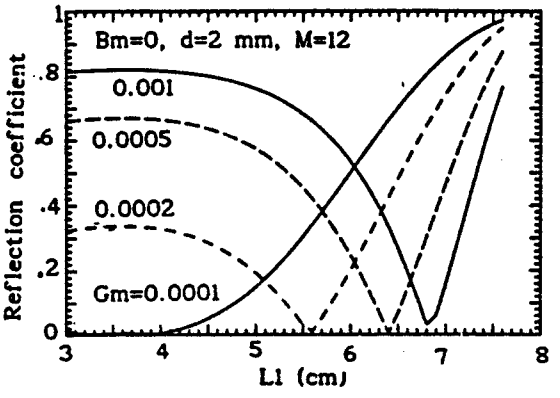


Figure 7. Reflection coefficient vs. gap position, L_1, and varying gap load conductance, Gm.

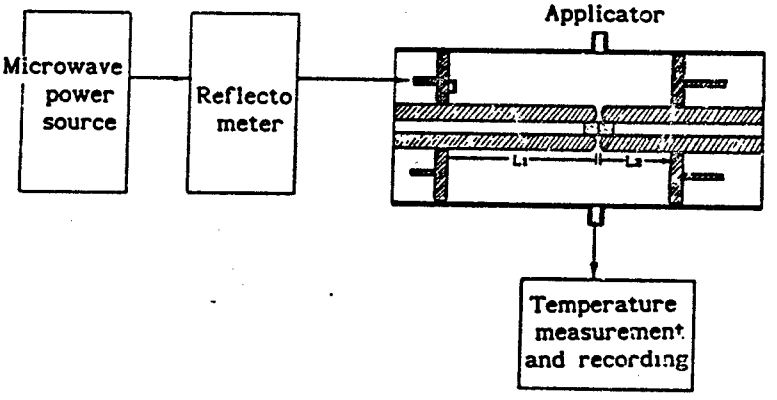


Figure 8. Schematic diagram of the experimental ceramic joining system

Two mullite rods of 3 mm and 5 mm in diameter were used as specimens. Their typical chemical analyses are listed in table 1.

Table 1. Typical Chemical Analyses of Mullite Rods.

Al_2O_3	SiO_2	MgO	Na_2O	CaO	Fe_2O_2	TiO_2	K_2O
55.4	42.0	0.04	0.5	0.1	0.8	0.5	0.7

The rods were first broken and then were joined at the natural broken surfaces without flux and other intermediates. A constant pressure

was applied though two fixed springs at the both ends of the sample. The rods were held at about 1500^0 C for 10 minutes using less than 60 W power. Azimuthal uniformity in the joining zone was achieved without rotating the specimen due to the azimuthally symmetric fields in the applicator. The boundary at the interface could not be detected visually after joining. Bending tests showed that the joined region was slightly stronger than the original rod for the 3 mm sample and 71% of the original strength for the 5 mm one. During the joining process, the required change in L_1 and L_2 was about 4 cm as the sample's temperature changed from room temperature to the highest joining temperature.

CONCLUSION

A new high temperature microwave applicator capable of being internally tuned and matched over a wide range of sample loading is proposed and analyzed. The artificial electric wall concept used in analyzing an arbitrarily positioned gap in the center conductor of a coaxial cavity is proven valid for small gap widths. Using this concept, a simple analytic equivalent circuit model was built to predict the input impedance of the applicator. The calculated results showed good agreement with experimental data. Owing to its good tuning and matching ability, a high heating efficiency has been achieved. Consequently, direct ceramic joining of thin rods can be accomplished with less than 60 W power at 915 MHz. This applicator can be used in various microwave high temperature material processing studies.

ACKNOWLEDGEMENT

This work was sponsored by the National Science and Engineering Research Council of Canada.

REFERENCES

1. W. R. Tinga, B. Q. Tian, W. A. G. Voss, "New High Temperature Multipurpose Applicator", Materials Research Society Proc. Symposium L, USA, April, 1990
2. N. Marcuvitz, Waveguide Handbook, McGRAW-HILL, New York, 1951, p 178.
3. Susanta Sen and P. K. Saka, "Equivalent Circuit of a Gap In the Center Conductor of a Coaxial Line", IEEE., Tran. on MTT, vol.30, pp2026-2029, Nov. 1982

EXPERIMENTAL EXAMINATION OF MATERIAL LOADED CYLINDRICAL APPLICATORS AND COMPARISON WITH THEORETICAL MODELS

J. Asmussen, Jr., B. Manring, R. Fritz, and M. Siegel
Michigan State University, Department of Electrical Engineering
East Lansing, MI 48824-1226

Microwave heating experiments are presented for several different applicator/load configurations. Techniques are described for measuring resonant frequency, cavity quality factor, and electric field at the applicator wall. Theoretical calculations of resonant frequency and field patterns for coaxially loaded rods are shown to compare very well with experiment. Placement and orientation of anisotropic graphite fiber reinforced epoxy composite wafers for maximum power absorption is established. Finally, a method for uniform heating of large materials by mode-switching is demonstrated for the case of nylon disks in TE_{111} and TE_{211} modes.

INTRODUCTION

It is well known that microwave applicators have an infinite set of resonant frequencies. These resonant frequencies provide the fundamental energy coupling windows into the cavity. Each single-mode window represents an electromagnetic field focus and allows energy input into the cavity at a small band of frequencies centered around the resonant frequency. When material loads are placed in the cavity, and when the material is heated, the coupling windows change from the empty cavity condition in a poorly understood manner.

In order to improve understanding of microwave heating and processing of materials it is necessary to understand the single-mode behavior of these material loaded resonances. Two methods of developing and understanding material loaded applicator resonances are theoretical modeling and experimental measurement. Methods of experimental measurement of single-mode material loaded resonances are described here.

EXPERIMENTAL SYSTEMS AND MEASUREMENT TECHNIQUES

The experiments described here were performed with a 6" diameter, variable eigenlength, variable coupling, circular cylindrical cavity applicator shown in Figures 1 and 2 [1], and with a similar 18" diameter cavity applicator not shown. As shown in Figures 1 and 2 the 6" cavity consists of a circular cylindrical waveguide with a fixed shorting plate on the bottom, an axially variable shorting plate on the top of the cavity region, and a variable penetration coupling probe in the side about one quarter of a wavelength from the bottom. Small diagnostic ports 2 mm in diameter are located on the waveguide and bottom shorting plate of the 6" cavity. These diagnostic ports are shown as dots on the cavity walls in Figures 1 and 2.

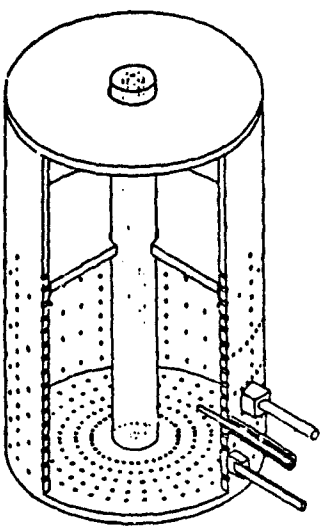


Figure 1. Rod-Loaded Cavity.

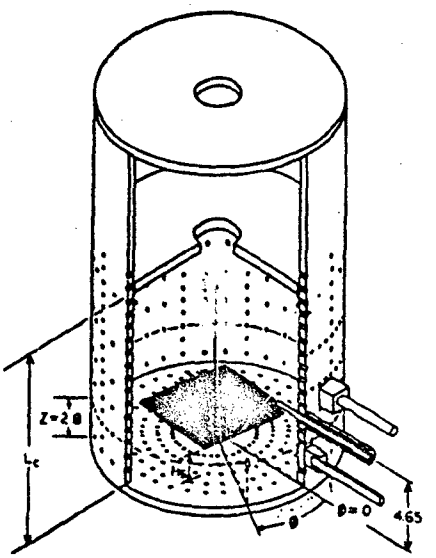


Figure 2. Anisotropic Wafer Loaded Cavity.

Resonant frequency and cavity quality factor measurements are performed using standard microwave circuitry and power absorption spectrum techniques, which together with the normal electric field measurements at the cavity wall, are described elsewhere [2]. Only a brief summary is given here. For low power experiments, microwave energy is provided by a sweep oscillator connected via a coaxial transmission line to the cavity coupling probe. Incident and reflected power are measured and displayed as a function of frequency on an oscilloscope. Resonant modes appear as inverted absorption dips on the display which vary in amplitude as functions of the

coupling. Critical coupling, i.e., zero reflected power, at a desired frequency is accomplished by iterative adjustment of the cavity length and coupling probe penetration.

Cavity quality factor, a measure of the ratio of energy stored in the cavity and load to the energy dissipated, is evaluated by measuring the width of the critically coupled power absorption curve at the half-power points. The cavity quality factor Q is then

$$Q = 2\,\frac{f_0}{\Delta f}, \tag{1}$$

where f_0 is the resonant frequency and Δf is the half-power bandwidth.

Electric field measurements in the interior of a resonant cavity are difficult to obtain since most measurement techniques disturb the cavity fields. However, it is possible to accurately measure the normal electric fields at the cavity wall using a microcoaxial probe. The microcoaxial probe, shown in Figure 3, is inserted into a small port in the cavity wall. The power coupled out by the probe is proportional to the square of the normal component of the electric field.

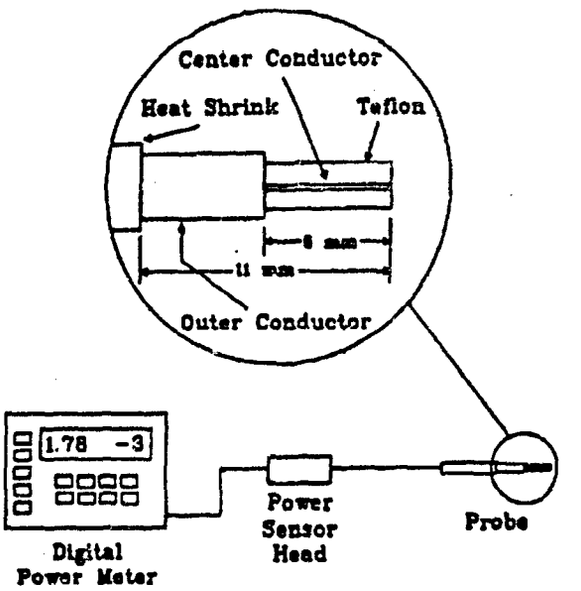


Figure 3. Microcoaxial Field Probe.

EXPERIMENTAL MEASUREMENTS

Cavity-Length Dielectric Rods

Resonant frequency, cavity quality factor, and field patterns were measured for a variety of homogeneous, isotropic dielectric rod loads located coaxially in the cavity and extending the cavity length as shown in Figure 1. Study of this configuration is useful for several reasons. Microwave processing of fibrous materials is often accomplished by drawing the fibers through the cavity coaxially in a continuous process, thus heating the material uniformly [3]. This configuration also lends itself to relatively simple numerical modeling of the electromagnetic fields in the cavity and material.

Resonant frequencies were measured for several different cavity lengths for alumina rod loads. Figure 4 is a graph of resonant frequency versus cavity length for a 6" diameter cavity loaded with a 0.25" diameter alumina load. The cavity was excited in the TM_{011} mode. Empty cavity and loaded cavity theoretical values are plotted for comparison. The theoretical model of this material loaded cavity is described in another paper in this proceedings [4]. As Figure 4 demonstrates, measurements are in excellent agreement with the theory.

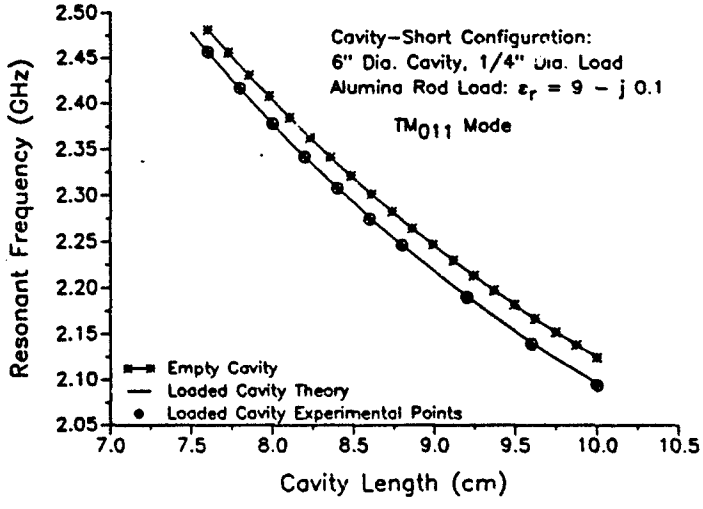


Figure 4. Resonant Frequency vs. Cavity Length for Alumina Rod Load.

The cavity quality factor was found to be 5,920 for the loaded cavity. When empty, the measured cavity quality factor was 6,120 for the TM_{011} mode. For the quality factor measurements, the cavity length was kept constant at the empty cavity 2.45 GHz resonant setting of 7.8 cm. The resonant frequency shifted down when the load was introduced. The quality factor can be considered a measure of the coupling efficiency of the applicator according to Equation (2),

$$Eff = 100\left[1 - \frac{Q_u}{Q_0}\right] \% \qquad (2)$$

where Q_u is the quality factor of the loaded cavity and Q_0 is the quality factor of the empty cavity. From Equation (2) the value of *Eff* for the measured quality factors given above is 3%, which is not unreasonable for a low loss load like sintered alumina, particularly when the load volume is much smaller than the cavity volume as in this case.

Micro-coaxial field probe measurements were made for a variety of rod-shaped material loads including quartz (ϵ_r=3.8-j0.00023), tefion (ϵ_r=2.1-j0.0003), nylon (ϵ_r=3-j0.039), ethyl alcohol (ϵ_r=6.5-j1.65), and ethylene glycol (ϵ_r=14.5-j14.6) along the axial direction for a cavity excited in the TM_{012} mode. Figure 5 shows the familiar standing wave pattern for the TM_{012} mode for loadings with moderate dielectric constant and low to high dielectric loss [5].

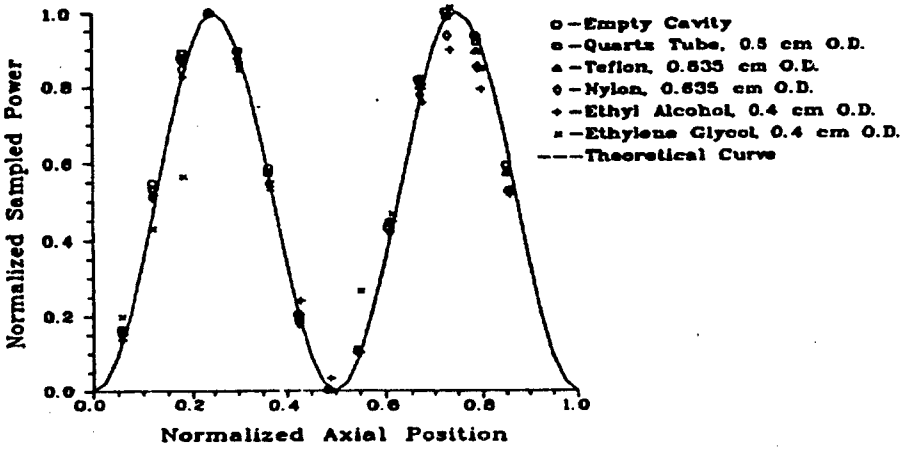


Figure 5. Normalized Axial Field Probe Measurements for Several Load Materials.

Field Patterns in a Composite Loaded Resonant Cavity

Theoretical models are very difficult to develop for certain material properties and shapes. One such material load, shown in Figure 2, is a 3" square 1/16" thick unidirectional graphite fiber reinforced epoxy composite wafer. This anisotropic material load dramatically changes the resonant frequencies of the empty cavity and experimental measurements are required to determine the material loaded resonances. Examples of single-mode measurements are presented here for the material loaded mode that is closely related to the empty cavity TE_{112} mode.

Measurements of the radial electric field patterns on the inside wall of the resonator are shown in Figure 2. The composite was supported in the cavity by thin rods so that its height and orientation could be continuously varied. The cavity was excited with a sweep oscillator at 2.45 GHz cw. Output from the microcoaxial field probe was displayed on a digital power meter.

It was observed that E_r was greatly reduced at the cavity wall when the composite sample was placed in the cavity. The sum of the field measurements around the circumference is plotted in Figure 6 for different sample heights, showing a minimum at about 1/2 cm for fiber orientation perpendicular to the input probe axis, and at about 3/4 cm for fibers parallel to the probe axis. The material loaded quality factor showed a minimum of 300 for a sample height of 1/2 to 3/4 cm when the fibers were parallel to the coupling probe, and less than 200 for any sample height when the fibers were perpendicular to the input probe, Figure 7. The input probe length did not show a well defined trend, as it was varied for loaded cavity impedance matching.

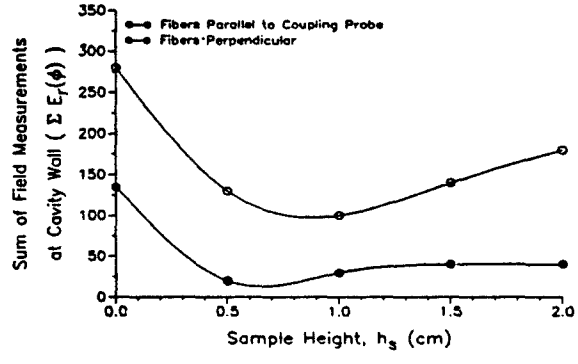


Figure 6. Sum of E_r measurements around circumference at 2.7 cm above the applicator bottom as a function of sample height.

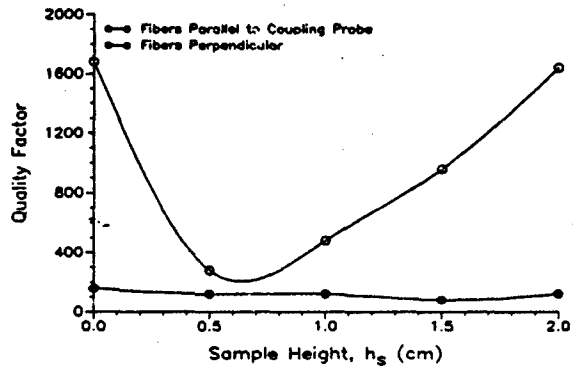


Figure 7. Cavity quality factor as a function of sample height. TE_{112} mode in a 6-inch diameter cavity.

Overall, measurements of the radial electric field component at the cavity wall and loaded cavity quality factor indicate a sample height of 1/2 to 3/4 cm for optimum energy coupling to the sample, as indicated by the reduction in the magnitudes of the field measured at the cavity wall and the quality factor. More energy was coupled to the sample when the fibers were perpendicular to the input probe, though power absorption was very high for either fiber orientation (loaded Q less than 300).

Figure 8 displays the resonant cavity length as the wafer was elevated in the cavity. When a dielectric is placed inside a resonant cavity the resonant length decreases. When a conductor is placed inside a resonant cavity the resonant length may either increase or decrease depending on where the sample is placed. Figure 8 shows that the conductivity of the graphite fibers dominated the dielectric constant of the epoxy, causing an increase in the cavity resonant length.

Investigation of Single-Mode Heating Patterns

A fundamental problem in microwave heating is nonuniform energy distribution leading to nonuniform heating patterns. One means of overcoming this difficulty is to process large materials using several different heating modes alternately. Since each mode has a unique energy distribution, switching in time between certain individual modes can provide a more uniform heating pattern than any one mode by itself. This mode-switching can take place by either excitation frequency switching or by length tuning the cavity. The following measurements demonstrate how the alternate use of two different modes to heat nylon disks can provide more uniform heating.

A 7" diameter nylon disk 0.25" thick was placed in the center of an 18" diameter cavity excited in the TE_{111} mode at 915 MHz with 40 W of input power. Figure 9

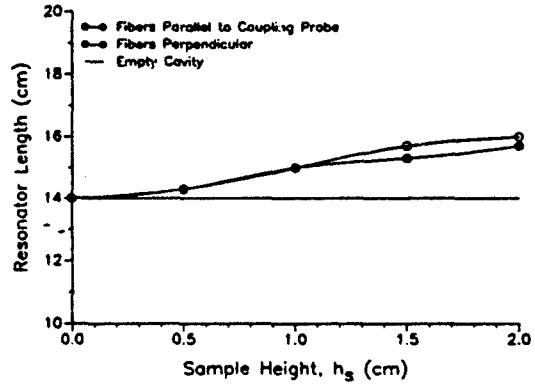


Figure 8. Cavity resonant length as a function of sample height for TE_{112} mode in a 6-inch diameter cavity.

shows a cross-sectional view of the cavity and disk with the temperature measurement positions, labeled 1 through 4, shown as oriented with respect to the coupling probe. Also shown in Figure 9 is a cross-sectional diagram of the field patterns for the TE_{111} mode; this diagram is oriented as the coupling probe in Figure 9 would excite the mode. The electric field is strongest in the center of the disk at position 1. 90° away from the coupling probe near the cavity wall, where there is no temperature measurement position for this configuration, the electric field is weakest.

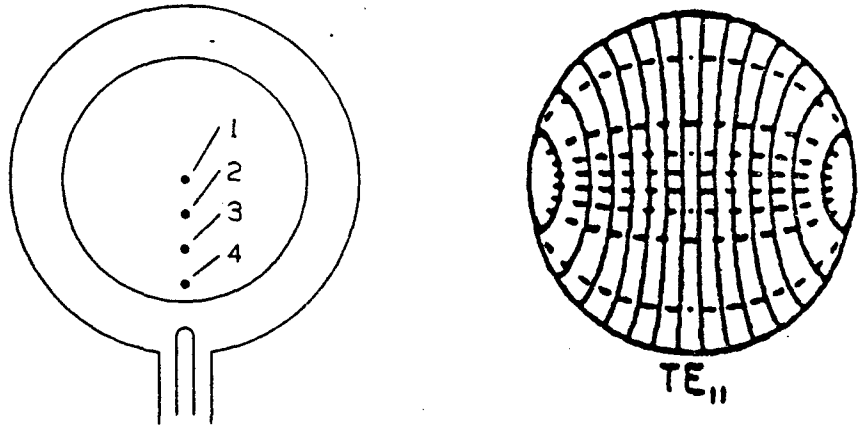


Figure 9. Nylon Disk Configuration for TE_{111} Heating.

Figure 10 is a plot of the measured temperatures versus time for the heating configuration shown in Figure 9. Temperature measurement positions corresponding to those shown Figure 9 are indicated in Figure 10. The temperature measurements correspond to what would be expected from the TE_{111} mode, with the highest temperature being in the center at position 1 and the lowest at position 4.

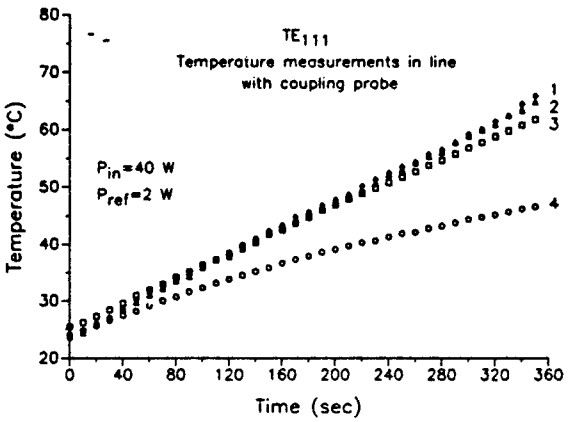


Figure 10. Temperature Measurements for Configuration Shown in Figure 9.

A similar experiment was conducted using the TE_{211} mode which has an electric field configuration and orientation with respect to the coupling probe as shown in Figure 11. For TE_{211}, the electric field is weakest in the center of the cavity, while for TE_{111} it was strongest. TE_{211} is better for heating the edges of the disk than the center.

The temperature measurements for the configuration of Figure 11 are plotted in Figure 12. Again, the expectation from examination of the electric field pattern of TE_{211} is borne out in the temperature measurements. Figure 12 shows that the lowest temperatures were toward the center of the disk while the warmest regions were on the edges. Other measurements, not shown here, for the same modes but for temperature measurement positions at different orientations with respect to the coupling probe, also demonstrate the heating pattern expected from examination of the modal electric fields.

These Figures demonstrate the complementary nature of single-mode heating with different modes. It is likely that a judicious combination of heating modes which will produce uniform heating under proper time constraints can be found for most cavity/load configurations. This procedure, called mode-switching, preserves the controllability and simplicity of single-mode heating while at the same time making it possible to heat many materials uniformly.

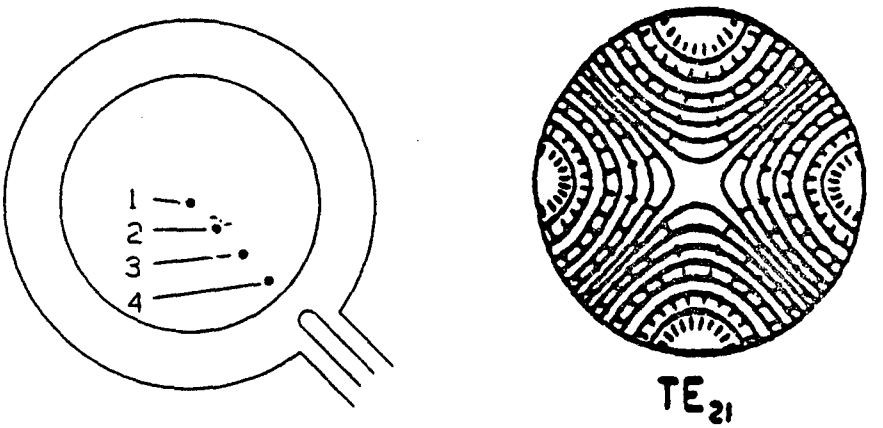


Figure 11. Nylon disk Configuration for TE_{211} Heating.

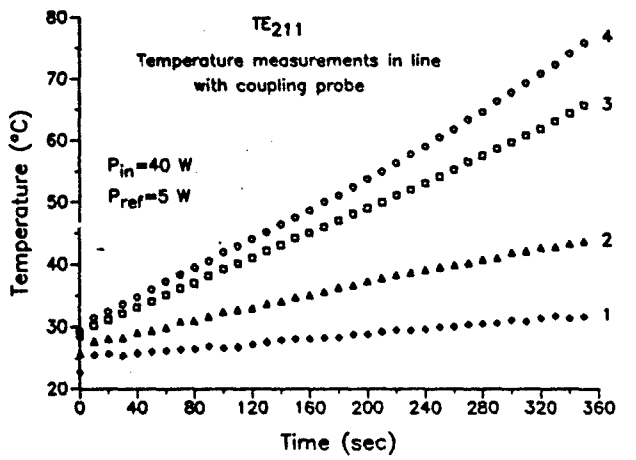


Figure 12. Temperature Measurements for Configuration Shown in Figure 11.

SUMMARY

Measurement techniques in lossy material-loaded cavity applicators have been described for a variety of applicator/load configurations and material properties. Even for highly lossy material loads with low cavity quality factors, it was still possible to

measure well-defined standing wave field patterns. Theoretical resonant frequency calculations were shown to compare very well with experimental measurements for rod loads extending the length of the cavity. Optimum energy coupling to unidirectional graphite fiber reinforced epoxy composite wafers was achieved by experimental trials of placement and fiber orientation. Finally, it was shown that single-mode heating patterns may be combined by mode-switching to uniformly heat large material loads.

---

1. Cavity drawings by Leonard Mahoney. A detailed description of the cavity and location of the diagnostic ports is given in L. Frasch, Ph.D. Dissertation, Michigan State University, 1987.

2. J. Rogers, Ph.D. Dissertation, Michigan State University, 1982.

3. Hua-Feng Huang, "Temperature Control in a Microwave Resonant Cavity System for Rapid Heating of Nylon Monofilament," *Journal of Microwave Power*, 11(4) 1976, 305-313.

4. B. Manring and J. Asmussen, Jr., "Electromagnetic Modeling of Single-Mode Excited Material Loaded Applicators," *Proceedings of the American Ceramic Society Symposium on Microwaves: Theory and Application in Materials Processing*, Cincinnati, Ohio, April 28-May 2, 1991.

5. L. Frasch, Ph.D. Dissertation, Michigan State University, 1987, 210.

TECHNIQUES TO IMPROVE THE PERFORMANCE OF MICROWAVE PROCESS SYSTEMS WHICH UTILIZE HIGH Q CAVITIES

John F. Gerling
Gerling Laboratories
Modesto, CA 95351

Gene Fournier
Wavemat, Inc.
Plymouth, MI 48170

ABSTRACT

Process systems utilizing high Q cavities can be subject to difficulty in tuning, resulting in reduced operational stability and power coupling. The relationships between magnetron operation and cavity Q are discussed, as well as the effects of insufficient magnetron isolation, varying magnetron output frequency and the phenomenon known as the long lines effect. Techniques to improve system performance are also discussed, including those for increased isolation, constant frequency operation and variable Q.

BACKGROUND

Most applications of microwave power in industrial heating processes involve the use of relatively crude and inefficient microwave process cavities. However, in recent years the development of microwave processes for a variety of new applications has led to new designs of high efficiency cavities. The need for such cavities stems from the desire to apply relatively large amounts of microwave power to materials which do not readily absorb such power. Examples of these "low loss" materials include high purity ceramics, certain plastics and other materials which can be characterized as having a loss tangent of less than 10^{-2} [1]. Even high loss materials can require a high efficiency cavity if the amount is small compared to the size and/or volume of the cavity.

The use of high efficiency cavities in conjunction with other equipment commonly found in industrial microwave process systems makes evident certain limitations in overall system performance which previously were seldom encountered. Operators of such systems have experienced difficulty in tuning a load to maximize power coupling and have experienced tuning instability once a match had been found. The use of a few relatively simple techniques involving common microwave system components can reduce or

eliminate many of these problems.

Cavity Q

Relating the difficulties and instabilities of tuning to the efficiency of a microwave process cavity can best be done by defining a quality factor, Q, in terms of the amount of energy stored in and lost to the cavity [2]. A microwave cavity can be described as a resonant circuit element in a microwave network, where the frequency of resonance of the element is a function of its characteristic complex impedance. The Q of any resonant circuit at the frequency of resonance is defined as

$$Q \cong 2\pi \times \frac{\text{Energy Stored}}{\text{Energy Dissipated}} \qquad (1)$$

When a load is present in the cavity the Q of the resonant circuit is a function of the total energy absorbed by both the cavity and the load. However, when the cavity is empty the Q is a function of the energy dissipated to the cavity itself.

In cases where the load is highly absorptive of microwave energy the total energy dissipated will be high, thus the Q will be low, regardless of the Q of the cavity. Otherwise, if the load does not readily absorb microwave energy then the Q of the resonant circuit will be more dependent upon the losses to, hence the efficiency of, the cavity.

Power Coupling

The Q of any resonant circuit can also be described in terms of the bandwidth of the circuit [3]. That is,

$$Q = \frac{\text{Resonant Frequency}}{\text{Half-Power Bandwidth}} = \frac{f_r}{(f_1 - f_2)} \qquad (2)$$

as illustrated in Figure 1. The maximum amount of the transmitted

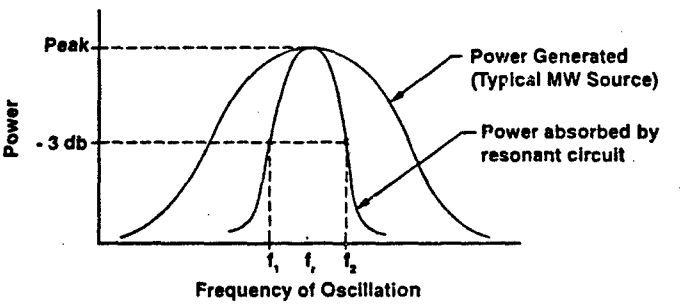


Figure 1. Bandwidth comparison between resonant cavity and microwave power source.

power which can be absorbed by the resonant circuit as a function of frequency is represented by the curve.

The importance of the above relationship is apparent when compared to the output frequency spectrum of a typical microwave power generator. The power output of the generator as a function of frequency is also represented by its output spectrum curve. If the Q of the loaded cavity is high then its bandwidth can be small as compared to the band of energy generated by the power source. The result is that only a small percentage of the power generated will be absorbed by the loaded cavity [4].

MAGNETRON OPERATION

A magnetron is also considered to be a resonant cavity [5]. Under normal operating conditions a magnetron's resonant frequency of oscillation is determined primarily by its physical characteristics of size, shape, materials of construction, etc. Other factors which can influence the output frequency include output power level, cooling temperature, waveform, age and reflected power. The output frequency of a typical magnetron operating nominally at 2.45 GHz can vary as much as +/- 30 MHz.

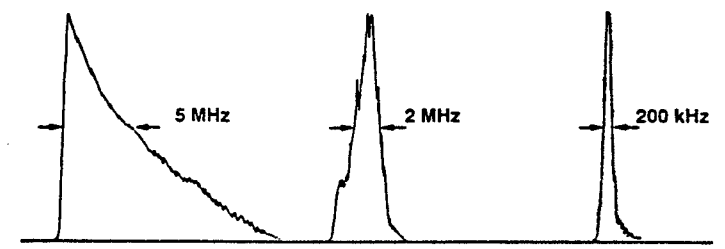


Figure 2. Magnetron output frequency spectrums.

Figures 2a thru 2c illustrate typical output frequency spectrums for magnetrons powered by different types of power supplies.

Because a magnetron is a resonant cavity it also has an associated Q which can vary depending on the conditions under which it is operating. Thus, the output frequency spectral bandwidth can vary depending on operating conditions.

The important relationship to consider is that between the output frequency and spectral bandwidth of the magnetron and the bandwidth of tuning of a resonant cavity. Figure 3 illustrates the relationship between a magnetron operating at 2.45 GHz with a spectral bandwidth as shown in Figure 2c and a cavity with a Q of 6,000. It is clear that power coupling can be reduced dramatically for relatively small shifts in output frequency.

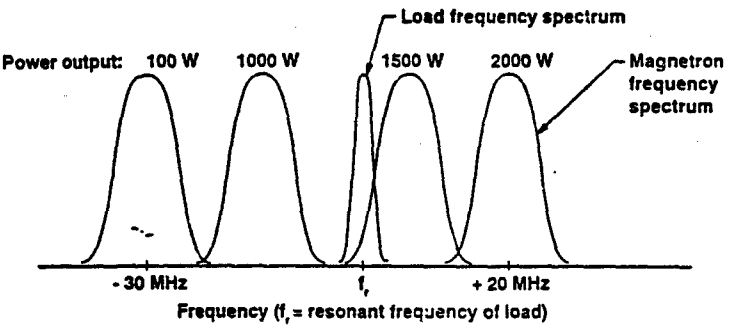


Figure 3. Magnetron output frequency operating range.

Reflected Power

The effect of reflected power on the operation of a magnetron can best be predicted using a Rieke Diagram [6] such as that shown in Figure 4. The Rieke Diagram describes, for a given plate voltage and current, the relationships between a magnetron's actual power output and oscillation frequency and the amplitude and phase of reflected power. The amplitude of reflected power is represented by annular rings in terms of VSWR while its phase with respect to the magnetron is represented by radial lines where a full 360 degrees equals one half wavelength.

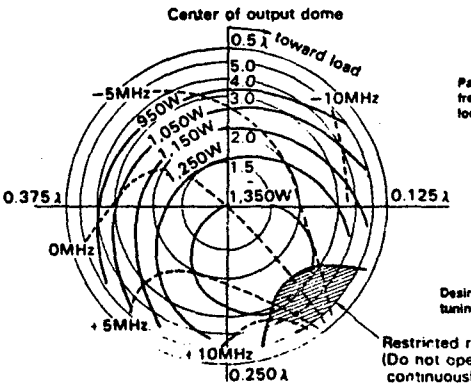


Figure 4. Rieke Diagram for 2M131 magnetron.

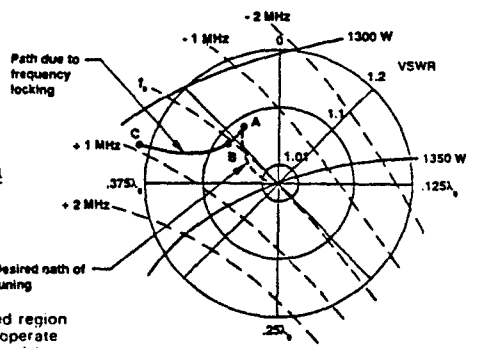


Figure 5. Magnetron frequency locking.

Reflected power for a particular case is represented by a point on the diagram which corresponds to its phase and Voltage Standing Wave Ratio (VSWR). The frequency and power lines which intersect that point represent the operating point of the magnetron. In the case of operation with a high Q cavity, a relatively small amount of reflected power can cause enough of a shift in output frequency to reduce power coupling to the load. The shift in output frequency is commonly referred to as "pulling" of the magnetron.

During the process of tuning the load the amplitude and/or phase of reflected power can change. Depending on the region of the Rieke Diagram in which this occurs, the result can be that of frequency locking which is characterized as a sudden loss of coupling after a small change in tuning. An example of this phenomenon is illustrated in Figure 5 where the desired path of tuning is from point A towards the center. At the beginning of the path the magnetron output frequency shifts enough to begin a reduction in coupling to the load. If tuning continues past point B then the change in frequency and the loss in coupling tend to reinforce each other causing an uncontrolled jump to point C.

Long Lines Effect

Instability of the magnetron output frequency can also occur in situations which allow the magnetron to operate at more than one nominal frequency. System configurations in which the actual distance between the magnetron and the load is significantly long can cause frequency jumping and/or a complete breakdown of the output spectrum [7]. The region of unstable magnetron operation as defined by the Rieke diagram becomes significantly enlarged when the magnetron is subjected to the long lines phenomenon [8].

TECHNIQUES TO IMPROVE PERFORMANCE

From the above discussions it is apparent there are several factors which affect the performance of high Q processing systems, primarily the spectral bandwidth of both magnetrons and cavities and the effect of reflected power on the operation of the magnetron. The following concepts can be implemented either individually or simultaneously to help improve overall system performance.

Magnetron Isolation

When operated into a matched load a magnetron's frequency performance is primarily determined by the magnetron power supply and cooling system. The adverse effects of reflected power on output power and frequency stability gives rise to the need for adequate magnetron isolation. The minimum isolation required for a certain situation depends upon factors such as magnetron output frequency spectral bandwidth, magnetron power output level, cavity Q and maximum expected reflected power.

The use of a 3-port circulator and dummy load to isolate the magnetron from reflected power is relatively common for high power processing systems [9] as shown in Figure 8. The performance of the circulator and dummy load together is determined by measuring the attenuation of reflected power (in db) for all phases of reflection. A typical circulator designed for industrial use provides 16 to 20 db of isolation while high performance circulators designed for laboratory use can provide 25 to 30 db of isolation at all phases of reflected power.

Figure 6a illustrates how the attenuation varies as a function of the phase of reflected power for a typical high performance circu-

lator and dummy load. For most applications an adjustment in the length of the waveguide between the circulator and the cavity may be necessary in order to maximize isolation for the specific phase of the load impedance.

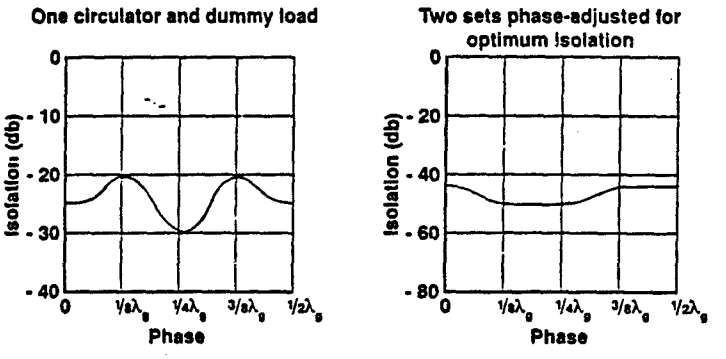


Figure 6. Circulator/dummy load performance vs phase of reflected power.

In some processes the complex impedance of a load can undergo a phase shift, for example as it is heated. It is possible to have sufficient isolation at the beginning of the process so that power is coupled to the load and then to lose isolation as the load impedance shifts in phase, thus causing a loss in power coupling.

It is for this reason that more than one circulator and dummy load combination has been used in a single system solely for the purpose of magnetron isolation. By adjusting the length of waveguide between the two circulators, the isolation can be maximized at all phases of reflection as shown in Figure 6b.

Constant Frequency Operation

A fundamental characteristic of all magnetrons is that their output center frequency varies with the level of output power as shown in Figure 7. As noted previously, such variation in output

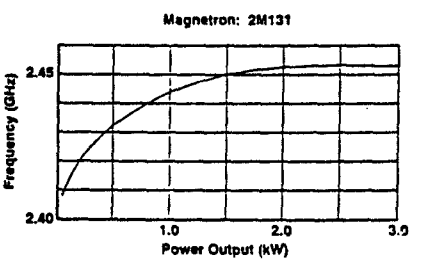


Figure 7. Magnetron power vs frequency.

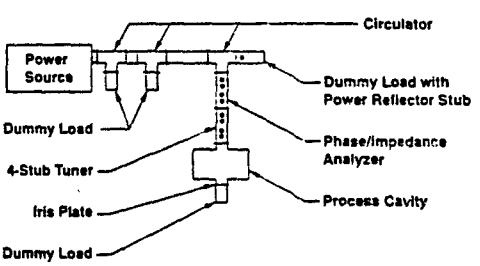


Figure 8. Typical MW system for laboratory use.

frequency is unacceptable for most high Q processes. However, variations in power level are a necessary requirement in many processes. One solution is to operate the microwave power source at full power and pulse the magnetron to achieve a variation in average power. This solution, however, may not be acceptable for reasons relating to process requirements.

An alternate technique which provides continuously variable power output at a fixed frequency also involves operation of the power source at full output. Figure 8 illustrates a configuration which utilizes an additional circulator. Instead of connecting the process cavity to port 2 as is usually the case, the load is connected to port 3. Connected to port 2 is a dummy load which is allowed to absorb all of the power generated by the power source operating at full output. By inserting a tuning stub into the waveguide of the dummy load, power is reflected back to the circulator where it is diverted to port 3. The power then exits port 3 and is applied to the load in the cavity.

Another advantage of the above technique is that it provides a waveform with a ripple content which is a fixed percentage of power applied to the load. The power supplies used to generate the frequency spectrums shown in Figure 2b and 2c provide a waveform ripple which has a fixed peak-to-peak amplitude, regardless of the level of power output. Without the use of the above technique the ripple may be acceptable at or near full power but perhaps not at some intermediate power level.

Magnetron Cooling System

As mentioned earlier, a magnetron's output frequency is effected by changes in the temperature of the cooling medium. All magnetrons require an external cooling system, usually either forced air or running water, to adequately dissipate the heat generated during operation. The output frequency of a typical magnetron can change by as much as 250 kHz per degree Celsius change in inlet temperature of the air or water. For this reason it is important that the cooling system be designed to ensure adequate temperature regulation. For the same reason it is important that the ambient conditions also remain as stable as possible.

Variable Q

Some situations can exist in which the cavity and load Q is so high that tuning and operational instability seems insurmountable. In such cases it may be possible to reduce the Q while maintaining vital process parameters, thereby improving both tuning and operational stability. Referring to equation 1, a reduction in Q can be achieved by increasing the amount of power dissipated by the system, either by increasing the size or loss characteristics of the load or by increasing the losses to the surroundings. The former may be unacceptable for process reasons while the latter can be accomplished using a few simple techniques.

Figure 8 shows a process cavity consisting of two ports. The

first port is used for power entry. A dummy load is connected to the second port and is used to increase the total amount of power absorbed by the cavity. By inserting an iris plate between the dummy load and the cavity the amount of power absorbed can be decreased, thereby increasing the overall Q of the cavity. The operator can experiment with irises of various sizes until the optimum Q of the cavity is reached.

The drawback of the variable Q technique is that the cavity field strength is decreased as Q is decreased. This can be made up for by increasing the power delivered to the cavity. The net result is a reduction in the overall efficiency of the system.

Waveguide Length

To avoid the problems associated with the long lines effect the microwave processing system should be designed to minimize the length of waveguide between the magnetron and the process cavity. The critical length, i.e. the length at which unstable operation begins to occur, depends upon factors such as magnetron operating characteristics, waveguide components utilized and waveguide size.

SUMMARY

The difficulties in tuning and operation of systems utilizing high Q cavities is caused primarily by a narrowing of the resonant bandwidth, thus creating difficulties in coupling power to the load. These difficulties can be overcome through stabilization of the operating frequency of the magnetron by sufficiently isolating it from reflected power, by allowing it to operate at a fixed level of power output and by stabilizing the external conditions under which the magnetron is operating. Alternately, by reducing the Q of the cavity the resonant bandwidth can be increased, thus offering greater ease in tuning and operational stability.

REFERENCES

1. A.C. Metaxas and R.J. Meredith, "Dielectric Properties," pg. 63 in *Industrial Microwave Heating*, Peter Peregrinus Ltd, London, UK, 1983.
2. P.A. Rizzi, "Microwave Resonators and Filters," pg. 412 in *Microwave Engineering*, Prentice-Hall, Inc., Englewood Heights, NJ, 1988.
3. Rizzi, pg. 413.
4. G.L. Ragan, "The Design of Microwave Filters," pg. 654 in *Microwave Transmission Circuits*, Radiation Laboratory Series, McGraw-Hill, New York, NY, 1948.
5. Ragan, "Elementary Line Theory," pg. 83.
6. Metaxas, "The Microwave Heating Circuit, Breakdown Phenomenon and Vacuum Processing," pg. 244.
7. J.E. Gerling, "System Design Considerations," pg. 12 in *Application Considerations for the Pulse Magnetron*, Litton Industries, San Carlos, CA, 1957.
8. Ragan, pg. 84.
9. Metaxas, pg. 251

MICROWAVE THERMOGRAVIMETRIC ANALYZER (MTGA)

Edmund H. Moore, Iftikhar Ahmad and David E. Clark
Department of Materials Science and Engineering
University of Florida
Gainesville, Florida 32611-2066

A Microwave Thermogravimetric Analyzer (MTGA) has been constructed, which allows for the measurement of weight change of a sample located within a 2.45 GHz microwave cavity, as a function of temperature. Samples in the powdered or compact form, are heated by microwave hybrid heating (MHH). These samples are placed inside an inert holder and subjected to a known reproducible thermal profile, which allows the material to be characterized. Changes in sample weight may occur due to oxidation, decomposition, reduction, volatilization, sublimation and/or reactions within the sample. Results of a binder removal study and the MTGA will be discussed.

INTRODUCTION

The processing and fabrication of materials with microwaves is becoming more important, and will become even more important over the next five to ten years. Potential advantages of microwave processing of materials, especially ceramic materials, include economic, ultra-rapid heating, uniform and volumetric heating [1,2]. Economic advantages may be realized in lower energy cost and shorter processing times. The ultra-rapid heating of materials may result in enhanced materials properties. Uniform and volumetric heating may result in materials being produced with fewer flaws and defects.

The overall objective of our research in the area of microwave processing of materials is to better understand how microwaves interact with materials. A more specific goal, of this paper, is to understand how microwaves interact with the polymethyl methacrylate (PMMA)/alumina system to effect the pyrolysis, decomposition, removal or burnout of the PMMA binder. Several binder removal studies have been done on polymeric binder(s) and alumina, including the PMMA/alumina system [3,4,5]. With this purpose in mind, a first generation MTGA apparatus has been developed.

The MTGA apparatus allows for a material to be characterized in a 2.45 GHz microwave cavity. The materials weight change may be monitored as a function of both time and temperature. Any process utilizing microwave energy as a heating source, that results in a weight change in the material, may be analyzed with a MTGA type apparatus. Future

additions of characterization equipment to the MTGA may allow chemical information to be obtained.

Since small samples are often hard to heat in a microwave cavity, a susceptor has been used to aid in heating the samples. Therefore, microwave hybrid heating (MHH), a combination of both thermal and microwave (MW) heating will be utilized for all samples placed into the MTGA apparatus.

EXPERIMENTAL PROCEDURE

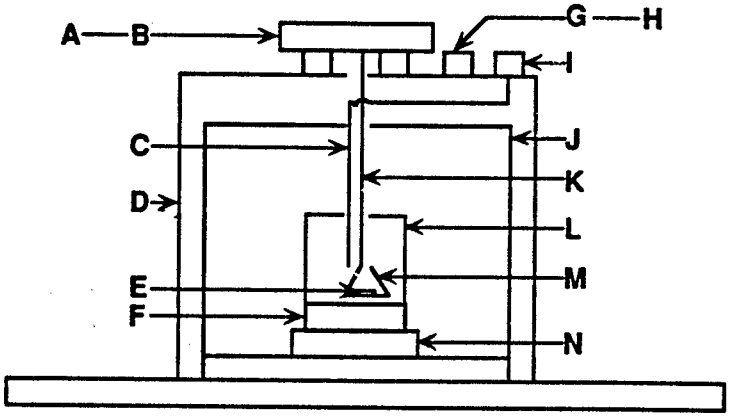
This section of the paper will essentially be written in two parts. The first part will cover the apparatus, that is the MTGA, and the second part will deal with experimental procedures.

Apparatus

Refer to Figure 1, which is a schematic of the MTGA apparatus. A Zenith[1] computer (A) has been interfaced with a Mettler[2] electronic balance (B) to record weight every 30 seconds. This data is sent directly into a spreadsheet program, in real time, and the weight versus time data can be plotted. A temperature display (G), that is an Omega[3] thermocouple thermometer, is connected to both a temperature controller (I) and a y-t plotter (H). The temperature controller is an Omega[4] microprocessor based temperature controller and the y-t plotter is a Fisher[5] y-t recorder. The y-t plotter allows temperature versus time data to be plotted and the temperature controller is interfaced with the electronic smart board of the G.E.[6] microwave oven (J) to control the processing temperature of the sample (E) being processed in the MTGA apparatus. The electronic balance (B), temperature display (G) and the temperature controller (I) are isolated from the microwave cavity (J) and supported by the cabinet (D). Holes have been drilled through the cabinet (D) and through the roof of the microwave cavity (J). A pyrex glass sample holder rod (K), with hooks on both ends, is suspended from the base of the electronic balance (B) into the microwave cavity (J). A pyrex glass sample holder (M) is connected to the sample holder rod (K) and samples (E) of either powders in a crucible or compacts may be suspended from the electronic balance (B). Alumina insulation (N) isolates the susceptor (L) and the susceptor base (F) from the floor of the microwave cavity (J). The susceptor (L) is simply a zirconia cylinder, with a thin coating of β-SiC paste on the inner walls of the susceptor (L). The susceptor (L) has been cut in half through the center of its top and a hole has been cut into the center of the top of the susceptor (L) to allow the sample holder rod (K) and the shielded K-type Omega[7] thermocouple (C) to be suspended inside of the susceptor (L). The thermocouple (C) is also

---

[1]Zenith Electronics Corp., Glenview, IL Model # ZF-158-42
[2]Mettler Instrument Co., Hightstown, NJ Model # PE 360
[3]Omega Engineering, Inc., Stamford, CT Model # 115 KC
[4]Omega Engineering, Inc., Stamford, CT Model # CN 9000
[5]Houston Instrument, Austin, TX Model # B5137-5I
[6]General Electric Co., Louisville, KY Model # JE1445
[7]Omega Engineering, Inc., Stamford, CT Part # XCIB-K-1-4-3



A - Computer
B - Electronic Balance
C - Thermocouple
D - Cabinet
E - Sample
F - Susceptor Base
G - Temperature Display
H - y-t Plotter
I - Temperature Controller
J - Microwave Cavity
K - Sample Holder Rod
L - Susceptor
M - Sample Holder
N - Insulation

Figure 1. Microwave Thermogravimetric Analyzer (MTGA).

connected to the temperature controller (I), used to monitor the samples (E) temperature and enters through a hole located in the back wall of the microwave cavity (J). The microwave cavity (J) has a power of 700 watts. The resolution of the electronic balance (B) is 0.001 milligrams and it has a 360 gram capacity.

Procedure

Refer to Figure 2, which is an Experimental Design Flowchart. Sumitomo[8] alumina powder, with a median diameter of 0.32 μm, as determined by x-ray sedigraph[9], was utilized in all sample preparations. The alumina powder was calcined at 1050°C for 24 hours in a 3500 watt Lindberg[10] Oven. DuPont[11] polymethyl methacrylate (PMMA) binder was used in all sample preparations, and was dried at 50°C for 24 hours, in a Blue M Oven[12]. The PMMA was mixed with chloroform in a Nalgene bottle. Both the solvent and the bottles, that is

[8]Sumitomo Chemical America, Inc., New York, NY Item # AKP-30
[9]Micromeritics Instrument Corp., Norcross, GA Model # SediGraph 5100
[10]Lindberg, Watertown, WI Type # 51894
[11]DuPont Co., Wilmington, DE Item # Elvacite 2010
[12]Blue M Electric Co., Blue Island, IL Model # OV-18A

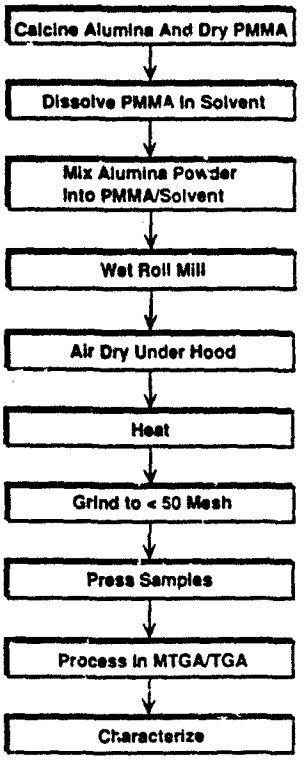


Figure 2. Experimental Design Flowchart.

chloroform[13] and Nalgene[14] bottles, respectively, were supplied by Fisher Scientific Inc. Once the PMMA dissolved in the chloroform, the alumina powder was mixed into the viscous solution and the mixture was wet roll milled for 24 hours on a U.S Stoneware[15] roll mill. The contents of the Nalgene bottle were then poured onto a sheet of mylar film, which covered a piece of plate glass. The PMMA, alumina and chloroform mixture was allowed to air dry under a hood for 24 hours. The mixture was then placed into a Blue M oven and dried at 50°C for 24 hours, to remove any residual solvent or moisture. The mixture was then ground to less than 50 mesh, which corresponds to less than 300 μm sized mesh openings, with a mortar and pestle. Either powder samples were used or compact samples were pressed, at

[13]Fisher Scientific Co., Fair Lawn, NJ Item # C-603
[14]Fisher Scientific Co., Fair Lawn, NJ Item # Nalgene 2104
[15]U.S. Stoneware, Mahwah, NJ Serial # CV89305

27.57 MPa (4000 psi), and used. Compact samples weighed either 2 grams or 4 grams and the weight percent (w/o) of PMMA binder used to make the samples was either 4 w/o or 8 w/o. The die used to press the compact samples was 1.27 cm (0.5 inches) in diameter. Samples were then processed or heated in a tube furnace, oven, thermogravimetric analyzer (TGA) and/or in a MTGA. In all cases, a static air atmosphere was used in the MTGA and the oven, whereas a flowing air atmosphere was utilized in the TGA and tube furnace. Usually, samples were processed in the MTGA first, then the heating schedule of the MTGA processed sample was mimicked with the TGA. However, for this paper, only TGA and MTGA data will be discussed.

RESULTS AND DISCUSSION

Results

Refer to Figure 3, which is a plot of TGA data, for two samples, and MTGA data for another sample. The upper plot shows sample temperature versus time and the lower one shows the corresponding change in weight % of the sample versus time. Sample composition was 4 w/o PMMA/alumina. Two samples, 1.27 cm in diameter, were pressed at 27.57 MPa. One was heated in the MTGA in a static air atmosphere. The other was sent to Harrop Inc., heated in a Harrop[16] TGA (with a Sartorius balance) and a flowing air atmosphere was used. The third one was a 64.51 milligram powder sample, heated in a DuPont[17] TGA (interfaced with a 1090 processor) and a flowing air atmosphere was used. The heating schedule of the MTGA processed sample was mimicked by the TGA processed samples. However, the MTGA processed sample was only heated to 400°C, at 18°C per minute, and processed for a total time of 60 minutes, which corresponds to a 45 minute isothermal hold at 400°C. The samples processed in the TGAs mimicked the MTGA sample for 60 minutes and were then heated to 1000°C at 18°C per minute. The compact sample was held at 1000°C for 30 minutes and the powder sample was heated to 1000°C.

Discussion

Microwaves have longer wavelengths and shorter frequencies than infrared radiation (thermal). In very simplified terms, infrared (IR) heating is accomplished by slow phonon conduction and microwave heating is accomplished by fast radiant conduction. MHH is just a combination of the two forms of heating. Calculations of the depth of penetration, which defines where 63% of the energy of the radiation is dissipated into a material as heat, were done using room temperature dielectric data [6,7]. The calculated depth of penetration for alumina is 581.4 cm (at 2.45 GHz) and 0.14 cm (at 10 THz). The calculated depth of penetration for PMMA was 209.4 cm (at 2.45 GHz) and 0.05 cm (at 10 THz). Samples of the size used in this initial investigation, in theory, should be heated more efficiently by infrared radiation and MHH, than by microwave heating. Figure 3 seems to indicate a delay in the removal of the binder, when using the MTGA apparatus as compared to the TGA. However, this data shows that the weight losses of all three samples are comparable. An apparent

---

[16]Harrop Industries, Inc., Columbus, OH Model # ST-712
[17]DuPont Co., Wilmington, DE Model # 951

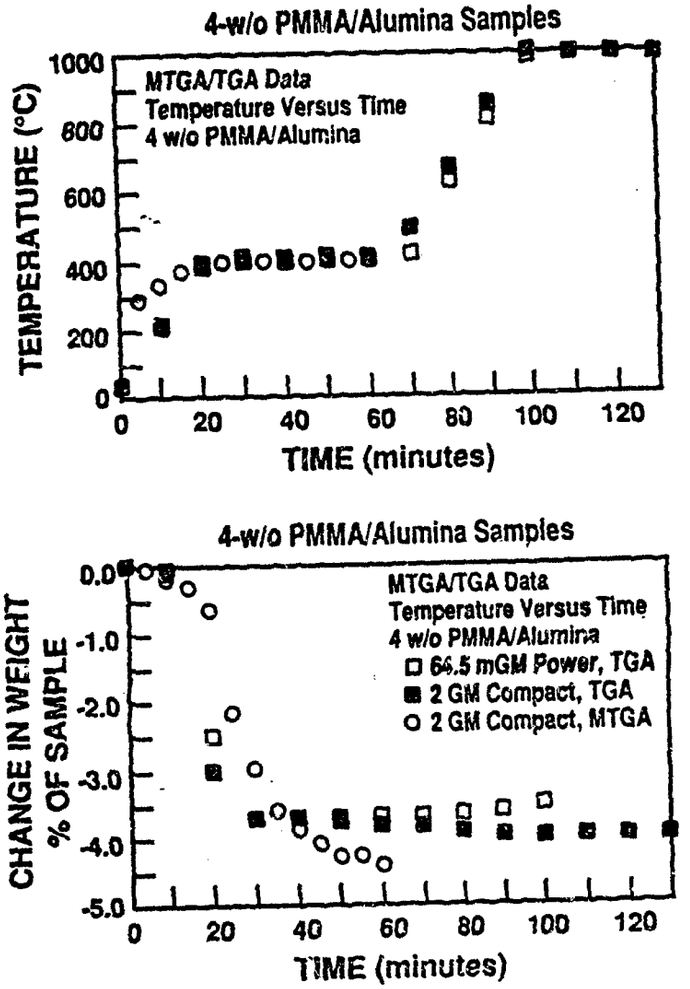


Figure 3. Temperature and Change in Weight % of a Sample versus Time for the 4 w/o PMMA/Alumina system (TGA and MTGA data).

delay in the binder removal and the heating schedule to 400°C, is artificial, as the average heating rate was used in programming the TGAs heating schedule. The TGAs heating schedules are linear, whereas the actual heating schedule of the MTGA is more of a parabolic curve (not linear).

Several other sets of experiments were conducted in the MTGA, but will not be included here. Essentially, these experiments demonstrated that the processing of samples in the MTGA are repeatable, the MTGA is reasonably stable, larger samples heat slower, binder removal from larger samples is delayed and other sample systems may be processed via MTGA.

CONCLUSIONS

As the sample size/weight increased, longer times were required to heat the samples under identical conditions. As the sample weight increased, a delay in the removal of binder was observed in the MTGA. There seems to be no major advantage or disadvantage to either MHH or IR heating of these samples. However, an advantage for MHH and/or microwave heating would be expected for much larger samples. A relation between the amount of binder in the samples and the extent of binder decomposition, under identical processing conditions, does not seem apparent.

ACKNOWLEDGEMENTS

The authors thank the University of Florida, DARPA and the United States Air Force for funding. Special thanks also goes out to the Department of Materials Science and Engineering, the Advanced Materials Research Center and the Department of Chemistry, all of which are located at the University of Florida.

REFERENCES

1. L.M. Sheppard. Manufacturing Ceramics With Microwaves: The Potential For Economic Production, Ceramic Bulletin, Volume 67, Number 10, pp. 1656-1662, 1988.
2. W.H. Sutton, Microwave Processing Of Ceramic Materials, Ceramic Bulletin, Volume 68, Number 2, pp. 376-386, 1989.
3. Y.-N. Sun, M.D. Sacks and J.W. Williams, Pyrolysis Behavior Of Acrylic Polymers And Acrylic Polymer/Ceramic Mixtures, pp. 538-548, Ceramic Transactions Ceramic Powder Science II Volume 1, First Edition, Edited by G.L. Messing, E.R. Fuller, Jr.and H. Hausner, Westerville, Ohio, 1988.
4. M.R. Barone, J.C. Ulicny, R.R. Hengst and J.P. Pollinger, Removal Of Organic Binders In Ceramic Powder Compacts, pp. 575-583, Ceramic Transactions Ceramic Powder Science II Volume 1, First Edition, Edited by G.L. Messing, E.R. Fuller, Jr. and H. Hausner, Westerville, Ohio, 1988.
5. G.W. Scheiffele and M.D. Sacks, Pyrolysis Of Poly(Vinyl Butyral) Binders: II, Effects Of Processing Variables, pp. 559-566, Ceramic Transactions Ceramic Powder Science II Volume 1, First Edition, Edited by G.L. Messing, E.R. Fuller, Jr. and H. Hausner, Westerville, Ohio, 1988.
6. S.J. Oda, B.G. Woods and J. Foster, Microwave/Infrared Drying Of Extruded Ceramic Forms, Journal Of The Canadian Ceramic Society, Volume 56, Number 4, pp. 70-73, 1987.
7. A.C. Metaxas and J.R. Meredith, Chapter 3 Dielectric Properties, pp. 28-32, Industrial Microwave Heating, Second Edition, No Editor, Peter Peregrinus Ltd., London U.K., 1983.

AN APPLICATOR DESIGN FOR PROCESSING LARGE QUANTITIES OF DIELECTRIC MATERIAL

Van Nguyen Tran
Deakin University
Victoria 3217
Australia

ABSTRACT

Knowledge of the dielectric properties of a material is essential for a proper design of an efficient applicator. The paper discusses the interaction of EM waves with a dielectric material. The analytical solution to the problem of a line source illuminating a cylinder is discussed. This then leads to a description of the technique of designing a new type of applicator for heating a large quantity of dielectric material. Experimental results are presented and discussed. The new applicator is capable of operating in a batch or continuous mode.

INTRODUCTION

The literature on dielectric properties and their measurements is very extensive. For instance, in a review of dielectric properties, Metaxas and Meridith [1] provide an extensive list of publications on the subject. Some recent techniques of broadband measurement are discussed by Bussey [2], Stuchly et al [3], Tran et al [4] and Gelinas et al [5].

Information such as the rate of power absorption, the depth of penetration, the transmitted power and the reflected power can be derived from the dielectric properties. Hence a knowledge of the dielectric properties is essential for any study of microwave heating or design of applicators.

This paper is not concerned with dielectric properties but is focused essentially on the electromagnetic (EM) field distribution inside and outside a dielectric cylinder and a technique of designing a new type of applicator which provides more uniform heating in a batch or continuous mode.

INTERACTION OF EM WAVES WITH A DIELECTRIC

The analysis of the interaction of EM waves in microwave dielectric heating seems to be confined to plane waves. Such an analysis provides at least an insight into the problem. However, the exact solution to many large scale microwave applicators is still too difficult and time consuming even on a large computer. Recently, an analysis was reported on the field distribution inside a simple multimode cavity such as a domestic microwave oven using a finite element technique [6]. A CRAY super computerwas required for the analysis.

Analyzing the interaction of EM waves with an arbitrary shaped lump of dielectric material is difficult. The problem becomes more compounded when one has to match the obtained solution with the boundary conditions of the metallic shielding enclosure.

Fortunately, the interaction of EM waves with an infinite lengtth dielectric cylinder is a problem to which the solution is available in the analytical form. There has been considerable interest in the solution for the field distribution in such a 2D problem. While the field outside the cylinder gives information on the reflected energy, ie., the efficiency of directing energy into the material, the inside field provides information on heating uniformity and the presence of hot and cold spots.

There are many industrial examples where the solution is applicable. These include drying of timber logs, curing of fibreglass masts for wind surf boards, sintering of ceramic cylinders and rods and investigating the biological effects on human parts.

The general solution to this 2D problem is described by Jones [7] as the solution for the scattering of EM waves (plane or cylindrical) by a dielectric cylinder.

The solutions for the fields inside and outside the cylinder must satisfy the boundary conditions at the interface, which depend upon the polarization of the incident EM field, viz. the electric field in parallel with or at right angles to the axis of the cylinder. If Ei is the field incident to the cylinder, Ec is the field inside the cylinder and Es is the scattered field on the outside, then Ei+Es is the standing wave outside the cylinder while Ec is the standing wave on the inside. Thus, by calculating the magnitude of these quantities, one obtains the reflection from the cylinder as well as the distribution of the magnitude of the field inside the cylinder. The expressions for Ei, Es and Ec are given by Jones [7]. For a given cylinder of dielectric, by applying the appropriate boundary conditions, one obtains the exact expressions for Es and Ec from Ei.

Furthermore, the power at each point inside the cylinder can be readily calculated by applying the Poynting's vector for power density. Thus the radial power component is given by:

$$Pr=i/(2we\ e\ )E^{*}dE/dr \qquad (1)$$

and the azimuthal component

$$Po=i/(2we\ e\ r)E^{*}dE/do \qquad (2)$$

If the diameter of the cylinder is small compared to the wavelength, the power distribution inside the cylinder is quite uniform. However, if the diameter is comparable or larger than the wavelength, uniform power distribution is most unlikely. There are also situations when the field at the axis of the cylinder is higher than the surrounding.

DESIGN PRINCIPLE FOR A NEW APPLICATOR

When the diameter of the dielectric cylinder is large compared to the wavelength, the above analysis shows that the power distribution inside the cylinder is not uniform when it is illuminated by a single line source. The degree of unevenness depends on the dielectric properties and the diameter of the cylinder. What one obtains from the analysis is the combined effect of power decaying with distance and the internal standing wave pattern.

One way of overcoming the uneven heating is to deploy more line sources around the cylinder. In biomedical applications, an experimental investigation has been carried out by Wyslouzil et al [8]. The authors demonstrated that an increase in the 'effective' depth of penetration is possible

when more than one source were used. If the applicators are fed from the same source, then the phase relationship between the different applicators have a very significant effect (in some cases disastrous effect) on the resulting heating patterns. It is reported that in the planar dielectric case, more applicators can be used to heat large areas with good uniformity. In the case of cylindrical surfaces, there appears to be considerable improvement in terms of

uniformity and penetration depth in going from one to two to four applicators.

The analysis for such a situation can be carried out as follows. If the solution for a single source is known, then the solution for many such sources deployed around a cylinder can be obtained by rotating the source and by using the principle of superposition. Some preliminary results from such an analysis were reported in a recent conference [9].

In practice, to prevent leakage and to provide adequate safety for operating personnel, the sources and the cylinder are placed inside a shielding metallic enclosure. The shielding enclosure may assume a

number of shapes such as cylindrical, rectangular or even arbitrary. However a better use of the enclosure can be made if its non absorbing but reflecting characteristics are integrated into the design of the applicator to create a more uniform heating applicator.

Assuming that the shielding enclosure consists of a number of reflectors and if each reflector is deployed on the opposite side to a source, then any unabsorbed power will be reflected back to the cylinder for further absorption. If the dielectric material is not very absorbent, a dangerous situation may arise: most of the incident power will find its way back to the magnetron! If the latter is not protected by a circulator, its operation will soon cease. The rule of thumb is as follows. For a given dielectric material, select a diameter such that after the first pass the power is reduced to at least 1/4. After reflection on the second pass the power will be reduced to 1/16. Reflected power at this level even if all of it finds its way back into the magnetron will not be sufficient to cause any damage to even an unprotected magnetron. Furthermore, the left over power after the second pass can be controlled in such a way that it combines destructively with the scattered power from the cylinder.

In this case, the reflection into the magnetron will become small (a very desirable situation). If the sources are directional, the mutual coupling will be small.

It has been found that the corner type of reflector is most appropriate and practical to use. For instance if five sources are used around a cylinder then there must be five corner reflectors. The shielding enclosure will then assume the shape of a pentagon.

The analysis for this problem becomes the superposition of many sources : those deployed and their images in the reflecting enclosure.

RESULTS

Figure 1 shows the general cross section of the applicator. Each source is a horn antenna approximating a parabolic shape to emulate a line source. The size of the enclosure is selected so that the standing wave in the horn antenna is minimum for a given dielectric material. Figure 2 gives the measured results for the following case. The material has a dielectric constant 7 and a loss factor 1.7, the cylinder diameter is 150mm and since the material is granular, it is kept inside a PVC pipe having the same inner diameter of 150mm. Only one source is energized in this experiment and the temperature distribution measured is quite interesting. Temperatue measurement is done by a fine Al/Cr thermocouple after each exposure. The exposure time is 60 seconds. The resulting heating pattern is due to the effects of the source plus the reflecting enclosure and any thermal conduction which may have occurred during the experiment and subsequent duration of the temperature measurement. The heating pattern has a higher temperature area around the axis of the cylinder. This result is different from the theoretical results shown in Figure 3.

Figure 3 shows the theoretical power contours obtained for the same dielectric cylinder illuminated by a single source but without the pentagon reflector system. The side facing the source is hotter and there is a depression or a colder spot on the opposite side. Thus it appears that the enclosure has a significant contribution to the overall heating pattern in this case. Further analysis results involving the enclosure are being investigated.

CONCLUSION

The design concept seems to work out well. So far a number of applicators hve been built for industries. One machine uses a conveyor belt, another uses a rotating drum, yet another uses a pump to push a slurry through the pipe vertically. It is totally flexible and can accomodate quite a range of materials and trnasport systems. Every system works satisfactorily with a coupling efficiency greater than 80% relative to the theoretical total microwave output of all the magnetrons in the system.

REFERENCE

[1] Metaxas A.C. and Meridith R.J. 'Industrial Microwave Heating', Chapter 3, pp26-69, IEE Power Engineering Series 4

[2] Bussey, H.E. 'Dielectric Measurements in a shielded open circuit coaxial line', IEEE Trans. Instrum. Meas., vol. IM-29, pp. 120-124, June 1980.

[3] Stuchly,S.S., Rzepecka,M.A., and Iskanda,M.F. 'Permittivity Measurements at Microwave Frequencies Using Lumped Elements', IEEE Trans. Instrum. Meas., vol. IM-23, pp. 56-62.

[4]Tran, V.N.,Stuchly,S.S., and Kraszewski,A.,"Dielectric Properties of Selected Vegetables and Fruits, 0.1-10 GHz', J. Microwave Power, 19(4), 1984, pp. 251-258.

[5] Gelinas, S.,Tran,V.N., Vaillancourt,R. 'Global Iterative Solution of Dielectric Spectroscopy Equations.' IEEE Trans. Instrum. Meas., vol IM-39, pp. 615-620.

[6] Yang,S. and Pearce,A. 'Boundary Condition Effects on Microwave Spatial Power Deposition Patterns.' Proceedings of the High Frequency/Micrwave Processing and Heating, Arnhem, The Netherlands, September 1989, pp 221-228.

[7] Jones, D.S. 'Theory of Electromagnetism' Pergamon Press (1964), Chapter 8, pp. 450-467.

[8] Wyslouzil,W., Kashyap, S, and Daien, D.M. 'Heating Patterns for an Array of 915 MHz Rectangular Waveguide Applicators', J. Microwave Power, pp 213-220.

[9] Tran, V.N., 'Dielectric Heating of an Infinite Cylinder' Proceedings of the 3rd Asia-Pacific Microwave Conference, Tokyo, September 1990, pp.1187-1189.

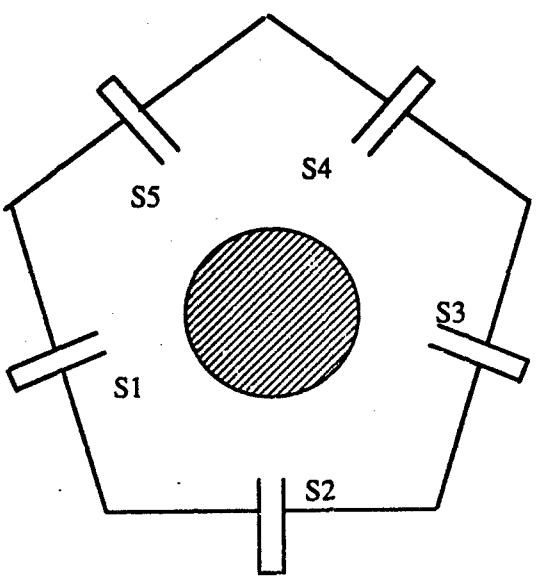


Figure 1. Pentagonic applicator

S1,S2,S3,S4,S5 : line sources

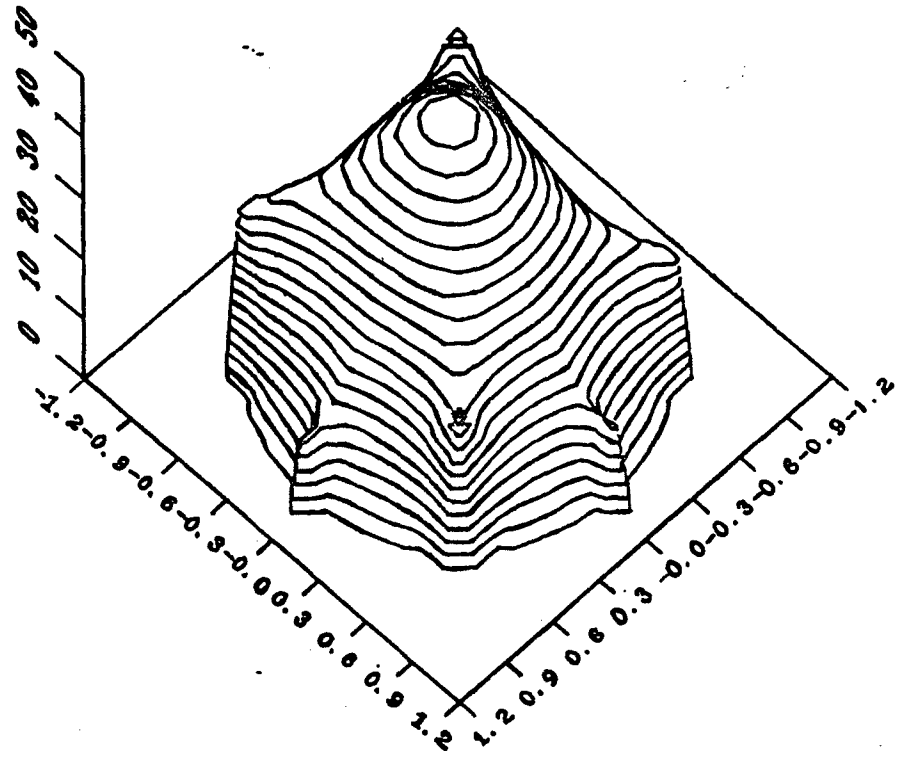


Fig.2 Heating Pattern from a single source in a pentagonic shielding enclosure.

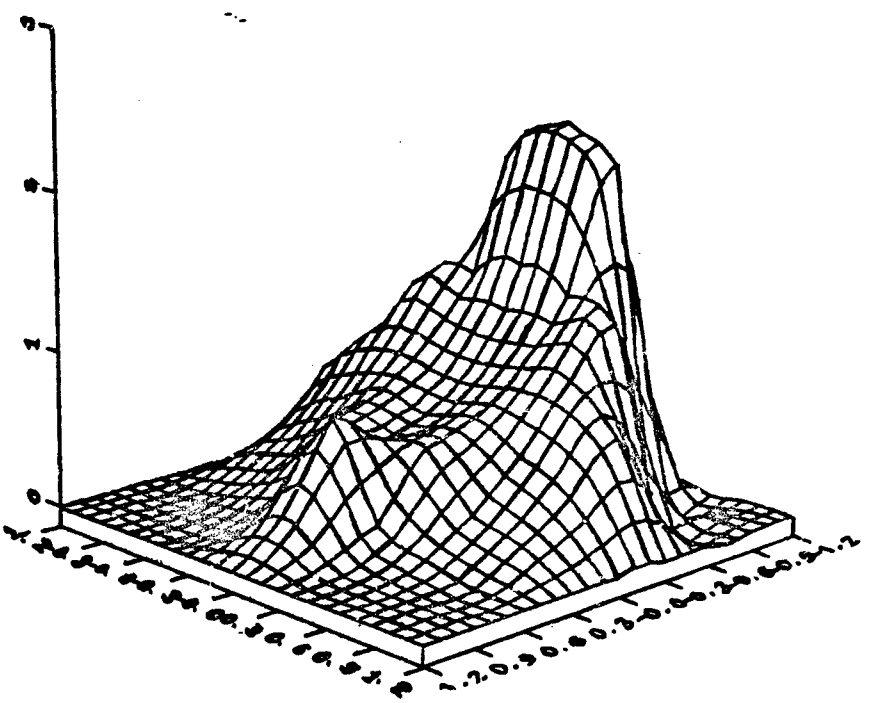


Fig.3 Power contours from a single source without the pentagon shield.

INDEX

1,2 dichloralethane, 203

Absorption, 523
Absorption mechanisms, 51
Activation energy, 107, 185
Active carbons, 467
Advanced ceramics, 3
Aerosol drying, 597
Agrawal, D.K., 349
Ahmad, I., 319, 329, 515, 605, 623, 675
Al-Assafi, S., 515
Al_2O_3:ZrO_2, 565
Alumina, 235, 301
Alumina powders, 225
Aluminum nitride, 421
Aluminium-tri-isopropanolate (ATIP), 631
Andrade, O., 35, 141
Anisotropic load, 547
Applicator design, 683
Asmussen, J., Jr., 159, 547, 655
Attenuation coefficient, 547

Balbaa, I.S., 475
Barmatz, M., 261, 271
Batch mode, 683
Bescher, E., 557
Binder, 675
Binder burnout, 29
Bioeffects, 125
Biological cell death, 125
Black, W.M., 487
Blake, R.D., 95, 487
Boltzmann thermal model, 185
Booske, J.H., 185
Boron carbide (B_4C), 375
Borosilicate glass, 441, 451
Bruce, R. W., 107
Burn thresholds, 125

Cadieux, J.R., 441
Calhoun, C.L., 311
Carbides, 387
Carbon, 387
Carbon-fiber composites, 539
Carbon fiber epoxy composites, 547
Carbon regeneration, 467
Carbothermal reduction, 387, 395
Catalyst-containing carbon, 467
Cavity perturbation theory, 261, 271
Cavity Q, 667
Cermets, 557
Chalcocite (Cu_2S), 203
Chalcopyrite (CuFeS), 203
Characteristic matrix, 159
Charge trapping, 225
Chemical strengthening, 623
Chemical synthesis, 3
Cheng, C., 35
Chiral composites, 523, 531
Chow, J.R., 235
Christiansen, D.E., 597
Chromium-alumina, 557
Clark, D.E., 29, 319, 329, 357, 451, 515, 605, 623, 675
Coax techniques, 235
Coaxial cavity, 215, 647
Coaxial line, 203
Coaxial load, 159
Coffey, D.W., 411
Combustion synthesis, 29, 487
Compaction pressure, 605
Complex dielectric constant, 261
Computational techniques, 141
Conducting load, 159
Conduction losses, 51
Constant frequency operation, 667
Contact exposures, 125
Contaminated soils, 459
Continuous mode, 683
Convective heat loss, 177
Conventional heating, 497
Conway, J.C., 507
Cooper, R.F., 185
Copper-alumina, 557
Coupling behavior, 235
Cozzi, A.D., 357
Cracking, 283

Crow, J.E., 613
Crucibles, 433
Cyclohexane, 203
Cylinder, 683
Cylindrical cavity, 159
Cylindrical cavities, 655

Dahimene, M., 301, 565
Dé, A., 319, 329
Decomposition, 675
Defects, 225
Defense Waste Processing Facility (DWPF), 441
Density, 203
Density measurements, 35
Detoxification, 459
Detoxification experiments, 467
Detoxification of TCE, 467
Dhulipala, R., 587
Dielectric constant, 203, 243
Dielectric measurements, 215, 587
Dielectric properties, 107, 203, 225, 235, 251, 623, 683
Dielectric properties measurements, 35
Diffusion, 95, 411, 515
Diffusion controlled reaction kinetics, 605
Diffusion paths, 507
Dipole reorientation, 51
Discontinuous grain growth, 225
Distribution of electric fields, 193
Dobson, I., 185
Dopants, 225
Dry air flow, 467
Dykes, N.L., 375
Dynamic heating and characterizing, 251
Dynamic sintering, 225

Eigenfrequencies, 159
Eisenhart, R.L., 235
Elastic oscillations, 185
Electric field strength, 167
Electric loss, 51
Electrical conductivity, 539
Electrical impedance, 539
Electro-optic ceramics, 29
Electromagnetic interference (EMI), 641
Electron microprobe analysis, 623
Electrophobia, 125
EMI immunity, 641
Energy consumption, 475
Environmental wastes, 3
Equivalent circuit, 251
Extent of cure, 587

Fan, J., 459
Fang, Y., 349
Fast firing, 329
Fathi, Z., 357, 451, 515, 623
FCA carbon, 467
Ferber, M.K., 411
Ferrimagnetic resonance, 51
Fiber-placement manufacturing, 539
Field distribution, 35
Field partitioning, 51
Field patterns, 655
Filament drying, 597
Finite-difference time-domain (FDTD), 35, 141
Finite element method, 193
Flaw control, 631
Folz, D.C., 29
Fournier, G., 667
Fracture toughness, 35
Free-space microwave set up, 243
Fringing capacitances, 203
Fritz, R., 547, 655

Gallerneault, C., 193
Gavulic, J., 301, 565
Gel, 515
George, C.E., 459
Gerling, J.F., 667
Ghodgaonkar, D.K., 243, 251
Gielisse, P.J., 613
Glass, 451
Glass melting, 29
Gold adsorption capacity, 475
Gold adsorption rate, 475
Grain growth, 411
Grain size, 349
Grain size distribution, 225
Grain structure, 81
Graphite, 387
Graphite fiber epoxy, 547, 655

Graphite fiber-reinforced epoxy composite, 547
Green state joining, 497
Guo, J.-K., 577

Hagenlocher, C.O., 271
Harris, N.H., 235
Hawley, M.C., 587
Hazardous wastes, 467
$HCl + Cl_2$, 467
Heat flow, 547
Heating distribution, 655
Heating rates, 329
High frequency dielectric heating, 523
High purity silicon, 403
High Q cavities, 667
High-temperature microwave dielectrometer, 215
High-temperature superconductors, 613
Holcombe, C.E., 375, 403
Hollinger, R.D., 243
Holt, R.T., 395
Hottong, Ursula, 587
Hubbard, C.M., 411
Hubbard, C.R., 403
Hydroxyapatite ceramics, 349
Hysteresis effect, 177

Ibarra, A., 225
Impedance analyzer, 251
Impedance method, 167
In situ measurement, 251
In situ monitoring, 243
Industrial microwave heating applications, 3
Infiltrated, 631
Infrared heating, 675
Interlaminar shear strength, 539
Interlayer materials, 487
Internal tuning and matching, 647
Ion diffusion, 185
Ion exchange, 623
Iris, 251
Iskander, M.F., 35, 141

Jackson, H.W., 261
Jang, S.J., 51
Janney, M.A., 311
Jantzen, C.M., 441
Johnson, D.L., 17, 365
Jones, D.K., 357
Jones, F., 51
Jun, I., 459

Kao, Y.H., 341
Katz, J.D., 95, 487
Kenkre, V.M., 69, 95
Kiggans, J.O., 403, 411
Kimrey, H.D., 35, 141, 311, 403
Kingon, A.I., 421
Knowlton, R., 35
Kozuka, H., 387
Kriegsmann, G.A., 177
Kumar, S.N., 395
Kurz, J.E., 539

Laminar flow, 421
Lamoreaux, S., 35, 141
Large quantity, 683
Leakage suppression, 125
Li, B.-S., 577
Lind, A.C., 539
Lodding, A.R., 623
Long lines effect, 667
Lorenson, C., 193
Loss factor, 523
Loss mechanisms, 95
Loss tangent, 203, 225, 243
Lossy dielectric spinere, 261, 271
Lossy dielectrics, 159

Ma, Y., 523
Mackenzie, J.D., 341, 387, 557
Magnetic field strength, 167
Magnetic loss, 51
Magnetite (Fe_3O_4), 341
Magnetometers, 613
Magnetron cooling system, 667
Magnetron isolation, 667
Manning, B., 159, 655
Materials consolidation, 341
Mathematical modeling, 193
Maxwell-Boltzmann distribution, 185
McCaughan, L., 185
McCurry, L.E., 117

Mechanical strength, 349
Meek, T.T., 81
Mehta, K., 35
Mehta, P., 421
Mershon, J., 641
Metal-ceramic composites, 557
Metallorganic, 631
Method of moments, 193
Mg-vacancy dipoles, 225
MgO-doped sample, 225
Microcircuitry, 613
Microstructural evolution, 225
Microstructural homogeneity, 319
Microstructural uniformity, 319
Microstructure, 349, 357, 411
Microwave absorption, 261, 271, 531
Microwave annealing, 411
Microwave applicator, 539, 647
Microwave cavity, 547, 597
Microwave couplers, 341
Microwave fusions, 441
Microwave heating, 17, 81, 167, 177, 341, 387, 403, 459, 467, 539, 557, 605, 675
Microwave hybrid heating (MHH), 29, 319, 329, 675
Microwave interactions, 69, 141
Microwave joining, 29, 487, 507, 515
Microwave melting metals, 433
Microwave reactivation, 475
Microwave resonance spectra, 51
Microwave sintering, 17, 35, 117, 301, 311, 319, 329, 341, 357, 365, 565, 577, 613
Microwave slurry vitrification, 441
Microwave thermogravimetric analyzer (MTGA), 29, 675
Minerals, 3, 203
Miranzo, P., 225
Mode matching, 159
Mode switching, 587, 655
Modeling, 167
Moist air flow, 467
Mollá, J., 225
Moore, E. H., 675
More, K.L., 411
Moreno, R., 225
Moya, J.S., 225
Mutsuddy, B.C., 301, 565

Nandi, S.P., 467
Nanophase, 395
NbC, 387
Network analyzer, 203
Network analyzer system, 251
Newnham, R.E., 51
Ng-Yellm, J., 395
Niculescu, H., 613
Nitridation, 403
Nonlinear finite element method, 167
Nonlinear skin effect, 177
Nonlinearity, 177
Nonsymmetric microwave radiation, 167
Nonthermal effects, 125
Nonthermal microwave plasma, 421
Nonthermal phonon distribution, 185
Nonuniform heating, 167
Nuclear waste, 441, 451
Nuclear waste glass, 433
Numerical modeling, 141, 159

Oda, S.J., 3, 475
Optical fiber temperature probes, 475, 547
Optical fiber thermometry (OFT), 641
Osepchuk, J.M., 125
Oxidative degradation, 467
Oxide, 81
Oxygen fugacity, 441
Oxygen vacancies, 225

Palaith, D., 487
Pant, A., 395
Particulate additives, 341
Patil, D.S., 301, 565
PEEK, 539
Penetration depth, 475, 547, 623
Perchloralethylene, 203
Permitivity, 225, 271
Pernambuco-Wise, P., 613
Photon/phonon coupling, 185
Pierce, B.M., 235
Plasma, 365
Plasma heating, 17
Plutonium dioxide, 117
Point defects, 185
Polarization mechanisms, 225

Polycrystalline alumina, 605
Polyester, 587
Polyester/glass composite, 587
Polymer-impregnated carbon fibers, 539
Polymethyl methacrylate (PMMA)/ alumina, 675
Polytypic modifications, 421
Porous ceramic matrices, 631
Potential energy barrier, 185
Powders, 421, 605
Power absorption, 531
Power coupling, 667
Power distribution, 547
Precursor gases, 421
Product gases, 467
Pyrochemical reactions, 117
Pyrolysis, 467
Pyrometer, 641

Quality factor, 655
Quasi-contact exposures, 125

Rader, M., 81
Radiation heat loss, 177
Radiation link elements, 167
Radiation/matter interaction, 193
Radiofrequency hazards, 125
Reaction bonded silicon nitride (RBSN), 403
Redox measurements, 441
Reference materials, 203
Reflected power, 667
Reflection coefficient, 203, 251
Relaxation spectra, 51
Remoted, 117, 433
Requena, J., 225
Resistance furnaces, 395
Resistive temperature detectors (RTDs), 641
Resonant cavity, 301, 547, 565
Resonant energy, 185
Resonant frequencies, 655
Ro, R., 531
Roy, B., 613
Roy, D.M., 349
Roy, R., 349

S-shaped response curve, 177
Sa'adaldin, H.S., 487
Safety standards, 125
Salsman, J.B., 203
Scanning acoustic microscope, 497
Scanning electron microscope, 497
Schulz, R.L., 451
Screen printing, 613
Selective enhancement of heating, 341
Self strengthened, 631
Shi, J.-L., 577
Si interlayer, 487
SiC, 387, 487
SiC whiskers, 387
Siegel, M., 655
Silberglitt, R., 487
Silicon carbide, 395
Silicon nitride, 235, 411
Simmons, J.H., 623
Simultaneous sintering and joining, 497
Singh, A.K., 421
Single crystal alumina, 605
Single mode microwave cavities, 17, 365
Single mode applicators, 159, 283, 301, 565
Single mode/controlled multimode, 547
Single mode microwave heating device, 251
Single mode microwave resonator, 271
Single mode rectangular cavity, 261
Sintering aid, 341
Skin effect, 547
Slip interlayer, 497
Smith, R., 35, 141
Soda-lime glass, 341
Sodium aluminosilicate, 623
Solid state reactions, 29, 605
Sood, R.R., 395
Space charge phenomena, 51
Spent carbon, 475
Spray-drying process, 597
Static sintering, 225
Steele, R.R., 403
Stuecken, E.F., 117, 433
Superconductors, 29, 357
Surface bonds, 185
Surface modification, 29, 623
Sweeney, M.P., 365

Sykora, G., 613
Synthesis, 421

TaC, 387
Tails from the infrared, 51
Tanner, C., 35
TCE adsorption, 467
TE_{011} mode cavity, 539
Teflon, 203
Temperature controller, 641
Temperature dependent dielectric properties, 167
Temperature gradients, 547
Temperature heterogeneity, 233
Temperature measurement, 467
Temperature profiles, 547
Thermal damage, 125
Thermal diffusivity, 35
Thermal partitioning, 185
Thermal runaway, 51, 69, 167, 177, 283
Thermocouple, 203, 641
Thermogravimetric analyzer (TGA), 675
Thick film sensors, 613
Thick-section composite, 547
Tian, B.Q., 647
Tian, Y.-L., 283, 577
TiC, 387
Tiegs, T.N., 403, 411
Tinga, W.R., 215, 647
Titanium diboride (TiB_2), 375
Toughening, 631
Tran, V.N., 683
Transmission electron microscopy, 395
Trichloroethylene (TCE), 467

Ultra-fine grain sizes, 577
Ultra-high temperature sintering, 375
Ultra-rapid heating, 319
Ultra-rapid sintering, 29, 283
Unruh, W.P., 597
Uranium oxides, 117

Vacuum, 459
Varadan, V.K., 167, 243, 251, 497, 507, 523, 531
Varadan, V.V., 167, 243, 251, 497, 507, 523, 531
Variable coupling, 655
Variable Q, 667
Variable short, 251
Varma, R., 467
Virkar, A., 35
Vitrification, 441
Vodegel, S., 631

Wahlers, R., 613
Water, 459
Watkins, J.L., 271
Waveguide techniques, 235
Wear, F.C., 539
Wei, J., 587
Weibull plots, 507
Whitewares, 29
Whitney, E. D., 319, 329
Wicks, G.G., 451
Willert-Porada, M.A., 631

Xi, W., 215
X-ray diffraction, 395
Xu, M., 51
Xu, Y.-P., 577

$YBa_2Cu_3O_{7-x}$, 29
Y-TZP (Y_2O_3 stabilized tetragonal ZrO_2 polycrystals), 577
Yen, D.-S., 577
Yiin, T.Y., 507
Yu, X.D., 167, 251, 497

Zhang, X., 81
Zirconia, 311
$ZnAl_2O_4$, 605

V

Published by
The American Ceramic Society, Inc.
Westerville, Ohio
ISBN 0-944904-43-2



END

FILMED

DATE: 9-92

DTIC